The Statistical Modelling of Production Processes of Biodegradable Aliphatic Aromatic Co-Polyester Fibres used in the Textile Industry

Basel Younes

Submitted for the degree of Doctor of Philosophy

Heriot-Watt University
School of Textiles and Design

April - 2012

ABSTRACT

Since the success of production processes in the textile industry depends on good planning and having a clear programme from the raw materials until the final product, the focus of this research is in the modelling of the production process of biodegradable aliphatic-aromatic co-polyester (AAC) fibres. The statistical modelling of the effects of the extrusion temperature profile and polymer grade on the properties of linear AAC as-spun fibres aims to find the better linear grade to be used. The investigation helped to establish a statistical method to optimize the extrusion temperature profile required for extrusion of AAC fibres. The effects of melt spinning conditions together with linear and branched grades of AACs on as-spun fibres were statistically modelled, programmed and evaluated. To identify the effect of the drawing process, the effect of multi stage hot and cold drawing process on AACs fibres has been statistically investigated and modelled. The additional effect gained from twisting the drawn fibres has been investigated in terms of process parameters interactions. Forecasting models have been set for optimizing and controlling the manufacturing of biodegradable AACs fibres. The novel statistical factorial method will help when taking the best experimental decision controlled by the design factors.

ACKNOWLEDGMENT

I wish to express my deep appreciation to **Dr. Alex Fotheringham**, Project Supervisor, for his encouragement, guidance, and greatly valued support throughout every phase of my MPhil/PhD program. Whenever I had a problem, his help was right there for me as an advisor and as a friend. Special thanks go to **The Syrian Capacity Building Project**, between the Syrian High Ministry of Education/Damascus University and British Council for supporting and funding, and to **Dr. Gassan Haddad** from FMEE-Damascus University for his internal supervision. I wish to express my sincere thanks to the **technicians, librarians and staff** in the School of Textiles and Design/Heriot-Watt University who have answered many questions that guided me along the way; my sincere thanks are also due to **Mr. James McVee** and previously to **Mrs. Magi Robson** for their much appreciated technical support on testing equipment. I want to give special thanks to **Dr. Robert .R Mather** from EPS/Heriot-Watt University for his helpful comments and stimulating discussions.

I also wish to thank the following: From Heriot-Watt University, **Mrs. Marian K Millar** from the School of Engineering and Physical Sciences for the technical support on the X-ray diffractometer, and **Dr. Christine D Taylor** from School of Mathematical and Computer Sciences for the technical support on programming; **Prof. Hassan M. EL-Dessouky** from School of Design, University of Leeds for their helpful comments and technical support on the Pluta microscope; from the STFC-Engineering Instrument Pool, **Mr. Peter Anthony** for their helpful comments and technical support in the Thermo-graphic measurement equipment, and **Dr. Alan Ruddell** for the results and helpful comments on the SKYSCAN Scanner. From Napier University, **Mrs. Lynn Chalmers**, polymer laboratory and **Mr. Colin S. Hindle** for the technical support on Brabender machine.

Lastly, and most importantly, my deepest thanks go to my wife ***Buthaina*** for her unconditional love, constant patience, encouragement and unlimited support. I also want to thank my lovely son, ***Yousef,*** who brings me so much fun and makes me happy. I would like to extend my gratitude to my **family** and **friends** in **Syria** and **Scotland** for their love and support.

TABLE OF CONTENTS

GLOSSARY OF TERMS

- Biomaterials: any synthetic or natural materials which interact with biological systems for construct artificial organs, rehabilitation devices, or prostheses and replace natural body tissues.
- Biomass: biological-based material from living, or recently living organisms.
- Bioplastics: a form of plastics derived from renewable biomaterial sources.
- Biodegradation: the chemical dissolution of materials where substances are broken down by bacteria, living organisms or other biological means
- Composite materials: engineered or naturally occurring materials made from two or more constituent materials with significantly different physical or chemical properties.
- Smart materials: materials composed of polymers which respond dramatically to very slight changes in their environment such as temperature, light, moisture, etc.
- Amorphous structure: structure with no long-range order where the atoms or molecules are not periodically located over large distances.
- Crystalline structure: structure with a unique arrangement of atoms or molecules.
- Moiety: a specific group of atoms within a molecule which is responsible for characteristic chemical reactions of that molecule.
- Uniaxial orientation: a method of orientation in which the orienting stress is applied in one direction only.
- Glass transition or liquid-glass transition: The reversible transition in amorphous materials (or in amorphous regions within semi-crystalline materials) from a hard and relatively brittle state into a molten or rubber-like state.
- Glass transition temperature (T_g): temperature at which an amorphous solid becomes soft upon heating or brittle upon cooling.
- Thermal recycling: method for breaking down polymeric materials simply by treatment at high temperature in an inert atmosphere.

LIST OF PUBLICATIONS

❖ **Publications**

1. B. Younes and A. Fotheringham, "Factorial Optimisation of the Effects of Extrusion Temperature Profile and Polymer Grade on As-spun Aliphatic-Aromatic Co-Polyester Fibres, II. Crystographic Order," Journal of Applied Polymer Science, 119:4 (2011), 1896-1904.
2. B. Younes, A. Fotheringham, and R. Mather, "Factorial Optimisation of the Effects of Melt Spinning Conditions on Biodegradable As-spun Aliphatic-Aromatic Co-Polyester Fibres II. Die head pressure, Crystallographic Order and Thermo-graphic Measurement," International Polymer Processing, 2011:2 (2011), 150-163.
3. B. Younes, A. Fotheringham, and H. M. EL-Dessouky, "Birefringent approach for assessing the influence of the extrusion temperature profile on the overall orientation of as-spun aliphatic-aromatic co-polyester fibres," Polymer Engineering & Science, 49 (2009), 2492-2500.
4. B. Younes, A. Fotheringham, H. M. EL-Dessouky, and G. Haddad, "Factorial Optimisation of the Effects of Melt Spinning Conditions on As-spun Aliphatic-Aromatic Co-Polyester Fibres I. Spin Draw Ratio, Overall Orientation and Drawability," International Journal of Polymeric Materials, 60:5 (2011), 316 - 339.
5. B. Younes, A. Fotheringham, and R. Mather, "Statistical Modelling of the Effect of Multi-Stage Hot Drawing on the Thermal Shrinkage and Crystallographic Order of Biodegradable Aliphatic-Aromatic Co-Polyester Fibres," Fibers and Polymers, 2011, 12:6 (2011), 778-788.
6. B. Younes and A. Fotheringham, "Factorial Optimisation of the Effects of Melt Spinning Conditions on Biodegradable As-Spun Aliphatic-Aromatic Co-Polyester Fibres III. Diameter, Tensile Properties and Thermal shrinkage," Journal of Applied Polymer Science, 122:2 (2011), 1434-1449.
7. B. Younes, A. Fotheringham, H. M. E. Dessouky, and G. Haddad, "The influence of multi-stage hot-drawing on the overall orientation of biodegradable aliphatic-aromatic co-polyester fibers," Journal of Engineered Fibers and Fabrics, In press (March, 2013).

8. B. Younes and A. Fotheringham, "Factorial Optimisation of the Effects of Extrusion Temperature Profile and Polymer Grade on As-spun Aliphatic-Aromatic Co-Polyester Fibres III. Mechanical Properties", The Journal of the Textile Institute, 103:2 (2012), 139-153.
9. B. Younes, A. Fotheringham, and H. M. EL-Dessouky, "Factorial Optimisation of the Effects of Extrusion Temperature Profile and Polymer Grade on As-spun Aliphatic-Aromatic Co-Polyester Fibres, I. Birefringence and Overall Orientation," Journal of Applied Polymer Science, 118:3 (2010), 1270-1277.

❖ **External Conferences**

1 B. Younes and A. Fotheringham, "Statistical modelling of the extrusion of biodegradable fibres, poster presentation," AUTEX 2008 Conference, World Textile Conference, Città Studi, Biella, Italy (June 24-26, 2008).

2 B. Younes and A. Fotheringham, "Statistical modelling of the thermal properties of extruded biodegradable fibres, poster presentation," The 5th International Speciality High Performance Polymer Fibres Conference, Polymer Fibres 2008, Weston Conference Centre, University of Manchester, UK (9-11 July, 2008).

❖ **Internal Conferences and seminars**

1 Process Modelling of Starch-Based Fibres for Weaving; Presentation in Research seminar: Talking of textiles, School of Textiles and Design - Heriot Watt University - UK, 31-May-07
2 Optimisation of Weaving Process for Biopolymers. International Journal of Clothing Science and Technology, Number 6 Volume 19 ISSN 0955-6222, 2007
3 Statistical Modelling of Melt-Spinning of Biodegradable Fibres; Presentation in Research in Information: Communication and Modelling, EBS Auditorium – Heriot Watt University – UK, 12-June-2008
4 A Systematic, Statistical Approach to Model The Relationship Between The Profiles of Extrusion Temperatures to The Control of Fibre Production; Poster in Research in Information: Communication and Modelling, EBS Auditorium – Heriot Watt University – UK, 12-June-2008

5 Biodegradable Fibres: Manufacturing, Optimisation and Applications; Presentation in Inspiring Yarns: a new research seminar programme, School of textiles and design – Heriot Watt University – UK, 11-February-2009

6 The Value of Statistical Modelling for The Extrusion of Novel Biodegradable Fibres; Presentation in Materials, Design and Sustainability, The Heriot-Watt Post-Graduate Research Conference – Heriot Watt University – UK, 4-June-2009

7 Production Approach for Assessing the Influence of the Process Parameters on the Properties of Biodegradable Aliphatic-Aromatic Co-polyester Fibres; The best poster. Materials, Design and Sustainability. The Heriot-Watt Post-Graduate Research Conference – Heriot Watt University - UK, 4-June-2009

8 Two runner up prizes for Infrared Image of Biodegradable Yarn in Hot Drawing Process & Cross Section of Biodegradable Aliphatic Aromatic Co-Polyester Yarn; SELEX Galileo - Scientific Photo Competition 2010 Sponsored by SELEX Galileo & School of EPS, Heriot-Watt University– UK, 12-May-2010

❖ **Patents**

After submitted business case, Biodegradable fibre optimization process, The Innovation Exploitation Board agreed that Project is to be protected by a GB patient filing. Paper work is under reviews:

Applicant: Heriot-Watt University – UK

Application number: GB1110799.2

Date: 24-06-2011

CHAPTER 1– INTRODUCTION

The goal of this thesis is the modelling of the production process of aliphatic-aromatic co-polyester fibres and yarns used in the textile industry for tomorrow's environment. A fully biodegradable petroleum linear aliphatic-aromatic co-polyester and branched aliphatic-aromatic co-polyester were used. The AAC textiles could be used for different applications, as an alternative to commercial chemical fibres at reasonable cost, leaving no environmental footprint.

The main positive points regarding the production process could be summarised by the low processing temperature which assists in energy saving, low material and manufacturing costs, leading to lower product cost and the forecasting program which simulates the relationship between the responses and the setting of the production processes of AACs. Appropriate statistical methods were applied and a model for specifying the direction of increasing or decreasing of the significant process parameters was identified. The novel statistical method for less experienced extrusion designers will help when taking the best experimental decision controlled by the design factors.

Theoretical technique and Factorial experimental design have been applied in the optimization process. Many tools, such as Pareto charts, main effect plots, interaction plots, normal probability plots, surface plots and analysis of variance are used in the statistical analysis of experimental design. All statistical-based plots in this study were constructed directly from the raw data. Multiple and individual regressions of independent variables employ fast linear forecasting models on independent variables. Simulations of statistical data and regression equations of simplified mathematical models were obtained; they merge the user's need with the technological capabilities and programs offered by Microsoft Visual studio program. A large amount of technical data from the effect of production process parameters could be obtained by using the designed process programme before moving to the production line.

1.1 Aims and Research Objectives

1. The present research:

- Relates to biodegradable textiles and supports the production process of environmentally friendly aliphatic-aromatic co-polyester fibres.
- Investigates and simulates the relationships between the fibres/yarn properties and the processing conditions by using factorial experimental design.
- Establishes programmed forecasting models and applications in the experimental ranges studied.

2. The enhanced factorial statistical models allow the control of:

- The extrusion temperature profile.
- The melt-spinning.
- The heat setting conditions.
- The blend ratio of AACs.
- The multi-stage hot or cold drawing parameters.
- The multi-stage hot or cold drawing and twisting parameters.

3. The main targets regarding the production process could be summarised by:

- The low processing temperature and torque study assist in energy saving.
- Low material and manufacturing costs minimize the enhanced product cost.
- The forecasting program simulates the setting of the production processes of AACs, and saves both time and cost which are critical resources in manufacturing.

1.2 Structure of The Thesis

The plan in this thesis is divided into 8 different chapters; the present biopolymer was selected because, although it is produced from oil, it is biodegradable and therefore has minimal environmental effects when sent to landfill, where it degrades naturally with no toxic by-products.

Chapter 1 gives a brief introduction about the work; it gives the aims and the objectives of this research and discusses the structure of this thesis.

Chapter 2 gives a brief background about environmentally friendly materials, the man-made fibres, modelling of the melt spinning process and theoretical consideration about extrusion basis, subsequent production processes and thermo-graphic theory; it also gives an overall background about experimental design techniques used.

Chapter 3 gives details about the materials and the instruments used to produce and characterize the studied samples, it also gives details about the programming and forecasting methods used.

In **Chapter 4**, two grades of linear as-spun aliphatic-aromatic co-polyester were extruded under a fractional factorial design as a function of the extrusion temperature profile and polymer grade using appropriate statistical methods. The relationship between the extrusion temperature profile and the polymer grade as well as the torque value and the extrusion productivity on the Brabender extruder machine was statistically modelled. Heaters (temperature) and screw driver energy (torque value) could be represented as energy cost; These aids in adjusting the balance between the energy cost and the extrusion productivity of the single screw extruder without the effect of the metering pump which is used later in the melt spinning machine. Following this, the properties of the as-spun fibres were quantitatively assessed as responses to polymer grades and extrusion zone temperature which affect the properties, productivity and cost of product. The optimization of processability and spin-ability shows the combination of factor levels which maximize and minimize the responses over the region indicated. This stage is important as it helps in selecting the temperature profile and one of the polymer grades for the extruder for melt spinning process. The forecasting statistical technique saves melt-extrusion energy and helps to simplify and speed up the modelling techniques. After the previous investigation to justify the extrusion temperature profile and to find a better linear aliphatic aromatic co-polyester grade, a grade with lower melt flow index should be selected for further works on modelling of the melt spinning, drawing and twisting process.

In **Chapter 5**, the effect of melt spinning conditions on the structural and physical properties of as-spun linear and branched aliphatic-aromatic co-polyester fibres were statistically investigated and modelled. Temperature profile and the linear grade were selected based on statistical experimental analysis and the results in chapter four. A structural analysis of the properties of linear grade, and thermo-graphic, thermal and physical analyses of properties of both linear and branched grades have been characterized and modelled. The effect of heat setting conditions on mechanical and thermal shrinkage properties gives information about the thermal behaviour of fibres. The influence of the blend ratio of AACs grades has been investigated to identify the blend ratio and as-spun fibres properties relationship. The regression equations obtained from statistical analysis form the source code for the forecasting programs designed.

Using previous forecasting statistical methods, the expected models form a major part in creating a planning programme and a plan for the production process regression. The forecasting program calculates the thermal, structural and physical properties of fibres (process-output data); It depends on the process conditions (process-input data) selected by the user. It provides more technical information for scientists and technologists so that they can produce the enhanced properties at suitable conditions related to final product cost and obtain environmentally friendly, economical, energy saving fibres. The program's result helps in achieving a balance between the enhanced properties and the fibre cost; it saves the processing cost required for enhanced fibres. For evaluation of the forecasting results obtained from melt spinning of LAAC and BAAC as-spun fibres, a set of conditions was selected for each in the ranges studied.

In **Chapter 6**, modelling of the effects of multi-stage hot drawing and twist processes' conditions on thermal and physical properties of linear (LAAC) and branched (BAAC) aliphatic-aromatic co-polyester fibres was statistically investigated and characterized. For technical and experimental reasons, the multi-stage hot drawing and twisting processes of as-spun AAC fibres were operated individually. The variation in drawing conditions could lead to the enhancement of single and simple untwisted or twisted yarns properties and the investigation sought to explain the main effects and interactions observed.

To identify the heat and annealing effects added in the hot drawing process, the effect of multi stage hot drawing process on linear and branched AACs fibres has been statistically investigated and modelled. The additional effect gained from adding twisting to the continuous drawn filament was investigated in terms of the interaction between processes. Temperature profile and spinning conditions were selected based on statistical experimental analysis and the results of the spinning study. A statistical experimental

design was used as a function of process parameters using statistical factorial methods. Optimization allows the production of a range of different properties from the same sample to suit different purposes. The statistical models covered the number of drawing stages, drawing temperature, total drawing ratio, plate temperature, spin finish application, relaxing stage ratio, relaxing temperature, twisting level and their interactions. The achieved models form a part in a forecasting program designed to optimize the drawing and twist processes of selected as-spun fibres. It could be connected with the control process system or TI-83 Plus Kit which is easy to use in the work place.

In **Chapter 7**, To separate the effect of temperature and the remaining factors in the hot drawing process, modelling of cold drawing was needed. Two general lines were used in this chapter to produce multifilament, single and simple untwisted or twisted yarns: first, for untwisted yarns, modelling the effect of the multi-stage cold drawing process on the thermal and mechanical properties of both drawn linear and branched aliphatic-aromatic co-polyester fibres were statistically investigated and characterized; secondly, for twisted yarns, selected continuous drawn filaments were gently twisted. Temperature profile and spinning conditions were selected based on statistical experimental analysis and the results of the spinning study. The additional effect gained from adding twisting to the continuous drawn filament was investigated in terms of the interaction processes. Modelling the effects of multi-stage cold drawing and twisting process conditions on the thermal and mechanical properties of drawn linear and branched aliphatic-aromatic co-polyester fibres were statistically analysed and characterized. In the programming process, the relationship between key inputs (factors) and performance measures (responses) using factorial statistical experimental design technology is reported using the Texas Instrument which could be connected to a control process system. The program includes the mathematical models which estimate the studied responses, depending on the modelling and controlling of the processes. **Chapter 8** gives the conclusion of all the research carried out, what has been achieved and future work.

CHAPTER 2– LITERATURE REVIEW AND BACKGROUND

Materials, technology and applications form the components of the textile industry, which is one of the oldest industries in the world. Textiles have played a significant role in the exchanging of goods, in technology, science and ideas between the east and the west, e.g. in the links of the Silk Road [1]. Since the early 1930s, when thermoplastic materials were first produced, many kinds of synthetic fibres have been manufactured. In the last three decades, the technology of man-made fibres has been developed and the use of novel materials has opened up a wide range of engineering applications. As a result, the replacement of chemical fibres with environmentally friendly fibres has become the major goal of the modern textile industries. The competition and/or the cooperation between the textile technologies and research into the new smart materials has drawn the attention of specialists to find where the science of fibre is now, where it should go and how it achieves the targets of the textile industry.

2.1 Waste Management and Environmentally Friendly Materials for the Textile Industry

Prior to 1884, all manufactured textiles were made from natural fibres [1]. The arrival of synthetic fibres began a revolution in textile industries and opened the door for the advance of structural, functional and bio-materials. The worldwide production of non-renewable and non-biodegradable, oil-based based plastics has increased and governments are searching for solutions to the disposal of biodegradable, renewable materials to solve the waste problems [2]. Finding successful applications of environmentally friendly textiles with low operational costs and energy consumption and reducing, reusing and recycling properties are the main goals for the sustainable textile industry [3].

Depending on the polymer nature and the application, there are various methods in which bio-polymers are processed, such as polymerization, crystallization and manufacturing. The material properties are highly dependent on the structure, because polymer materials are solid, non-metallic compounds of high molecular weights [4]. The intent to reduce plastic waste began in the 1960s; waste management in textiles has become a large and expensive issue. Textile recycling after the 20th century is becoming more difficult,

because of increasing of fibre strength and fibre blends. Most textile waste is composed of natural and synthetic polymeric material [5]; the recycling resources can be thermal, material or chemical. Although thermal recycling is used in textile industries, it does not mean the recycling of the resource. It recovers polymers from fibres, but the materials obtained are not high quality. Chemical recycling is the method of the future, because it recovers monomers from fibres by polymer decomposition and pure monomers can be obtained. Alternatively, other approaches of fibre recycling technologies exist, such as pyrolysis and hydrolysis which convert the plastic wastes into basic chemicals or fuels, or burning the fibrous solid waste and utilizing the materials generated. By energy recycling, the material generates heat after its destruction [6] and the decomposition rate increases with increasing temperature.

Natural-based textiles are nearly 100% recyclable; recycling in biopolymer textiles allow environmental protection, energy and resource saving. Recycling is not the final solution for waste management. However, biodegradable products do solve the problem. The biodegradable materials and the technical progress in melt spinning processing technologies have achieved both qualitative and quantitative improvement in fibre manufacturing. The key studies on structural changes in melt spinning focus on the reinforced fibres by improving the relationship between the material properties and the process parameters. Biopolymers reduce the environmental pollution; the natural fibres could be added to biopolymers for reinforcements such as flax[7], cellulose acetate[8], ramie [9, 10], jute [11], bamboo [12], pineapple [13], kenaf [14], henequen [15], sisal[16] and hemp [17, 18]. Many scientists have worked to produce and develop new biodegradable polymers to be used in commercial products, such as ball-point pens, toothbrushes, bulk packaging, fishing lines, tennis racquet strings and wrapping paper...etc.

2.2 Biopolymers and Classification

The use of composite materials is increasing by more than 10% per year [19]. The production of novel and biodegradable fibres from biomass feed stocks has been facilitated by biotechnology that is used to produce the biodegradable biopolymers. Biodegradable polymers are friendly materials based on petroleum, agricultural or animal sources (see Table 2.1) [19]. They are classified into synthetic origin biopolymers from synthetic monomers and natural origin biopolymers from polysaccharides, protein, lipids and polyesters [20].

Biopolymers are broken down in the environment by microorganisms such as bacteria and fungi. The technique of life cycle analysis is a good method of examining the practicality of further development of biopolymer materials; biopolymers appear to be a win-win opportunity for the economy and the environment [21]. Several standardized test methods using mixed cultures for evaluation of the biodegradability and compost-ability of plastics have recently been established [22-27]. Plasticizers are added to some biopolymers during the extrusion process to reduce the intermolecular hydrogen bonds, to stabilize product properties and to limit microbial growth [28]. Biotechnology techniques are currently being used in many areas, such as tissue culture (plant, animal tissue or cells fragments), food and agriculture to develop plants [29, 30].

Classification of Biopolymers			
Natural Origins		Synthetic Origins and Synthetic monomers	
Polysaccharides	Starch, cellulose, lignin and chitin	Aliphatic Polyesters	Polyglycolic acid, Polybutylene succinate and polycaprolactone
Proteins	Gelatine, casein, silk and wool	Aromatic Polyesters	Polybutylene succinate terephthalate
Lipids	Plate oil including castor oil and animal fats	Aliphatic-Aromatic co-Polyesters	
Polyesters 1- from micro-organism or plants	1-polyhydroxyalcanoates, poly-3-hydroxybutyrate	Polyvinyl-alcohols	
2- from bio derived monomers	2- polylactic acid	Modified Polyolefin	Polyethylene or polypropylene with specific agents

Table 2.1. Classification of Biopolymers

The textile industry has been impacted by novel techniques through the development of more environmentally friendly manufacturing processes such as production of novel hygiene and infection control textiles [31]. The two main factors in increasing the market scope and size of biodegradable polymers are material properties and cost [32]. The development stages of the main bio-based polymer types, such as polymers from biomass, microbial production and polymers conventionally and chemically synthesised from renewable resources are listed in Figure 2.1.

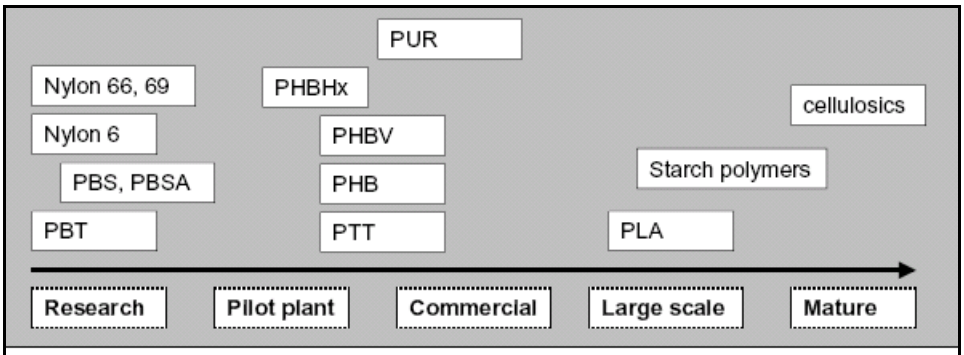

Abbrev.	Class Name
Nylon	Polyamide
PLA	Polylactic acid
PTT	Polytrimethyleneterephthalate
PBT	Polybutyleneterephthalate
PBS	Polybutylene succinate
PBSA	Polybutylene succinate adipate
PHB	Polyhydroxybutyrate (type of PHA)
PHBV	Polyhydroxybutyrate-co-hydroxyvalorate (type of PHA)
PHBHx	Polyhydroxybutyrate-co-hydroxyhexanoate (type of PHA)
PUR	Polyurethanes

Figure 2.1. The development stages of main bio-based polymer types [33]

Synthetic, biodegradable polyesters are produced in two broad types: aliphatic (linear) highly amorphous, flexible polyesters with properties similar to low density polyethylene (LDPE), and aromatic (aromatic rings) semi-crystalline, rigid polyesters with properties similar to polypropylene (PP), polyester (PS) or polyethylene telephthalate (PET), shown in Figure 2.2. They could be made from a biomass such as the agro-polymers from agro-resources (starch and cellulose), or obtained by microbial production, e.g. the polyhydroxy-alkanoates (PHA, PHB and PHBV). Some of them are conventionally and chemically synthesised, and their monomers are obtained from agro-resources, e.g. poly (lactic acid) or by chemical synthesis (PCL, aliphatic co-polyester, aromatic co-polyester) [34]. Polyesters have in their structure the potentially hydrolysable ester bond, and the corresponding enzyme responsible for the primary degradation is hydrolase [19]. Synthetic aliphatic polyesters are more expensive and lack mechanical strength compared with some conventional plastics such as polyethylene [35]. Among petroleum based biopolymers and by combining the biodegradability of aliphatic unit with the beneficial physical properties of aromatic unit, great interest has been given to aliphatic-aromatic copolymers. Recently, there has been an increasing interest in applying biodegradable aliphatic/aromatic multi-block co-polyesters for biomedical [36, 37] and agricultural [38-41] applications using non-woven technology. They are widely used for paper coating, fibres, refuse bags, disposable wipes, seed mats and erosion control items [42, 43].

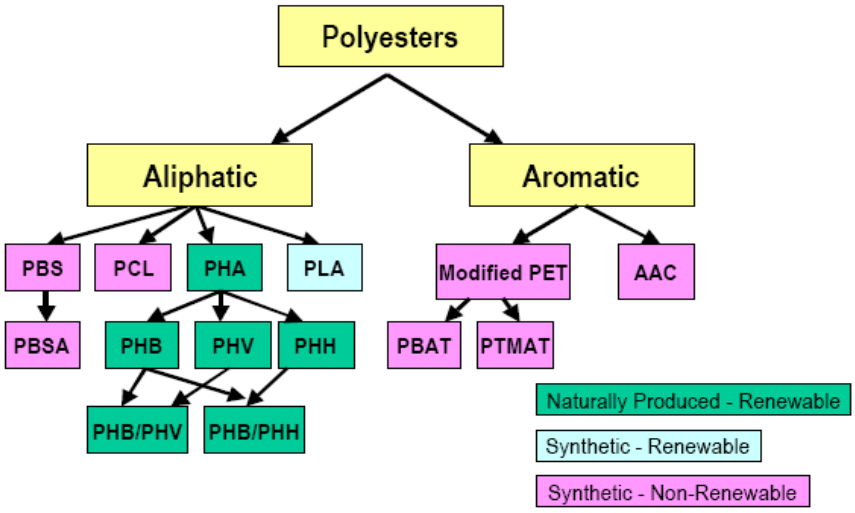

PHA – polyhydroxyalkanoates (micro-organisms- obtained by extraction)
PHB – polyhydroxybutyrate
PHH – polyhydroxyhexanoate
PHV - polyhydroxyvalerate
PLA – polylactic acid (conversional synthesis from bio-derived monomers)
PCL – polycaprolactone
PBS – polybutylene succinate
PBSA - polybutylene succinate adipate
AAC – Aliphatic-Aromatic Co-polyesters (conversional synthesis from synthetic monomers)
PET – polyethylene terephthalate
PBAT – polybutylene adipate/terephthalate
PTMAT- polyethylene adipate/terephthalate

Figure 2.2. Classification of polyesters [35]

2.3 Review on Aliphatic Aromatic Co-Polyesters

The development of biodegradable aliphatic-aromatic co-polyesters (AAC) started with different modes of degradation [44, 45]. Several AACs have been developed during the last 10 years [46, 47] and a successful future is promised for the low product cost and the excellent properties [48, 49]. AACs have lower prices with economic benefits, widely available and lower priced monomers, such as butanediol, adipic acid and terephthalic acid. Aliphatic polyesters are biodegradable and sensitive to hydrolysis; their flexible chain fits into the active site of the enzyme [50]. They are obtained by the combination of diols, such as 1, 2-ethanediol, 1, 3-propanediol or 1, 4-butadenediol, and dicarboxylic

acid (adipic, sebacic or succinic acid). Aromatic polyesters have an excellent pattern of physical properties, being strongly resistant to hydrolysis, bacterial and fungal attack [51], but they can be degraded when they are copolymerized with aliphatic polyesters [52]. When aromatic monomer groups are incorporated into the main chain of aliphatic polyesters, the mechanical properties are improved [53].

Polyethylene terephthalate (PET) and polybutylene terephthalate (PBT) are technical application aromatic polyesters [44]. Compared with aliphatic polyester, the aromatic form is often based on terephthalic diacid which strongly influences the degradation behaviour [54]; e.g. as the percentage of the terephthalic acid unit increased, a decrease in melting temperature was observed [55].

Aliphatic-aromatic co-polyesters (AAC) could be made from petroleum with stable physical and chemical properties with comparable cost to other plastic polymers. They combine the biodegradable properties of aliphatic polyesters with the strength and performance properties of aromatic polyesters and leave no environmental footprint. Scientists have tried to increase the strength of bio-plastics and their properties without affecting their biodegradability. However, the balance between the improvement of mechanical properties and the biodegradability needs to be investigated [56]. Copolymers generally showed higher solubility, less moisture absorption and greater thermal stability than other biopolymers [57].

Synthetics biodegradable poly (α-ester)s (poly-lactic acid and poly-glycolic acid and copolymers) have been manufactured for biomedical uses since the 1970s. Other researchers produced non-biodegradable aliphatic-aromatic co-polyester fibres in 1981 [58]. The properties and the degradation rate of blended polymers determine the final degradation of the final mix [59]. Studies on co-monomer compositional distribution of the bacterial poly(3- hydroxybutyric acid-co-3-hydroxypropionic acid)s, crystal and thermal characteristics of their fractionated component co-polyesters have been done [60]. Co-polyesters containing an aromatic segment and aliphatic segment structure could be synthesized from bis(hydroxyethyl)arylate (BHEA) and bis (hydroxymethyl - cyclohexane) arylate (BHCA) [57]. A series of biodegradable aliphatic-aromatic co-polyesters (PBHTL) was synthesized, in the development of catalyst free synthesis of high molecular weight co-polyesters with biodegradable and aromatic moieties [61]. It has been found that with the increase of lactide moieties, the crystalline structures of poly (4, 40 isopropylidenediphenyl terephthalate)-co-poly (hexylene terephthalate)-co-polylactide (PBHTL) are gradually destroyed as a result of the spatial effect of lactide. With the increase of lactide and hexylene content, the co-polyesters show better

biodegradability [61]. Thermal stabilities of the poly (butylenes succinate-co-butylene terephthalate) (PBST) co-polyesters were much better in nitrogen than in air [62]. A co-polyester, poly(butylene succinateco- ethylene succinate-co-ethylene terephthalate) (PBEST), was synthesized via direct polycondensation from three prepolymers of butylenes succinate, ethylene succinate and ethylene terephthalate [63]. Another technique has been recently used for the preparation of poly(1,4-butylene succinate)/poly-(1,4-butylene terephthalate), poly(1,4-butylene adipate-co-succinate)/poly(1,4-butylene terephthalate) and poly(1,4-butylene glutarate-co-adipate-co-succinate)/ poly(1,4-butylene terephthalate) co-polyesters [64]. Random aliphatic-aromatic co-polyesters are synthesized from 1,4-butanediol, adipic acid and terephthalic acid (BTA) [65]. Other researchers have derived aliphatic-aromatic co-polyesters from 2,2,4,4-tetramethyl-1,3-cyclobutanediol [66]. Based on the data obtained, it can be concluded that biodegradable aliphatic aromatic copolyester (AAC) does not improve the thermal stability of poly(3-hydroxybutyrate) [67]. An ideal random copolymer PBTSA, exhibits a rubber-like stress–strain curve; a part of the aliphatic units (BA,BS) must be in a common crystal lattice with the BT unit, where BA and BS units are incorporated into the crystal lattice of BT units [68]. AAC could be a probable modification of the basic BTA structure and become commercialized [69].

AAC biodegradation behaviour, application and properties have been reported by many researchers [70]. The biodegradation behaviour of the aliphatic-aromatic co-polyesters is strongly influenced by their co-monomer composition [71]. Biodegradability is a function of a chemical structure, an origin and degrading environment. With increasing butylene terephthalate content in the co-polyesters, the rate of biodegradation decreases [72].

This is a result of the influence of the chemical structure on biological resistance which overrides the biodegradability of the co-polyesters; Co-polyesters are affected by average block length of the aromatic unit [55]. A family of biodegradable polymers can be created by modifying aromatic polyesters by adding aliphatic groups. An aromatic ring adds to the polymer a good resistance to hydrolysis and chemical agents; the material becomes stiffer, and has more strength and less elongation [73]. With increasing poly (tetramethylene glycol) content, the toughness and breaking strain of the copolymers increased [74]. Because the melting point of AAC is relatively 100 ^{o}C and for certain applications, their properties are better than that of other polymers with low melt point, such as PCL. The fibres have low glass transition (T_g); a low processing temperature could be used in a narrow temperature range. Because the glass transition temperature is

notably below room temperature; AAC products will be soft and thermally unstable at standard processing temperatures.

AAC grades could be classified depending on the structural chain design, such as linear or branched grades. Linear AAC is highly linear in structure and has good contact clarity and adhesion properties, low stiffness and poor melt strength [75]. The branched grade contains a long-chain branching which is added to aliphatic molecular chains to improve the mechanical properties.

Because of their flexibility, linear AACs such as Bionolle and Easter Bio are potential candidates for making staple fibres for various non-woven materials, including spun-bonded and melt-blown, particularly for disposable use in medicine and agriculture.

The branched aliphatic-aromatic co-polyester is resistant to water; it has many applications owing to its moderate water and vapour permeability. Branched AACs consist of several polyester units, 1, 4-butanediol and the dicarbonic acids, adipic acid and terephthalic acid such as Ecoflex made by BASF [76]. It can be fully degraded in an environmentally safe manner in a composting process; its biological degradation was investigated by evaluating the degree of degradation during the degradation process and the intermediates formed [77]. Ecoflex has a long-chain branched structure [78]. Under each product name there are several specific grades and each grade of polymer has been designed with controlled branching and chain lengthening to match its particular application. Biodegradable copolymer poly(butylene adipate-co-terephthalate), with 44 mol% butylene terephthalate (BT), was meltspun into fibers [76]. The Novamont and Ulice companies make a polymer as a mixture of rigid corn starch PLA as well as flexible and soft co-polyesters to produce Semi-flexible and impact resistant materials which improve the mechanical properties and the processability of the melt and products. With low softening temperature of the co-polyester component, AAC (co-polyester-PTAT)/ PP fibres were used as binder fibres in non-woven fabrics. Cotton/(co-polyester/PP) nonwoven has good flexural rigidity and absorbency with better mechanical properties than that of cotton/co-polyester nonwoven [79-81], but the non-woven contains PP which is not biodegradable. Other researchers have produced biodegradable cotton-based, non-woven by using blends of cotton, flax and a biodegradable thermoplastic fibre act as the binders [82].

To reduce the cost of the nonwoven process, researchers have made a pure nonwoven material from co-polyester by a direct melt-blowing process [83]. With regard to the biodegradability, 40% of the initial weight was lost after 8 weeks in compost, while in water the decrease amounted to only 23% after 10 weeks of biodegradation [84]. Some

researchers have made fibre comprising starch and biodegradable polymers StarDri 100 glycerine with/without PLA and sorbital [85]. Various blending ratios of regular (25% amylose) and waxy corn starches with co-polyester were extruded into loose-fill foams [86]. Others studied the properties of the blend ratio and the degradation process on biopolymers [87-89].

The American Society for Testing of Materials (ASTM) and the International Standards Organization (ISO) define degradable plastics as plastics which undergo a significant change in chemical structure under specific environmental conditions. According to the ASTM standard, D-5488-94d and BS EN 13432:2000, biodegradable means capable of undergoing decomposition into methane (oxygen absent: anaerobic), water (in the presence of oxygen: aerobic), carbon dioxide, inorganic compounds and biomass over specific periods of time reflecting available disposal conditions, by a significant change in the material chemical structure and leaving no visually distinguishable or toxic residues. ACCs fully biodegrade to carbon dioxide, water and biomass; they become invisible to the naked eye within 12 weeks in an active microbial environment [54]. Table 2.2 shows how the degradation results depend on biodegradation type.

Original substrate	Biodegradation Type	Converted into
Polymer	Aerobic	CO_2 & H_2O & (Biomass & Residue)*
	Anaerobic	CH_4 & CO_2 & H_2O & (Biomass & Residue)*
*The biomass yield is (10-40) % depending on converted substrate; residual consists of un-degraded test item/parent compound or metabolites; complete degradation occurs when no residues remains [44].		

Table 2.2. Degradation results depending on biodegradation type

Biodegradation is a process which occurs within the biosphere, in which the organic chemicals are converted to simpler compounds, mineralized and redistributed through the carbon, nitrogen and sulphur cycles [44]. Biodegradation of the natural and synthetic polymers can be made via two methods: microorganisms (by fungi or bacteria) and by enzymes. The biodegradation starts in the amorphous regions and then continues into the crystalline regions [51]. The exposure conditions include moisture, pH, temperature and aerobic or anaerobic conditions of the soil and thickness, size, manufacturing method and shape of the exposed item [90]. The organism type determines the appropriate degradation temperature. The disposal site must be in the presence of oxygen, moisture and mineral nutrients; the process leaves behind carbon dioxide and water [91]. The

degree of randomness of the co-polyester chains and the block length distribution help to understand the biodegradation behaviour of aliphatic-aromatic co-polyesters[92]. It was expected that the degradability of the oligomers would decrease with increasing chain length [93] and the amorphous part of the polymer is preferentially degraded [94].
Block-length is the key point of the aromatic group which should be no more than a trimer. An increase of terephthalic acid content tends to decrease the degradation rate [95]. Aliphatic co-polyesters degrade totally in the microorganisms' environment [96].

2.4 Biopolymer Applications

Depending on the sources of biopolymers, their properties have an effect on their shelf-life and biodegradability. During usage, the biopolymers should keep their functionality, disintegrate in the specific environment in a time frame and be transformed into natural occurring metabolic products. Some of the major biodegradable polymers based on renewable resources in the marketplace are provided by many companies such as Novamont, Plantic Technologies Ltd, Rodenburg, Natureworks LLC, Innovia Films, Procter & Gamble and others.
The common commercial uses of biodegradable polymers are for paper coating, packaging and life-bags, textiles, medical and agriculture applications, catering and fast-food containers, food packaging, lawn and garden waste bags, agricultural films, commercial food wrap, toys, leisure, medical products, disposable wipes, seed mats and erosion control. Biopolymer fibres with typical morphology find applications in bone tissue engineering [97] and a degradable nano-fibre for bone tissue engineering [98]. Some researchers have used natural fibres to improve the mechanical properties of biopolymers; with adding the natural fibres to the biopolymer fibres or their composites, the strength is increased without affecting the biodegradability [99-102]. Some biodegradable fibres have been made to blend with other fibres, such as PLA, thermoplastic starch, polycaprolactones and natural fibres, to improve their properties. The non-woven webs and disposable articles may contain other synthetic or natural fibres [103]. A biodegradable thermoplastic polymer and a plasticizer could be used to produce the starch matrix of the finely attenuated fibre; environmentally degradable non woven webs and articles are disclosed [104]. Biopolymers could be used as the base of oiling agents for processing glass fibres [105]. There is good compatibility between chitosan obtained from a shrimp shell and starch-based polymers [106]. By dry jet-wet spinning

and using celluloses/hydrolyzed starch-grafted-polyacrylonitrile solution, the mechanical properties of lycell fibres are improved [107].

2.5 Man-Made Fibres, Production Techniques and Textiles

The manufacturing of synthetic fibres began in 1885; the first commercial manmade fibre was artificial silk (rayon), made in 1925 [108]. Textile materials are generally classified as shown in Figure 2.3 [109, 110]. Fibres comprise long chain molecules which give the fibres properties such as length, thickness, strength and flexibility. A typical process schedule of fibres during production processes is summarized in Table 2.3; it gives a clear idea about the differences between spinning systems [111, 112]. The influence of the spinning process on the yarn properties depends on the process parameters used and the polymer properties [113]. Regenerated and synthetic manmade fibres form high percentage of yarn fibres in the world; fibres can be mixed or blended to make a mixture of fibre characteristics [114]. The simplest and the most economical method of fibre formation is melt-spinning [115]. In this process, shearing of the molten granules destroys their organized structure and crystallinity. Melt spun fibres have higher specific strength, temperature and chemical resistance in comparison to some natural fibres. Some researchers use the integrated control system, which manages the production of synthetic fibres from fibre formation, stretch and orientation, finishing and preparation for extra processing [116].

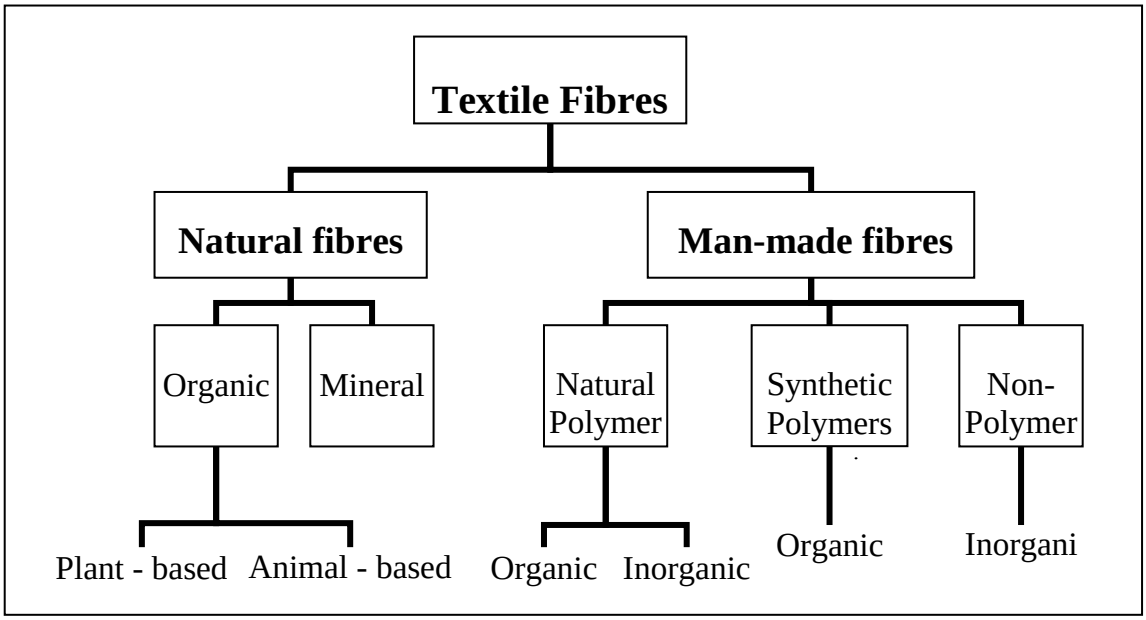

Figure 2.3. Major textile fibre types

Melt spinning with its inherent high processing speeds and capacities gives many economic advantages. It contains propulsion compression, heating working, filtration and metering, extrusion of the polymer through the spinneret, then the quenching, drawing and winding [112]. The structure of as-spun fibre such as molecular orientation or degree of crystallinity is developed through melt-spinning processes. Hot water provides a slower quench, leading to larger and more crystal development; it can be used to draw the filaments to reduce the filament diameter [117].

The formation of synthetic fibres with high take-up speed leads to uniaxial orientation of chain segments and orientation-controlled crystallization [118]. Process conditions affect the viscosity of molten material, the flow rates and the yarn properties. The crystallization dynamics of polymers strongly depend on the temperature, cooling rate and the application of a flow field [119].

The structure of spun fibres should be drawn easily to extend the chain and to obtain a high orientation along the fibre's axis. The processing conditions such as heat, humidity and mechanical stress affect the filament properties [120].

<table>
<tr><th></th><th>Nylon filament textured yarn</th><th>Nylon two staple yarn</th><th>Polyester staple yarn</th><th>Cotton staple yarn</th><th>Wool staple yarn</th></tr>
<tr><td rowspan="4">Fibre Processes</td><td colspan="3">Extrusion</td><td>Harvesting</td><td>Shearing</td></tr>
<tr><td colspan="2">Drawing</td><td>Cutting</td><td rowspan="2">Ginning</td><td>Sorting</td></tr>
<tr><td rowspan="2">Winding</td><td rowspan="2">Stretch-break</td><td>Crimping</td><td>Scouring</td></tr>
<tr><td colspan="3">Baling</td></tr>
<tr><td rowspan="7">Mill Processes</td><td rowspan="6">Texturing</td><td rowspan="3">↓</td><td colspan="3">Opening</td></tr>
<tr><td rowspan="2">↓</td><td colspan="2">Cleaning</td></tr>
<tr><td>↓</td><td>Scouring</td></tr>
<tr><td colspan="3">Carding</td></tr>
<tr><td colspan="4">Drawing</td></tr>
<tr><td colspan="4">Roving</td></tr>
<tr><td colspan="4">Spinning</td></tr>
<tr><td colspan="5">Winding</td></tr>
</table>

Table 2.3. The typical process schedule of fibre and mill processes

Theoretically, the fibres or fibre textiles for industrial use are classified as follows [121]:

1. High tenacity and high modulus fibres:
   - Organic such as polyester and aromatic.
   - Inorganic such as carbon and glass.
2. High resistance fibres:
   - Organic such as phenolic, aramid and fluorocarbon.
   - Inorganic such as rock.
3. Separation function fibres:
   - Activated carbon.
   - High water absorption.
   - Deodorisation.
   - Filters.
   - Reverse osmosis.
   - Blood dialysis.
   - Ultra-filtration.
   - Gas separation.
4. Light conduction fibres:
   - Communication.
   - Image transfer.
   - Sensor.
   - Optical guide.
   - Illumination.
5. Other function fibres:
   - Adhesive.
   - Fibrillation/ degradation / soluble.
   - Electrically conductive.
   - Colour rising.
   - DNA analysis.
6. Special fibres:
   - Vinylal.
7. Functionally modified fibres:
   - High tenacity.
   - Flame retardant etc.
8. End use oriented fibres:
   - Fibrefill use.
   - Tyre use.
   - Carpet use.
   - Mesh cloth use …etc.
9. Fibre reinforced composites products such as construction, civil engineering, electrical, information technology, hygienic/medical, transport, safety/protection, environment/resource, biodegradable fibres, agriculture, marine, packaging, industry, sport, leisure.

To produce a good fabric, the relationship between the fabric and the yarn should be characterised and adjusted. The fabric takes its shape and character from the fibres; the overall orientation of the molecule chains and crystanallity of the fibres form an important part in this field. The number of the filaments and the plies determine the thickness and the weight of the fabric [114]. Figure 2.4 shows seven major headings containing many attributes in speciality apparel textiles [121]. In conclusion, fabric properties are affected by fibre filament, yarn count and fabric specification.

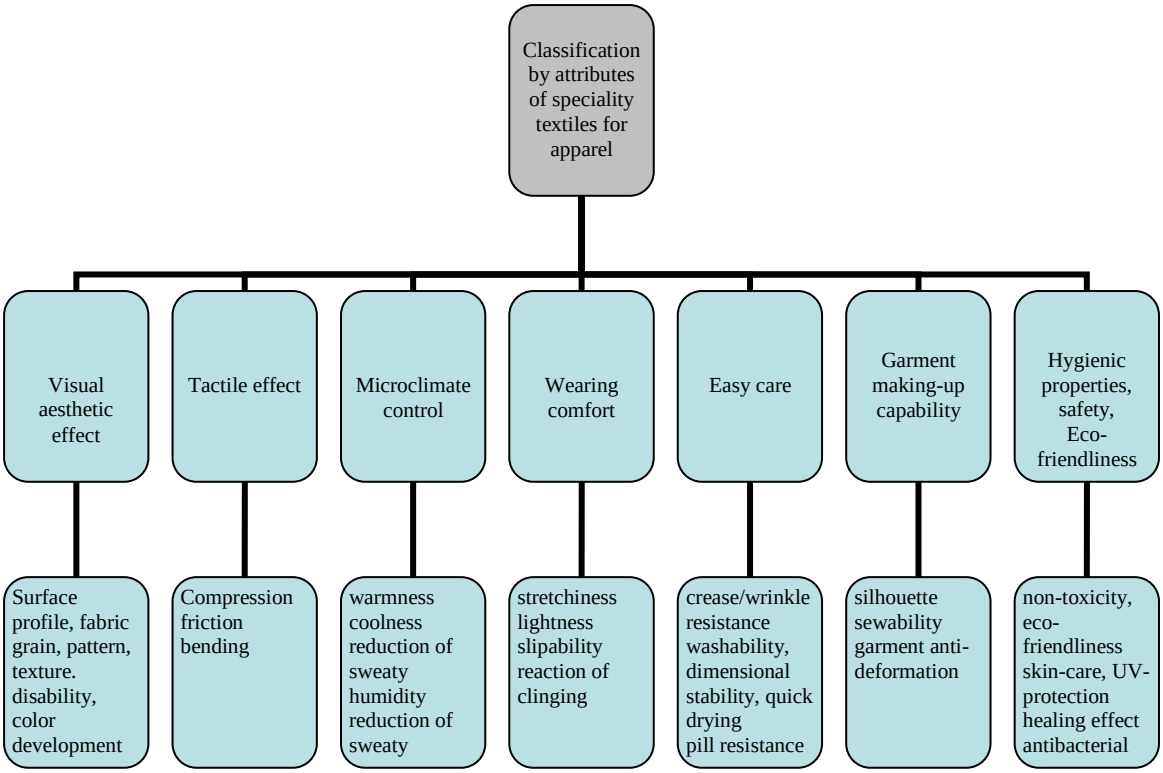

Figure 2.4. Classification of speciality apparel textiles [121]

2.6 Development in Biodegradable Fibres Extrusion

Between percent limitation and future textiles, environmentally friendly fibres are needed. Biodegradable fibres may be natural, regenerated or synthetic. In fibre spinning, many biodegradable polymers, such as PHB-PHV, PLA, PCL, PTMAT, PVA, PP, (PE + agents) and (Starch +PVA) may be found.

There are some commercial biodegradable fibres, such as Ingeo (Natureworks), LLC produced from corn, a biodegradable thermoplastic polyatide (PLA), Lenpur produced from wood pulp of harvested tree clippings of white pine trees, Modal and Tencel/Lyocell produced by Lenzing from wood pulp of beech and eucalyptus trees and biodegradable aliphatic/aromatic multi-block co-polyesters. A green fibre has a shorter life cycle than oil-based fibres. A green life cycle is given in Figure 2.5 [122].

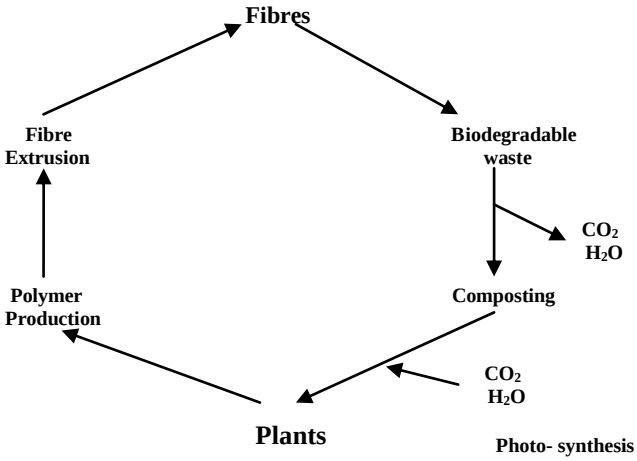

Figure 2.5. Life cycle of compostable biodegradable fibres

As the use of composite material increases every year in developed countries, biopolymer fibres may be used to make textiles for tissue and cell engineering and incorporated into wound dressings[122]. Some of those materials are even more costly than the traditional polymers; the huge rate of production will reduce prices and increase availability of novel industrial fibres made from renewable biomass sources. To improve the properties of biodegradable polyesters, researchers have made crimp natural stable fibres for use with other biodegradable based fibres to make medical products, disposable wipes, seed mats and materials for erosion control [43].

2.7 Modelling of The Melt Spinning Process

Measurement, feedback and adjustment, prediction and correction are the main elements in online quality control [123]. The practical software-based approach has improved the confidence benefits of experimental design and simulation [124]. The key point is how to apply those techniques on many applications for manufacturing the novel product; it helps the engineering by reducing the target value variation in processes [125]. The quality control is the major element in the production process; it helps to meet the customers' requirements and expectations.

Commercially, it is a challenge to develop a new competitive product in business [126]. All the production process parameters must be controlled to build the quality and then the significant main factors must be analyzed [127]. Many textiles researchers have applied the experimental design and statistical analysis theories in their research.

Some researchers evaluated the melt spinning of fibres using the finite element modelling software; others used the experimental design to evaluate and simulate the melt spinning process. Table 2.4 shows some research works on statistical analysis, mathematical simulation and modelling of the processes of fiber formation and some examples of their post-processes.

	Subject	Ref.
Melt spinning	The influence of fiber processing parameters on the structural properties of as-spun polypropylene fibers: A factorial design approach	[128]
	Lab-Scale Fiber Spinning Experimental Design Cost Comparison	[129]
	Dynamic modelling of melt spinning	[130]
	Model of steady-state melt spinning at intermediate take-up speeds	[131]
	Viscoelastic Effect in the Non-Isothermal Melt Spinning Processes	[132]
	Processing, structure, and mechanical properties of as-spun polypropylene filaments—A systematic approach using factorial design and statistical analysis	[133]
	Modeling of pneumatic melt spinning processes	[134]
	Modelling of rapid solidification by melt spinning: effect of heat transfer in the cooling substrate	[135]
	Mathematical modelling for polymer processing	[118]
	Multifilament Model of PET Melt Spinning and Prediction of As-spun Fiber's Quality	[136]
	Two Dimensional Modelling of PET Melt Spinning: The effects of heat transfer limitations on the quality of PET yarn produced during melt spinning	[137]
	Simulation of Multifilament Semicrystalline Polymer Fiber Melt-Spinning	[138]
	Mathematical Modelling of the Pneumatic Melt Spinning of Isotactic Polypropylene. Part III. Computations of the Process Dynamics	[139]
	Modelling the melt spinning of polyethylene terephthalate	[140]
	Process analysis and optimization for the ionic interactions of quaternary ammonium salts with nylon 66 fibers using statistical experimental design	[141]
	Modelling and optimization of nozzle design in planar flow melt spinning	[142]
	Mechanical Behavior of Irregular Fibers, Part I: Modeling the Tensile Behavior of Linear Elastic Fibers	[143]
	Simulation of melt spinning including flow-induced crystallization: Part I. Model development and predictions	[144]
Fibre Post-processes	Modelling and predicting textile behaviour	[145]
	Adsorption modelling of textile dyes by sepiolite	[146]
	Brilliant Yellow dye adsorption onto sepiolite using a full factorial design	[147]
	Multivariate analysis of anionic, cationic and nonionic textile surfactant degradation with the H 2 O 2 /UV-C process by using the capabilities of response surface methodology	[148]
	Color removal from textile dyebath effluents in a zeolite fixed bed reactor: Determination of optimum process conditions using Taguchi method	[149]
	The influence of technological parameters on the filtration efficiency of electret needled non-woven fabrics	[150]
	Fabrication of electrospun poly(methyl methacrylate) nanofibrous membranes by statistical approach for application in enzyme immobilization	[151]
	Ink-jet printing process for lyocell and cotton fibres. Part 2: The relationship of colour strength and dye fixation to ink penetration	[152]

Table 2.4. Examples of the modelling of the melt spinning and some fibre post-processes

2.8 Extrusion Basics and Subsequent Production Processes

2.8.1 Extrusion Theory

Polymers are supplied to the extrusion machine, either from the chemical reactor or as polymer chips. The extruder contains a special form of rotation screw (or multi screws) in a heated barrel (or a cylinder) and the die-head on the end of the barrel. The hard chromic plated die head consists of a die block which supports a woven wire filter, a breaker plate, a copper seal and a spinneret. The molten material is pumped through the filter back and die-head directly or by using several types of pumps. The screw contains three zones: feed zone, compression or transition zone and metering or melt zone, as shown in Figure 2.6 [153]. The screw may be a single start flight or more start flights. The diameter and the length of the screw are the major factors determining the volumetric capacity in transferring the temperature from the barrel wall to the material, and in generating the temperature from friction and shear. Each extruder temperature zone has at least one heater controlled by an individual thermocouple.

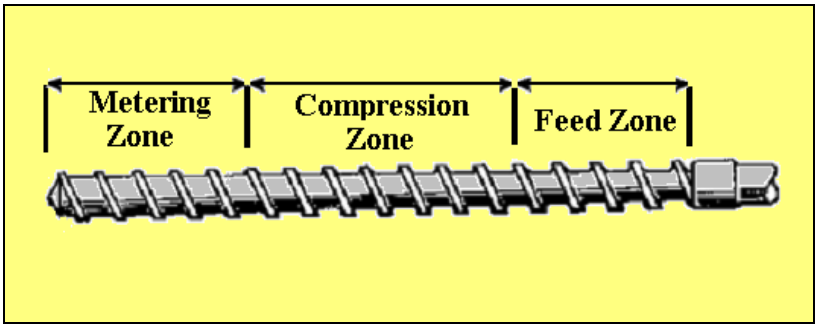

Figure 2.6. The zones of the extruder screw.

The screw takes the material chips from the hopper through the heated barrel zones either to the metering pump to help in controlling the liquid flow rate in the die, or directly to the die. The screw plays a major role like a pump and acts to make the material homogeneous; it is an important part of a heat exchanger [112]. The part between the hopper and the heated part of the feeding zone is cooled with water during the operation to facilitate the forward feeding of the polymer granules and to prevent the polymer pre-melting and sticking to the feeding zone surface.

The feed zone transfers the cold material from the hopper to the second zone. Sometimes it helps in drying the materials and is the most critical area in the screw. The feed section should be calculated to give the best feeding with a good cross section which does not affect the screw strength. In that area, the entire torque and the fraction of the total torque

have to be transmitted [154]. In the second zone, the root diameter of the screw will be increased till the diameter of the third zone is reached. It helps in pushing any occluded air back to the feed zone and compacts the material [155]. The compression ratio of the second zone is the ratio of the clearance between the barrel and screw root of the feed section; between the barrel and the screw root of the metering section. The higher compression ratio gives a more stable flow [156]. The flow in the compression and metering sections is Non-Newtonian and not isothermal [155]. The third zone works as a metering pump and gives the material constant volume and pressure through its pass to the die [153]. The suggested place for measuring the die head pressure is between the last flight and the screen peak. The material is heated by the hot barrel, the electrical resistance heaters, and the internal friction between the material and the barrel which is more than the friction between the material and the screw. Decreasing the melt temperature leads to higher viscosity and higher resistance to flow in the die, as well as lower leak pressure flow in the extruder [117]. The friction generated heat could be controlled by the speed of the screw. The shear forces will increase with the increasing of the rotational screw speed. A low rotational speed affects the homogeneity of the material, resulting in the lower capacity of mixing [157].

The output of the machine depends on the temperature generation and screw design; the increase in screw speed does not necessarily mean an increase in the output [153]. Figure 2.7 shows an example of the screw design, the pitch and the flight form of the screw thread, including the helix angle and the depth of the flight. Screw design affects the extrusion capacity; it determines the output of the machine and controls the friction and the shear applied to the material. A long screw gives more time for heat transferring, and the larger length to diameter ratio allows more output of the machine [153].

The movement of the material is caused as a composed form from three types of melt flow in the single screw machine (Figure 2.8). In terms of the die head pressure, pressure flow rises when a die, valve or any part is fixed at the end of the barrel; the velocity of the material will be half of that of the moving surface [153]. The three types are pressure flow (1), drag flow (2) and leak flow (3). Drag flow takes place when the material sticks to the fixed barrel and the moving screw. Leak flow is caused by the pressure gradient along the screw and between the land of the flight and the barrel.

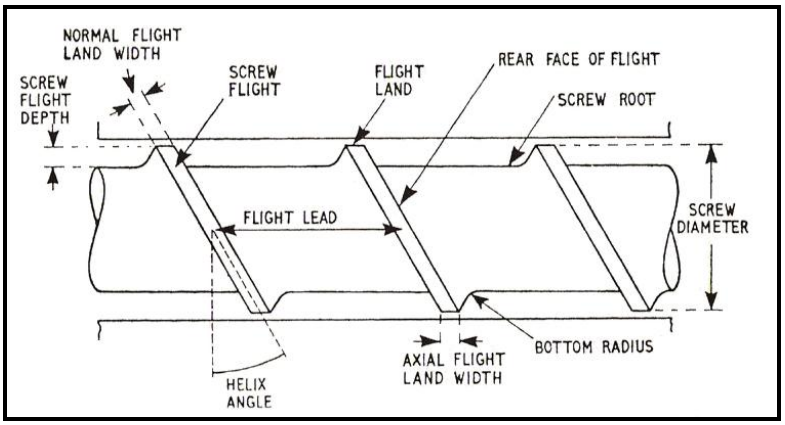

Figure 2.7. Topical screw design

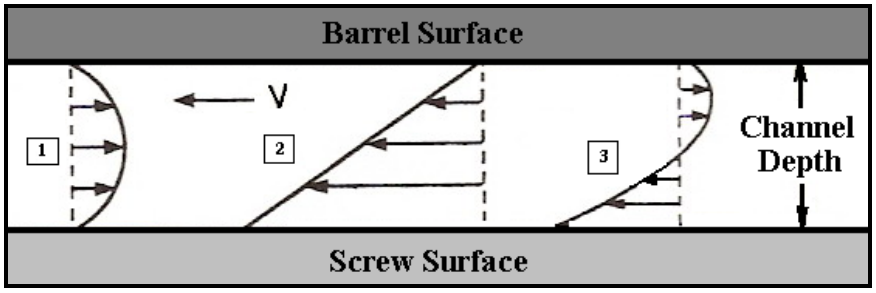

Figure 2.8. Three types of the melt flow in the single screw machine.

The drag flew of (Q_D) will have the opposite signs to both the pressure flow (Q_P) and the leak flow (Q_L). The output of the machine is equal to the sum of the previous three flows, Equation 2.1 [153]:

$$Q = Q_D - Q_P - Q_L \quad (2.1)$$

The power required to heat the polymer from the feed through to the melt state could be calculated as the difference between energy required to heat polymer from feed to melt temperature ($M.C_P.\Delta T$) and fusion heat of polymer ($M.\Delta H$) (where M is the mass flow rate [kg/hr], C_P is the heat capacity [kJ/kg.°C], ΔT is the difference in temperature between the feed and the melt temperature [°C] and H is the heat of fusion of polymer [kJ/kg]). More details about the physical effects and causes that determine the extrusion mechanical design and construction are shown in Figure 2.9 [153].

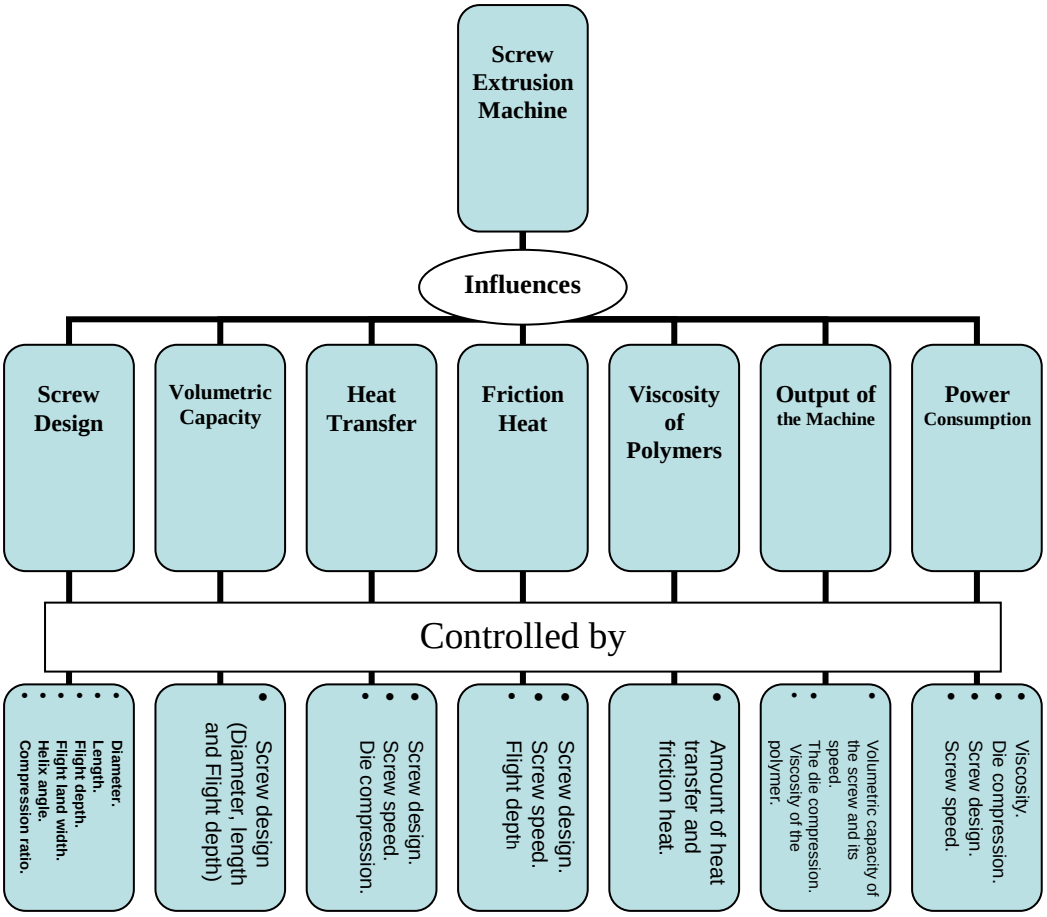

Figure 2.9. The physical effects and causes determining the mechanical design and construction

2.8.2 Extrudeability in Practice

The extrudeability or processability measurements in the extrusion systems present the flow of different materials in practice simulation conditions. Extrusion could be simulated for thermoplastics, thermo settings, elastomers and many other plastics or plastifiable materials. For some polymers, the production must be at a high temperature from oxidation which causes changes in viscosity, cross linking or deterioration in the final product. Extrusion temperature profile of the extruder affects on the local pressure, specific volumes, coefficient of friction and the viscosities of the melt [112]. Power is related to material behaviour and properties as well as the machine design. For example, the power requirement to drive the screw for some biopolymers is decreased with increasing temperature, but it is increased with the high moisture [155].

The relationship between the torque speed characteristic and the power speed characteristic is determined by the torque and power relationship in Equation 2.2 [154]:

$$P = T.\omega = C\ T\ N \quad (2.2)$$

Where (P) power, (T) torque, (ω) angular frequency [radians/s], (N) screw or motor speed [rpm], (C) a constant [$C = 2\pi/60 \approx 0.1$]. As the torque is constant and the screw speed is increased, the power is increased. The full speed gives the maximum power, which explains why the extruder output is power limited. That could be controlled by mechanical solutions based on the motor, the gearbox and the screw design [154].

2.8.3 Dynamics of the Melt Spinning Process

Theoretically, fibres are assemblies of macromolecules in the form of multi individual chemical units, covalently bonded together one after another. There are three types of polymers: homopolymers, copolymers and block polymers. In homopolymers, which is the most common type, one chemical compound repeats itself along the polymer chain. In copolymers, two or more monomers comprise the polymer chain. In block polymers, blocks comprising homopolymers are repeated along the polymer chain. Within fibres adjacent polymers are found tightly packed together in specially ordered crystalline regions and further apart in amorphous regions. The degree of polymerization describes the number of times the monomer is repeated along the chain which specifies the polymer length. The fibre made of long chain polymer is generally stronger, extends a shorter distance at a given load and requires more force to cause elongation [158].

In melt spinning and after the filament leaves the spinneret, it passes through the spin line environment including the extrusion speed, take-up speed and medium of quenching. By increasing the speed and essentially owing to air resistance and inertia force, the filament is subjected to increasing stress. Solidification conditions determine the structure of spun fibres which affect the subsequent post-spinning operations. The spinline stress decreases as the melt flow index increases; the wind up controls the draw and tension on the material from the extruder exit through the cooling and solidification steps [117]. There are inertial, gravitational and air filament drag forces which affect the filament flow in the non-isothermal process [140]. The total spinline force (except the gravity force at any spinline position) equals the sum of spinline force at position of maximum die swell (rheological drag), force caused by acceleration of spinline (inertia), force caused by surface tension and force caused by air drag (skin friction) [159].

The orientation dynamics of polymers strongly depends on the temperature, cooling rate and the flow field in melt spinning [119]. Cooling rate controls the crystal size in the final product [117]. The cooling must be done slowly to improve the crystallinity and crystal size; it is determined by throughput rate, yarn cross section and cooling medium temperature. The flowing air must be at a temperature below the solidification temperature of the polymer [120]. If the cooling is not uniform, some filaments will be more likely to break than others; the speed of filaments affects the quenching rate, which helps in determining the morphology of the partially oriented yarn [112].

The formation of synthetic fibres with high take-up speed leads to the uniaxial orientation of chain segments and orientation-controlled crystallization [160]. The orientation of molecular chains could be achieved by increasing the ratio between the take-up speed and the extrusion speed; a drawing process is needed to complete the process [161]. With higher draw down ratio or higher spinline stress, the orientation in melt spun fibres will increase. A high degree of extension could give higher tenacity together with lower elongation at break (high modulus) and via versa.

The special design of the spinnerets with the funnel shape entrance of the nozzles does not allow any dead volume in the polymer path [142]. The spinneret consists of a large number of fine holes; the filament takes the shape of the cross section of the spinneret nozzle [153]. The spinneret is defined by its dimension, especially length to diameter nozzle ratio. With a large nozzle ratio, the back pressure in the die increases. Over-orientation increases with shear rate associated with a small spinneret orifice size, resulting in an increase in fibre strength and reduction in elongation at break. The ultimate radial expansion will appear depending on the elastic properties of the melt polymer [162]. The group (die, filter and break plate) placed at the end of the extruder creates a back pressure and greater mixing movement to the materials and large shear; it gives the material the homogeneous state and the free-state from the foreign particular [153]. The die pressure must be high, and it depends on the high melt viscosity [156]. The die head temperature presents the spinning or extrusion temperature.

The change in the flow velocity profile gives rise to molecular relaxation outside the die and the resultant extrudate swell; the main factor that affects the die swell is the shear rate in the die, the melt temperature, die land length and reservoir length [117].

Molecular weight, the degree of chain branching, crystallinity and the heat transfer in polymer processing affect the ability of the polymer's melt to flow under pressure; the higher melt flow index means the lower resin velocity and molecular weight [163]. As the molecular weight increases, the process ability decreases and the property performance

increases; low polymer molecular weight polymers have low viscosity [117]. With the change in pressure, the volumetric flow rate changes and the flow rate jumps. The main factors playing a role in this are the shear rate in the die, the melt temperature, die land length and reservoir length. The spin finish coats the fibres with a thin surface to impart the correct friction and adherence properties[164], to prevent build-up of electrostatic charge during processing and to offer sufficient protection to the filament without damage [165]. In conclusion, as-spun fibres should have a structure that can be drawn easily and also be conducive to the formulation of an extended chain and high orientation along the fibre axis. Undrawn fibres exhibit low tenacity and high elongation percentage; the drawing process aligns the molecular chain and affects the degree of crystallinity along the fibre axis. The melt spinning systems have two or more draw zones; drawing may be made during texturing or out near the extrusion operation. An optimal qualities approach for determining the parameter values in melt spinning processes could be achieved [166].

2.8.4 Dynamics of Fibre Drawing

Drawing is the major stage in the manufacturing of synthetic fibres, because it stabilizes the molecular structure and strengthens the yarn by improving the molecular orientation and crystallinity [112]; the drawing ratio depends on the drawing conditions and original structure of filaments [167]. Cold drawing takes place in temperatures lower than the transformation temperature T_g, while hot drawing takes place at temperatures above T_g in the phase of the so-called rubber-like increase in the degree of molecular orientation. By heat setting, an increase in the molecular mobility and the relaxation of internal stress are achieved [159]. The fibre diameter plays a role in crystallization during drawing which leads the material to stay warm for long periods. The structural changes involve alignment of the molecular chain along the fibre axis and an improving in the degree of the crystallographic order. The high crystalline and orientated fibre is stronger, stiffer and has lower elongation at break [158]. More uniform fibres are produced as the draw ratio increases. Drawing tension is related to the stability of drawing conditions; it is an increase with reduction of drawing temperature or increasing of drawing ratio. If the draw ratio is under the natural draw ratio, the neck is moved down along the drawing line and un-drawing section will appear. Otherwise the neck will move up along the line and regular technical drawing has been achieved. Homogenous drawing and heterogeneous drawing are two important cases in drawing technology [167] (Figure 2.10).

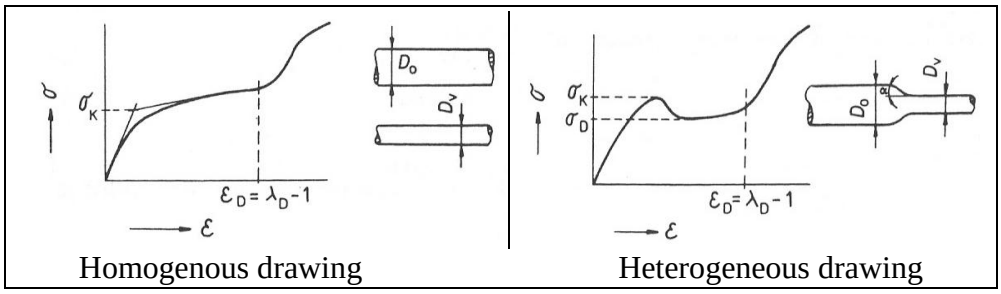

Homogenous drawing Heterogeneous drawing

Figure 2.10. Homogenous and heterogeneous drawing

Homogenous drawing appears at high temperature and a low speed of deformation; it is of only small practical significance. The diameter D_O decreases continuously to value D_V and the high configured structure prevents the tension concentration from making a collar. In heterogeneous drawing, which is the most frequently used in filaments drawing, the filaments are deformed homogenously till the tension reaches the yield point σ_k. After the collars are formed, the drawing tension is dropped and the local plastic deformation begins. This collar with constant collar angle $\boldsymbol{\alpha}$ travels along the filaments with a practically constant value of drawing tension till the sample is fully drawn. After the deformation $\varepsilon_D = \lambda_D - 1$, the deformation takes place in the homogeneous way until the breakage and the diameter D_V does not change [167]. In the continuous process, experiments must be conducted first to investigate the drawability of as-spun fibre. The critical draw ratio varies according to material and processing conditions; filaments should not slip during drawing. The actual/calculated draw ratio is less than the nominal/measured draw ratio, because the draw line shrinks when tension is removed.

In internal structure analysis, drawing aligns the molecules in a more parallel arrangement and brings them close together to be more crystalline and oriented [108]. Crystallinity and orientation affect strength, elongation at break, moisture absorption, absorption resistance and dye-ability; high orientation reduces molecular mobility and the dye-ability [168]. Cold drawing disrupts the crystalline structure, introduces defects, strains and reduces the crystalline size. High crystallinity is difficult to obtain from melt or solution for most flexible polymers; the crystallinity of the nonflexible polymer of the liquid crystal type is very high [168]. The structure formation in the spinning process is very complex because of the crystallization, phase separation and glass transition occurring in the process. Highly oriented fibres are highly crystalline but fibres that are highly crystalline are not necessarily highly oriented. There are different regions in the fibre structure (Figure 2.11); amorphous chain (A) with random way and molecular chains (B) are parallel to each other (crystalline but not oriented), and oriented and crystalline area (C) (molecular chain are parallel and oriented to the fibres length wise axis) [108].

In drawing, molecules may be pulled out of the lamellar crystals, and molecules in the amorphous regains are extended. The higher draw ratio causes the higher internal stress to decrease by the heat setting. The annealing process of the filament partially relaxes the frozen internal stress and decreases the residual shrinkage. At the setting mechanism, polymers are deformed and the internal stresses are relaxed to let the new form stabilize by recrystallization [169]. Geometrically, a long filament drawing could occur as a non-uniform, non-isothermal elongated flow. In case of non-linear viscoelastic behaviour, the necking effect could be obtained. The velocity is neither steady nor uniform and a kinematics problem of continuous drawing arises [159].

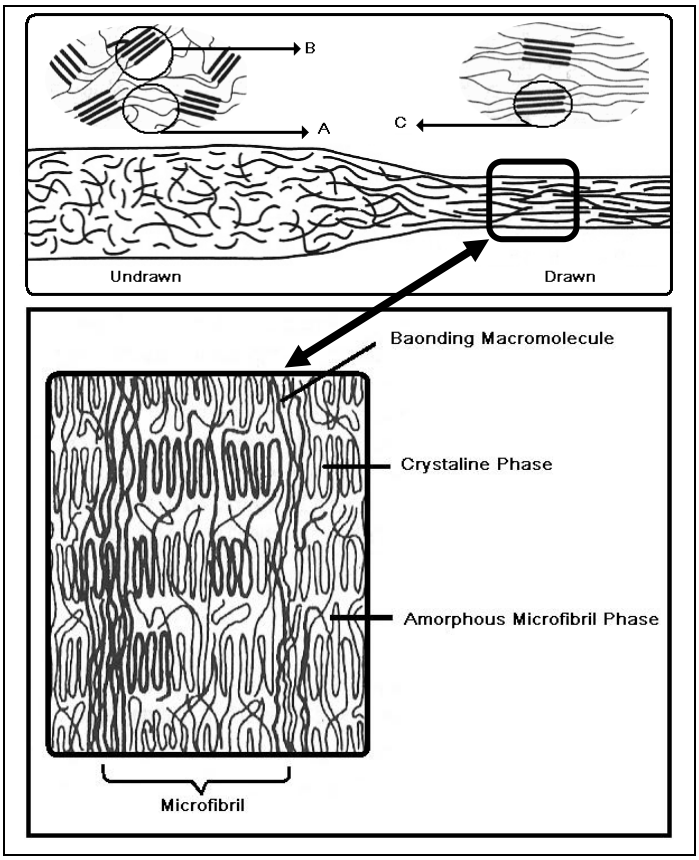

Figure 2.11. Effect of drawing on as-spun fibre and the final regions in drawn fibres [167]

After drawing, the relaxing process is necessary to obtain thermal stability in semi-crystalline fibres. In the relaxing process, the key is to expose the fibre in processing to a temperature lower than Tg which plasticizes the glassy regions. With a small percentage of relaxing to occur, it is necessary to use this step to obtain thermal stability in semi-crystalline fibres. There will be some losing of orientation in the amorphous (non-crystalline) regions [115]. By the improving of the thermal stability under controlled tension or in free-state, the internal tensions are eliminated by readjustment of

intermolecular chemical links and the crystallization degree. Treatment could be done to reduce the movement freedom of the chains and set in particular form [170]. If the setting temperature can be determined before or after weaving, shrinkage behaviour has been studied for some synthetic fibres under dry heating conditions [170].

The effective glass transition temperature (Tg) is below the normal operation temperature, so the crystallization will go to equilibrium only very slowly. It is necessary to heat the moulded polymers (anneal) in an inert atmosphere at some temperature between Tg and melting (Tm) in order to stabilise the polymer [171]. Some unstable fibres could be related to the machine faults, such as variations of drawing, feed velocity, temperature, guides or pins wearing out [159].

2.8.5 Dynamics of Fibre Twisting

Yarn, the major unit of the textile structure, is made by either stretching the staple fibres and twisting them into a regular yarn, or by twisting continual filaments [114]. In continuous filament yarns, the twist keeps the filaments together but with the increasing twist the strength is reduced [172]. The change in mechanical properties and the structure of as-spun filaments could be determined after the filaments are drawn and twisted to obtain continuous filament twisted yarn [173]. When the twist increases, the internal force is increased and the fibre angle with the yarn axis increases. According to the variability of individual filament strength, applying the twist supports the weaker filaments and increases the strength.

The theoretical maximum strength is realised with the aligned parallel filament to the yarn axis; the filaments are given axial strength and lateral pressure with the increasing of the twisting. The yarn strength has an optimum value less than the sum of strength of fibres in a cross section. Above the optimum twist, the yarn fails and a snap can be heard when the yarn breaks; otherwise, no snap can be heard [112].

Twist is defined as the number of the turns around the axis per unit of length (twist ratio per length unit); the twist factor defines the number of the twists per length unit. It gives the angle of the fibre position depending on the straight axes of the straight axis of the yarn [114]. The main factors affecting the twist are the linear velocity of the strand and the rotation speed of the twist. Twist density is calculated from the ratio of the twist constant and the number of teeth in the twist gear [112]. Twist direction is determined by the centre position of the letter S or Z; the yarn can be twisted in Z direction and plied in S direction. Twist affects some physical characteristics, which are bending behaviour,

resistance to creasing, resistance to abrasion, drapability, elastic performance, impact strength and stress distribution. As the twist level in a yarn is increased, the yarn properties are affected, such as yarn with a harder feel, the access of water to the yarn interior is restricted, pilling is prevented, the thickness and the light reflecting properties are affected, change in yarn diameter and absorption and appearance of fabric made of the twisted yarn [174]. Twisting generates irregular deformation and irregular tightness of the elementary filament; the outer filament processes a higher level of tightness than that nearer to the filament's bundle axis. There is another effect from the fractional resistance between the fibres, because it transfers the forces between the fibres and raises the friction. [170]. There are up twist and down twist, up twist to wind yarn from a package but down twist to wind yarn onto a package. Two for one twisting is applied in plying doubling from package to package [112].

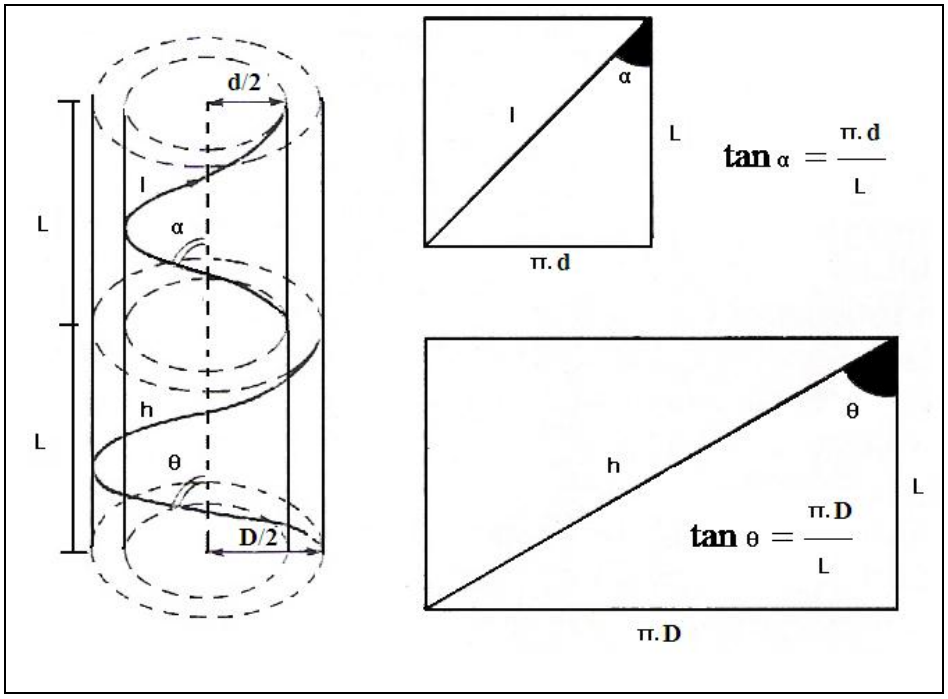

Figure 2.12. A helical shape of twisted filaments

The helix angle of the filament is very important when determining the strength of the yarn; the same twist angle and the twist factor have different numbers of terns per length unit. Low twist factor and low twist level will give softness and lightness of the fibres, while the higher twist gives crease resistance and clearer woven structure [114]. In Figure 2.12, the fibrils take on a helical shape; the number of turns per unit length is independent of radius [173]. Fibres at the centre are straight and the helix angle reaches a maximum value at the yarn's outer layer. Diagrammatically, a fibre takes one turn of twist in a

length of yarn L and the angle between the fibre and the yarn axis is θ; the angle is a function of the twist level [172], as shown in Equation 2.3:

$$\tan\theta = \frac{\pi D}{L} \tag{2.3}$$

The range of the angle α is from zero at the centre of the yarn to θ at the yarn's outer layer; with the increasing of yarn diameter, θ produced at one turn of twist is increased. With twisting, the length of drawn filaments will decrease and the diameter will increase. A higher twisting rate creates a mechanical structure of filaments; the outside tension strain leads to the irregular tension strain of individual filaments [167], depending on the radius. The theoretical and experimental theories of structure and properties of fibres and fibre assemblies employ novel mechanical, mathematical and numerical methods [145].

2.8.6 Thermo-Graphy Theory

Thermography is designed to meet demanding thermal analysis requirements in scientific, target signature and non-destructive testing applications. ThermaCAM researcher measurement methods allow extensive thermal analysis [175]. According to thermography theory, the electromagnetic spectrum is divided arbitrarily into a number of wavelength regions distinguished by the methods used to produce and detect radiation. The radiation of object surface temperature calculates and displays at determined emissivity by the equipment and software available [176, 177]. Radiation originates from the surroundings; it is reflected in the object and affected by the absorption of the atmosphere. Radiation is controlled by the emissivity of the object, the reflected temperature, the distance between the object and the camera as the transmittance drops with distance, atmospheric humidity and temperature. The camera receives radiation from the object and the surroundings reflected via the object surface, and the radiation contribution from the atmosphere itself. Accepting the description above, the true description of the real condition in Figure 2.13 below was used to derive a formula for the calculation of the fibre surface temperature from the calibrated camera output.

The received radiation power, W, from the blackbody source of temperature over a short distance generates a camera output signal, U. That is proportional to the power input, $U_{SOURCE} = CW(T_{SOURCE})$, with a simplified notation, $U_{SOURCE} = CW_{SOURCE}$, where C is a constant. With the received radiation of a graybody source with emittance ε, the received radiation would consequently be εW_{source}. With the total received radiation

power of the three collected radiation power terms (the fibre, reflection from ambient sources and the atmosphere) and by multiplying each term by the constant C and replacing the CW products by the corresponding U, the calculated camera output voltage for a blackbody of fibre temperature can be calculated by means of Equation 2.4 [176]:

$$U_{fibre} = \frac{1}{\varepsilon\tau} U_{total} - \frac{(1-\varepsilon)}{\varepsilon} \tau U_{refl} - \frac{(1-\tau)}{\varepsilon\tau} U_{atm} \qquad (2.4)$$

The previous measurement formula was applied in the system thermographic equipment used; the voltages of the formula are:

U_{fibre} : The calculated camera output voltage for a blackbody of fibre temperature and that voltage were converted into the true requested fibre temperature.

U_{total}: Measured camera output voltage for the actual case.

U_{refl} : Theoretical camera output voltage for a blackbody of temperature according to the calibration.

U_{atm} : Theoretical camera output voltage for the atmosphere.

τ : is the transmittance of the atmosphere.

ε : is the emittance of the fibre.

$(1-\varepsilon)$: is the reflectance of the fibre.

$(1-\tau)$: is the emittance of the atmosphere.

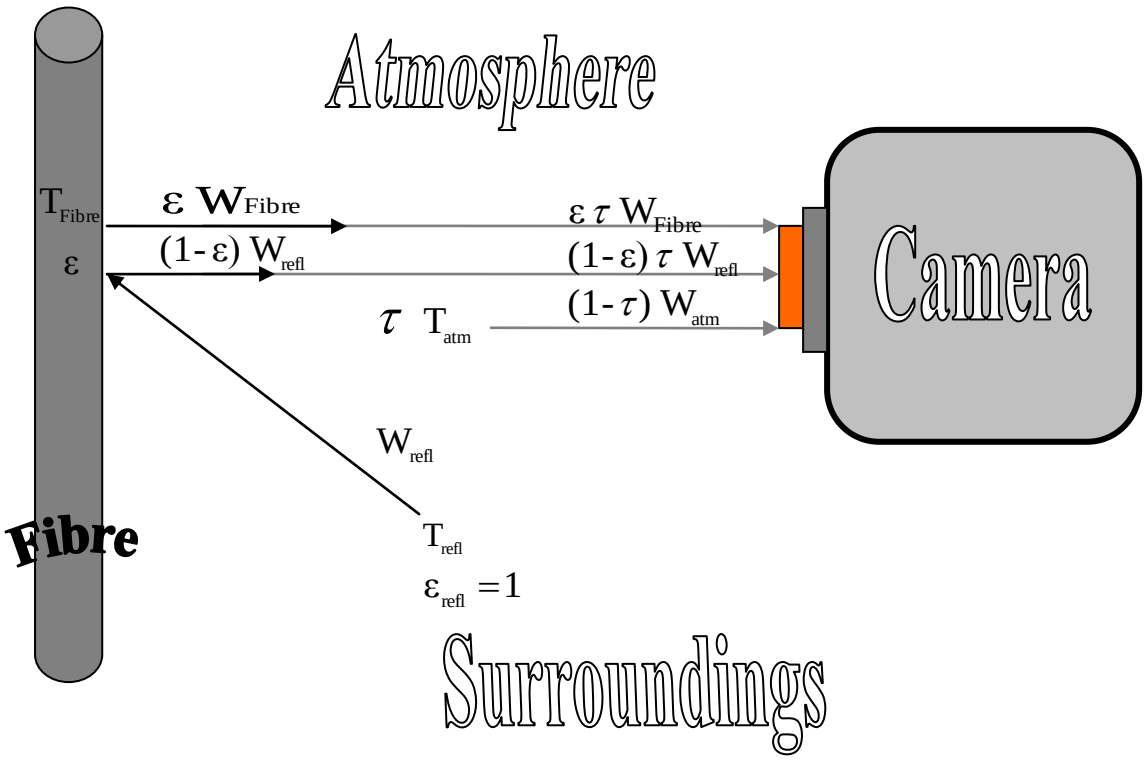

Figure 2.13. Schematic representation of the thermographic measurement situation of the fibre surface temperature

2.9 Experimental Design Techniques in Statistical Practice

Modelling, optimization and calibration are the most significant issues in any analytical methodology. Although the development of the process is achieved by experienced engineers without specific methods, using statistical experimental design is an efficient technique for reducing the time and the cost required in creating and/or improving the quality of consistent and economical products. Statistical experimental design (SED) and modelling are very powerful problem solving techniques; they assist industrial operators in tackling quality control problems effectively and economically [178].

2.9.1 Factorial Experimental Design, History and Theory

Statistical experimental design, which has been used for many years, is a novel technique developed by Sir Ronald Fisher in his agriculture research in the UK in the 1920s. Then it was used in technological studies in the early 1950s [179]. In similar fields and since the 1950s, Tanguchi has been working on his quality improvement ideas. In the early 1980s, Tanguchi methods became known outside Japan [180]. The progress was very rapid, through the use of statistical methods to meet the customers' requirement and expectations [181].

Statistical experimental design analysis solves the problems that arise in traditional analyses depending on the one factor-at-a-time method [182]. The process factors are classified as controllable, noise and constant factors. The noise factors are classified thus [183]: first, external factors which are environmental noise factors like temperature, humidity, dust, supply voltage, electromagnetic interaction, vibrations of instrument supports or in the sunlight intensity through the windows and human errors; secondly, unit-to-unit variations like resistance; finally, deterioration in the product as time passes. The focus of SED is the optimizing of the average response values depending on the factors and their levels. Design and analysis of experimental methods add additional advantage to the analysis of manufacturing processes such as a 'fibre-to-fabric engineering' approach [184]. The use of experimental design ideas is still limited on large industrial scale applications, for many reasons [185] such as inadequate education, familiarity with home-grown solutions, lack in understanding of the statistical experimental design method and lack in collaboration between academic and industrial fraternities. Experimentation could require massive resources to identify the optimum settings of the factors affecting the production process.

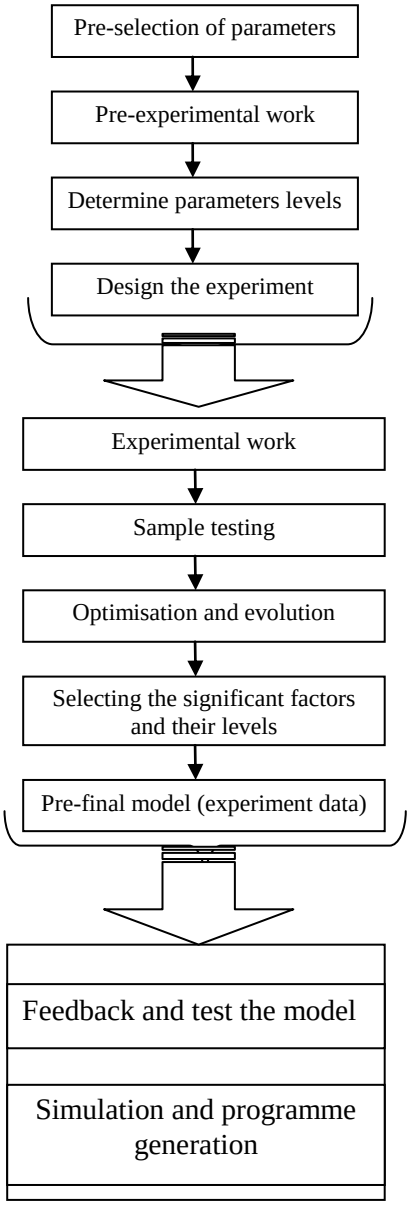

Figure 2.14. Schematic programme for experimental plan

Figure 2.14, shows a schema of the research work plan translating how to get the best model at low costs and in the required time. The process involves the selection of the control factors, the number of levels, the design matrix and the number of trials. Fewer levels are used at the pre-experimental stage to identify the significant factors, the levels of significant factors are increased later for optimisation. After the pre-experimental work, the system database is collected to determine the number and the levels of factors that will help in preparation of the matrix design. Then, the sample and its data are analysed and the significant factors are determined to develop the process design of factory production [186]. The regression model gives information about the significant main factors and their interaction. Regression is a statistical procedure for estimating the

parameters necessary in order to use a certain relationship in prediction applications. The theoretical technique for a two-level design structure is provided below; it gives an idea about the methodology on which the used software is based. All statistical-based plots in this study were constructed directly from the raw data using STATGRAPHICS Plus Version 5.1 and MINITAB 15.1 programs [187, 188].

2.9.2 Theoretical Case Study for Two-Level Design Structure

The design matrix must be understood; in the case of K factors and M levels coded as +1 (or H) for high level and -1 (or L) for low level, M^K trials must be conducted. The two levels of each parameter are separated as far apart as possible from one another. The level range should be small to delete any non-linear effect, if some factors are related to quality characteristics in a non-linear fashion. For example, Table 2.5 shows the design used for three factors A, B and C with two levels for each; 8 ($8 = 2^3$) trials should be conducted in this case. To reduce the number of trials (M^K) to one half, (M^{K-1}) must be applied and to reduce to one quarter (M^{K-2}) must be applied and so on. In the matrix design inTable 2.5. for three factors, the first three columns contain the factors (A, B, C) and the columns from 4 to 7 contain the interaction between the factors. If there are four factors, the fourth factor D=ABC will be in the seventh column and 8 ($= 2^{4-1}$) trials could be conducted. The interaction effect will be between the factors; for example in the first trial the interaction AB=A.B=-1*-1=1. The sum of +1s and the -1s is zero in each column for factors or the interactions. In Table 2.5, both the factors and the interactions between the factors are displayed. Generally, the generated matrix clusters all factors to be controlled, as all factors levels appear the same number of times in each column, and allows all individual factors and their interactions to be analysed statistically and evaluated independently.

The unsuspected factors which change with time may distort the analysis and result in misleading conclusions such as moisture, temperature and voltage. Because of the unsteady errors, the standard order should be randomly assigned [182]. It is always good practice to randomize the order in which the systematic of the designs are performed. The randomization can be performed by either writing the trial numbers on pieces of paper, drawing them one at a time and putting the new order in the order in which the pieces were taken up, or by using a special table of experimental ordering using statistical programs. If the time does not allow doing the whole work in the same day, blocking is needed. The trials could be divided into 2, 4 or more blocks and the effect of the block will be analyzed in the same way as the main factors; a new column will be added as a block effect which will be another experimental factor added to the experiment. The

block effect does not interact with other factors, so any interaction containing the block effect will be ignored [127]. Again, randomization must be applied within each block. Sometimes the replication of the experiments is applied to delete the experimental error, or the effect of a factor in the experiment by using the sample mean [127]. Replicating estimates the so-called pure error in the experiment. To have the required matrix design, the same method, as explained previously, is applied by using STATGRAPHICS Plus Version 5.1 and MINITAB 15.1 programs. Many tools, such as Pareto chart, main effect plot, interaction plot, normal probability plot, surface plot and analysis of variance are used in the statistical analysis of experimental design.

Standard Order	Factors						
	A	B	C				D
	NUMBER OF FACTORS						
	1st	2nd	3rd				4th
	Factors Interactions						
	= BCD	= ACD	= ABD	= AB CD	= AC BD	= BC AD	= ABC
	Column Number						
	1	2	3	4	5	6	7
1	-1	-1	-1	+1	+1	+1	-1
2	-1	-1	+1	+1	-1	-1	+1
3	-1	+1	-1	-1	+1	-1	+1
4	-1	+1	+1	-1	-1	+1	-1
5	+1	-1	-1	-1	-1	+1	+1
6	+1	-1	+1	-1	+1	-1	-1
7	+1	+1	-1	+1	-1	-1	-1
8	+1	+1	+1	+1	+1	+1	+1

Table 2.5. The matrix design and the interactions between the factors

2.9.3 Pareto Chart

For the two-level experiments, factors and interaction effects are determined as the difference between the average responses at the low and high level of the factors. The design lies in the restricted numbers of runs through mathematical interactions. The Pareto chart is a means of effect estimate plotting similar to a horizontal diagram. The Pareto Chart for response (Figure 2.15) shows the significant arrangement of factors and their interactions in decreasing order (y-axis) depending on the significant effect (x-axis)

for their positive (+) and negative (-) effects on the response. The plot shows how each of responses' effect is affected as the factors are changed from low level to high level.

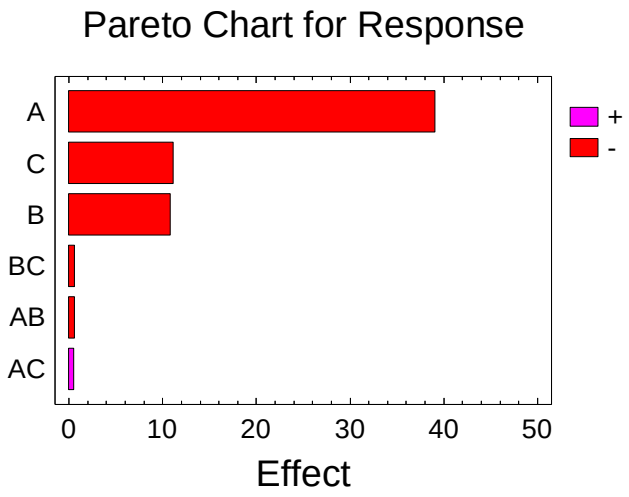

Figure 2.15. A ranked list of significant arrangement effects and interactions for response (Pareto chart)

2.9.4 Main Effects and Interaction Plots

The main effects and interaction plots help to determine the level of influence of the effects caused by the main factors and their interactions on response. In the effects plot, shown in Figure 2.16, the factor effect between the average responses of the low and high levels of the factors is presented, with the capital letters along the horizontal axis representing the main factors. The response at low level is the point on the left and that of the high level on the right; the effect line connects the two points [127]. The effect line determines the effect of the factors from the slope of the line between the two levels. The steeper the slope, the more significant is the factor effect. The direction of the effect is determined by the direction of slope of the line; a positive effect is obtained when the line increases from the left to the right and vice versa.

To determine the form of the interaction effect between two factors together and how the direction of change of the interacting factors influences the change on response, an interaction plot is needed. In Figure 2.17, all the interactions could be simulated as the plot shows the existence or otherwise of the interaction between both factors. For example, the interaction between A and B is presented as AB on the plot. The first factor (A) is presented on the x-axis from low level (left) to high level (right) and the second factor (B) is shown as two different lines, one for low level coded as (-) and another for high level coded as (+). The parallel lines confirm the absence of an intersection; the

interactions will show no significant interaction effect because of the parallel or small angle between lines in the interaction plots. The response is influenced by the change direction of the interaction factors [127]. The y-axis shows the averages of the measured response. When the low level of A is paired with the low level of B, the maximum response is obtained.

Figure 2.16. The main effects plot for the response

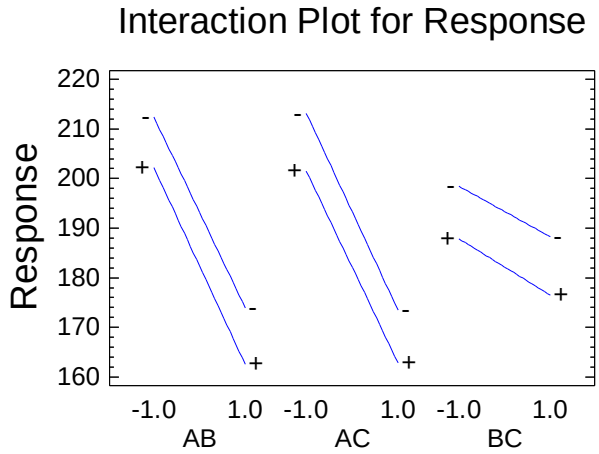

Figure 2.17. The interaction plot for the response

2.9.5 Normal Probability Plot (Daniel's Plot)

To explain a normal probability plot (Daniel's plot) theoretically, the response table for a three factor experiment will depend on the design matrix, as described previously (Table 2.6) [127]. After obtaining the statistical standardized and percentage order values for factors and their interactions, they are plotted on X and Y axes respectively to generate a normal probability plot (Daniel's plot).

Random Order Trial Number	Standard Order Trial Number	Response Observed Values Y	Response column (i)					
			1		2		3…	
			A		B		A*B…	
			1	2	1	2	1	2
	1	Y_1	Y_1		Y_1		Y_1	
	2	Y_2	Y_2		Y_2			Y_2
	3	Y_3	Y_3			Y_3	Y_3	
	4	Y_4	Y_4			Y_4		Y_4
	5	Y_5		Y_5	Y_5		Y_5	
	6	Y_6		Y_6	Y_6			Y_6
	7	Y_7		Y_7		Y_7	Y_7	
	8	Y_8		Y_8		Y_8		Y_8
Total		Sum of measurements in columns above goes here						
Number Of Values		8	4	4	4	4	4	4
Average		$\overline{Y}$	$\overline{A_1}$	$\overline{A_2}$	$\overline{B_1}$	$\overline{B_2}$	$\overline{A_1 * B_1}$	$\overline{A_2 * B_2}$
Effect (Estimated Value E)			$\overline{A_2} - \overline{A_1}$		$\overline{B_2} - \overline{B_1}$		$\overline{A_2 * B_2} - \overline{A_1 * B_1}$	

Table 2.6. The response table for a three factors experiment

Percentage order values (normal scores) are calculated as $P_i = 100(\frac{j-0.5}{m})$ where j is rank order, and m is the number of estimated effects (observations). Y_i is response observed value; for example for factor A see Equations (2.5-2.7) [124]:

$$\overline{A_1} = \frac{\sum_{i=1}^{i=4} Y_i}{4} \qquad (2.5)$$

$$\overline{A_2} = \frac{\sum_{i=5}^{i=8} Y_i}{4} \qquad (2.6)$$

$$E1 = \overline{A_2} - \overline{A_1} \qquad (2.7)$$

E(j) is statistical standardized (effect estimate) could be obtained from Table 2.6. In practice, a STATGRAPHICS program calculates and plots a normal probability or Daniel's plot. This technique separates the factors into important/unimportant categories and illustrates further details about whether the factor's effect is positive or negative [124]. The straight line represents the empirical principle in the middle of the range; the significant effect for both positive and negative effects could be reflected in deviation of the data points from the straight line. The further the deviation, the greater the statistical significance. If responses follow a normal distribution pattern, there are no statistically significant factor effects in the experiment. Figure 2.18 displays the normal probability

(Daniel's) plots and shows the percentage and standardized effects. The data points appear on or close to the straight line; these are normal data, in other words no significant effect but the outlier points have a significant effect [127].

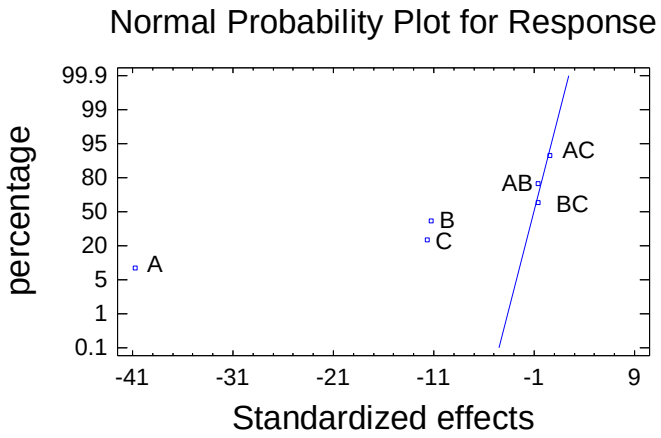

Figure 2.18. Normal Probability Plot

2.9.6 Analysis of Variance (ANOVA) Principle

In order to determine the factor effects in terms of statistical significance, analysis of variance (ANOVA) of the data was conducted. The ANOVA method, designed by Sir R. A. Fisher, is a mathematical method [127]. It compares the response data with the error data and determines the significant effect of the independent factors or their interactions. ANOVA depends on the F test, the F-ratio being obtained from statistical F tables at the appropriate level $\alpha = 0.05$ [183]. The F value is the ratio of the mean square caused by regression to the mean square resulting from the real error. ANOVA depends on the F test that compares the actual F value of the factor effects with the critical F value in the statistical F tables. For example, $F_{\mu 1,\ \mu 2,\ \alpha} = F_{3,\ 12,\ 0.05} = 3.49$: $\mu 1$: degree of freedom of the factor, $\mu 2$: degree of freedom of error, α: confidence limit. If F value is greater than the critical F value in the statistical F tables, its factor has a significant effect on the response. After calculating the F value, the P value is determined using the graphic method ($P \equiv \alpha$-significance level) and can be obtained from most modern statistical analysis programs. A probability or P-value used in ANOVA provides quantitative and objective criteria for judging the statistical significance of the effects. Each factor has a P-value less than 0.05, indicating that the factor effect is significantly different from zero at the 95.0% confidence level; the smallest p-value indicates high significance of the corresponding coefficient. An error could come from either assignable causes that represent variation

resulting from changes in the independent factors, or random causes that signify uncontrolled variation. The ANOVA table partitions the variability in response into separate parts for each effect then tests the statistical significance of each effect by comparing the mean square against the experimental error. In traditional techniques for analysis (one factor at time methods) variation may be caused by the influence of operator, specimen size and the conditions (temperature, humidity, speed and pressure, and the type of equipment). The standard deviation measures the spread of results about the mean value [172]. Table 2.7 shows the explanation of the elements for ANOVA.

Factor (Source)	**Response table column (i)**	**Effect estimate E**	**Estimated squared E^2**	**Sum of squares SS**	**Mean of square MS**	**Degree of freedom DF**	**F Value**	**P Value**
A	**1**	E_1		SS_A	MS_A	1		
B	**2**	E_2				1		
A*B	**3**	E_3		SS_{AB}		1		
No effect (Error)			E^2_{Error}			4		
Total				$\mathbf{SS_T}$	$\mathbf{MS_T}$	**7**		

Table 2.7. Results from analysis of variance (ANOVA) of the data identifying the statistical significance of factor

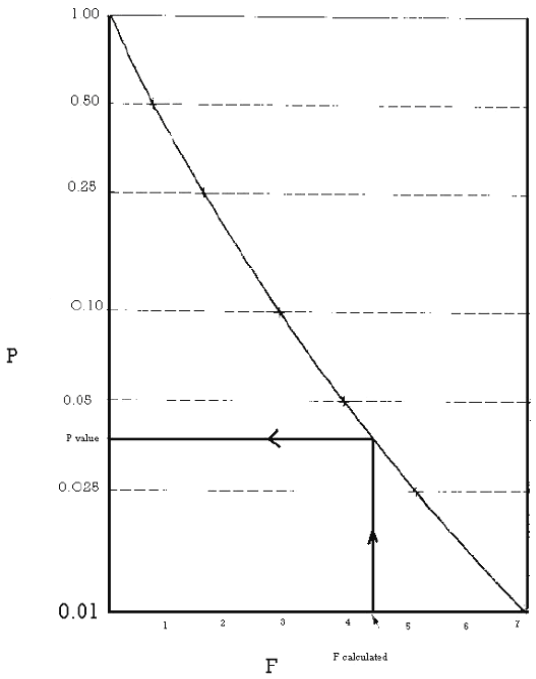

Figure 2.19. Calculating the P value using the graphic method.

The degree of freedom for the no effect (DF) is the number of independent comparisons available to estimate a parameter; in other words, it is the model parameters minus 1 ,(K-

1) or the number of free choices to estimate a parameter [189]. Error comes from either assignable causes i.e. variation resulting from changes in the independent factors, or random causes such as uncontrolled variation. After calculating the F Value, the P value (P ≡ α-significance level) can be obtained using the graphical method, as shown in Figure 2.19 [189].

2.9.7 Regression Equation and Estimation Results

Based on the analysis of the fraction factorial experimental design results and using STATGRAPHICS program, a simplified mathematical model was fitted. The regression equation (Equation 2.8) was fitted to the experimental data. The forecasting model includes all interaction terms regardless of their significance. It is a sufficient basis for interpretation of the obtained relationships Y= *f* (A, B, C):

$$\mathbf{R} = a_0 + b_1A + b_2B + b_3C + b_{12}AB + b_{13}AC + b_{23}BC \quad (2.8)$$

The model evaluates the significance effect of each independent variable to a predicted response, depending on the coefficient constant for the linear effects of independent factors, and the coefficient constant for the interactions effects. Where R is predicted response, A, B and C are independent factors; a_0 is the coefficient constant for the offset term; b_1, b2 and b_3 are the coefficient constant for linear effects and b_{12}, b13 and b_{23} are the coefficient constant for interactions effects. The model was limited to only two-parameter interactions, since interactions of more than two parameters are not useful in practice.

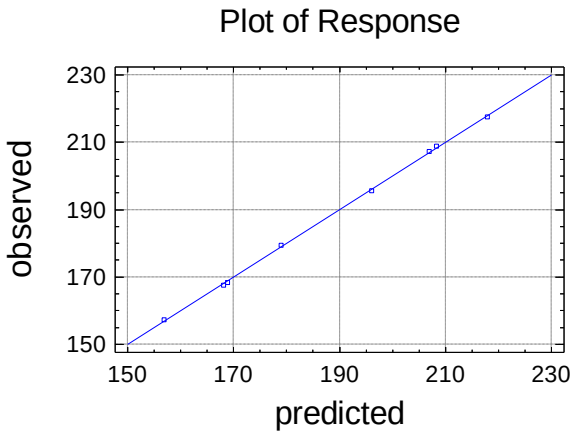

Figure 2.20. Experimental observed results and calculated fitted results plot for response

The mathematical model was driven from the experimental data and the residual plot was analyzed to validate the regression formula. Figure 2.20 shows the experimental observed

results and calculated fitted results plot of response using the last fitted models for each trial. Experimentally observed results are plotted on the Y axis and the response for calculated fitted results generated using the last fitted model are plotted on the X axis for each trial. In Figure 2.20, while the point estimate gives the best possible prediction, the prediction could be not perfect. The error in prediction could be incorporated by using interval estimates rather than point estimates or further regression.

Theoretically, the software gets the standard deviation of the mean values. Then, estimates what range of values would encompass the predicted and observed values. A new name is assigned to the standard deviation of the means which is the standard error. Standard Deviation reflects the variability of individual data points, and the Standard Error is the variability of calculated and predicted values of the responses. To find how accurate is the estimate, Model Standard Error (MSE) for forecasts statistic in Table 2.8.

By itself, the MSE is used in constructing confidence intervals (CIs), which indicate a range of values within which the "true" value lies. It shows how accurate the estimates of the population values actually are. Both statistical significance testing and CIs are useful because they assist the reader in determining the meaning of the results. MSE is calculated by the used software; the intervals bound the sampling error in the estimates and judge how precisely each response's mean.

2.9.8 Surface Plot (3D-Surface Response Diagrams), Square and Cube Plots

To determine the behaviour of the interaction between factors, a surface plot may be used. The surface plot can be visualized as a three-dimensional (3D) plot that presents the predicted responses as a function of two factors, while keeping other factors constant on their middle levels. The pattern of estimated responses is based on the assumed model derived from the experimental observations. The geometric result of plotting a response variable is as a function of two factors and the interaction appears with the surface twist (bend). If the surface is flat, there is no significant interaction. Figure 2.21 shows estimated response surface plots (3D-surface response diagrams) for interactions A & B, the surface plot between two factors, the first interaction factor (A) on the X-axis with low and high levels, the second interaction factor (B) on the Y-axis with low and high levels, and the Z-axis shows the averages of the measured response. Estimated response surface plots show significant twist and significant effect as a result of these interactions. For the surface plot, the high response results from the low level of factor A and the low level of the factor B.

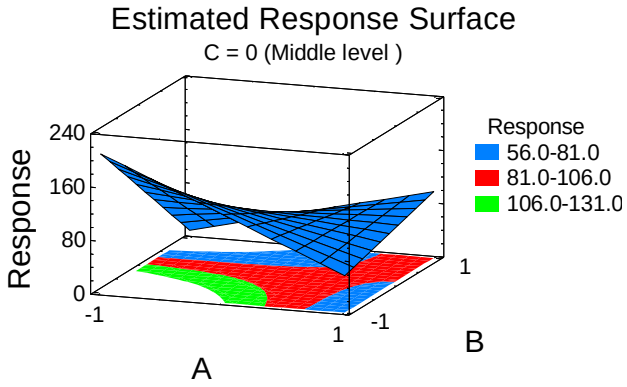

Figure 2.21. Estimated response surface A&B

Square and Cube plots (Figure 2.22) are fast and flexible forecasting tools used to summarize predicted values for the dependent variable by giving the respective high and low setting of factors. The square plot shows the predicted values for the respective low and high settings for each of the two factors (variables) at a time; the cube plot shows the predicted values for the respective low and high settings for three factors at a time.

In Figure 2.22 a, and depending on the regression equation, each value corresponds to the values of the experimental factors A and B at the middle level of C range between -1 and +1, which is 0. There are two axes: the first factor A is on the X-axis with low and high levels, and the second factor B is on the Y-axis with low and high levels.

In Figure 2.22 b, and depending on the regression equation, each value corresponds to the values of the experimental factors A, B and C at the middle level of other factors ranging between -1 and +1, which is 0. There are three axes: the first factor A is on the X-axis with low and high levels, the second factor B is on the Y-axis with low and high levels and the third factor C is on the Z-axis with low and high levels.

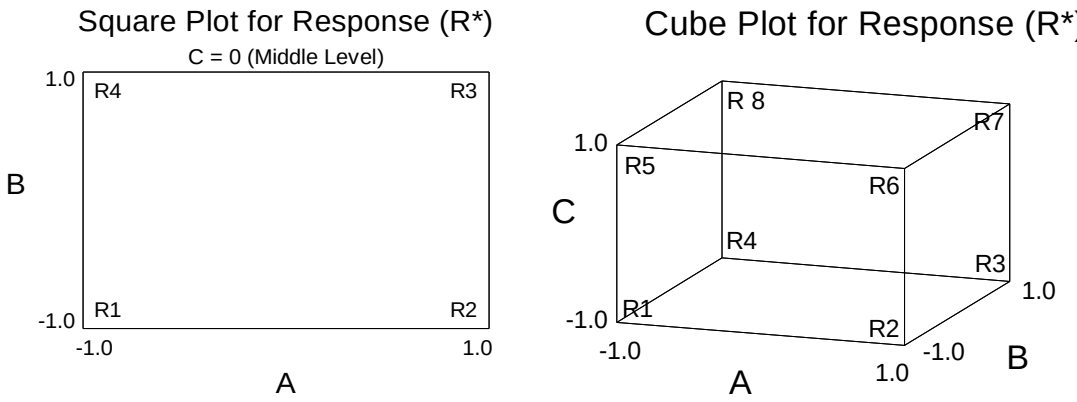

(a) (b)

Figure 2.22. Square and Cube plots of the estimated effects for the high and low studied factor settings (R1-R8, response values)

2.9.9 Statistical Model for Optimisation

The responses of the statistical models derived here could be explained scientifically by related theories and the knowledge of the influence of the involved parameters on the production process. For the final optimization of the studied responses,Table 2.8 shows the combination of factor levels which maximize and minimize responses over the indicated region. In the course of response optimization, the mathematical statistical model was derived from the experimental data. The statistical model covers all the factors and their interactions; The Model Standard Error (MSE) value listed in Table 2.8 indicates the dispersion of predicted and observed values around the theoretical fitted line generated using the fitted model for each trial.

Factor	Optimum Model for Response	
	MSE Value	
	Optimum Value	
	Maximum	Minimum
A	L	H
B	H	L
C	H	H

Table 2.8. The combination of factor levels which maximize and minimize response over the indicated region (L: Low Level, H: High Level, MSE: Model Standard Error)

CHAPTER 3 - MATERIALS AND METHODS

3.1 Materials, Structure and Properties

As environmentally friendly materials, fully biodegradable polymers were used in this research. Their properties are listed below:

3.1.1 Linear Aliphatic Aromatic Co-polyester (LAAC)

Fully biodegradable, petrochemical-based, linear aromatic-aliphatic co-polyesters were used in this research. In terms of structure (Figure 3.1), the two grades of LAACs used in this stage were coded as MFI1 and MFI2, depending on their melt flow index [MFI is described in section 3.2.1]. The supplier datasheet does not show the details related to the copolymerization ratio, because it is a commercial sample (Table 3.1). Each grade was optimized by the manufacturer to be mixed with starch-based polymers (Solanyl Rigidity Component) by controlled chain length. Granules were dried at 60^{o}C for 6 hours to avoid possible hydrolysis during the extrusion process.

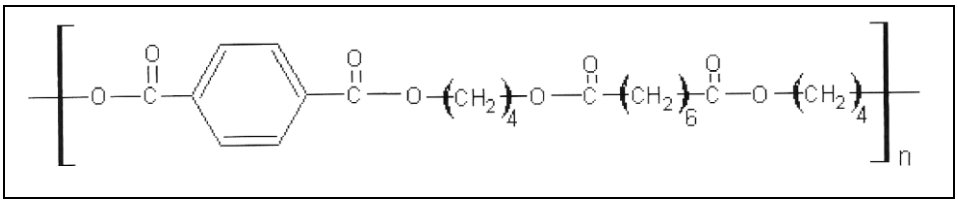

Figure 3.1. Chemical structure of linear aliphatic aromatic co-polyester

3.1.2 Branched Aliphatic Aromatic Co-polyester (BAAC)

Petrochemical-based, fully biodegradable, branched, modified aliphatic-aromatic co-polyester was used also in this research (Figure 3.2). The grade used was optimized by the manufacturer for film extrusion and extrusion coating by controlled branching and chain length by the manufacturer (Table 3.1). The BAACs met the requirement of the European Norm EN 13432, entitled "Requirements for packaging recoverable through composting and biodegradation - Test scheme and evaluation criteria for the final

acceptance of packaging". Granules were dried at 60°C for 6 hours to avoid possible hydrolysis during the extrusion process regarding the supplier datasheet.

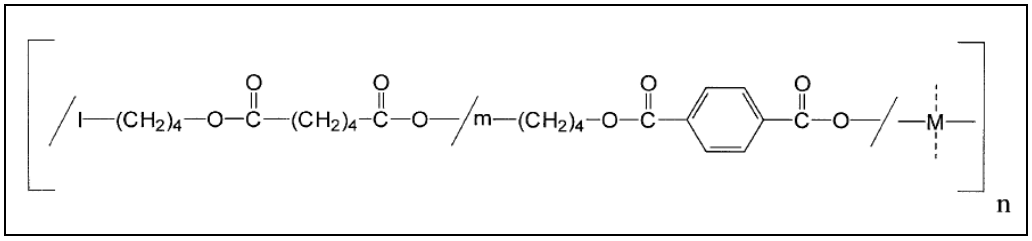

Figure 3.2. Chemical structure of branched aliphatic aromatic co-polyester (Ecoflex), M=modular component, e.g. monomers with a branching or chain extension effect [77].

Material	Linear AAC	Branched AAC
Supplier	Made by Eastman (USA) Supplied by the Rodenburg in the Netherlands	Made by BASF (Germany) Supplied by FKuR in Germany
Trade name	Solanyl Flexibility Component	Ecoflex F BX 7011
Chemical basis	1,4-benzenedicarboxylic acid, polymer with 1,4-butanediol and hexanedioic acid	1,4-butanediol,adipic acid, terephthalic acid (42-45% mol)
Density	1.2-1.22 (g/cm^3)	1.25-1.27 (g/cm^3)
Melting Temperature	110 to115 (°C)	110-120 (°C)
Glass Transition Temperature	-30 to -32 (°C)	-30 (°C)
Melt Flow Index (2.16 kg/130°C)	MFI1 = 6-8 (g/10 min) MFI2 = 12-14 (g/10 min)	2.7- 4.9 (g/10 min)
The polymer shape and dimension	A spherical granule resin Diameter of 3-5 mm	A spherical granule resin Diameter of 3-5 mm
Granule colour	White (MFI1), Cream (MFI2)	White
Toxic effects	No	No
Preparation before use	Dried at 60°C for 6 hours	Dried at 60°C for 6 hours

Table 3.1. The two main types of commercial AAC bio-plastics

3.2 Material Characterization

Characterization of materials used is needed to understand their flow behaviour and properties and to identify their fibre-forming properties [159]. Since the polymer melts differ in size, weight and degree of freedom, the microstructure of the materials has to be taken into account in order to describe typical features of non-Newtonian fluid behaviour. The characterization methods used are described below:

3.2.1 Melt Flow Index and Rheological Properties

A Ray-Ran 5 Series Advanced Melt Flow System was used to measure the melt flow index (MFI) [190]. MFI (g/10 min) measures the mass in grams of a thermoplastic material through a standard size capillary at known temperature for 10 minutes [191]. MFI values according to ASTM D-1238 for AACs are listed in Table 3.1. In the rheological studies, different pressures were applied to the melt via a piston using different loads of total mass (F) of 2.16, 3.16 and 5.00 kg at different temperatures of 120, 125, 130 and 135°C. A schematic diagram of the pressure distribution in the reservoir and the capillary is shown in Figure 3.3. The piston diameter (D = 9.5504 mm) was bigger than the capillary diameter (d = 2.0955 ± 0.0051) and the pressure dropped along the capillary (ΔP). L is the capillary length (L= 8.000 ± 0.0250 mm, L/d =3.8177) and P (I=0) is the atmospheric pressure. When the piston was moved down by the weight, the molten polymer was forced through the die.

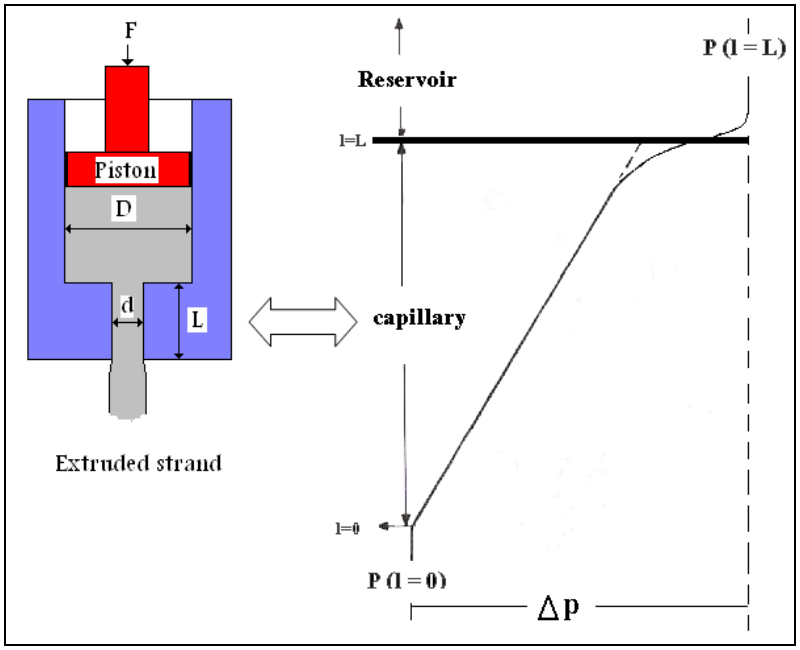

Figure 3.3. The melt index tester with schematic diagram of the pressure distribution in the capillary

In Newtonian fluids, it is possible to calculate the flow properties via equations from the literature [192, 193]. As the piston diameter (D) is bigger than the capillary diameter (d), the wall shear stress τ in the capillary can be related to the force on the piston, and the entrance effects are ignored, the wall shear stress can be calculated then using the following equation: $\tau = \frac{\Delta P\, d}{4\, L}$ where: ΔP is the pressure dropped along the capillary and L

is capillary length, [192], ΔP can be calculated by the equation $\Delta P = \frac{4F}{\pi.D^2}$ Where: F is the weight on the plunger in grams . The shear stress τ at the capillary wall is determined by equation 3.1

$$\tau = \frac{F.d}{\pi.L.D^2} = 8.97\,F \quad (pa) \tag{3.1}$$

Where: F is the weight on the plunger in grams.

The flow rate (υ, cm^3/s) is determined by the area (cm^2) and the piston velocity (v, cm/s) or by the MFI value and the melt density at the current temperature (ρ_t) [154]:

$$\upsilon = \frac{MFI}{600 \times \rho_t} \ (g/s) \tag{3.2}$$

The apparent shear rate γ_{app} at the capillary wall can now be expressed as a function of the MFI as flow rate υ through the capillary [154] by equation 3.2:

$$\gamma_{app} = 1.845\,\upsilon \quad (s^{-1}) \tag{3.3}$$

The apparent η_{app} viscosity can be determined by dividing the shear stress by the apparent shear rate [154] as shown in equation 3.4:

$$\eta_{app} = \frac{4.86\,F}{\upsilon} (pa.s) \tag{3.4}$$

The viscoelastic effect and the slip of polymer on solid walls could be noted in the simulation of polymer processing operations of thermoplastic materials [194, 195]. The viscosity ratio affects the capillary instability of fluid jets and helps in determining melt spinning conditions. If the entrance effect is considerable, there are errors in the expression for the wall shear stress and the apparent viscosity. This drawback is negated by running the melt indexer with several different weights. In non-Newtonian fluids, the actual value of the shear rate at the capillary depends on the fluid behaviour as a power law fluid with power law index; the viscosity curves of viscosity and shear rate are converted to true viscosity curves using the Rabinowitsch correction [171].

3.2.2 Thermal Analysis Using Differential Scanning Calorimetry (DSC)

Differential scanning calorimetry (DSC) is a thermal analysis used to determine physical changes, chemical changes or the degree of the crystallinity of the polymers through

measuring the enthalpy and comparing it with the enthalpy of a crystalline sample of the same material [196]. The differential scanning calorimetry thermal trace of the exothermic heat flow contains the transient, the glass translation, crystallization and melting point peaks (Figure 3.4). The area between the profile and the baseline, which is between the limits of temperature of a particular feature, is related to the enthalpy-change for the corresponding transition in the polymer sample.

METTLER- TA Instrument and METTLER –TOLEDO –TA89E System Software were used to determine the thermal curves of the AAC polymer. The sample and the reference have the same heat input, and the same temperature must be in both through maintaining the temperature by the servo-system supplying the energy input to each. The instrument was equipped with an extra gas inlet and used water as a cooling liquid. A 5-10 mg weight of the specimen was put in a supplied standard aluminium pan in a free state. The heating rate applied was $10^{o}C.\ min^{-1}$; the gas used was nitrogen at a flow rate 45-50 $cm^{3}.min^{-1}$. An average of three replicates scanned for each sample was used.

The melting point (T_m) appeared as a peak in the melting endotherm in a thermal melting apparatus, depending on the chemical structure, molecular weight and degreed branching. T_m was lower than theoretically predicted; that depends on crystallite size and the heating rate; for flexible polymers there is a range of melting - as much as $10^{o}C$ [168]. The glass transition temperature (Tg) is a conventional criterion used to assess segmental mobility for a given polymer or miscibility for an investigated polymer blend in the amorphous state [197]. If the Tg is lower than room temperature, the polymer is crystallisable and kinetically unstable at spinning temperatures, the same as polyolefines.

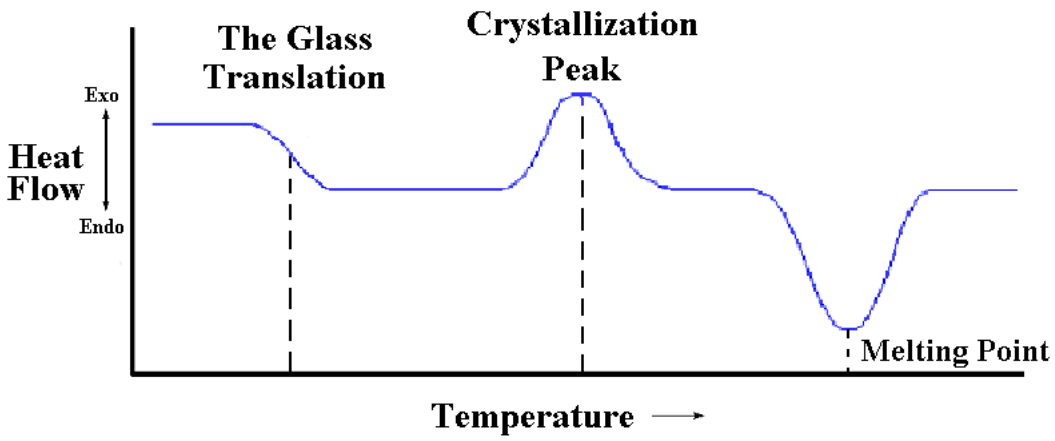

Figure 3.4. The differential scanning calorimetry (DSC) thermal trace

3.2.3 Extrudability and Productivity Analysis Using a Brabender Machine

A Brabender machine with an extruder attached and a torque recording rheometer (Plasti-Corder) was used to measure the extrudability and productivity and their effects with the extrusion temperature profile of a single screw extruder, which was not connected to a metering pump. Using a Brabender machine helps to investigate torque and throughput by optimising the processing temperature profile in barrel zones for the fibre extrusion and to understand the relationship between the extrusion temperature profile, extrudability and the productivity of polymer, a measure of output from the extrusion process per minute (g. min^{-1}). The extrusion productivity was measured by weight of the extrudate each minute, 5 times for each. The machine consists of a specially designed laboratory extruder with four heating zones and a vibratory feed hopper (Figure 3.5). The measuring head is mounted against the rotating screw. The temperature zones in the extruder are the three barrel zones (T1, T2 and T3) and the die head zones (T4); all heating zones are electrically heated and controlled independently and are supplied with thermocouples. Theoretically and by increasing the screw speed, the temperature is increased as a result of the increase in shear viscous dissipation [198].

For all experiments, shift position was 0 and the connector setting was 1.5; indicator adjustment for measuring systems ×5, with screw speed of 7 rpm and the die nozzle diameter was 2 mm. Torque unit (force by distance, g×m) can be converted to N m , 1 N m =1 g m * 0.001*9.81, to describe the resistance to turn the screw.

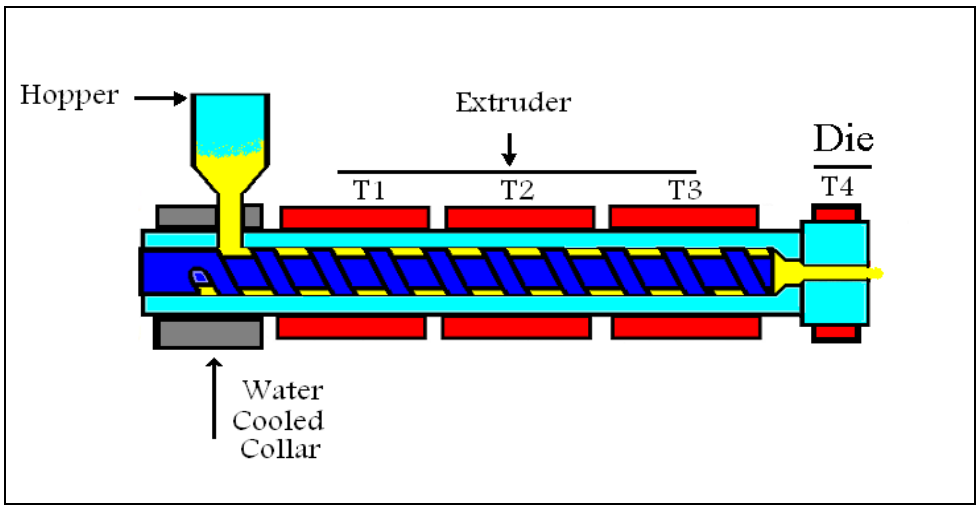

Figure 3.5. Schematic diagram of the Brabender extruder

3.3 Filament Production

3.3.1 Melt Spinning of As-Spun Fibres

Fibres were extruded via a melt spinning on Lab-Spin machine (Figure 3.6). The Lab-Spin machine consists of a single screw extruder barrel (25 mm screw with length-to-diameter ratio 20:1), a metering pump (capacity of 2.4 $cc.rev^{-1}$), a die head, a cooling window (1.5 m length) with a cross flow air quench, a spin finish application system (capacity of 0.146 $cc.rev^{-1}$), godet roller of 66 cm circumference and Leesona winder (spindle diameter of 143 mm) used for both spinning and drawing experiments. The godets and the winder speed were controlled independently by DC motors. Cooling air was provided by means of a centrifugal fan powered by 1.5 Kw AC motor and static invertors speed control for varying cooling air velocity. The rate and stability of the cooling process was controlled by a transverse air flow distributed through a distribution sock. The spinneret is defined by its dimension, especially length to diameter nozzle ratio. Two special designed spinnerets were used: a 55 capillary circular cross section holes spinneret (diameter of 0.40 mm and length to diameter ratio 4:1) for temperature profile studies and 30 capillary circular cross section holes spinneret (diameter of 0.40 mm and length to diameter ratio 2:1) for spinning and drawing studies, it is designed with lower l/d ratio as with a large l/d ratio, the back pressure in the die increases and makes die swell.

The temperature in the extruder was controlled by three barrel zones (T1, T2 and T3), metering pump zone (T4) and two die head zones (T5 and T6). All heating zones were electrically heated and the six zone temperatures controlled independently by thermocouples. The energy required to melt the polymer came from both external heating and the internal friction [118]. Dried granules are fed through the hopper into the extruder without any additives, then mechanically compressed and melted. The molten polymer is forced through spinneret as fine jets with different speeds adjusted and metered by the metering pump speed. As the polymer was extruded, the pressure built up at the end of the extruder. The temperature of the feeding zone was kept above $100^{o}C$ to prevent any moisture from forming.

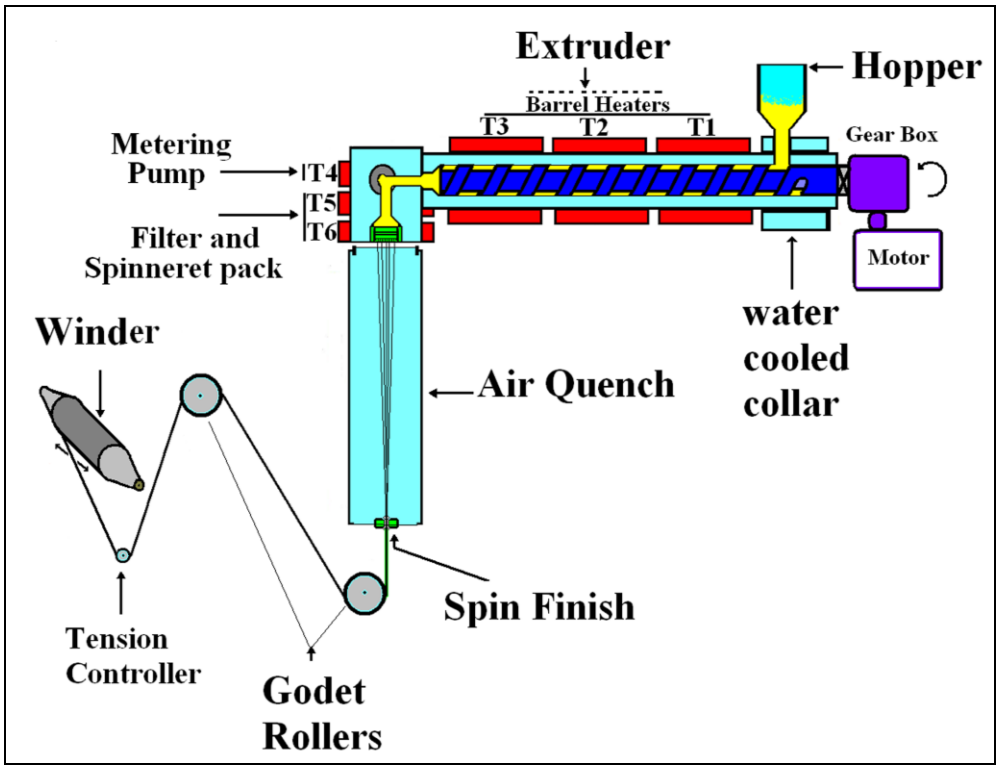

Figure 3.6. Schematic diagram of the melt spinning equipment

The filaments cooled and hardened through the air cooling quench at ambient temperature progressively to emerge as solid filaments. The spin finish available in the extrusion lab (VICKERS, 1031) was diluted five times with water before use and applied through a ceramic thread guide. The filaments were collected on a tube using the Leesona winder. The tension in the Leesona winder was controlled automatically by a tension controller to obtain good package build up and also to avoid the tension variation which could affect the filament properties during package diameter changing. All the speeds were measured by a laser source digital tachometer. The laboratory working conditions were measured using a digital hygro-thermometer; the temperature was between 18^{o} and 23^{o} C, and the relative humidity was between 45 and 75 %. Spin-draw ratio (SDR) or draw-down ratio (DDR) is the ratio between the speed of the initial fibre (take up or winding speed) to that of the melt coming out of the spinneret (extrusion speed) by keeping the tension constant in the take up line [199]. It may also be obtained from the diameter of the filament at maximum die swell (D) and that of the produced fibre (d), as in Equation 3.5:

$$SDR = V_{take\ up} / V_{extrusion} = D^2/d^2 \quad (3.5)$$

More details could be obtained by calculating polymer flow rate and extrusion speed from the literature [161]. If the take-up speed is greater than the extrusion speed, the filament is elongated uniaxially [160]. The molecular orientation of the fibre during spinning

(i.e. draw-down ratio) was less than that produced during post drawing (solid state draw ratio).

3.3.2 Multi-Stage Drawing Process Equipment and Procedure

Multi-stage cold and hot drawing was carried out on an ESL drawing frame (Extrusion Systems Limited, UK). The multi-position draw frame consisting of four hot rollers (160 mm) with a freely rotating separator (35mm) was used to separate the filaments bundle on each roller, three hot plates (495×30 mm), a spin finish applicator (capacity of 0.292 cc.rev^{-1}) and the Leesona winder (spindle diameter of 143 mm), Figure 3.7. For technical reasons, the spinning and the drawing were separated.

The temperature and speed of the four roller motors were adjusted separately and the spin finish (VICKERS 1031) was diluted five times with water before use and supplied to the filaments through a ceramic thread guide before the last roller. Filaments were wound five times around each roller and its separator to prevent slippage and to obtain the actual draw ratio. Theoretically, there are the solid-state (actual) draw ratio R_D and adjusted (machine) drawing ratio R, as Equation 3.6 [167]:

$$R = \frac{L_2}{L_1} = \frac{d1}{d2}(actual) \Leftrightarrow R_D = \frac{V_2}{V_1}(adjusted) \tag{3.6}$$

Where V_1 is the speed of the first drawing roller (m min^{-1}), V_2 is the speed of the second drawing roller (m min^{-1}), L_1 is the fibre length before drawing, L_2 is the fibre length after drawing, d1 is the fibre diameter before drawing and d2 is the fibre's diameter after drawing.

Drawability is the surface speed of the draw roller at break to the surface speed of the feed roller at break ratio. For measuring the drawability value of as-spun fibres at constant feeding speed roller, hot plate temperature and constant drawing speed, the speed of the draw roller was increased gradually until the yarn eventually broke. Then the current draw ratio was measured which is the drawability value of the as-spun fibres. After analysing the result and obtaining the correct processing conditions and drawability value, end use fibres could be produced directly from a continuous process, as shown in Figure 3.8.

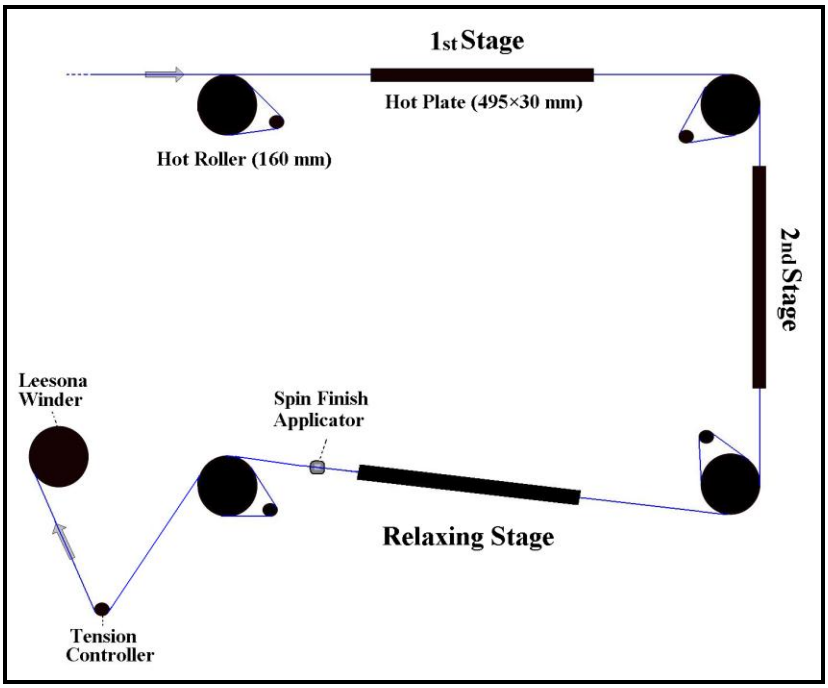

Figure 3.7. Schematic diagram of the multi-stage drawing equipment

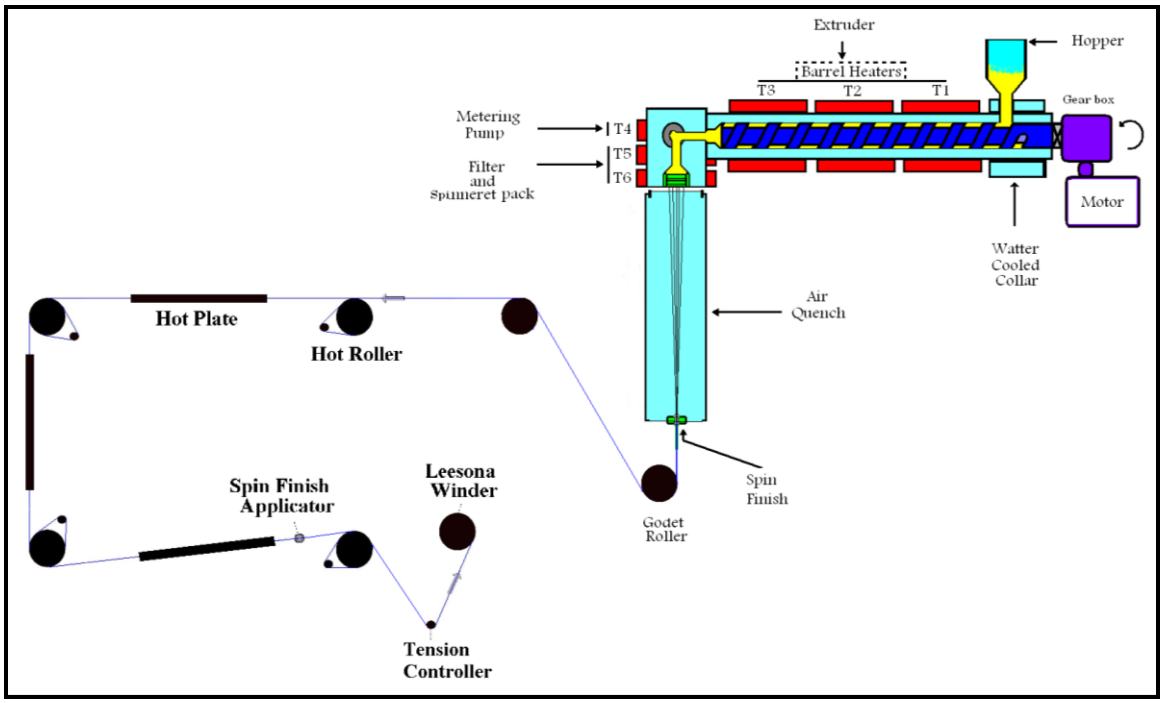

Figure 3.8. Schematic diagram of the continuous melt spinning and drawing processes

3.3.3 Twisting Equipment and Procedure

Twisting was carried out by a J.T Boyd twisting machine, in which the yarn runs downwards and is then taken up by rotating spindles through a ring/traveller system. Twist was applied on the continuous drawn filaments at different twist levels and a constant spindle speed (316 rpm) at ambient temperature (Figure 3.9).

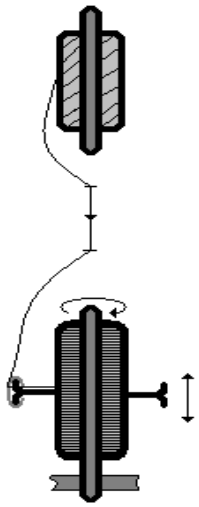

Figure 3.9. Schematic diagram of the ring/traveller twisting system

The angular velocity of the traveller correlated the yarn twists by the different angular velocity between the traveller and the spindle; twist direction was S direction[200]. In the case of incompletely drawn filaments, the effect of additional drawing occurring during twisting must be considered. The producer twist reduced the amount of filaments or loops protruding from the yarn [112]. Because the inter-filament pressure depends on the level of twist, the filaments were increasingly less able to resist the tension, leading to a reduction tensile strength with increasing twist for some fibres.

3.4 Thermo-Graphic analysis (Infrared Imaging and Measurement Equipment)

Surface temperature was calculated and displayed by advanced ThermaCAM SC 3000 - FILR SYSTEMS and the ThermaCAM research Professional 2.7 program. The system deals with a live infrared (IR) image arriving through ThermaCAM SC 3000 Quantum Well Infrared Photodetector (QWIP) System [176]. The system includes IR camera with a 20° lens, high capacity PC card, remote control, cables, connectors, power supply and a range of optional hardware and software accessories. It offers superior thermal sensitivity, broad dynamic range, extraordinary long-wave (8 to 9μm) imaging performance and high speed data acquisition capabilities. The electromagnetic spectrum was divided arbitrarily into a number of wavelength regions distinguished by the methods used to produce and detect radiation. Depending on pre-experimental work, an infrared image was designed to calculate the temperature of filaments indicating five line readings coded as L01 (the die head temperature), L02, L03, L04 and L05. Their distances from the spinneret surface are 0, 25, 80, 170 and 285 mm respectively, as shown in Figure 3.10. Each line put on the

image gives the temperature profile on the profile scale connected to the IR image, which helps in finding the heat transfer effect found in fibre spinning [177]. The temperature scale is in the top left corner and image colours correspond to the temperature scale on the right.

The temperature profile is a useful tool for illustrating the temperature variation across or along an object in the image. The software provides several layout options, such as the IR image, the profile layout options and the histogram; the camera measures and images the infrared radiation emitted from the filaments. Temperature (^{o}C) vs. time (sec) data was analyzed using the plot module, as shown in Figure 3.11 (a-c). In Figure 3.11, a, temperature (^{o}C) vs. time (sec) data with no filament and no cooling applied gives valuable information about each line. Differences in analysed data could be noted when the filament started extruding (Figure 3.11, b), so that more thermal balance could then be achieved when the air quench speed was applied (Figure 3.11, c). That will be investigated in Chapter 5, to find the effect of processing conditions and how they could be optimized, forecasted and controlled.

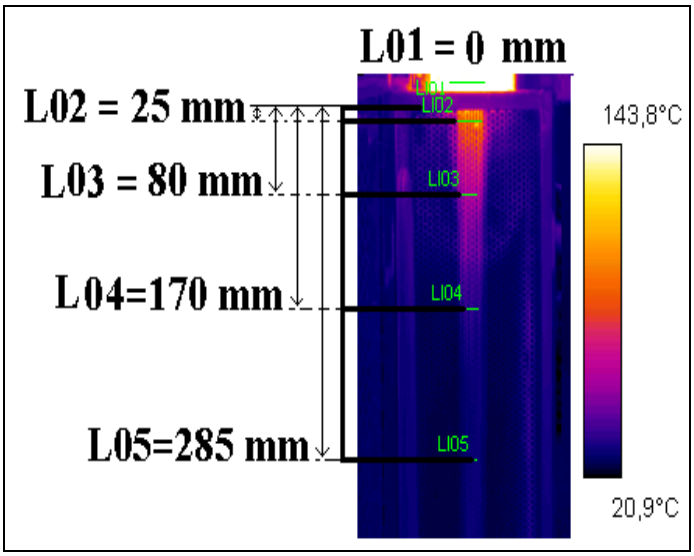

Figure 3.10. Infrared image of filaments
(Image colours correspond to the temperature scale)

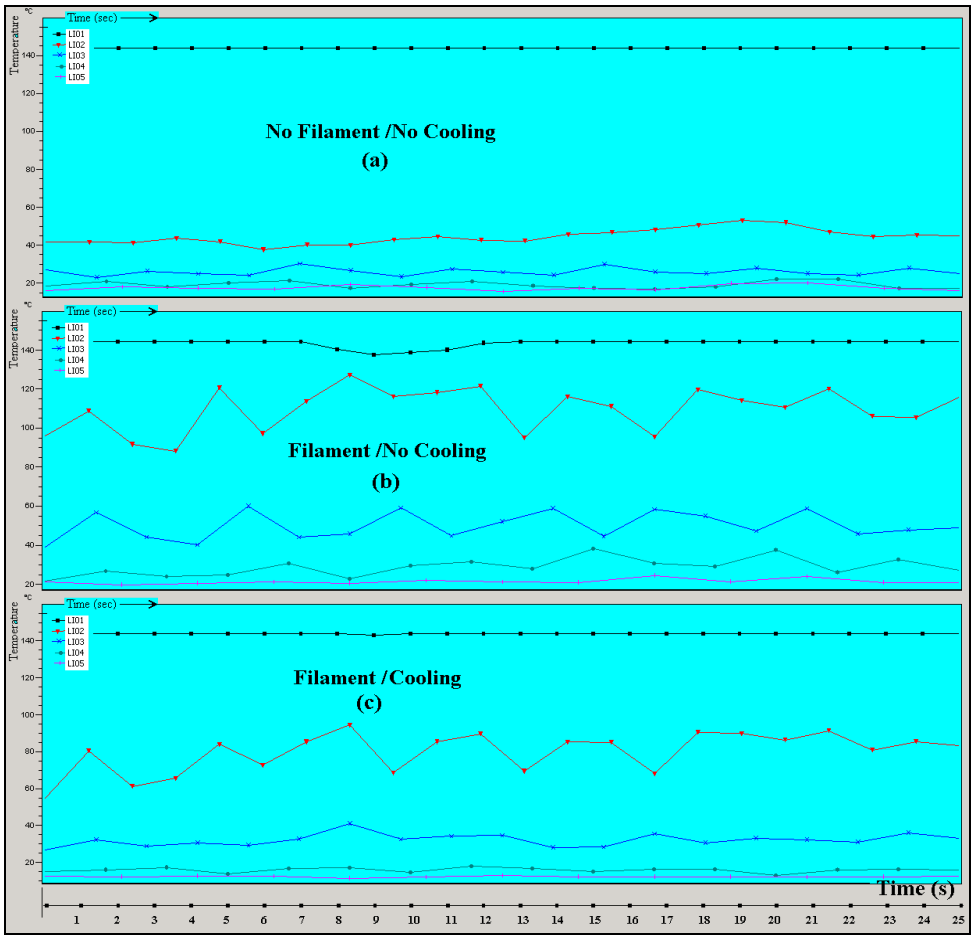

Figure 3.11. Temperature vs. time plots

3.5 Filament and Yarn Characterization

Fibre properties are determined by physical structure, chemical composition and the molecular arrangement. The textiles take their shape and character from the yarn design and structure. Fibres with a longer chain (higher molecular weight) are stronger and more difficult to pull apart than fibre with a shorter chain (lower molecular weight). Finer fibres are more flexible and more easily damaged [112]. Yarn spun from staple fibres has more flexibility and durability than that from the filament fibres, which will give stiffer fabric.

3.5.1 Optical Microscope

The diameter, surface and cross section of fibres affect the yarn volume, handle, insulating ability, lustre and working performance in processing. A Leitz Diaplan optical microscope connected to Digital Olympus ALTRA 20 camera with Olympus Imaging Software was used to characterize the diameter, surface and cross section of the fibres.

Fibre samples were selected randomly and put onto a yarn holder and eyepiece. The fibre diameter was measured in five various axial positions for 10 individual fibres selected randomly and the mean values and deviations of diameter were calculated. The effect of fineness could essentially be regarded as an effect of changing filament diameter.

3.5.2 Linear Mass Density (Count)

Yarn count was determined by weighing a 100 m length; the samples were conditioned in the conditioned laboratory at standard testing atmosphere, the temperature of 20 ± 2^{o} C and the relative humidity of 65 ±5%. The result was converted to denier (the mass in grams per 9,000 meters) or tex (the mass in grams per 1,000 meters). Linear mass density was determined using a balance accurate to one milligram; the reported results were the average values of five repeated measurements. Denier per filament (dpf) was calculated by dividing the yarn size by the number of filaments. Theoretically, the fibre mass could be calculated from the cross section area of fibre, fibre length and density.

3.5.3 Optical Birefringence and Overall Orientation Technique

Birefringence manifests itself as a splitting of a light ray into components having different vibration directions transmitted at different velocities. Optical birefringence was determined using a polarizing interference microscope, depending on the strong relationship between birefringence and molecular orientation [201]. The value of the measured birefringence reflects the overall orientation or the alignment of the fibre molecules around its axis. As is known, low birefringence fibers have low orientation and would be more drawable than the higher values and via versa.

The double refracting polarizing interference (Pluta) microscope was designed, developed and applied by Pluta [202]. It is especially suitable for microinterferometry of birefringent fibers. This microscope was used to conduct observations of various micro-objects that produce a shift in either the phase or amplitude of light waves being transmitted. This microscope also measures the optical path difference, refractive index and birefringence.

The Pluta microscope, as a non-destructive tool, was the interferometric technique available and used in the study. It is a useful technology for measuring the fibre's birefringence. It was used to measure the refractive indices between the values of fibre refractive index in case the light used polarized parallel to the fibre axis, and the value of

fibre refractive index in case the light used polarized perpendicular to the fibre axis at the same time from one mirointerferogram.

In this work, the subtractive position is applied to give the non-duplicated images for the direct measurement of the fibre's birefringence (Δn). The direct measurement of Δn is most desirable using the Pluta microscope (subtractive position). For accurate and less time-consuming measurements, this Pluta microscope was equipped with a computerized unit consisting of a CCD micro-camera, PC computer and digital monitor (Figure 3.12). The measured parameter can be analyzed by using this unit and the microinterferogram of fibers [203].

The birefringence (Δn) of the fibre can be determined indirectly by calculating the difference between the refractive indices ($n^{\parallel}$ - $n^{|}$) of the fibre. Here $n^{\parallel}$ and $n^{|}$ are the refractive indices of fibre, in case of the light polarising parallel and perpendicular to the fibre axis, respectively but it can be measured directly using the subtractive mode of Pluta microscope via the following Equation 3.7 [204]:

$$\Delta n = \frac{t.\lambda}{h.d} \tag{3.7}$$

Where, *t* is the apart of the fringe shift., λ is the wavelength of the light used., *h* is the interfringe spacing and *d* is the fibre diameter.

The error of measuring the optical path difference (Z λ/b) using the interference Pluta microscope ranges from ±0.001 to ± 0.003 [205]. The bigger the molecular orientation leads to the higher the value of The overall orientation factor F = Δn / Δṅ, where Δṅ is the intrinsic birefringence.

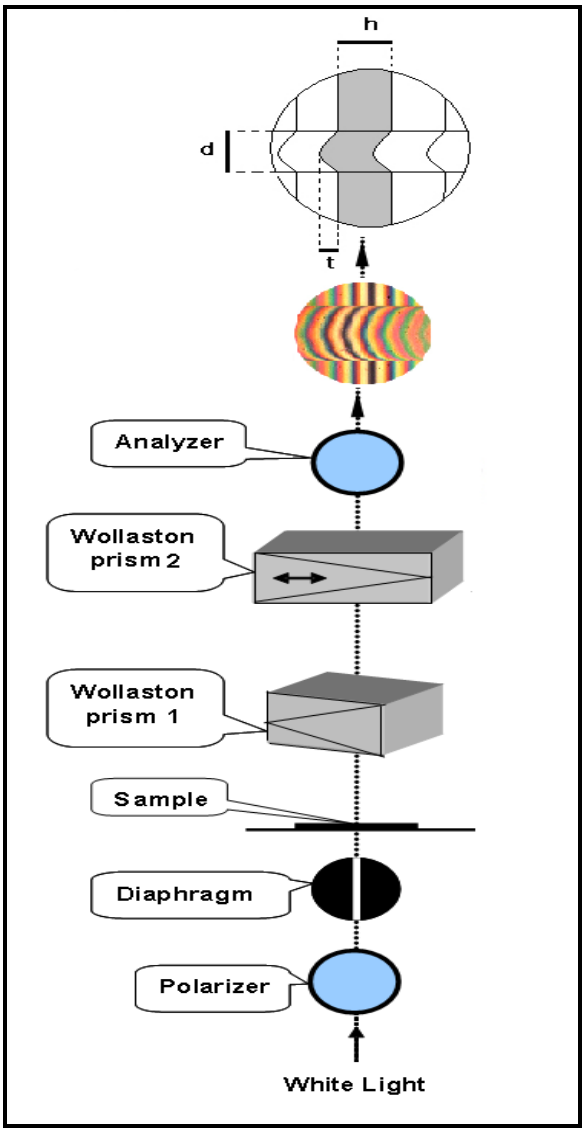

Figure 3.12. Diagram of the Pluta microscope

3.5.4 Wide Angle X-Ray Diffraction (WAXS)

The X-Ray diffraction method is a physical technique for investigating the atomic and molecular structure of the fibres [206]. Theoretically, X-Ray diffraction establishes standards for assessing crystal structure and crystallinity, the fine structure of matter states of an atomic order, lattice spacing, crystallite form and size and crystallite orientation [207]. In 1912, Bragg recognized a predictable relationship between the wavelength, the (d-spacing) inter-atomic spacing and the diffraction angle which are combined in Bragg's law. The diffraction occurs when the path length difference between the two beams is an integral multiple of the wavelength. A scan of intensity vs. angle θ gives a number of peaks; from the knowledge of the crystal structure, the positions of the

peaks can be calculated. In Figure 3.13, the two parallel incident rays a and b make an angle (θ) with these planes. A reflected beam of maximum intensity will result if the waves represented by a' and b' are in phase. The difference in path length between a to a' and b to b' must then be an integral number of wavelengths (λ); this relationship is expressed mathematically in Bragg's law. The beams that appear to be reflected beams are in-phase (Bragg's law), the beam incident at an angle $\boldsymbol{\theta}$ on a set of atomic plans has spacing d between successive planes of the lattice; the scattered beam from the first plane is regarded as a reflection of the incident X-ray beam.

Both rays lie in the same plane perpendicular to the diffracting plane and the incident angle that is equal to the diffraction angle. With diffracted rays with different path-length they will differ in phase and will cancel one another. The more rigorous method leads to exactly the same relation, Equation 3.8 [206] :

$$n * \lambda = 2\, d * \sin(\theta) \qquad (3.8)$$

Where, n is an integer., λ is the wavelength in angstroms, d is the (d-spacing) inter-atomic spacing in angstroms, θ is the diffraction angle in degrees which is called theta angle and d*sin (θ) is the length of segment a or b.

The 2- theta angle is measured twice that of theta angle; The fixed wavelength depends on the distance between successive lattice planes, not on the atomic arrangement.

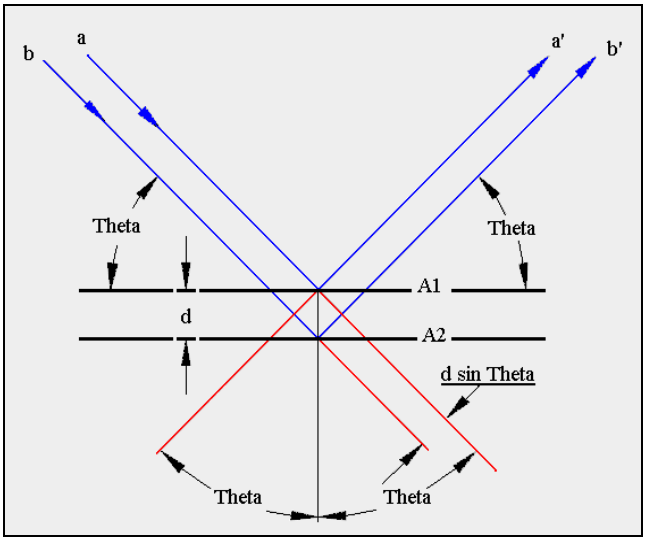

Figure 3.13. Diffraction in path length of X-ray beam according to Bragg's law

In practice, in X-Ray Diffractometer (XRD) characterization of fibres, the transmission x-ray diffractometer used was a Bruker D8Discover. The Discover uses a copper k-alpha target and transmits x-rays through the sample. For the X-ray test, the fibres were cut up very finely with particle dimensions of less than 1 mm using sharp blade and compacted

into sample PMMA (acrylic) holders with a diameter of 25 mm and 3mm depth to form discs; the detector was placed beneath the holder. As the x-ray source moves theta degrees, the detector stays in conjunction with it by 2 theta degrees ($2\theta^0$) throughout the scan. The raw data were then processed using DIFFRAC plus EVA software (a Bruker Evaluation package 2007, V13). Full-width half-maximum (FWHM) of the diffractometer spectra of the obtained wide angle x-ray scattering (WAXS) traces was obtained using EVA software to calculate intensity; the degree of blackening. FWHM is a function of the internal strain state in the material investigated [208]. Scherrer (1918) observed that small crystal size could give rise to peak broadening.

According to the Debye-Scherrer formula (Equation 3.9), the lower value of FWHM, the higher degree of crystallographic order and vice versa [209]:

$$t = \frac{k.\lambda}{B.\text{Cos}\,\theta} \tag{3.9}$$

Where: t is the averaged dimension of the crystallite or the length of the column of coherently diffracting plane in the crystallite [210], K is the crystallite shape constant that may range depending on the specific geometry of the scattering objects, λ is the wavelength of the x-ray source, θ is the Bragg diffraction angle in degrees and B is the diffraction peak width proportional to FWHM located at 2 θ (Figure 3.14).

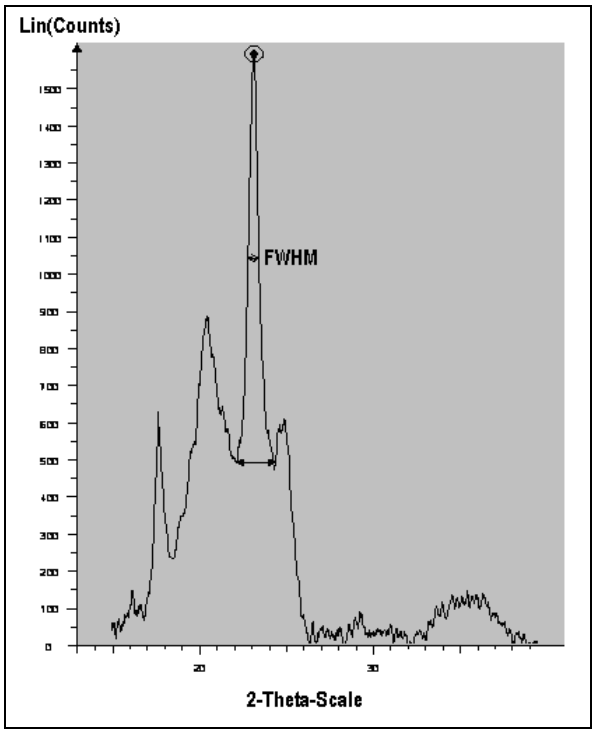

Figure 3.14. Schematic illustration of FWHM of WAXS peaks of AAC fibre

That formula provides a crystallite size from the measured FWHM of one diffraction peak [207]. Thus, K is assumed to be the same amongst all the fibres for which FWHM is determined. The degree of the crystalographic order increases with the increase in the intensity of crystalline peaks, decrease in peak width and decrease in the background area of the scattering profile. A higher size of the crystallite and the higher degree of crystalographic order are reflected qualitatively in a decrease in FWHM value, and vice versa. Comparing the half-height widths of an X-ray scattering profile directly draws conclusions about the relative crystalographic order within a series of fibres [207]. The percentage crystallinity could be estimated from the relative areas under the peaks(crystalline region/ amorphous and crystalline regions).

3.5.5 Thermal Analysis Using Differential Scanning Calorimetry (DSC)

METTLER- TA Instrument and METTLER –TOLEDO –TA89E System Software were used to determine the thermal curves of AAC fibres which were cut to very short lengths (<1mm). The 5-10 mg weight of the specimen was put in a supplied standard aluminium pan in a free-state and scaled with a lid. The software offers the DSC graphic, the gas used was nitrogen at a flow rate 45-50 cm3 min-1, and an average of three replicates scanned for each sample was used for the calculation.

3.5.6 Scanning Electron Microscopy (SEM)

A scanning electron microscope was used to determine the eventual surface defects and morphology. Optimal images formed in SEM are characterized by high resolution, substantial depth of field, high contrast, high intensity and low specimen charged.

The specimen is coated by a thin layer of conductor, commonly gold, to assure conductivity, to avoid charging effects of the electron beam and to improve the secondary electron yield by using SEM Sputter coater, A Polaron THERMO VG SCIENTIFIC SC 7620. Argon atoms introduced into the evacuated chamber were ionised to positive charges by means of a high voltage. These struck a negatively charged gold target and released gold atoms. Gold atoms fell onto the specimen in a conductive layer of controlled thickness which was proportional to the coating time period. The coating thickness for fibres and yarn samples should be adjusted; a thin layer would not reduce charging sufficiently and the thick layer would obscure surface details. Samples were

coated with a gold palladium target for 45 seconds under 18 mA current and in argon medium.

SEM studies were taken with a Cold Field Emission Scanning Electron Microscope HITACHI S-4300, Figure 3.15. It consists of electron gun and a filament (Wehnelt cylinder and anode (+); a high voltage feeds an electrical circuit containing a tungsten hairpin-shaped filament which heats up by voltage increasing and thermionic emission takes place), electromagnetic lens system, condenser lens, final objective lens (used to reduce the probe (spot) size to nm dimensions at specimen, allowing high resolution imaging), scan system (a set of deflection coils enables the electron probe to be restored a cross the specimen allowing a specimen image to be built up), electron collection (the particles and electromagnetic radiations are produced after the electron collision with specimen), the Everhart-Thornely detector (positively charged collector cage which attracts the electrons into the detector), specimen stage (platform located below final lens as a significant portion of specimen chamber) and vacuum system with combination of pumping mechanisms (a rotary oil mechanical pump to protect the hot filament from oxidation and burning out, and to remove any moisture corrosion or charged dust particles and keep the beam well focussed). Image quality could be altered by control accelerating voltage, working distance and/or final aperture size.

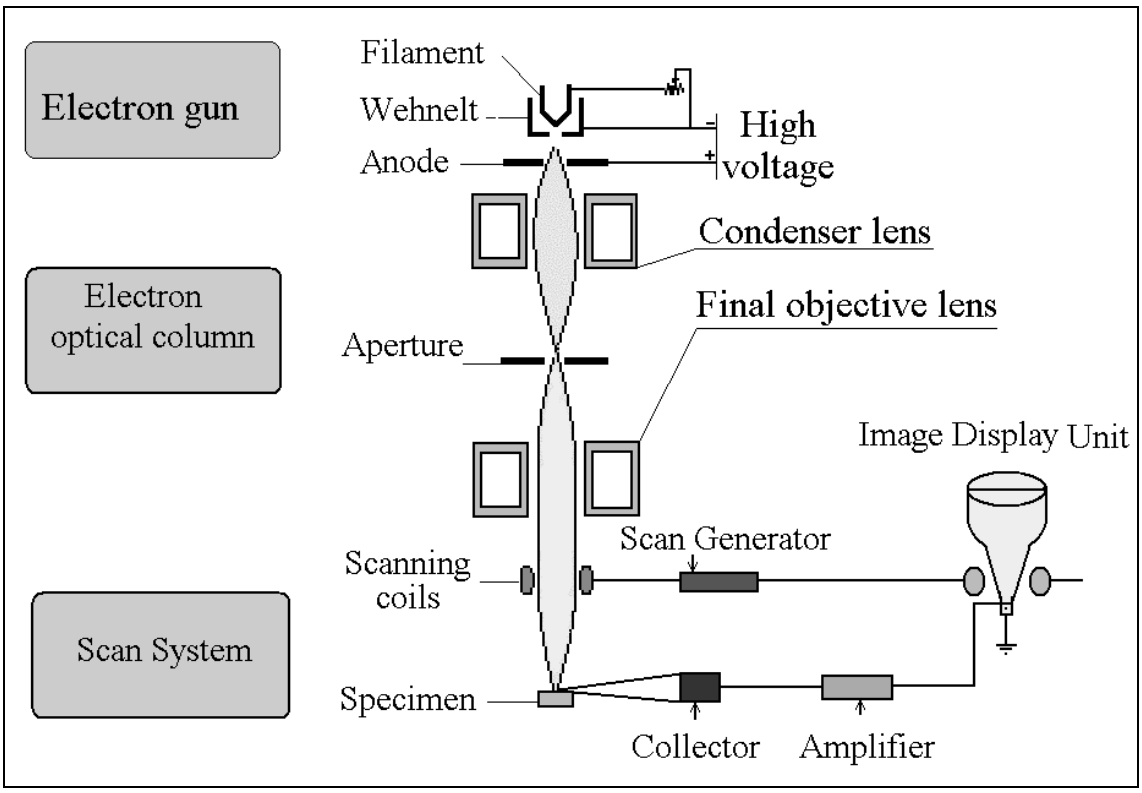

Figure 3.15. Diagram of scanning electron microscopy

3.5.7 Characterization of Tensile Properties

Tensile testing of fibres was carried out using an Instron tester (model 3345) connected to Instron Bluehill V 2.21 software at a temperature of 20 ±2 ^{o}C and relative humidity 65 ±5 %. The initial gauge length 20 mm was stretched at a constant cross head speed of 200 mm/min. Pre-tension of 0.005 N/tex was applied to the yarn to give a reproducible extension value; the samples were conditioned for 48 hours before testing. Twisted fibres were attached to a cardboard frame to prevent untwisting of the specimen. After securing the specimen in the grips, the cardboard frame was cut along the cutting line and the fibre was then loaded until it was fractured. The reported results were the average values of five repeated measurements and the results were averaged to obtain a mean value. Samples were taken from different parts of a package and the elongation at break was measured as a percentage of the original length.

The stress-strain curve can be used to describe and classify the material qualitatively. Stress strain curve, Figure 3.16, must be understood to decide the best strength and elongation for the yarn which is good for the weaving process [168]. When testing the fibres until they break, they pass through many regions including elastic region, yielding, strain hardening, necking and failure. It should be emphasized that the extent of each region in stress-strain space is material dependent and not all materials exhibit all of the regions. At the yield point, the tensile filament starts to neck down and continues necking till the sample ruptures in the elastic region.

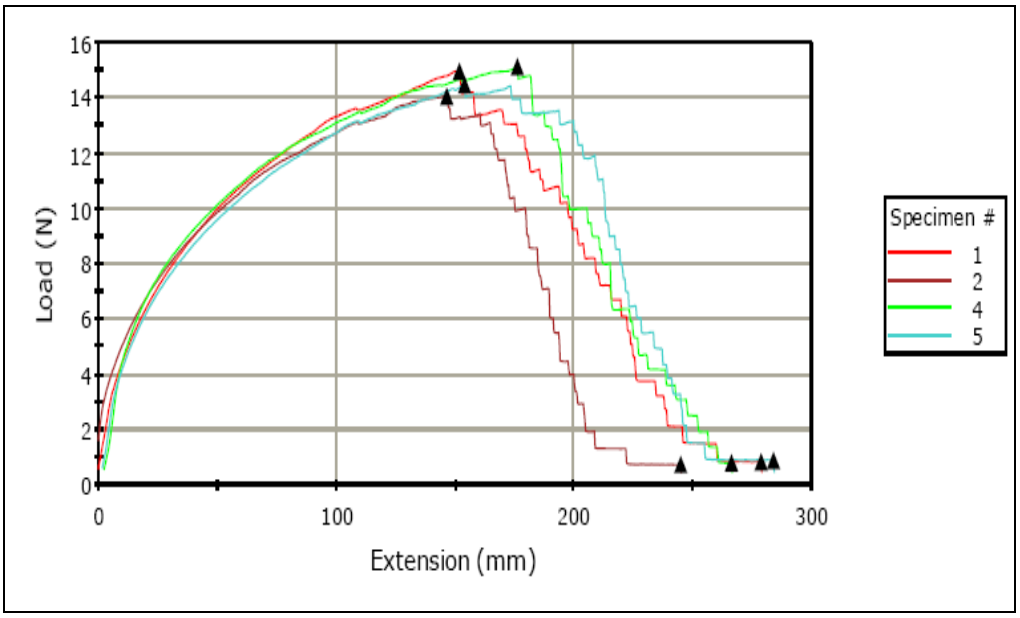

Figure 3.16. The stress-strain curve for draw fibres

3.5.8 Thermal Shrinkage

Textile fibres with thermoplastic properties have created the need for the testing of shrinkage or extension of yarns and fabrics when subjected to heat. At high temperature, adhered locations created in the yarn or fabric will affect the character of the textile [170]. The thermal shrinkage test was carried out using the Testrite Thermal Shrinkage Oven, MK IV Shrinkage-Force from Testrite Ltd UK.

The instrument (Figure 3.17) comprises the heating chamber zone (250×110×80 mm), temperature controller, computer micro processor, L.E.D readouts for results and the sliding carriage (which affords the means of mounting the test sample and presenting it to the heated zone), plus a load cell and free shrinkage attachment. The loaded threads carrier consisted of a jaw/clamp on one end and the free shrinkage drum with low torque potentiometer fitted to give the results on the other end. Using a load cell of 10 g and a shrinkage pot, the computer micro-processor determines the results shown on the front display panel; the movement expressed as a % of the sample length is related to shrinkage/extension under a constant tension during heating. Samples were heated for 2 minutes at 60 ^{o}C.

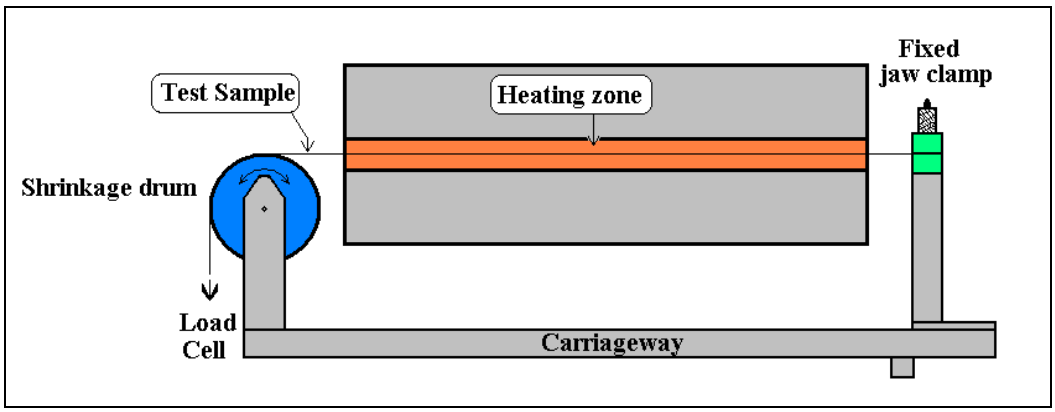

Figure 3.17. Diagram of thermal shrinkage tester

The thermal shrinkage is calculated as $100 \times (L_0-L_1)/L_0$, where L_0 is the original sample length and L_1 is the shrinkage/ extension sample length under a constant tension. The thermal stability is affected by influences of medium, sample weighting, temperature, time subjection to heat, count and structure of the sample, associated substances and evaluation parameter [170]. There is another effect from the fractional resistance between the fibres that transfers the forces between the fibres and raises the fraction.

3.5.9 Abrasion Testing Procedure

The measurement of abrasion resistance of yarn is desirable for the prevention of broken yarns in the production processes, such as weaving and knitting where the yarn is subject to rubbing, abrasion and strain forces. The Shirley Yarn Abrasion Tester (Y027 – SDL) was used to determine the abrasion resistance of yarns (Figure 3.18). The yarn abrasion tester is commonly used for determining the abrasion resistance of traditional yarns after sizing and prior to weaving. The instrument is capable of making up to ten simultaneous tests on individual threads; the yarns (1-10) are threaded from left to right. This is done by lifting the sprung-loaded peg and placing the yarn underneath to secure onto the free block (A), then attaching the other end onto the bar (B) on the right-hand side of the instrument in the same way. When the required numbers of threads are fitted and by pressing the start button, the abrasion bars will then start to rotate and begin to abrade the yarn. When a thread fails, the free block falls and a signal is sent from the appropriate sensor to the microprocessor which records the exact number of rubs for that particular yarn. The abrasion paper is Naylobon Waterproof Paper (P600 GB 701 4).

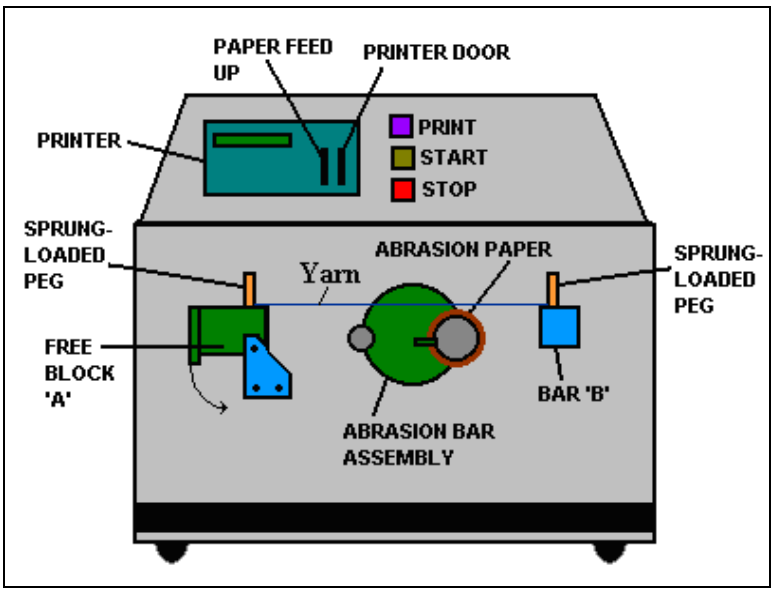

Figure 3.18. Diagram of Abrasion Tester

3.5.10 X-Ray Micro-CT Scanning Procedure

Internal and hidden features and behaviours of fibres and fibres in fabric samples were investigated using the Skyscan 1174 X-Ray Micro-CT Scanner, a sealed cabinet device designed for desktop operation in a normal laboratory environment. X-ray

microtomography (micro-computed tomography or micro-CT) is identical in its basic principles to medical CT scanning [211], and has been increasingly utilized in non-clinical research.

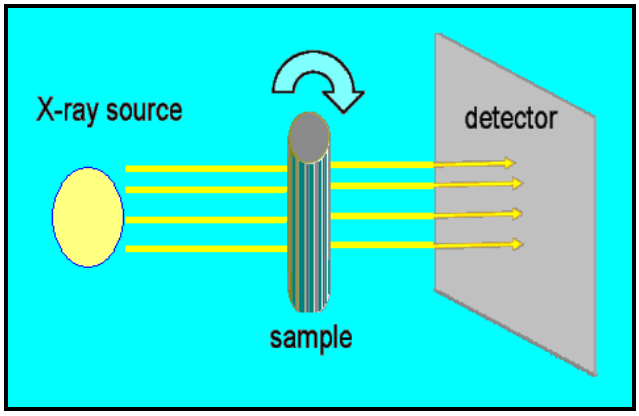

Figure 3.19. Diagram of X-ray tomography

The sample (fibre or fabric) was fixed on the precision rotation stage using a minimum amount of material with low x-ray absorption; a drinking straw or araldite was used on the sample edges for support and it should be prepared with an aspect ratio (width/thickness) less than 20. After this, the sample was placed in the path of an x-ray beam to form a projection image on x-ray-sensitive detector array, rotated and imaged at many angles value (Figure 3.19).

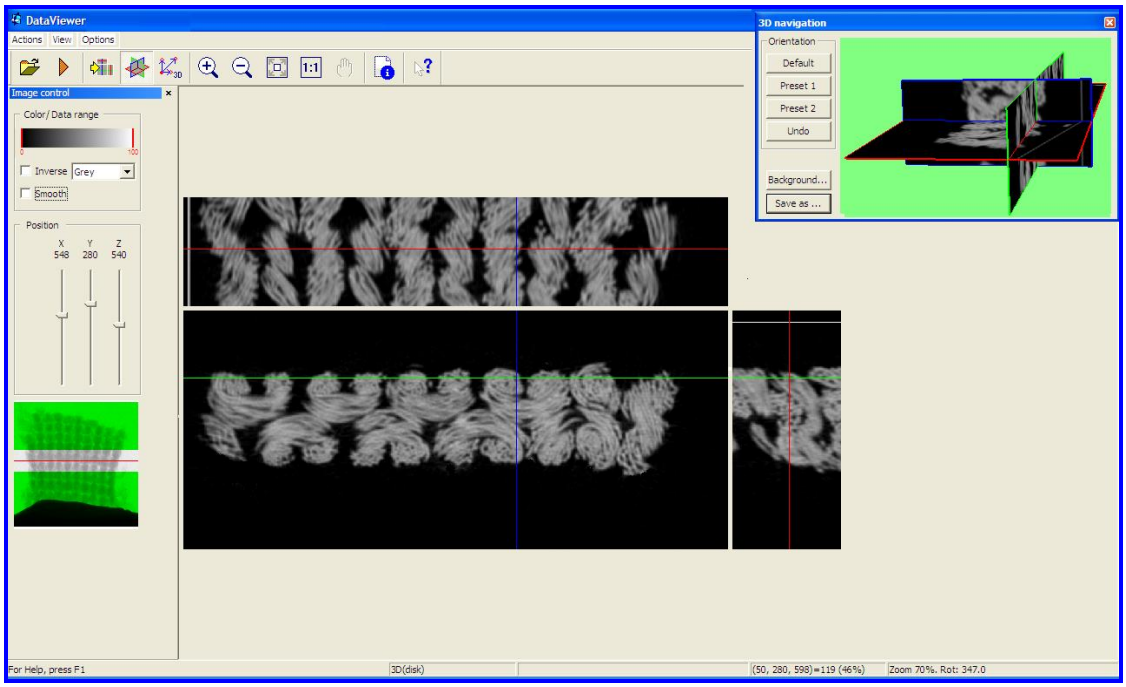

Figure 3.20. Knitted AAC fabric scanned with the SkyScan 1174 System
(Three orthogonal virtual slices)

The sample stages were controlled by the software independent of the main scanner control program. The data were reconstructed using the software and exported for further processing. The scanner uses an x-ray source; the x-ray image detector is a 1.3 Mpixel CCD coupled to a scintillator via a zoom lens. The variable magnification (6-30 µm pixel size) and object positioning (50mm vertical travel) allows a selection of the volume to be scanned. The scanner is controlled by a desktop PC via two control cables and a FireWire (IEEE1394) input. Software is provided allowing fast volumetric reconstruction, 2D / 3D quantitative analysis and realistic 3D visualization. The scanner provides high resolution 3D imaging down to 6µm for fibres inside the fabric and shows the effect of processing on the fibre's response, surface and appearance. The data can be used to create realistic 3D images and to calculate internal morphological parameters using the software attached to the scanner, (Figure 3.20).

3.5.11 Yarn Tension Meter

A Yarn Tension Meter (Wira, 0-120 grams) from Thorn Automation Nottingham, England, was used to measure the yarn tension during the extrusion process. The Yarn Tension Meter gives steady readings of the average tension in a running yarn, even if the tension fluctuates. The yarn passes alternately over and under three pulleys, the centre one of which is carried on a flexible strain-gauge cantilever beam. The output is read on the display of the instrument which is calibrated to represent the average yarn tension.

3.6 Programming and Forecasting Program

The key features of the need for the forecasting program include the ease and flexibility of input to provide user-friendly instrument for the 'non-statistician'. Figure 3.21 shows a flow chart for the methodologies used for obtaining the program, starting from the data and statistical modelling methods. Multiple and individual regressions of independent variables employ linear quick forecasting models on independent variables. Based on the analysis of the fraction factorial experimental design results and using STATGRAPHICS program, Simulations of statistical data and regression equations of simplified mathematical models were obtained; they merge the user's need with the technological capabilities and programs offered by Microsoft Visual studio program. It could be

connected with the control process system or TI-83 Plus Kit which is easy to use in the work place. The applications optimise the quality required for various applications and identify the effects of the factors and their interactions.

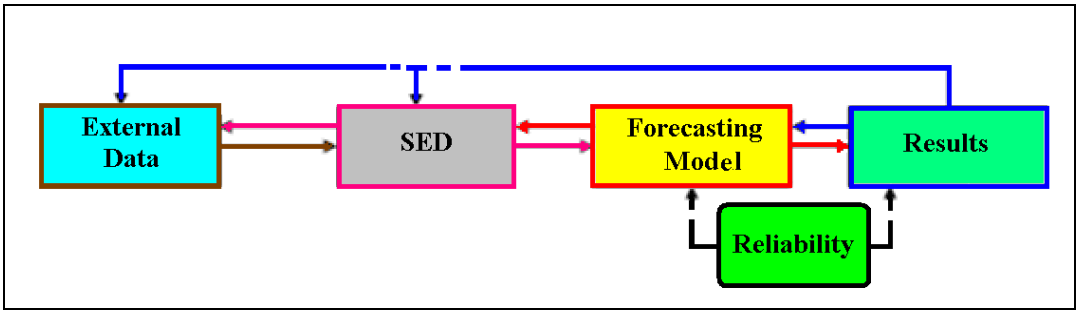

Figure 3.21. The flow chart of the statistical method

(SED: Statistical Experimental Design)

3.6.1 Programming Using Microsoft Visual Basic

Microsoft Visual Basic (2008) was used to write a forecasting program for the melt spinning process of as-spun aliphatic aromatic co-polyesters fibres. Unlike other programming languages, Visual Basic provides a high degree of simple automatic programming. The program offers the management of regression models of responses based on statistical factorial design, design analysis and process simulation. The simulation and the optimization of statistical database were achieved in many stages; it includes the design specification, definition, implementation and control.

The program was set at two interfaces: the first interface is the input window for process conditions; each factor is represented as a record and it may be owned by more than one record, leading to a network-like structure. The regression models obtained using statistical technique form the source code for the forecasting programme. The second interface is the output result window. The programmed application powerfully supports product development, design process control, quality assurance and product performance evaluation. All factors and dependencies between factors of the reality could be stored in the data model; it is structurally identified by their domains (names and kind of values). Each factor is represented as a record and relationships by a matrix design representing the relationship between factors. Results obtained should answer the fairly complex demands posed by multi-applications running concurrently with the application programs (or processes) in the computer.

3.6.2 Programming Using a Texas Instrument

A Texas Instrument with TI-83 Plus Software Development Kit (SDK) was used in the work to write calculator programs (as forecasting applications) using a variety of the calculator's internal functions (Figure 3.22). This Texas Instrument offers the ability to load and debug programs, applications and breakpoint.

The Texas Instrument was connected to PC simulation tools of the TI-83 Plus, including keyboard and display. Because software engineering programs do not reflect the need by industry for practising software, the Texas Instrument could develop suitable applications, which could be connected to melt spinning specifications and requirements for embedded real-time systems.

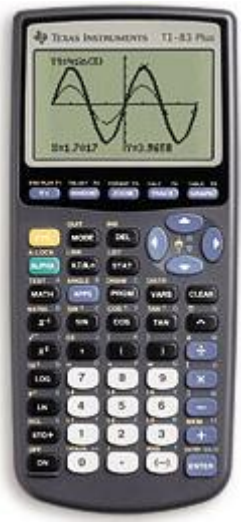

Figure 3.22. Texas Instrument TI-83 Plus

Using the Texas instrument covers the need for a fast and accurate technique to calculate without the need for further statistical background and computing equipment; it is a different style of programming suite for the task selected. The key features of the need of the Texas instrument inside the lab/plant include the ease and flexibility of data input and the user-friendly instrument for the non-statistician. TI-GRAPH LINK is the software for connectivity between the instrument and the computer.

CHAPTER 4- STATISTICAL MODELLING OF THE EFFECTS OF EXTRUSION TEMPERATURE PROFILE AND POLYMER GRADE ON THE PRODUCTION PROCESS AND THE PROPERTIES OF LINEAR AS-SPUN ALIPHATIC-AROMATIC CO-POLYESTER FIBRES

4.1 Introduction

In the fibre extrusion process, many factors, such as extrusion temperature profile, screw speed, metering pump speed, cooling system and winding up speed, affect the quality of the manufactured fibres. Spinning or extrusion temperature is considered as an important parameter in the melt spinning process of synthetic fibres; it cannot be too low or too high, as the energy required to melt the polymer comes from both external heating and the internal friction. The extrusion temperature profile controls the quality and the cost of manufactured fibres; the energy saving is achieved by balancing between the quality and the processing temperature profile. Because textile fibres are made up of long chain molecules, the chemistry and the molecular structure of the polymers play a role in the fibre production and treatment processes [112]. The main activity within the polymer processing research is the mathematical modelling and the numerical simulation of the industrial processes [118].

Pre-experimental work was conducted to find the rheological data of the molten polymer at different temperatures and to determine the enhanced melt spinning conditions. The results obtained from the melt flow indexer and differential scanning calorimetry give an explanation for the character of rheological properties and surface shape. Following this, the relationship between the extrusion temperature profile and the polymer grade denoted by melt flow index (MFI) as well as the torque value and the extrusion productivity on Brabender extruder machine is statistically modelled. This aids in adjusting the balance between the energy cost and the extrusion productivity of the single screw extruder without the effect of the metering pump which is used in the melt spinning machine. Depending on both the rheological and Brabender extrusion analysis results and by using factorial experimental design, the statistical modelling of the relationship between the extrusion temperature profile and the polymer grade as well as the structural and physical properties of linear as-spun aliphatic-aromatic co-polyester (LAAC) fibres have been proposed. The aim of the statistical analysis is to obtain an insight into the relationship between the visco-elastic properties and morphology of linear as-spun aliphatic-aromatic co-polyester (LAAC) which can be used to select the extrusion temperature profile and one of the polymer grades for the extruder for the melt spinning process.

The obtained models allow a fast simulation to describe the behaviour of the factor-response relationship through mathematical interactions. With the advantages of the factorial experimental design in the development of fibre process technology, the enhanced statistical approach specifies the direction of change of the polymer's grade and extrusion temperature profile for the studied responses. The produced as-spun linear aliphatic aromatic co-polyester fibres are an environmentally-friendly fibres; they are attractive alternative to conventional chemical fibres for different applications.

4.2 Rheological and Thermal Characterizations of LAAC

To study the effects of extrusion temperature profile and polymer grade on the production process and the properties of linear as-spun aliphatic-aromatic co-polyester fibres, two grades of linear AACs were used at this stage. They are coded as MFI1 (AAC1) and MFI2 (AAC2) depending on their melt flow indices; the measured melt flow index MFI does not fully present the properties of the polymer.

The annealing/drying stage is important for the quality control of the polymer process. To avoid possible hydrolysis during the rheological analysis and extrusion process, AACs were dried at 60^{o}C for 6 hours before use. Because the effective glass transition temperature is below the normal operation temperature, the crystallization will go to equilibrium very slowly. To avoid this problem, it is necessary to heat the moulded polymers (anneal) in an inert atmosphere at a temperature between Tg and Tm ($T \approx (Tg + Tm)/2$) to stabilise the polymer [171]. The overall thermal behaviour of the polymer used in this work suggests that the processing temperature range is slightly wide (20-25 °C). According to the differential scanning calorimetry (DSC) results in Figure 4.1, the thermal diagrams of the two grades show that a broad temperature range of melting (about 100-135°C) was observed for the polymer samples. According to the DSC results for the two grades studied, an optimum temperature window was found taking all factors into account because the polymer does not melt over a narrow range and does not melt completely below 120^{o}C. The multiple melting phenomena observed could be attributed to the compositional heterogeneity of the co-polyester. Based on this fact, it can be confirmed that LAAC is a mixture composed of a number of components with different melting points. The large peaks around -30^{o}C could be related to the glass transition temperature Tg of the polymer; moisture content is indicated at the large peaks of the start of the curve.

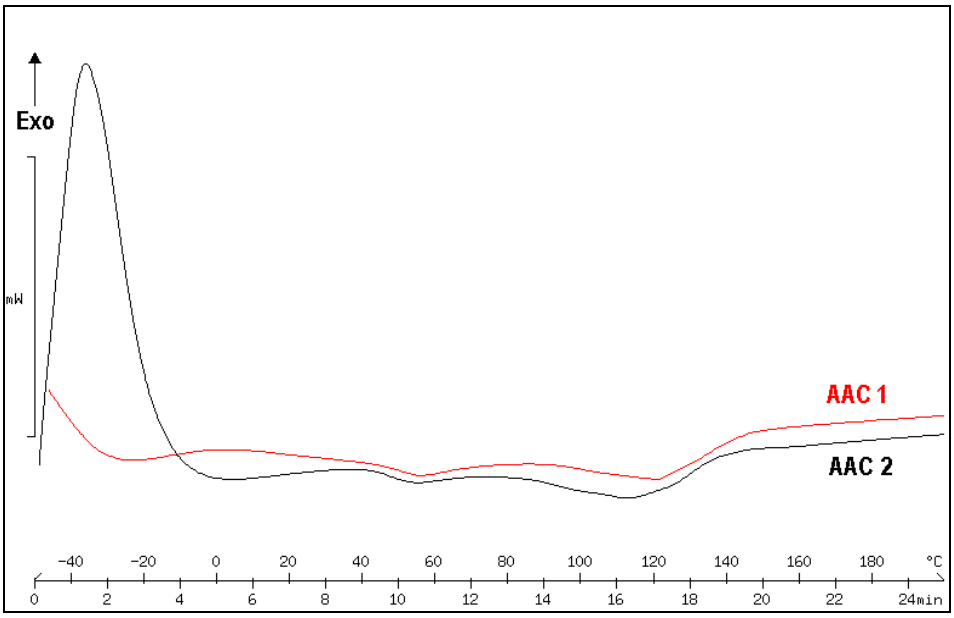

Figure 4.1. Thermal diagram of LAACs

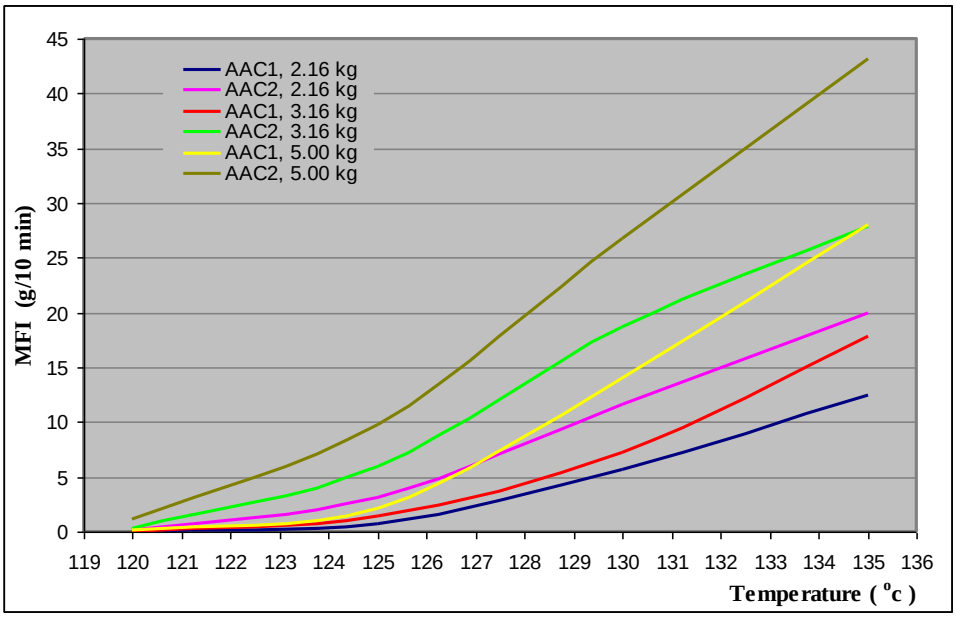

Figure 4.2. The relationship between MFI (AAC1 and AAC2), the pressure and temperature

In Figure 4.2, the MFI was measured at different loads (2.16, 3.16 and 5 Kg) and temperatures (120-135°C). The relationship between flow (MFI), pressure and temperature is not linear and is related to the nonlinear change in viscosity with change in pressure and/or temperature. Within a considerable range of melting temperatures, the difference between MFI1 and MFI2 increased as the temperature increased. Viscosity varies inversely with the temperature and pressure and that is clear from the increase in MFI with the increase of both temperature and pressure. Alternatively, the productivity (a measure of throughput per minute (g. min^{-1})) will be increased if the temperature or the pressure is increased and will be limited depending on the polymer degradation. The

apparent extrudate swell depends on the die entry and the die exit and possible slip at the polymer-wall interface [212].

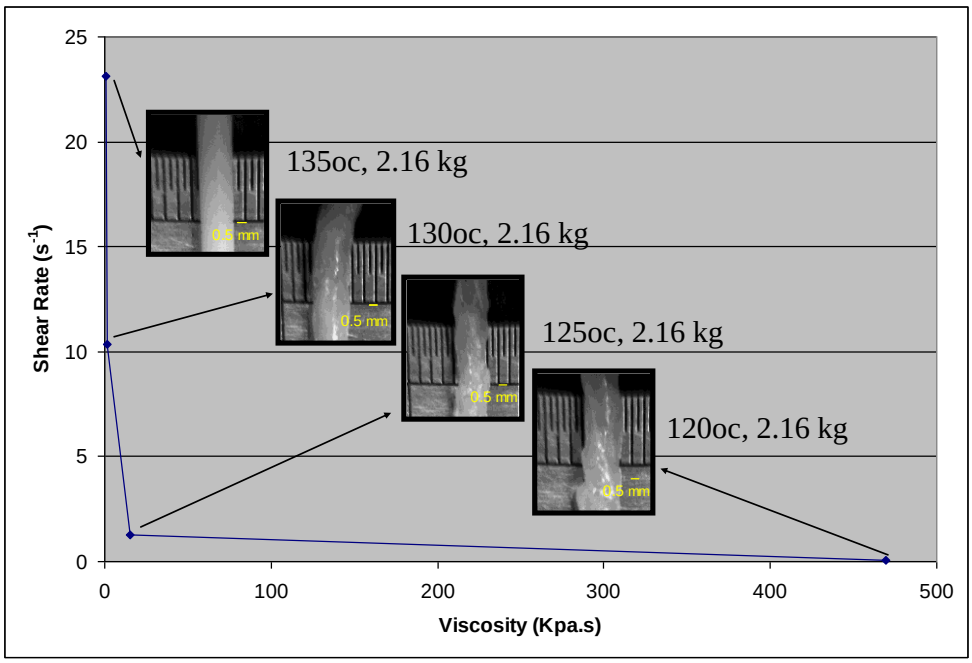

Figure 4.3. The surface shape at different temperature, viscosity, and shear rate at load of 2.16 kg for LAAC1

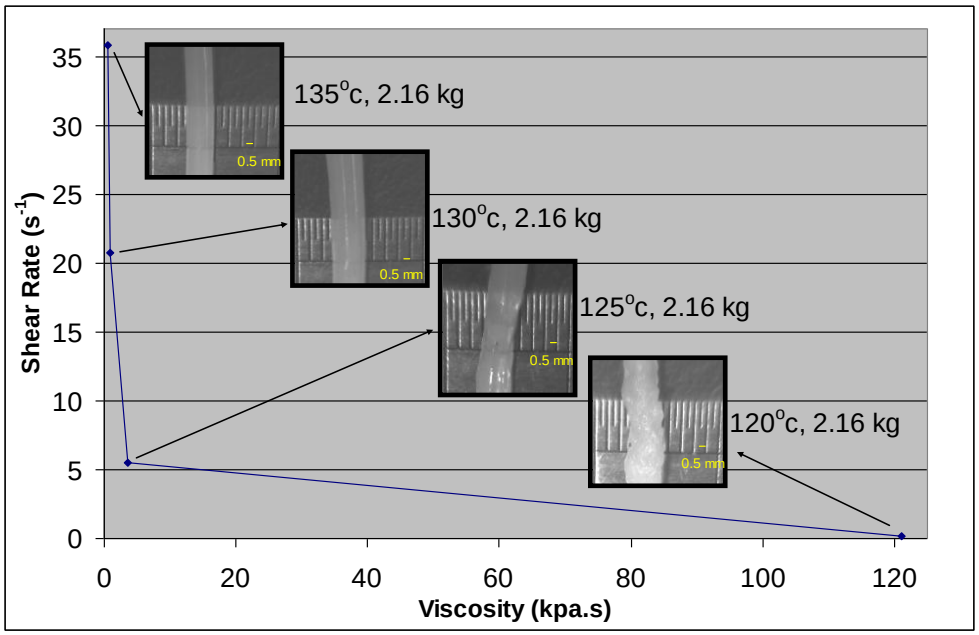

Figure 4.4. The surface shape at different temperature, viscosity, and shear rate at load of 2.16 kg for LAAC2

Figure 4.3 and Figure 4.4 show the extrudates' appearance at different temperatures, apparent shear rate and viscosity. The analysis will give an explanation for the character of the rheological and thermal properties and surface shape at the different conditions in

which recent analysis was performed. In terms of extrudate surface analysis for both grades, smooth extrudate can be observed above 130 ^{o}C and 'shark skin' extrudate between 125 and 130^{o}C. A 'shark skin' surface was formed by a series of ridges aligned perpendicular to the flow direction. It could be distinguished from an elastic turbulence, which belongs to the material nature and sometimes to the polymer-die metal adhesion [171]. Stick-slip or oscillating melt extrudate appears at 125^{o}C, and gross melt fractured extrudate was found at 120^{o}C; it could be observed at the lower extrusion rate and depended on the temperature, as described previously. Melt instability can be caused by an excusive increase in shear stress and stick-slip, or the shark-skin effect will appear. Depending on theoretical formulas and MFI results analysis, at higher temperatures the viscosity decreased and the material flowed easily. At shear rates more than 5s^{-1}, the extrudate surface was practically smooth and quite smooth up to 15s^{-1}, whereas smoother extrudates were obtained at shear rates of more than 15s^{-1}. Under processing, the visco-elastic nature of polymeric fluids of some materials has many complex effects on the flow stability [160] and the other properties, such as molecular mobility and dye-ability of produced synthetic fibres [168, 213]. If the local power law index can be obtained, the viscosity curves of viscosity and shear rate (Figure 4.5) could be converted to true viscosity curves using the Rabinowitsch correction.

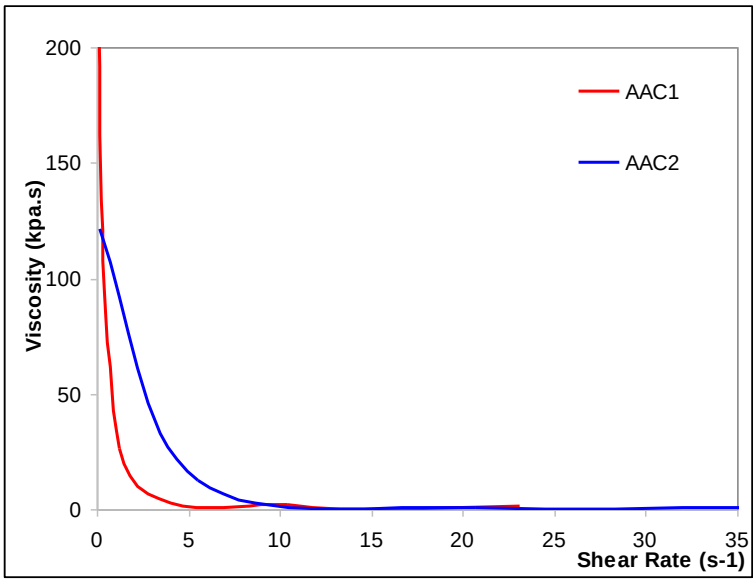

Figure 4.5. Viscosity– Shear rate curve at load of 2.16 kg

Analysis of Figure 4.5 shows that, as the temperature increases, the shear decreases and the shear rate increases as a result of the viscosity decreases. Thus, the increasing in shear rate results in a decrease in the viscosity for a particular temperature. At the same load

and as MFI increases, the piston speed (or extruder screw speed) is increased as the shear rate increases as a result of the die head pressure and the shear stress (load) increasing. Occasionally the melting temperature does not necessarily include the processing temperature, as was found on the extrusion machine, because flow of the molten polymer also depends on its viscosity. The overall thermal behaviour of the LAAC grades used in this work allows the conclusion that the processing window is quite wide. Therefore, the co-polyester can be safely extruded from 130^{o}C. The decrease in viscosity improves the material flow and leads to more uniform extrudate (or filaments); hence additional information about the processing window can be obtained. In Figure 4.6 (a), the elongation flow behaviour of polymer melts (coded as **B**) could be determined, the melt will construct its own boundary leaving a slowly re-circulating dead zone (**A**) where the taper should give minimum pressure. The kinematics are determined by the flow rate and the shape of the central core regain [212]. The zone will be bigger after increasing the difference between the resistance to shear and elongation[214]. This phenomenon happens in the die head when using different polymers, for example using AAC after cleaning the extruder using polypropylene (PP) without taken the die head off, as shown in the Figure 4.6 (b).

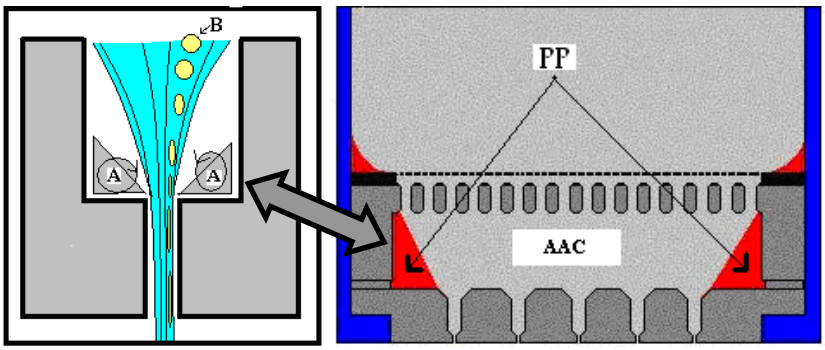

Figure 4.6. Elongational flow in a convergent channel (a) and die head (b)

After the spinneret temperature comes down to AAC processing temperature and when the AAC flows through the spinneret, a ring of the polypropylene (PP) placed in the dead zone around the spinneret, just as in the case of the vortex, regains **A** (Figure 4.6 (a)). That causes blocking to some surrounding nozzles in the spinneret because of the difference between the melting temperatures of the polymers. Melt fracture occurs when the temperature is too low or if the orifice shear rates are too high. The machine and the die head should be cleaned completely from PP before each run.

After the visco-elastic and morphological characteristics had been identified, the rheological data were used to determine the enhanced extrusion temperature profile of the six heating zones.

4.3 Experimental Design

Experimental design analysis is a technique for obtaining information about the significant main factors and the interactions through optimisation of the average response values, depending on the factors and their levels. After pre-experimental work had been done to determine the number and the levels of factors, the matrix design and the number of trials were selected as in sections 4.3.1 and 4.3.2.

4.3.1 Selected Factors and their Levels for the Branbender Machine Experiment

A Brabender machine with an extruder attached and a torque value recording rheometer (Plasti-Corder) was used to measure the extrude-ability of polymers and extruder torque value by measuring torque value, temperature and pressure of the melt along the barrel.
The experiments conducted involved four factors at two levels, as given in Table 4.1. The two grades of linear LAACs were used, coded as MFI1 and MFI2. The temperature zones in the Brabender machine (Figure 4.7) are barrel zones (feeding zone temperature T1, compression zone temperature T2 and metering zone temperature T3) and die head zone temperature (T4). Depending on the Brabender machine design and results obtained of pre-experimental work, the four temperature zones were condensed into three heating zones to decrease the unstable flow and to simplify the experiment. Because of the viscosity and temperature interaction between feeding and compression zones, the first two zones in the extruder were combined and considered as one: i.e. Z1=T1+T2. Z2 represents the metering zones of the screw (Z2 = T3), and Z3 represents the melt extrusion temperature (Z3 = T4). Some interactions could be found because of a continuous flow of the molten polymer in the extruder zones, and the heat diffusion between the metering zones of the screw and the die head zone which could not be controlled separately regarding to the machine head design.
A full factorial experimental design (L16) for a simple experiment of four factors at two levels with random order was designed using the STATGRAPHICS program; the detailed experimental arrangement of the sixteen trials is given in Table 4.2. The designed matrix clusters all experimental conditions to be controlled and allows all individual factors and

their interactions to be analysed statistically and evaluated independently. The experiments were conducted in two blocks for the polymer grade (MFI) because of the difficulty of cleaning the machine after each run. This justification allowed the temperature profile to continue to increase from the screw feeding zone to the die head. AACs are poor conductors of heat and would need time to cool down.

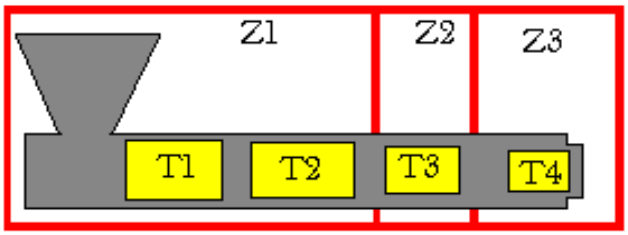

Figure 4.7. Schematic diagram of temperature zones in the Brabender machine

Level	Factor				
	MFI	Z1		Z2	Z3
		T1	T2	T3	T4
-1 (Low)	MFI 1	110	115	125	130
+1 (High)	MFI 2	115	120	130	145

Table 4.1. Factors and their levels for the Brabender machine (Temperature values, ^{o}C).

Trial Number	Block	MFI	Z1	Z2	Z3
1	2	+1	+1	-1	+1
2	1	-1	-1	+1	-1
3	1	-1	+1	+1	+1
4	1	-1	+1	-1	-1
5	2	+1	-1	-1	-1
6	2	+1	+1	+1	-1
7	2	+1	-1	+1	+1
8	1	-1	-1	-1	+1
9	2	+1	-1	+1	-1
10	2	+1	+1	-1	-1
11	1	-1	-1	+1	+1
12	1	-1	+1	+1	-1
13	1	-1	-1	-1	-1
14	2	+1	+1	+1	+1
15	2	+1	-1	-1	+1
16	1	-1	+1	-1	+1

Table 4.2. L16 Experimental matrix with the random order for the Brabender machine

4.3.2 Selected Factors and their Level for Melt Spinning Experiment

Fibres were extruded via melt spinning on a Lab-spin machine. The molten polymer was forced through the spinneret (55 holes) as fine jets with speed adjusted by the metering pump (fixed at 4 rpm, capacity of 2.4 cc rev^{-1}), which generates the high pressure during metering. The air cooling quench speed was set at 37 % of total blower fan air output. The spin finish application speed was set at 0.4 rpm. The filaments were collected from the godets set at 36 m min^{-1} without tension between them and the winder. The main theme here is to lower the fibre tension affecting the fibre's structure and causing undesirable structural changes and to balance the factors' effects with regard to the material's rubbery behaviour. Alternatively, the high speed with wide range will omit the effect of other factors that need to be investigated. The low speed in such processes is compensated by use of a very large number of nozzles per spinneret; as a result, the comparable throughput can be obtained relative to the high speed process, such as upward and downward spinning processes. Figure 4.8 shows IR images of the die head and the spinneret; the image colours corresponding to the temperature scale on the right. The IR image illustrates the temperature variation on each point on the thermo image to obtain the temperature profile scale along or across the studied object. The fibre extrusion experiments conducted involved four factors at two levels: the polymer grade (MFI) and the extruder temperature zones, as given in Table 4.3.

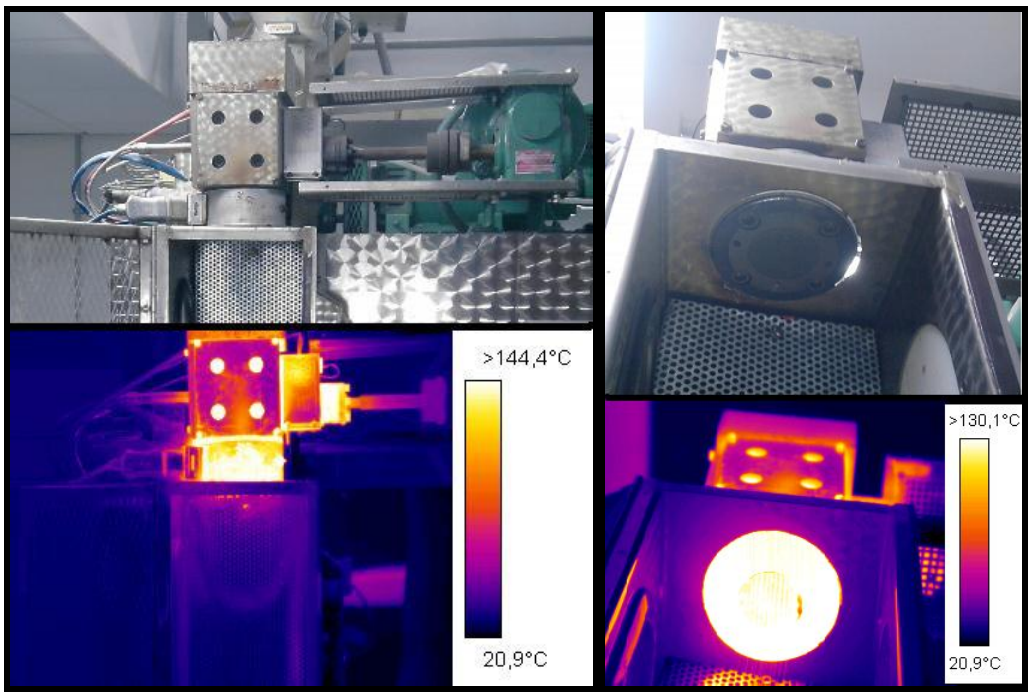

Figure 4.8. IR images of the die head and the spinneret of Lab-spin machine

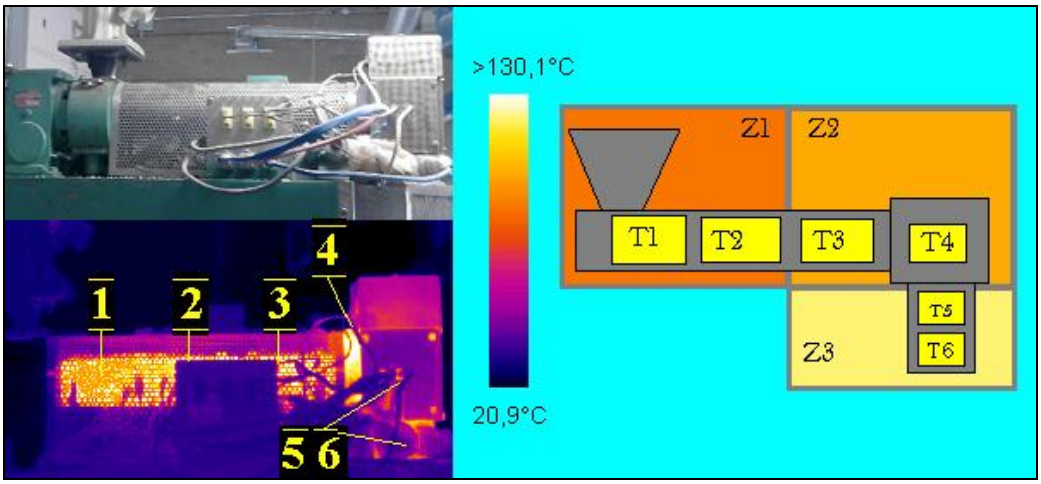

Figure 4.9. IR Image of lap-spin machine and schematic diagram of temperature zones

Level	Factors						
	MFI	Z1		Z2		Z3	
		T1	T2	T3	T4	T5	T6
-1 (Low)	MFI 1	110	115	120	125	130	130
+1 (High)	MFI 2	115	120	125	130	145	145

Table 4.3. Factors and their levels for the lab-spin machine (Temperature values, ^{o}C)

Trial Number	Block	MFI	Z1	Z2	Z3
1	1	-1	+1	+1	+1
2	1	-1	-1	-1	+1
3	2	+1	+1	-1	+1
4	2	+1	+1	+1	-1
5	1	-1	+1	-1	-1
6	2	+1	-1	-1	-1
7	1	-1	-1	+1	-1
8	2	+1	-1	+1	+1
9	1	-1	+1	-1	+1
10	2	+1	+1	+1	+1
11	2	+1	-1	-1	+1
12	1	-1	-1	-1	-1
13	2	+1	+1	-1	-1
14	2	+1	-1	+1	-1
15	1	-1	-1	+1	+1
16	1	-1	+1	+1	-1

Table 4.4. L16 Experimental matrix with the random order for melt spinning

Two grades of linear AAC (AAC1 and AAC2) were used in this stage. The two grades are coded as MFI1 and MFI2, depending on their measured melt flow index (MFI); MFI does not present the properties of the polymer fully which is related to the copolymerization ratio. The temperature zones in the extruder (Figure 4.9) are barrel

zones (feeding zone temperature T1, compression zone temperature T2 and metering zone temperature T3), metering pump temperature (T4) and temperature of die head zones (T5 and T6). Depending on related work on the Brabender machine and in order to simplify the experiment, each two zones were combined and considered as one, i.e. Z1=T1+T2, Z2 =T3+T4 and Z3 =T5+T6. Z3 represent the melt-spinning temperature or melt extrusion temperature. The six temperature zones were condensed into three zones to decrease the unstable flowing resulting from viscosity and temperature interaction because of the continuous flowing of the molten polymer between the die head zones (T5+T6) and the heat diffusion between the metering zone of the screw (T3) and the metering pump (T4) which could not be controlled separately. A full factorial experimental design (L16) for a simple experiment of four factors at two levels with random order was designed using STATGRAPHICS software; the detailed experimental arrangement of the sixteen trials for the melt spinning machine is given in Table 4.4. The generated matrix (L16) clusters all experimental conditions to be controlled, as all factors levels appear the same number of times in each column, and allows all individual factors and their interactions to be analysed statistically and evaluated independently. The experiments were conducted in two blocks for the polymer grade (MFI) because of the difficulty of cleaning the machine after each run. The used justification in the experimental arrangement matrix allowed keeping the temperature profile increasing from the screw feeding zone until the die head. That because polymers are bad conductors of heat and would need more time to cool down, that make a decrease in the temperature from zone to another is not possible**.**

4.4 Experimental Results

The results of the effects of extrusion temperature profile and polymer grade for both the Brabender and melt spinning experiments are given in Table 4.5. The as-spun fibres' results have acceptable standard deviations as a result of blocked nozzles in the spinneret; the rubbery behaviour of AACs caused a non-uniform flow which decreased at high temperature, tension during the spinning or preparing the sample for the test, machine error variation or variation in cooling rate through the filaments bundle. Because the unsuspected factors' change with time may distort the analysis and result in misleading conclusions in the program results, randomly unsteady errors could be separately distributed. A Brabender machine measured the extrude-ability of LAAC and the machine torque value depending on temperature and pressure of the melt along the barrel. The torque-time curves (Figure 4.10) of aliphatic-aromatic co-polyesters obtained from

constant extruding speed at 7 rpm but at different temperature zone profiles (see Table 4.2) give an idea about the influence of extruding temperature profile on torque value. The torque value is decreased with an increase in the temperatures. The torque value measured at higher temperature decreased faster than those at lower temperature. Generally, the required torque value decreased with the increase in extruding temperature. The results indicated how the temperature profile could potentially affect the productivity, a measure of output per minute (g min^{-1}). Note that there was no metering pump connected to the Brabender machine extruder. While the Brabender machine controls the throughput through the die by keeping the extruder screw speed constant, the melt spinning machine guaranteed the pressure/speed control for constant filling of the gear pump by adjusting the screw speed automatically. The output rate of the polymer is controlled by the metering pump arranged between the metering zone of the extruder and the extrusion die to reduce polymer shear in the melt spinning machine. The extruder was subjected to lower mechanical stresses than the Brabender machine without a pump, low-shear production and therefore enhanced quality in the produced extrudate. Heaters (temperature) and screw driver energy (torque value) could be represented as energy cost; the achieved model will help to adjust the balance between the energy cost and the productivity.

An interferometric technique was employed for measuring the fibre birefringence; the overall orientation of the spun filaments was analysed. As shown from the microinterferograms obtained (Figure 4.11), the fringe shifts seemed uniform and regular and this uniformity reflect the shape of the fibre cross section. As is known, if the fringe shift has non-uniform (irregular) shape, this implies that the fibres have irregular cross sections of the spun fibres which take the same cross section of the circular holes of the spinneret. Figure 4.11 shows the recorded microinterferograms of fibres using the polarizing (Pluta) microscope using light of wavelength (λ = 550nm). The results of the first block of fibres (MFI1) show higher birefringence, overall orientation and consistency than those of the second block (MFI2).

A range of crystallographic orders for as-spun linear aliphatic-aromatic co-polyester fibres have been characterized with the aid of wide angle X-ray diffraction measurements which calculate the value of full-width half-maximum of an x-ray scattering profile (FWHM) in terms of crystallographic orders analysis.

Results of x-ray diffractometer traces (Figure 4.12) reveal that some traces are similar to each other (a). Some of them have significant differences, including the overall shape, the positions and the numbers of peak(b). In Figure 4.12 (a) which presents typical x-ray

diffractometer traces for the first block (MFI1), there are five major crystalline diffraction peaks with different full-width half-maximum (FWHM) of an x-ray scattering profile observed at 2θ° = 16, 17.5, 20.5, 23 and 24.5. Figure 4.12 (b), which presents typical x-ray diffractometer traces for the second block (MFI2), the same previous noted five peaks and an additional peak at 2θ° = 21.5 were observed.

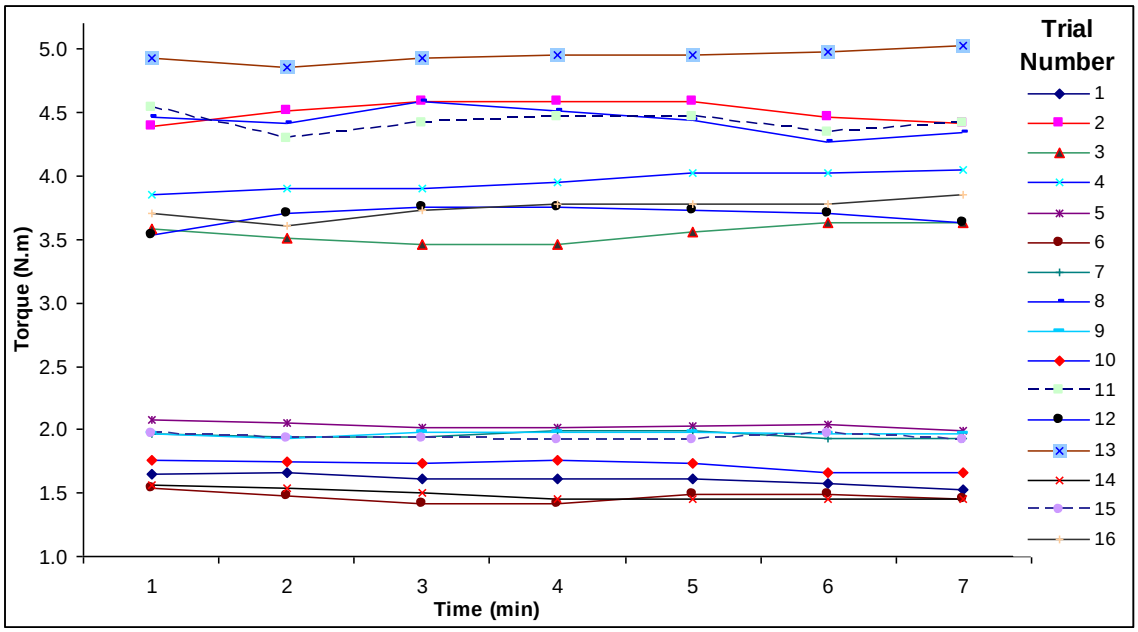

Figure 4.10. Torque value-time curve

The gradual structural change is attributed to the polymer grade and the extrusion temperature profile. The peaks observed at 2θ° = 16, 20.5, 21.5 and 24.5 are very wide and less intense due to low tension applied. The peaks at 2θ° = 17.5 and 23 are slightly sharper, more intense and smaller in width. An increase in structure order is obtained in an increase in the peak intensity; a decrease in the peak width and a decrease in the background area. Such a quantification of structure order as a response parameter makes it possible to conduct the analysis of the polymer grade and the temperature profile on the fibre structure and to facilitate optimization and analysis of melt spinning process. The peak at 2θ° = 23 was fitted using DIFFRAC plus EVA software to compare the half-height widths (see Ch. 03). From it, conclusions were drawn about the relative crystallographic order within a series of the sixteen samples. The FWHM results of the sixteen trials are listed in Table 4.5; the results analysis helps in the evaluation of the effect between as-spun fibre structur to enhance improved drawn fibres. The optimization of tenacity, elongation at break, modulus, spinning productivity and processability helps to understand and control the properties most desired in the produced fibre for different

applications. Tested fibres are as-spun fibres with a very high elongation at break; they are akin to a rubbery material because the glass transition temperature is below room temperature, around -30^{o}C. The elongation at break values is related to two grades: the first grade coded as MFI1 has elongation at break from 438 to 748 % and the second grade MFI2 has elongation at break from 633 to 1150 %.

Trial Number	Results								
	Brabender Machine		Melt spinning						
	Torque value N.m	Productivity g/min	Birefringence $\times 10^{-3}$	FWHM*	Tenacity (g/den)	Elongation at break (%)	Modulus (g/den)	Productivity (g/min)	Count (dpf)
1	1.544	5.09	38.0	0.630	0.320	748	0.178	7.27	32.2
2	4.488	5.61	22.0	0.628	0.300	748	0.164	7.31	32.3
3	3.544	5.50	3.7	0.579	0.238	1150	0.160	8.87	40.3
4	3.949	5.20	21.7	0.597	0.140	675	0.162	8.75	39.8
5	2.034	5.17	43.0	0.590	0.230	471	0.218	7.82	34.6
6	1.558	4.62	22.1	0.602	0.172	696	0.187	8.59	39.1
7	1.919	5.36	39.0	0.621	0.224	438	0.208	7.85	34.7
8	4.427	5.70	0.0	0.606	0.179	1046	0.188	8.89	40.4
9	1.962	5.15	19.0	0.652	0.279	715	0.158	7.38	32.6
10	1.702	4.98	3.0	0.646	0.209	1141	0.175	8.56	38.9
11	4.415	5.82	9.3	0.596	0.243	1134	0.184	8.75	39.8
12	3.642	5.43	44.0	0.615	0.288	534	0.187	7.40	32.6
13	4.942	5.81	17.1	0.602	0.161	633	0.161	8.32	37.8
14	1.500	5.04	10.5	0.591	0.130	704	0.177	8.22	37.4
15	1.948	5.15	28.0	0.639	0.336	738	0.167	7.35	32.5
16	3.728	5.42	38.0	0.607	0.226	488	0.223	7.66	33.9

Table 4.5. The experimental results

*****FWHM: Full-width half-maximum of an x-ray scattering profile (^{o})

In Figure 4.13, no appreciable changes of relative intensity of the peaks in the endotherm are observed in the as-spun fibres; the multiple melting phenomena observed is attributed to the compositional heterogeneity of the co-polyester. Based on this fact, it can be suggested that LAAC is a mixture composed of a number of components with different melting points. The endothermic curves of fractions indicate that they are in amorphous states. As-spun fibres of LAAC show a small exothermic peak associated with crystallisation, implying incomplete crystallisation during the formation of the as spun fibres as a result of extrusion temperature values. Ko and Chen *et al.* [215] relate the complex melting behaviour as a result of the melting of different populations of lamellar

crystals and/or the melting-recrystallization-remelting processes. That could be related to a large variation between the lengths and the nature of the constituent polymer chains.

Figure 4.14 shows SEM images (at 1 mm scale) of selected fibres from both grades; it shows a uniform cross section and acceptable surface of each of the fibres. Based on DSC and XRD, the two grades used show differences in crystallization and rheological behaviours.

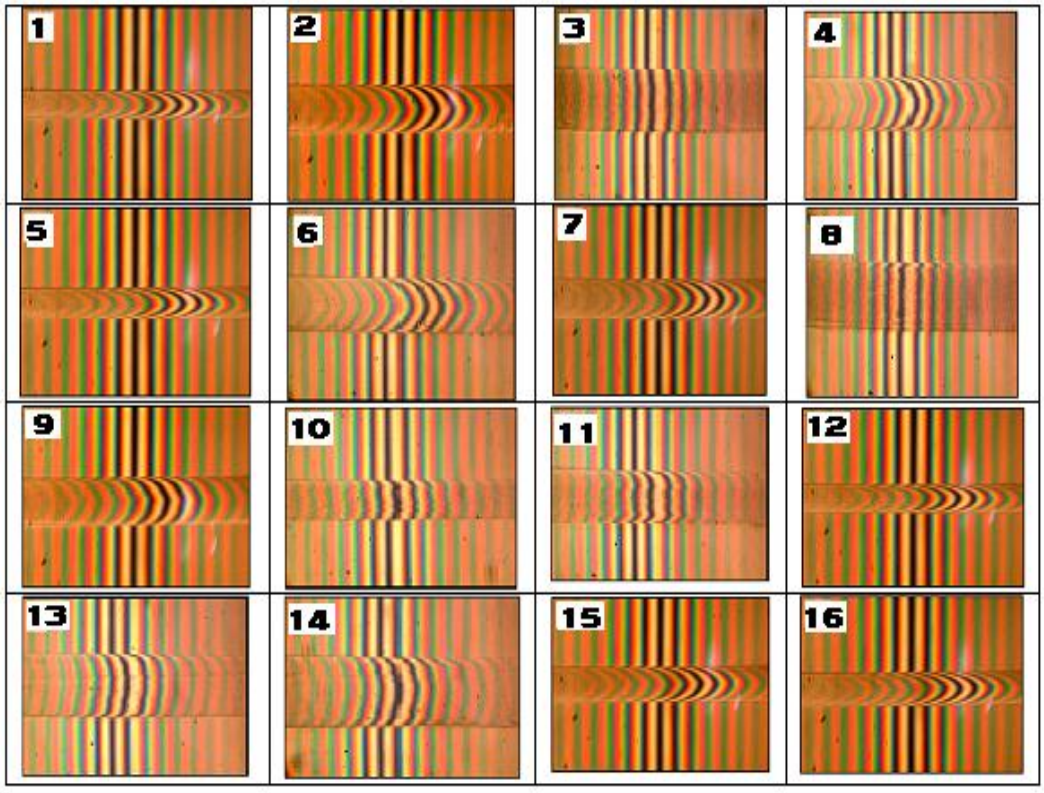

Figure 4.11. Microinterferograms of birefringence using a Pluta microscope

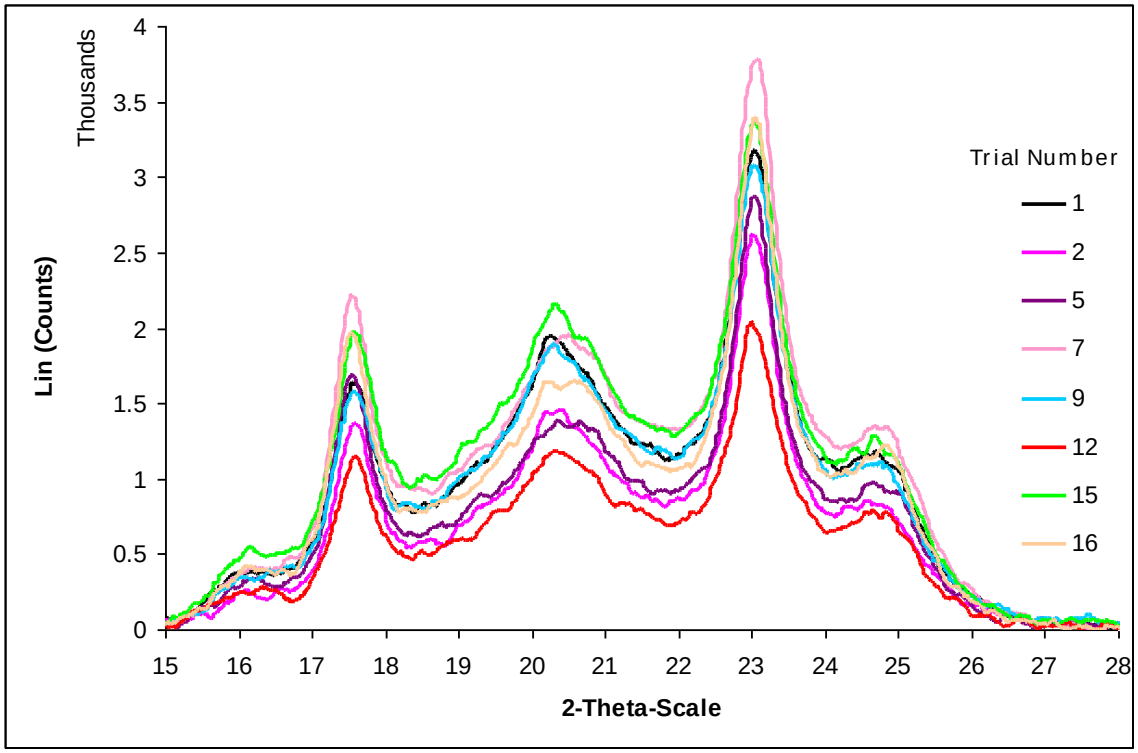

(a)

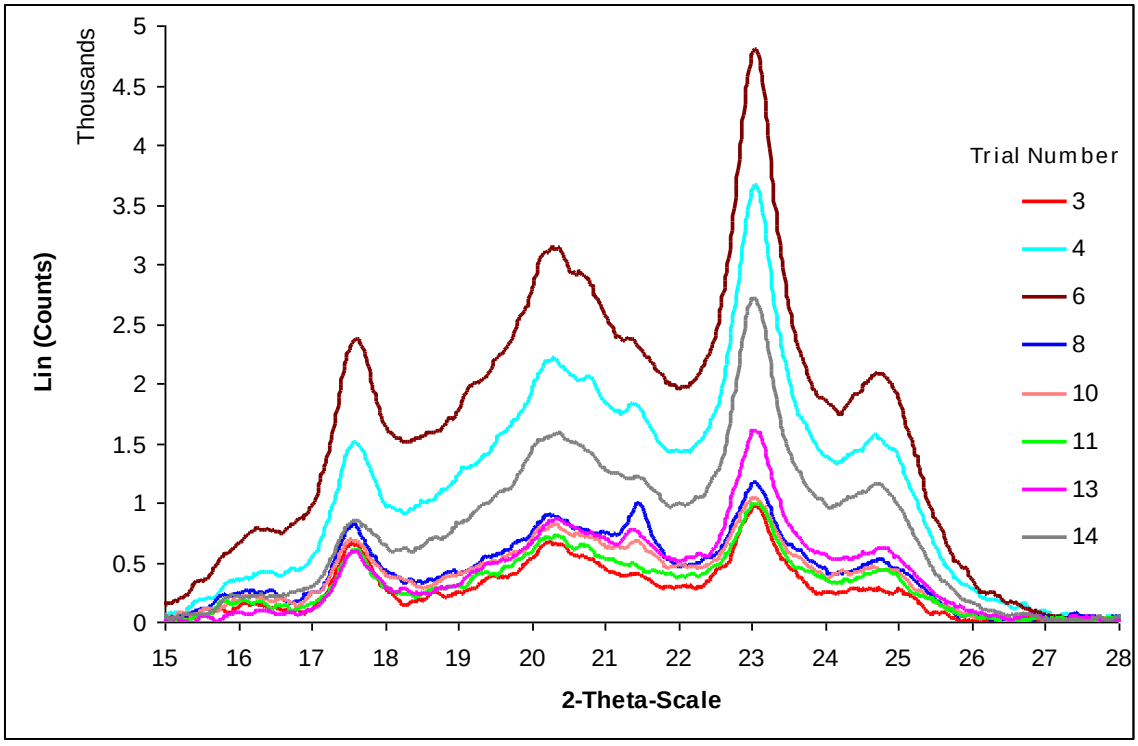

(b)

Figure 4.12. WAXS traces of LAAC fibres for first (a) and second (b) blocks

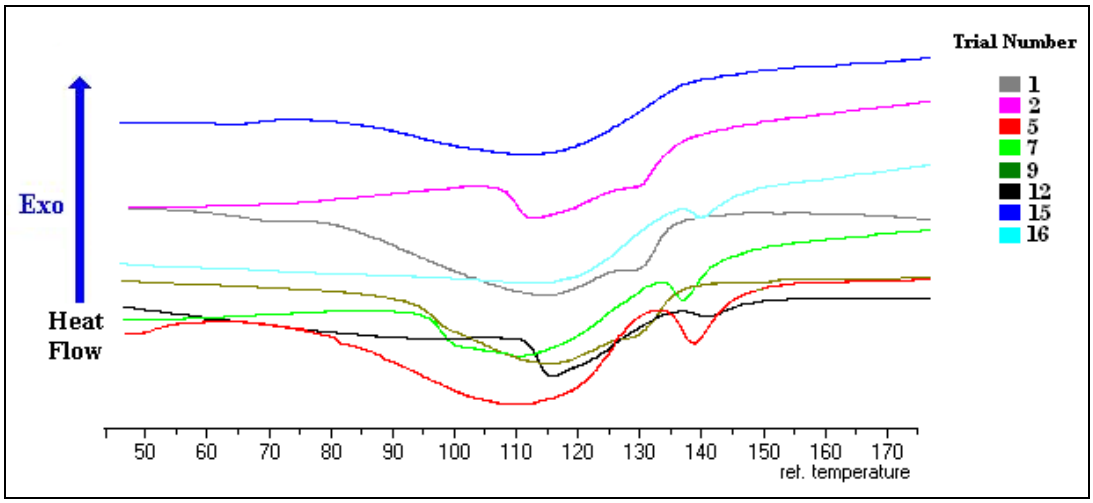

(a)

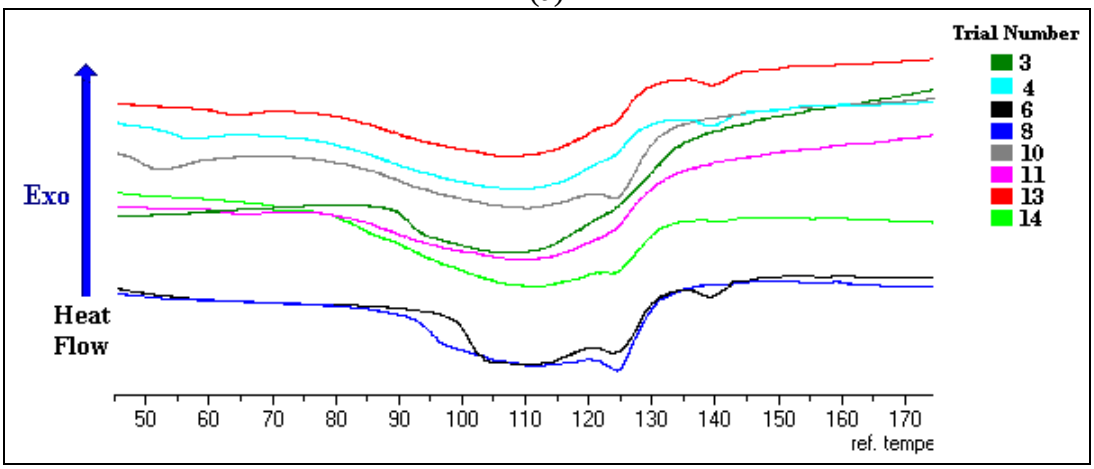

(b)

Figure 4.13. Thermal diagrams of fibres for first (a) and second (b) blocks

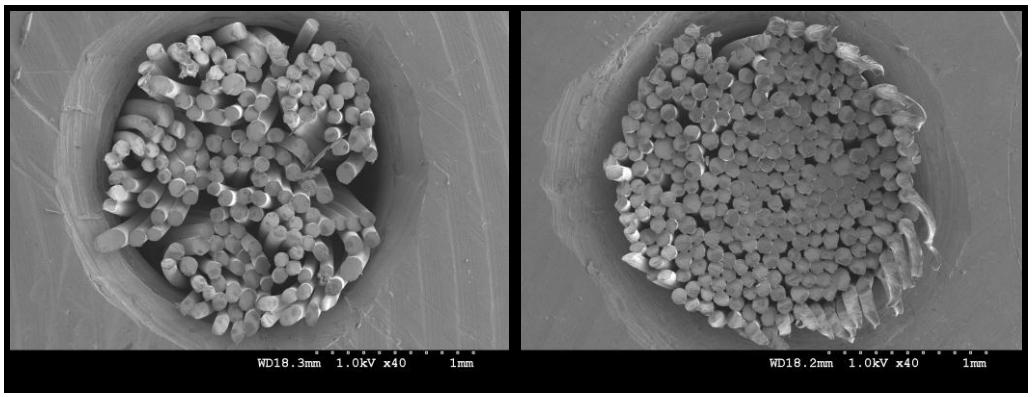

(a) (b)

Figure 4.14. SEM Images of selected fibres from first (a: LAAC1) and second (b: LAAC2) blocks (19:1magnification ratio)

4.5 Statistical Analysis and Discussion of Results

After testing the samples, the results were analysed to determine the significant factors which develops the process. Many tools, such as the Pareto chart, the effect plot, interaction plot, normal probability plot, surface plot and analysis of variance ANOVA, were used in the statistical analysis of the results of 16-run design. It should be borne in mind that the other parameters in section 4.3.1 (which are not included in Table 4.1 and Table 4.3) were set on selected values and any changing of those values could lead to different results and models.

4.5.1 Process-ability of LAACs Using a Brabender Machine

As a two-level experiment, a factor effect and interaction effect could be determined as the difference between the average responses at the low and the high level of the extrusion temperature profile zones and polymer grades. Orthogonal arrays were constructed to model the extrusion temperature profile and polymer grade effects to optimise the fibre's properties required for various applications as in Ch 03. Using a full design approach, the model expected should be able to control torque value and productivity by optimising the processing temperatures profile in barrel zones and polymer grade. The statistical model will identify the significant factors affecting the process as well as any interactions which may exist between them. This is important, as it will help later when selecting the temperature profile for the extruder for melt spinning process. The Pareto chart for torque, Figure 4.15 (a), shows the significant arrangement of factors and their interactions in decreasing order depending on the significant effect [216]. They present details about the importance and direction of the effect, and the way that the factors interact with one another. The decreasing order is MFI, Z1, MFIZ1, Z3, Z2, Z2Z3, MFIZ2, MFIZ3, Z1Z3 and Z1Z2. The polymer grade effect and the temperature of the feeding and the compression zones play an important role in torque required to extrude the materials. As the die-head temperature is increased, the viscosity of the material changes and that helps the extrudate to leave the machine and to reduce the die head pressure, which negatively affect the internal pressure and the material flowing in the extruder then on the torque required. The Pareto chart for extrusion productivity, Figure 4.15 (b), shows the significant arrangement of factors and their interactions in decreasing order, depending on the significance effect. The decreasing order is MFI, Z1, Z3, Z2Z3, Z1Z3, MFIZ2, MFIZ3, MFIZ1, Z1Z2 and Z2. More torque

leads to more productivity but the first zone temperature should not be raised very high to achieve the lower torque, as it will cause the melt of the material in very early stages and lower the friction between the granulate and the screw and negatively affect the productivity. Lower temperatures in the feeding zone will lead to high torque, high fraction (between the polymer and the feeding zone in the screw) and high productivity. The best selected temperature profile and polymer grade help in balancing the torque and productivity required and should be analysed, as will be described later.

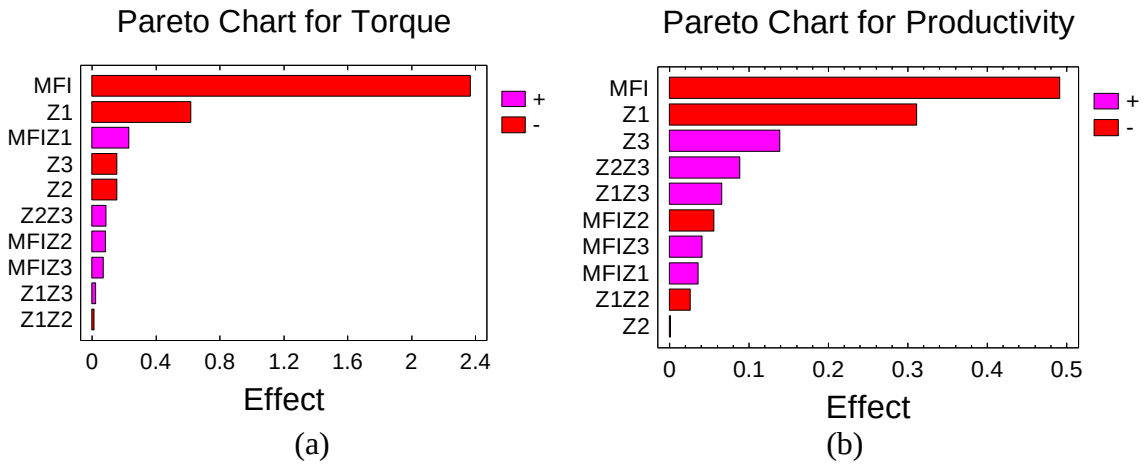

Figure 4.15. A ranked list of significant arrangement effects and interactions for Torque and Productivity (Pareto chart)

Figure 4.16 shows the main effect and interaction plots of the statistical analysis of the effects caused by the main factors and their interactions on torque value and extrusion productivity. From the effects plots (Figure 4.16 (a and b)), it can be seen that the main effect of MFI and Z1 (the feeding and compression zone in the barrel) and their interactions have a significant effect on torque - more than the other factors Z2 and Z3 which have a notable effect because of the flowing of the molten polymer through the metering zone and the die head, as their lines are longer and their slip is sharper than that of the other factors in addition to the angle between their interaction lines. As the viscosity changes with the high temperature, the high temperature will help the material to flow and will reduce the toque required to overcome the pressure generated inside the machine. An interaction plot is needed to determine the form of the interaction between each two factors together and how the direction of change of the interacting factors influences the change on torque. All the interactions could be simulated, as the plot shows the existence or otherwise of each two factors interaction. For example, in Figure 4.16 (b), the interaction between MFI and Z1 is presented as MFIZ1 on the plot. The first factor (MFI) is presented on the x-axis from low level to high level, and the second factor (Z1) is shown as two different lines, one for low level coded as - and another for high

level coded as +. The y-axis shows the averages of the measured responses. The interaction between the polymer grade (MFI) and the die head temperature (Z3) is relatively easy to understand. When the low level of the die head temperature is paired with the lower MFI grade, the maximum torque is obtained. The parallel lines confirm the absence of intersection. The other interactions between factors have no significant effect because the interaction lines are parallel in some interactions and a small angle between them in others. Torque increases either by decreasing the temperature of the barrel and the die head or by using the lower melt-flow index grade (MFI1).

Figure 4.16 (c) and Figure 4.16 (d) show the main effect and interaction plots of the statistical analysis of the effects caused by the main factors and their interactions on the extrusion productivity. From the effects plot (Figure 4.16, c), the main effect of MFI and Z1 (feeding and compression zones in the extruder barrel) can be seen, as their lines are longer and their slip is sharper than that of other factors. Other noted interactions between factors have no significant effect because of the parallel nature of the interaction lines in some interactions and the small angle between them in others.

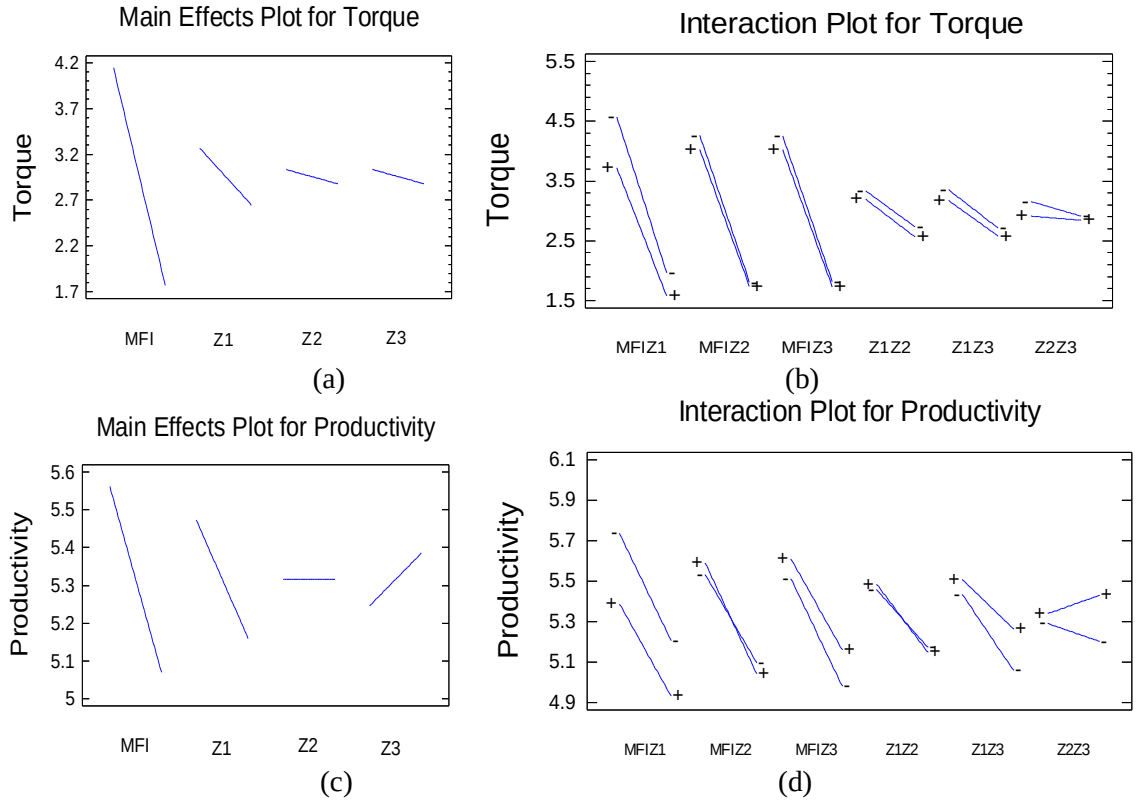

Figure 4.16. The effect and interaction plots for the torque value (the main factors (a) and their interaction (b)) and the extrusion productivity (the main factors (c) and their interaction (d))

Statistical standardized and percentage order factors and their interaction values were calculated and then plotted on X and Y axes respectively to generate a normal probability plot or a Daniel's plot, by using STATGRAPHICS. The Daniel's plot (Figure 4.17) helps in the separation process of factors into important/unimportant categories and illustrates further details concerning if the factor's effect is positive or negative. Figure 4.17 (a) displays the normal probability (Daniel's) plot of torque and productivity. The negative effects from polymer grade and Z1 are prominent; the negative effects from the Z2, Z3 and the positive effect of the interaction MFI Z1 are less prominent; more details can be obtained from analysis of variance. Figure 4.17 (b) displays the normal probability plots for extrusion productivity. The negative effects from polymer grade and Z1 are again prominent; the effects from the Z2, Z3 and the interactions are less prominent.

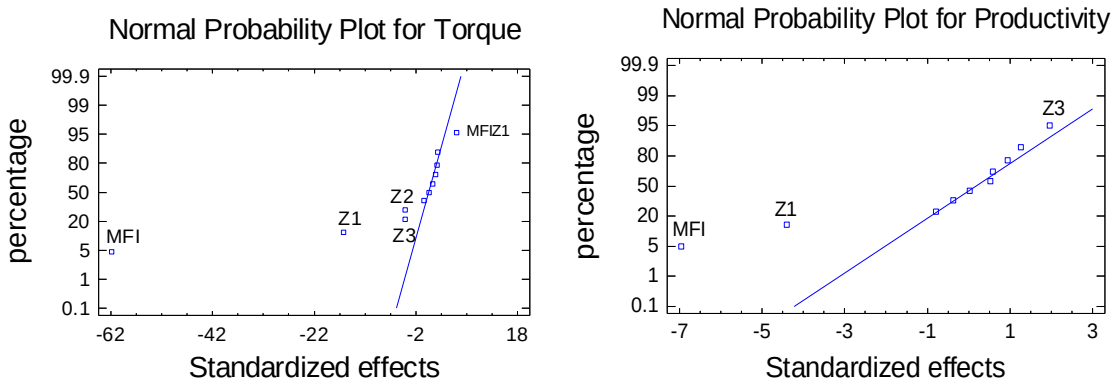

(a) (b)

Figure 4.17. The normal probability plot for the torque value (a) the productivity (b)

4.5.1.1 Analysis of Variance (ANOVA) for Torque and Productivity

In order to determine the factor effects in terms of statistical significance, analysis of variance (ANOVA) of the data was conducted. ANOVA depends on the F test, the F-ratio being obtained from statistical F tables at the appropriate level $\alpha = 0.05$. If the F value is greater than the critical F value, F= 6.61 for this design, its factor has a significant effect on the response. A probability or P-value provides quantitative and objective criteria for judging the statistical significance of the effects. Each factor has a P-value less than 0.05, indicating that the factor effect is significantly different from zero at the 95.0% confidence level. Analyses of variance (ANOVA) of the torque and extrusion productivity data were conducted to determine the factor effects in terms of statistical significance; the results are listed in Table 4.6 and Table 4.7.

Source	Sum of Squares	Degree of Freedom	Mean Square	F-Ratio	P-Value
MFI	22.4866	1	22.4866	3468.25	0.0000
Z1	1.54256	1	1.54256	237.92	0.0000
Z2	0.0970322	1	0.0970322	14.97	0.0118
Z3	0.097969	1	0.097969	15.11	0.0116
MFI Z1	0.213906	1	0.213906	32.99	0.0022
MFI Z2	0.027889	1	0.027889	4.30	0.0928
MFI Z3	0.0197403	1	0.0197403	3.04	0.1414
Z1Z2	0.000784	1	0.000784	0.12	0.7422
Z1Z3	0.00207025	1	0.00207025	0.32	0.5964
Z2Z3	0.031329	1	0.031329	4.83	0.0793
Total error	0.0324177	5	0.00648355		
Total	24.5523	15			

Table 4.6. Results from ANOVA identifying the statistical significance of factor effects on torque value. P-Value is the smallest risk level α at which the data are significant. F (1, 5) =6.61 at α=0.05 under the conditions

Source	Sum of Squares	Degree of Freedom	Mean Square	F-Ratio	P-Value
MFI	0.965306	1	0.965306	48.44	0.0009
Z1	0.387506	1	0.387506	19.45	0.0070
Z2	0.00000625	1	0.00000625	0.00	0.9866
Z3	0.0770062	1	0.0770062	3.86	0.1065
MFI Z1	0.00525625	1	0.00525625	0.26	0.6294
MFI Z2	0.0126563	1	0.0126563	0.64	0.4616
MFI Z3	0.00680625	1	0.00680625	0.34	0.5843
Z1Z2	0.00275625	1	0.00275625	0.14	0.7252
Z1Z3	0.0175562	1	0.0175562	0.88	0.3910
Z2Z3	0.0315063	1	0.0315063	1.58	0.2641
Total error	0.0996312	5	0.0199262		
Total	1.60599	15			

Table 4.7. Results from ANOVA identifying the statistical significance of factor effects on productivity: P-Values is the smallest risk level α at which the data are significant.

To provide quantitative and objective criteria for judging the statistical significance of the effects on toque, the significance of studied factors will then be MFI (P_{MFI} = 0.0000) >Z1 (P_{Z1} = 0.0000) >Z3 (P_{Z3} = 0.0116) ≈ Z2 (P_{Z2} = 0.0118). Because there is continuous flow of the molten polymer in the extruder parts and the sensitivity of the material to the temperature, an understanding of the interactive relationships between the factors is very important to manage the melt spinning process through the fibre quality. The interaction MFIZ1 has P-value (P_{MFIZ1}= 0.0022) lower than 0.05 and so there is a significant effect for the interaction MFIZ1. There are no significant effects of the other interactions within the range of factors in the experiments from which it is possible to provide quantitative

and objective criteria for judging the statistical significance of the effects on extrusion productivity (Table 4.7). The significant factors are MFI (P_{MFI}= 0.0009) and Z1 (P_{Z1}= 0.0070). There are no significant effects of the other factors and interactions within the range of factors in the experiments. The quantitative ANOVA results are consistent with quantitative conclusions derived from the effects plots and Daniel's plots. The polymer grade effect and the temperature of the feeding and the compression zones play an important role in torque required to extrude the materials. More torque leads to more productivity; lower temperature in the feeding zone will lead to high torque, high friction and high productivity.

4.5.1.2 The regression Equation and Estimation Results for Torque Value and Extrusion Productivity

Based on the analysis of the full factorial experimental design (L16) results and using STATGRAPHICS software, simplified models were fitted by the regression equations (4.1 and 4.2) for torque value and extrusion productivity which were fitted to the experimental data. The regression equations in terms of the previous coded values in Table 4.1 are as follows:

Torque Value = 2.95638 - 1.1855*MFI - 0.3105*Z1 - 0.077875*Z2 - 0.07825*Z3 + 0.115625*MFI*Z1 + 0.04175*MFI*Z2 + 0.035125*MFI*Z3 - 0.007*Z1*Z2 + 0.011375*Z1*Z3 + 0.04425*Z2*Z3 (4.1)

Extrusion Productivity = 5.31563 - 0.245625*MFI - 0.155625*Z1 + 0.000625*Z2 + 0.069375*Z3 + 0.018125*MFI*Z1 - 0.028125*MFI*Z2 + 0.020625*MFI*Z3 - 0.013125*Z1*Z2 + 0.033125*Z1*Z3 + 0.044375*Z2*Z3 (4.2)

Each regression equation is a sufficient basis for interpretation of the relationships obtained $\Delta n = f$ (Z1, Z2, Z3, MFI), see section 2.9.7. The model evaluates the significance effect of each independent variable to a predicted response, depending on the coefficient constant for the linear effects of independent factors and the coefficient constant for the interactions effects, where 2.95638 (for Torque) and 5.31563 (for productivity) are the coefficient constants for the offset term. Figure 4.18 shows the experimental results observed and calculated fitted results plots of torque and productivity using the last fitted models for each trial. Experimentally observed results were plotted on the Y axis and torque or productivity for calculated fitted results generated using the last fitted model were plotted on the X axis for each trial. Their Model Standard Error (MSE) values listed in Table 4.11 indicate the dispersion of predicted and observed values around the theoretical fitted line generated using the fitted model for each trial. The predictive model

gave useful results, with acceptable variation because of the rubbery nature of the LAACs.

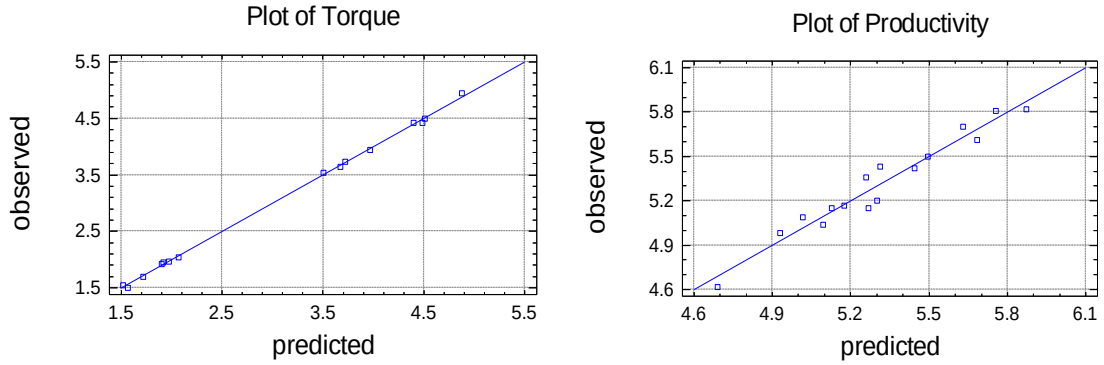

(a) (b)

Figure 4.18. Estimation results for the torque value (a) the productivity (b)

Cube plots (Figure 4.19) are fast forecasting tools used to summarize predicted values for the dependent variable by giving the respective high and low selected setting of factors. The cube plot shows the predicted values for three factors at a time. Depending on the regression equation, each value corresponds to the values of the experimental factors Z1, Z2 and MFI at the middle level of Z3 range (between -1 and +1); that is 0 for torque and Z1, Z3 and MFI at the middle level of Z2 range for productivity. The flat temperature profile does not reduce polymer viscosity sufficiently to pass through the barrier section. Too high viscosity then causes high barrel pressures, which accelerates screw and probably barrel wear. Proper setting of barrel temperatures could help reduce screw and barrel wear caused by forcing cold polymer into the barrier section of the screw. As the die-head temperature is increased, the viscosity of the material changes and that helps the extrudate to leave the machine and to reduce the die head pressure, which negatively affects the internal pressure and the material flowing in the extruder and then on the torque required.

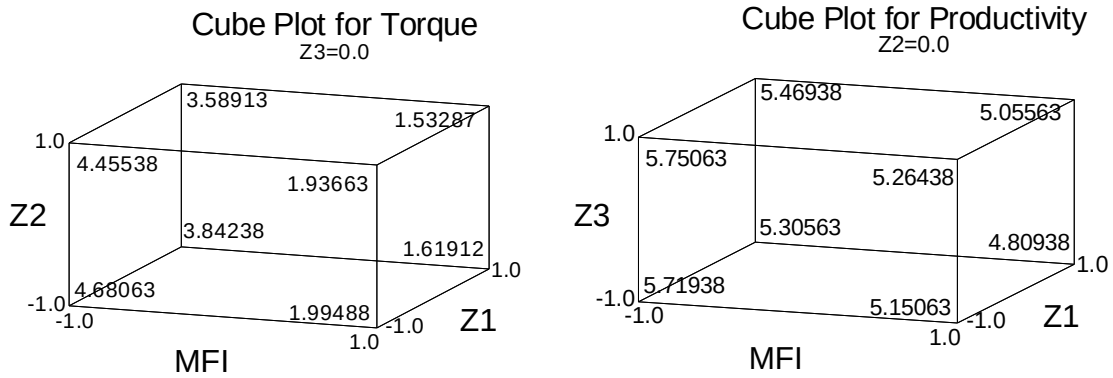

(a) (b)

Figure 4.19. Cube plots of the estimated effects for the high and low settings of selected factors for torque (a) and productivity (b)

In conclusion, if the feeding zone temperature is too hot, the friction between the polymer granules and the barrel wall will decrease because of the lubrication film generated on the barrel wall, leading to granule slippage. If the temperature is too low, the molten polymer external friction drops with poorer solid conveying. The ideal temperature is expected to allow the granules surface to be tacky with high generated internal friction, which moves the polymer forward as a plug with screw rotation. The models achieved could help in forecasting and controlling the friction between barrel and granules, as well as the friction between granules and friction between the root of the screw and granulate through statistical optimization of the torque and the productivity values obtained and with the rheological data calculated previously. The relationship between the extrusion temperature profile and the polymer grade as well as the torque value and extrusion productivity of the Brabender machine has been characterised and modelled; polymer flow depends on the temperature and the die head pressure. As a result, the feeding and metering zones temperature and the LAACs grade have the most significant effect on the process-ability (torque and productivity). The interaction between polymer grade and the temperature of feeding and compression zones is related to the material supply action in the feeding zone and to the friction between the screw and the material. Metering zone temperature and die head temperature exhibit little prominence effect on torque, as they affect the viscosity leading to a decrease in the torque needed to run the screw. The best value helps in balancing the torque and productivity required, which should be analysed as described later in sections 4.6.

4.5.2 Overall Orientation of As-Spun Fibres

The Pareto chart for birefringence (Figure 4.20) shows the significant arrangement of factors and their interactions in decreasing order (y-axis), depending on the significant effect (x-axis). The value of the birefringence reflects the overall orientation or the alignment of the molecules along the fibre axis. The decreasing order is MFI>Z3>>Z1Z2>>MFIZ2> Z1Z2>> Z1>Z2> MFIZ3> MFIZ1> Z1Z3. The polymer grade and the temperature of the die head control the overall orientation of the chains inside the fibres. As the die-head temperature is increased, the viscosity of the material changes, which helps the fibres to leave the machine and negatively affect their overall orientation. There is a recognized interaction effect between Z1 and Z2 because of the flowing of the molten polymer through the barrel zones and the metering pump speed.

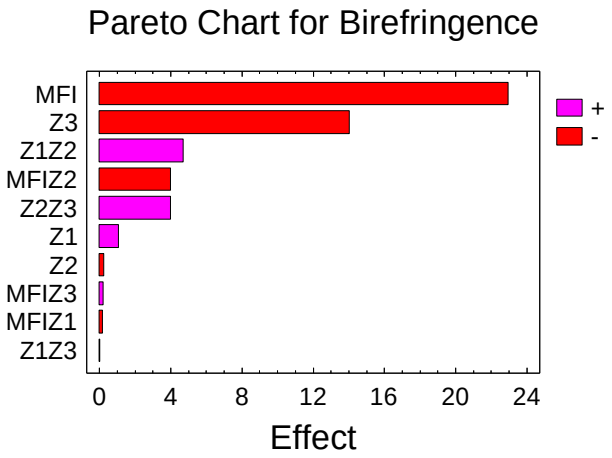

Figure 4.20. A ranked list of significant arrangement effects and interactions for Birefringence (Pareto chart)

Figure 4.21 shows the main effects and interaction plots of the statistical analysis of the effects caused by the main factors and their interactions on birefringence. In the effect plot, Figure 4.21(a), the factor effect between the average response of the low and high level of the factors is presented, the capital letters along the horizontal axis representing the main factors. It is obvious that die head temperature Z3 (T5&T6) and the polymer grade (which is coded as MFI) are the most significant effects on the overall orientation of fibres; i.e. MFI has a negative effect as it decreases from left to right. The other main factors, Z1 and Z2, exhibit little prominence. Birefringence increases either by decreasing the temperature of the die head or by using the lower melt-flow index grade which affect the spin line tension. To determine the form of the interaction between each two factors together and how the direction of change of the interacting factors influences the change on birefringence, an interaction plot is required. In Figure 4.21 (b), all the interactions could be simulated as the plot shows the existence or otherwise of the interaction between each two factors. For example, the interaction between MFI and Z3 is presented as MFIZ3 on the plot. The first factor (polymer grade coded as MFI) is presented on the x-axis from low level to high level; the second factor (die head temperature coded as Z3) shows as two different lines, one for low level coded as - and another for high level coded as +; The parallel lines confirm the absence of intersection. The y-axis shows the averages of the measured response, birefringence. It is a useful method for rendering the interaction between the polymer grade (MFI) and the die head temperature (Z3) relatively easy to understand. When the low level of die head temperature is paired with the lower melt flow index grade, the maximum birefringence is obtained. The interaction noted between Z1 and Z2 will be discussed separately below to find any significance that may arise from the usual experimental error. The small effect of Z2 interaction with Z3 is

related to the heat diffusion between the metering pump and die head as a result of the continuous flowing of the molten polymer, both parts are connected together. The other interactions show no significant interaction effect because of the parallel nature of the lines in the interaction plots and the small interaction angle in the others.

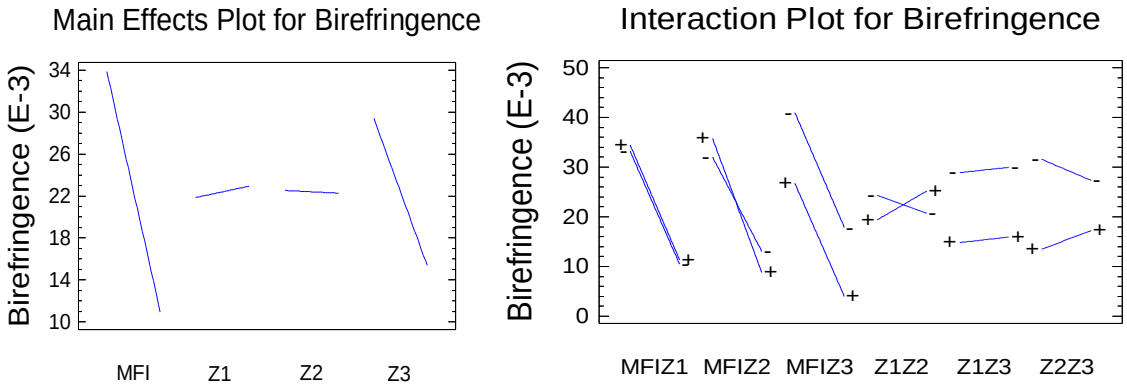

(a) (b)

Figure 4.21. The main effects and interaction plots for the birefringence for the main factors (a) and their interaction (b) respectively

STATGRAPHICS was used to calculate the statistical standardized and percentage order factors and their interactions values and then to plot them on X and Y axes respectively to generate a normal probability plot or a Daniel's plot. Figure 4.22 displays the normal probability (Daniel's) plots. The negative effect from polymer grade and die head temperature are again prominent. Other effects of factors and interactions agree with the last results; more details can be obtained from analysis of variance.

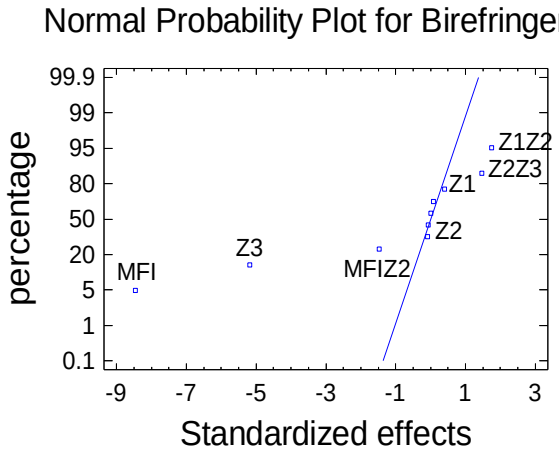

Figure 4.22. Statistical standardized and percentage order values of factors and their interactions for the birefringence (normal probability plot).

4.5.2.1 Analysis of Variance (ANOVA) for Birefringence

In order to determine the factor effects in terms of statistical significance, analysis of variance (ANOVA) of the data was conducted. Analysis of variance (ANOVA) of the birefringence data was conducted to determine the factor effects in terms of statistical significance. The ANOVA results are listed in Table 4.8. The P-Value is the smallest risk level α at which the data are significant; F-Ratio F (1, 15) is 4.54 at α =0.05 under the selected conditions. The significance of the studied factors will then be MFI (P_{MFI} =0.0004) >Z3 (P_{Z3} =0.0035). P-values of Z1, Z2 and all interactions are greater than 0.05, thus their effects are not significant. There are no significant effects of the other interactions within the temperature range in the experiments. The quantitative ANOVA results are consistent with quantitative conclusions derived from the effects plots and Daniel's plots. The pattern of the 3D estimated responses is based on the assumed regression model derived from the experimental observations. The geometric result of plotting a response variable is as a function of two factors, and the interaction appears with the surface twist. Figure 4.23 shows the estimated response surface plots for interactions Z1Z2 (a), Z2Z3 (b) and MFIZ2 (c). The small notable effect of the Z1 interaction with Z2 (Figure 4.23, a) is related to the heat diffusion between the metering zone and the compression zone as a result of the continuous flowing of the molten polymer; that unexpected diffusion generates an experimental error. As no significant interactions were found for interactions Z2Z3 (Figure 4.23, b) and MFIZ2 (Figure 4.23, c), the estimated response surface plots show no significant twist and no significant effect as a result of these interactions. Furthermore, this agrees with the previous statistical analysis results of the interaction plot and ANOVA derived from the experimental data.

Source	Sum of Squares	Degree of Freedom	Mean Square	F-Ratio	P-Value
MFI	2106.81	1	2106.81	71.61	0.0004
Z1	4.62	1	4.62	0.16	0.7082
Z2	0.25	1	0.25	0.01	0.9301
Z3	789.61	1	789.61	26.84	0.0035
MFI Z1	0.12	1	0.12	0.00	0.9511
MFI Z2	64.0	1	64.0	2.18	0.2002
MFI Z3	0.16	1	0.16	0.01	0.9441
Z1Z2	89.30	1	89.30	3.04	0.1419
Z1Z3	0.003	1	0.003	0.00	0.9930
Z2Z3	64.0	1	64.0	2.18	0.2002
Total error	147.1	5	29.42		
Total (corr.)	3265.98	15			

Table 4.8. Results from analysis of variance (ANOVA) of the data identifying the statistical significance of factor

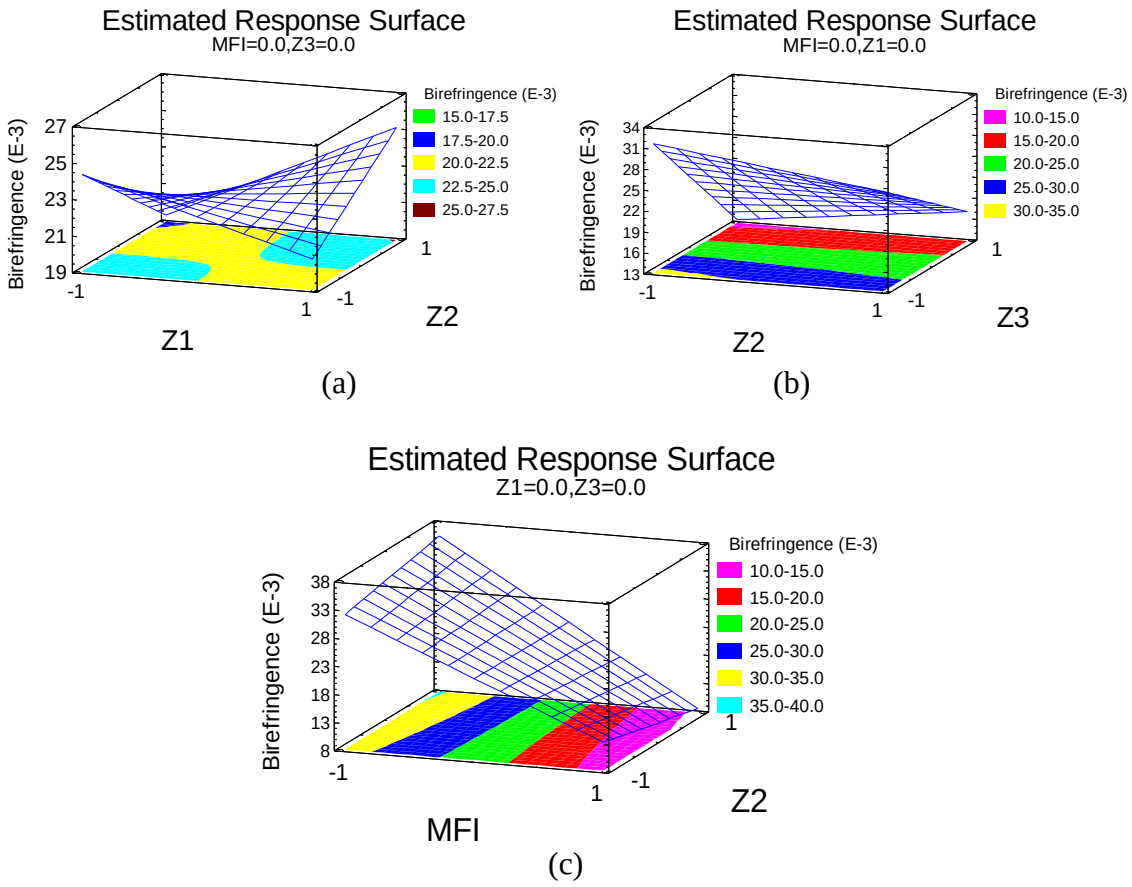

Figure 4.23. Estimated response surface Z1Z2 (a), Z2Z3 (b) and MFIZ2 (c)

4.5.2.2 The Regression Equation and Estimation Results for Birefringence

Based on the analysis of the full factorial experimental design (L16) results and using STATGRAPHICS, a simplified model was fitted by the regression equation (Equation 4.3) which was fitted to the experimental data. The regression equation in terms of the previous coded values in Table 4.3 is the following:

$$\mathbf{\Delta n\ (10^{-3})} = 22.4 - 11.475*MFI + 0.5375*Z1 - 0.125*Z2 - 7.025*Z3 - 0.0875*MFI*Z1 - 2.0*MFI*Z2 + 0.1*MFI*Z3 + 2.3625*Z1*Z2 + 0.0125*Z1*Z3 + 2.0*Z2*Z3 \quad (4.3)$$

This regression equation is a sufficient basis for interpretation of the relationships obtained $\Delta n = f$ (Z1, Z2, Z3, MFI). The model evaluates the significance effect of each independent variable to a predicted response, depending on the coefficient constant for the linear effects of independent factors and the coefficient constant for the interactions effects, where 22.4 is the coefficient constant for the offset term. Figure 4.24 shows the experimental observed results and calculated fitted results plot of birefringence using the last fitted models for each trial. Its Model Standard Error (MSE) values listed in Table

4.12 indicate the dispersion of predicted and observed values around the theoretical fitted line generated using the fitted model for each trial. The predictive model gave useful results with an acceptable level of variation for reasons such as blocked nozzles in the spinneret due to the nature of this polymer and the nonuniform flow, the tension during producing or preparing the sample for the test. The interaction Z2Z3 effect is related to the heat diffusion between the metering pump and die head as a result of the continuous flowing of the molten polymer.

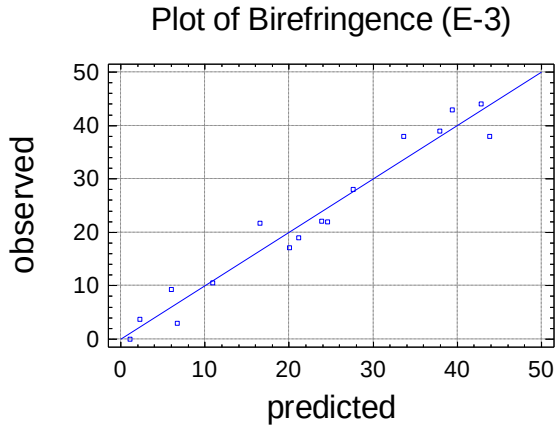

Figure 4.24. Experimental observed results and calculated fitted results plot for birefringence

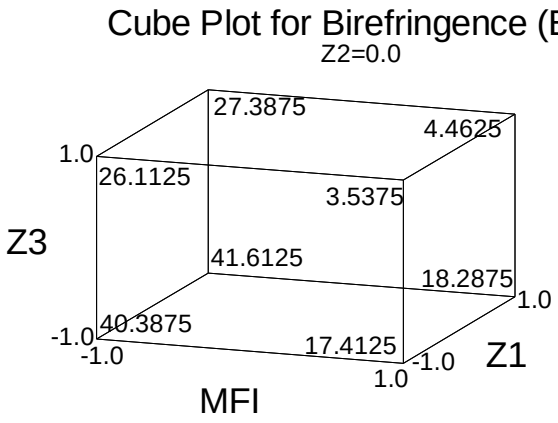

Figure 4.25. Birefringence cube (MFI, Z1 and Z3) plot of the estimated effects for the high and low studied factor settings.

The cube plot, Figure 4.25, was used to summarize predicted values for the dependent variable by giving the respective high and low setting of factors. The cube plot shows the predicted values for three factors at a time. Depending on the regression equation, each value corresponds to the values of the experimental factors Z1, Z3 and MFI at the middle level of Z2 range (0). There are three axes: the first factor Z1 is on the X-axis with low and high levels, the second factor Z2 is on the Y-axis with low and high levels and Z-axis shows the averages of the measured birefringence. The experimental results obtained here

can be used in practice for more economic operation of extrusion equipment in the production of fibres for different applications. In conclusion, there are two significant factors affecting the overall orientation: the LAACs grade used and the die head temperature (or the extrusion temperature Z3) at which the polymer melt passes through the spinneret.

4.5.3 Crystallographic Order of As-Spun Fibres (FWHM)

Figure 4.26 shows the Pareto chart for Full-Width Half-Maximum of an x-ray scattering profile (FWHM) of the fibre samples. The lower value of FWHM leads to the higher size of the crystallite and the higher degree of crystallographic order and vice versa, as mentioned previously. The decreasing order of the factors and the interactions effect on Full-Width Half-Maximum of an x-ray scattering profile are MFI>Z3>>MFIZ3>Z2> Z1Z3> Z2Z3> MFIZ1> MFIZ2> Z1Z2>>Z1. The effects of the polymer grade and the extrusion temperature on crystallographic order are permitted.

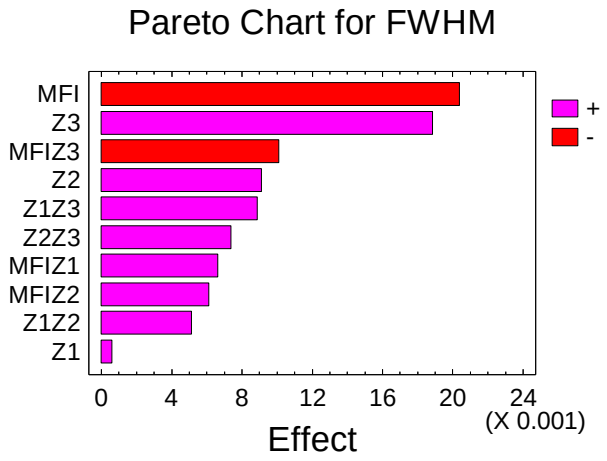

Figure 4.26. A ranked list of significant arrangement effects and interactions for FWHM (Pareto chart)

Figure 4.27 shows the main effects and interaction plots of the statistical analysis of the effects caused by the main factors and their interactions on FWHM. In the effect plot, Figure 4.27 (a), the main effects of MFI and Z3 (die head and spinneret temperature) are more pronounced than the other factors, Z1 and Z2, as their lines are longer and their slope sharper than that of the other factors. FWHM increases either by increasing the temperature of the die head or by using the lower melt-flow index grade. In other words, increasing the temperature of die head or using the lower melt-flow index grade decreases

the degree of crystallographic order. The lower value of FWHM leads to the higher size of the crystallite and the higher degree of crystallographic order and vice versa. To determine the form of the interaction between each two factors together and how the direction of change of the interacting factors influences the change on FWHM, an interaction plot is needed. In Figure 4.27 (b), all the interactions may be simulated as the plot shows the existence or otherwise of the interaction of each two factors. For example, the interaction between MFI and Z3 is presented as MFIZ3 on the plot. The first factor (polymer grade coded as MFI) is presented on the X-axis from low level to high level, the second factor (die head temperature coded as Z3) shows as two different lines, one for low level coded as - and another for high level coded as +. The nonparallel lines confirm the presence of the intersection MFIZ3. The Y-axis shows the averages of the measured response, FWHM. It is a useful method for rendering the interaction between the polymer grade (MFI) and the die head temperature (Z3) relatively easy to understand. When the high level of die head temperature is paired with the lower MFI grade, the maximum FWHM (or lower degree of crystallographic) is obtained. However, there are two noteworthy interactions, MFIZ3 and Z1Z3; their significance should be investigated because of the small angles between the interaction lines. It would be advisable to assess the major factors influencing FWHM value further to understand their influence more fully. The small effect of Z2 and its interaction with Z3 are related to the heat diffusion between the metering pump and die head as a result of the continuous flowing of the molten polymer.

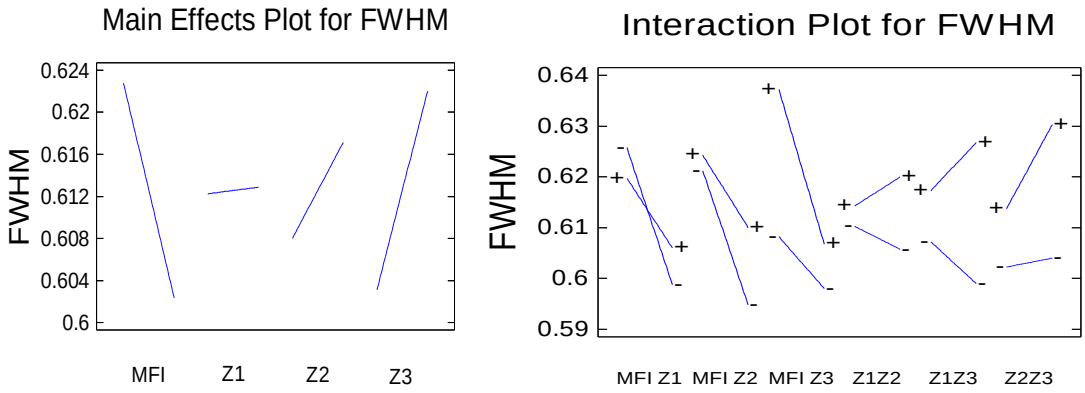

Figure 4.27. The effect and interaction plots for FWHM, (a) and (b), are for the main factors and their interaction respectively.

The normal probability plot of the derived effect estimated (Figure 4.28) illustrates further details about the normal distribution for the data. The effects from MFI and Z3

and their interaction are again prominent; the effects from Z1, Z2 and other interaction are less notable.

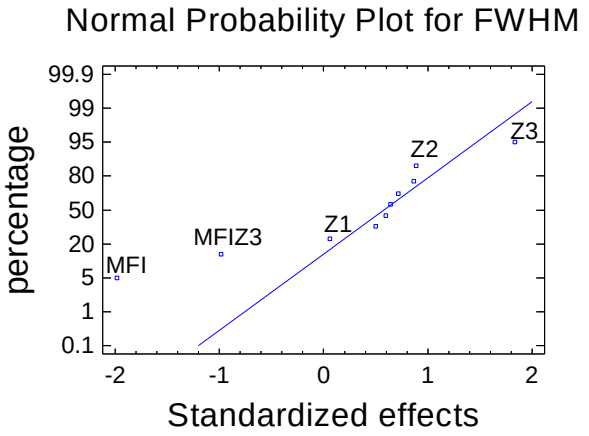

Figure 4.28. Statistical standardized and percentage order values of factors and their interactions for the FWHM (Normal Probability Plot).

4.5.3.1 Analysis of Variance (ANOVA) for FWHM

The ANOVA table partitions the variability in FWHM into separate parts for each effect, and then tests the statistical significance of each effect by comparing the mean square against the experimental error. The results are listed in Table 4.9. The significance of the studied factors will then be MFI (P_{MFI} =0.0330) >Z3 (P_{Z3} =0.0453). There is an interaction between MFI and Z3 as mentioned before; its P-value (P_{MFIZ3} =0.2514) is larger than 0.05. As a result, the interaction MFIZ3 has no significant effect. There are no significant effects of the other interactions within the temperature range in the experiments.

Source	Sum of Squares	Degree of Freedom	Mean Square	F-Ratio	P-Value
MFI	0.00166056	1	0.00166056	5.94	0.0330
Z2	0.000333063	1	0.000333063	1.19	0.2985
Z3	0.00142506	1	0.00142506	5.09	0.0453
MFI Z3	0.000410063	1	0.000410063	1.47	0.2514

Table 4.9. Results from analysis of variance (ANOVA) of the data identifying the statistical significance of factor

The pattern of estimated responses is based on the assumed model derived from the experimental observations. The geometric result of plotting a response variable is as a function of two factors and the interaction appears with the surface twist. In order to determine the direction of the interaction MFIZ3, the estimated response surfaces of FWHM were used, as shown in Figure 4.29. There are three axes: the first factor MFI is

on the X-axis with low and high levels, the second factor Z3 is on the Y-axis with low and high levels and Z-axis shows the averages of the measured MFIZ3. The estimated response surface is based on the assumed regression model. As the surface is flat with no twist found in the surface, no significant effect was detected between MFI and Z3. That agrees with the previous statistical analysis results of the interaction plot and ANOVA derived from the experimental data.

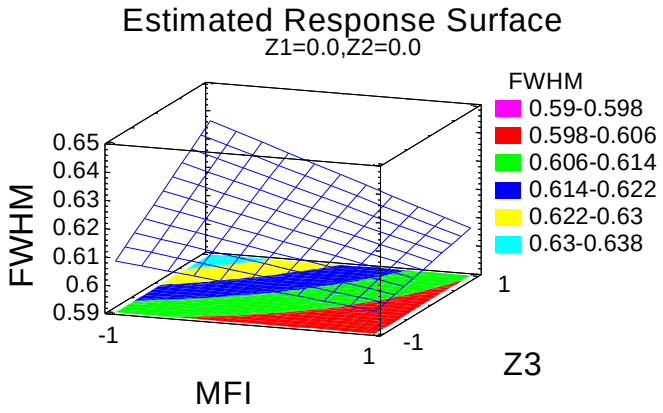

Figure 4.29. Estimated response surface between MFI and Z1

4.5.3.2 The Regression Equation and Estimation Results for FWHM

Based on the analysis of the fraction factorial experimental design (L16) results and using STATGRAPHICS, simplified model was fitted by the regression equation (4.4) which was fitted to the experimental data. The regression equation in terms of the previous coded values in Table 4.3 is the following:

FWHM = 0.612562 - 0.0101875*MFI + 0.0003125*Z1 + 0.0045625*Z2 + 0.0094375*Z3 + 0.0033125*MFI*Z1 + 0.0030625*MFI*Z2 - 0.0050625*MFI*Z3 + 0.0025625*Z1*Z2 + 0.0044375*Z1*Z3 + 0.0036875*Z2*Z3 (4.4)

The model evaluates the significance effect of each independent variable to a predicted response depending on the coefficient constant for the linear effects of independent factors and the coefficient constant for the interactions effects, where 0.612562 is the coefficient constant for the offset term.

Figure 4.30 shows the experimental observed results and calculated fitted results plot of FWHM. Experimentally observed results are plotted on the Y axis and FWHM for calculated fitted results generated by the last fitted model are plotted on the X axis for each trial. Its Model Standard Error (MSE) values listed in Table 4.12 indicate the dispersion of predicted and observed values around the theoretical fitted line generated

using the fitted model for each trial. The predictive model gave acceptable variation for reasons such as blocked nozzles in the spinneret because of the nature of this polymer and the nonuniform flow, the tension during the spinning or preparing the sample for the test. The interaction Z2Z3 effect is related to the heat diffusion between the metering pump and die head as a result of the continuous flow of the molten polymer.

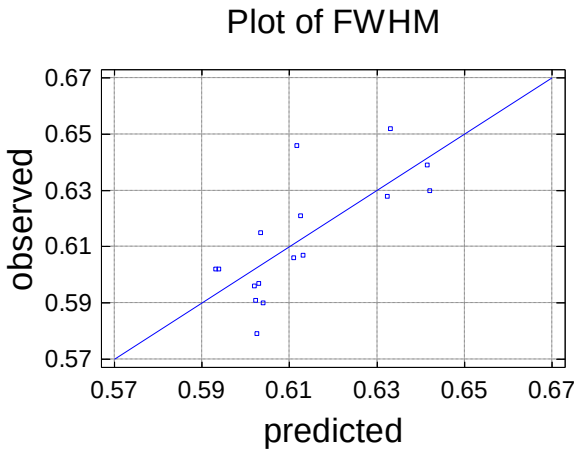

Figure 4.30. Experimental observed results and calculated fitted results plot for FWHM

Square and cube plots are fast tools used to summarize predicted values for the dependent variables by giving the respective high and low settings of factors. The cube plot shows the predicted values for three factors at a time and the square plot shows the predicted values for two factors at a time. In Figure 4.31 a and, depending on the regression equation, each value corresponds to the values of the experimental factors Z2, Z3 and MFI at the middle level of Z1 range (between -1 and +1) that is 0. In Figure 4.31 b, the square plot illustrates further details about the relationship between Z3 and MFI at the middle levels of both Z1 (0) and Z2 (0) ranges.

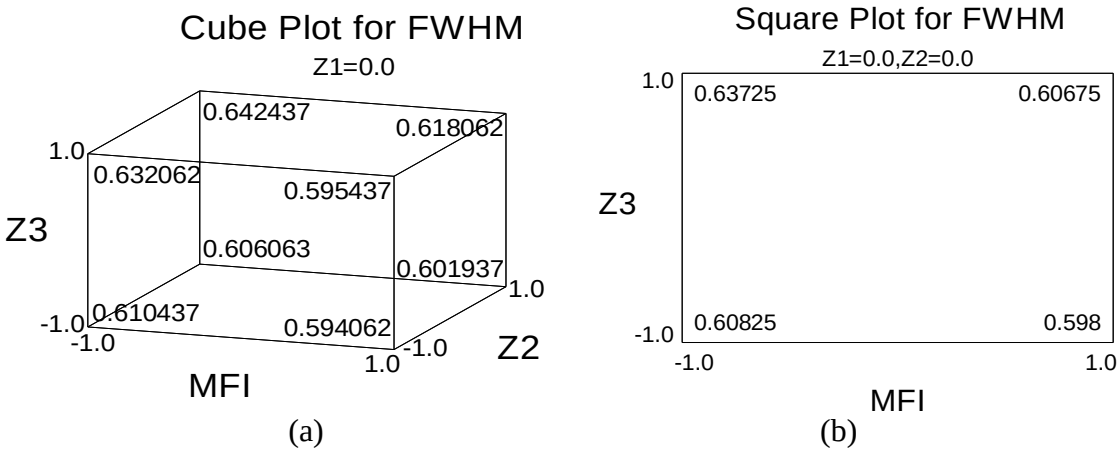

Figure 4.31. FWHM cube (MFI, Z2 and Z3) plot (a) and square (MFI and Z3) plot (b) of the estimated effects for the high and low studied factor settings.

The experimental results indicated that the apparent viscosity was significantly affected by shear rate, melt temperature and polymer grade. In conclusion, the two significant factors affecting the crystallographic order are the LAACs grade used and the die head temperature (Z3) at which the polymer melt passes through the spinneret. Statistical experimental design is a useful method for rendering the relationship between the polymer grade (MFI) and the die head temperature (Z3) relatively easy to understand. For example, when the high level of die head temperature is paired with the lower MFI grade, the maximum FWHM (or lower degree of crystallographic) is obtained. These are shown as active and reactive relationships between the heating zones and that is clear at higher temperatures.

4.5.4 Tenacity, Elongation at Break, Modulus and Spinning Productivity of As-Spun Fibres

The Pareto chart (Figure 4.32) clearly shows the arrangement of the factors depending on the significant effect for both positive and negative effects. The two significant factors affecting the tenacity, elongation at break, modulus and spinning productivity are the LAACs grade used and the die head temperature (or extrusion temperature Z3) at which the molten polymer passes through the spinneret and their interaction (MFIZ3). Other factors and interactions seem to be notable but not significant.

Figure 4.33 shows the effect plots of the statistical analysis of the effects caused by the main factors on tenacity, elongation at break, modulus and productivity. It is clear that filament tenacity, elongation at break and modulus are significant influenced by polymer grade and die head temperature Z3 (T5&T6) as main factors. The remaining main factors (Z1 and Z2) have a small notable effect but it is not significant. In terms of productivity, it can be seen that the MFI has a greater effect than the other factors, as the MFI line is longer and the slope is steeper than that of the other factors and that could be related to the material density. MFI shows a similar negative effect on tenacity and modulus but a positive effect on elongation at break and productivity. However, the polymer grade demonstrated an adverse effect on tenacity and elongation at break; in other words, the higher MFI grade gives lower tenacity and higher elongation at break and via versa. It is interesting to note that lower MFI leads to higher tenacity, lower elongation at break and productivity which could be related to the polymer properties.

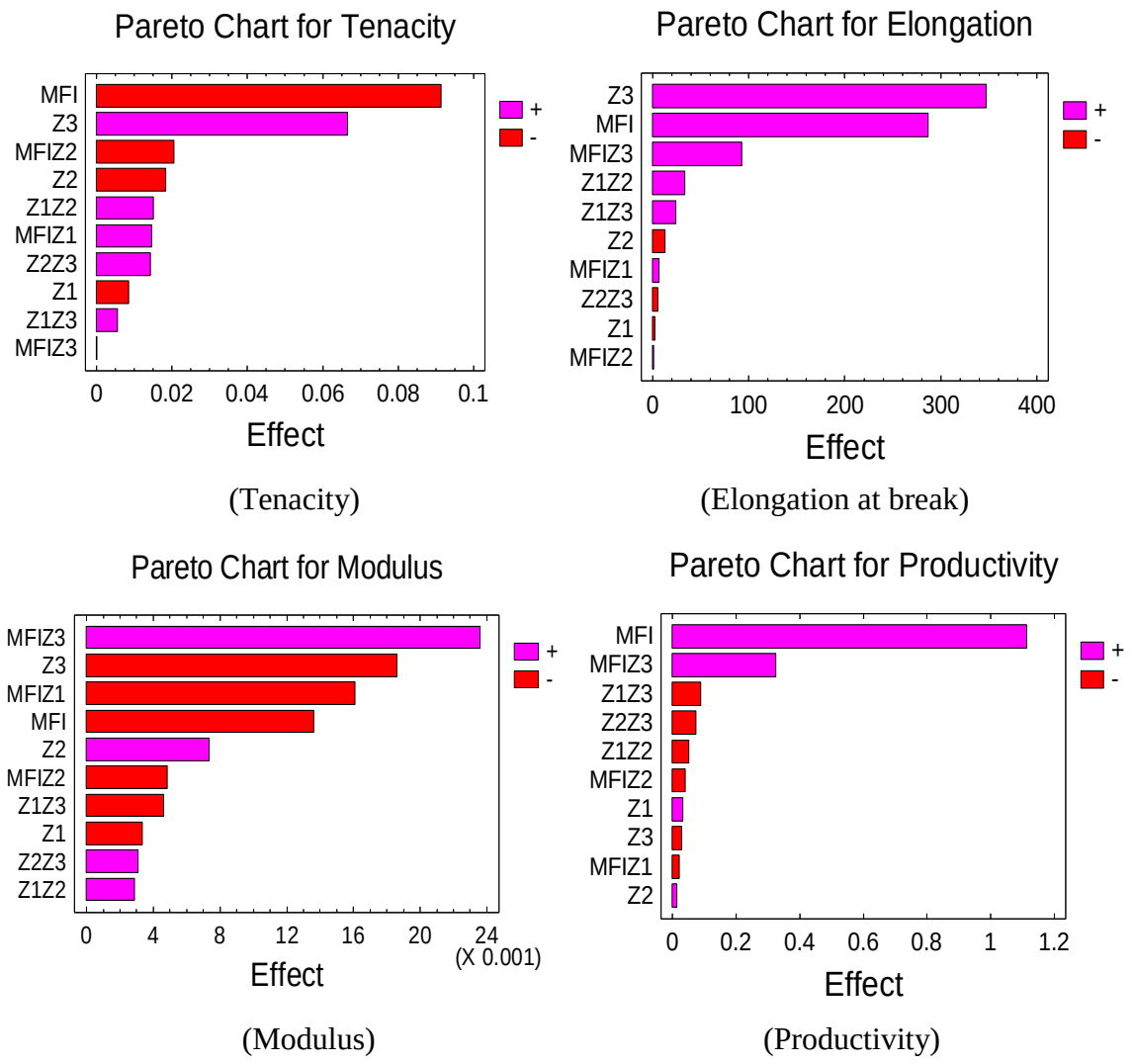

Figure 4.32. A ranked list of significant arrangement effects and interactions for tenacity, elongation at break, modulus and productivity (Pareto chart)

Figure 4.34 shows the interaction plots of the statistical analysis of the effects caused by the factors interactions on tenacity, elongation at break, modulus and productivity. Furthermore, there are noted interactions (MFIZ3, Z1Z3, Z1Z2 and Z2Z3) in the interaction plots for tenacity, elongation at break and productivity and additional noted interaction MFIZ1 in the interaction plot for modulus. Because of small interaction angles between interaction lines and the parallel nature of others, some interactions seem not to have a significant effect. The significance of those interactions needs to be further investigated later by using analysis of variance (ANOVA) which will help in giving accurate numerical results. As an alternative to an effects plot, a Daniel's plot can be used to assess the significance of the effects of the factors.

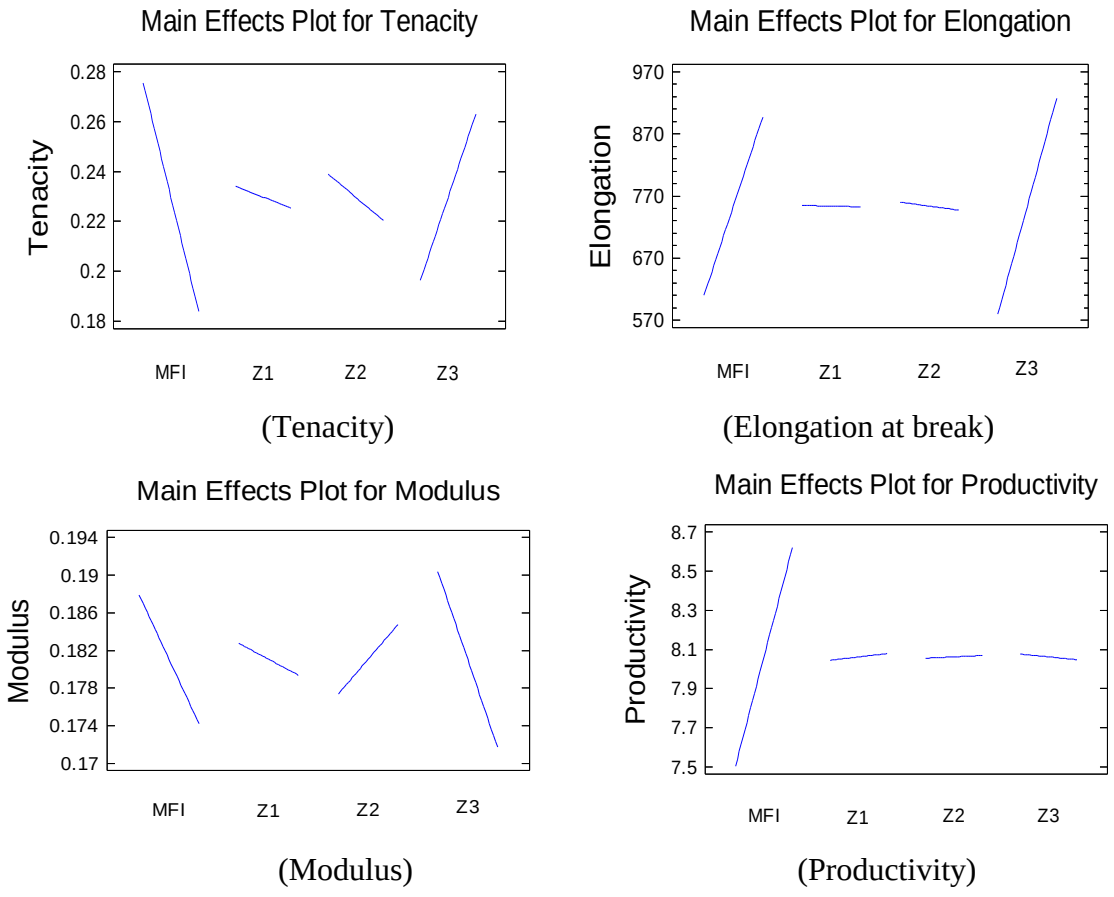

(Tenacity) (Elongation at break)

(Modulus) (Productivity)

Figure 4.33. The effect plots for tenacity, elongation at break, modulus and productivity

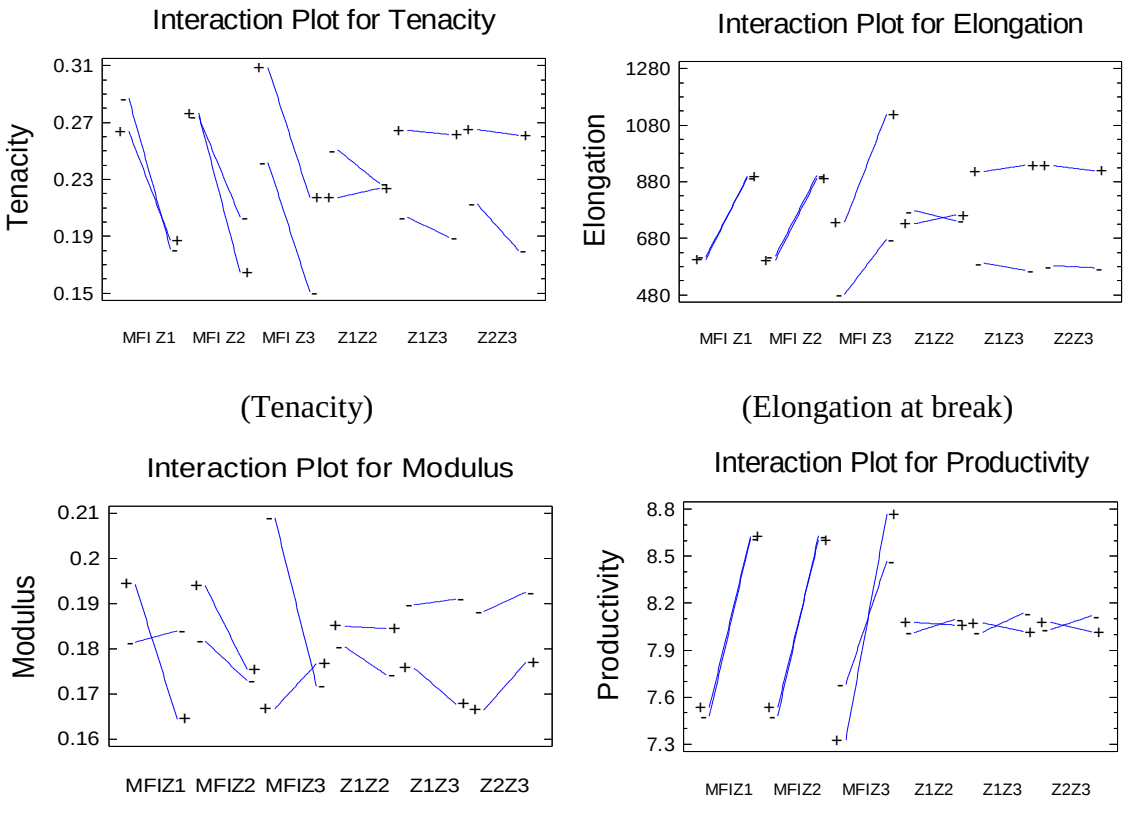

(Tenacity) (Elongation at break)

(Modulus) (Productivity)

Figure 4.34. The interaction plots for tenacity, elongation at break, modulus and productivity

Figure 4.35 displays the normal probability plots and shows the percentage and standardized effects. The points located on the right of the straight line give a positive effect and the points on the left give a negative effect. Normal probability plots lead to the same conclusion; the effects from polymer grade and extrusion temperature and their interaction are prominent, as the points representing MFI and Z3 are located far away from the straight line. The effects from Z2, Z3 and other interactions are less prominent. The interaction MFIZ3 is more significant in terms of elongation at break, modulus and productivity.

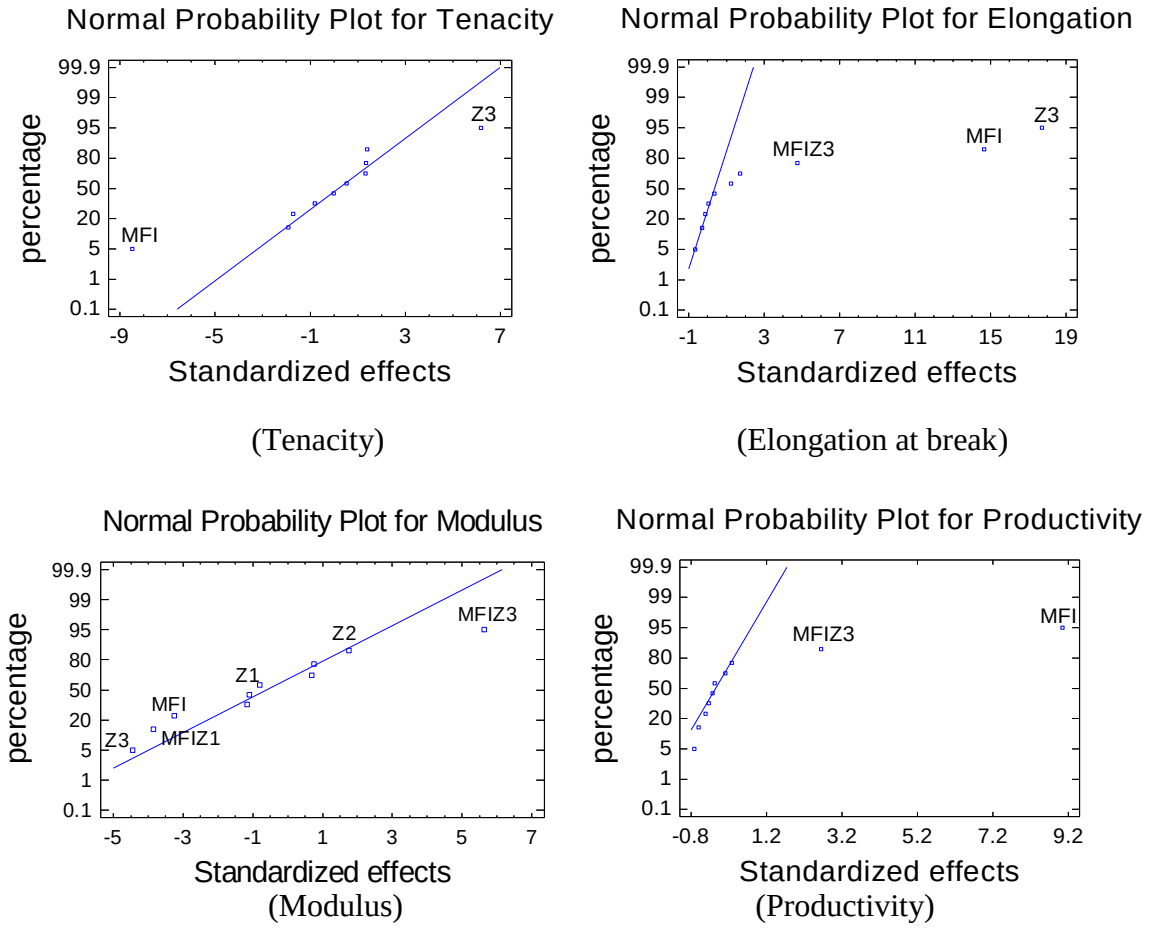

Figure 4.35. Statistical standardized and percentage order values of factors and their interactions for tenacity, elongation at break, modulus and productivity

(Normal Probability Plot)

4.5.4.1 Analysis of Variance (ANOVA) for Tenacity, Elongation at Break, Modulus and Spinning Productivity

In order to determine the factor effects in terms of statistical significance, analysis of variance (ANOVA) of the data was conducted. The ANOVA table partitions the variability in tenacity, elongation at break, modulus and productivity into separate parts

for each effect and then tests the statistical significance of each effect by comparing the mean square against the experimental error. ANOVA results are listed in Table 4.10. Depending on the tenacity analysis, MFI and Z3 are the most significant factors (P_{MFI} = 0.0004, P_{Z3}= 0.0016) and the remaining factors and their interactions are not significant. In elongation at break analysis, MFI, Z3 and MFIZ3 are the most significant (P_{MFI} = 0.0000, P_{Z3} = 0.0000 and P_{MFIZ3} = 0.0051) and the remaining factors and their interactions are not significant. In modulus analysis, MFI, Z3, MFIZ1 and MFIZ3 are the most significant (P_{MFI} = 0.0226, P_{Z3} = 0.0067, P_{MFIZ1}= 0.0120 and P_{MFIZ3} = 0.0024). The remaining factors and their interactions are not significant. The interaction between MFI and Z1 is related to the material supply action in the feeding zone and the friction between the screw and the material affected by heating action and the molten material behaviour. Analysis of the productivity shows that MFI (P_{MFI} = 0.0003) is the most significant factor and the interaction between MFI and Z3 (P_{MFIZ3} = 0.0454) is the most significant interaction influencing the productivity. Overall, these results are consistent with those from the effects plots and normal probability plots. It should be noted that, with the metering pump and the die head pressure controller, the effect of the feeding zone on the productivity is overcome. The effect of the interaction between MFI and Z1 on the modulus is related to the material supply action in the feeding and compression zones and the friction between the screw or barrel and the material. This is affected by heating action and unsteady viscosity– shear rate, which generates an error resulting from the pre-pump pressure changing.

Source	P-Value			
	Tenacity	**Elongation at break %**	**Modulus**	**Productivity**
MFI	0.0004	0.0000	0.0226	0.0003
Z1	0.4600	0.9179	0.4566	0.7949
Z2	0.1490	0.5405	0.1383	0.9154
Z3	0.0016	0.0000	0.0067	0.8246
MFI Z1	0.2330	0.7402	0.0120	0.8697
MFI Z2	0.1139	0.9565	0.2966	0.7512
MFI Z3	0.9912	0.0051	0.0024	0.0454
Z1Z2	0.2196	0.1471	0.5227	0.6945
Z1Z3	0.6241	0.2733	0.3194	0.5033
Z2Z3	0.2399	0.7857	0.4889	0.5752

Table 4.10. Results from analysis of variance (ANOVA) of the data identifying the statistical significance of factor

#

In order to determine the direction of the interactions, the estimated response surfaces for the responses elongation at break (a), productivity (b) and modulus (c and d) are shown in

Figure 4.36. By connecting between the points of the surface and the response, the factor values can be estimated to obtain the enhanced response values. The twist in the 3D-surface response diagrams confirms the MFIZ3 interaction effect on elongation at break (a), productivity (b) and modulus (c) and the MFIZ1 interaction effect on modulus (d) as mentioned previously.

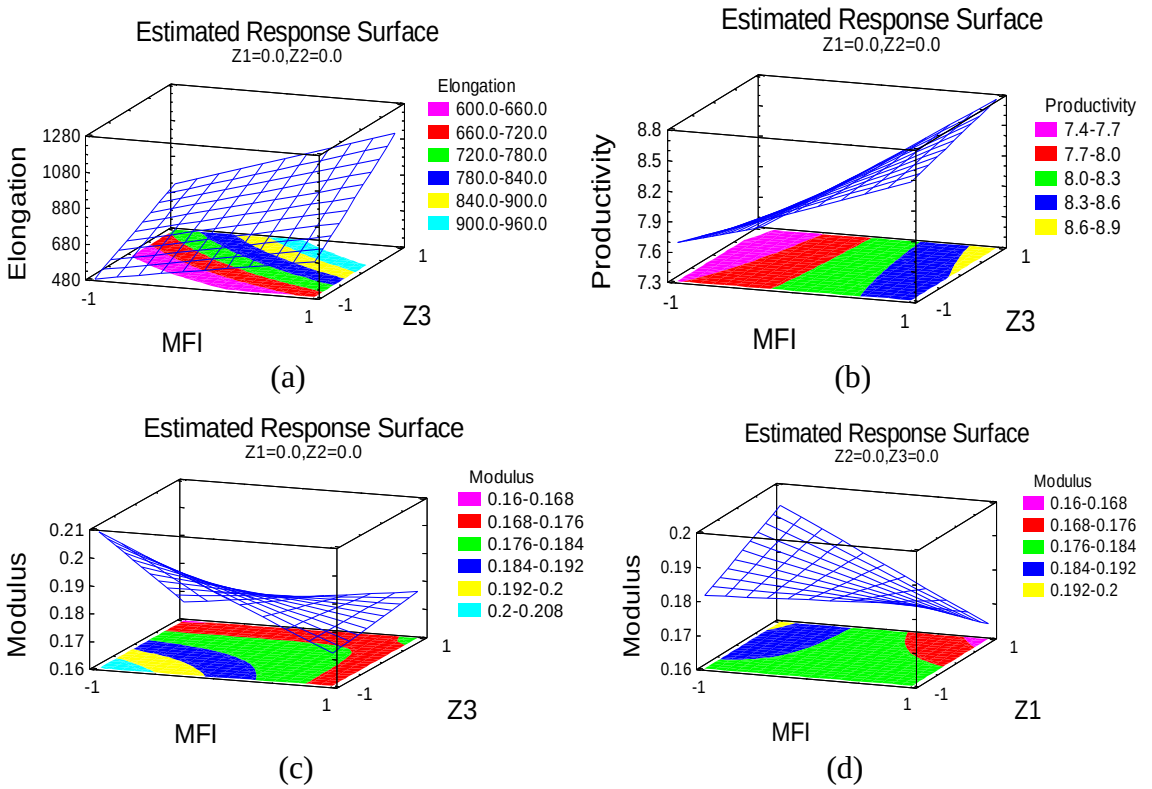

Figure 4.36. Estimated response surface between MFI and Z3 of elongation at break (a), productivity (b) and modulus (c), and between MFI and Z1 of modulus (d)

4.5.4.2 The Regression Equation and Estimation Results for Tenacity, Elongation at Break, Modulus and Spinning Productivity

Based on the analysis, a simplified model was fitted by the regression equations (4.5-4.8) which were fitted to the data of tenacity, elongation at break, modulus and productivity. The regression equations in terms of the previous coded values in Table 4.3, which include all interaction terms regardless of their significance, are the following:

Tenacity = 0.229687 - 0.0456875*MFI - 0.0043125*Z1 - 0.0091875*Z2 + 0.0333125*Z3 + 0.0073125*MFI*Z1 - 0.0103125*MFI*Z2 - 0.0000625*MFI*Z3 + 0.0075625*Z1*Z2 + 0.0028125*Z1*Z3 + 0.0071875*Z2*Z3 (4.5)

Elongation at break = 753.688 + 143.688*MFI - 1.0625*Z1 - 6.4375*Z2 + 173.813*Z3 + 3.4375*MFI*Z1 + 0.5625*MFI*Z2 + 46.5625*MFI*Z3 + 16.8125*Z1*Z2 + 12.0625*Z1*Z3 - 2.8125*Z2*Z3 (4.6)

Modulus = 0.181062 - 0.0068125*MFI - 0.0016875*Z1 + 0.0036875*Z2 - 0.0093125*Z3 - 0.0080625*MFI*Z1 - 0.0024375*MFI*Z2 + 0.0118125*MFI*Z3 + 0.0014375*Z1*Z2 - 0.0023125*Z1*Z3 + 0.0015625*Z2*Z3 (4.7)

Productivity = 8.06187 + 0.556875*MFI + 0.016875*Z1 + 0.006875*Z2 0.014375*Z3 - 0.010625*MFI*Z1 - 0.020625*MFI*Z2 + 0.163125*MFI*Z3 0.025625*Z1*Z2 - 0.044375*Z1*Z3 - 0.036875*Z2*Z3 (4.8)

As can be seen, the predicated values reasonably match experimental values; this model is a sufficient basis for interpretation of the relationships obtained $\Delta n_1 = f$ (Z1, Z2, Z3, MFI). The model evaluates the significance effect of each independent variable to a predicted response, depending on the coefficient constants for the linear effects of independent factors and the coefficient constant for the interactions effects.

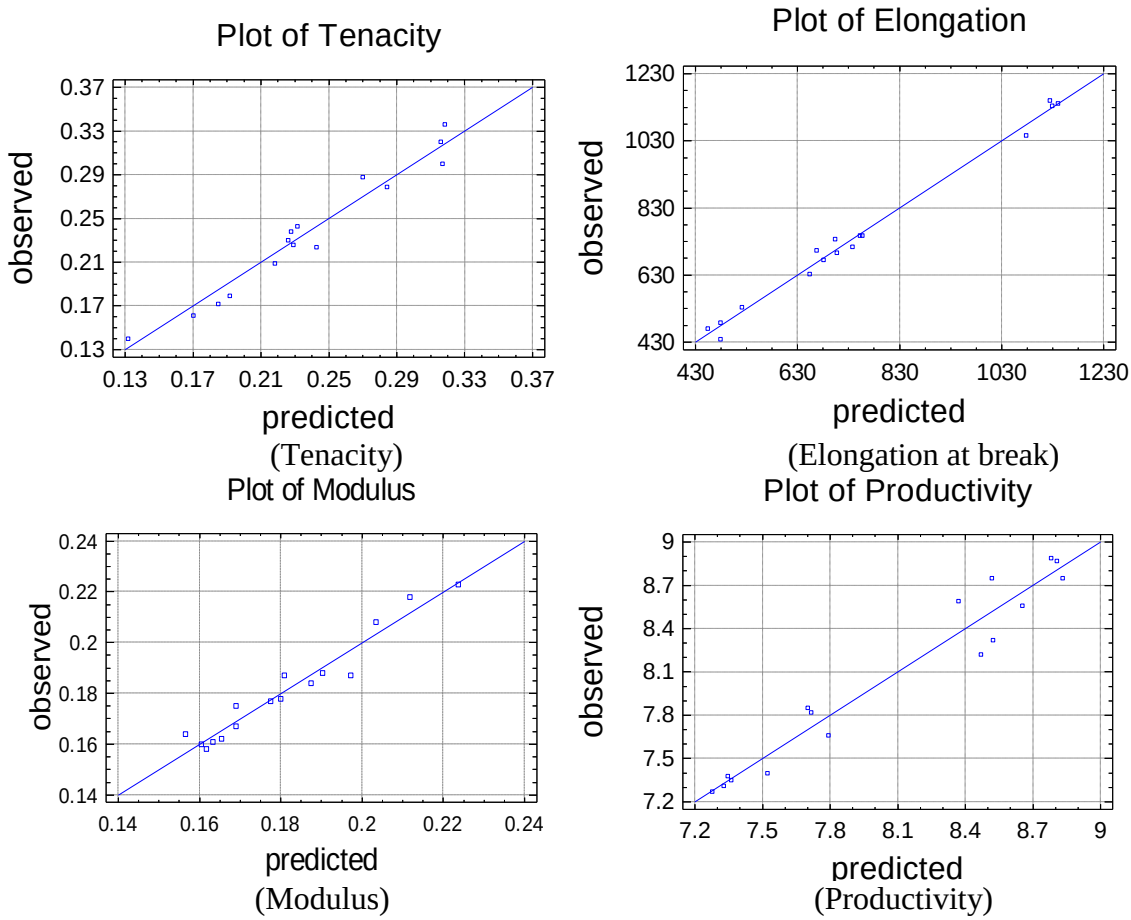

Figure 4.37. Experimental observed results and calculated fitted results plot for tenacity, elongation at break, modulus and productivity

Figure 4.37 shows the observed results and fitted results generated using the last fitted model of tenacity, elongation at break, modulus and productivity for each trial. Their Model Standard Error (MSE) values listed in Table 4.12 indicate the dispersion of

predicted and observed values around the theoretical fitted line generated using the fitted model for each trial. The model gave useful results. Each value corresponds to the values of the experimental factors in a specific row of the data file in the cube plot, depending on the regression equation. Depending on the regression equation, the square plots (Figure 4.38) for tenacity, elongation at break, modulus and productivity give more details about the relationship between Z3 and MFI at the middle of the level range of both Z1 (Z1=0) and Z2 (Z2=0). It is fast tool which helps technicians to forecast the response values in the studied range. In conclusion, the two significant factors affecting the tenacity, elongation at break, modulus and spinning productivity are the LAACs grade used and the die head or extrusion temperature (Z3) at which the molten polymer passes through the spinneret and their interaction (MFIZ3). There is an effect obtained from the interaction between MFI and Z1 on the modulus related to the material supply action in the feeding and compression zones and the friction between the screw or barrel and the material.

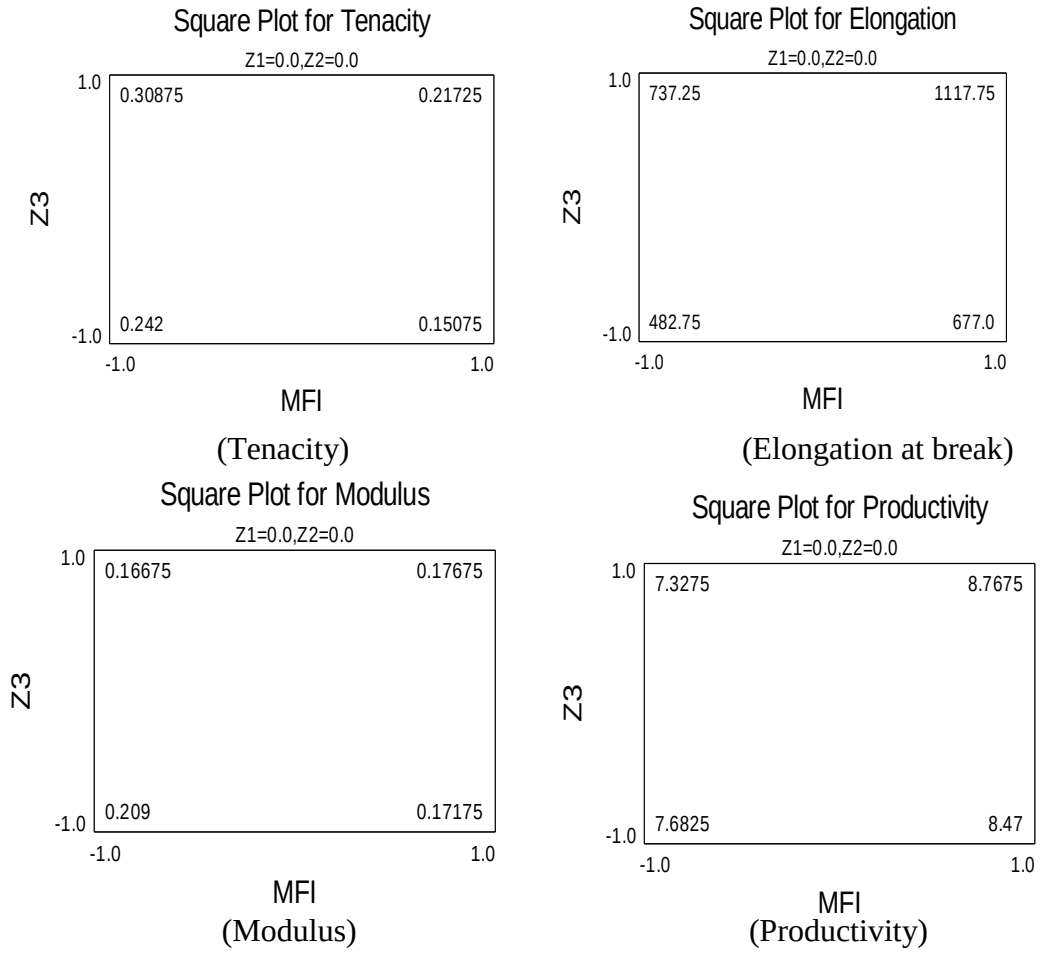

Figure 4.38. Square (MFI and Z3) plots of the estimated effects for the high and low studied factor settings for tenacity, elongation at break, modulus and productivity

4.6 Conclusion and Statistical Model for Optimisation

In this chapter, as-spun linear aliphatic-aromatic co-polyester fibres were spun under a statistical factorial design as function of the extrusion temperature profile and polymer grade using appropriate statistical methods. The properties of the as-spun fibres were quantitatively assessed as responses to polymer grades and extrusion zone temperature. That is important as it helps in selecting the extrusion temperature profile and one of the polymer grades for the extruder for melt spinning process. The spinning temperature affects the properties, productivity and cost of product.

The apparent viscosity was significantly affected by shear rate, melt temperature and polymer grade. The increasing in shear rate results in a decrease in the viscosity for a particular temperature. Depending on theoretical formulas and MFI results analysis, at higher temperature the viscosity was decreased and the material flowed easily; smooth extrudate could be observed above 130^{O}C. Based on DSC and XRD data, the two grades used show differences in crystallization and rheological behaviours; it can be suggested that LAAC is a mixture composed of a number of components with different melting points. The torque value required for extrusion process decreases with an increase in the temperature profile; it depends scientifically on the temperature profile and its relationship with the melt viscosity. The feeding zone temperature allows the granulate surface to be tacky with high generated internal friction. The flat temperature profile will not decrease polymer viscosity sufficiently to pass through the barrel sections. The interaction between MFI and Z1 is related to the material supply action in the feeding zone and to the friction between the screw and the material. The metering zone temperature and die head or extrusion temperature exhibit little prominence effect on torque, as they affect the viscosity leading to decrease the torque needed to run the screw because of decreasing of the die head pressure.

In spinning experiments, the overall orientation and the crystallographic order of as-spun fibres are affected by the LAACs grade and the die head temperature (spinning or extrusion temperature, Z3) at which the polymer melt passes through the spinneret's nozzles. It has been noted that the die head temperature, the polymer grade and their interaction are the most significant factors affecting the mechanical properties and spinning productivity. There is an interaction between polymer grade and feeding zone temperature which is related to the granules feeding action in the feeding zone; an increase in feed zone temperature significantly affects the shear rate. The friction between the screw and the material is affected by heating action, which affects the moisture

content in the granuals feeded and the molten material rheology. It can be seen that the properties have deviations for reasons such as blocked nozzles in the spinneret at lower spinning temperature because of the nature of this polymer and the non-uniform flow which reduces at high temperature, tension during the spinning (machine setting error) or some tension during the preparation of the sample (human error) for the test and difference in cooling rate through the filaments' bundle.

The optimization of process-ability and spin-ability shows the combination of factor levels which maximize and minimize the responses over the region indicated. It summarises the main conclusion of the responses results in a concise statistical model which covers the identified significant main and interaction factors and specifies the combinations of factor levels for enhancing torque value and productivity. The models take account of interaction effects as well as main effects. It is shown that the models are consistent with the experimental results derived. In the optimization of the studied responses, Table 4.11 and Table 4.12 show the combination of factor levels which maximize and minimize responses over the indicated region, depending on the experimental data which were analyzed to validate the regression models for both the Brabender and melt spinning experiments respectively, and show the Model Standard Error (MSE) values described previously. The results in the table describe the best results could be achieved by taking in all the factors and their interactions, some time the interaction effects change the individual factor effect. Through analysis, the combination of factor levels which maximize and minimize results over the indicated region, die head temperature, the polymer grade and their interaction are the most significant effects. For the spinning machine, the noted interaction effect between Z1 and Z2 could be related to the sensitivity of the material to the temperature. The interaction between Z2 and Z3 is related to the heat diffusion between the metering pump and die head as a result of the continuous flowing of the molten polymer. In other words, it is shown as a reactive relationship between the heating zones which will be clearer at higher temperatures than lower temperature due to melt viscosity changes. An understanding of the interactive relationships between the factors is very important when managing the melt spinning process through the fibre quality. The fibres spun at relatively high spinning temperature had a better developed, more highly oriented structure than that of lower temperature as fund in the results. The more significant effect factor should be adjusted in the optimization of the effect of temperature profiles and polymer grades on physical and structural properties and the process productivity to improve process performance.

Factor	Optimum model			
	Torque value (N.m)		Productivity (g/min)	
	MSE= 0.31		MSE=0.081	
	Optimum Value		Optimum Value	
	Max	Min	Max	Min
MFI	MFI 1	MFI2	MFI 1	MFI2
Z1	L	H	L	H
Z2	L	H	H	H
Z3	L	L	H	L

Table 4.11. The combination of factor levels for Brabender machine
(L: Low Level, H: High Level, MSE: Model Standard Error)

Factor	Optimum model											
	Birefringence $\times 10^3$		FWHM (^{o})		Tenacity (g/den)		Elongation at break (%)		Modulus (g/den)		Productivity (g/min)	
	MSE=3.688		MSE=0.0054		MSE=0.0157		MSE=59.9		MSE=0.0051		MSE=0.155	
	optimum value		optimum value		optimum value		optimum value		optimum value		optimum value	
	Max	Min	Max	Min	Max	Min	Max	Min	Max	Min	Max	Min
MFI	**MFI 1**	**MFI 2**	**MFI 1**	**MFI 2**	**MFI 1**	**MFI 2**	**MFI 2**	**MFI 1**	**MFI 1**	**MFI 1**	**MFI 2**	**MFI 1**
Z1	H	L	H	L	L	L	H	H	H	L	L	H
Z2	H	H	H	L	H	H	H	L	H	L	L	H
Z3	L	H	H	H	H	L	H	L	L	H	H	H

Table 4.12. The combination of factor levels which maximize and minimize results over the indicated region
(L: Low Level, H: High Level, MSE: Model Standard Error)

Current results assist the understanding of the processing of LAAC fibres; melt spinning of LAAC is easily processed by common techniques involving melt pumping and die-forming, depending on melt rheology data. The fibres made of the low melt flow index grade have better and more consistent structure and mechanical properties than that made of the higher MFI grade. In Table 4.12, module of LAAC fibres is affected by spinning temperature more than the material itself and that could explain why we could get the lowest and the highest value from the lower MFI grade.

After the previous investigation, a grade with lower melt flow index should be selected for further works on modelling of the melt spinning, drawing and twisting process. LAAC has good spinning properties; the processing temperatures profile must be at the values which are good for the spinning process with good interaction with the other considered parameters. The current results and analyses allow a fast simulation to describe the behaviour of a factor-response relationship. The models help processing scientists and technologists in industry to obtain the enhanced fibre properties at suitable conditions

related to final product cost to obtain environmentally friendly, economical, energy saving fibres; fibre science should be connected with statistics results to achieve the best results. Using the statistical forecasting models, the production process cost is controlled by adjusting the extrusion temperature profile and selecting the required polymer grade. Finished LAACs fibres are potential candidates to make continuous or staple fibres for knitted and woven fabrics, particularly for disposable use in medical and agricultural, horticultural and other non-traditional applications such as seed mats, erosion and seasonal weed control ground covers and other non-traditional fibres and fabric applications.

CHAPTER 5- STATISTICAL MODELLING OF THE EFFECTS OF MELT SPINNING CONDITIONS ON LINEAR AND BRANCHED AS-SPUN ALIPHATIC-AROMATIC CO-POLYESTER FIBRES

5.1 Introduction

After optimizing the effects of the extrusion temperature profile and polymer grade on the melt spinning process and the properties of linear as-spun aliphatic-aromatic co-polyester fibres, the optimum melting conditions were determined and the lower melt flow index grade (LAAC1: MFI1) was utilized.

In this chapter, the effects of melt spinning conditions on the structural and physical properties of as-spun linear (LAAC) and branched (BAAC) aliphatic-aromatic co-polyester fibres were statistically investigated and modelled. The effects of heat setting conditions on mechanical and thermal shrinkage properties give information about the thermal behaviour of fibres, then the investigation of the blend ratio effect of fibre properties can take place. Appropriate statistical methods were applied and a model for specifying the direction of increasing or decreasing of the significant process parameters was identified. The regression equations obtained from statistical analysis form the source code for the forecasting programs designed. Actual and forecasting results were evaluated and the fitted model was designed to obtain the accurate responses. Because AAC fibres has thermoplastic properties, that is created the need for the thermal study. Thermal study is important for identifying the thermo conditions for thermal-based treatment processes, washing or ironing processes. The results will also help researchers in the balance between the biodegradability of fibres and their structure, because the biodegradability of polymers is influenced by the chemical structure of the polymer chains, crystallinity, chain orientation and other morphological properties [51]. Some researchers have conducted work to model the extrusion processes for polymer melts in order to find the mathematical models and the numerical simulations of the industrial processes [118]. Others have tried to simulate the melt spinning process in term of quench air flow [217], or have established computer simulation of the melt spinning of isotactic polypropylene[139]. Based on melt spinning dynamic model and theory, some researchers establish a basic model of superfine denier polyester multifilament [138].

In order to optimize the melt spinning process and properties of as-spun linear and branched aliphatic-aromatic co-polyester fibres, different samples of aliphatic-aromatic co-polyester fibres were spun at different process profiles to determine the parameters and

their interaction effects and to generate the forecasting regression equations. Spin-draw ratio, optical birefringence, drawability, die head pressure of the extrusion machine, a range of crystallographic orders (FWHM) for as-spun fibres, thermo-graphic measurement of extruded filaments in the air quench cooling window, tensile and thermal shrinkage behaviour were measured and analysed. Because of the difficulty of the design and production of manufactured fibres, experimental design techniques are a useful practice.

5.2 Rheological and Thermal Characterizations

A fully biodegradable petroleum linear aliphatic-aromatic co-polyester (the lower melt flow index grade – the Solanyl flexibility component used in Chapter 4) and branched aliphatic-aromatic co-polyester (Ecoflex F BX 7011) were used to study the effects of the melt spinning process on the production process and the properties of fibres. They are coded as LAAC and BAAC respectively. To avoid possible hydrolysis during the rheological analysis and extrusion process, they were dried at 60^{o}C for 6 hours before use. The recent analysis gives an explanation for the character of surface shape at different conditions, on which the recent analysis was performed. According to the differential scanning calorimetry (DSC) results in Figure 5.1, the thermal diagrams of the LAAC and BAAC show broad temperature ranges of melting. The large peaks around the measurement start stage could be related to the moisture content. The range for melting temperatures for LAAC is 110-135^{o}C, and the range of melting temperatures for BAAC is 110-150^{o}C. These temperature ranges do not necessarily include the processing temperature as was found on the extrusion machine, because the extrusion flow of the molten polymer also depends on its viscosity. Therefore, the linear grade can be melt processed from 130^{o}C and the branched grade can be melt processed from 145^{o}C. The processing window is slightly wide and it could be around 15 degrees for each grade.

Based on the DSC results, the melt flow indices are measured at different loads (2.16, 3.16 and 5 Kg) and temperatures (from 120 to 135°C for LAAC and from 135 to 150°C for BAAC) as shown in Figure 5.2. The relationship between the melt flow index (MFI), pressure (load) and temperature is not linear and is related to the nonlinear change in viscosity with change in pressure and/or temperature, as Non-Newtonian flow behaviour.

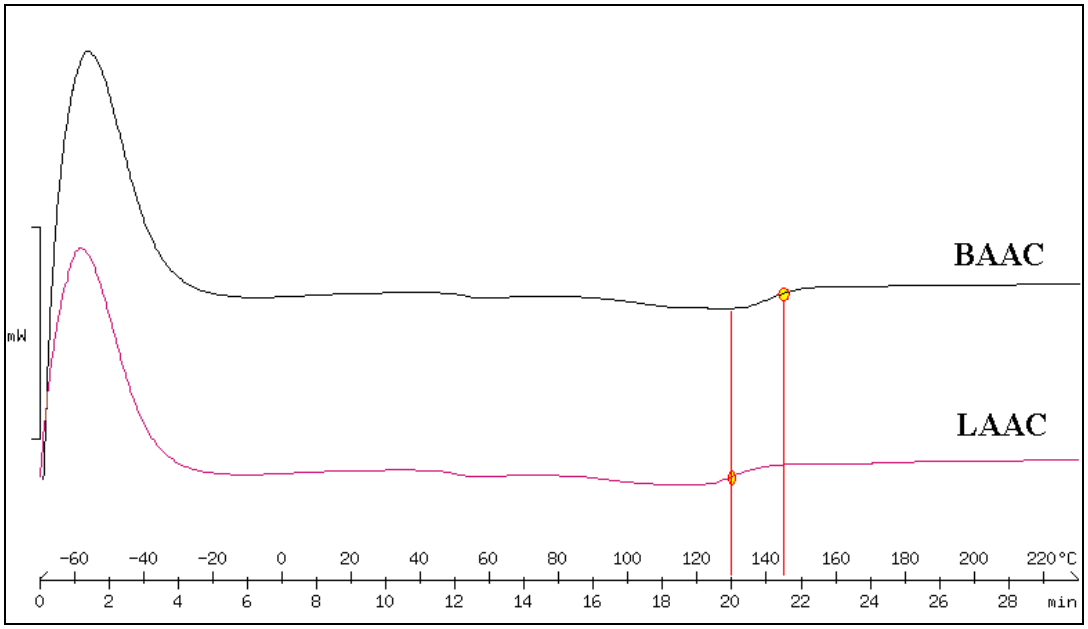

Figure 5.1. Thermal diagram of LAAC and BAAC

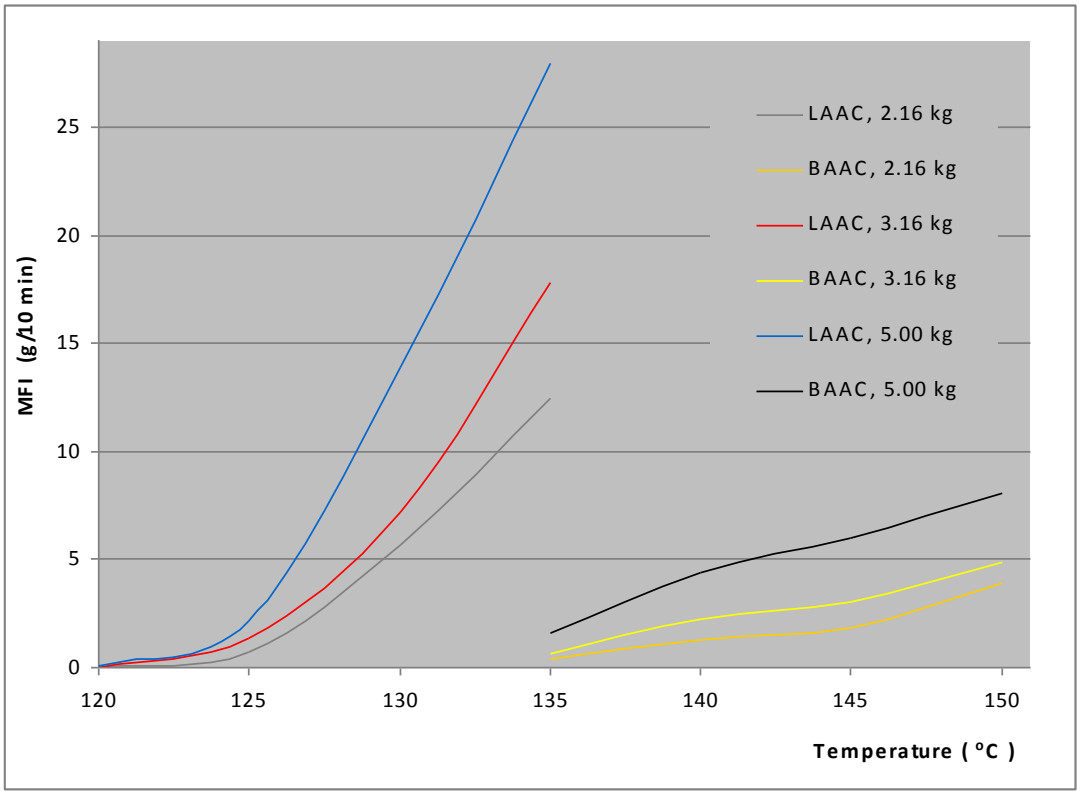

Figure 5.2. The relationship between polymer (LAAC and BAAC), the pressure and temperature

In terms of the extradite surface observation, smooth extrudate can be observed above 130^{o}C for LAAC (see description in Chapter 4 related to Figure 4.3) and above 145^{o}C for BAAC (Figure 5.3). For BAAC, stick-slip or oscillating melt extrudate appears at 140^{o}C and gross, melt-fractured extrudate was found at 135^{o}C. The apparent extrudate swell could be related to the die entry and the die exit and possible slip at the polymer-wall

interface. Figure 5.3 shows the appearance of the extrudates at the different temperatures, apparent shear rate and viscosity. Depending on theoretical formulae [218] and MFI results analysis at higher temperatures, the viscosity was decreased and the material flowed easily. At shear rate more than $2.3s^{-1}$, the extrudate surface was practically smooth. It is relatively smooth up to $3.1s^{-1}$shear rate, whereas smoother extrudates were obtained at shear rates greater than $4.5s^{-1}$.

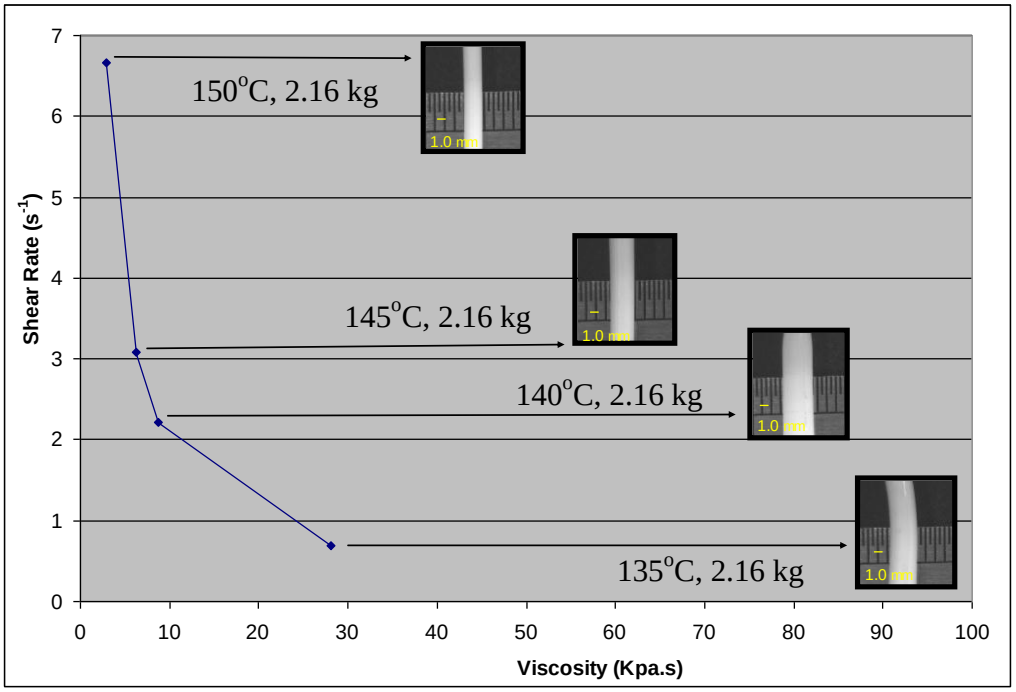

Figure 5.3. The surface shape at different temperature, viscosity, and shear rate at load of 2.16 kg for BAAC

The curves in Figure 5.4 for viscosity and shear rate can be converted to true viscosity curves using the Rabinowitsch correction [218]. Analysis of Figure 5.4 shows that as the temperature increases as the shear rate increases. The shear rate increases as a result of the reduction of viscosity. Thus, the increasing shear rate results in a decrease in the viscosity for a particular temperature. As the piston speed is increased (or extruder screw speed increases), the shear rate increases as a result of the die head pressure and the increasing shear stress (load). The decrease in viscosity improves the material flow and leads to more uniform extrudate/filaments. Viscosity varies inversely with the temperature and pressure, which is clear from the increase in MFI with the increase of both temperature and pressure. Alternatively, the productivity or throughput (MFI) will be increased if the temperature or the pressure is increased, as described in Chapter 3. The productivity or throughput will be affected depending on the polymer degradation and the properties of the enhanced product.

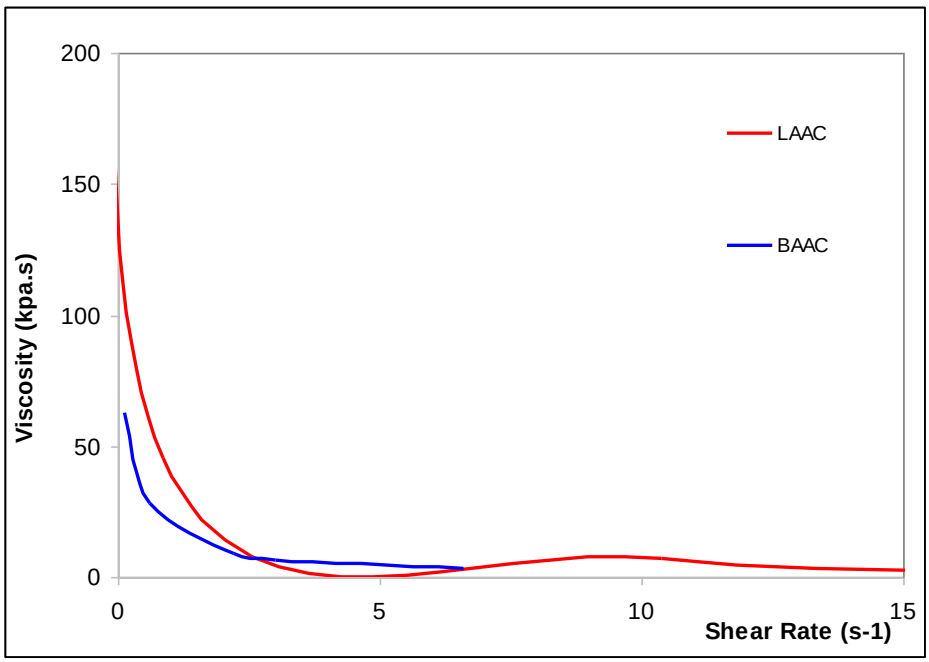

Figure 5.4. Viscosity– shear rate curve at load of 2.16 kg and different temperature

5.3 Factorial Experimental Design for Melt Spinning of As-Spun Fibres

Experimental design gives information about the significance of the main effect factors and their interactions then provides further information on how to optimize the average response values depending on the factor levels. The design for this experiment was limited to two-parameter interactions only, since interactions of more than two parameters are not useful in practice [186]. After the rheological study and pre-experimental work had been done for the branched grade BAAC and using the results obtained of Chapter 4, the number and the levels of factors were determined and the matrix design and the number of trials were prepared.

A full factorial experimental design (L32) with random order for the thirty-two screening trials involving five control parameters and two levels for each parameter was used for both LAAC and BAAC as-spun fibre analysis. The five control parameters for the lab-spin machine are metering pump speed (MPS), melt-spinning temperature (or melt extrusion temperature) (T), quenching air speed (QA), applied speed of spin finish (SF) and winding speed (WS). The specially designed spinneret of 30 holes was used in this chapter. For LAAC, the heating zones for the barrel and the metering pump in the extrusion machine profile were 115, 120, 125 and 130^{o}C. For BAAC, the heating zones for the barrel and the metering pump in the extrusion machine profile were 120, 125, 135 and 140^{o}C.

The two levels of each parameter were separated as far apart as possible from one another, as shown in Table 5.1; the experiments were conducted in one block. The AACs were dried at 60^{o}C for 6 hours before use.

The study describes the melt spinning of aromatic-aliphatic co-polyester within the low range of take-up velocities (50-100 m/min). The main purpose here is to lower the fibre tension which affects the fibre's properties and causes undesirable structural changes regard to the material's rubbery behaviour. Alternatively, the high speed with wide range omits the effect of other factors that need to be investigated. The low speed is compensated by using a very large number of nozzles per spinneret; as a result, the comparable throughput can be obtained relative to the high speed processes, such as the upward and downward spinning processes. The temperature of the feeding zone was maintained above 100^{o}C to prevent any moisture from forming during the extrusion process. The detailed experimental arrangement of the trials is shown in Table 5.2. The sample data were analysed and the significant factors were determined to develop the process design.

The matrix design, statistical analysis and represented analysis plots are constructed directly from the raw data using STATGRAPHICS programs. Many tools, such as the Pareto chart, the main effect plot, interaction plot, normal probability plot, surface plot and analysis of variance ANOVA, are used in the statistical analysis of experimental design.

Factor abbreviation	**Factor name**	**Low Level ↓**	**High Level ↑**
T	Melt-Spinning Temperature, ^{o}C of LAAC	*130*	*145*
	Melt-Spinning Temperature, ^{o}C of BAAC	*145*	*160*
MPS	Metering Pump Speed, rpm (2.4 cc.rev^{-1})	*6*	*12*
QA	Quench Air Speed, % (Transverse air velocity m/sec)	*35*	*50*
SF	Spin Finish Speed, rpm (0.146 cc.rev^{-1})	*0.35*	*0.50*
WS	Winding Speed, m.min^{-1}	*50*	*100*

Table 5.1. Factors and their levels for the spinning experiments of LAAC and BAAC as-spun fibres

Trial Number	T	MPS	QA	SF	WS
1	H	H	H	H	L
2	L	L	H	H	L
3	H	H	H	H	H
4	H	H	H	L	H
5	L	L	H	L	H
6	L	H	L	H	L
7	H	L	L	H	L
8	H	L	H	H	L
9	L	L	L	H	H
10	L	L	H	L	L
11	L	L	L	L	H
12	H	H	H	L	L
13	H	H	L	H	H
14	H	H	L	L	L
15	L	H	H	L	H
16	L	H	H	H	L
17	L	L	H	H	H
18	L	H	H	L	L
19	H	L	H	L	H
20	L	L	L	H	L
21	H	L	H	L	L
22	H	L	H	H	H
23	L	H	H	H	H
24	L	H	L	L	H
25	L	L	L	L	L
26	H	H	L	L	H
27	H	H	L	H	L
28	H	L	L	L	H
29	L	H	L	L	L
30	H	L	L	H	H
31	L	H	L	H	H
32	H	L	L	L	L

Table 5.2. L32 Experimental design array for the melt spinning experiments

(H = High, L = Low)

5.4 Experimental Results of Melt-Spinning of LAAC Fibres

The experimental design with random order was used for the thirty-two screening trials (L32) involving five control parameters (Table 5.1), as represented in Table 5.2. The detailed experimental arrangement of the calculated results of spin draw ratio, birefringence, drawability, die head pressure, full-width half-maximum (FWHM), filament temperature averages (at L02, L03, L04 and L05), count, tensile properties,

diameter and thermal shrinkage are shown Table 5.3 and Table 5.4. The as-spun fibre results have acceptable standard deviations generated from blocked nozzles in the spinneret; the rubbery behaviour of AACs caused a non-uniform flow which decreases at high temperature, tension during the spinning, machine error variation or variation in cooling rate through the filament bundle.

Figure 5.5 shows the recorded microinterferograms of the 32 samples of based fibres using the polarizing (Pluta) microscope. The measured values of birefringence were the average of the repeated measurements for each sample and could be related to Figure 5.5 (Table 5.3).Typical x-ray diffractometer traces showed five major crystalline diffraction peaks with different FWHM of an x-ray scattering profile observed around 16, 17.5, 20.5, 23 and 24.5 2θ° (Figure 5.6), it shows relative crystallographic order of fibres relating to the sharpness of the peaks and the area under the traces.

The peaks observed at 16, 20.5 and 24.5 2θ° are very wide and weak; the peaks at 17.5 and 23 2θ° are slightly sharper, more intense and smaller in width. The peak at 23 2θ° was fitted using DIFFRAC plus EVA software to compare the half-height widths. An increase in structure order is obtained in an increase in the peak intensity; a decrease in the peak width and a decrease in the background area. Conclusions were drawn about the relative crystallographic order within a series of the 32 samples (Table 5.3). The lower value of FWHM leads to the higher size of the crystallite and the higher degree of crystallographic order and vice versa, as mentioned previously. For measuring of drawability value of as-spun fibres at constant feeding speed roller, hot plate temperature and constant drawing speed, the speed of the draw roller was increased gradually until the yarn eventually broke. Then the current draw ratio was measured, which is the drawability value of the as-spun fibres (see chapter 3).

The thermo-graphic measurement shows the recorded results of the 32 samples of spun fibres using the ThermaCAM SC 3000 and ThermaCAM research program at L01=0 (die head or extrusion temperature), L02 = 25 mm, L03 =80 mm, L04=170 mm and L05=285 mm. The cooling ratio affects of the relative crystallographic order, it could be controlled by spinning temperature, and winding speed and air quench speed. The values of responses were averages of the repeated measurements for each sample represented by the order number in the first column in the designed matrix. Infrared (IR) images of filaments indicating five line temperature readings are shown in Figure 5.7, with the image colours corresponding to the temperature scale on the right of the image. The IR image illustrates the temperature variation along each line put on the thermo image to obtain the temperature profile scale along or across the studied object. It was found that

the temperature decreases and the speed increases with the increase of the distance from the spinneret. In Figure 5.8, temperature and trial number are plotted along a selected area of filaments using the profile function of a camera.

Depending on decreasing of the filament heating content, the trials could be divided to three groups: low (for trial numbers 1, 3, 4, 12, 13, 14, 26 and 27), high (for trial numbers 2, 5, 9, 10, 11, 17, 20 and 25) and medium (for the remaining trials) groups. By investigating the relationship between the thermo-graphic measurement results and the matrix design presented factors and their levels, it becomes clear that the combination between the higher throughput flow rate (or metering pump speed) and the high spinning (or extrusion) temperature in the filaments' extrusion will lead to a decrease in the filament heating content and vice versa. The combination of the higher throughput flow rate controlled by metering pump speed and the low melt-spinning temperature, or of the low throughput flow rate (metering pump speed) and the high spinning temperature in filaments extrusion leads to medium decreasing in the filament heating content. There are temperature variations in each group related to the effect of the other factors; the relationship between the factors and their interactions will be investigated later using a full factorial experimental design which will help to identify their effects on the cooling process variations in each group.

Further work could be done with air quench temperature variation, if applied. The air quench effect will be explained in detail in the statistical analysis of the results later, which will give a better insight into the relationship between melt spinning process parameters and LAAC fibre properties; a programme and plan for the production process will be created using forecasting statistical methods.

A broad range of melting temperature (100-135°C) was observed for the as-spun fibres(Figure 5.9). The relationship between drawing temperature and drawability (Figure 5.10) shows that the drawability decreases regularly with increasing drawing temperature as a result of the low glass transition temperature of AAC. In addition to the interaction between thermal and mechanical properties of the fibres, the fibres will break if they are heated under high drawing tension.

In terms of influence of the process parameters on the filament the surface microstructure and cross section, Figure 5.11 shows an SEM photomicrograph of the surface and cross-section of the fibres. Fibres have a uniform circular cross section with acceptable uniform surface as seen in Figure 5.11, which is in agreement with previous results.

Trial Number	Spin Draw Ratio	Birefringence *1000	Drawability	Die Head Pressure (dpi)	FWHM (^{o})	Filament Temperature Average (^{O}C)			
						L02	L03	L04	L05
1	13.4	10.0	5.7	1000	0.610	82.8	48.7	25.3	20.3
2	22.0	48.0	3.3	1300	0.577	51.7	26.4	20.2	19.3
3	28.6	24.0	4.2	1100	0.631	80.4	46.9	25.4	18.4
4	26.4	19.0	4.3	1150	0.616	80.4	46.9	25.4	18.4
5	42.9	36.0	2.9	1300	0.485	49.1	24.7	20.4	18.4
6	13.2	12.0	5.8	1600	0.593	68.4	41.9	26.1	20.6
7	25.4	19.0	4.4	700	0.633	72.6	37.5	22.1	15.6
8	23.8	10.0	5.7	750	0.643	67.0	35.2	18.7	16.3
9	45.2	41.0	2.9	900	0.627	54.7	27.3	19.8	17.6
10	21.8	44.0	3.9	1200	0.499	51.7	26.4	20.2	19.3
11	45.8	35.0	2.9	900	0.523	54.7	27.3	19.8	17.6
12	14.1	9.0	6.0	1000	0.592	82.8	48.7	25.3	20.3
13	27.7	30.0	4.4	1150	0.658	85.4	50.0	29.2	21.2
14	13.7	6.0	6.5	1000	0.581	87.8	54.0	29.6	19.9
15	24.5	26.0	3.9	1600	0.643	62.7	39.1	27.0	20.8
16	12.9	14.0	5.1	1500	0.630	65.8	39.9	25.2	21.2
17	44.8	34.0	2.9	1100	0.539	49.1	24.7	20.4	18.4
18	12.9	12.0	5.1	1600	0.600	65.8	39.9	25.2	21.2
19	45.5	44.0	2.9	700	0.630	66.5	36.6	20.5	14.6
20	22.7	22.0	3.8	1200	0.582	54.4	30.2	22.0	15.9
21	22.8	28.0	4.4	750	0.636	67.0	35.2	18.7	16.3
22	49.0	56.0	2.9	750	0.603	66.5	36.6	20.5	14.6
23	23.6	26.0	4.0	1450	0.559	62.7	39.1	27.0	20.8
24	25.9	23.0	3.9	1100	0.632	68.8	40.9	26.3	19.2
25	22.5	14.0	3.7	1200	0.644	54.4	30.2	22.0	15.9
26	26.2	16.0	4.4	1100	0.629	85.4	50.0	29.2	21.2
27	14.4	12.0	6.2	1000	0.631	87.8	54.0	29.6	19.9
28	49.6	47.0	3.0	750	0.530	68.0	39.4	25.1	15.2
29	12.9	27.0	5.1	1600	0.585	68.4	41.9	26.1	20.6
30	44.7	44.0	3.0	750	0.358	68.0	39.4	25.1	15.2
31	24.6	16.0	3.9	1300	0.551	68.8	40.9	26.3	19.2
32	25.9	17.0	4.2	700	0.457	72.6	37.5	22.1	15.6

Table 5.3. Response data of spin draw ratio, birefringence, drawability, die head pressure, full-width half-maximum FWHM and filament' temperature average (at L02, L03, L04 and L05) for the experiment of spinning of LAAC

Trial Number	Count denier	Tenacity g/den	Elongation at break %	Modulus g/den	Diameter µm	Thermal shrinkage %
1	3079.5	0.351	910	0.181	109.2	-0.50
2	1878.6	0.285	600	0.163	85.3	-0.25
3	1445.7	0.422	605	0.194	74.8	-1.00
4	1569.3	0.405	640	0.192	77.9	-1.20
5	963.9	0.358	420	0.273	61.1	-0.83
6	3133.5	0.32	900	0.196	110.1	+0.17
7	1630.8	0.38	766	0.182	79.4	-1.00
8	1738.8	0.42	700	0.189	82.0	-0.75
9	915.9	0.338	390	0.227	59.5	-0.58
10	1900.8	0.284	572	0.176	85.8	+0.00
11	904.2	0.327	380	0.237	59.1	+0.33
12	2928.9	0.369	876	0.178	106.5	+0.00
13	1493.4	0.415	728	0.210	76.0	-1.25
14	3030.3	0.371	976	0.181	108.3	-0.15
15	1691.4	0.34	570	0.197	80.9	+0.00
16	3219	0.318	860	0.163	111.6	-0.25
17	923.7	0.347	386	0.301	59.8	-0.25
18	3198.6	0.331	924	0.176	111.2	+0.57
19	909.6	0.649	390	0.244	59.3	-1.58
20	1819.2	0.29	594	0.236	83.9	+0.00
21	1813.5	0.391	668	0.158	83.8	-1.00
22	845.1	0.651	460	0.277	57.2	-2.17
23	1753.2	0.308	556	0.223	82.4	+0.00
24	1597.2	0.334	662	0.224	78.6	-0.17
25	1842.3	0.301	638	0.221	84.4	0.00
26	1581.6	0.392	706	0.179	78.2	-0.83
27	2872.8	0.369	970	0.176	105.4	-0.17
28	834.9	0.623	412	0.231	56.8	-2.17
29	3204	0.321	964	0.163	111.3	+1.00
30	926.1	0.486	673	0.228	59.9	-2.17
31	1683.3	0.33	630	0.221	80.7	+0.00
32	1596	0.397	670	0.182	78.6	-1.42

Table 5.4. Response data of diameter, tenacity, elongation at break, modulus and thermal shrinkage for the experiment of spinning of LAAC

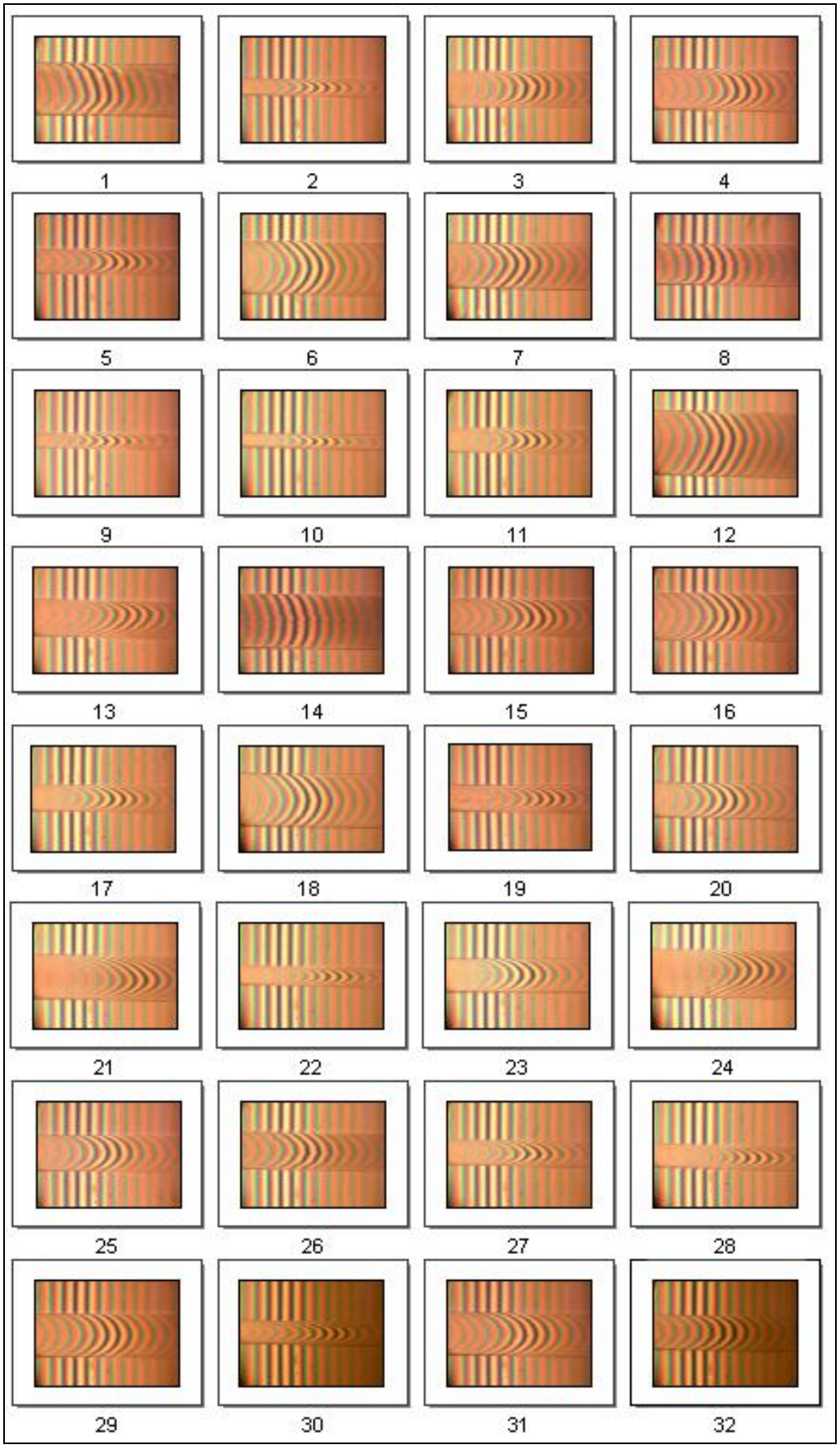

Figure 5.5. The microinterferograms of LAAC fibres using Pluta microscope

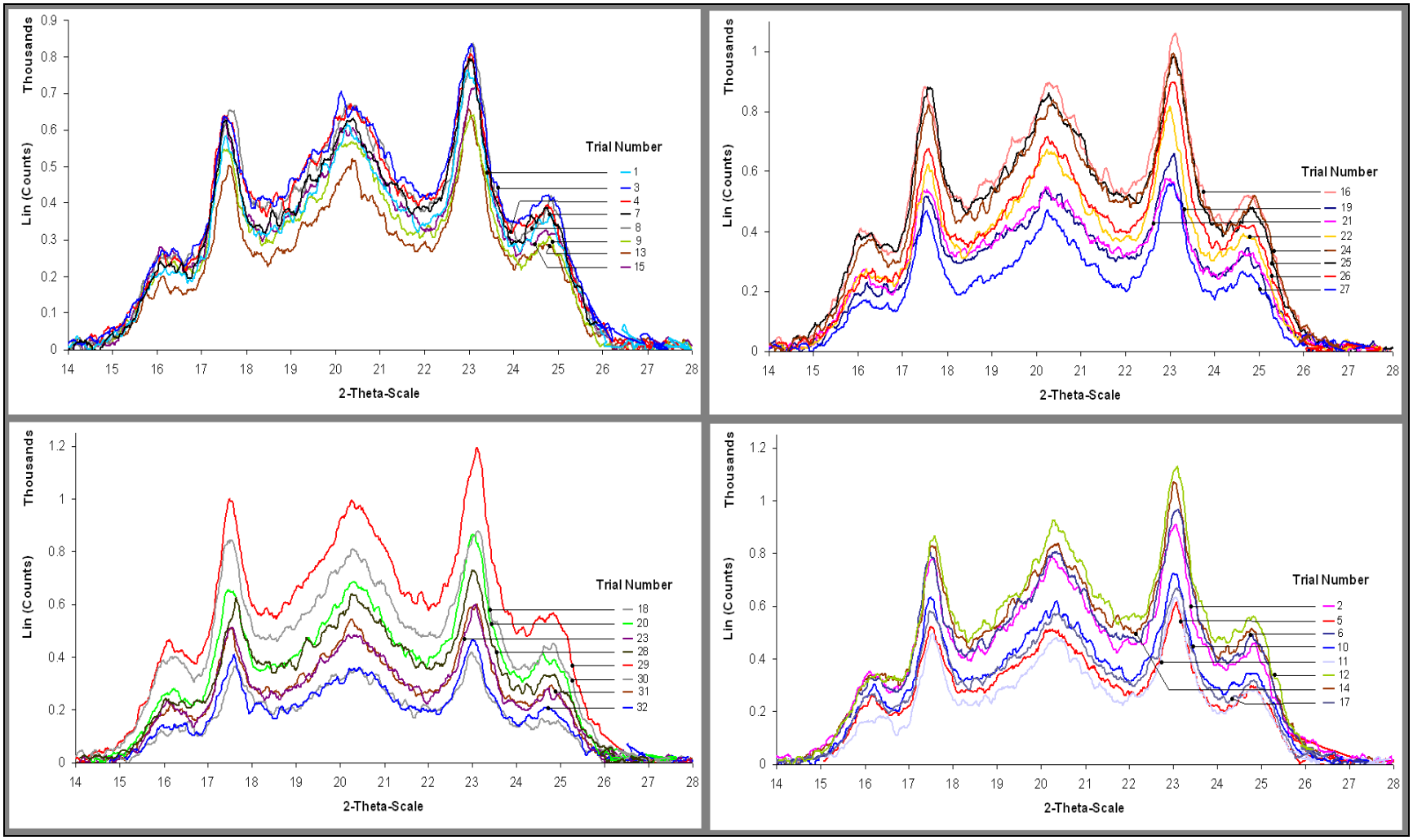

Figure 5.6. WAXS traces of 32 trials for LAAC fibres

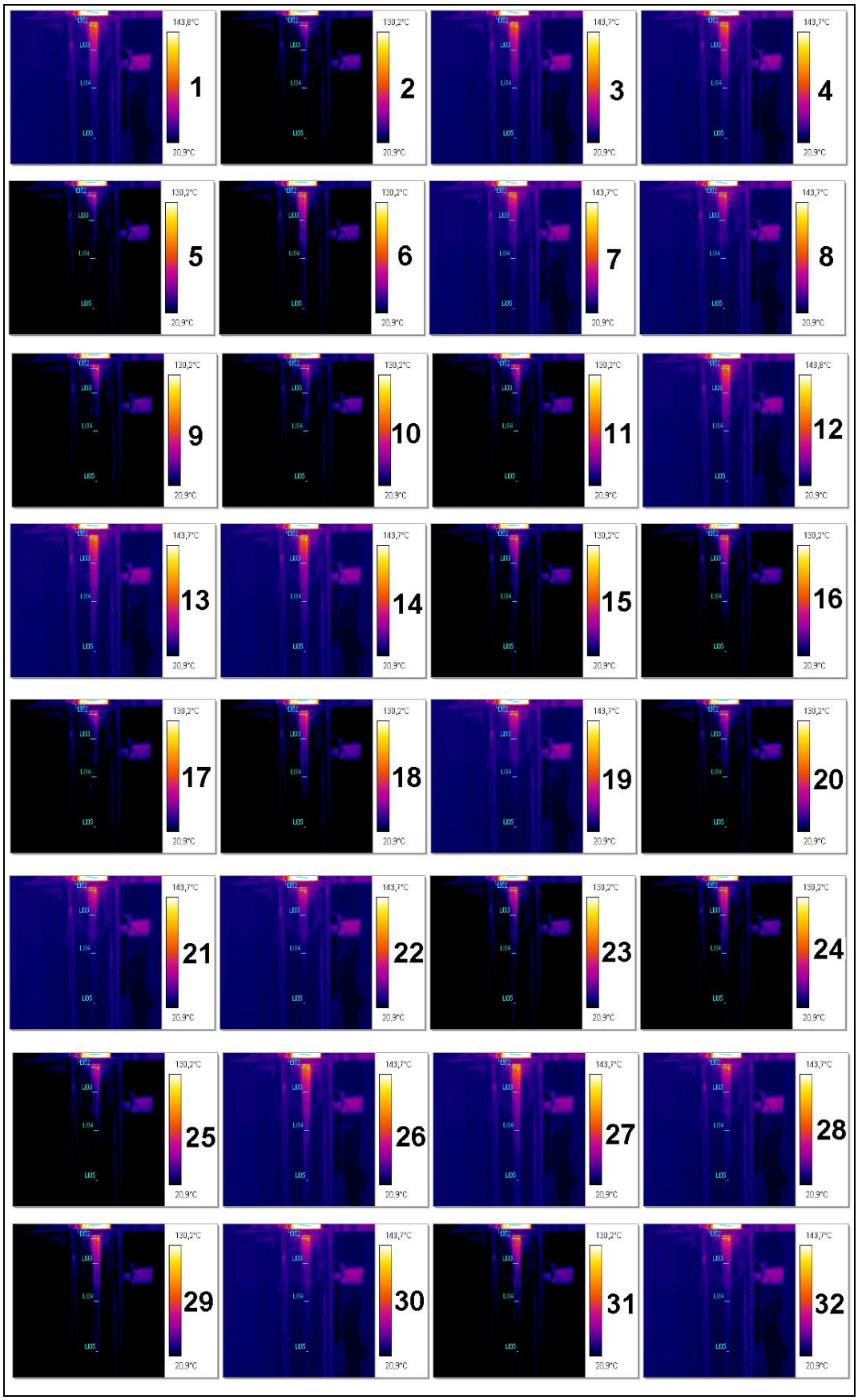

Figure 5.7. IR images of LAAC filaments indicating five line temperature readings.

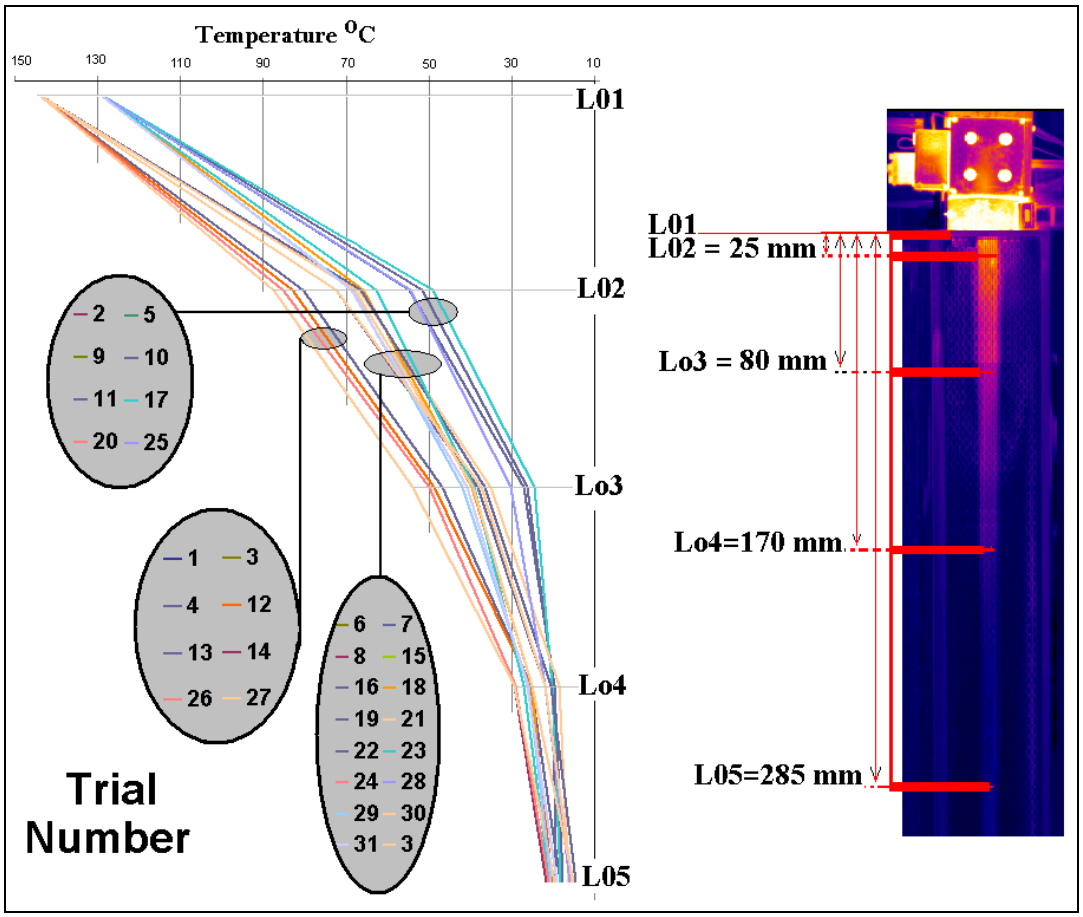

Figure 5.8. Temperature vs. trial number plot along the selected area of LAAC filaments.

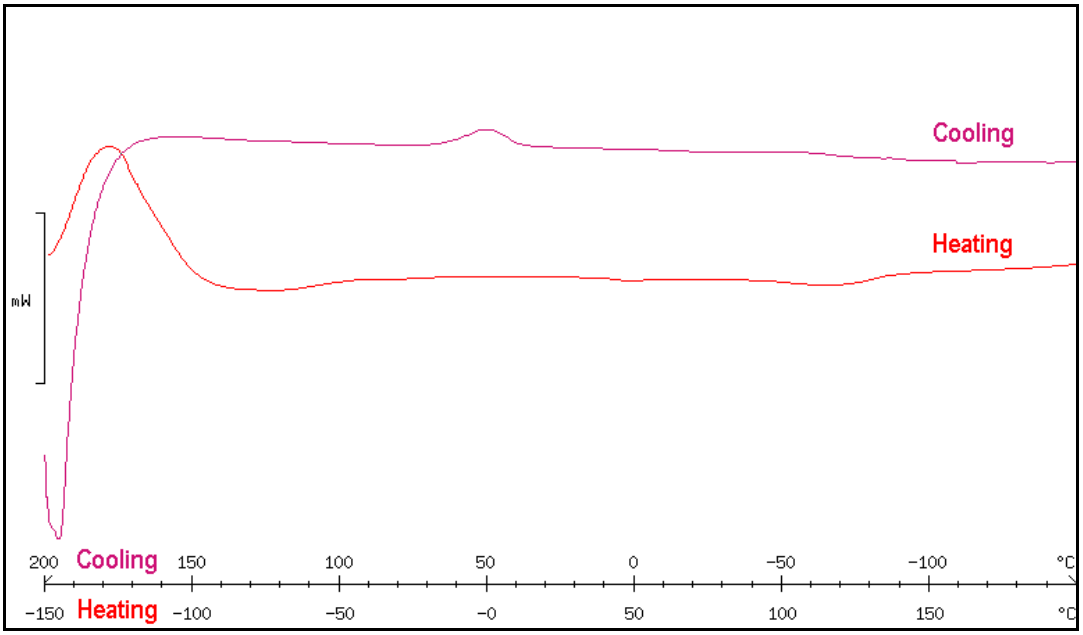

Figure 5.9. DSC curves show the heating and the cooling diagrams of LAAC fibres produced

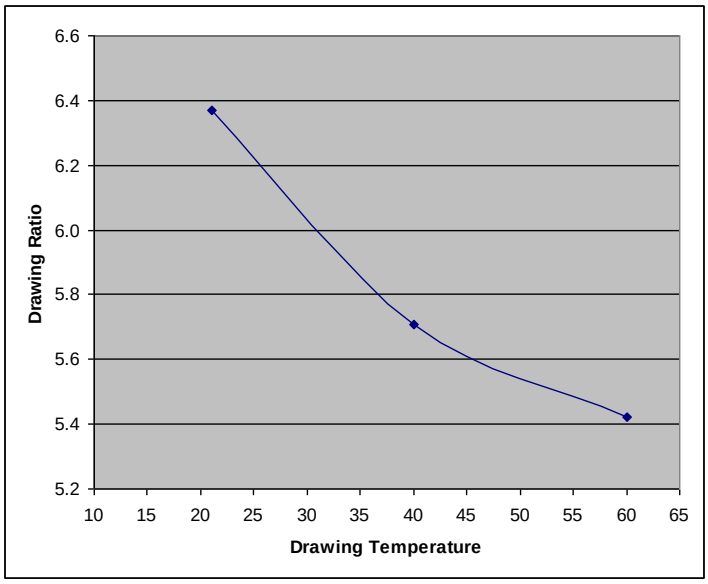

Figure 5.10. The relationship between drawing temperature and draw ratio

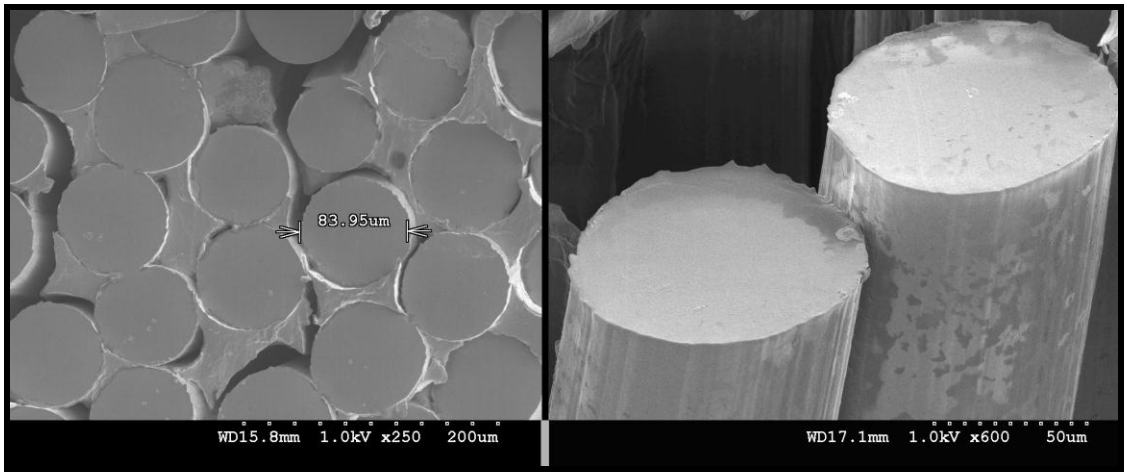

Figure 5.11. SEM Photo of the surface and cross section of the LAAC fibres

5.5 Statistical Analysis and Discussion of LAAC Fibres

5.5.1 Spin Draw Ratio, Overall Orientation and Drawability

According to the spin draw ratio, overall orientation and drawability characterization (described in Chapter 3), as-spun fibres should have a structure that can be drawn easily and be conducive to form a good chain orientation along the fibre axis. The structural changes involve alignment of molecular chain and crystallinity along the fibre axis and an increase in the degree of the crystallographic order. Crystallinity and orientation affect strength,

elongation at break, moisture absorption, absorption resistance and dye-ability; high orientation reduces molecular mobility and the dye-ability depending on the process parameters used and the polymer properties [168]. Over-orientation increases with shear rate associated with a small spinneret orifice size and high l/d ratio, resulting in an increase in fibre strength and reduction in elongation at break.

The Pareto charts (Figure 5.12) for the spin draw ratio (a), birefringence (b) and drawability (c) show the arrangement of the factors and their interactions in decreasing order, depending on the effect. The Pareto chart for spin draw ratio (SDR) clearly shows that metering pump speed and winding speed are the most important factors affecting the spin draw ratio, followed by their interaction, extrusion temperature and the other factors and interactions. High spinning temperature allows the chains to be flexible for longer time than lower temperature, as a result high spinning temperature interacts with the winding speed; the variation between the extrusion speed (metering pump speed) and the winding speed causes notable effect on the dawn draw ratio.

The Pareto chart for birefringence shows that metering pump speed and winding speed are the most important factors affecting the overall orientation, followed by the interaction between the extrusion temperature and the winding speed and the other factors and interactions. The Pareto chart for drawability shows that winding speed, metering pump speed and extrusion temperature are the most important factors affecting the drawability, followed by the interaction between the extrusion temperature and the winding speed and then the other factors and interactions. There is a clear relationship between spin draw ratio and the improvement of the overall orientation of the fibres; it has a significant effect on the drawability. In other words, the increasing in spin draw ratio increases the overall orientation of the fibres and decreases the drawability ratio. Temperature has a significant effect on the spin draw ratio and drawability which affects the flow rate and tension value.

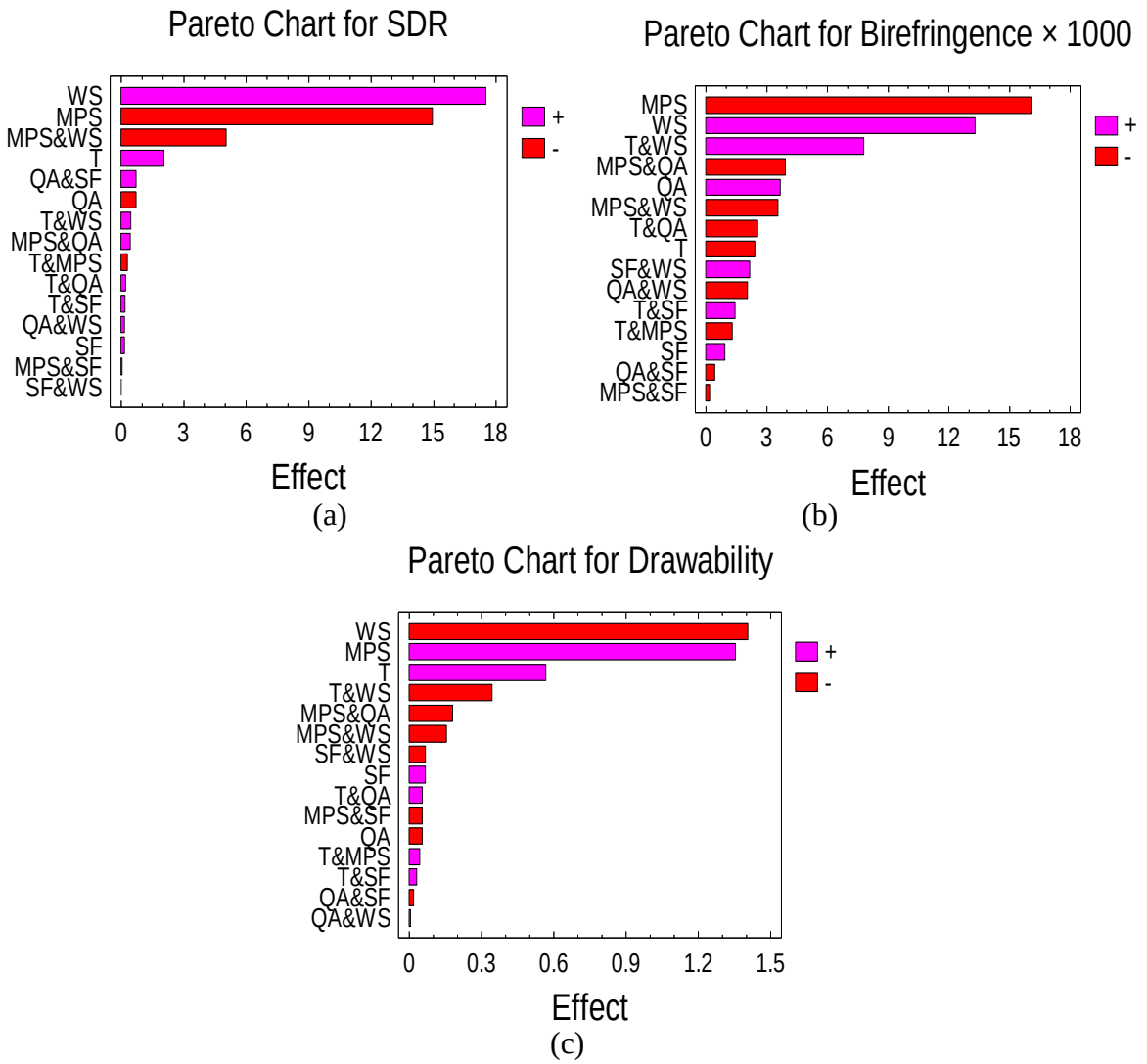

Figure 5.12. A ranked list of significant arrangement effects and interactions (Pareto charts) for the spin draw ratio (a), birefringence (b) and drawability (c)

Figure 5.13 and Figure 5.14 show the effect plots of statistical analysis of the effects caused by the main factors and their interactions on the spin draw ratio, birefringence and drawability of as-spun fibres obtained using the design matrix. The statistical analysis of the effects caused by the main factors effect and their interactions on SDR shows that, for the main effect plots the effects from the extrusion temperature, the flow rate represented as metering pump speed and the take-up speed are significant; quench air speed and spin finish speed applicator show no significant effect (Figure 5.13 (a)). No significant interactions can be detected apart from the interaction between metering pump speed and winding speed (Figure 5.14 (a)).

Birefringence is strongly affected by winding speed and metering pump speed. No significant effect has been reported for other factors (Figure 5.13 (b)). Birefringence is affected by the interaction between extrusion temperature and winding speed and no significant effect has been reported for other interactions (Figure 5.14 (b)). The degree of drawability (Figure 5.13) is affected by the extrusion temperature, metering pump speed and winding speed (c). In Figure 5.14 (c), a significant interaction is demonstrated between extrusion temperature and winding speed related to the viscosity and flowing rate relationship inside the die head as a result of the heating effect on the flowing and the stretching of the filaments.

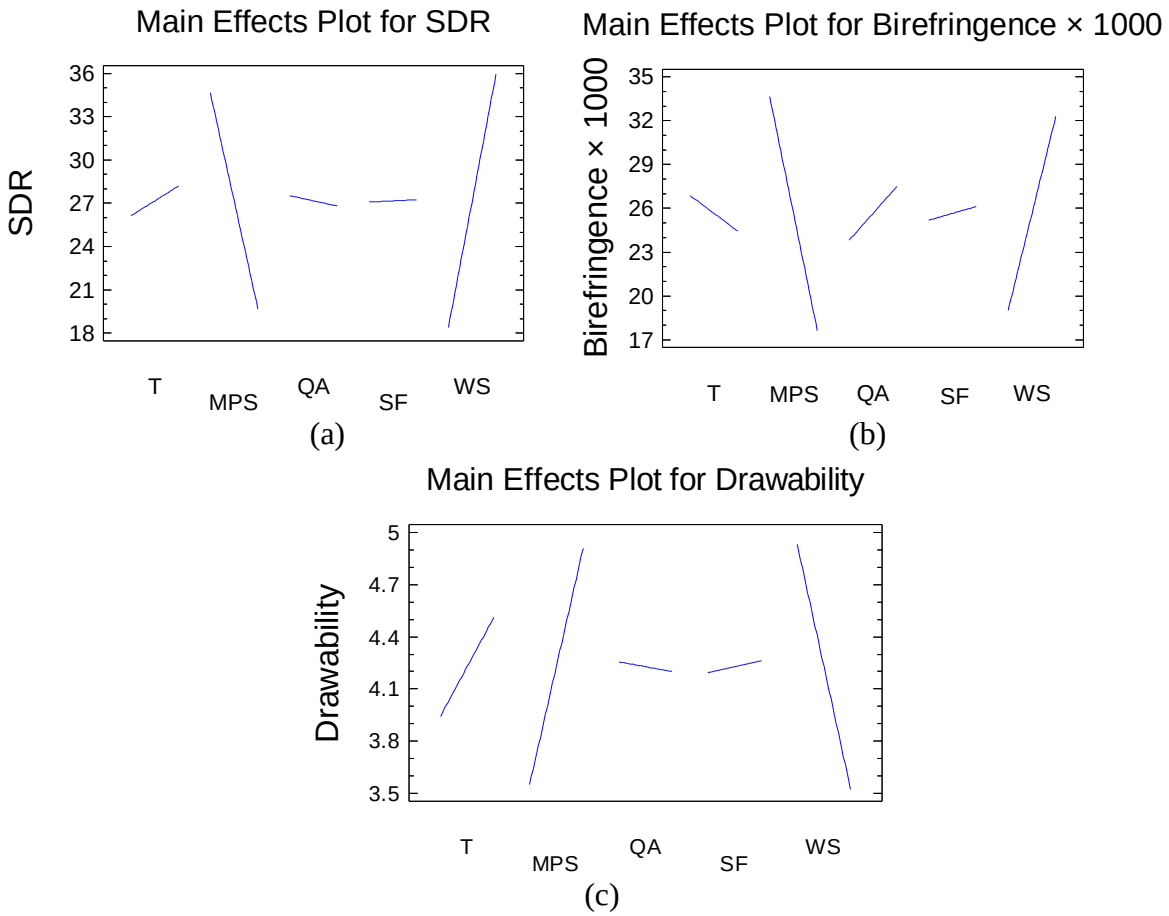

Figure 5.13. Effect plots for the spin draw ratio (a), birefringence (b) and drawability (c)

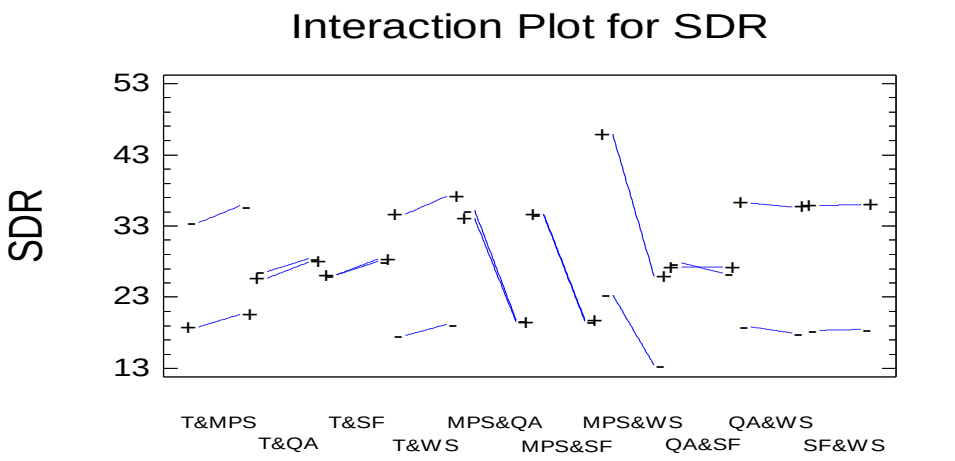

(a)

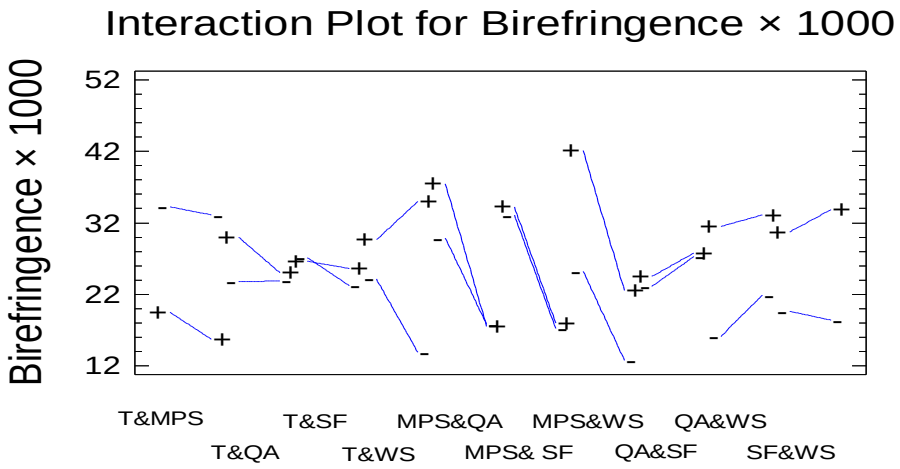

(b)

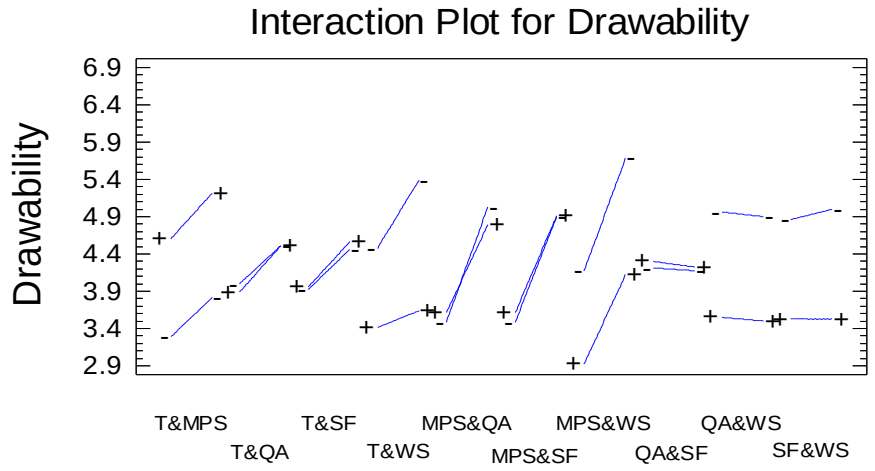

(c)

Figure 5.14. The interaction plots for the spin draw ratio (a), birefringence (b) and drawability (c)

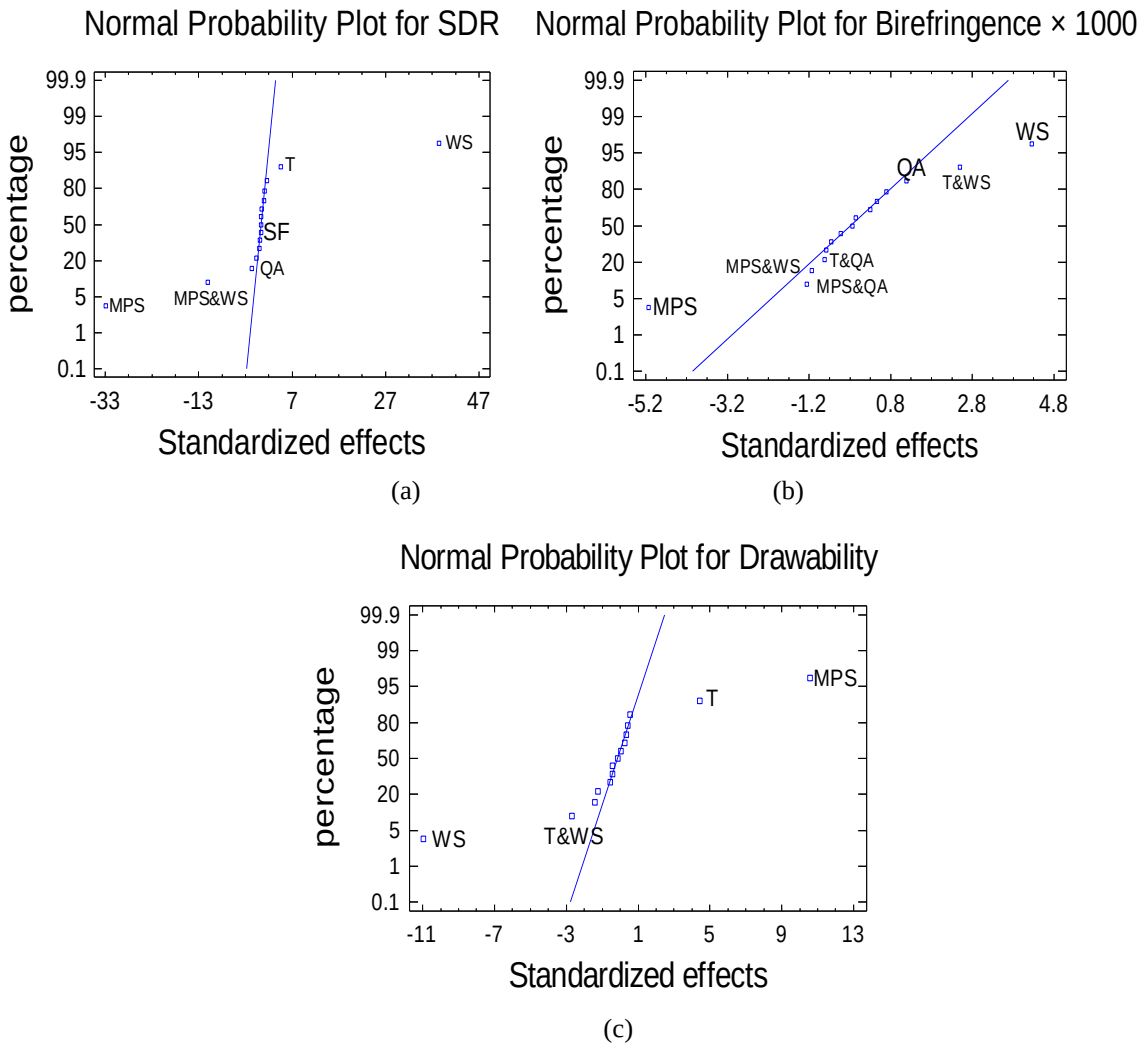

Figure 5.15. Normal probability plots for the spin draw ratio (a), birefringence (b) and drawability (c)

As an alternative plot of effects, Figure 5.15 displays the normal probability plots with the percentage and standardized effects. From the normal probability plot for SDR (Figure 5.15 (a)), it is noted that the negative effect from metering pump speed and the interaction MPS&WS and the positive effect from WS are prominent. Birefringence (Figure 5.15 (b)) is affected negatively by metering pump speed and positively by winding speed. In the interaction between T&WS, a small effect of the interactions MPS&QA (negatively), MPS&WS (positively) and T&QA (negatively) was observed; this will be investigated later using ANOVA. When the drawability is described (Figure 5.15 (c)), the positive effect of MPS and the negative effect of winding speed, extrusion temperature and the interaction T&WS are notable. Temperature plays an important role in controlling the fibre structure as well as affecting the drawability.

5.5.1.1 Analysis of Variance (ANOVA)

In order to determine the factor effects in terms of statistical significance, analysis of variance (ANOVA) of the data was conducted. F-ratio is a statistic in ANOVA; the factor has significant effect if the ratio is much larger than the circuital value (F= 4.49 at the appropriate level α =0.05); or has P-value smaller than 0.05. ANOVA results from the experiments are listed in Table 5.5. The spin draw ratio is significantly affected by winding speed (P_{WS} 0.000) > metering pump speed (P_{MPS} = 0.000) > extrusion temperature (P_T = 0.000) and the interactions WS&MPS ($P_{WS\&MPS}$ = 0.000). There are no significant effects of the other factors and interactions. Note that even when P_{MPS} = P_{WS} = P_T = 0.000, the order of the significance is obtained depending on F-Ratio listed. Birefringence is significantly affected by metering pump speed (P_{MPS} = 0.000), winding speed (P_{WS} 0.000) and the interaction T&WS ($P_{T\&WS}$ = 0.024). The achieved model is formulated to describe the melt spinning of LAAC within the low range of take-up velocities (50-100 m/min), while synthetic fibres' formation with high take-up speed leads to uniaxial orientation of chain segments and orientation-controlled crystallization [118]. There are no significant effects of the other factors and interactions on birefringence. In the drawability analysis, the significance of factors are then winding speed (P_{WS} 0.000)> metering pump speed (P_{MPS} = 0.000)> extrusion temperature (P_T = 0.000) while there is no significant effect due to other factors. Because the interaction T&WS has a P-value (0.016) which is lower than 0.05, the interaction between extrusion temperature and winding speed is significant. There are no significant effects for the other interactions.

The quantitative ANOVA results are consistent with quantitative conclusions derived from the effects plots and Daniel's plots. According to the previous analyses, the most effective and significant parameters are the extrusion temperature (T), the metering pump speed (MPS) and the winding speed (WS). Metering pump speed plays an interactive role with winding speed; that relationship orients the fibre chains and adds different spin draw ratio which has an effect on drawability later.

Source	SDR		Birefringence *1000		Drawability	
	F	P	F	P	F	P
T	20.5	0.000	0.6	0.447	19.7	0.000
MPS	1078.1	0.000	26.4	0.000	112.1	0.000
QA	2.4	0.138	1.4	0.256	0.2	0.666
SF	0.1	0.726	0.1	0.768	0.3	0.599
WS	1481.1	0.000	18.1	0.001	120.5	0.000
T &MPS	0.5	0.503	0.2	0.681	0.1	0.737
T & QA	0.2	0.647	0.7	0.425	0.2	0.666
T& SF	0.2	0.686	0.2	0.652	0.1	0.810
T& WS	1.1	0.301	6.2	0.024	7.2	0.016
MPS& QA	0.9	0.351	1.6	0.226	2.0	0.176
MPS& SF	0.0	0.893	0.0	0.953	0.2	0.666
MPS& WS	122.2	0.000	1.3	0.272	1.5	0.240
QA & SF	2.6	0.125	0.0	0.891	0.0	0.885
QA & WS	0.1	0.726	0.4	0.519	0.0	0.962
SF& WS	0.0	0.979	0.5	0.495	0.3	0.599

Table 5.5. ANOVA Results identifying the statistical significance of factor effects on the spin draw ratio, birefringence and drawability

5.5.1.2 The Regression Equation and Estimation Results

Based on the analysis, the simplified models were fitted by the regression equations below which were fitted to the experimental data. The regression equations forecast the fibre properties in order to achieve the most satisfactory properties in the final desired fibre for different applications. The regression equations in terms of the previous coded values (Table 5.1) are given as follows:

Spin draw ratio = 26.4583 - 0.0486111*T + 0.507639*MPS - 0.705833*QA - 51.1944*SF + 0.454417*WS - 0.00694444*T*MPS + 0.00188889*T*QA + 0.166667*T*SF + 0.0013*T*WS + 0.00972222*MPS*QA + 0.138889*MPS*SF - 0.0335833*MPS*WS + 0.655556*QA*SF + 0.000433333*QA*WS + 0.00333333*SF*WS (5.1)

Birefringence (×1000) = 102.278 - 1.0375*T + 7.01042*MPS + 4.74306*QA - 192.917*SF - 2.39875*WS - 0.0291667*T*MPS - 0.0227778*T*QA + 1.27778*T*SF + 0.0208333*T*WS - 0.0875*MPS*QA - 0.416667*MPS*SF - 0.02375*MPS*WS - 0.388889*QA*SF - 0.0055*QA*WS + 0.583333*SF*WS (5.2)

Drawability = -8.20486 + 0.0648611*T + 0.394792*MPS - 0.0304167*QA - 0.152778*SF + 0.114375*WS + 0.000972222*T*MPS + 0.0005*T*QA + 0.0277778*T*SF - 0.000916667*T*WS - 0.00402778*MPS*QA - 0.125*MPS*SF - 0.00104167*MPS*WS - 0.0166667*QA*SF + 0.0000166667*QA*WS - 0.0183333*SF*WS (5.3)

For the measured and fitted results generated for each trial (Figure 5.16), the models gave useful results for the birefringence (a), spin draw ratio (b) and drawability (c). Their Model Standard Error (MSE) values listed in Table 5.10 indicate the dispersion of predicted and observed values around the theoretical fitted line generated using the fitted model for each trial.

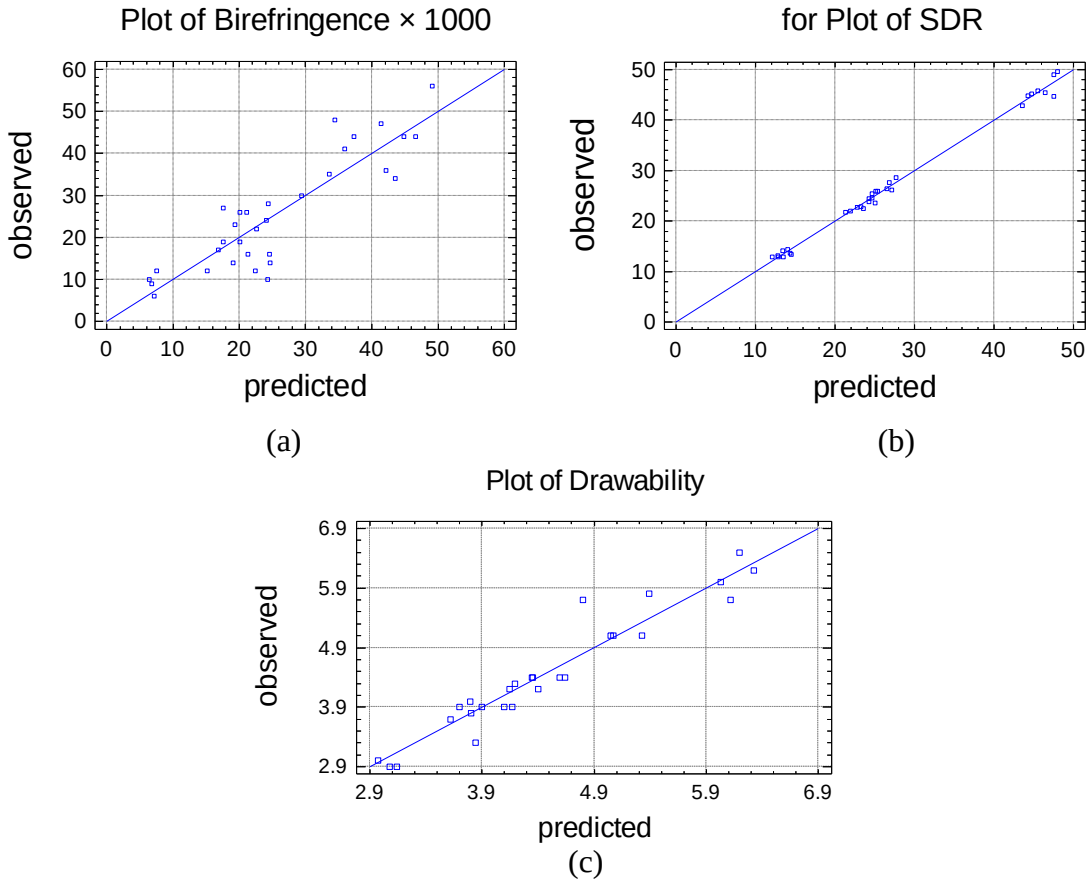

Figure 5.16. Experimental observed results and calculated fitted results plot for the birefringence (a), spin draw ratio (b) and drawability (c)

To determine the direction of the significant interactions, the estimated response surfaces are shown in Figure 5.17. Because of the twist found in the 3D surface response diagrams MPS& WS, the detected effect is found to be significant and confirmed the last analysis of the results. The twist in the surface in other plots (Figure 5.17, a and b) confirms the interaction effect as mentioned previously in the previous statistical analysis results. Those interactions

will affect the structure of as-spun fibres and help to extend the chains to obtain high orientation along the fibre axis.

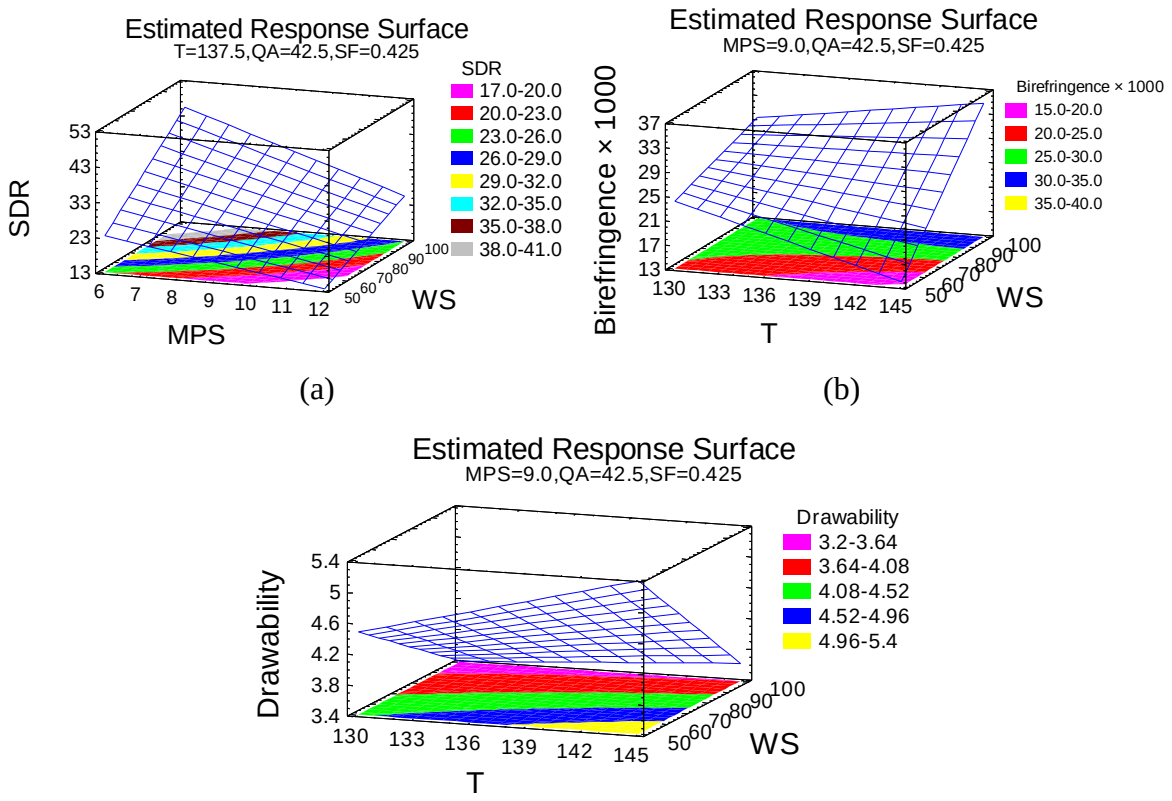

Figure 5.17. Estimated response surface for the spin draw ratio (a), birefringence (b) and drawability (c)

The cube plots is fast forecasting tool for technical fields, plots in Figure 5.18 show the cube plots for the spin draw ratio (a), birefringence (b) and drawability (c). Each value in the cube plot corresponds to the values of the experimental factors WS, T and MPS at the middle levels of QA of 42.5 and SF of 0.425 and depending on the regression equation.

In conclusion, the interaction found between extrusion temperature and winding speed is related to the viscosity and flowing rate relationship inside the die head. Because extrusion temperature affects the flow rate and tension value in the spinline, it has a significant effect on the spin draw ratio and drawability. Metering pump speed plays an interactive role with winding speed as the relationship between the output of the machine and the collection at different speeds.

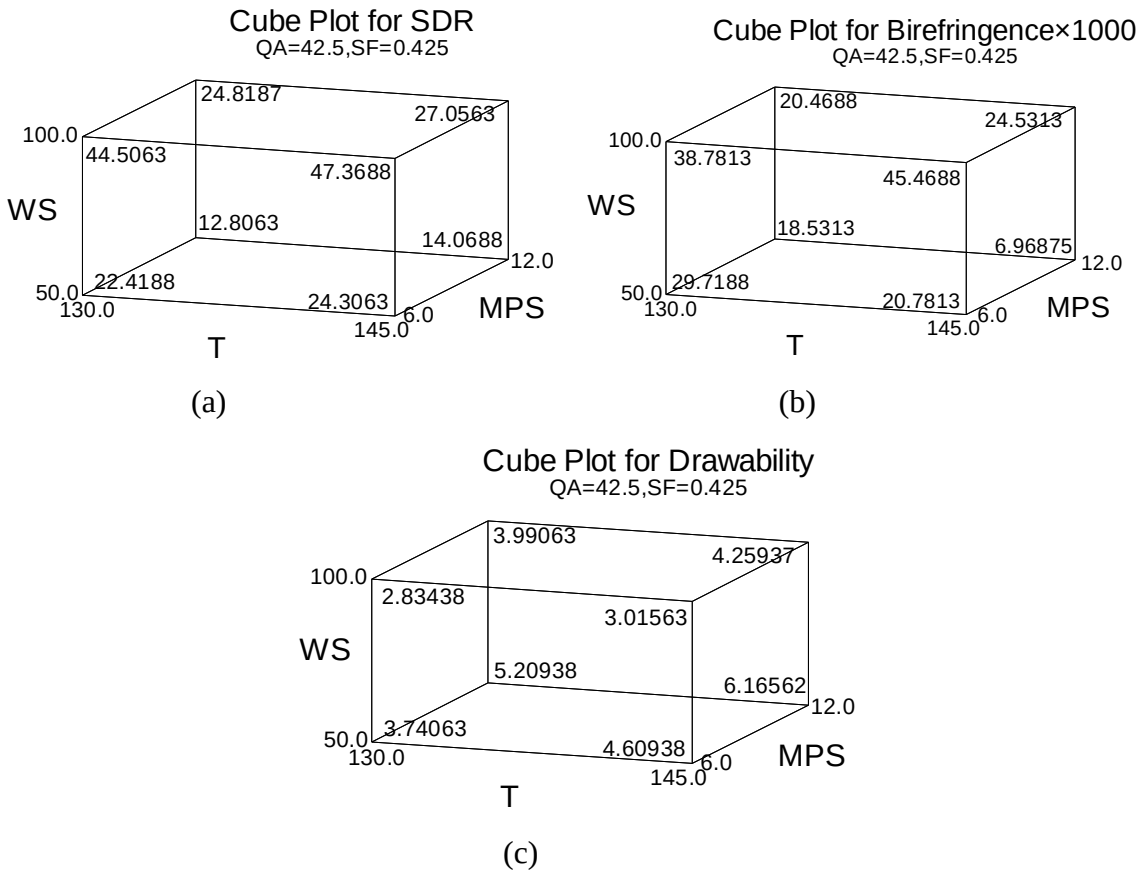

Figure 5.18. Cube plots of the estimated effects for the spin draw ratio (a), birefringence (b) and drawability (c)

5.5.2 Die Head Pressure, Crystallographic Order and Thermo-Graphic Measurement

Die head pressure, crystallographic order and thermo-graphic measurement analyses explain the relationship between the fibre cooling ratio affected by process conditions and the crystallographic structure of the fibres and also identify any interactions which may exist between flow ratios and die head pressure. There are inertial, gravitational and air filament drag forces which affect the filament flow in the non-isothermal process [140]. Crystallization is a mechanism of phase change in polymeric materials; the crystalline phase has a higher orientation degree than does the amorphous. The structural changes involve alignment of crystals and molecular chains along the fibre axis and an increase in the degree of the crystallographic order [159]. This analysis was applied to establish the degree of crystallographic order as a function of the processing parameters as their interactions. Some researchers have studied the simulation of the fibre spinning process through the quench air

flow and the spinneret to show the filament behaviour along the spinning line and the relationship with the quench air flowing around it [217]. Fibres are also affected by high extrusion speed at which the shear rate affects the morphological structure [112]. Others have reported a notable difference of the air temperature before and behind some filaments [159]. As the fibre's properties depend on the micro and the crystallographic structure improving the fibre's properties, the target is to demonstrate how variation in spinning conditions could lead to the formation of crystalline, monoclinic or paracrystalline structures and their relationship with thermo-graph measurement.

The Pareto charts (Figure 5.19) for die head pressure (a), FWHM (b), filaments' temperature average at L03 (c) and filaments' temperature average at L04 (d) show the significant arrangement of factors and their interactions in decreasing order (y-axis) depending on the significant effect (x-axis). The Pareto chart for die head pressure confirms that extrusion temperature, metering pump speed and quench air speed are the most important factors affecting the die head pressure, followed by the interactions T&QA, MPS&QA and T&MPS. The Pareto chart for FWHM shows that metering pump speed and the interaction T&QA are the most important factors affecting the FWHM, followed by the interactions MPS&WS and SF&WS, quench air speed, winding speed and other factors and interactions. The Pareto chart for filaments' temperature average at L03 shows that metering pump speed, extrusion temperature and quench air speed are the most important factors affecting the filaments' temperature average at L03, followed by winding speed, the interactions MPS&WS, T&WS, T&QA and other factors and interactions. The Pareto chart for filaments' temperature average at L04 shows that, as the filaments leave the spinneret, the effect of the spinning or extrusion temperature (T) on the fibre temperature decreases, while the effect of the quench air speed increases. This is noted from the factors' significant arrangement which is metering pump speed, quench air speed, extrusion temperature, winding speed, the interactions T&QA, T&WS and QA&WS and other factors and interactions.

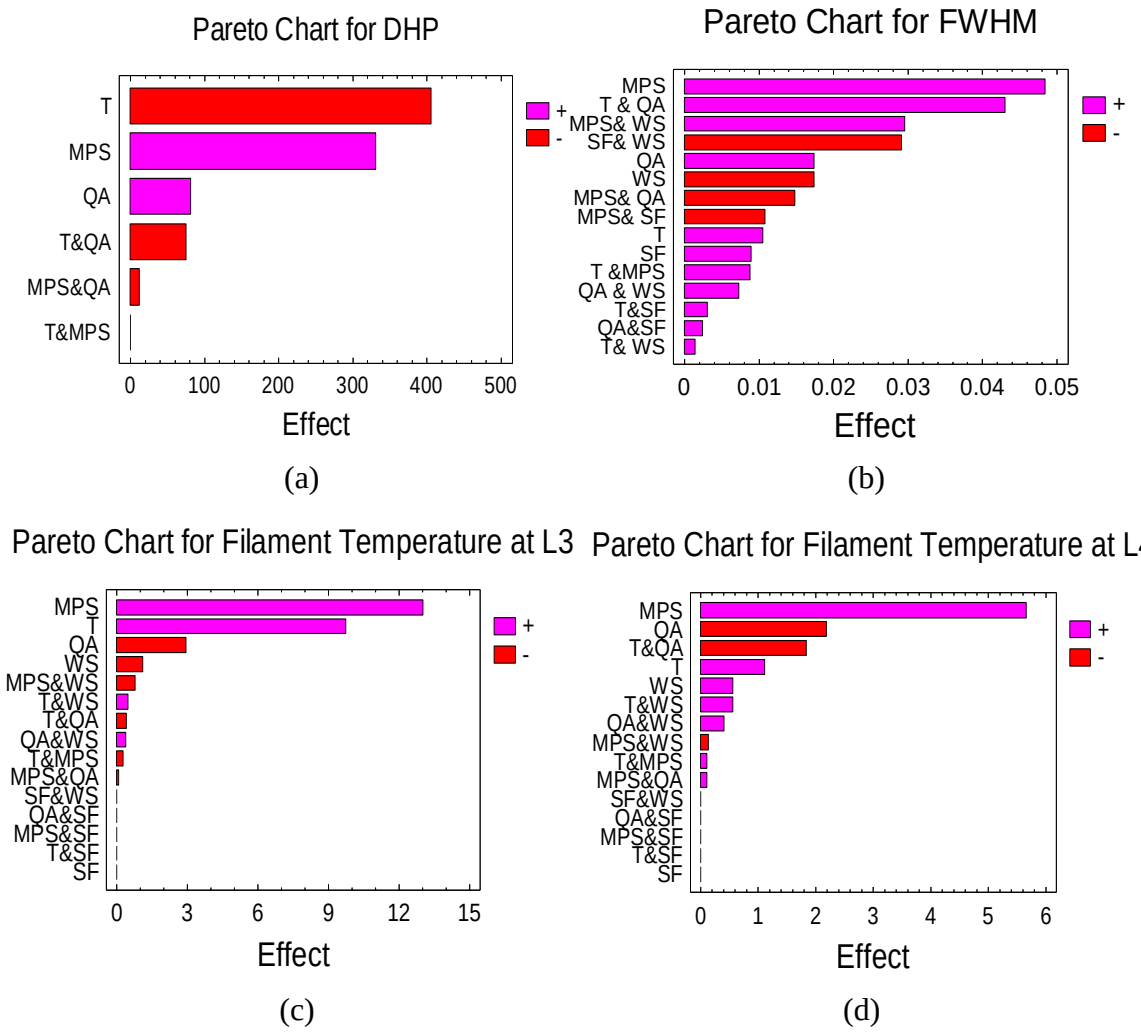

Figure 5.19. A ranked list of significant arrangement effects and interactions (Pareto chart) for die head pressure (a), FWHM (b), filament' temperature average at L03(c) and filament' temperature average at L04 (d).

Figure 5.20 and Figure 5.21 shows the effect plots of statistical analysis of the effects caused by the main factors and their interactions on the die head pressure, FWHM, filaments' temperature average at L03 and filaments' temperature average at L04 of as-spun fibres obtained using the design matrix.

Statistical analysis of the effects caused by the main factors effect (Figure 5.20, a) and their interactions (Figure 5.21, a) on die head pressure shows that, for the main effect plots, the effects from the temperature T and the flow rate represented as metering pump speed are significant. Quench air speed and the factor interactions show no significant effect, except for small noted interactions which can be detected between extrusion temperature and quench air speed.

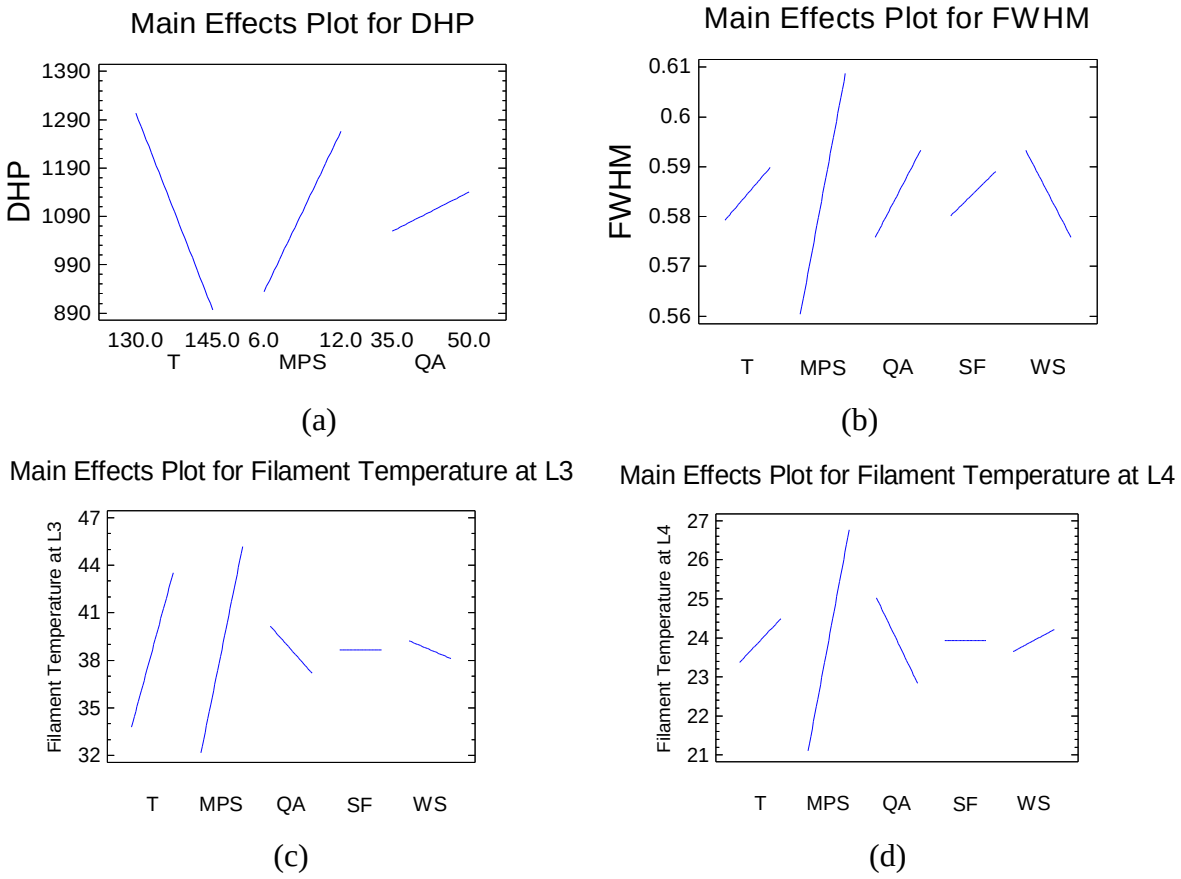

Figure 5.20. The effect and interaction plots die head pressure (a), FWHM (b), filament' temperature average at L03 (c) and filament' temperature average at L04 (d).

The main factors' effects (Figure 5.20, b) and their interactions (Figure 5.21, b) for FWHM are strongly affected by metering pump speed and the interaction between extrusion temperature and quench air speed which are on the borderline of significance. There is no significant effect identified for other factors. The interactions MPS&WS and SF&WS need to be further investigated; there is no significant effect reported for other interactions. The filaments' temperature average at L03 (Figure 5.20, c) was affected by metering pump speed, extrusion temperature, quench air speed and winding speed.

The viscosity was affected by die head pressure, die head temperature and the molten polymer flow ratio (described as metering pump speed). The relationship between the output of the machine and the collection at different speeds affects the throughput flow rate and the spin draw ratio of the filaments. The filament diameter decreases by increasing spin draw ratio, then the filament heating content is affected.

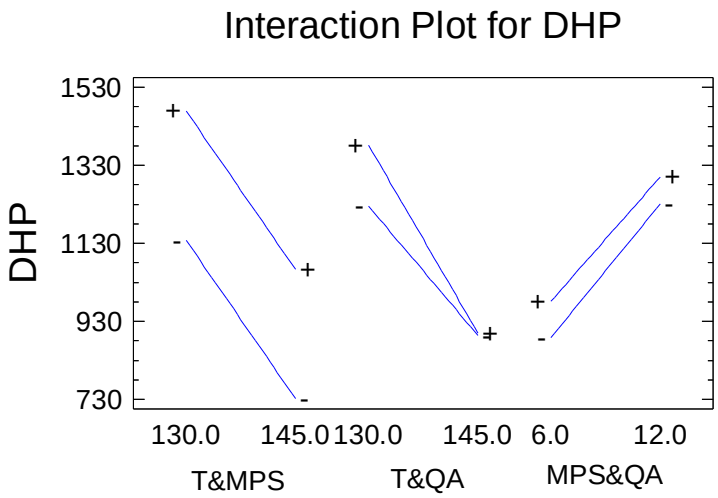

(a)

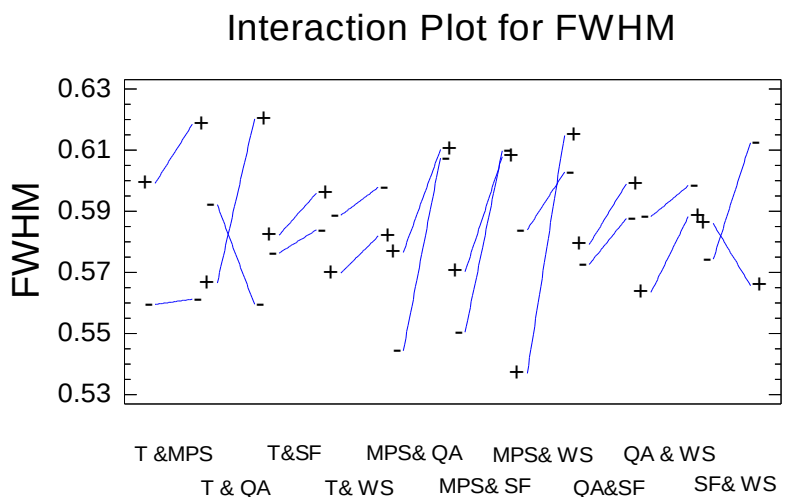

(b)

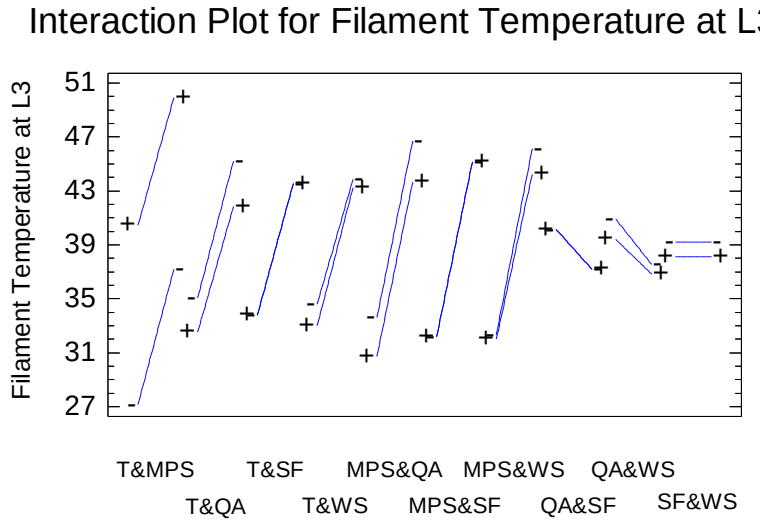

(b)

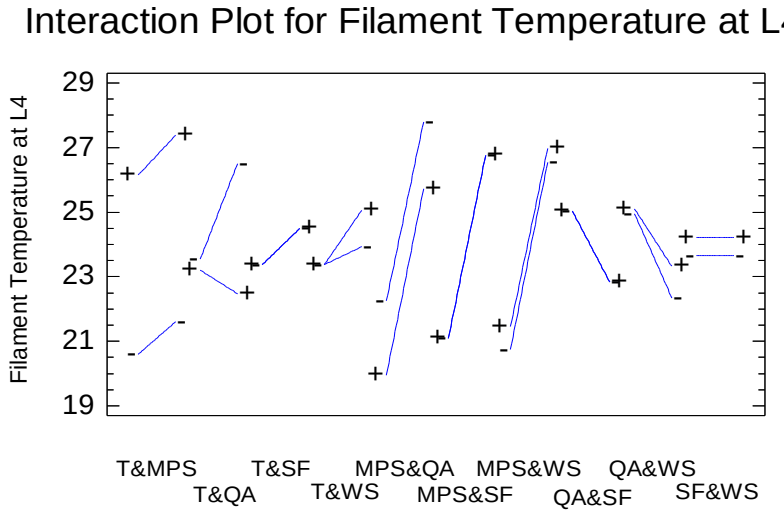

(d)

Figure 5.21. The effect and interaction plots die head pressure (a), FWHM (b), filament' temperature average at L03 (c) and filament' temperature average at L04 (d).

The filaments' temperature average at L04 (Figure 5.20, d) was affected by metering pump speed, quench air speed and extrusion temperature. A significant interaction was found between the extrusion temperature and quench air speed (Figure 5.21, d), as spinning temperature plays an interactive role with quench air cooling speed on the filament cooling speed then solidification and the internal structure of filaments. The interactions QA & WS and T&WS were detected and need to be further investigated, but no significant effect was found for other factors and interactions.

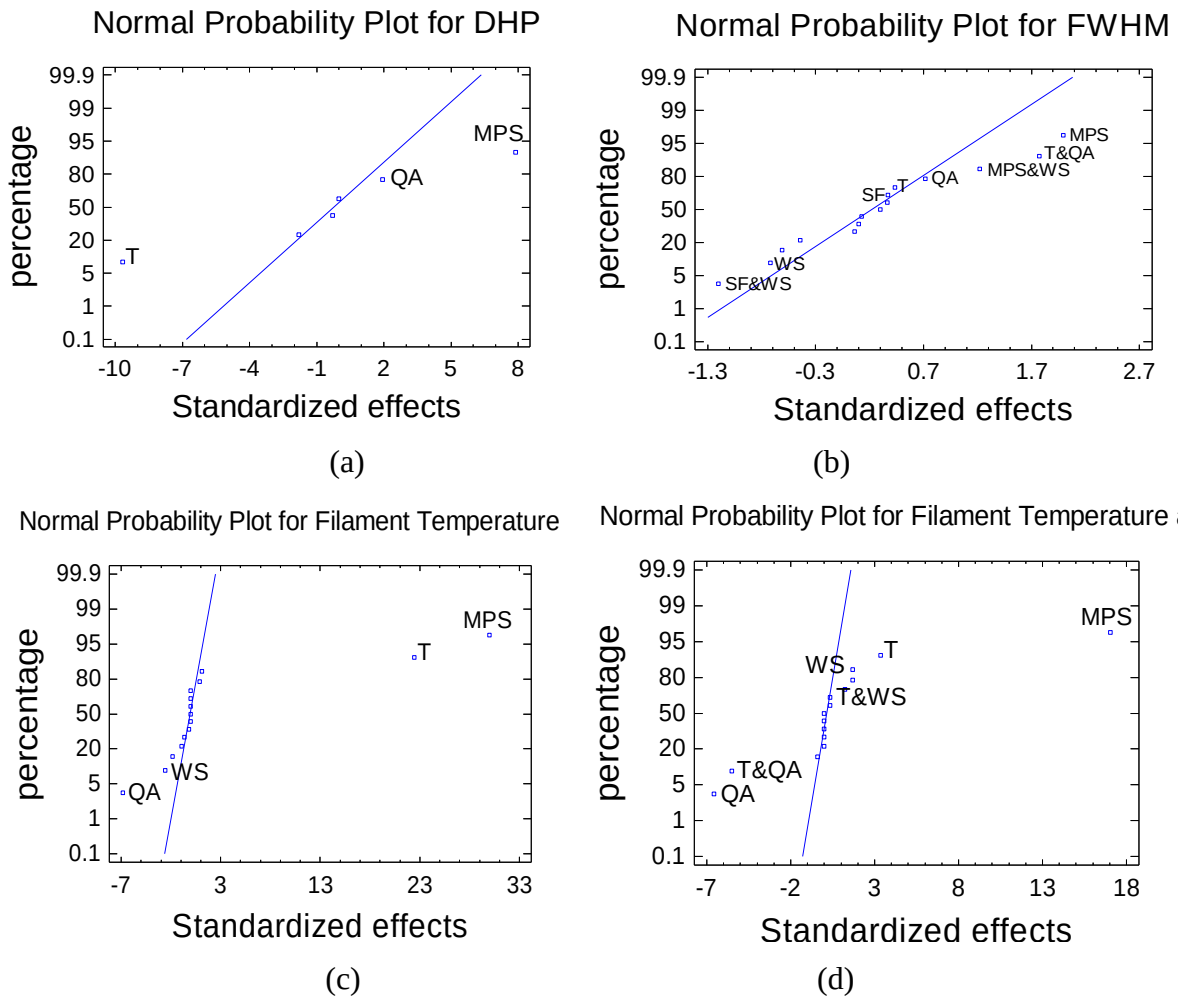

Figure 5.22. Statistical standardized and percentage order values of factors and their interactions (The normal probability plot) for die head pressure (a), FWHM (b), filament' temperature average at L03(c) and filament' temperature average at L04 (d).

Figure 5.22 displays the normal probability plots for die head pressure (a), FWHM (b), filament' temperature average at L03 (c) and filaments' temperature average at L04 (d) of as-

spun fibres. Die head pressure (a) is affected by metering pump speed and quench air speed which has a positive effect and decrease with extrusion temperature which gives a negative effect. From the x-ray diffraction results (b), it is clear that the crystallinity (FWHM) is affected positively by MPS and negatively by the interaction T&QA. Winding speed, quench air speed and the interactions MPS&WS and SF&WS will be investigated later using ANOVA to provide quantitative and objective criteria for judging the statistical significance of the effects. The filaments' temperature average at L03 of as-spun fibres (c) is affected positively by metering pump speed and extrusion temperature and negatively by winding speed and quench air speed respectively. From a normal probability plot for the filaments' temperature average at L04 of as-spun fibre (d), it can be noted that the positive effects from metering pump speed and extrusion temperature and the negative effect from quench air and T&QA are prominent. Winding speed and T&WS effects will be investigated later using ANOVA to determine if there is a statistical significance of the effects.

5.5.2.1 Analysis of Variance (ANOVA)

ANOVA results are listed in Table 5.6; the significance of studied factors on die head pressure will be T (P_T 0.000)> MPS (P_{MPS} = 0.000). No significant effect of QA (P_{MPS} = 0.064>0.05) and other interactions were detected. Note that, even when $P_{MPS} = P_T = 0.000$, the order of the significance is obtained depending on F-Ratio listed.

FWHM is significantly affected by MPS (P_{MPS} = 0.049). There are no significant effects of the other factors and interactions. Even the interaction T&QA seems to be statistically significant; it has a P-value (0.076>0.05) so it has is no significant effect.

Filaments' temperature average at L03 of as-spun fibres is significantly affected by MPS (P_{MPS} = 0.000) > T (P_T = 0.000) > QA (P_{QA} = 0.000) > WS (P_{WS} 0.021). There are no significant effects of the other factors and interactions. In the filaments' temperature average at L04 of as-spun fibres analysis, the significance of factors will then be MPS (P_{MPS} = 0.000)>QA (P_{QA} = 0.000)> T (P_T = 0.004). There is no significant effect for other factors. Because the interaction T&QA ($P_{T\&QA}$ = 0.000) has P-value of 0.000 which is lower than 0.05, the interaction T&QA is significant. There are no significant effects of the other interactions. The quantitative ANOVA results are consistent with quantitative conclusions derived from the effects plots and Daniel's plots.

Source	DHP		FWHM		Filament Temperature			
					at L03		at L04	
	F	P	F	P	F	P	F	P
T	93.6	0.000	0.2	0.650	502.9	0.000	11.2	0.004
MPS	62.2	0.000	4.5	0.049	897.9	0.000	290.1	0.000
QA	3.7	0.064	0.6	0.456	46.5	0.000	43.3	0.000
SF	-	-	0.2	0.701	0.0	1.000	0.0	1.000
WS	-	-	0.6	0.456	6.6	0.021	2.9	0.110
T &MPS	0.0	1.000	0.2	0.705	0.4	0.517	0.1	0.740
T & QA	3.2	0.086	3.5	0.076	0.9	0.356	30.6	0.000
T& SF	-	-	-	-	0.0	1.000	0.0	1.000
T& WS	-	-	0.0	0.895	1.3	0.278	2.9	0.110
MPS& QA	0.1	0.768	0.4	0.526	0.0	0.843	0.1	0.739
MPS& SF	-	-	0.2	0.642	0.0	1.000	0.0	1.000
MPS& WS	-	-	1.7	0.213	3.3	0.089	0.2	0.685
QA & SF	-	-	-	-	0.0	1.000	0.0	1.000
QA & WS	-	-	0.1	0.753	0.8	0.385	1.5	0.233
SF& WS	-	-	1.6	0.219	0.0	1.000	0.0	1.000

Table 5.6. ANOVA results identifying the statistical significance of factor effects on the die head pressure, FWHM, filament temperature averages at L03 and L04

5.5.2.2 The Regression Equation and Estimation Results

Based on the analysis, the simplified models were fitted by the regression equations which were fitted to the experimental data. The regression equations forecast die head pressure, FWHM and temperature averages at L03 and L04 in order to achieve the most satisfactory properties in the final desired fibre for different applications.

The regression equations in terms of the previous coded values (Table 5.1) are given as follows:

DHP = 94.7917 + 1.25*T + 67.0139*MPS + 99.5833*QA + 0.0*T*MPS - 0.666667*T*QA - 0.277778*MPS*QA (5.4)

FWHM = 2.81277 - 0.0187708*T - 0.00943403*MPS - 0.0508903*QA + 0.393194*SF - 0.000170417*WS + 0.000195833*T*MPS + 0.000382778*T*QA + 0.00272222*T*SF + 0.00000383333*T*WS - 0.000329167*MPS*QA - 0.0240278*MPS*SF + 0.000197083*MPS*WS + 0.00216667*QA*SF + 0.0000195*QA*WS - 0.00778333*SF*WS (5.5)

Filament temperature at L3 = -76.9687 + 0.765*T + 3.52361*MPS + 0.246667*QA + 0.0*SF - 0.197667*WS - 0.00638889*T*MPS - 0.00366667*T*QA + 0.0*T*SF + 0.0013*T*WS - 0.00194444*MPS*QA + 0.0*MPS*SF - 0.00525*MPS*WS + 0.0*QA*SF + 0.00103333*QA*WS + 0.0*SF*WS (5.6)

Filament temperature at L4 = -62.4479 + 0.633333*T + 0.5625*MPS + 1.995*QA + 0.0*SF - 0.2335*WS + 0.0025*T*MPS - 0.0163333*T*QA + 0.0*T*SF + 0.0015*T*WS + 0.0025*MPS*QA + 0.0*MPS*SF - 0.000916667*MPS*WS + 0.0*QA*SF + 0.0011*QA*WS + 0.0*SF*WS (5.7)

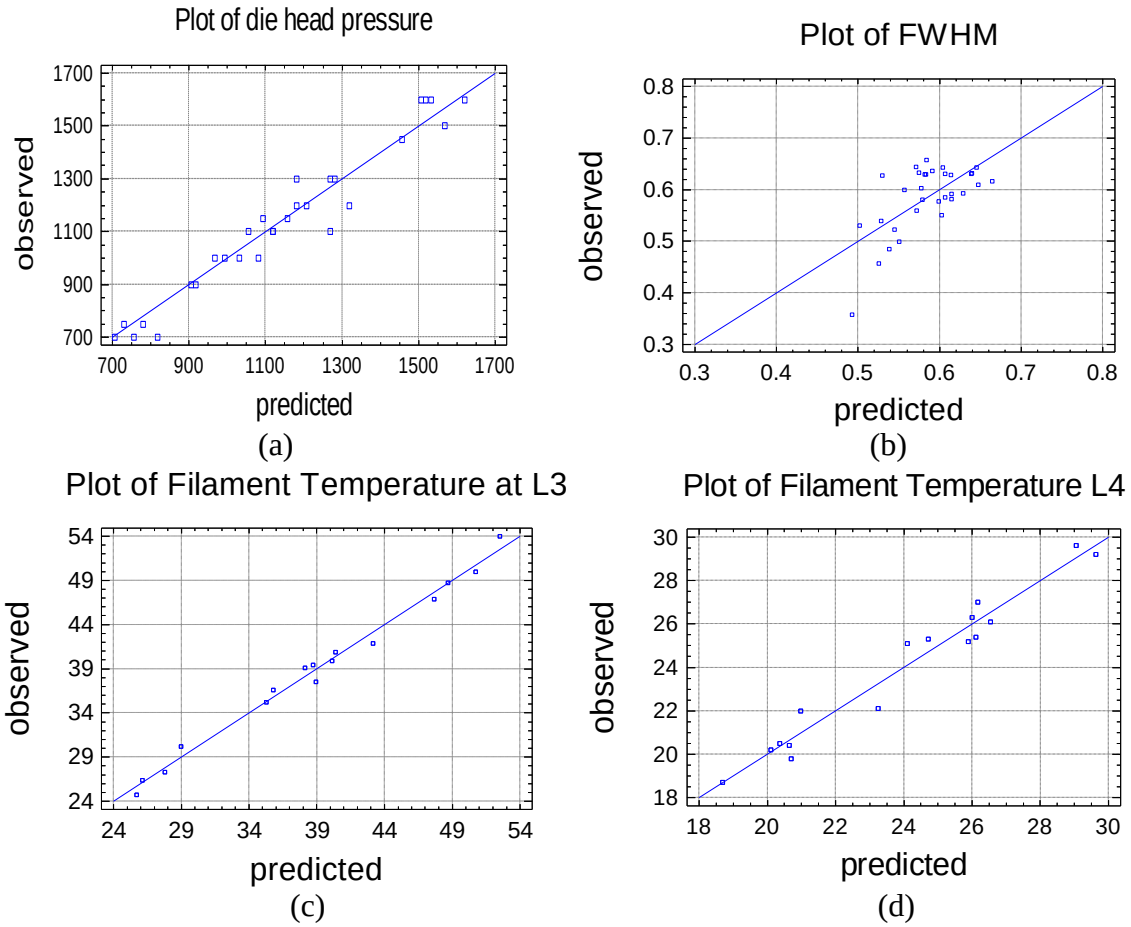

Figure 5.23. Experimental observed results and calculated fitted results plot for die head pressure (a), FWHM (b), filament' temperature average at L03 (c) and filament' temperature average at L04 (d).

For the observed and fitted results generated for each trial (Figure 5.23), the models gave useful results for the die head pressure (a), FWHM (b) and temperature averages at L03 (c) and temperature averages at L04 (d). The biggest scatter of points seems to be for FWHM as expected, because the measurement of FWHM is probably subject to the most error and number of sample tested. Their Model Standard Error (MSE) values listed in Table 5.10 indicate the dispersion of predicted and observed values around the theoretical fitted line

generated using the fitted model for each trial. There is some difference in cooling rate through the filament bundle in the melt spinning process; non-uniform structure and properties could be found from one filament to another.

There are small variations related to extrusion machine setting-based variation, the nature of this polymer and the nonuniform flow, the winder tension variation, tension during the preparation of the sample for the test or the interactions T&QA and its effect on the air cooling temperature then on FWHM .

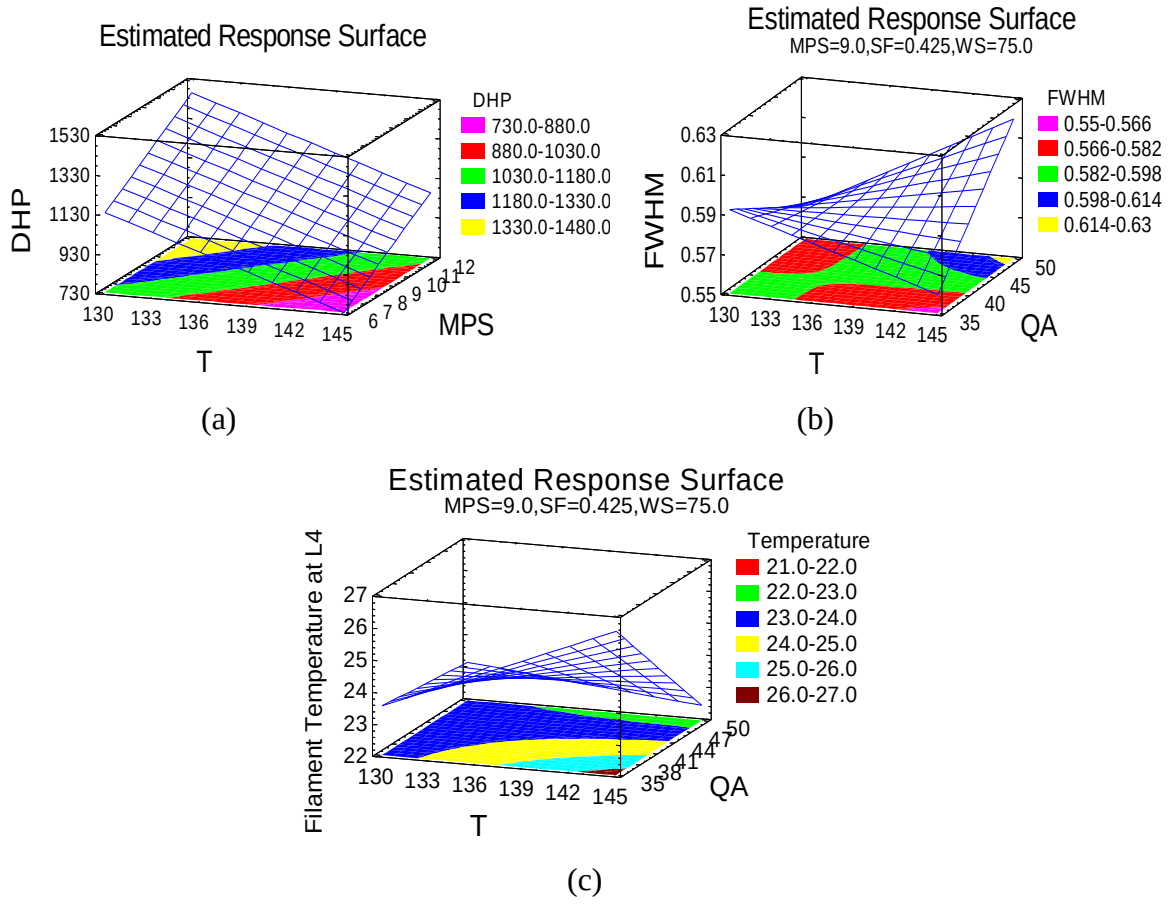

Figure 5.24. Estimated response surface between MPS and T die head pressure (a), FWHM (b) and filament' temperature average at L04 (c)

The geometric result of plotting a response variable is as a function of two factors and the interaction appears with the surface twist. In order to determine the direction of the interaction T& MPS on die head pressure, in the estimated response surfaces of count as shown in Figure 5.24 (a), the remainder of the factors are fixed on the middle of their range: for example, the middle of the temperature range is T = 130 + (145-130)/2 = 137.5 ^{O}C.

Because of the twist found in the 3D surface response diagrams, the detected effect is found to be significant and confirmed the last analysis of the results. The twists in estimated response surfaces between QA and T for FWHM (b) and between QA and T for filament' temperature average at L04 (c) confirm the interactions mentioned in the previous statistical analysis results.

In the cube plots (Figure 5.25) for the die head pressure (a), FWHM (b) and filament temperature averages at L03 (c) and temperature averages at L04 (d) and depending on the regression equation, each value corresponds to the values of the experimental factors MPS, T and QA at the middle levels of WS and SF.

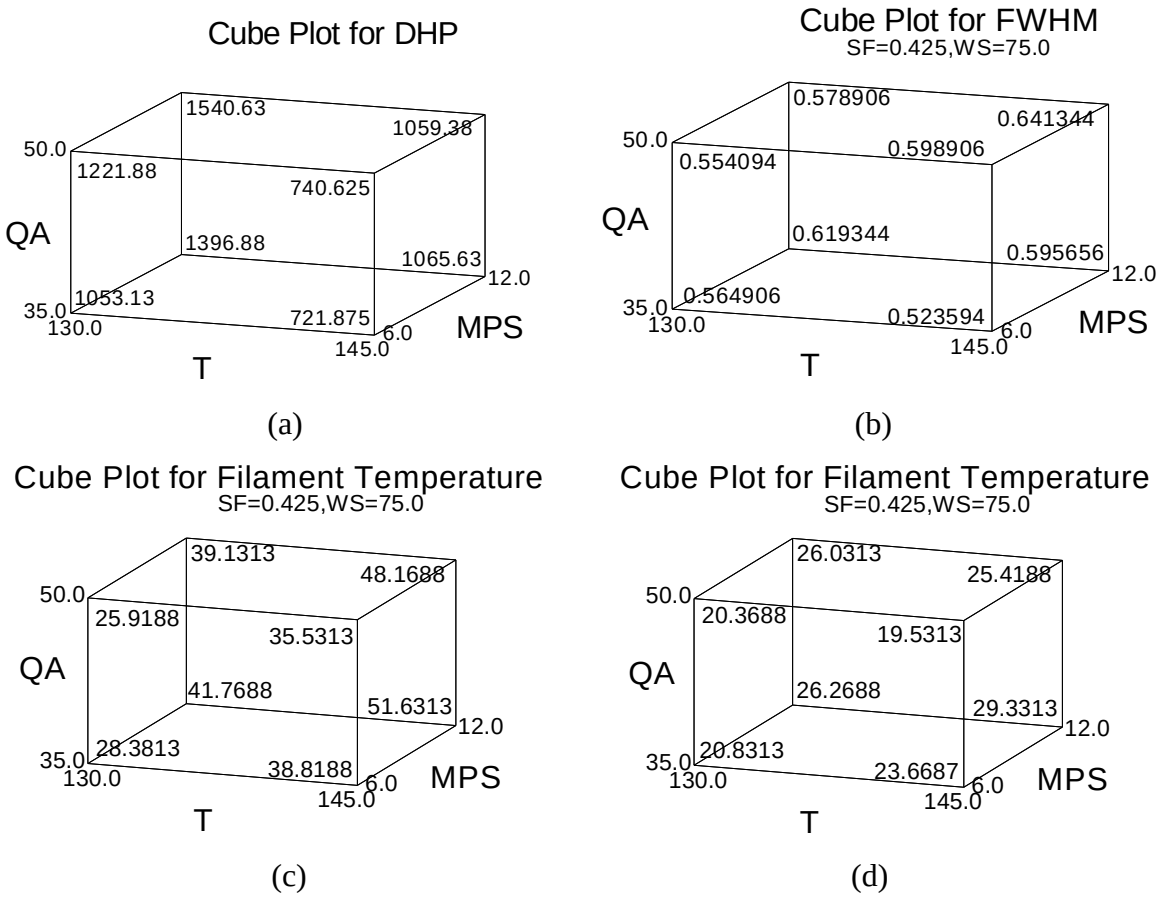

Figure 5.25. Cube plots of the estimated effects for the high and low settings of MPS, T and QA die head pressure (a), FWHM (b), filament' temperature average at L03 (c) and filament' temperature average at L04 (d)

The cooling must be designed to improve the crystallinity and crystal size that is affected by throughput rate, yarn cross section and air cooling temperature. The wind-up speed controls

the spin draw ratio and tension on material from the spinneret through the cooling and solidification steps. Decrease of spinning temperature leads to higher viscosity, higher flow resistance through the spinneret's nozzle and high die head pressure. The auto-mode in the extrusion machine controls the feeding action and the die head pressure. This is affected by heating action and unsteady viscosity-shear rate (see chapter 3), which could generate an error resulting from the pre-pump pressure changing. It can be seen that the properties have deviations for reasons such as blocked nozzles in the spinneret because of the rubbery nature of this polymer and the non-uniform flow which reduces at high temperature, tension during the spinning, cooling rate difference through the filaments bundle or some tension during the preparation of the sample for the test. The cooling ratio affects the crystallinity; cooling time is affected by extrusion rate, fibre cross section and air cooling temperature.

5.5.3 Diameter, Tensile Properties and Thermal Shrinkage

Applied statistical techniques on physical properties indicate how to optimize the fibre proportions in order to produce the most satisfactory properties in the extruded fibre for different applications. The target here is to demonstrate how variations in spinning conditions can affect the physical and thermal properties, giving a better insight into the relationship between melt spinning process parameters and produced as-spun fibre properties. After different samples of linear as-spun aliphatic-aromatic co-polyester fibres were spun at different process parameters (Table 5.2), their control effects were determined and modelled.
As a two-level experiment, a factor effect and interaction effect could be determined as the difference between the average responses at the low and the high level of the studied factors. In Figure 5.26, Pareto charts for diameter (a), tenacity (b), elongation at break (c), modulus (d) and thermal shrinkage (e) show the significant arrangement of factors and their interactions in decreasing order. The Pareto chart for diameter clearly shows that winding speed, metering pump speed, MPS&WS and T are the most important factors affecting the diameter. The Pareto chart for tenacity clearly shows that extrusion temperature, winding speed, metering pump speed and the interactions T&MPS, MPS&WS and T&WS are the most important factors affecting the tenacity, followed by other factors and interactions.

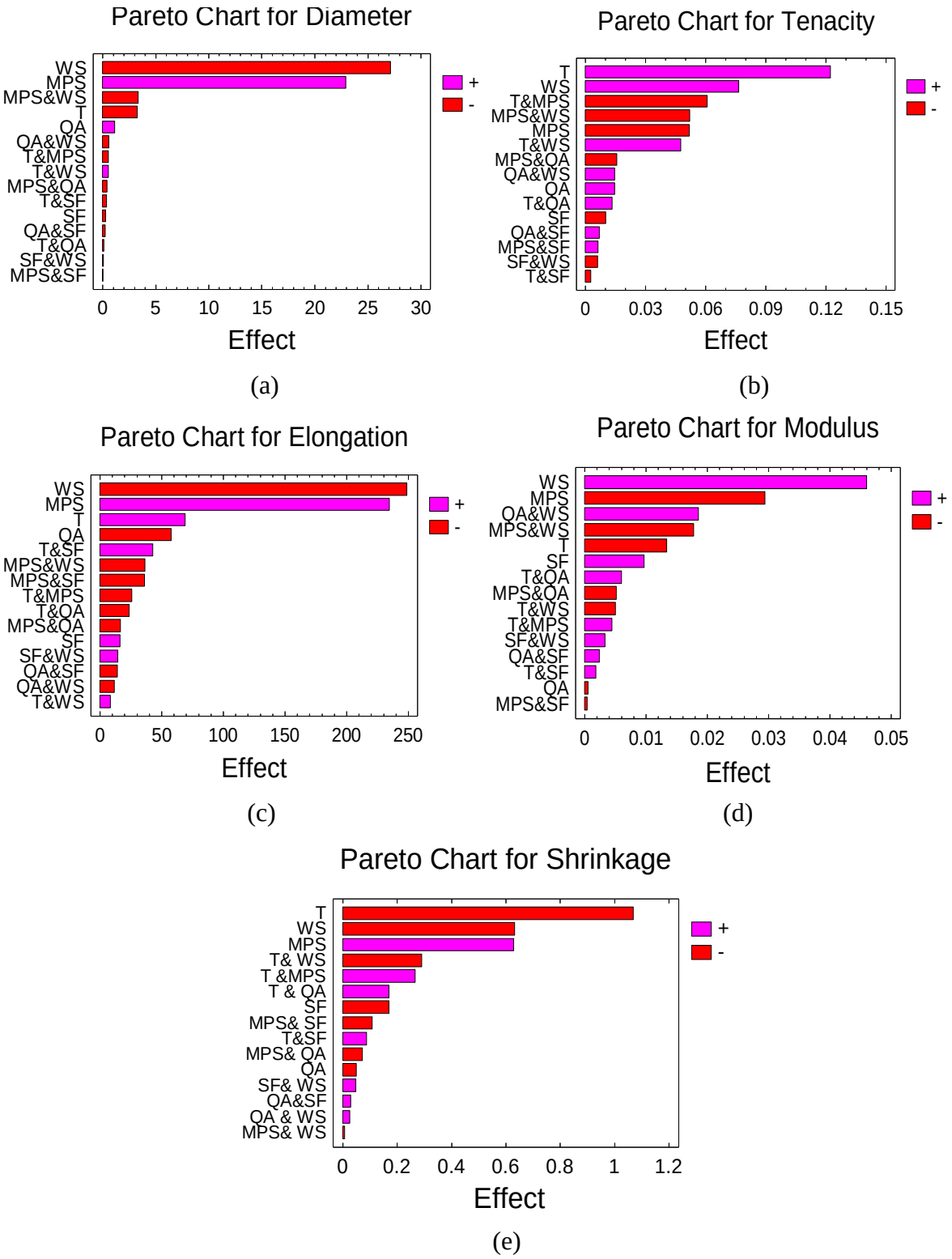

Figure 5.26. A ranked list of significant arrangement effects and interactions (Pareto chart) for diameter (a), tenacity (b), elongation at break (c), modulus (d) and thermal

shrinkage (e)

The Pareto chart for elongation at break clearly shows that winding speed, metering pump speed, extrusion temperature, quench air speed and the interactions T&SF, MPS&WS and

MPS&SF are the most important factors affecting the elongation at break, followed by the interactions T&MPS, T&QA and other factors and interactions.

The Pareto chart for modulus shows that winding speed, metering pump speed, extrusion temperature, spin finish speed applicator and the interactions QA&WS, MPS&WS, T&QA, MPS&QA and T&WS are the most important factors affecting the modulus, followed by the interactions T&MPS, SF&WS and other factors and interactions. The Pareto chart for thermal shrinkage clearly shows that extrusion temperature, winding speed, metering pump speed, spin finish speed applicator and the interactions T&WS, T&MPS and T&QA are the most important factors affecting the thermal shrinkage, followed by other factors and interactions. Figure 5.27 and Figure 5.28 show the effect plots of statistical analysis of the effects caused by the main factors and their interactions on the diameter, tenacity, elongation at break, modulus and thermal shrinkage of as-spun fibres obtained using the designed matrix. The statistical analysis on diameter (Figure 5.27, a and Figure 5.28, a) shows that the effects from the temperature winding speed, metering pump speed, extrusion temperature and the interaction between winding speed and metering pump speed are significant.

The interaction between metering pump speed and winding speed is related to the relationship between the output of the machine and the collection at different speeds, which affect the throughput flow rate and the spin draw ratio of the filaments and then changes the filament diameter. The main factor effect for tenacity (Figure 5.27, b and Figure 5.28, b) is strongly affected by extrusion temperature, metering pump speed and winding speed. The interactions T&MPS, T&WS and WS&MPS are significant. The interactions QA&WS and SF&WS need to be further investigated. From results, no significant effect has been reported for other factors and interactions. Elongation at break (Figure 5.27, c and Figure 5.28, c) was affected by metering pump speed, winding speed, quench air speed and extrusion temperature. The interactions T&SF, MPS&SF and MPS&WS and T&MPS need to be further investigated; statistical analysis ANOVA is given in next section. No significant effect was reported for other factors and interactions. Modulus (Figure 5.27, d and Figure 5.28, d) was affected by main factors metering pump speed, winding speed and extrusion temperature. The interactions MPS&WS and QA&WS affect the modulus; T&QA are on the borderline of significance and need to be investigated. Thermal shrinkage (Figure 5.27, e and Figure 5.28, e) is strongly affected by extrusion temperature, winding speed and metering pump speed; the interactions T&MPS and T&WS strongly affect the thermal shrinkage and

need to be investigated. All previous factors and interactions which are on the borderline of significance will be further investigated later using ANOVA.

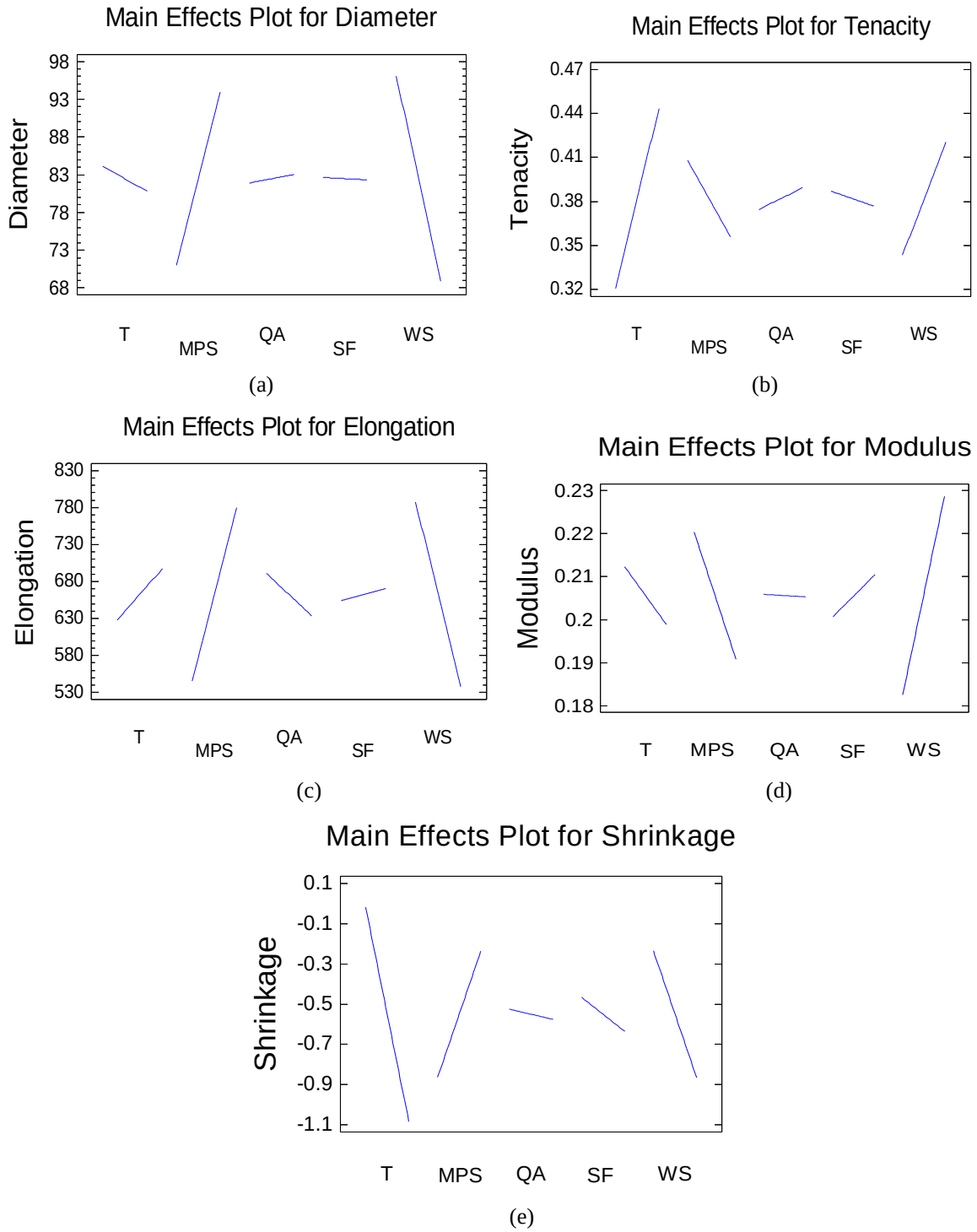

Figure 5.27. The main affect plots for diameter (a), tenacity (b), elongation at break (c), modulus (d) and thermal shrinkage (e)

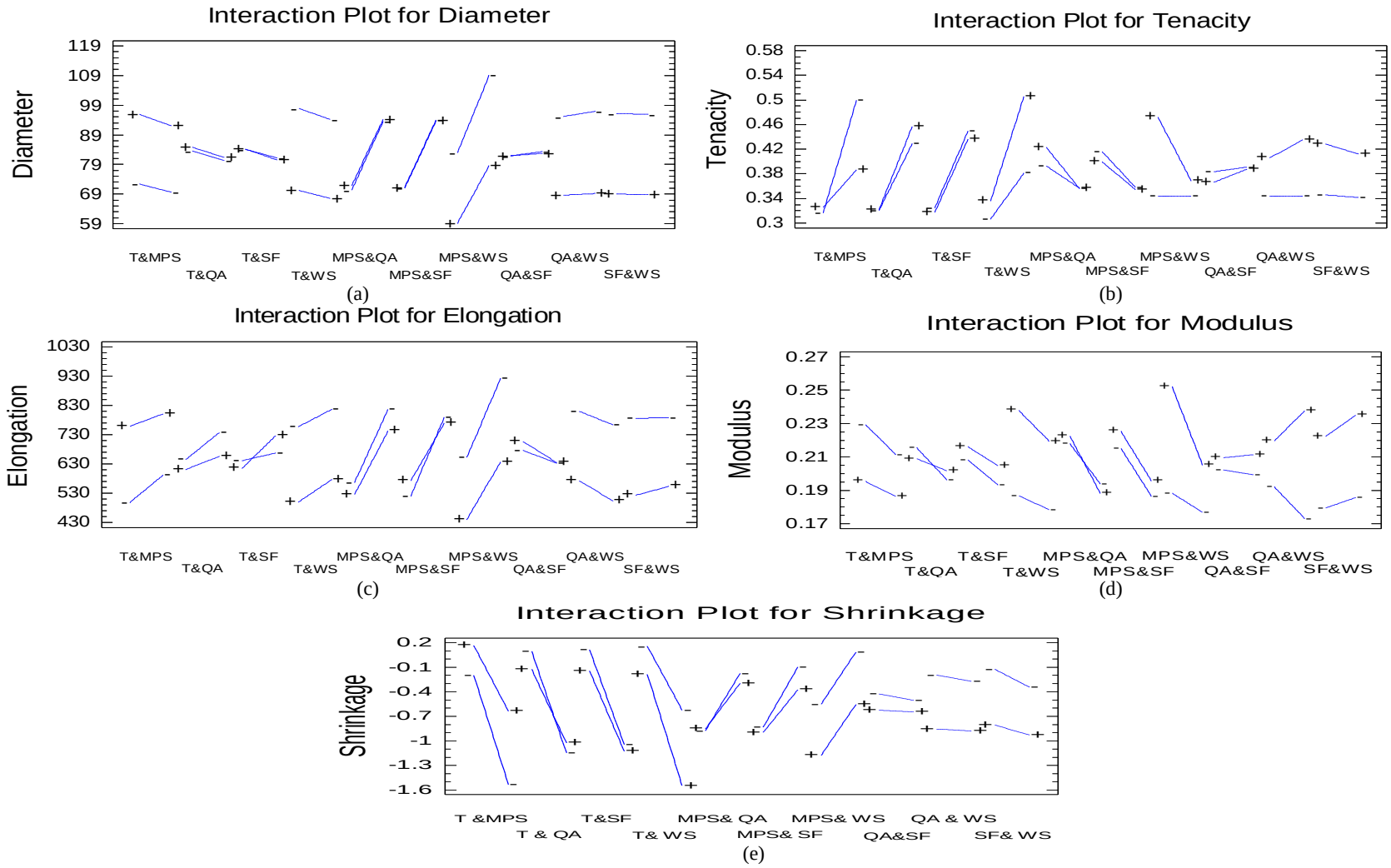

Figure 5.28. The interaction plots for diameter (a), tenacity (b), elongation at break (c), modulus (d) and thermal shrinkage(e)

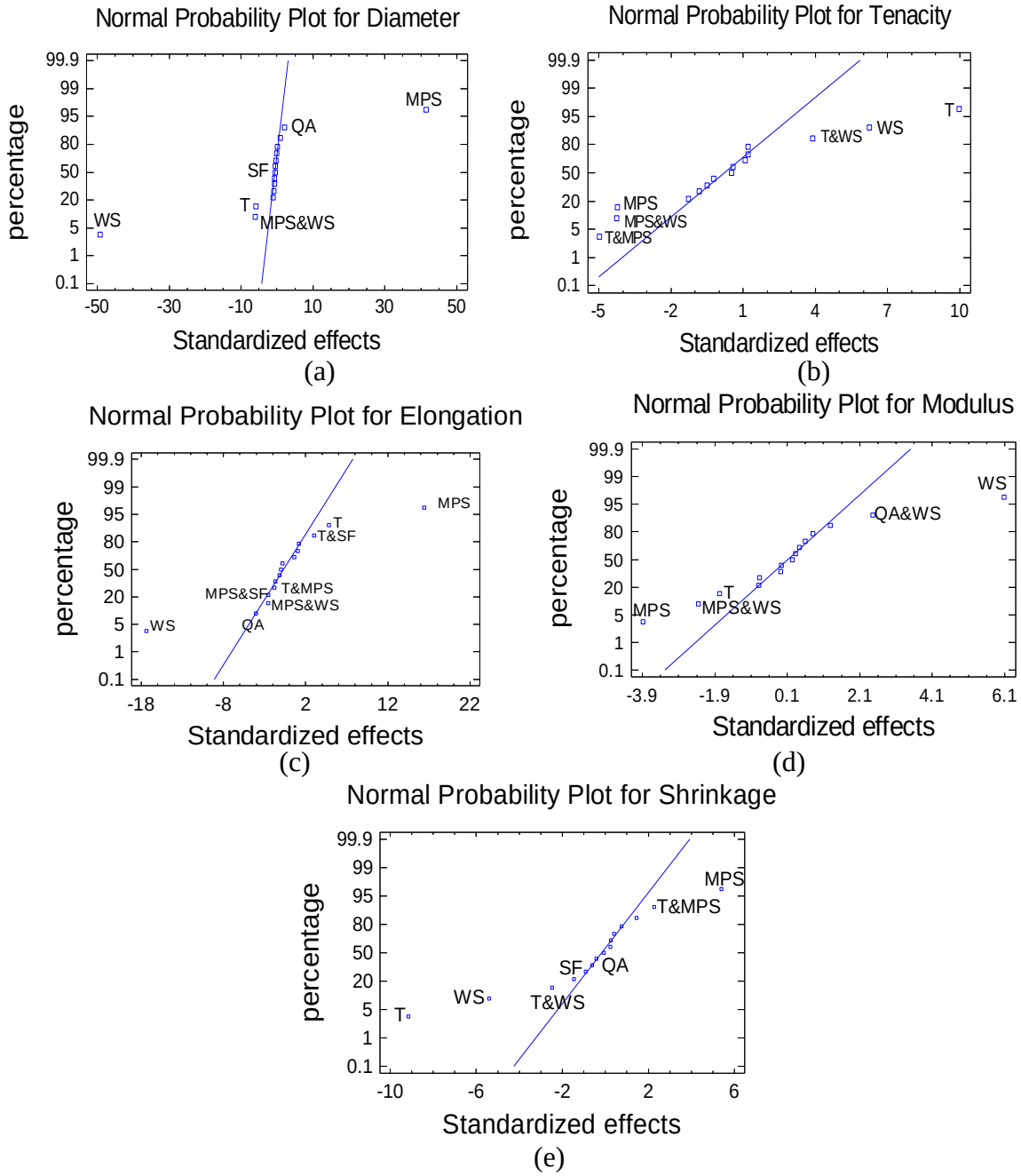

Figure 5.29. Statistical standardized and percentage order values of factors and their interactions (the normal probability plot) for the diameter (a), tenacity (b), elongation at break (c), modulus (d) and thermal shrinkage (e)

Figure 5.29 displays the normal probability plots for the diameter, tenacity, elongation at break, modulus and thermal shrinkage of as-spun fibres obtained using the design matrix, and also shows the percentage and standardized effects. The normal probability plot for diameter (a) shows the clear a positive effect of metering pump speed and negative effect of winding speed and their interaction on the diameter. Other effects appear for extrusion temperature and quench air speed which could be related to the effect of these factors on the down draw

ratio, as has been noted. Tenacity (b) is affected positively by extrusion temperature, winding speed and the interaction T&WS and negatively by metering pump speed and the interactions WS&MPS and T&MPS. Together with the main effects of extrusion temperature, winding speed and metering pump speed, the interactions T&SF and MPS&WS affect the elongation at break (c), which can be related to the interaction effect on the spin draw ratio which decreases the elongation at break ratio. In the modulus analysis (d), winding speed and the interaction QA&WS have a positive effect on the modulus but metering pump speed, extrusion temperature and the interaction MPS&WS have a negative effect on the modulus. The thermal shrinkage (e) is affected negatively by extrusion temperature, winding speed and the interaction T&WS, and positively by metering pump speed and its interaction with spinning temperature. The normal probability charts give more details explaining the parameter effect on different responses. For example, spinning temperature has a negative effect on modulus, thermal shrinkage and diameter and a positive effect on tenacity and elongation at break.

5.5.3.1 Analysis of Variance (ANOVA)

ANOVA results for diameter, tenacity, elongation at break, modulus and thermal shrinkage of as-spun fibres are listed in Table 5.7. The significant factors on the diameter are WS (P_{WS} 0.000)> MPS (P_{MPS} = 0.000)> T (P_T = 0.000). No significant effect of SF and QA was found. The interaction MPS& WS has significant effect ($P_{MPS\&WS}$= 0.000). There are no significant effects of the other interactions on diameter. On the mechanical properties, tenacity is significantly affected by T (P_T = 0.000) >WS (P_{WS} 0.000)> MPS (P_{MPS} = 0.001) and the interactions T&MPS ($P_{T\&MPS}$ = 0.000) >MPS&WS ($P_{MPS\&WS}$ 0.001)> T&WS ($P_{T\&WS}$ = 0.001). There are no significant effects of the other factors and interactions. Elongation at break is significantly affected by WS (P_{WS} 0.000)> MPS (P_{MPS} = 0.000)> T (P_T = 0.000)> QA (P_{QA} = 0.001) and the interactions T&SF ($P_{T\&SF}$ = 0.008) > MPS&WS ($P_{MPS\&WS}$ = 0.021) > MPS&SF ($P_{MPS\&SF}$ = 0.022). There are no significant effects of the other factors and interactions. Modulus is significantly affected by WS (P_{WS} 0.000)> MPS (P_{MPS} = 0.001) and the interactions QA&WS ($P_{QA\&WS}$ = 0.026) > MPS&WS ($P_{MPS\&WS}$ = 0.032). There are no significant effects of the other factors and interactions. Thermal shrinkage is significantly affected by T (P_T = 0.000) >WS (P_{WS} 0.000)> MPS (P_{MPS} = 0.000) and the interactions

T&WS ($P_{T\&WS}$ = 0.025) >T&MPS ($P_{T\&MPS}$ = 0.037). There are no significant effects of the other factors and interactions.

Source	Diameter		Tenacity		Elongation at break		Modulus		Thermal shrinkage	
	F	P	F	P	F	P	F	P	F	P
T	35.3	0.000	99.3	0.000	23.3	0.000	3.2	0.095	83.7	0.000
MPS	1727	0.000	17.9	0.001	269.9	0.000	15.1	0.001	29.0	0.000
QA	4.2	0.056	1.4	0.249	16.3	0.001	0.0	0.942	0.2	0.674
SF	0.3	0.596	0.7	0.419	1.3	0.269	1.6	0.219	2.1	0.165
WS	2417	0.000	39.0	0.000	303.0	0.000	37.1	0.000	29.3	0.000
T &MPS	1.0	0.338	24.6	0.000	3.3	0.089	0.3	0.566	5.2	0.037
T & QA	0.1	0.801	1.2	0.290	2.8	0.114	0.6	0.435	2.1	0.165
T& SF	0.5	0.490	0.1	0.830	9.1	0.008	0.1	0.814	0.6	0.465
T& WS	0.9	0.346	15.1	0.001	0.4	0.559	0.5	0.513	6.2	0.025
MPS& QA	0.6	0.458	1.6	0.220	1. 35	0.262	0.5	0.503	0.4	0.544
MPS& SF	0.0	0.924	0.3	0.607	6.4	0.022	0.0	0.955	0.9	0.371
MPS& WS	36.9	0.000	18.1	0.001	6.5	0.021	5.5	0.032	0.0	0.950
QA & SF	0.2	0.673	0.3	0.573	1.0	0.335	0.1	0.752	0.1	0.809
QA & WS	1.1	0.304	1.4	0.249	0.7	0.431	6.0	0.026	0.1	0.825
SF& WS	0.0	0.901	0.3	0.621	1.1	0.319	0.2	0.667	0.2	0.682

Table 5.7. ANOVA results identifying the statistical significance of factor effects on the diameter, tenacity, elongation at break, modulus and thermal shrinkage

5.5.3.2 The Regression Equation and Estimation Results

Based on the analysis, the simplified models were fitted by the regression equations which were fitted to the experimental data. The regression equations forecast for diameter, tenacity, elongation at break, modulus and thermal shrinkage in order to achieve the most satisfactory properties in the final desired fibre for different applications. The regression equations in terms of the previous coded values (Table 5.1) are given as follows:

Diameter = 61.3105 - 0.0162222*T + 7.61583*MPS + 0.539278*QA + 54.3222*SF - 0.479967*WS - 0.0121111*T*MPS - 0.00125556*T*QA - 0.346667*T*SF + 0.00143*T*WS - 0.00933333*MPS*QA - 0.119444*MPS*SF - 0.0223667*MPS*WS - 0.211111*QA*SF - 0.00156333*QA*WS + 0.0186667*SF*WS (5.8)

Tenacity = -0.724049 + 0.00675139*T + 0.212372*MPS - 0.0179125*QA - 0.01125*SF - 0.0137837*WS - 0.00135417*T*MPS + 0.000119444*T*QA - 0.00238889*T*SF + 0.000127167*T*WS - 0.000348611*MPS*QA + 0.0143056*MPS*SF - 0.000347917*MPS*WS + 0.00627778*QA*SF + 0.0000391667*QA*WS -0.00165*SF*WS (5.9)

Elongation at break = -128.163 + 0.828917*T + 186.364*MPS + 36.3343*QA - 4184.63*SF - 6.27401*WS - 0.575*T*MPS - 0.212222*T*QA + 38.2589*T*SF + 0.0227767*T*WS - 0.369444*MPS*QA - 80.4639*MPS*SF - 0.243608*MPS*WS - 12.63*QA*SF - 0.0307767*QA*WS + 3.922*SF*WS (5.10)

Modulus = 0.766958 - 0.00374583*T - 0.00424653*MPS - 0.0110431*QA - 0.306528*SF + 0.00136708*WS + 0.0000986111*T*MPS + 0.0000538889*T*QA + 0.00161111*T*SF - 0.0000135*T*WS - 0.000115278*MPS*QA - 0.000972222*MPS*SF - 0.00011875*MPS*WS + 0.00216667*QA*SF + 0.0000495*QA*WS + 0.000883333*SF*WS (5.11)

Thermal shrinkage = 22.1331 - 0.163778*T - 0.535*MPS - 0.212722*QA - 11.7389*SF + 0.0856333*WS + 0.00591667*T*MPS + 0.00151111*T*QA + 0.0777778*T*SF - 0.000773333*T*WS - 0.00161111*MPS*QA - 0.238889*MPS*SF - 0.00005*MPS*WS + 0.0255556*QA*SF + 0.00007*QA*WS + 0.013*SF*WS (5.12)

For the observed results and fitted results generated for each trial (Figure 5.30), the models gave useful results for the diameter (a), tenacity (b) and elongation at break (c), modulus (d) and thermal shrinkage (e). Their Model Standard Error (MSE) values listed in Table 5.10 indicate the dispersion of predicted and observed values around the theoretical fitted line generated using the fitted model for each trial. The fractional resistance between the fibres that transfers the forces between the fibres and raises the fraction could play a role in small tenacity variation resulting from the material nature.

The model gave useful results with small variation related to extrusion machine setting based variation, the nature of this polymer and the nonuniform flow, the winder tension variation and tension during preparation of the sample for testing. In order to determine the direction of the interaction MPS&WS, the estimated response surfaces of diameter were used, as shown in Figure 5.31. There are three axes: the first interaction factor MPS is on the X-axis and low and high levels, the second interaction factor WS is on the Y-axis with low and high levels and the Z-axis shows the averages of the measured diameter. A small twist was found in the surface and as a result, a significant effect was detected between MPS and WS, which confirms the previous analysis results. In a similar analysis (Figure 5.32), the estimated response surfaces for tenacity, elongation at break modulus and thermal shrinkage show the relationship between them and the previously studied affected interactions. The results obtained agree with the conclusions from the previous analysis.

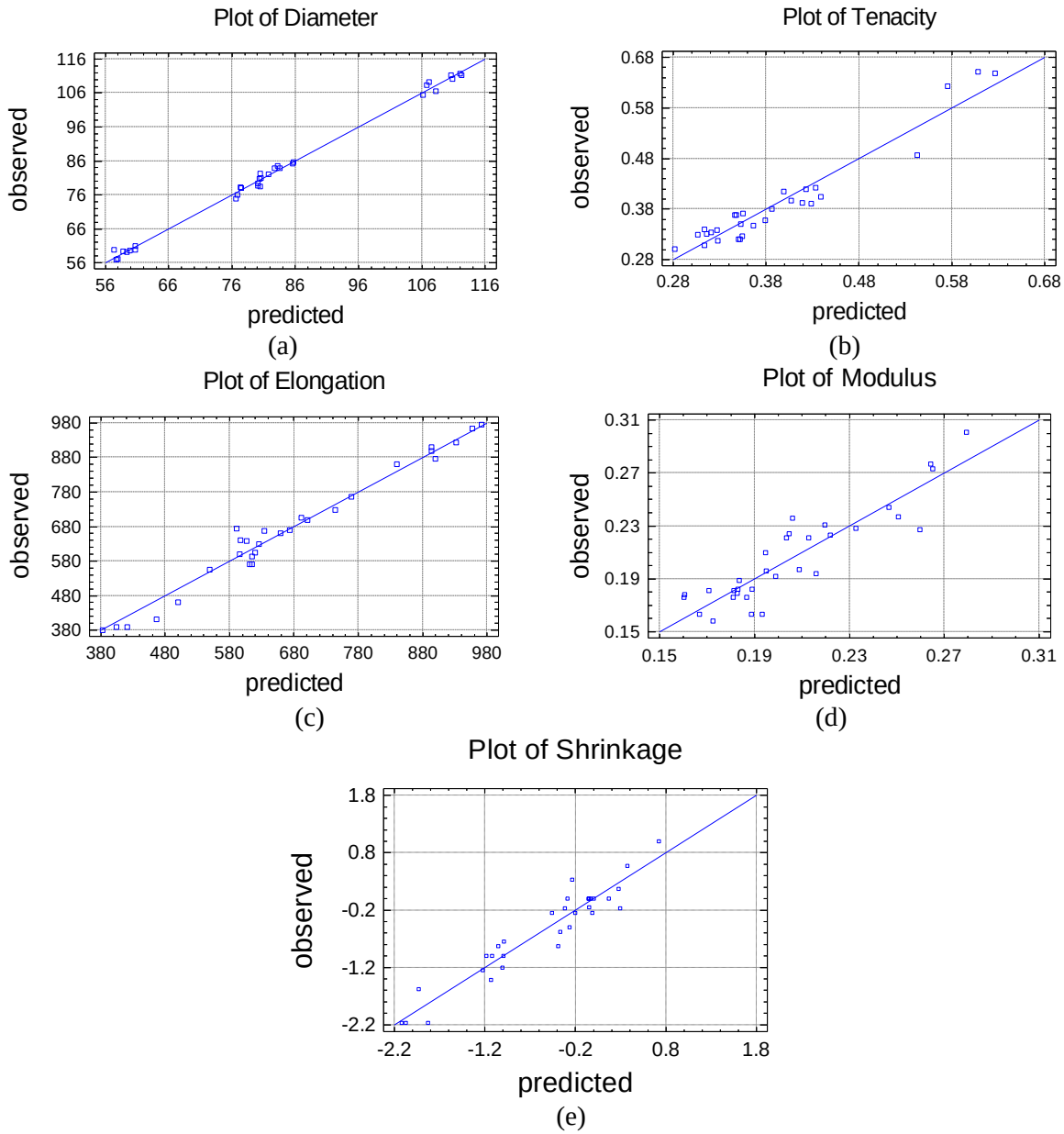

Figure 5.30. Experimental observed results and calculated fitted results plot for the diameter (a), tenacity (b), elongation at break (c), modulus (d) and thermal shrinkage (e)

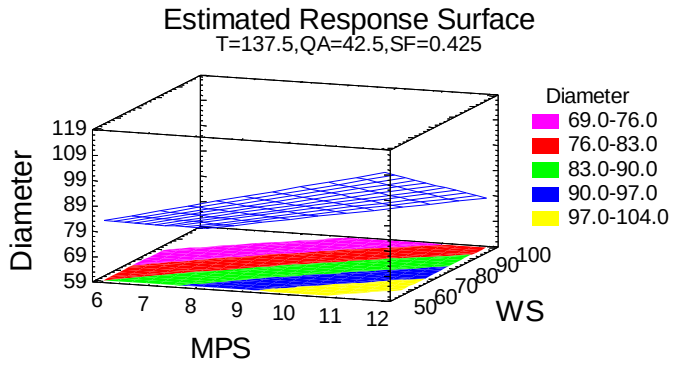

Figure 5.31. Estimated response surface between MPS and WS for diameter

The cube plots (Figure 5.33) for the diameter (a), tenacity (b), elongation at break (c), modulus (d) and thermal shrinkage (e) depend on the obtained regression equation; each value corresponds to the values of the experimental factors MPS, T and WS at the middle levels of QA and SF range, which are 42.5 and 0.425 respectively. The mathematically concise statistical models predict the diameter, tenacity, elongation at break, modulus and thermal shrinkage of the as-spun fibres in terms of random variables and their associated probability distributions. A high degree of extension gives higher tenacity together with lower elongation at break (high modulus) and vice versa [168]. The increased modulus and tensile strength could be related to the increasing of down draw ratio. The stress-strain behaviour is used to describe and classify qualitatively the polymer and its fibre properties and behaviour. In a thermosetting mechanism, fibres could be deformed and the internal stresses relaxed to let the new form stabilize by re-crystallization [170]. A clear relationship between the factors affecting the physical and internal structural properties could be noted; the connections between statistical and experimental results gave a description about the effect of the parameters through the selected ranges on the manufactured fibres.

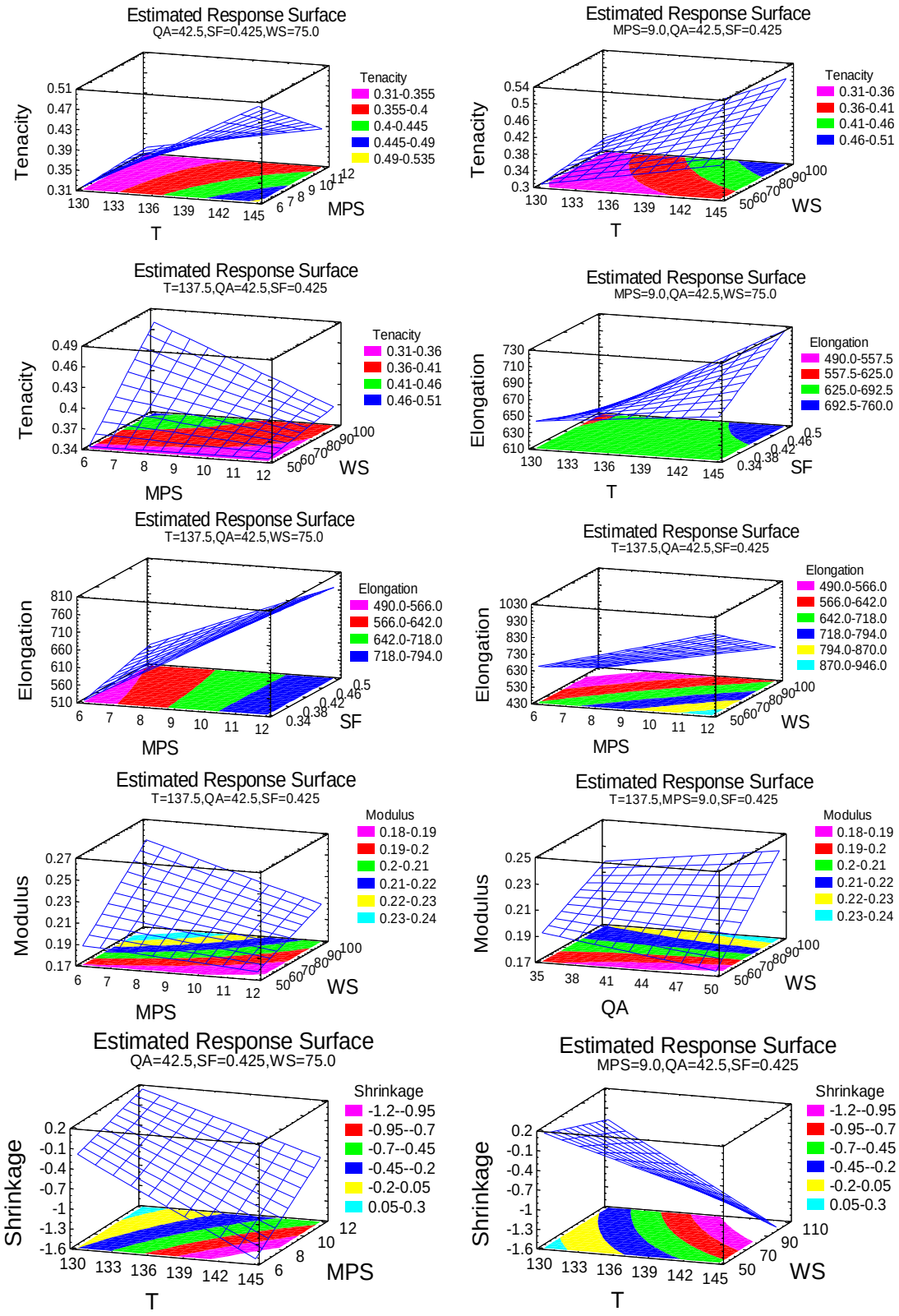

Figure 5.32. Estimated response surface between WS and T for tenacity, elongation at break, thermal shrinkage and modulus

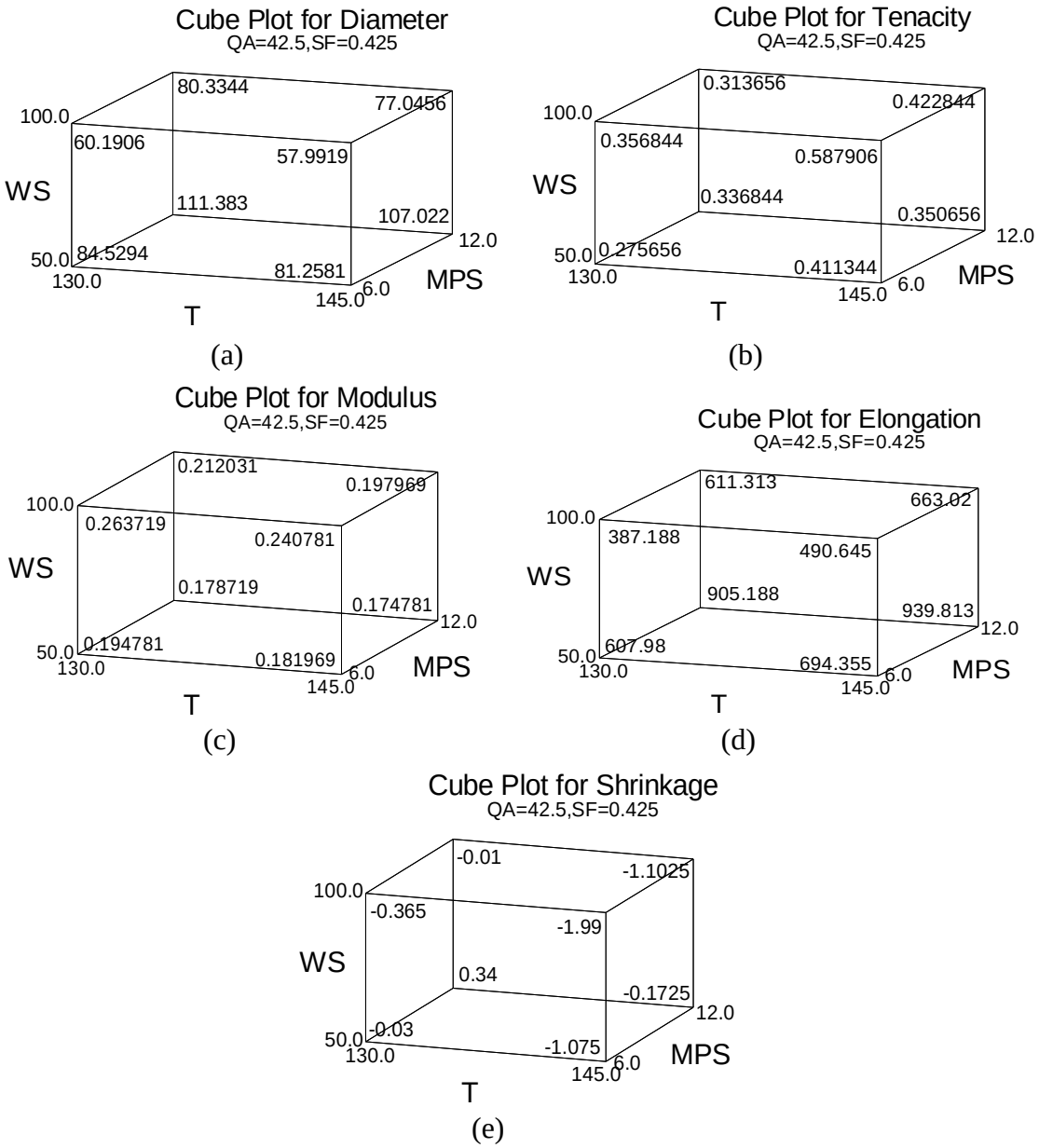

Figure 5.33. Cube plots of the estimated effects for the high and low settings of MPS, T and WS for diameter (a), tenacity (b), elongation at break (c), modulus (d) and thermal shrinkage (e)

5.5.4 The Effect of Heat Setting Conditions on The Thermal Shrinkage and Mechanical Properties of LAAC Fibres

Textile fibres with thermoplastic properties have created the need for the testing of thermal shrinkage or extension of yarns and fabrics made from such materials subjected to heat, which is important for identifying the thermal conditions for thermal treatment processes. If the fibres are heated unconstrained, the internal stress produces a higher shrinking. Thermal

shrinkage leads to annealing of the filament to relax at least partially the frozen internal stress and decrease the residual thermal shrinkage. Some instability could be obtained when the fibres are heated to practical application temperatures, such as during washing and ironing processes [159]. Thermal stability is affected by the influences of temperature, time and tension subjection to heat, structure of the sample, associated substances and evaluation parameters [170]. The prediction of yarn properties can thus be fulfilled through a prediction model.

5.5.4.1 Results

A new fibre for this experiment was extruded via melt spinning on the same lab-spin machine. The temperature zones in the extruder are barrel zones (T1=115^{o}C, T2=120^{o}C and T3=125^{o}C), metering pump zone (T4=130^{o}C) and die head zones (T5=130^{o}C and T6=130^{o}C). The molten polymer was forced through a spinneret of 55 holes with speed adjusted by the metering pump (6 rpm). The air cooling quench speed was set at 35 % of total blower fan air output. The spin finish (Vickers) was diluted fivefold with water before use with application speed of 0.35 rpm. The filaments were collected from the godets set at 50 m.min^{-1}. As-spun fibres were hot drawn at drawing ratio of 3 and drawing temperature of 60^{o}C. In the heat setting experiments, testing was carried out using the Testrite Thermal Shrinkage Oven. Filaments were heat set over a range of temperatures between 40 and 80°C for times ranging from 1 to 3 minutes, while the yarn was held taut at constant length using weight from 5 to 20g. After the samples had been heat treated, they were left to cool in ambient temperature. The loaded filaments carrier consisted of a jaw/clamp on one end and the free drum with low torque potentiometer fitted to give the results on the other end.
The heat setting experiments conducted involved three factors at three levels, as given in Table 5.8.

Trial Number	**Level 1**	**Level 2**	**Level 3**
Temperature (^{o}C**)**	40	60	80
Weight (g**)**	5	10	20
Time (Sec**)**	60	120	180

Table 5.8. Factors and their levels for the annealing experiment

A full factorial experimental design (L27) for a simple experiment with random order was used, as shown in Table 5.9, and designed using STATGRAPHICS software. The designed matrix clustered all experimental conditions to be controlled and allowed all individual factors and their interactions to be analysed statistically and evaluated independently. This procedure performs a multifactor analysis of variance for responses; it constructs various tests and graphs to determine which factors have a statistically significant effect on responses.

5.5.4.2 Statistical Analysis and Discussion

The experimental design array for the spinning experiment and response data is represented in Table 5.9. The properties of the taut-annealed samples showed small but significant differences. The predominant role of the temperature of heat setting on thermal shrinkage and mechanical properties of fibres are discussed in detail. By the combination of factor levels which obtain the desirability function over the indicated region, the factor optimization which achieved the selected properties, higher tenacity and modulus with lower shrinkage and elongation at break, is setting the fibres at a temperature of 40 ^{o}C for 63 seconds at tension of 19.99 gram, which is trial number 12 in the design (Table 5.9).

The relationship between the weight and the temperature is explained to give a realistic analysis of thermo-mechanical behaviour of the fibres. In the setting mechanism, the fibres were deformed and the internal stresses relaxed to let the new form stabilize. The factors affecting the results are sample weighting, operating temperature, duration of test and count of samples. In order to determine the factor effects in terms of statistical significance, analysis of variance of the data was conducted. Tenacity is affected negatively by temperature increasing and positively by time and weight increasing. Elongation is affected negatively by time and temperature increasing and positively by weight decreasing. Thermal shrinkage is affected negatively by temperature increasing and positively by time and weight increasing. From the ANOVA results, thermal shrinkage is significantly affected by temperature (P_{tem} 0.000) > weight (P_w = 0.000) and their interactions Tem&W ($P_{Tem\&W}$ = 0.000) (Figure 5.34). There are no significant effects of the other factors and interactions. The interaction plot (Tem & W) will help in interpreting the significant effects. Tenacity is significantly affected by Weight (P_w = 0.0024). Temperature is not significant (P_{Tem} = 0.0770).There are no significant effects of the other factors and interactions. In the elongation

at break analysis, although there is an effect from temperature and its interaction with time effect, this is not significant. Modulus is significantly affected by temperature (P_{tem} 0.002) > Weight (P_w = 0.0394). There are no significant effects of the other factors and interactions.

Trial Number	Temperature (^oC)	Weight (g)	Time (s)	Thermal shrinkage %	Tenacity g/den	Elongation at break %	Modulus g/den
1	80	20	60	2.7	0.87	184.8	0.43
2	40	20	180	0.0	0.96	172.7	0.63
3	60	05	180	12.5	0.76	193.9	0.36
4	40	20	120	0.0	0.94	190.9	0.83
5	60	10	60	6.3	1.00	179.5	0.50
6	40	10	120	5.0	0.90	159.1	0.40
7	80	20	120	3.0	0.85	169.7	0.43
8	60	10	120	6.5	0.87	195.5	0.43
9	40	05	60	0.7	0.82	134.8	0.73
10	80	10	180	12.7	0.88	225.8	0.40
11	60	05	120	11.8	0.82	183.3	0.40
12	40	20	60	0.0	0.84	170.5	0.73
13	80	05	120	20.3	0.69	187.9	0.23
14	60	20	180	2.5	0.90	177.3	0.56
15	40	05	180	1.3	0.87	157.6	0.63
16	40	05	120	1.3	0.89	213.6	0.63
17	80	10	60	12.8	0.82	197.0	0.36
18	40	10	180	0.7	0.99	183.3	0.73
19	60	20	120	2.5	0.95	328.8	0.46
20	80	20	180	2.7	1.03	224.2	0.46
21	60	20	60	2.8	0.93	193.9	0.53
22	80	05	60	20.5	0.81	297.0	0.26
23	40	10	60	0.3	0.87	153.8	0.73
24	80	05	180	20.8	0.70	215.2	0.26
25	60	05	60	10.8	0.83	183.3	0.40
26	60	10	180	6.3	0.89	177.3	0.46
27	80	10	120	12.8	0.87	203.0	0.36

Table 5.9. L32 Experimental design array for the spinning experiment and responses data

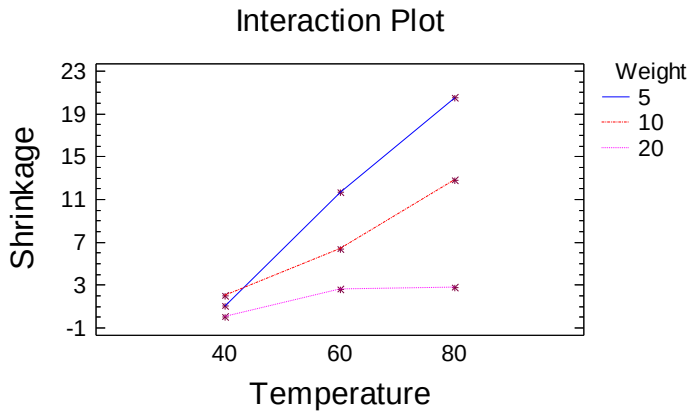

Figure 5.34. The interaction plot between weight and temperature

The regression equations for thermal shrinkage, tenacity, elongation at break and modulus are given as follows:

Thermal shrinkage = -3.05556 + 0.275*Temperature + 0.00240741*Time - 0.606984*Weight (5.13)

Tenacity = 0.861111 - 0.0015556*Temperature + 0.0001759*Time + 0.007143*Weight (5.14)

Elongation at break = 123.578 + 0.0302778*Time + 1.02306*Temperature + 0.513175*Weight (5.15)

Modulus = 0.885 + 0.0255556*Weight - 0.000462963*Time - 0.0236111*Temperature (5.16)

After heat setting affects on the internal structure of the fibres, temperature affects positively on the elongation at break and thermal shrinkage and negatively on the tenacity and the modulus of the fibres. Weight affects negativity on the thermal shrinkage and positively on the tenacity and the modulus of the fibres. A small effect of weight has been identified on elongation at break and small effect of time has been identified on all responses. Thermal properties are important if the fibres undergo heat treatment during processing as well as in use. Many important physical properties are affected when fibres are thermally set. With increasing mobilization of chains, the thermodynamically beneficial random coil state is approached; heat causes a softening of the non-crystalline region [115].

The temperature and the weight are the more significant factors controlling the thermal shrinkage and mechanical properties. There is a small effect from the heat setting time. Those factors are affected by temperature, stress and moisture. Other factors, such as chain stiffness, cross linking, crystallization, chemical cross links and impregnation with matrix

could have an effect within the fibres. In twisted fibres, the fractional resistance between the fibres transfers the forces between the fibres and raises the fraction [170]. As a result and at high setting temperature, adhered locations are created in the yarn or fabric which will affect the character of the textile.

5.5.5 General Conclusions about LAAC Fibre Analyses

In this section, different samples of as-spun linear aliphatic-aromatic co-polyester fibres were spun at different melt spinning conditions to determine their effects. The aim was to show how variation in spinning conditions could lead to a better insight into the relationships between melt spinning process conditions and the fibre properties produced. Not only the extrusion temperature profile affects the properties, productivity and product cost but also the other melt spinning parameters can do so. Spin-draw ratio, the overall orientation, drawability of the spun filaments, die head pressure, FWHM, temperature averages at L03, temperature averages at L04 of the spun filament, the diameter, tenacity, elongation at break, modulus and thermal shrinkage of fibres were modelled. A production process of biodegradable linear aliphatic-aromatic co-polyester fibre was optimized.

It is clear that the combination between the higher metering pump speed and the high spinning temperature in filaments extrusion leads to low reduction in the filament heating content and vice versa. That depends on the fibres diameter and then on their heat content and its effect by cooling ratio. The combination between the higher metering pump speed and the low spinning temperature or between the low metering pump speed and the high spinning temperature in filaments extrusion leads to medium reduction in the filament heating content resulting from the material nature. No appreciable changes of relative intensity of the peaks in the endotherm (DSC) were observed in different samples for the same trial. An SEM photomicrograph of the surface and cross section of the fibre shows uniformity and the circular cross section of the as-spun fibres. There is a clear relationship between spin draw ratio and the improvement of the overall orientation of the fibres which has a significant effect on the drawability. In other words, the increase in spin draw ratio increases the overall orientation of the fibres and decreases the drawability ratio. Spinning temperature has a significant effect on the spin draw ratio and drawability, which are affected on the flow rate and tension value. Metering pump speed plays an interactive role with winding speed as the

relationship between the output of the machine and the collection at different speeds which affects the tension in the spinline. This controls the fibre orientation chains and adds different spin draw ratios which have a negative effect on drawability. Temperature plays an important role in controlling the fibre structure as well as affecting the drawability.

Spinning temperature and metering pump speed are the most important factors affecting the die head pressure. Crystallographic order is significantly affected by metering pump speed, as metering pump speed is increased, the fibre diameter is increased; that increases the heat content inside the fibre and affects the cooling ratio. The interaction between the spinning temperature and the quench air cooling speed seems to have an effect on crystallographic order but is not statically significant. Metering pump speed, spinning temperature, winding speed and quench air cooling speed are the most important factors affecting the filaments' temperature average at L03. The throughput flow rate (metering pump speed) and the collection at different speeds affect the filament diameter and the filament heating content.

In the filaments' temperature average at L04 analysis, the significant factors will be metering pump speed, quench air cooling speed, spinning temperature and the interaction between the spinning temperature and the quench air cooling speed. The cooling ratio affects the crystallinity; cooling time is affected by extrusion rate, fibre cross section and air cooling temperature. The high wind-up speed adds tension to the filaments from the spinneret through the cooling and solidification stages. Decrease of spinning temperature leads to higher viscosity, higher flow resistance through the spinneret's nozzle and high die head pressure. Melt extrusion temperature, metering pump speed, winding speed and the interaction between the metering pump and the winding speeds are the most important factors affecting the diameter.

Extrusion temperature, winding speed and metering pump speed are the most important factors affecting the mechanical properties and thermal shrinkage, as described previously. Regarding the heat setting effects on the internal structure of the fibres, temperature positively affects the elongation at break and thermal shrinkage and negatively on the tenacity and the modulus of the fibres. Weight negatively affects the thermal shrinkage and positively on the tenacity and the modulus of the fibres. The small effect of weight was identified on elongation at break and the effect of heat setting time was identified on all responses.

Response	MSE	Optimum model	The combination of factor levels (↓: Low Level, ↑: High Level)				
			T	MPS	QA	SF	WS
Spin Draw Ratio	2.136	Maximum	↑	↓	↓	↓	↑
		Minimum	↓	↑	↑	↓	↓
Birefringence × 1000	2.41	Maximum	↑	↓	↑	↑	↑
		Minimum	↑	↑	↑	↑	↓
Drawability	0.193	Maximum	↑	↑	↓	↑	↓
		Minimum	↓	↓	↓	↓	↑
DHP (dpi)	51.7	Maximum	↓	↑	↑	-	-
		Minimum	↑	↓	↓	-	-
FWHM (^{o})	0.012	Maximum	↑	↑	↑	↓	↑
		Minimum	↑	↓	↓	↑	↑
Filament' Temperature at L3 (^{o}C)	1.498	Maximum	↑	↑	↓	↓	↓
		Minimum	↓	↓	↑	↓	↑
Filament' Temperature at L4 (^{o}C)	0.596	Maximum	↑	↑	↓	↑	↑
		Minimum	↑	↓	↑	↑	↓
Diameter (μm)	3.23	Maximum	↓	↑	↑	↓	↓
		Minimum	↑	↓	↓	↑	↑
Tenacity (g/den)	0.0169	Maximum	↑	↓	↑	↓	↑
		Minimum	↓	↓	↓	↑	↓
Elongation at break (%)	33.03	Maximum	↑	↑	↓	↑	↓
		Minimum	↓	↓	↑	↓	↑
Modulus (g/den)	0.0063	Maximum	↓	↓	↑	↑	↑
		Minimum	↓	↑	↑	↓	↓
Thermal shrinkage (%)	0.139	Maximum	↓	↑	↓	↓	↓
		Minimum	↑	↓	↓	↓	↑

Table 5.10. The combinations of factor levels and the obtained responses (MSE: Model Standard Error)

Table 5.10 summarises the main conclusion of the results in a concise statistical model, and shows the Model Standard Error (MSE) values described previously. The optimization of structural, thermal and physical properties presents the combination of factor levels which maximize and minimize responses over the indicated region. The model covers the identified significant main and interaction factors and specifies the combinations of factor levels for enhancing responses of as-spun linear aliphatic-aromatic co-polyester fibres. The lower value of FWHM leads to the higher size of the crystallite and the higher degree of crystallographic order and vice versa, as mentioned previously. Each of the statistical analysis methods provides information which supports each other for the significant factors effect and no

pivotal contradictions were detected. The models gave useful results with some expected scatter of points which could be due to experimental and testing errors. The theoretical regression models obtained form the main source code in the enhanced forecasting program, which will be presented later the melt spinning process of aromatic-aliphatic co-polyester fibre.

In addition to creating group trials of data with similar characteristics, the predictive method decreases the number of factors and responses to a small set of meaningful measures. It helps in understanding the melt spinning process and properties of LAAC fibres and also provides more technical information for scientists and technologists in order to have the enhanced properties at suitable conditions related to final product cost.

After drawing and preparing, fibres could be used in agricultural, horticultural and other textile applications as environmentally friendly, economical, energy saving fibres. Using forecasting statistical methods, the achieved models play a major role in creating a planning program and a plan for the production process regression.

5.6 Experimental Results of Melt-Spinning of BAAC Fibres

The five control parameters for the extrusion experiments were metering pump speed (MPS), spinning temperature (T), quenching air speed (QA), applied speed of spin finish (SF) and winding speed (WS). In Table 5.1, the two levels of each parameter were separated as far apart as possible from each other. The same factorial experimental design (L32) was used for the thirty-two screening trials in this experiment, involving five control parameters and two levels for each parameter (Table 5.2); the experiments were conducted in one block. A total of 32 experiments were performed. The detailed experimental arrangement of the calculated results of spin draw ratio, die head pressure, filament' temperature average (at L02, L03, L04 and L05), count, tensile properties, diameter and thermal shrinkage are shown in Table 5.11 and Table 5.12. The results have small standard deviations which could be related to extrusion machine setting based variation; the rubbery behaviour of AACs caused a non-uniform flow which decreases at high temperature, tension during the spinning or preparing the sample for the test, machine error variation or variation in cooling rate through the filament bundle. The thermo-graphic measurement in Figure 5.35 shows the recorded results of the 32 samples of spun fibres using the ThermaCAM SC 3000 and ThermaCAM research program at L01=0 (die head or extrusion temperature), L02 = 25 mm, L03 =80 mm, L04=170 mm and L05=285 mm. IR images of filaments indicated five line temperature readings (Figure 5.35), the image colours corresponding to the temperature scale on the right of the image. The IR image illustrates the temperature variation along each line put on the thermo image to obtain the temperature profile scale along or across the studied object. From the physical aspects, it was found that the temperature decreases and the speed increases with the increase of the distance from the spinneret. Temperature and trial number were plotted using the plot module along a selected area of filaments using a camera's profile function (Figure 5.36). Depending on decreasing of the filament heating content in Figure 5.36, the trials could be divided to three groups: low (for trial numbers 3, 7, 10, 13, 20, 21, 26 and 32), high (for trial numbers 5, 6, 8, 11, 18, 22, 23 and 30) and medium (for the remaining trials) groups.

By investigating the relationship between the thermo-graphic measurement results and the matrix design represented factors and their levels, it is clear that the combination between the higher metering pump speed and the high extrusion or spinning temperature in filaments

extrusion leads to low decreasing in the filament heating content and vice versa. The combination between the higher metering pump speed and the lower extrusion temperature or between the lower metering pump speed and the higher spinning temperature in filaments extrusion leads to medium decreasing in the filament heating content. The relationship between factors and their interactions will be investigated later using a full factorial experimental design to identify the temperature variations in each group. Air quench effect will be explained later in detail in the statistical analysis. To identify the effects on the cooling process variations in each group, air quench temperature variation could be applied.

According to the DSC results, the fibre does not melt completely below 140^{o}C. A broad range of melting temperature (100^{o}C to 150°C) was observed for the as-spun fibres (Figure 5.37). The interaction between thermal and mechanical properties of the BAAC fibres regularly decreases the drawability. As-spun fibres will be broken if they are heated under high drawing tension. The surface and cross section of the fibre were investigated by an SEM photomicrograph (Figure 5.38). The outer surface and the cross section of photographs show useful results as they are uniform without any deformation. From the structural point of view and owing to the limitation of funding needed for the X-ray and the polarizing (Pluta) microscope tests in this project, 2 samples (1 and 19) were selected and characterized, comparing the similar factor levels in Table 5.2. Typical x-ray diffractometer traces (Figure 5.39) showed five major crystalline diffraction peaks with different FWHM of an x-ray scattering profile observed around 16, 17.5, 20.5, 23 and 24.5 2θ°. The peaks observed at 16, 20.5 and 24.5 2θ° are very wide and weak; the peaks at 17.5 and 23 2θ° are slightly sharper, more intense and smaller in width. The peak at 23 2θ° was fitted using DIFFRAC plus EVA software to compare the half-height widths. From results, it was found that with (FWHM $_{LAAC1}$ (0.610 ^{o}) > FWHM $_{BAAC1}$ (0.562 ^{o}), FWHM $_{LAAC19}$ (0.630 ^{o}) > FWHM $_{BAAC19}$ (0.546 ^{o})), the lower value of FWHM leads to the higher size of the crystallite and the higher degree of crystallographic order and vice versa, as mentioned previously. Figure 5.40 shows the recorded microinterferograms of the selected samples. The measured values of birefringence are averaged from the repeated measurements: Birefringence $_{LAAC1}$ (0.010) < Birefringence $_{BAAC1}$ (0.062) and Birefringence $_{LAAC19}$ (0.044) < Birefringence $_{BAAC19}$ (0.051). Generally, the results of the BAAC fibres show more crystalline, birefringent, overall orientation and consistency than those of the LAAC fibres.

Trial Number	SDR	Die Head Pressure (dpi)	Filament Temperature Average (^{o}C)			
			L02	L03	L04	L05
1	48.2	1250	106.1	41.1	21.7	14.2
2	48.2	1250	96.4	43.6	19.9	17.9
3	27.3	1600	128	71.9	39.5	29
4	25.5	1250	99.2	45.5	25.1	16
5	32.4	1500	62.5	31	20.1	15.9
6	24.7	1500	75	33.8	19.5	15.8
7	13.7	1500	120.3	69.9	39.8	27.6
8	36.3	1500	76.3	29.2	18.9	15.3
9	46.9	1250	106.1	41.1	21.7	14.2
10	27.1	1600	128	71.9	39.5	29
11	35.8	1500	76.3	29.2	18.9	15.3
12	25.1	1250	99.2	45.5	25.1	16
13	27.9	1600	119.8	66.9	31.1	21.3
14	27.5	1900	99.6	60.5	32.8	21.5
15	47.3	1250	96.4	43.6	19.9	17.9
16	25.3	1250	97.7	49.7	23.1	17.3
17	13.9	1900	103.1	64.6	27.7	23.5
18	25.6	1500	79.2	36.5	23.4	15.9
19	13.7	1900	95.2	54.3	31.4	19.6
20	13.8	1600	120.3	69.9	39.8	27.6
21	27.7	1600	119.8	66.9	31.1	21.3
22	19.5	1500	79.2	36.5	23.4	15.9
23	25.1	1500	75	33.8	19.5	15.8
24	13.7	1900	95.2	54.3	31.4	19.6
25	28.1	1900	99.6	60.5	32.8	21.5
26	14.0	1600	123.8	72.3	41.5	26.5
27	24.7	1250	97.7	49.7	23.1	17.3
28	27.4	1900	104.6	43.8	22.7	18.3
29	28.0	1900	104.6	43.8	22.7	18.3
30	27.3	1500	62.5	31	20.1	15.9
31	14.5	1900	103.1	64.6	27.7	23.5
32	13.9	1600	123.8	72.3	41.5	26.5

Table 5.11. Response data of spin draw ratio, die head pressure and filament' temperature average (at L02, L03, L04 and L05) for the experiment of melt spinning of BAAC

Trial Number	Count denier	Tenacity g/den	Elongation at break %	Modulus g/den	Diameter µm	Thermal shrinkage %
1	965.9	1.1	116	1.13	57.61	4.00
2	965.9	1.1	96	1.37	57.61	4.00
3	1707.7	0.9	129.33	0.72	76.6	3.67
4	1829.7	0.9	138.67	0.62	79.29	3.33
5	1437.4	0.9	116	0.89	70.28	3.50
6	1882.4	0.8	158.67	0.79	80.43	3.33
7	3405.5	0.7	146.67	0.41	108.18	3.00
8	1282.4	1.0	116	1.10	66.38	4.00
9	992.3	1.1	116	1.20	58.39	3.50
10	1720.9	0.9	141.33	0.67	76.9	3.83
11	1302.2	1.0	124	1.10	66.89	3.75
12	1856.0	0.9	138.67	0.65	79.86	3.67
13	1668.1	1.0	158.67	0.72	75.71	3.92
14	1694.5	0.9	173.33	0.69	76.31	3.25
15	984.4	1.0	124	0.17	58.16	4.00
16	1842.9	0.9	150.67	0.64	79.58	3.50
17	3362.6	0.7	164	0.43	107.5	2.17
18	1823.1	0.9	156	0.80	79.15	3.50
19	3392.3	0.7	153.33	0.43	107.97	2.67
20	3381.8	0.7	157.33	0.44	107.8	2.83
21	1684.6	1.0	156	0.73	76.09	3.83
22	2383.5	0.6	196	0.53	90.5	2.42
23	1859.3	0.9	158.67	0.79	79.93	3.75
24	3395.6	0.7	157.33	0.43	108.02	2.08
25	1654.9	0.9	172	0.73	75.41	3.25
26	3329.7	0.7	156	0.00	106.97	2.42
27	1882.4	0.8	161.33	0.61	80.43	3.33
28	1697.8	0.9	164	0.82	76.38	3.33
29	1661.5	0.9	166.67	0.81	75.56	3.33
30	1704.4	0.8	116	0.85	76.53	3.50
31	3211.0	0.8	153.33	0.44	105.04	2.17
32	3352.7	0.7	157.33	0.40	107.34	2.42

Table 5.12. Response data of diameter, tenacity, elongation at break, modulus and thermal shrinkage for the experiment of melt spinning of BAAC

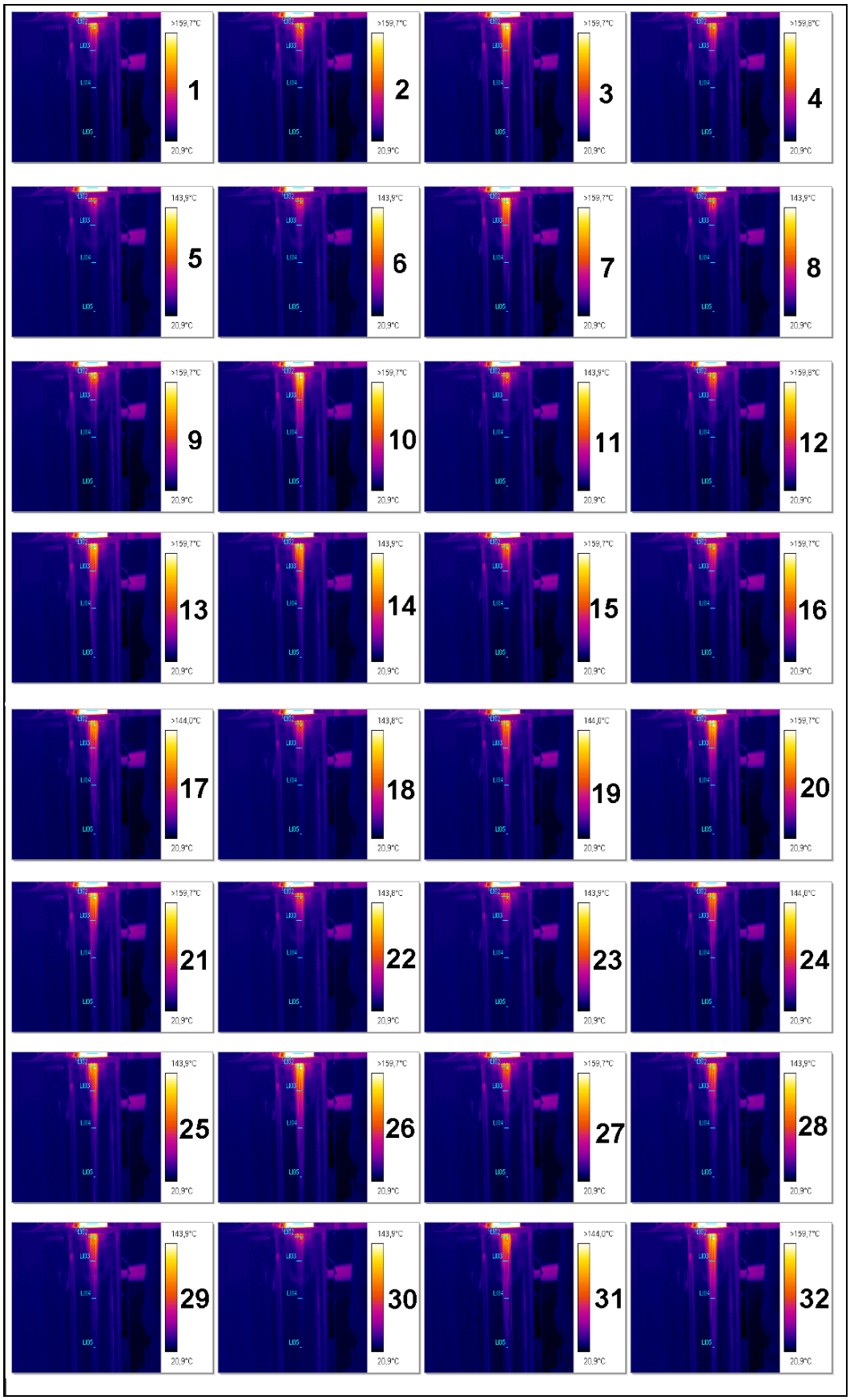

Figure 5.35. IR images of BAAC filaments indicating five line temperature readings.

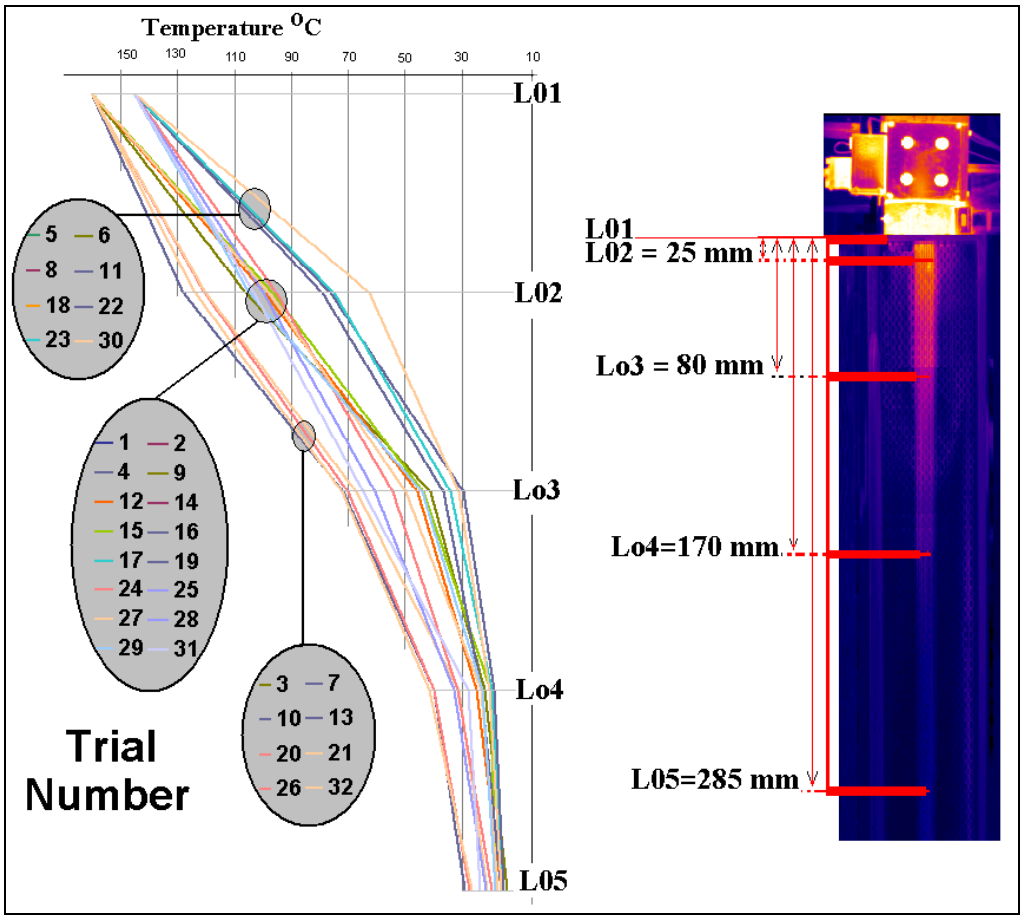

Figure 5.36. Temperature vs. Trial number plot along the selected area of BAAC filaments.

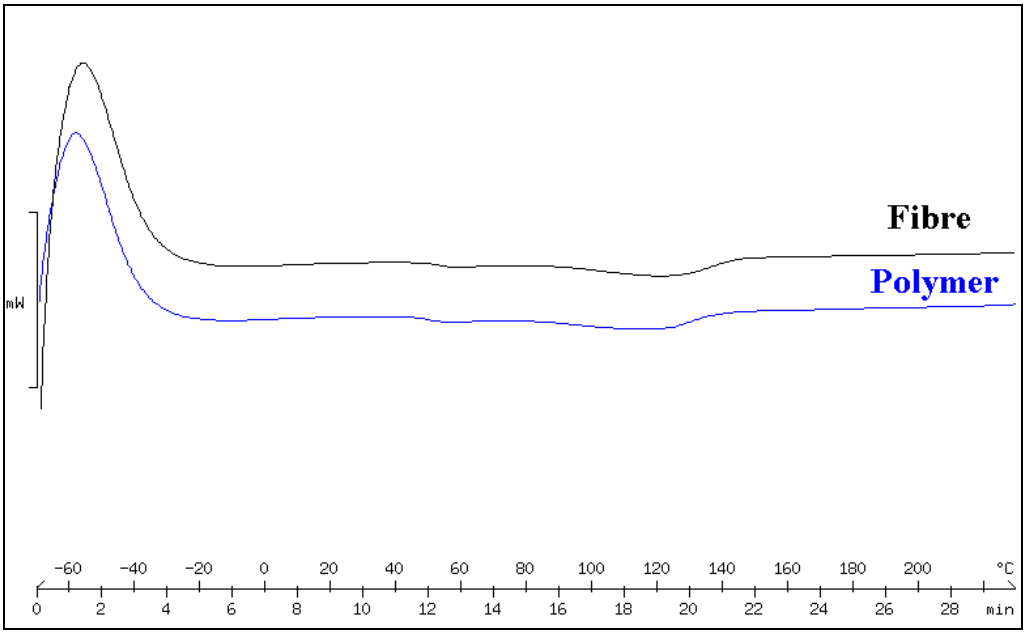

Figure 5.37. DSC curves of BAAC polymer and fibres produced

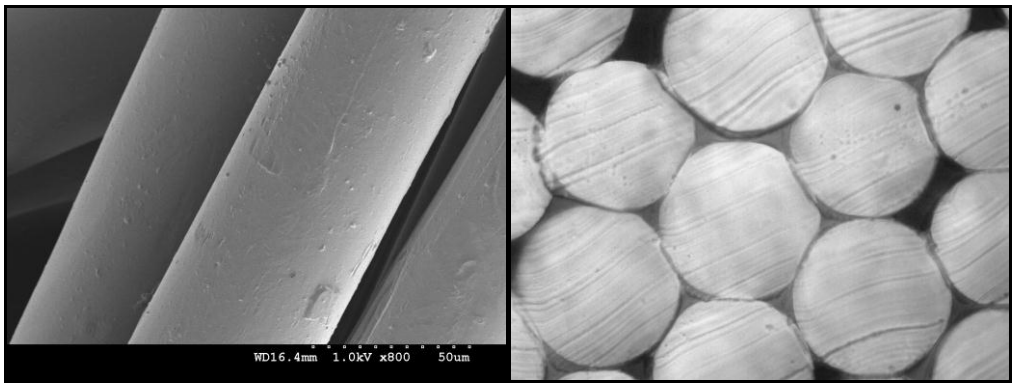

Figure 5.38. SEM Photo of surface and cross section of BAAC fibres

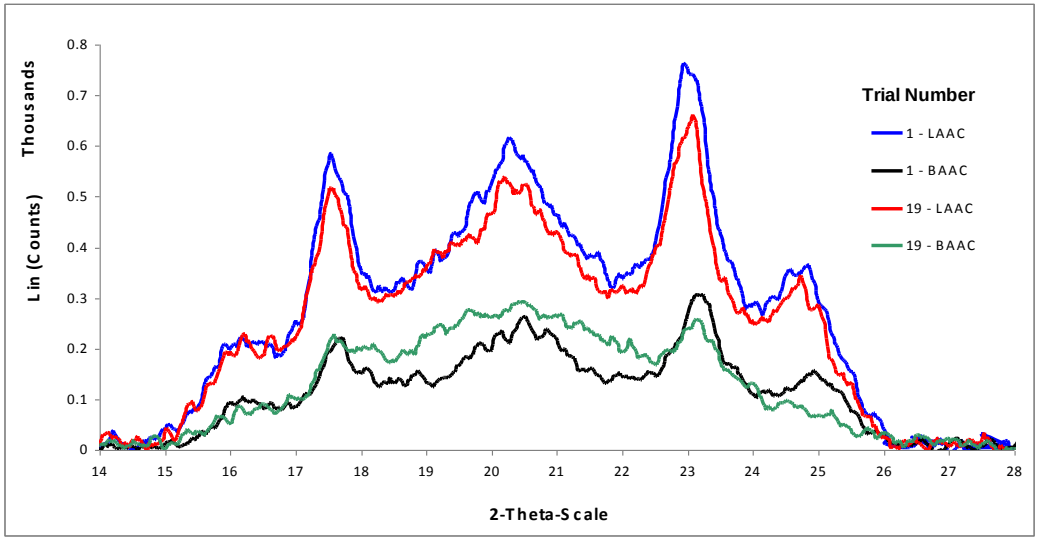

Figure 5.39. WAXS traces of selected fibres

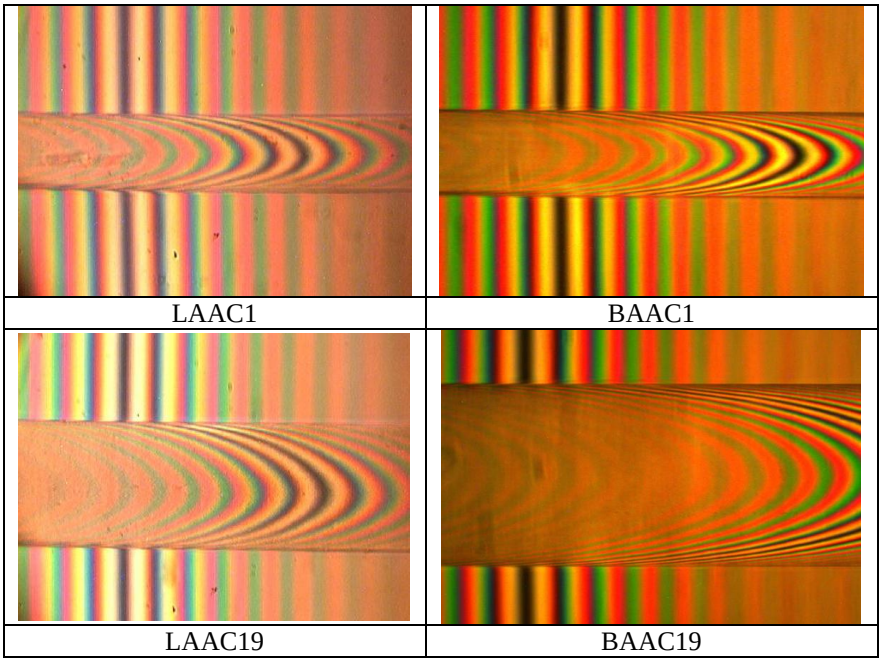

Figure 5.40. The microinterferograms of selected fibres using a Pluta microscope

5.7 Statistical Analysis and Discussion of BAAC Fibres

5.7.1 Spin Draw Ratio, Die Head Pressure and Thermo-Graphic Measurement

Because melt spinning parameters affect the properties, productivity and product cost, different samples of branched as-spun aliphatic-aromatic co-polyester fibres were spun with different process parameters (Table 5.2) and their effects determined. By connecting spin draw ratio, die head pressure and thermo-graphic measurement, the relationship between the interaction between rheology and process-ability of as spun fibres could be understood (Table 5.11). The results analyses will also explain the relationship between the air cooling, flow rate and die head pressure. The results determine the easily drawn structure and a better orientation along the fibre axis. The Pareto charts in Figure 5.41 show the spin draw ratio (a), die head pressure (b), filament' temperature average at L03(c) and filament' temperature average at L04 (d). The Pareto chart for the spin draw ratio (a) clearly shows that winding speed and metering pump speed are the most important factors affecting the spin draw ratio, followed by extrusion temperature and the interactions T& MPS and T&WS. Depending on drawing ratio applied, the structure changes involve alignment of the molecular chain and crystallinity along the fibre axis. High temperature allows the chains to interact with the winding speed. The variation between the extrusion speed (metering pump speed) and the winding speed causes notable effect on the dawn draw ratio. Spin line stress increases as spin draw ratio increases. The Pareto chart for die head pressure clearly shows that metering pump speed, extrusion temperature and their interaction are the most important factors affecting the die head pressure. The viscosity is affected by die head pressure and temperature and the molten polymer flow ratio relationship (described as metering pump speed) inside the die head as a result of the relationship between the output of the machine and the collection at different winding speeds. This relationship affects the extrusion speed and the spin draw ratio of the filaments. The Pareto chart for filament' temperature average at L03 clearly shows that metering pump speed, extrusion temperature, the interaction MPS&QA, winding speed and quench air speed are the most important factors affecting the filaments' temperature average at L03, followed by the interactions T&QA, T&WS and T&MPS. The Pareto chart for filament' temperature average at L04 shows the same effect of the factors noted in the filaments' temperature average at L03. The significant arrangement

of the factors will be metering pump speed, extrusion temperature, winding speed, quench air speed, the interactions T&MPS, QA&WS, MPS&QA and T&WS. The fibres diameter obtained by down draw ratio applied plays an important role in the thermal-content, as thicker fibres stay warm for long periods.

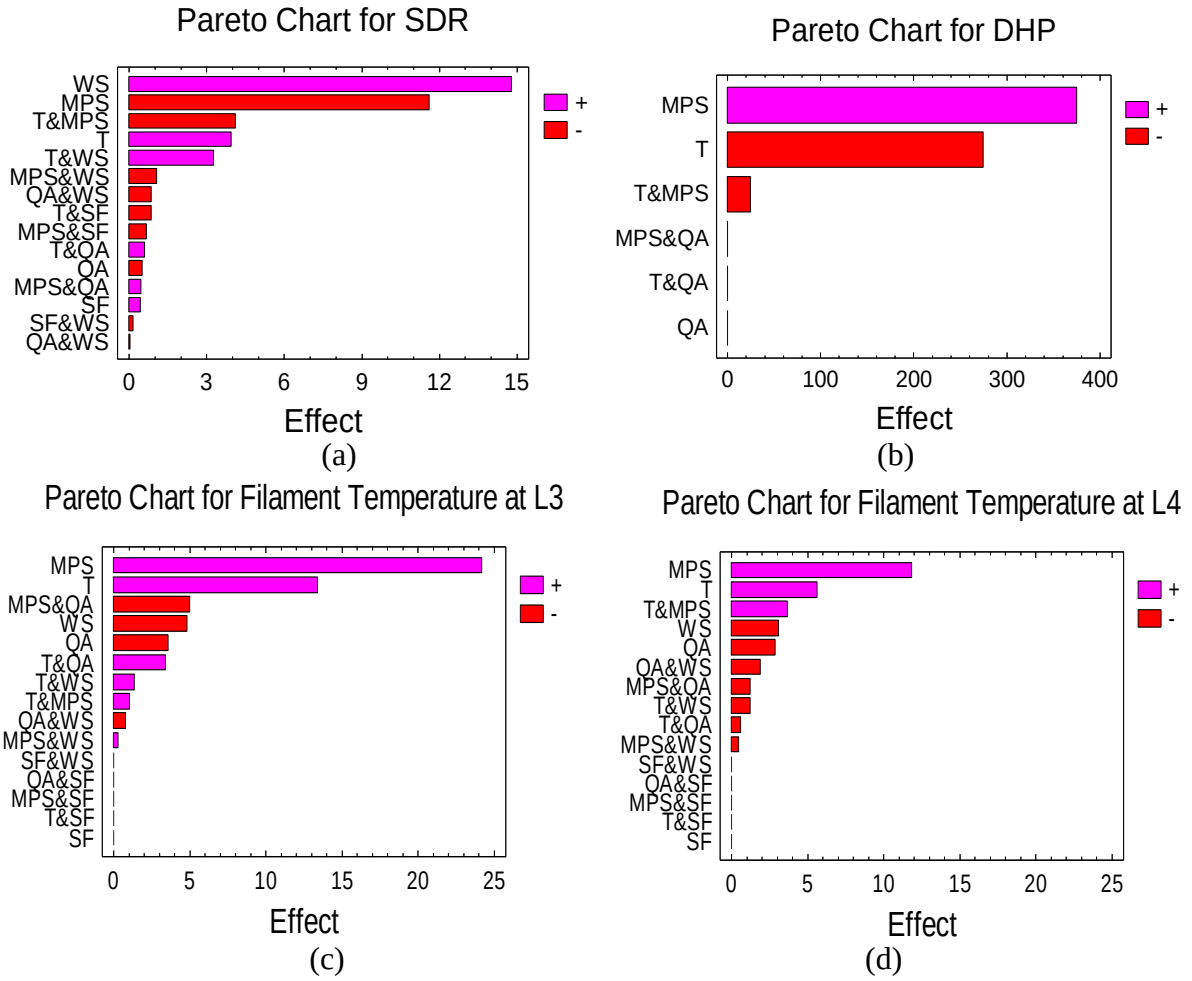

Figure 5.41. A ranked list of significant arrangement effects and interactions (Pareto chart) for the spin draw ratio (a), die head pressure (b), filament' temperature average at L03(c) and filament' temperature average at L04 (d).

Figure 5.42 and Figure 5.43 show the plots of statistical analysis of the effects caused by the main factors and their interactions on the spin draw ratio, die head pressure, filament' temperature average at L03 and filament' temperature average at L04 of as-spun fibres. From the statistical analysis of the effects caused by the main factors and their interactions on spin draw ratio (Figure 5.42, a and Figure 5.43, a), it can be noted that the effects from winding speed, metering pump speed, extrusion temperature and the interactions T&MPS and T&WS are prominent. Statistical analysis of the effects caused by the main factors and their

interactions on die head pressure (Figure 5.42, b and Figure 5.43, b) shows that, for the main effect plots, the effects from the extrusion temperature and the metering pump speed are significant. The filament' temperature average at L03 (Figure 5.42, c and Figure 5.43, c) was affected by metering pump speed, extrusion temperature, winding speed, quench air speed and the interactions MPS&QA, T&WS and T&QA. The viscosity, spinning temperature and flow rate relationship inside the die head could be understood by the connections between the studied responses results.

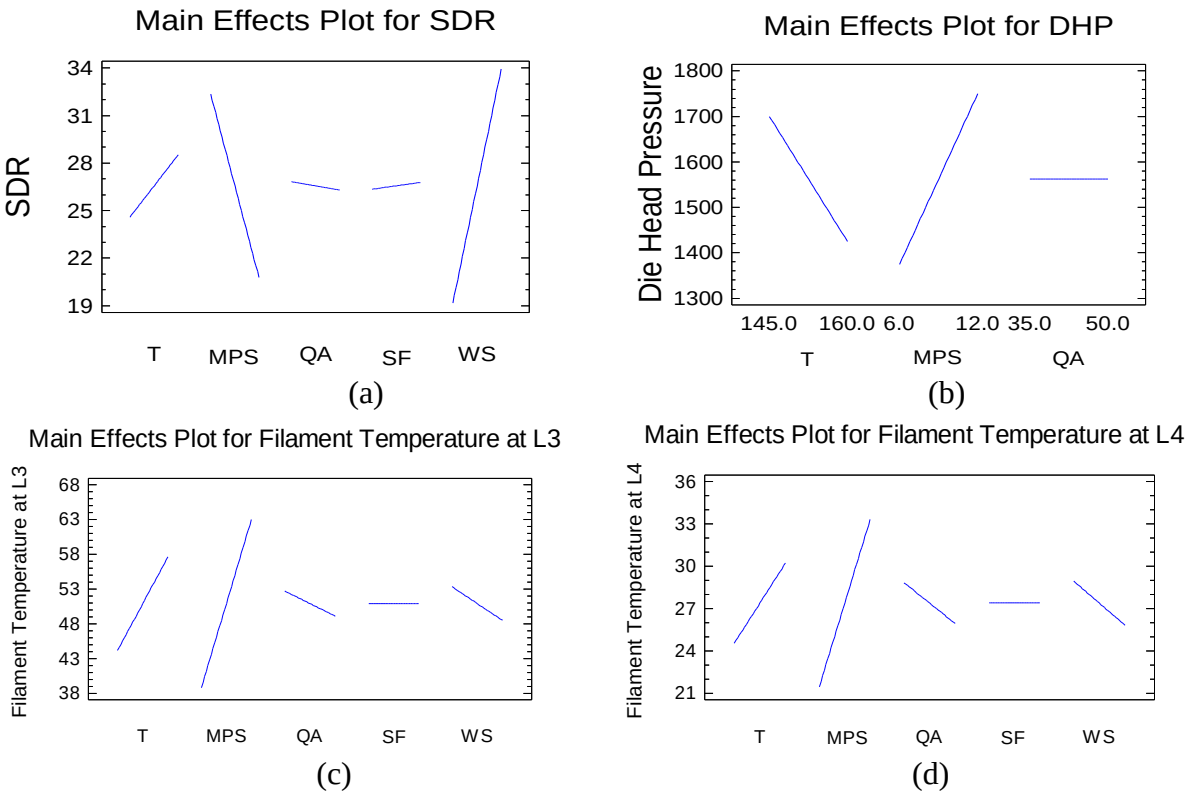

Figure 5.42. The effect plots for the spin draw ratio (a), die head pressure (b), filament' temperature average at L03 (c) and filament' temperature average at L04 (d)

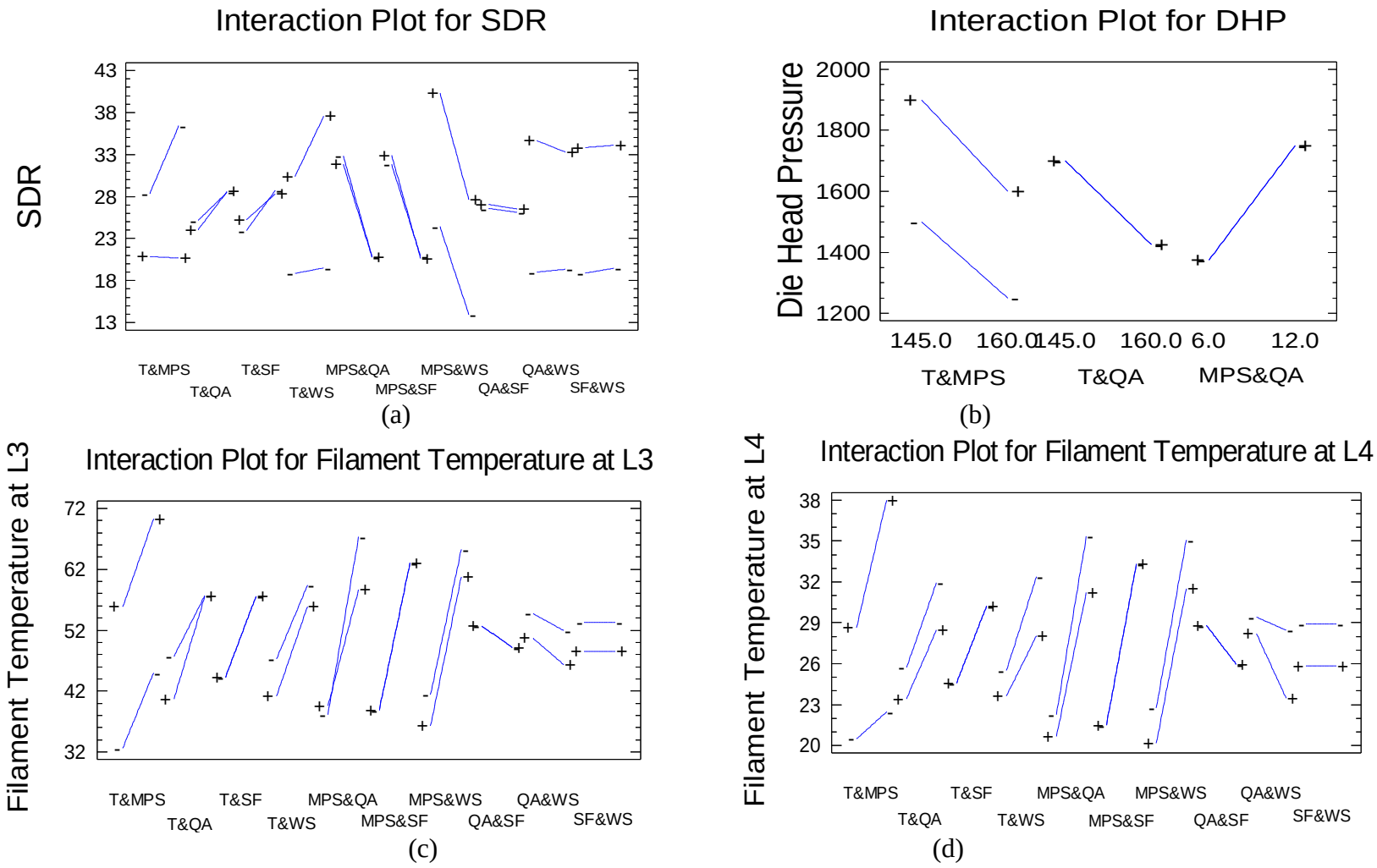

Figure 5.43. The interaction plots for the spin draw ratio (a), die head pressure (b), filament' temperature average at L03 (c) and filament' temperature average at L04 (d)

The filament' temperature average at L04 (Figure 5.42, d and Figure 5.43, d) was affected by metering pump speed, quench air speed, winding speed, extrusion temperature and the interactions T &MPS and QA&WS. These relationships affected the throughput flow rate and the spin draw ratio of the filaments to reduce the filament diameter; then the filament heating content needed to be cooled. Spinning temperature plays an interactive role with quench air cooling speed on the filament cooling speed and then solidification and the internal structure of filaments. Winding speed could control the cooling speed because it controls the cooling time leading to controlling the cooling ratio through the fibre bundle in the cooling window. The internal structure and crystallization will be significantly affected by the cooling process. Spin finish could affect the high temperature and could add cooling action on the fibres produced in addition to its main use.

Figure 5.44 displays the normal probability plots for SDR (a), die head pressure (b), filament' temperature average at L03 (c) and filament' temperature average at L04 (d) of as-spun fibres, and shows the percentage and standardized effects. From the normal probability plot for spin draw ratio (a), the positive effects from winding speed, extrusion temperature and their effects can be noted. The negative effects of metering pump speed and its interaction with spinning temperature are also prominent. As a result of rheological changes, the die head pressure (b) is significantly affected by metering pump speed which has a positive effect and decreases with extrusion temperature which gives a negative effect.

The filament' temperature average at L03 of as-spun fibres (c) is affected by metering pump speed, extrusion temperature, winding speed and quench air speed and the interactions T&QA and MPS&QA. From the normal probability plot for the filament' temperature average at L04 of as-spun fibre (d), it is noted that the effects from metering pump speed, extrusion temperature, winding speed, quench air speed and the interaction T&MPS are prominent. Extrusion temperature plays an important role in controlling the fibre structure as well as affecting the spin draw ratio.

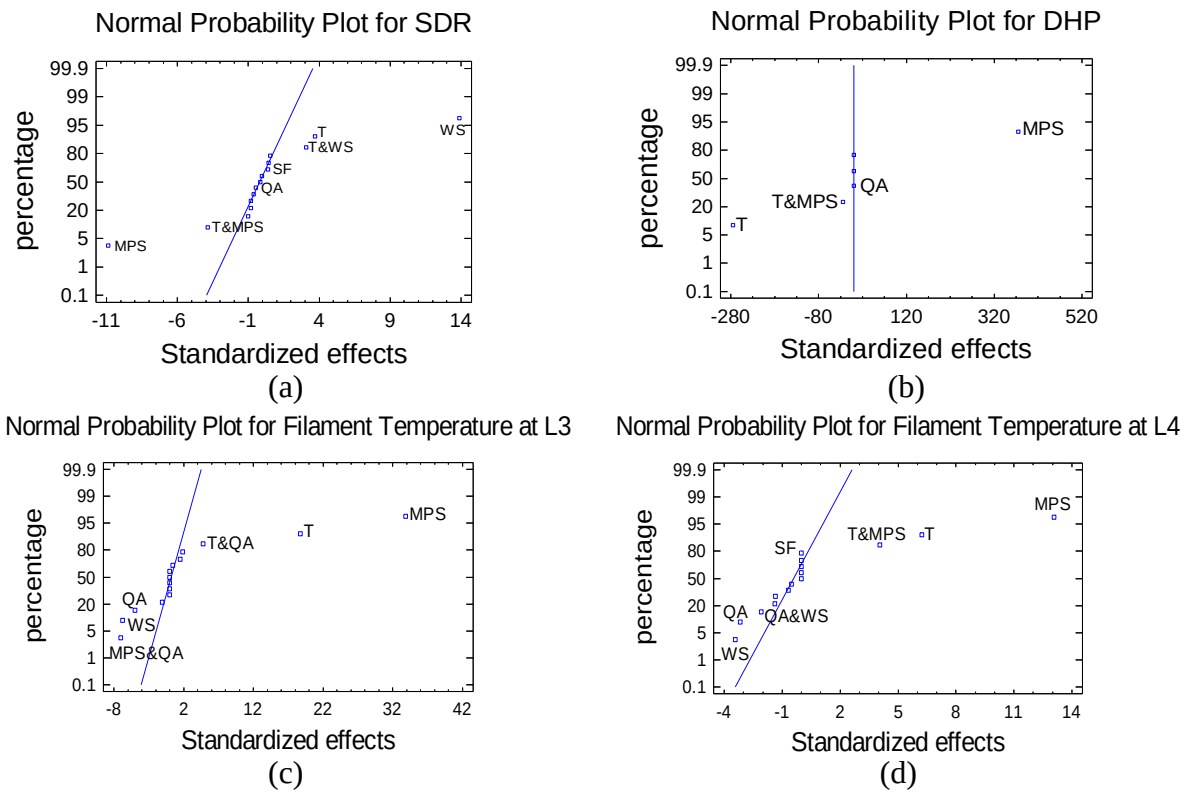

Figure 5.44. Statistical standardized and percentage order values of factors and their interactions (the normal probability plot) for the spin draw ratio (a), die head pressure (b), filament' temperature average at L03 (c) and filament' temperature average at L04 (d).

5.7.1.1 Analysis of Variance (ANOVA)

The ANOVA results are listed in Table 5.13. The factor has a significant effect if its F ratio is much larger than the circuital value (F=4.49), which was obtained from F tables at the appropriate level α =0.05, or its P-value is smaller than 0.05. Spin draw ratio is significantly affected by winding speed (P_{WS} 0.000) > metering pump speed (P_{MPS} = 0.000) > extrusion temperature (P_T = 0.002) and the interactions T&MPS ($P_{T\&MPS}$ = 0.001) and T&WS ($P_{T\&WS}$ = 0.007). There are no significant effects of the other factors and interactions. Note that, although $P_{MPS} = P_{WS}$ = 0.000, the order of the significance is obtained depending on F-Ratio listed. The significant studied factors on die head pressure are metering pump speed (P_{MPS} = 0.000)> extrusion temperature (P_T 0.000)>T&MPS ($P_{T\&MPS}$ 0.000). No significant effect of QA (P_{MPS} = 0.3269>0.05) and other interactions were detected. Filament' temperature average at L03 of as-spun fibres is significantly affected by metering pump speed (P_{MPS} = 0.000) > extrusion temperature (P_T = 0.000) > MPS&QA ($P_{MPS\&QA}$ 0.000)> winding speed (P_{WS} 0.000)> quench air speed (P_{QA} = 0.000) >T&QA ($P_{T\&QA}$ 0.000). There are no significant

effects of the other factors and interactions. In the filament' temperature average at L04 of as-spun fibres analysis, the significance of factors will then be by metering pump speed (P_{MPS} = 0.000) > extrusion temperature (P_T = 0.000) > T& MPS ($P_{T\&MPS}$ 0.009)> winding speed (P_{WS} 0.035). There are no significant effects of the other factors and interactions. The quantitative ANOVA results are consistent with quantitative conclusions derived from the effects plots and Daniel's plots. The filament diameter decreases scientifically by spin draw ratio increasing; then the filament heating content needs to be cooled. The cooling ratio is affected by throughput rate, yarn cross section and air cooling temperature.

Source	SDR		DHP		Filament Temperature			
					at L03		at L04	
	F	P	F	P	F	P	F	P
T	13.7	0.002	2025	0.000	351.19	0.000	38.89	0.0000
MPS	119.0	0.000	3481	0.000	1147.8	0.000	171.06	0.0000
QA	0.2	0.633	1.0	0.3269	25.00	0.000	10.07	0.0059
SF	0.2	0.691	-	-	0.00	1.000	0.00	1.0000
WS	193.3	0.000	-	-	45.53	0.000	11.71	0.0035
T &MPS	15.0	0.001	25	0.000	2.16	0.161	16.45	0.0009
T & QA	0.3	0.585	1.0	0.3269	22.61	0.000	0.44	0.5173
T& SF	0.7	0.433	-	-	0.00	1.000	0.00	1.0000
T& WS	9.5	0.007	-	-	3.56	0.077	1.83	0.1952
MPS& QA	0.2	0.665	1.0	0.3269	49.39	0.000	1.90	0.1867
MPS& SF	0.4	0.531	-	-	0.00	1.000	0.00	1.0000
MPS& WS	1.0	0.330	-	-	0.21	0.656	0.27	0.6073
QA & SF	0.0	0.968	-	-	0.00	1.000	0.00	1.0000
QA & WS	0.7	0.433	-	-	1.17	0.295	4.40	0.0522
SF& WS	0.0	0.885	-	-	0.00	1.000	0.00	1.0000

Table 5.13. ANOVA results identifying the statistical significance of factors' effects on the die head pressure, FWHM, filament temperature averages at L03 and L04

5.7.1.2 The Regression Equation and Estimation Results

Based on the analysis, the simplified models were fitted by the regression equations which were fitted to the experimental data. The regression equations forecast SDR, die head pressure and temperature averages at L03 and L04 in order to achieve the most satisfactory

properties in the final desired fibre for different applications. The regression equations in terms of the previous coded values (Table 5.1) are given as follows:

Spin draw ratio = -74.6535 + 0.529583*T + 12.7587*MPS - 0.745417*QA + 137.347*SF - 0.859625*WS - 0.0915278*T*MPS + 0.00527778*T*QA - 0.761111*T*SF + 0.00875*T*WS + 0.0104167*MPS*QA - 1.51389*MPS*SF - 0.007125*MPS*WS - 0.0388889*QA*SF - 0.00228333*QA*WS - 0.0416667*SF*WS (5.17)

Die head pressure = 3033.33 - 13.3333*T + 147.222*M+ 0.0*Q - 0.555556*T*M+ 0.0*T*Q + 0.0*M*Q (5.18)

Filament temperature at L3 = 116.949 - 0.871111*T + 5.0625*MPS - 3.68722*QA + 0.0*SF - 0.577167*WS + 0.0233333*T*MPS + 0.0302222*T*QA + 0.0*T*SF + 0.0036*T*WS - 0.111667*MPS*QA + 0.0*MPS*SF + 0.00216667*MPS*WS + 0.0*QA*SF - 0.00206667*QA*WS + 0.0*SF*WS (5.19)

Filament temperature at L4 = -23.7875 + 0.113333*T - 9.06111*MPS + 1.25167*QA + 0.0*SF + 0.68*WS + 0.0816667*T*MPS - 0.00533333*T*QA + 0.0*T*SF - 0.00326667*T*WS - 0.0277778*MPS*QA + 0.0*MPS*SF - 0.00316667*MPS*WS + 0.0*QA*SF - 0.00506667*QA*WS + 0.0*SF*WS (5.20)

For the observed and fitted results generated for each trial, shown in Figure 5.45, the models gave useful results for the spin draw ratio (a), the die head pressure (b) and temperature averages at L03 (c) and temperature averages at L04 (d). Their Model Standard Error (MSE) values listed in Table 5.15 indicate the dispersion of predicted and observed values around the theoretical fitted line generated using the fitted model for each trial. There are small variations related to extrusion machine setting based variation, the nature of the polymer and the nonuniform flow, the tension winding system variation, tension during the preparation of the sample for testing, and the difference in the cooling rate through the filament bundle.

Again, the geometric result of plotting a response variable is as a function of two factors and the interaction appears with the surface twist. In order to observe the direction of the interactions T&WS and T&MPS for SDR and DHP, the estimated response surfaces are shown in Figure 5.46. Because of the twist found, the effects detected are significant and they confirm the previous statistical analysis.

The twist in the surface in plots seen in Figure 5.47 confirms the interaction, as mentioned before in the previous statistical analysis results. The twists in estimated response surfaces T&QA and MPS&QA for filament temperature at L3 (a-b) and T&MPS and QA&WS for filament' temperature average at L04 (c-d) confirm the interactions, as described before in

the previous statistical analysis results. In the cube plots (Figure 5.48) for the SDR (a), die head pressure (b) and filament temperature averages at L03 (c) and temperature averages at L04 (d) and depending on the regression equation, each value corresponds to the values of the experimental factors WS, T and MPS at the middle levels of QA and SF. The wind up speed controls the spin draw ratio and tension on material from the spinneret through the cooling and solidification steps. A decrease of spinning temperature leads to higher viscosity, higher flow resistance through the spinneret's nozzle and higher die head pressure. Form the relationship between the extrusion speed and take up speed and by connecting them with the material rheology and thermal content, a clear physical image could be obtained. Because the difference of the velocity field and the pressure around the bundle sides, non-uniform structure and properties could be obtained. The cooling ratio affects the crystallinity; cooling time is affected by extrusion rate, fibre cross section and air cooling temperature

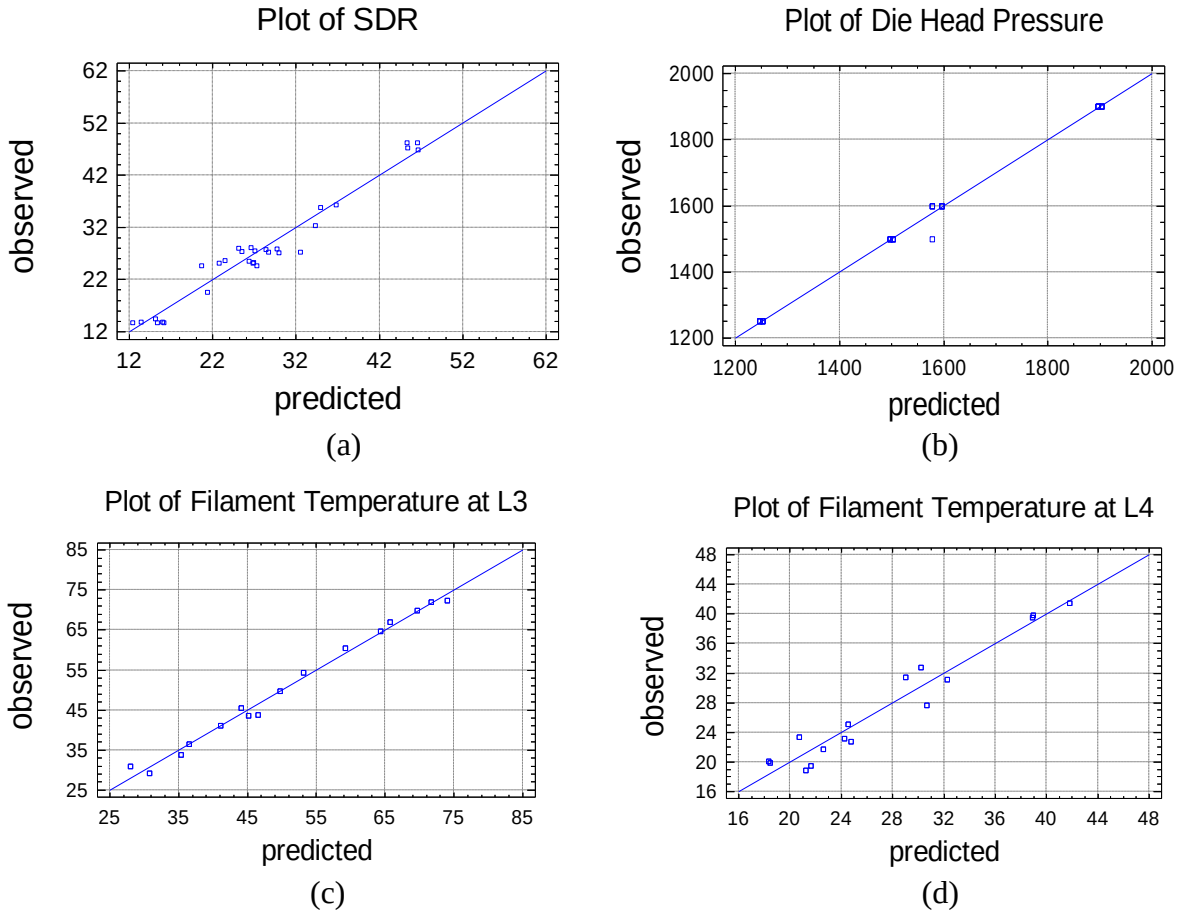

Figure 5.45. Experimental observed results and calculated fitted results plot for the spin draw ratio (a), die head pressure (b), filament temperature average at L03(c) and filament temperature average at L04 (d).

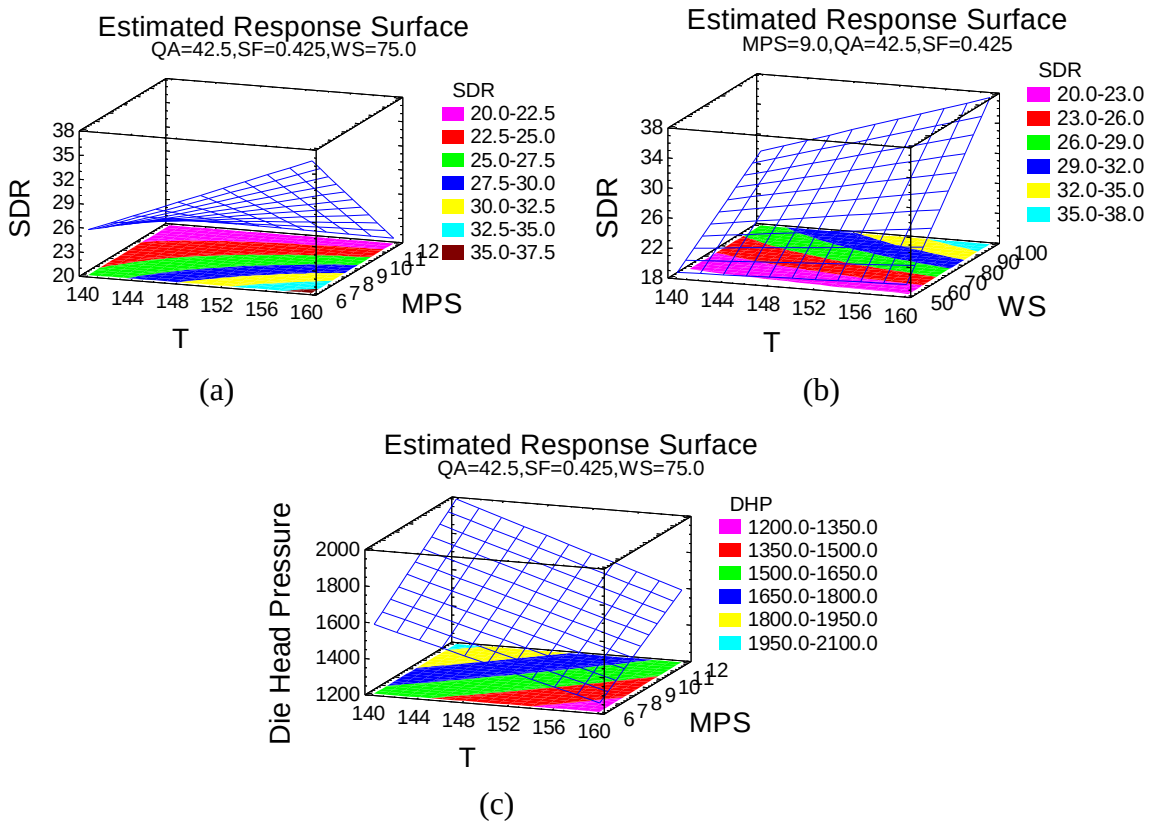

Figure 5.46. Estimated response surface for the spin draw ratio (a-b) and DHP(c)

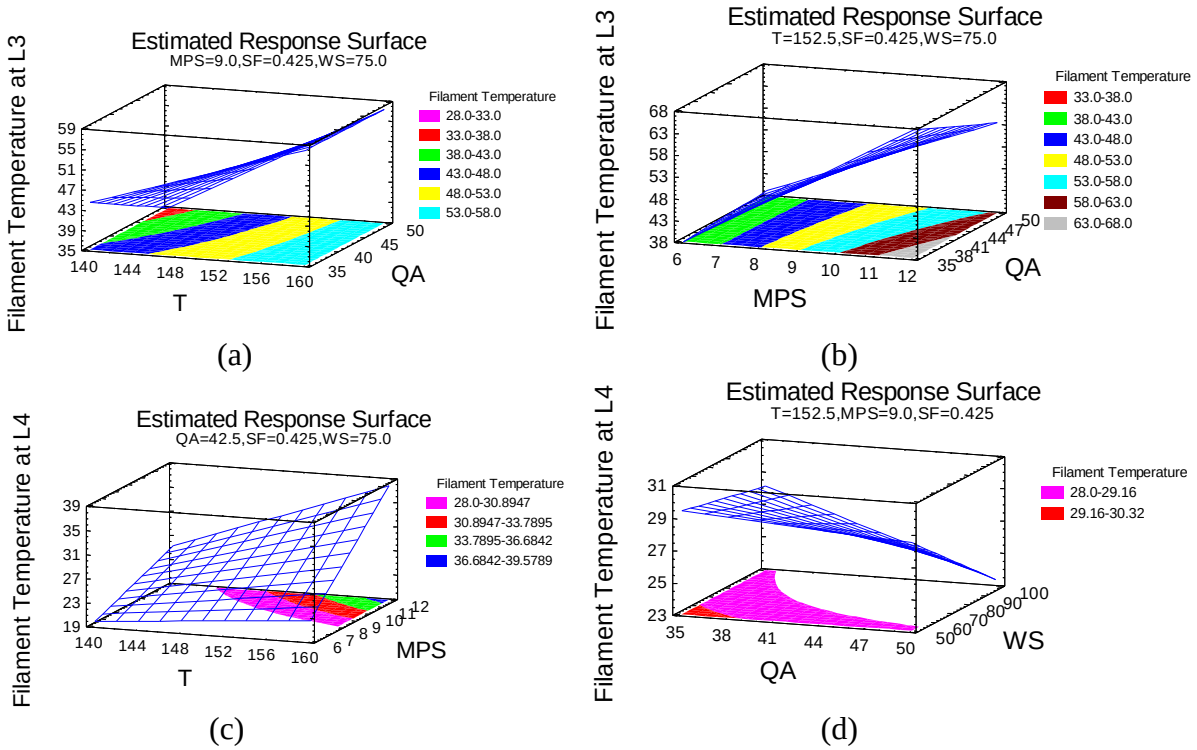

Figure 5.47. Estimated response surface for filament' temperature average at L03 (a-b) and L04 (c-d)

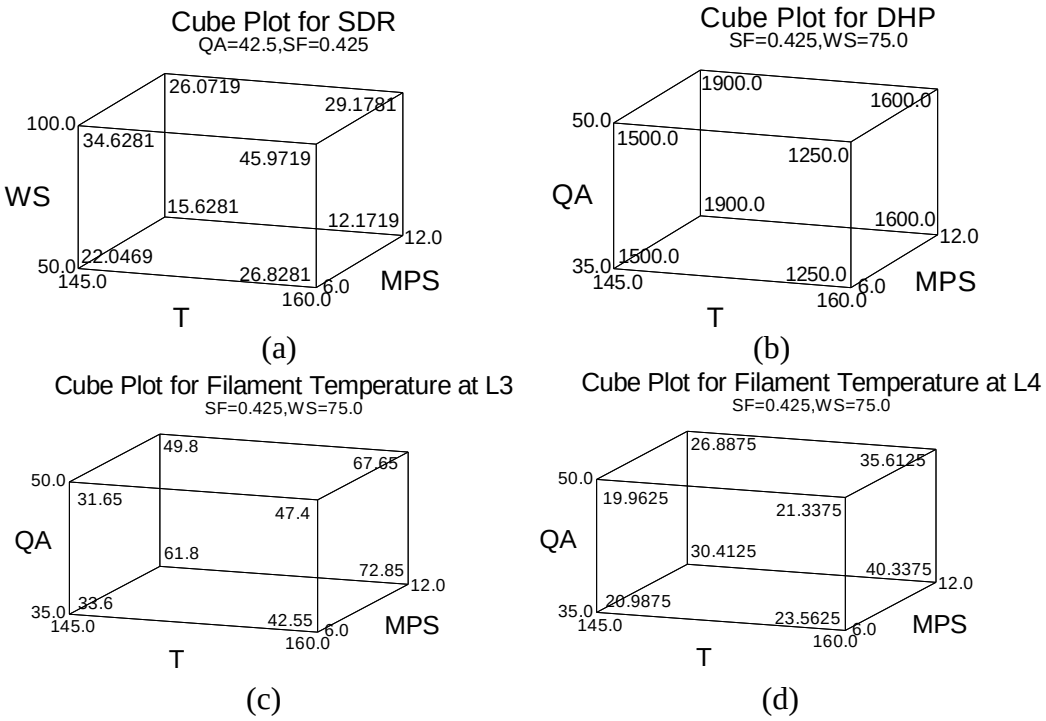

Figure 5.48 show the cube plots of the estimated effects for the high and low settings of MPS, T and WS for the spin draw ratio (a), and cube plots of the estimated effects for the high and low settings of MPS, T and QA for die head pressure (b), filament temperature average at L03 (c) and filament temperature average at L04 (d).

5.7.2 Diameter, Tensile Properties and Thermal Shrinkage

The mathematically concise statistical models predict the diameter, tenacity, elongation at break, modulus and thermal shrinkage of the spun fibre in terms of random variables and their associated probability distributions. The relationships between those proportions give the most satisfactory properties in the extruded fibre for different applications. The percentage of fibre extension could be limited by cross-linking of the polymer structure which will affect the biodegradability of the fibres [219].

Because used fibres have thermoplastic properties, the testing of thermal shrinkage or extension of yarns and fabrics made from such materials is required. Different samples of branched as-spun aliphatic-aromatic co-polyester fibres were spun at different process parameters to determine and model their effects. The aim was to demonstrate how variation in spinning conditions can affect the diameter, tensile properties and thermal shrinkage and that give a better insight into the relationship between melt spinning process parameters and fibre properties. After different samples of branched as-spun aliphatic-aromatic co-polyester

fibres were spun at different process parameters (Table 5.2), their effects were determined and modelled (Table 5.12).

The Pareto chart (Figure 5.49), for diameter (a), tenacity (b), elongation at break (c), modulus (d) and thermal shrinkage (e) shows the significant arrangement of factors and their interactions in decreasing order. The Pareto chart for diameter shows that winding speed, metering pump speed, extrusion temperature and the interactions MPS&WS, T&MPS and T&WS are the most important factors affecting the diameter. Winding speed, metering pump speed, extrusion temperature and the interactions T&MPS, T&WS and T&SF are the most important factors affecting the tenacity, followed by other factors and interactions. The Pareto chart for elongation at break clearly shows that the interaction MPS&WS, metering pump speed, winding speed, extrusion temperature and the interaction T&QA are the most important factors affecting the elongation at break, followed by the interactions QA&SF and T&SF, and other factors and interactions.

The interaction between metering pump speed and winding speed is related to the relationship between extrusion speed and the collection at different speeds, which affects the throughput flow rate and the spin draw ratio of the filaments and then changes the filament diameter. The Pareto chart for modulus shows that winding speed, metering pump speed, extrusion temperature and the interactions QA&SF, MPS&QA, SF&WS, QA&WS and MPS&SF are the most important factors affecting the modulus followed by the interactions T&SF and T&WS. The Pareto chart for thermal shrinkage clearly shows that winding speed, metering pump speed, extrusion temperature, quench air speed and the interactions MPS&WS, SF&WS and T&SF are the most important factors affecting the thermal shrinkage. The factors increasing the down draw ratio negatively affect the elongation at break. Figure 5.50, Figure 5.51 and Figure 5.52 show the effect plots of statistical analysis of the effects caused by the main factors and their interactions on the diameter, tenacity, elongation at break, modulus and thermal shrinkage of as-spun fibres obtained using the designed matrix. The statistical analysis of the effects caused by the main factors effect and their interactions on diameter (Figure 5.50) shows that the effects from the winding speed, metering pump speed, extrusion temperature and the interactions T&MPS, MPS&WS and T&WS are significant.

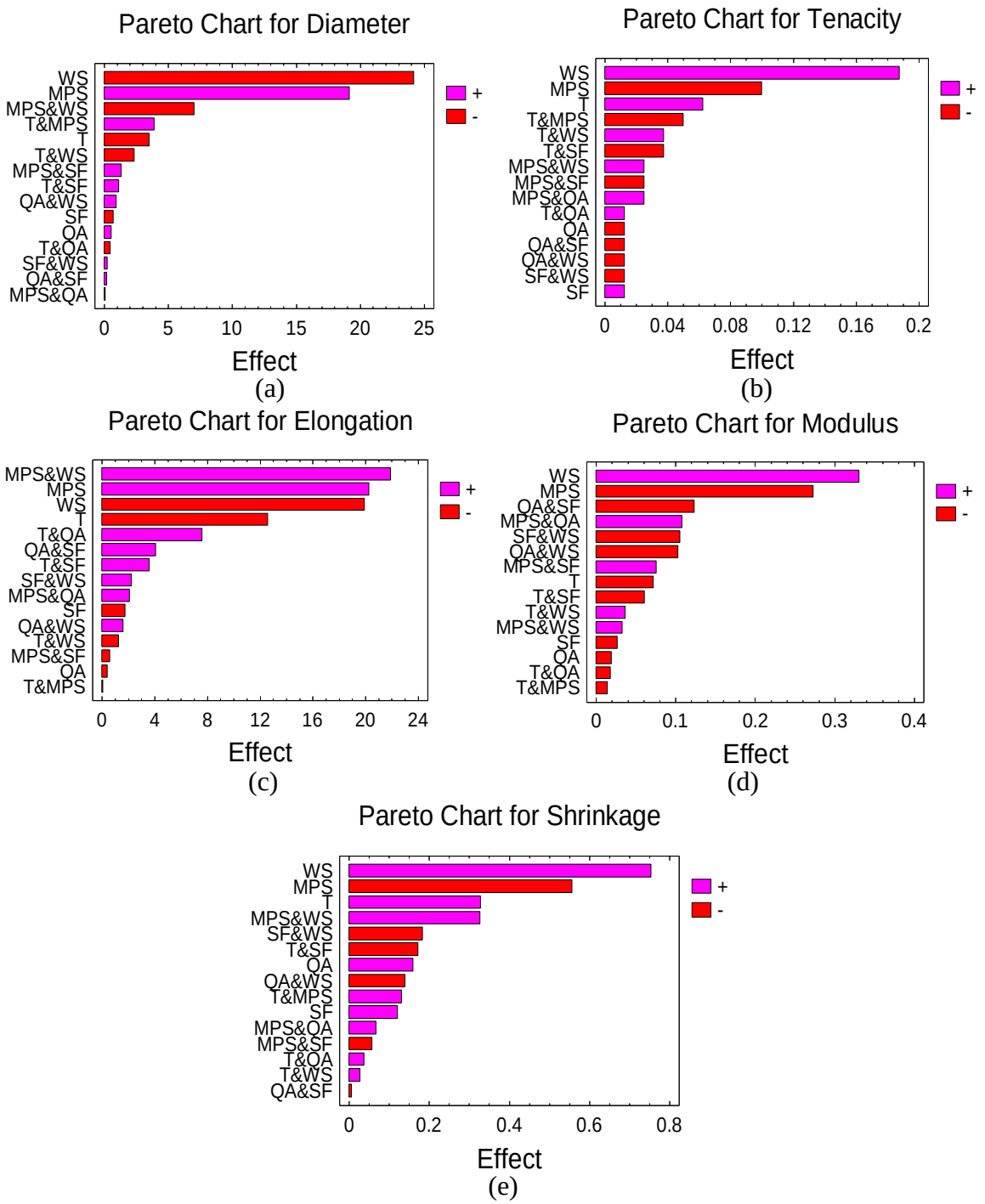

Figure 5.49. A ranked list of significant arrangement effects and interactions (Pareto chart) for diameter (a), tenacity (b), elongation at break (c), modulus (d) and thermal shrinkage (e)

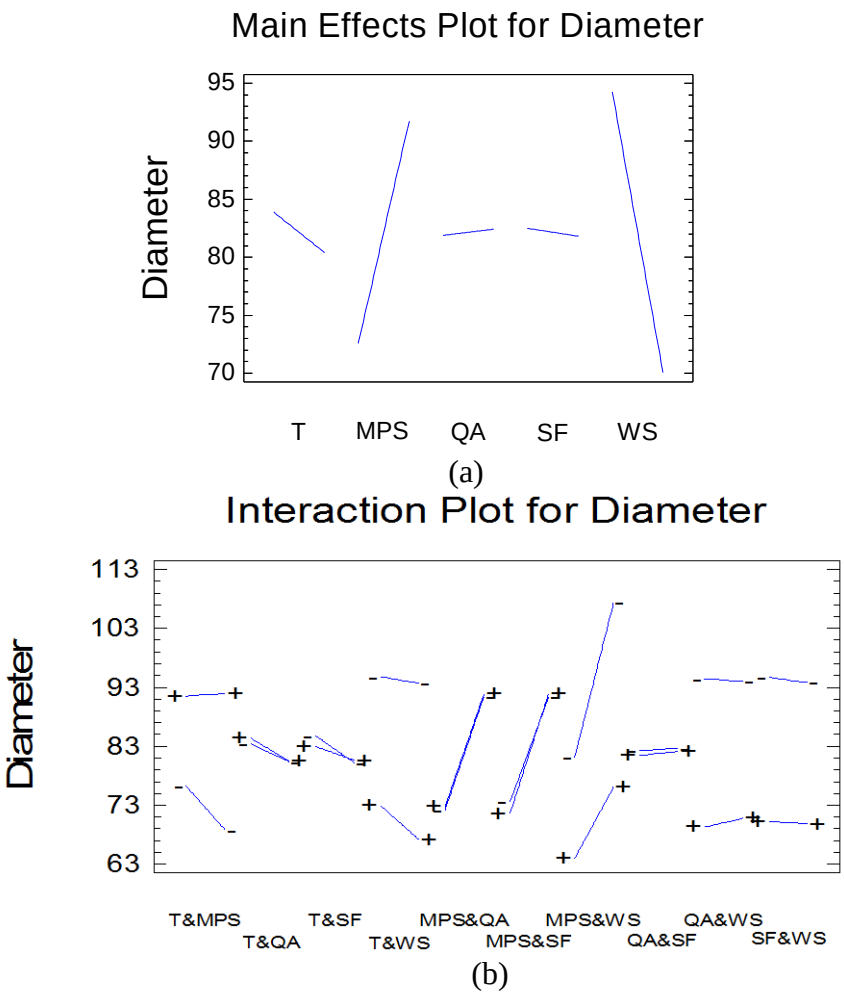

Figure 5.50. The main effect and interaction plots for diameter

The interaction between metering pump speed and winding speed could be related to the relationship between the output of the machine, viscosity change of molten polymer, the melt temperature and the collection at different speeds. It affects the throughput flow rate and reduces the filament diameter. The main factor effect for tenacity (Figure 5.51 and Figure 5.52, a) is strongly affected by extrusion temperature, metering pump speed and winding speed. The interaction of T&MPS needs to be further investigated. No significant effect was reported for other factors and interactions. Elongation at break (Figure 5.51 and Figure 5.52, b) was affected by metering pump speed, winding speed and extrusion temperature. The interactions T&QA, T&SF, QA&SF and MPS&WS need to be further investigated; statistical analysis ANOVA is given in next section. No significant effect was reported for other factors and interactions. Modulus (Figure 5.51 and Figure 5.52, c) was affected by the main factors metering pump speed and winding speed. The interactions of MPS&QA, QA&WS and QA&SF affect the modulus and statistical analysis; their statistical analysis

ANOVA is given in next section. Thermal shrinkage (Figure 5.51 and Figure 5.52, d) is strongly affected by extrusion temperature, winding speed and metering pump speed, while the interactions T&SF, QA&WS, T&MPS, MPS&WS and SF&WS strongly affect the thermal shrinkage and need to be investigated. The effects of interactions on thermal shrinkage could be related to the effect of these factors on the down draw ratio, as noted previously.

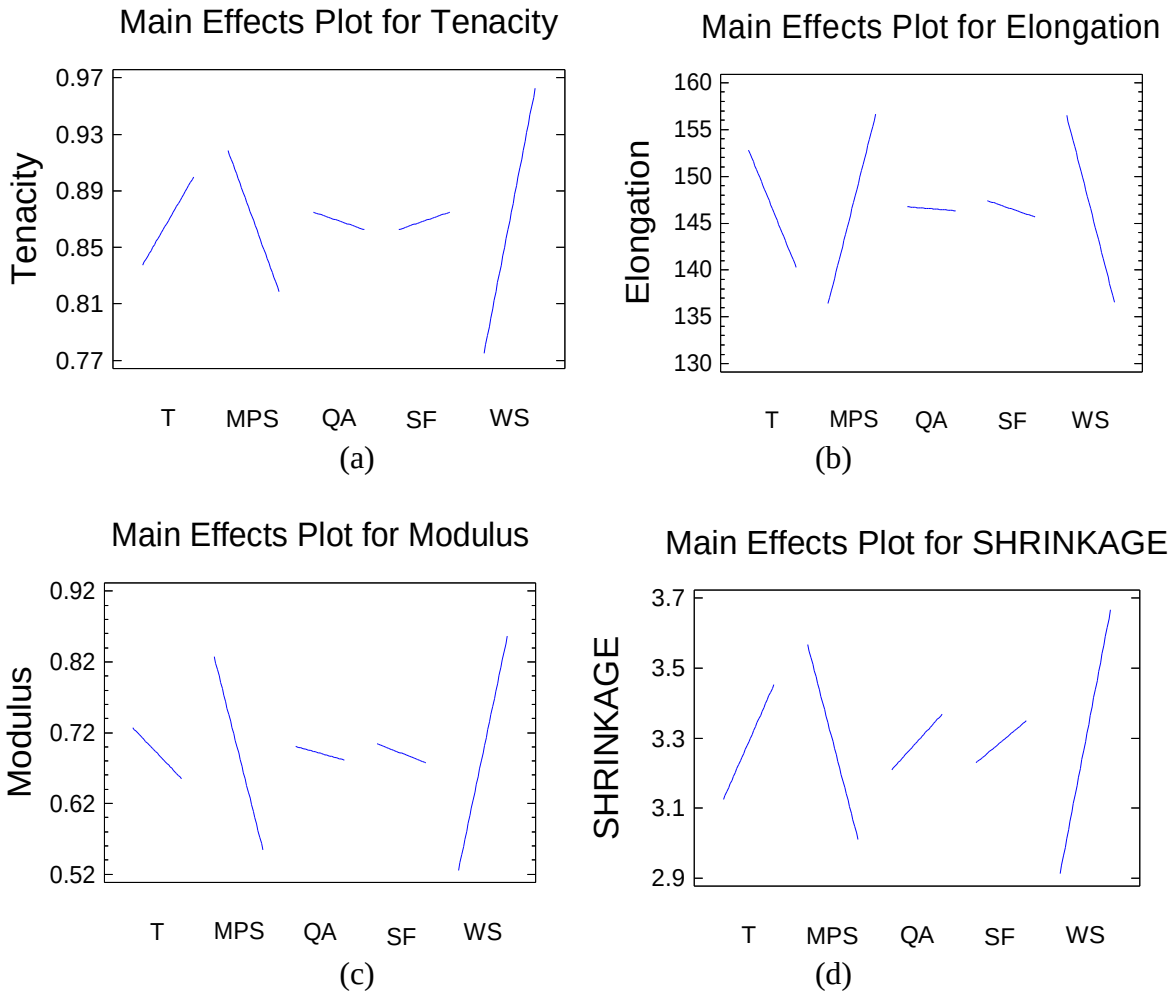

Figure 5.51. The main effect plots for tenacity (a), elongation at break (b) modulus (c) and thermal shrinkage (d)

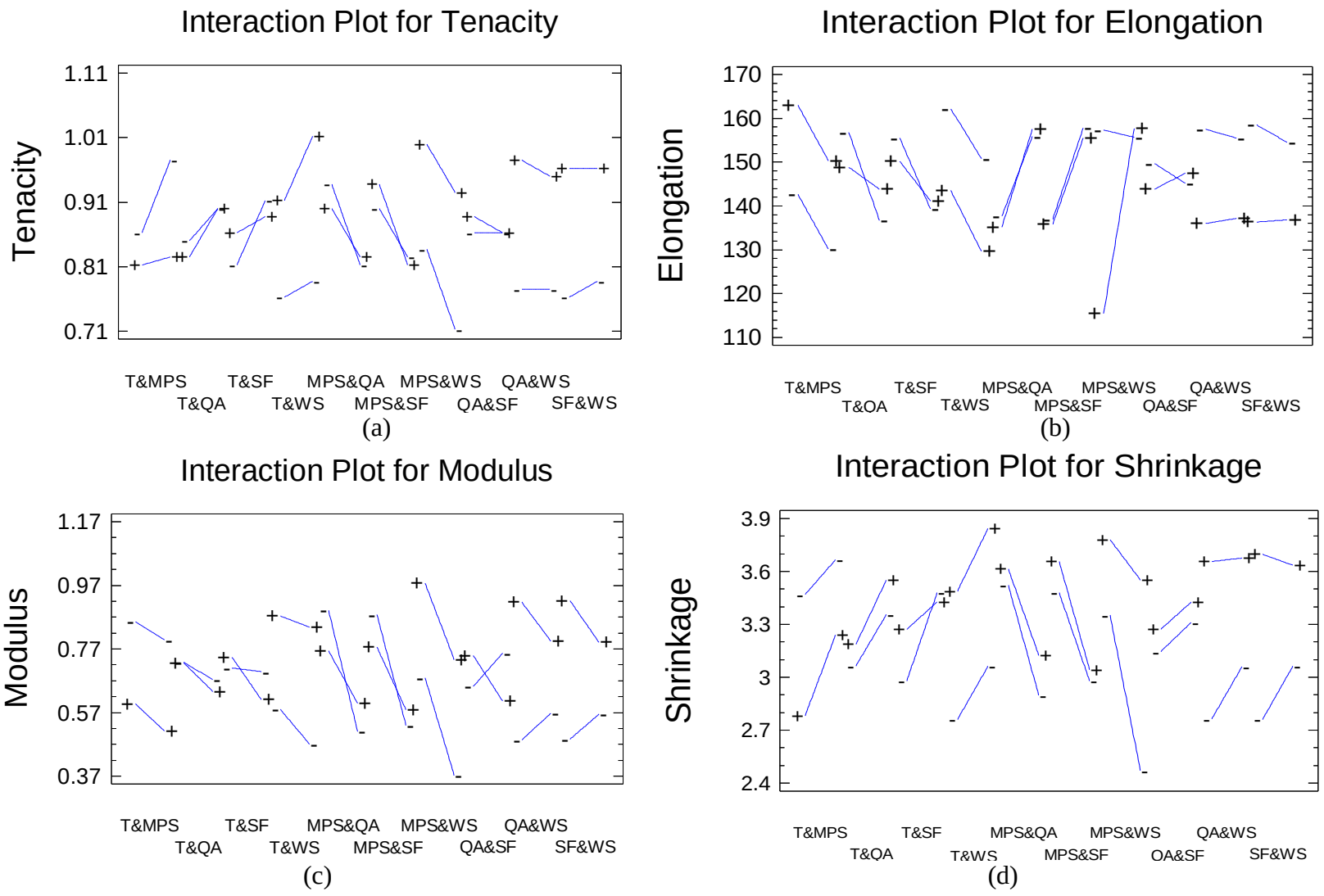

Figure 5.52. The interaction plots for tenacity (a), elongation at break (b) modulus (c) and thermal shrinkage (d)

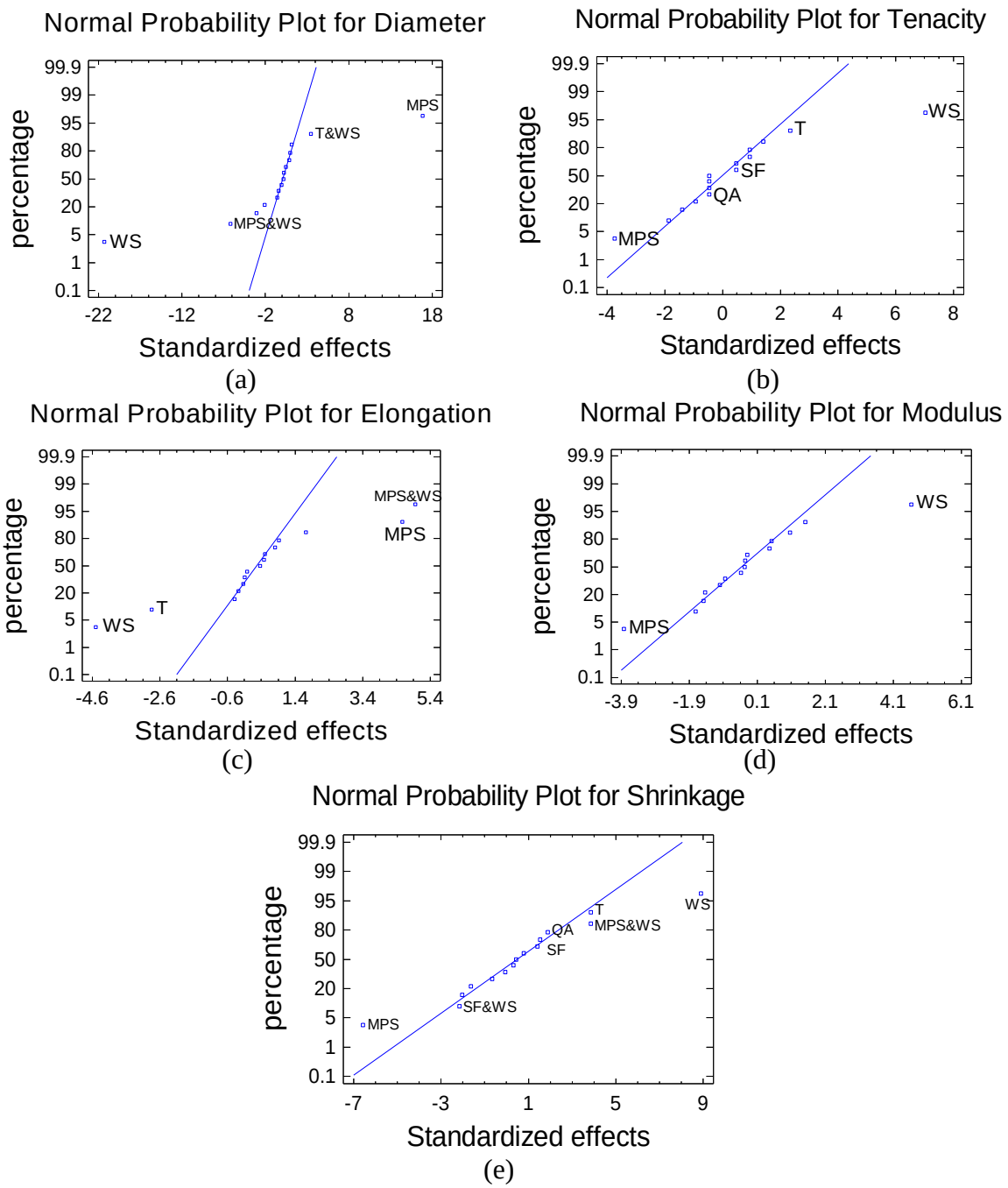

Figure 5.53. Statistical standardized and percentage order values of factors and their interactions (the normal probability plot) for the diameter (a), tenacity (b), elongation at break (c), modulus (d) and thermal shrinkage (e)

Figure 5.53 displays the normal probability plots for on the diameter, tenacity, elongation at break, modulus and thermal shrinkage of as-spun fibres obtained. The diameter plot (a) shows the positive effects of metering pump speed and T&WS and the negative effect of winding speed and its interaction with the metering pump speed on the diameter. Tenacity (b) is affected positively by winding speed and extrusion temperature and negatively by the

metering pump speed. Extrusion temperature and winding speed negatively affect the elongation at break. Metering pump speed and its interaction with winding speed positively affect the elongation at break (c). This could be related to the interaction effect on the spin draw ratio which decreases the elongation at break ratio. In the modulus analysis (d), it is significant that winding speed has a positive effect and metering pump speed has a negative effect on the modulus. The thermal shrinkage (d) is positively affected by winding speed, the interaction MPS&WS, extrusion temperature and the interaction SF&WS and it is negatively affected by metering pump speed increasing.

5.7.2.1 Analysis of Variance (ANOVA)

The ANOVA results for diameter, tenacity, elongation at break, modulus and thermal shrinkage of as-spun fibres are listed in Table 5.14. The significant factors on the diameter are winding speed (P_{WS} 0.000)> metering pump speed (P_{MPS} = 0.000)> extrusion temperature (P_T = 0.007). No significant effects of spin finish applicator or quench air speed were found. The interactions MPS&WS ($P_{MPS\&WS}$= 0.000) and T&MPS ($P_{T\&MPS}$= 0.003) have significant effects. There are no significant effects of the other interactions on diameter.

On the mechanical properties, tenacity is significantly affected by winding speed (P_{WS} 0.000) > metering pump speed (P_{MPS} = 0.002) > extrusion temperature (P_T = 0.033) and the interactions T&MPS ($P_{T\&MPS}$ = 0.000) >MPS&WS ($P_{MPS\&WS}$ 0.001)> T&WS ($P_{T\&WS}$ = 0.001). There are no significant effects of the other factors and interactions. Elongation at break is significantly affected by metering pump speed (P_{MPS} = 0.000)> winding speed (P_{WS} 0.000)> extrusion temperature (P_T = 0.012)> QA and the interaction MPS&WS ($P_{MPS\&WS}$ = 0.000). There are no significant effects of the other factors and interactions. Modulus is significantly affected by winding speed (P_{WS} 0.000)> metering pump speed (P_{MPS} = 0.001). There are no significant effects of the other factors and interactions. Thermal shrinkage is significantly affected by winding speed (P_{WS} 0.000)> metering pump speed (P_{MPS} = 0.000) > extrusion temperature (P_T = 0.001) and the interactions MPS&WS ($P_{MPS\&WS}$ = 0.001) >SF&WS ($P_{SF\&WS}$ = 0.046). There are no significant effects of the other factors and interactions.

Source	Diameter		Tenacity		Elongation at break		Modulus		Thermal shrinkage	
	F	**P**	**F**	**P**	**F**	**P**	**F**	**P**	**F**	**P**
T	9.4	0.007	5.5	0.033	8.1	0.012	1.01	0.329	15.0	0.001
MPS	284.4	0.000	14.0	0.002	21.0	0.000	14.58	0.001	43.2	0.000
QA	0.2	0.646	0.2	0.646	0.0	0.926	0.07	0.789	3.5	0.078
SF	0.4	0.557	0.2	0.646	0.2	0.697	0.14	0.712	2.0	0.174
WS	453	0.000	49.3	0.000	20.3	0.000	21.37	0.000	79.2	0.000
T &MPS	11.8	0.003	3.5	0.080	0.0	0.985	0.04	0.843	2.4	0.143
T & QA	0.2	0.693	0.2	0.646	2.9	0.105	0.06	0.803	0.2	0.669
T& SF	1.0	0.336	2.0	0.179	0.7	0.429	0.72	0.409	4.1	0.060
T& WS	4.3	0.055	2.0	0.179	0.1	0.781	0.27	0.613	0.1	0.755
MPS& QA	0.0	0.947	0.9	0.363	0.2	0.644	2.29	0.150	0.6	0.442
MPS& SF	1.3	0.269	0.9	0.363	0.0	0.897	1.12	0.306	0.5	0.512
MPS& WS	38.3	0.000	0.9	0.363	24.6	0.000	0.21	0.649	14.9	0.001
QA & SF	0.0	0.860	0.2	0.646	0.9	0.369	2.96	0.105	0.0	0.948
QA & WS	0.7	0.418	0.2	0.646	0.1	0.725	2.08	0.169	2.7	0.120
SF& WS	0.0	0.844	0.2	0.646	0.3	0.618	2.18	0.159	4.7	0.046

Table 5.14. ANOVA results identifying the statistical significance of factor effects on the diameter, tenacity, elongation at break, modulus and thermal shrinkage

5.7.2.2 The regression Equation and Estimation Results

Diameter, tenacity, elongation at break, modulus and thermal shrinkage were fitted with the regression equations which were fitted to the experimental data. The regression equations in terms of the previous coded values (Table 5.1) are given as follows:

Diameter = 203.829 - 0.798167*T - 7.69403*MPS + 0.404944*QA - 195.822*SF + 0.760183*WS + 0.0868889*T*MPS - 0.00406667*T*QA + 1.00333*T*SF - 0.00626333*T*WS - 0.00172222*MPS*QA + 2.89167*MPS*SF - 0.0468917*MPS*WS + 0.181111*QA*SF + 0.00252333*QA*WS + 0.0606667*SF*WS (5.21)

Tenacity = -2.02014 + 0.0161111*T + 0.140278*MPS - 0.0155556*QA + 6.38889*SF - 0.0101667*WS - 0.00111111*T*MPS + 0.000111111*T*QA - 0.0333333*T*SF + 0.0001*T*WS + 0.000555556*MPS*QA - 0.0555556*MPS*SF + 0.000166667*MPS*WS - 0.0111111*QA*SF - 0.0000333333*QA*WS - 0.00333333*SF*WS (5.22)

Elongation at break = 1092.27 - 4.79049*T - 8.72052*MPS - 12.5833*QA - 684.96*SF - 1.63933*WS - 0.00184722*T*MPS + 0.0674056*T*QA + 3.185*T*SF - 0.003335*T*WS + 0.0463194*MPS*QA - 1.29583*MPS*SF + 0.146121*MPS*WS + 3.62944*QA*SF + 0.004225*QA*WS + 0.599833*SF*WS (5.23)

Modulus = -4.42444 + 0.0204583*T - 0.18691*MPS + 0.0687917*QA + 13.2903*SF + 0.0132875*WS - 0.000319444*T*MPS - 0.000161111*T*QA - 0.0538889*T*SF + 0.0000983333*T*WS + 0.00240278*MPS*QA + 0.168056*MPS*SF + 0.000220833*MPS*WS - 0.109444*QA*SF - 0.000275*QA*WS - 0.0281667*SF*WS (5.24)

Thermal shrinkage = -5.38583 + 0.041375*T - 0.708368*MPS - 0.0227361*QA + 29.1153*SF + 0.0210958*WS + 0.00290278*T*MPS + 0.000327778*T*QA - 0.152778*T*SF + 0.0000716667*T*WS + 0.00148611*MPS*QA - 0.126389*MPS*SF + 0.00217917*MPS*WS - 0.005*QA*SF - 0.000371667*QA*WS - 0.0488333*SF*WS (5.25)

For the observed results and fitted results generated for each trial (Figure 5.54), the models give useful results for the diameter (a), tenacity (b) and elongation at break (c), modulus (d) and thermal shrinkage (e). The mathematically concise statistical models predict the diameter, tenacity, elongation at break, modulus and thermal shrinkage of the as-spun fibres in terms of random variables and their associated probability distributions. Their Model Standard Error (MSE) values listed in Table 5.15 indicate the dispersion of predicted and observed values around the theoretical fitted line generated using the fitted model for each trial.

There are small variations related to the extrusion machine setting based variation and the nature of this polymer and the nonuniform flow. In order to determine the direction of the interactions T&MPS and MPS&WS, the estimated response surfaces of diameter were used, as shown in Figure 5.55. A small twist was found in the surface and as a result a significant effect was detected between the factors which confirm the previously analysed results. In a similar analysis, the estimated response surfaces for elongation at break (MPS&WS) and thermal shrinkage (the interactions MPS&WS and SF&WS) show the relationship between them and the previously studied interactions. The results obtained are in agreement with the conclusions from previous analysis.

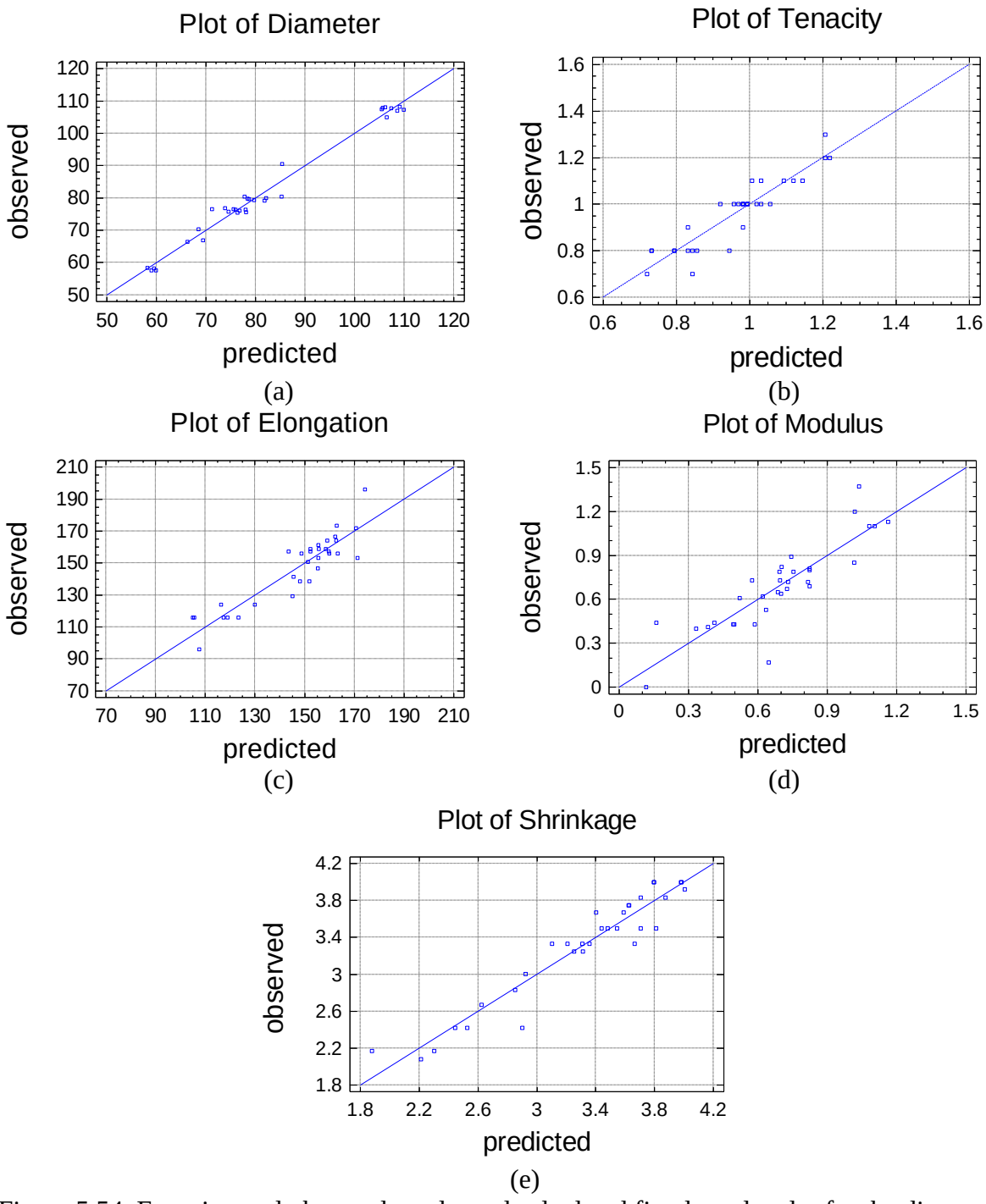

Figure 5.54. Experimental observed results and calculated fitted results plot for the diameter (a), tenacity (b), elongation at break (c), modulus (d) and thermal shrinkage (e)

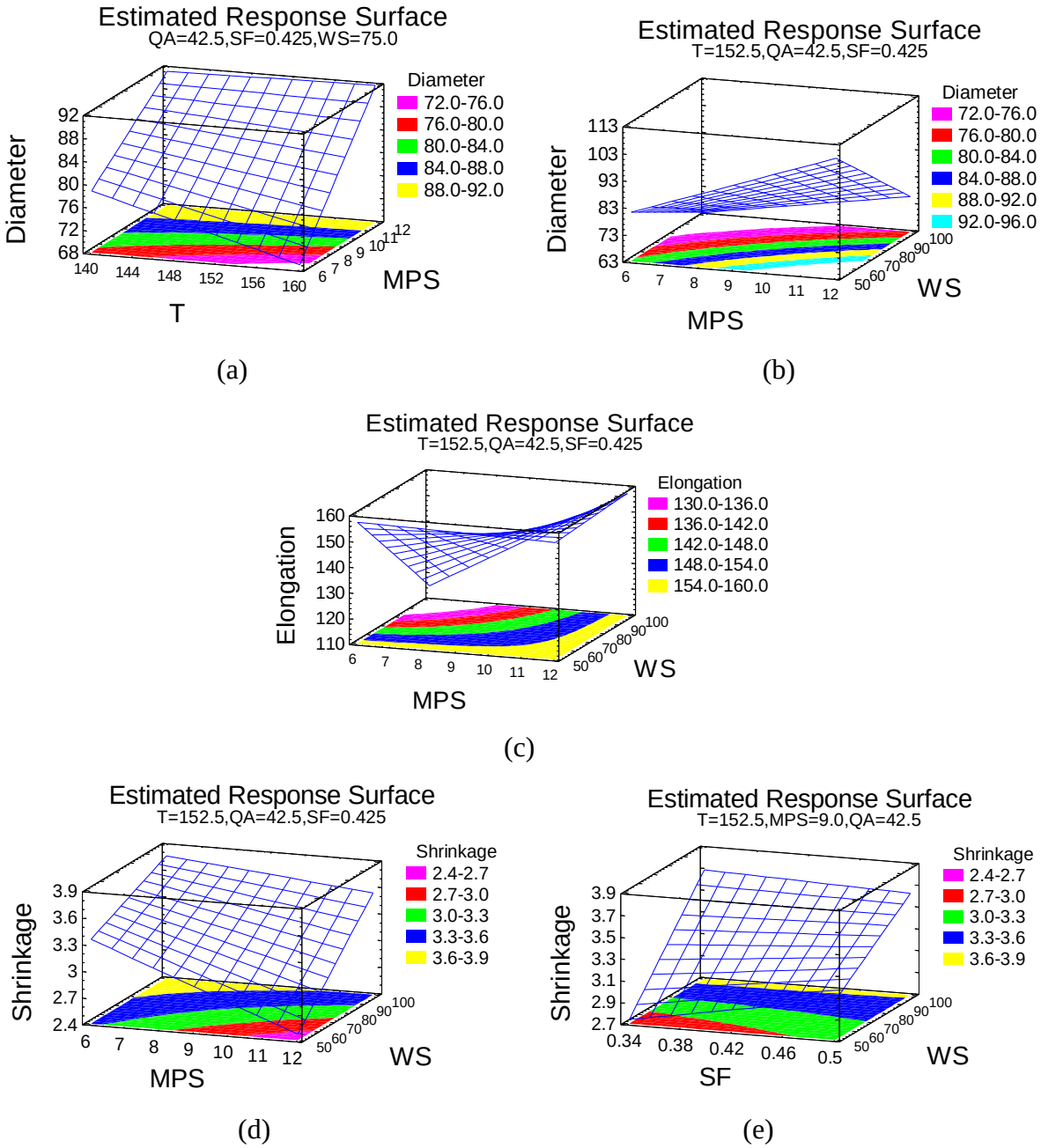

Figure 5.55. Estimated response surface for diameter (a-b), elongation at break(c) and thermal shrinkage (d-e)

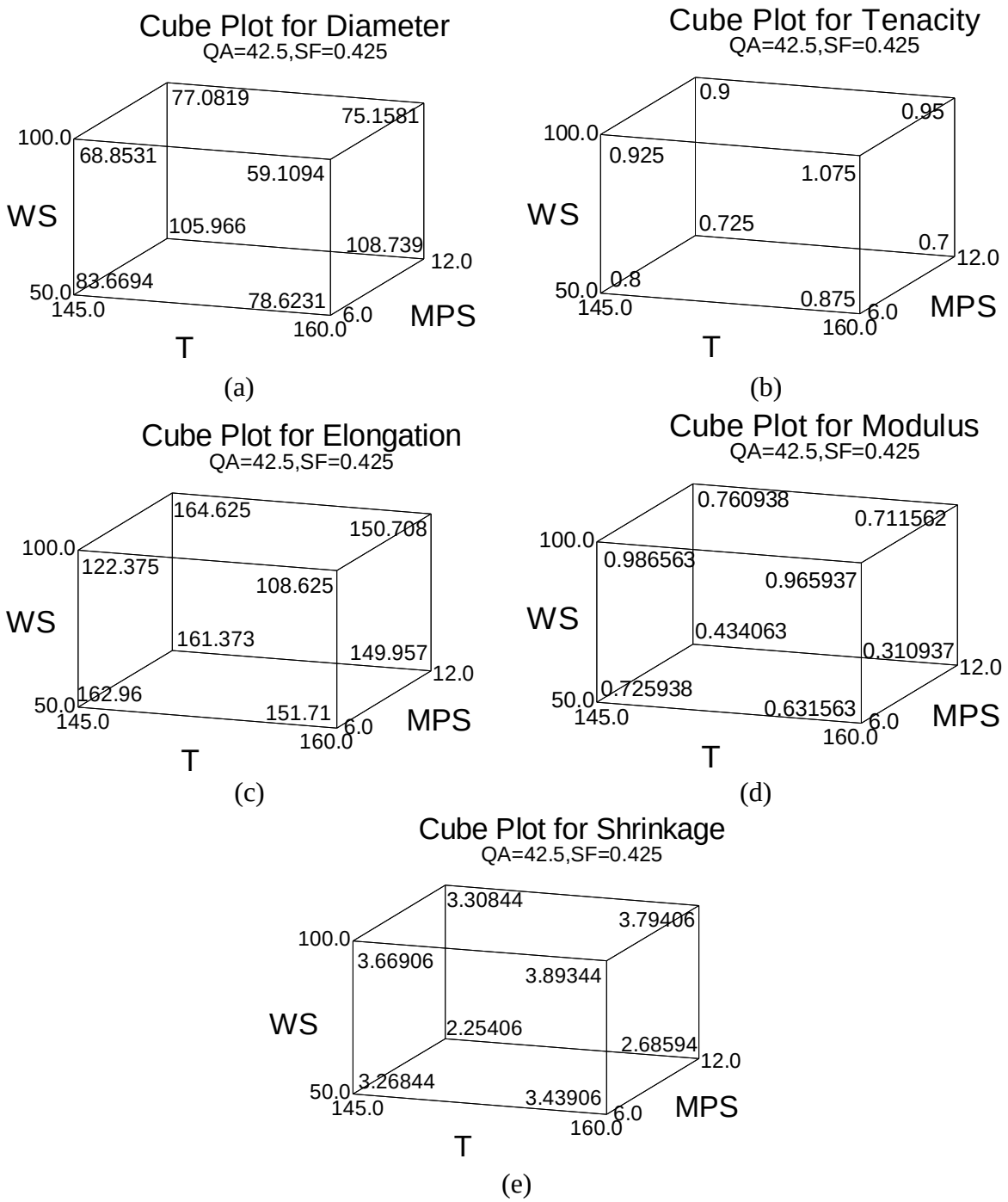

Figure 5.56. Cube plots of the estimated effects for the high and low settings of MPS, T and WS for diameter (a), tenacity (b), elongation at break (c), modulus (d) and thermal shrinkage (e)

In the cube plots in Figure 5.56, the diameter (a), tenacity (b), elongation at break (c), modulus (d) and thermal shrinkage (e) depend on the obtained regression equation. Each value corresponds to the values of the experimental factors MPS, T and WS at the middle levels of QA and SF range, which are 42.5 and 0.425 respectively.

5.7.3 General Conclusions about BAAC Fibre Analyses

In this section, different samples of as-spun branched aliphatic-aromatic co-polyester fibres were spun in different melt spinning conditions. A production process of biodegradable branched aliphatic-aromatic co-polyester fibre was analysed and regression models was estimated. The relationship between factors and their interactions was investigated using a full factorial experimental design to establish the temperature variations in each group. Spin-draw ratio, die head pressure, temperature averages at L03, temperature averages at L04 of the spun filament, the diameter, tenacity, elongation at break, modulus and thermal shrinkage of fibres were investigated and modelled. A decrease of spinning temperature leads to higher viscosity and higher flow resistance through the spinneret's nozzle and increases die head pressure which should be noted in the production stage. From an investigation of the thermo-graphic measurement results, it is clear that the combination between the higher metering pump speed and the high spinning temperature in filament extrusion leads to thicker filaments resulting to higher filament heat content and vice versa. There are small variations related to the extrusion machine-setting based variation, the rubbery nature of this polymer causing nonuniform flow, the tension winding system variation, tension during the preparation of the sample for testing. The spin draw ratio is significantly affected by winding speed, metering pump speed, spinning temperature and the interactions between them. Metering pump speed plays an interactive role with winding speed in the relationship between the extrusion speed and the collecting at different speeds that affects the spin line tension and related properties. The wind up speed controls the spin draw ratio and tension on material from the spinneret through the cooling and solidification stages. Spinning temperature and metering pump speed have a significant effect on die head pressure. Spinning temperature plays an important role in controlling the fibre structure as well as affecting the drawability; it affects the overall orientation of the produced fibre and its drawability.

The filament temperature average at L03 of as-spun fibres is significantly affected by metering pump speed, spinning temperature, winding speed, quench air speed and the interactions between quench air speed, spinning temperature and metering pump speed. The filament temperature average at L04 of as-spun fibres is affected by metering pump speed, spinning temperature, their interaction and winding speed. The cooling ratio is affected by throughput rate, yarn cross section and air cooling temperature.

The diameter value is positively affected by metering pump speed and the interaction between the spinning temperature and the winding speed and negatively affected by winding speed and its interaction with the metering pump speed. The cooling ratio affects the crystallinity; cooling time is affected by metering pump speed, fibre cross section and fibre temperature. Alternatively, low spinning temperature leads to high die head pressure. The high wind up speed adds tension to filaments from the spinneret through the cooling and solidification stages. Tenacity is affected positively by winding speed and spinning temperature speed and negatively by the metering pump speed. Together with the negative effects of spinning temperature and winding speed, metering pump speed and its interaction with winding speed positively affect the elongation at break. The friction effect on the spin draw ratio may decrease the elongation at break ratio. It is significant that winding speed has a positive effect and metering pump speed has a negative effect on the modulus. The thermal shrinkage is positively affected by winding speed, spinning temperature, the interaction between winding speed and metering pump speed and the spin finish application, which could be related to its cooling action on the material leading to structural effects. Thermal shrinkage is negatively affected by metering pump speed increasing.

Table 5.15 summarises the main conclusions of the results in a concise statistical model, which presents the combination of factor levels which maximize and minimize responses over the region indicated. It also shows the Model Standard Error (MSE) values described previously. The model covers the identified significant main and interaction factors and specifies the combinations of factor levels for enhancing responses of as-spun branched aliphatic-aromatic co-polyester fibres. The models achieved were used to calculate various statistics, including correlations, co-variances and partial correlations. Using the obtained regression equations, the models help in understanding the relationship between the melt-spinning process conditions and properties of BAAC fibres. It also provides more technical information for scientists and technologists so that they can produce the enhanced properties at suitable conditions related to final product cost and obtain environmentally friendly, economical, energy saving fibres. Additionally, creating group trials of data can be created with similar characteristics, developing a predicting method, reducing the number of factors and responses to a small set of meaningful measures, determining which combinations of the factors and responses determine most of the variability in analysed data and finding combinations of the factors and responses related to each other.

Response	MSE	Optimum model	The combination of factor levels				
			T	MPS	QA	SF	WS
DHP (dpi)	41.8	Maximum	↓	↑	↓	-	-
		Minimum	↑	↓	↑	-	-
Diameter (µm)	2.2925	Maximum	↑	↑	↓	↑	↓
		Minimum	↑	↓	↓	↑	↑
Tenacity (g/den)	0.0235	Maximum	↑	↓	↓	↓	↑
		Minimum	↑	↑	↓	↑	↓
Elongation at break (%)	3.87	Maximum	↓	↓	↓	↓	↓
		Minimum	↑	↓	↓	↓	↑
Modulus (g/den)	0.0518	Maximum	↑	↓	↓	↓	↑
		Minimum	↑	↑	↓	↓	↓
Thermal shrinkage (%)	0.105	Maximum	↑	↑	↑	↓	↑
		Minimum	↓	↑	↓	↓	↓
Spin Draw Ratio	1.838	Maximum	↑	↓	↓	↑	↑
		Minimum	↑	↑	↓	↑	↓
Filament Temperature at L3 (^{o}C)	2.62	Maximum	↑	↑	↓	↓	↓
		Minimum	↓	↓	↑	↑	↑
Filament Temperature at L4 (^{o}C)	1.344	Maximum	↑	↑	↓	↓	↓
		Minimum	↓	↓	↑	↑	↑

Table 5.15. The combinations of factor levels for t levels and the responses obtained (↓: Low Level, ↑: High Level, MSE: Model Standard Error)

In conclusion, the optimization of melt spinning process conditions and BAAC fibres properties help in producing the most satisfactory properties in the final textile product. The achieved mathematical models form the main part in creating a planning programme and a plan for the production process depending on forecasting. After the BAAC fibres have been drawn and prepared, they could be used for different applications such as agricultural, horticultural and other textile applications, as an alternative to commercial chemical fibres.

5.8 Investigation of The Influence of Blend Ratio on The Properties of Blend AAC Fibres

This section will explain the influence of blend ratios on the physical properties of the as-spun and drawn fibres composed of different grades of aliphatic aromatic co-polyesters. The three grades were used in this investigation AAC1 (coded previously as LAAC1), AAC2 (coded previously as LAAC2) and AAC3 (coded previously as BAAC). Using previous

forecasting statistical methods, the expected models form a major part in creating a planning programme and a plan for the production process regression.

5.8.1 Effect of AAC Blend Ratio on The Mechanical Properties of As-Spun Fibres

5.8.1.1 Results

Fibres were extruded via melt spinning on the Lab-spin machine. The temperature zones in the extruder are barrel zones (T1=120, T2=135 and T3=135), metering pump zone (T4=135) and die head zones (T5=140 and T6=145). The selected control factors covered the polymer grades (MFI) and the extruder temperature zones. Polymer granules were fed through the hopper into the extruder and then mechanically compressed and melted. The molten polymer was forced through the spinneret of 30 holes with speed adjusted by the metering pump (10 rpm). The air cooling quench speed was set at 50 % of total blower fan air output. The spin finish (Vickers) was diluted fivefold with water before use, with application speed set at 0.35 rpm.

Trial Number	AAC1 (%)	AAC2 (%)	AAC3 (%)
1	25	75	0
2	0	75	25
3	25	50	25
4	50	0	50
5	0	100	0
6	50	25	25
9	25	25	50
10	50	50	0
11	0	50	50
12	100	0	0
13	0	0	100
14	75	0	25
15	75	25	0
16	25	0	75
17	0	25	75

Table 5.16. L17 Experimental design array for the blending experiment

The filaments were collected from the godets set at 100 m min^{-1}. Samples were heated for 2 minutes at 60^{o}C when the thermal shrinkage test was carried out using thermal shrinkage tester with a load cell of 10 g. The detailed experimental arrangement of the seventeen trials

is listed in Table 5.16. The fibre properties (Table 5.17) were evaluated using tenacity, modulus, elongation at break, thermal shrinkage and count; in addition to the tension in the spin line and the die head pressure.

Trial Number	DHP (dpi)	Tension (gms)	Thermal shrinkage (%)	Tenacity (g/den)	Elongation at break (%)	Modulus (g/den)	Count (den)
1	450	8	-0.7	0.3	575	0.10	1321.74
2	600	25	3.1	0.4	335.8	0.22	1616.4
3	675	25	1	0.4	314.2	0.28	1748.16
4	1000	45	1.4	0.6	186.7	0.21	1739.88
5	450	5	-2.5	0.2	574	0.21	1237.86
6	800	30	1.6	0.4	365	0.24	1680.48
9	1000	45	1.5	0.5	433.3	0.57	1719.0
10	550	15	0.9	0.2	223.3	0.26	1348.2
11	900	50	1.5	0.5	265	0.12	1763.46
12	680	20	0.7	0.3	797.9	0.32	1535.76
13	1700	80	1.3	0.8	170.8	0.90	1888.92
14	750	25	1.3	0.4	299.2	0.26	1634.04
15	600	12.5	2.8	0.2	317.5	0.33	1349.28
16	1400	63	1.4	0.6	225.8	0.29	1815.48
17	1300	70	1.9	0.7	171.9	0.63	1749.6

Table 5.17. Experimental responses data of as-spun fibres

5.8.1.2 Discussion

From Table 5.17, it could be summarized that when the AAC3 blend ratio is above 50%, the die head pressure and the spin line tension values will be greater than the values of other blend ratios. At 100% of AAC2, the fibre extension will be 2.5% and it decreases as the AAC1 ratio increases. At blend ratio 25/75 in an AAC1/AAC2, extension decreases and at blend ratio 75/25 as an AAC2/AAC3, the maximum thermal shrinkage (3.1%) will be obtained. Statistically it is noted that the thermal shrinkage is increasing with decreasing the AAC2 blend ratio. Thermal shrinkage will increase with AAC2 ratio decreasing and thermal shrinkage value depends on AAC1 and AAC3 ratios. When the AAC3 blend ratio in any blend is more than 50%, the tenacity will increase to reach the largest value on 100% of AAC3. Maximum modulus value was obtained with 100% ratio in an AAC3, blend ratio 25/75 in an AAC2/AAC3 or blend ratio 25/25/50 in an AAC1/AAC2/AAC3. AAC2 affects negatively the tenacity and modulus values. Elongation at break is affected negatively with

decreasing the AAC2 blend ratio and by increasing the AAC3 value. As the density of AAC3 is greater than density of AAC1 or AAC2, the increasing of the AAC3 ratio will affect positively the count of the yarn produced.

In conclusion, the AAC3 blend ratio positively affects the count, tension and die-head pressure. AAC2 blend ratio affects negatively the count, tension and die-head pressure. The AAC1 blend ratio has a small effect on the count, tension and die-head pressure. The count, tension and die head pressure are affected by rheology and density of the polymer, which explains the significant effect of the branched grade on those properties. The AAC3 blend ratio positively affects the tenacity and the modulus and it affects negatively the elongation at break, with a small effect on thermal shrinkage. The AAC2 blend ratio affects negatively the tenacity, modulus and thermal shrinkage. It affects positively elongation at break. The AAC1 blend ratio has a small negative effect on the tenacity and modulus. It affects positively the elongation at break, with a small effect on thermal shrinkage.

5.8.2 Effect of AACs Blend Ratio on The Mechanical Properties of Drawn Fibres

5.8.2.1 Results

For technical reasons, the spinning and drawing are considered as separate processes. Fibres produced (Table 5.16) were drawn at the draw ratio (1.5) to reduce factor interactions; drawing took place at a temperature of 40^{o}C. At a constant roller speed, hot plate temperature and constant drawing speed and spin finish applicator speed sets at 1.5 rpm. The detailed experimental arrangement of the seventeen trials is given in Table 5.16. The fibre properties (Table 5.18) are evaluated using tenacity, modulus, elongation at break, thermal shrinkage and count results.

Trial Number	Thermal shrinkage (%)	Tenacity (g/den)	Elongation at break (%)	Modulus (g/den)	Count (den)
1	9.2	0.38	286.7	0.21	935.10
2	9.4	0.44	474.0	0.18	1011.15
3	3.1	0.49	379.2	0.44	1570.50
4	8.7	0.50	226.7	0.77	1303.38
5	8.6	0.40	343.3	0.35	1009.08
6	5.5	0.57	225.8	0.61	1430.28
9	10.3	0.34	247.5	0.4	922.68
10	8.8	0.33	175.8	0.48	1268.46
11	4.3	0.50	315.0	0.6	1468.80
12	7.3	0.31	82.5	0.64	1211.76
13	5.9	1.01	102.5	1.79	1476.54
14	9.2	0.45	365.0	0.52	1069.20
15	7.5	0.45	169.8	0.66	1247.94
16	1.5	0.72	158.3	0.57	1719.90
17	8.3	0.69	143.3	1.25	1308.42

Table 5.18. Experimental responses data of drawn fibres

5.8.2.2 Discussion

Table 5.18 shows that, at blend ratio 25/25/50 in an AAC1/AAC2/AAC3, the fibre thermal shrinkage was 10%, and it decreased as the AAC1 and AAC3 ratio increased. Statistically, when the AAC3 blend ratio in any blends is more than 50%, the tenacity and the modulus will increase to be at the greatest value on 100% of AAC3. AAC2 affects negatively the tenacity and modulus values. Elongation at break is affected negatively with the decreasing of the AAC2 blend ratio and with the increasing AAC3 value. As the density of AAC3 is greater than the density of AAC1 or AAC2, increasing the AAC3 ratio will affect positively the count of the yarn produced. In conclusion, the AAC3 blend ratio mechanically improves the fibre properties. After drawing and when heat setting and draw ratio have affected the internal structure of the fibres, the AAC3 blend ratio positively affects the count and negatively the thermal shrinkage properties of the fibres. The AAC2 blend ratio affects negatively the count and positively the thermal shrinkage properties. The AAC1 blend ratio has a small effect. The AAC3 blend ratio positively affects the tenacity and the modulus and it affects negatively elongation at break. The AAC2 blend ratio affects negatively the tenacity and modulus. It has a positive effect on elongation at break. The AAC1 blend ratio has a negative effect on the elongation at break. It has a small effect on tenacity and modulus.

5.9 Forecasting Program for Melt Spinning of As-Spun AAC Fibres

Because the modelling and controlling of the processes within the engineering aspects are complex tasks, an effective program involves controlling not only the product data but also the processes affecting the fibre properties. The relational data, hierarchical data and network data models are three major models which are used in the modern database analysis systems [220]. With different programming language, different styles of programming could suit the same task selected. The details look different in different languages for the same program, but a few basic instructions, functions and method mechanisms appear in just about every language. The programming stage is very important for developing a forecasting application depending on previous results and their optimization. The theoretical regression models obtained form the main source code in the enhanced forecasting program, which will present the melt spinning process of aromatic-aliphatic co-polyester fibre. In the programming process, the relationship between key inputs (factors) and performance measures (responses) using factorial statistical experimental design technology is reported. The statistical data and regression formulas are represented as a computer vision application. For this chapter, the programming stage is very important for developing a forecasting application depending on previous results and their optimization. The program includes the mathematical models which estimate the studied responses. The program provides a communication environment between the industrial application and research results. Once models presenting the relationship between response values and the factors and their levels have been identified, forecasting can be accomplished based on a statistical methodologies program. Setting up, performing and analysing the results do not require special computational or mathematical skills. Any technician is able to realize the full potential of the simulator. Additionally, the application runs on inexpensive hardware (e.g. personal computer).

5.9.1 Forecasting Program Based on Visual Basic/C++ Program

The multiple regression analysis and previous forecasting models (4.1-4.12 and 4.17-4.25) provide a basis for identifying the relationship between process-input and process-output data. It is based on regression formulas and limited by the regions of the studied factors between the factor levels. All obtained models are summarized using a visual basic program.

It is easy to understand the designed computer vision application and to obtain results from regression analysis and forecasting. The forecasting program calculates the thermal, structural and physical properties of fibres (process-output data). It depends on the process conditions (process-input data) selected by the user. The program's result helps in achieving a balance between the enhanced properties and the fibre cost; it saves the processing cost required for enhanced fibres. The first step is the C++ source code design; the C++ source code is represented in Appendix A. By converting the previous source code to a simple flow chart, the flow chart summarizing the C++ source code can be drawn (Figure 5.57).

In Figure 5.57 and after selecting the polymer grade, the program requests the parameters values and calculates the responses' values by using the regression equations, and then gives the results. The input conditions data were used to obtain the structural, mechanical and physical data. Using Microsoft Visual Studio 2008, the forecasting program for melt spinning of AACs fibres was written and designed. Visual Basic makes the creation of applications with graphical user interface easier and faster with the use of the graphical tools to build the user interface of a visual basic program. In the input interface/window, the program obtains the selected grade (LAAC or BAAC) and the preferred process conditions from the keyboard or other device (Figure 5.58). Spinneret used in this programme is 30 hole spinneret (diameter is 0.4 mm, l/d ratio is 1.2). After checking for certain conditions and executing the appropriate sequence of statements, the output interface/window displays data on the screen or sends data to a file or other devices. Figure 5.59 shows the output interface/window for filament temperature in the machine's cooling window, and the fibre's structural, mechanical and physical properties.

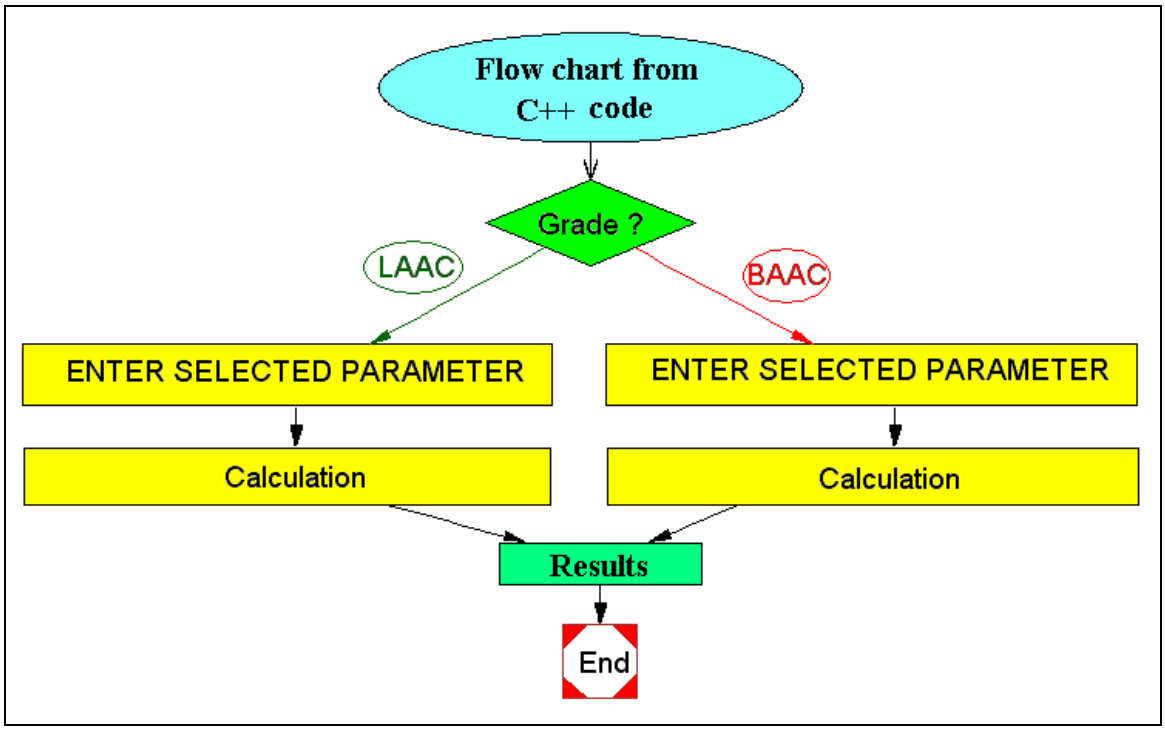

Figure 5.57. Schematic program process

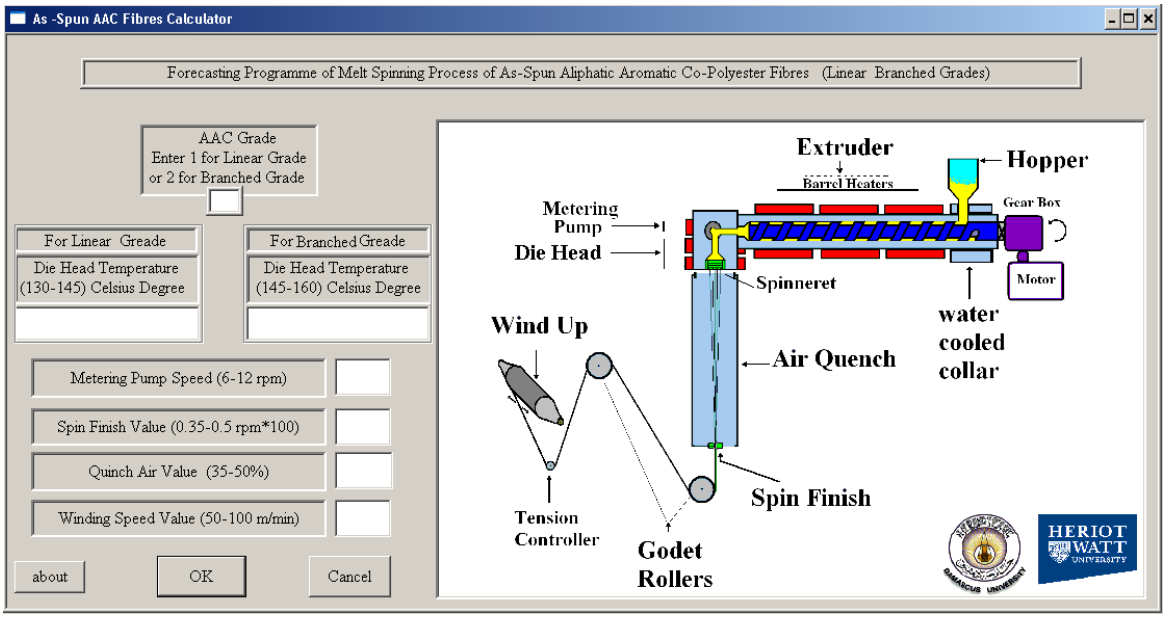

Figure 5.58. The main input interface/window for process conditions input.

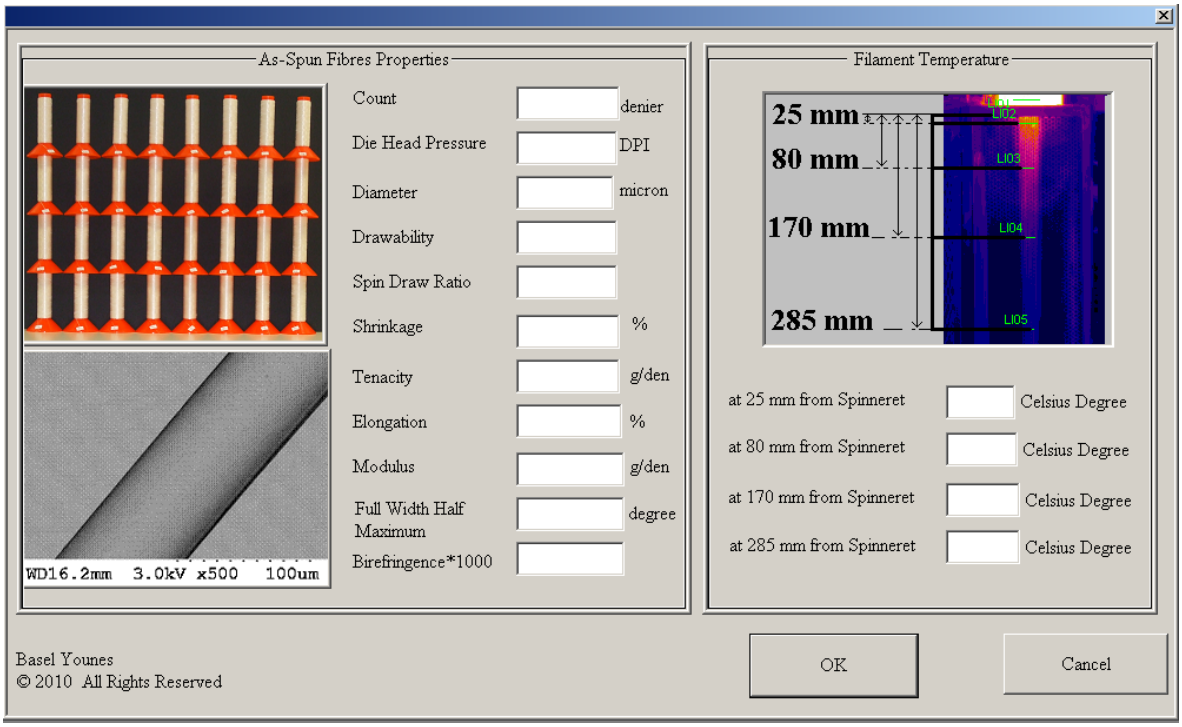

Figure 5.59. The output interface/window for filament temperature in the machine's cooling window and the fibre's structural, mechanical and physical properties.

5.9.2 Forecasting Program Based on the Texas Instrument

The Texas instrument covers the need for a fast and accurate technique to calculate without the need to further statistical background and computing equipment. It is a different style of programming suite for the task selected. The details could look different for the same program, but the basic instructions and method mechanism are the same in general. The key features of the need of the Texas instrument inside the lab/plant include the ease and flexibility of data input and the displayed user-friendly results for the non-statistician. The TI-83 programs are outlined in Appendices B (for melt spinning of LAAC) and C (for melt spinning of BAAC). Program listed in appendix D shows the TI-83 program of melt spinning of blended AACs fibres.

5.9.3 Results and Evaluation of The Forecasting Program

For evaluation of the forecasting results obtained from melt spinning of LAAC and BAAC as-spun fibres, a set of 10 selected conditions was selected for each in the ranges studied (Figure 5.60); LAAC and BAAC as-spun fibres were processed as shown in Table 5.19.

The results of the trials for the LAAC and BAAC as-spun fibres experiments are given in Table 5.20 and Table 5.21. The estimates should be sufficiently accurate for practical application; the simulation results are in agreement with available data and within acceptable variation.

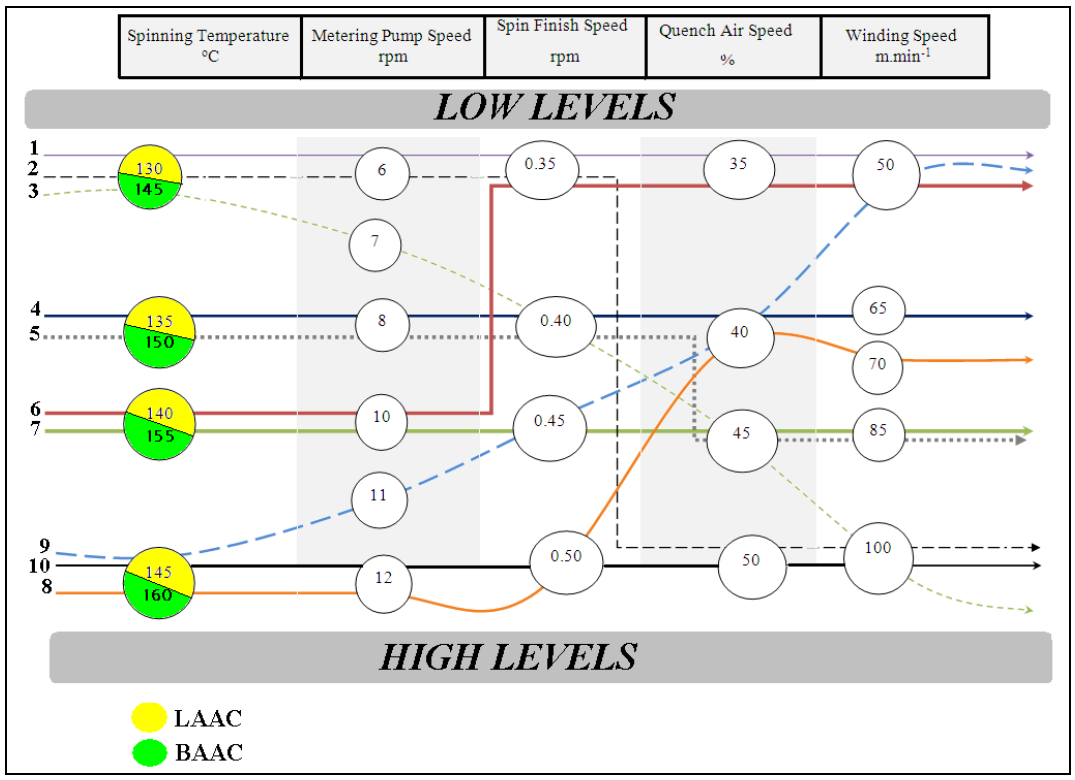

Figure 5.60. Method used for selecting the conditions

Trial No	T		MPS	SF	QA	WS
	Linear Grade	Branch grade				
1	130	145	6	0.35	35	50
2	130	145	6	0.35	50	100
3	130	145	7	0.40	45	100
4	135	150	8	0.40	40	65
5	135	150	8	0.40	45	85
6	140	155	10	0.35	35	50
7	140	155	10	0.45	45	85
8	145	160	12	0.5	40	70
9	145	160	11	0.45	40	50
10	145	160	12	0.5	50	100

Table 5.19. Selected experimental conditions for LAAC and BAAC grades

Responses*		1	2	3	4	5	6	7	8	9	10
Count (den)	P	1805	949	1062	1905	1486	2591	1732	2372	2742	1520
	O	1814	977	1116	1980	1567	2863	1817	2412	2904	1668
Tenacity (g/den)	P	0.28	0.38	0.36	0.35	0.39	0.36	0.41	0.37	0.36	0.43
	O	0.21	0.32	0.33	0.29	0.34	0.32	0.36	0.31	0.32	0.39
Elongation (%)	P	606	368	418	663	552	861	651	858	917	620
	O	720	428	473	820	787	907	720	920	1067	720
Modulus (g/den)	P	0.20	0.27	0.26	0.20	0.22	0.19	0.21	0.19	0.18	0.22
	O	0.22	0.22	0.21	0.17	0.20	0.17	0.19	0.16	0.16	0.19
DHP (dpi)	P	1053	1222	1220	1094	1131	1061	1096	1064	1008	1059
	O	1050	1190	1150	1100	1100	1090	1090	1100	1090	1100
Drawability	P	3.6	2.8	3.0	4.1	3.6	5.3	4.2	5.5	5.9	4.2
	O	3.4	2.9	3.2	3.9	3.4	4.8	4.1	4.8	5.3	3.8
Diameter (µm)	P	83.2	60.8	63.7	84.2	74.1	99.1	80.1	94.5	102.4	76.5
	O	82.8	60.8	64.9	87.0	77.7	107.5	87.3	95.4	110.0	80.3
FWHM (^{o}C)	P	0.57	0.54	0.55	0.58	0.57	0.57	0.60	0.61	0.61	0.64
	O	0.60	0.58	0.60	0.60	0.55	0.61	0.63	0.62	0.60	0.61
Shrinkage (%)	P	0.17	-0.39	-0.31	-0.31	-0.56	-0.09	-0.78	-0.66	-0.37	-1.12
	O	0.15	0.15	-0.10	0.25	0.27	0.00	0.25	0.34	-0.25	-1.19
Spin Draw Ratio	P	23.6	43.6	41.0	25.7	32.9	17.6	28.2	19.4	15.9	27.7
	O	23.3	43.4	38.2	22.0	28.0	13.8	21.0	17.6	13.2	25.0
Birefringence	P	24.6	42.1	36.6	25.2	31.7	13.5	25.9	15.3	9.2	24.1
	O	29.0	37.0	39.0	7.0	11.0	6.0	8.0	6.0	4.0	22.0

Table 5.20. The experimental results for predicted and observed value of LAAC as-spun fibres properties (* P: Predicted and O: Observed)

Responses*		1	2	3	4	5	6	7	8	9	10
Count (den)	**P**	1991	1369	1336	1965	1568	2689	1719	2504	2933	1495
	O	1933	1119	1244	2089	1540	2943	1880	2499	2958	1617
Tenacity (g/den)	**P**	0.77	0.87	0.90	0.84	0.90	0.74	0.90	0.77	0.72	0.92
	O	0.73	0.78	0.82	0.77	0.75	0.66	0.76	0.66	0.65	0.81
Elongation (%)	**P**	174	117	128	152	139	157	146	148.5	149	160
	O	181	131	155	178	150	181	178	160	190	180
Modulus (g/den)	**P**	0.64	1.02	0.95	0.68	0.81	0.30	0.68	0.48	0.36	0.58
	O	0.54	0.85	0.86	0.53	0.63	0.26	0.48	0.39	0.26	0.48
DHP (dpi)	**P**	1500	1500	1567	1544	1544	1577	1578	1600	1542	1600
	O	1430	1430	1520	1500	1480	1500	1500	1550	1480	1540
Diameter (µm)	**P**	85.4	71.2	70.9	84.2	75.9	99.1	79.7	96.2	104.0	76.7
	O	85.0	68.0	65.7	88.8	76.3	108.9	85.0	97.2	110.9	80.0
Shrinkage (%)	**P**	2.90	3.55	3.57	3.13	3.45	2.54	3.45	3.05	2.76	3.71
	O	2.40	2.90	2.70	3.00	3.00	1.25	2.80	2.60	1.75	2.86
Spin Draw Ratio	**P**	21.3	32.5	32.6	24.7	30.1	16.9	28.1	18.3	14.3	28.4
	O	22.2	35.6	34.1	20.3	27.5	15.0	24.0	16.9	13.0	25.0

Table 5.21. The experimental results for predicted and observed value of BAAC as-spun fibres properties (* P: Predicted and O: Observed)

5.9.4 Discussion

In Figure 5.61, Figure 5.62 and Figure 5.63, the results were plotted with the predicted (calculated) values on the X–axis and the actual (observed) values on the Y–axis for all selected trials. The outputs were plotted versus the targets as red dots. A blue line indicates the linear fit. The fitted line plot command provides not only the scatter plot of the data adorned with the estimated regression function but also an estimated regression function. The most useful aspects of these plots are their ability to show nonlinear relationships between variables. The predictive models gave useful results for physical properties and notable variation for structural related properties; that could be related to the limitation of funding needed for the X-ray and the polarizing (Pluta) microscope tests in this project. Low number of samples from each trial were selected and characterized and that affects the model results relating to the structure analysis. More certainty for the corresponding models should be improved in future work with testing more samples. R-squared or the coefficient of determination is the ratio of the sum of squares explained by a regression model and the "total" sum of squares around the mean. A high R-squared value does not guarantee that the model fits the data well. To increase the precision of R-squared, the adjusted R-squared

should be used to reflect both the number of independent variables in the model and sample size; it will always be less than or equal to R-squared. Adjusted R-squared is a modification of R-squared that adjusts for the number of explanatory terms in the model. Using a model that does not fit the data well cannot provide good answers to the underlying engineering or scientific questions under investigation. ANOVA is the proportion of variance and it explains the model's terminology and significance. The correlation coefficient (R-squared) between the outputs and targets is a measure of how well the variation in the output is explained by the targets to show the correlation between targets and outputs depending on the fit model generated. By using the obtained approaches and by applying regression equations (Table 5.22), regression analysis results have an acceptable fitting on the levels selected. Structural related properties (FWHM, shrinkage and birefringence) have bigger variation between the studied properties. By using the obtained approaches and by applying the regression equation (Table 5.23), regression analysis results have an acceptable fitting on the levels selected. Shrinkage and elongation at break have the higher variation between the studied properties.

As described previously, different samples of aliphatic-aromatic co-polyester fibres were spun at different process profiles to determine the control parameters and their interaction effects and to test the forecasting regression equations. Spin-draw ratio, optical birefringence, drawability, die head pressure of the extrusion machine, a range of crystallographic orders (FWHM) for as-spun fibres, thermo-graphic measurement of extruded filament in the air quench cooling window, tensile and thermal shrinkage behaviour were measured and characterised. In conclusion, this chapter starts from the optimization of the production process to establish the forecasting program. The importance of achieved models and designed programs lie in controlling the production process to optimize and enhance fibre properties which may improve the quality and give reasonable cost to biodegradable fibres. Because of the difficulty of designing and producing manufactured fibres, experimental design techniques are a useful practice. The statistical optimization of fibre properties helps to produce the most satisfactory properties in the final fibres as an environmentally friendly attractive alternative to commercial chemical fibres. Due to their relationship with the internal structure of the fibres, the mechanical and thermal shrinkage properties of AACs fibres have a central role in the production processes.

Regarding the thermo-graphic measurement of extruded filaments in the air quench cooling window, the rate of heat flow away from the extruded filaments leaving the spinneret could provide information about the morphological structure of the crystallinity and overall

orientation of fibres. The responses of the statistical models derived can be explained by general extrusion theories and the knowledge of the influence of the involved parameters on the studied responses.

LAAC	Observed value =	R-Sq %	R-Sq % (adj)	ANOVA P-value
Count	- 39.82 + 1.075 Predicted Value	98.0	97.9	0.000
Tenacity	- 0.1035 + 1.145 Predicted Value	94.5	93.9	0.000
Elongation	+100.0 + 1.007 Predicted Value	90.4	89.2	0.000
Modulus	+0.05635 + 0.6221 Predicted Value	59.8	54.8	0.009
DHP	606.9 + 0.4533 Predicted Value	71.7	68.1	0.002
Drawability	+0.7651 + 0.7530 Predicted Value	97.4	97.2	0.000
Diameter	- 7.512 + 1.134 Predicted Value	96.3	95.9	0.000
FWHM	0.4186 + 0.3121 Predicted Value	17.6	7.3	0.228
Shrinkage	0.2567 + 0.6099 Predicted Value	23.7	14.2	0.154
SDR	- 3.616 + 1.023 Predicted Value	95.5	95.0	0.000
Birefringence	- 8.654 + 1.029 Predicted Value	59.7	54.7	0.009

Table 5.22. Regression analysis results for LAAC fibres: observed values versus predicted values

BAAC	Observed value =	R-Sq %	R-Sq % (adj)	ANOVA P-value
Count	- 192.2 + 1.111 Predicted Value	95.9	95.4	0.000
Tenacity	+0.1211 + 0.7417 Predicted Value	80.8	78.4	0.000
Elongation	+30.82 + 0.9332 Predicted Value	65.8	61.5	0.004
Modulus	- 0.03266 + 0.870 Predicted Value	95.2	94.7	0.000
DHP	- 300.7 + 1.157 Predicted Value	89.8	88.5	0.000
Diameter	- 21.47 + 1.281 Predicted Value	94.6	94.1	0.000
Shrinkage	- 1.470 + 1.245 Predicted Value	70.4	66.7	0.002
SDR	- 3.213 + 1.075 Predicted Value	89.7	88.5	0.000

Table 5.23. Regression analysis results for BAAC fibres: observed values versus predicted values

Theoretically, the obtained statistical based models could be tested regarding the reported dynamic modelling of melt spinning process [159, 221] and crystallization dynamics [222] through a set of rate equations. Input and output values should be adjusted according to the material properties and the process conditions which aids in finding the general effect with some numerical differences in the results of the regression method obtained from such theoretical models [134]. In dry-laid or air-laid based non-woven technologies, short staple aliphatic-aromatic co-polyesters fibres could be used to produce various non-woven webs for

medicine and agricultural applications. Post processes include the preparation of the fibres as new and smart friendly fibres to be weave-able, such as drawing, twisting, plying and the preparation processes for weaving. Aliphatic-aromatic co-polyesters are potential candidates to make staple fibres for various non-woven materials, particularly for disposable uses in medicine and agriculture. A balance between the improvement of mechanical properties and the biodegradability needs to be taken into account and requires further investigation in future work.

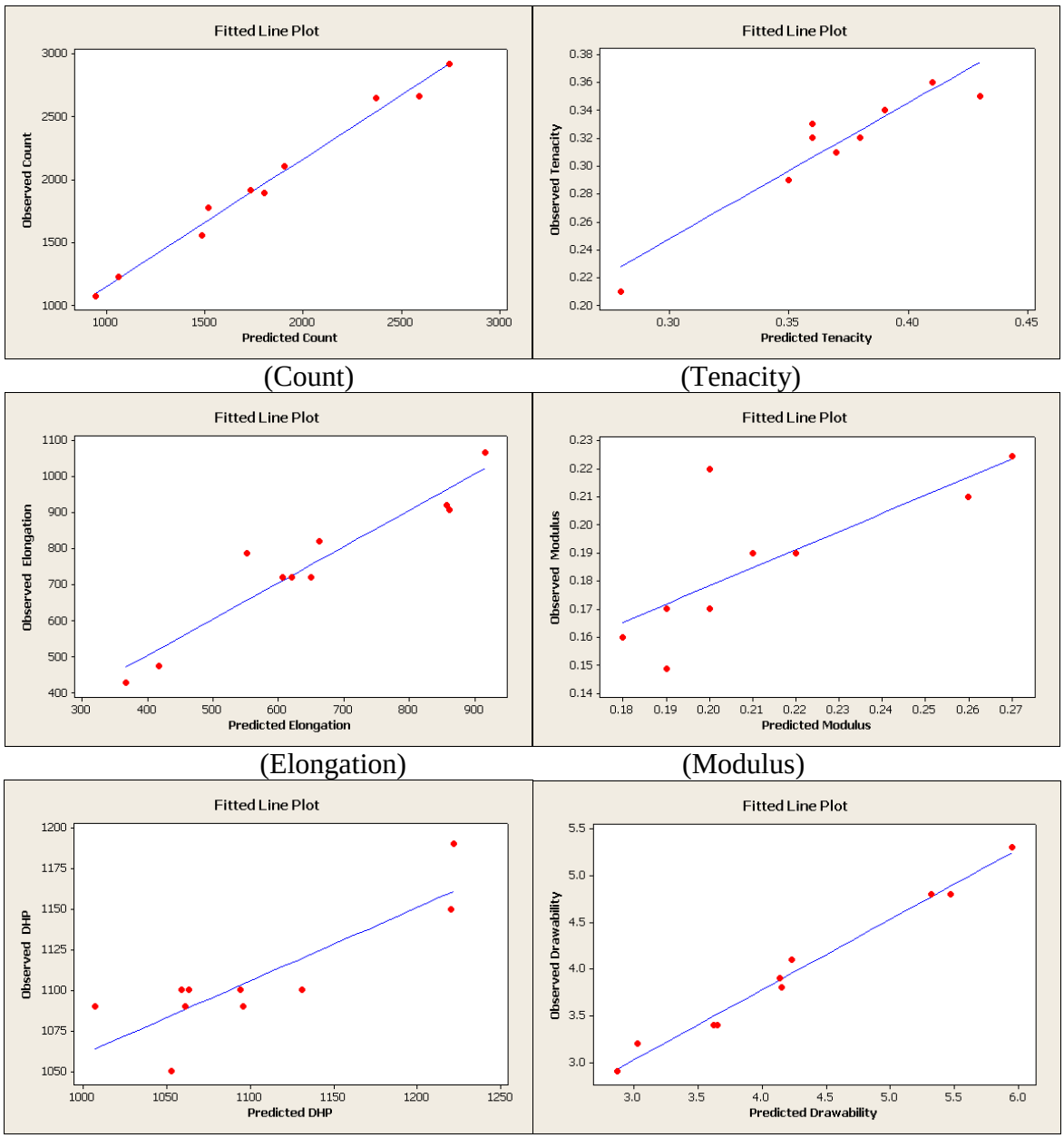

Figure 5.61. Fitted line plots between experimental observed results and theoretical predicted results for count, tenacity, elongation, modulus, die head pressure and drawability of LAAC fibres

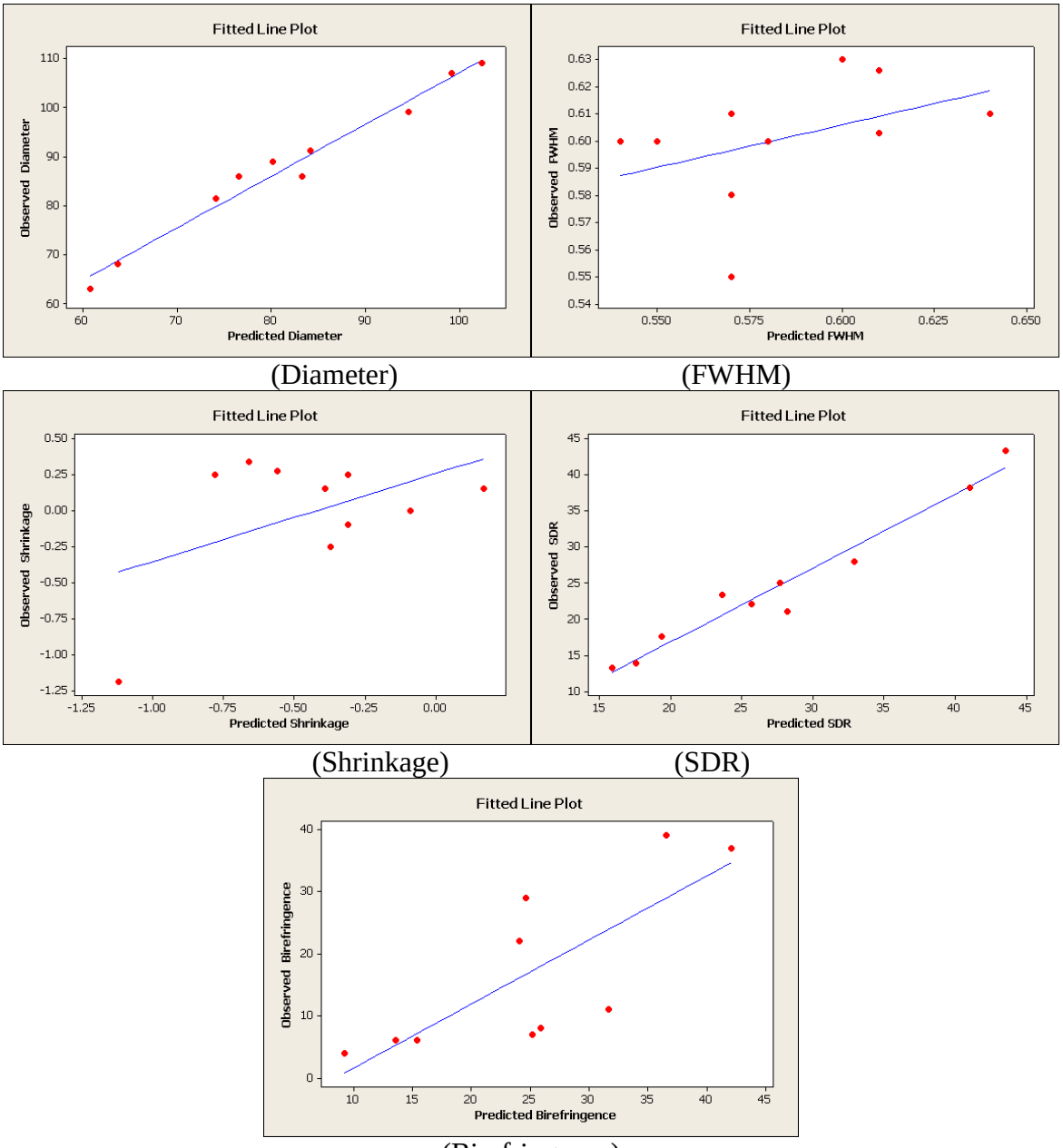

Figure 5.62. Fitted line plots between experimental observed results and theoretical predicted results for diameter, FWHM, shrinkage, SDR and birefringence of LAAC fibres

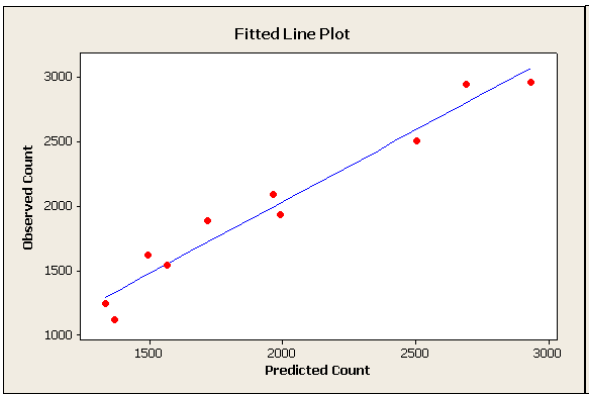

(Count)

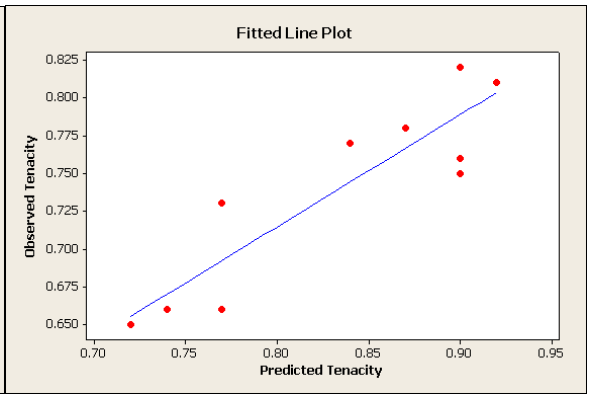

(Tenacity)

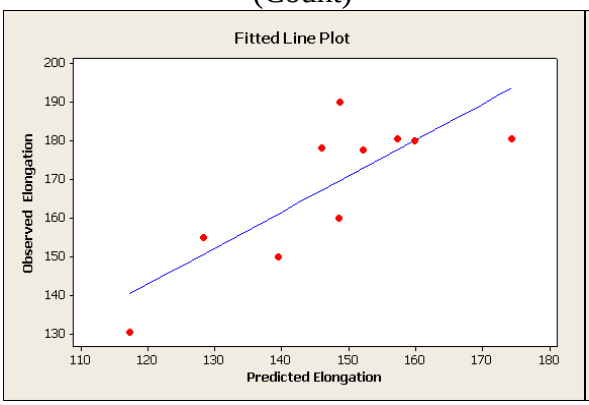

(Elongation)

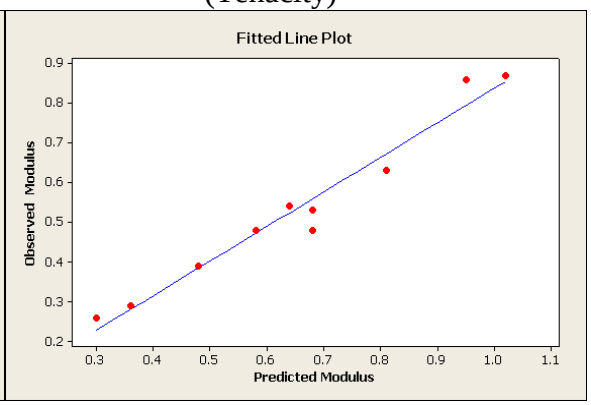

(Modulus)

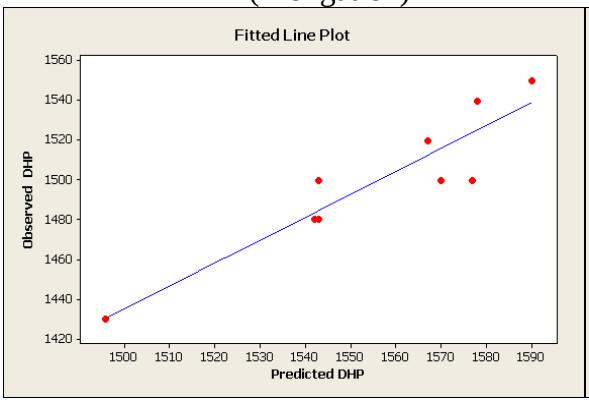

(DHP)

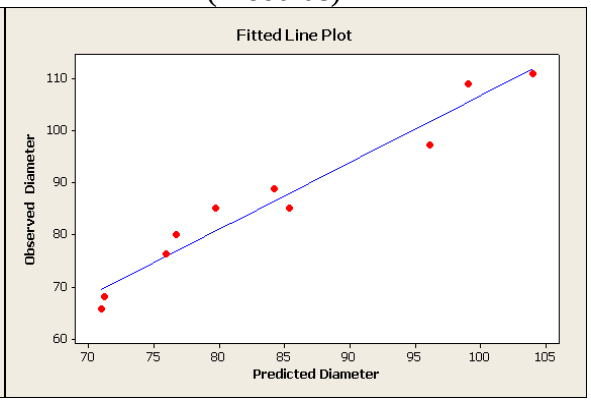

(Diameter)

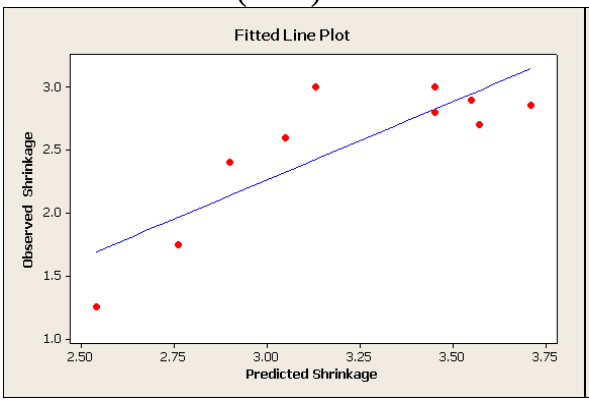

(Shrinkage)

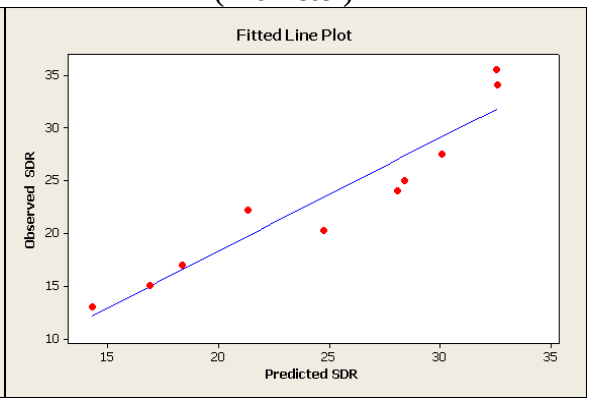

(SDR)

Figure 5.63. Fitted line plots between experimental observed results and theoretical predicted results for count, tenacity, elongation, modulus, die head pressure, diameter, shrinkage and SDR of BAAC fibres

CHAPTER 6 - STATISTICAL MODELLING OF THE EFFECT OF MULTI-STAGE HOT DRAWING AND TWISTING ON LINEAR AND BRANCHED ALIPHATIC-AROMATIC CO-POLYESTER FIBRES

6.1 Introduction

All the as-spun fibres produced at different conditions could not be drawn to the same maximum draw ratio; each polymer has its natural draw ratio [112]. The drawability value of the as-spun fibres plays an important role in identifying the levels of the hot drawing parameters in the fraction factorial experimental design matrix. The heating during the drawing process increases polymer chain mobility and elongates the chains in the direction of the fibre's axes [117]. The hot drawing process helps to produce super fine filaments; hot drawing of as-spun fibres can increase the tenacity, decrease the fibre elongation and control the overall orientation. In the case of non-linear visco-elastic behaviour and necking effect, the velocity was neither steady nor uniform and there was a kinematics problem of continuous drawing [159]. Overall orientation was improved during hot drawing; molecules were pulled out of the lamellar crystals and molecules in the amorphous regions were extended [161]. The mechanical properties depend on the drawing conditions and the original structure of un-drawn fibre which may be para-crystalline or amorphous. The mechanical properties of drawn fibres are determined by the orientation, crystallinity and morphological structure produced in drawing. In fact, the drawing process could be done at a higher speed than the melt spinning speed; therefore the drawing process is a separate operation from the spinning line [223]. With twisting, each yarn runs from a supply drawn yarn bobbin via a supply roller through a yarn guide into the twisting balloon and then through a round running traveller tangentially onto the bobbin. As twist was applied to multifilament yarn, the freedom of the filament to move was reduced as the yarn was given stiffer cohesion and the filaments away from its original axis were forced to stretch [168]. Twist caused the outer filaments to press on inner filaments (filaments exert a pressure on each other). Twist helps the filaments to share the load and increase the strength. When one of the filaments is broken, its friction with the neighbouring filaments enables the broken filament to carry load a short distance away from the break.

A fractional factorial statistical experimental design was used in this chapter as a function of the process parameters using statistical factorial methods. The aliphatic-aromatic co-polyester (AACs) fibres were spun, hot drawn, twisted, characterised and analysed under a fractional factorial design as a function of the process parameters using appropriate statistical methods to model the process parameters' effect. The results and statistical analysis helped in designing a combination of factor levels controlling the production processes of environmentally friendly biodegradable fibre. The additional effect gained from adding twisting to the continuous drawn filament was investigated in terms of the process parameters interactions. A new forecasting data source were achieved to optimize the hot drawing and twist of as-spun aliphatic-aromatic co-polyesters (AAC) fibres and to specify the direction of increasing or decreasing of the significant process parameters.

Two general lines were used in this chapter to produce multifilament, single and simple untwisted or twisted yarns: first, for untwisted yarns, modelling the effect of the multi-stage hot drawing process on crystallographic order and chain orientation of only drawn linear (LAAC), and on the thermal and mechanical properties of both drawn linear (LAAC) and branched (BAAC) aliphatic-aromatic co-polyester fibres were statistically investigated and characterized; secondly, for twisted yarns, selected continuous drawn filaments were twisted. That will help to find the effect of twisting on the fibres properties and to find the twist interaction with the drawing conditions. A combination of factor levels was designed for controlling the properties using the regression equations obtained by using Statographic Software. Generated regression model formed a part of a forecasting program for environmentally-friendly biodegradable fibre production.

6.2 Preparation of As-Spun AAC Fibres For Hot Drawing Without/With Twisting

The same sample of as-spun AACs fibres was extruded via melt-spinning using the Lab-Spin machine for hot drawing without / with twisting. The specially designed spinneret of 30 holes was used. New temperature profile and spinning conditions were selected based on statistical experimental analysis and the results of the spinning study (Section 5.9.3). The temperature of the feeding zone was kept above 100^{o}C to prevent any moisture from forming. For LAAC fibres made of Solanyl flexibility component, the six heating zones in the extrusion machine profile were 115, 120, 125, 130, 140 and 140^{o}C. The metering pump was fixed at 12 rpm at

pre pump pressure of 1000 psi. The air cooling quench speed percentage was set at 73%. The spin finish application speed was set at a speed of 0.3 rpm; the godets and the Leesona winder were set at a speed of 50 m min^{-1}. For BAAC fibres made of Ecoflex, the six heating zones in the extrusion machine profile were 120, 125, 135, 140, 150 and 150^{o}C. The metering pump was fixed at 8 rpm at a pre pump pressure of 1000 psi. The air cooling quench speed percentage was set at 35%. The spin finish application speed was set at a speed of 0.3 rpm, the godets and the Leesona winder were set at a speed of 50 m min^{-1}. The godets and the Leesona winders were controlled independently by DC motors; all speeds were confirmed by the laser digital tachometer. The as-spun fibres drawability value played an important role in identifying of the levels of hot drawing parameters in the fraction factorial experimental design matrix.

6.3 Experimental Design for Hot Drawing of Aliphatic-Aromatic Co-Polyester Fibres

Hot drawing was carried out on the ESL draw frame described previously in Chapter 3. Figure 6.1 shows an infrared image of a multi-stage hot drawing frame and one of the drawing rollers. For technical and experimental reasons, the spinning and multi-stage hot drawing processes of as-spun AAC fibres were operated individually.

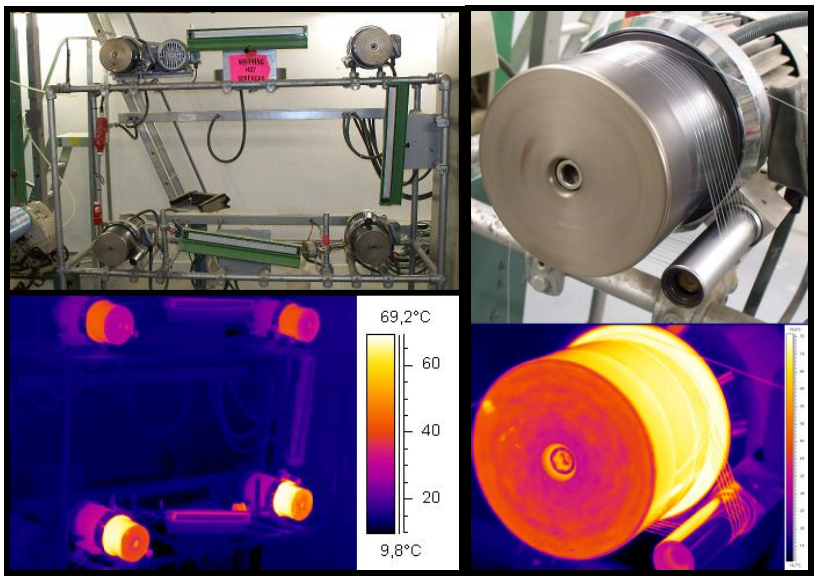

Figure 6.1 Infrared image of multi-stage hot drawing frame and one of the drawing rollers. Image colours correspond to the temperature scale on the right.

Factor abbreviation	Factor name	Level	
		Low	High
A : DS	Total drawing stages number	1	2
B : DT	Drawing temperature (^{O}C)	40	60
C : DR	Total drawing ratio for LAAC	3.5	5.0
	Total drawing ratio for BAAC	1.6	2.6
D : PT	Plate temperature (^{O}C)	40	60
E : SF	Spin finish (rpm, 0.292 cc/rev)	1.5	3.0
F : RS	Relaxing stage ratio (%)	0.04	0.08
G : RT	Relaxing temperature (^{O}C)	40	60

Table 6.1 Factors and their levels for the multi-stage hot drawing experiments

Trial Number	DS	DT	DR	PT	SF	RS	RT
1	L	H	H	L	L	L	H
2	H	L	H	L	H	L	H
3	H	H	L	H	L	L	H
4	L	H	H	H	L	L	L
5	H	H	H	L	L	H	L
6	H	H	L	H	H	L	H
7	H	L	L	H	H	H	L
8	L	H	L	H	H	H	L
9	H	L	H	H	H	L	L
10	H	L	L	H	L	H	L
11	L	H	L	H	L	H	L
12	H	H	L	L	H	L	L
13	H	L	H	H	L	L	L
14	L	H	L	L	H	H	H
15	L	L	L	L	H	L	L
16	H	L	L	L	L	H	H
17	L	H	L	L	L	H	H
18	L	L	L	L	L	L	L
19	H	H	H	L	H	H	L
20	L	L	L	H	H	L	H
21	L	L	L	H	L	L	H
22	H	L	H	L	L	L	H
23	H	H	H	H	L	H	H
24	H	H	H	H	H	H	H
25	L	H	H	L	H	L	H
26	L	L	H	L	L	H	L
27	L	L	H	L	H	H	L
28	L	H	H	H	H	L	L
29	L	L	H	H	H	H	H
30	L	L	H	H	L	H	H
31	H	H	L	L	L	L	L
32	H	L	L	L	H	H	H

Table 6.2 L32 Experimental design array and results for the multi-stage hot drawing experiments (L: Low, H: High)

To investigate the influence of hot-drawing conditions on the structural and physical properties of LAAC and BAAC fibres, a fraction factorial experimental design was used. The factors are listed with their abbreviations in Table 6.1; the seven control parameters for the hot drawing experiments were the total number of drawing stages (DS), drawing temperature (DT), total drawing ratio (DR), plate temperature (PT), spin finish application speed (SF), relaxing stage ratio between relaxation process rollers (RS) (where speed of the second roller = RS * speed of the first roller) and relaxing temperature (RT). The two levels of each parameter were separated as far apart as possible from one another. The total drawing ratio (DR = DR1*DR2=V2/V1 *V3/V2 = V3/V1) used in the optimization represents the ratio between the speed of the second roller (V3) of the second stage to the speed of the first roller of the first stage (V1). The speed of the second roller of the first stage equals the speed of the first roller of the second stage, V2. The draw ratio of first stage (DR1:V2/V1) is larger than that of the second stage (DR2:V3/V2); the DR1 to DR2 ratio is 2 to 1. The speed of the first roller was 35 m min^{-1} allowing the fibre to receive more heat which reduced the variation; the temperature rise should be similar, as the draw ratio is affected by the temperature at which the drawing is carried out. In two drawing stages; the same drawing temperature was applied for both the first and the second stages which decreased the number of interactions between the factors achieved; as a result of the ability of the software used, the relaxing stage helped in the deformability of the fibre by decreasing the internal stress inside the fibre. As a function of hot-drawing conditions, a fractional factorial design with random order (L32; $2^{7-2} = 2^5 = 32$) was used for the thirty-two screening trials in this experiment, involving the mentioned seven control parameters as shown in Table 6.2, designed using the STATGRAPHICS program.

6.4 Statistical Modelling of The Effect of Multi-Stage Hot Drawing on Linear Aliphatic-Aromatic Co-Polyester Fibres (LAAC)

6.4.1 Experimental Results

The experiments in Table 6.2 were randomly conducted in one block involving control factors and their levels (Table 6.1). The birefringence, full-width half-maximum (FWHM) of an x-ray scattering profile, thermal shrinkage and mechanical properties for fibres were measured and the data obtained are listed in Table 6.3. The means of measured data of the specimens have acceptable standard deviations which may be related to the draw frame setting based variation, the tension or slippage on the drawing roles or tension during the preparation of the sample for testing. Figure 6.2 shows the recorded microinterferograms of the 32 samples of LAAC fibres using the polarizing (Pluta) microscope. The measured values of birefringence were averaged from three repeated measurements for each sample, Table 6.2. With heating, the chain will be flexible and will take the opportunity for a new and ordinary arrangement to be arrived at the achieved structure. The fibre diameter affects the crystallization during drawing; the high value of fibre diameter leads the fibre to stay warm for longer period. The stability will be less, with more internal strain, looking to get the original position and behaving like rubber. As the hot drawing parameters changed, the fibre structure was expected to change and that will be seen in the intensity and the width of the crystalline peaks of x-ray diffraction traces. Wide angle x-ray scattering (WAXS) traces were obtained; the scan range was 15~28 ($2\theta^{o}$). In x-ray diffraction traces, the degree of crystallographic order increased with the increase in the intensity of crystalline peaks, decreased in peak width and decreased in background area of the scattering profile. A higher size of crystallite and the higher degree of crystallographic order were reflected qualitatively in a decrease in FWHM value and vice versa.

Figure 6.3 presents typical x-ray diffractometer traces. There are five major crystalline diffraction peaks with different full-width half-maximum (FWHM) of an x-ray scattering profile observed at $2\theta^{\circ}$ = 16, 17.5, 20.5, 23 and 24.5. An X-ray scattering profile will facilitate the optimization and modelling of the overall process; the gradual structural change is attributed to the setting of the drawing process. The process conditions affect the crystallinity of the fibre and that could be noted from the sharpness of the peaks and the area under the traces.

The peaks observed at 2θ° = 16, 20.5, 21.5 and 24.5 are relatively wide and not obvious. The peaks at 2θ° = 17.5 and 23 are slightly sharper, more intense and smaller in width. The peak at 2θ° = 23 was fitted using DIFFRAC plus EVA software to compare the half-height widths. From it, conclusions were drawn about the relative crystallographic order within a series of the 32 samples. For all trials, the analysis explained the gradual change in the factors and the structure obtained. Detailed comparisons of each trace revealed that some traces were more similar to each other than to others, with slightly significant differences including the overall shape, the numbers and the positions of peak. Figure 6.4 shows the recorded x-ray diffractometer traces of the 3 selected samples of LAAC fibres, which present low, middle and high FWHM values for trials 10, 17 and 18 respectively. Such a quantification of structure order as a response parameter makes it possible to conduct systematic analysis of processing factors on the fibre structure. FWHM and birefringence results analysis helped in the evaluation of the effect between drawn fibre structure and the thermal shrinkage to better enhance fully drawn fibres in the practical stage. Each thermal shrinkage test was carried out using a MK IV Shrinkage-Force Tester; samples were heated for 2 min at 60^{o}C under a load cell of 10g.

To find the effect of hot drawing on the thermal properties of drawn fibres, Figure 6.5 shows DSC curves for four selected samples produced with different hot drawing conditions for trials 4, 13, 23 and 30. No significant effect was reported in their thermal properties but the mechanical properties were better with the relaxation stage. A broad range of melting temperature (about 100-135°C) was observed for the fibres. According to the DSC results, the fibre did not melt completely below 120 °C, as an optimum temperature window was found taking all factors into account. No appreciable changes of relative intensity of the peaks in the endotherm were observed in different samples for the same trial. Figure 6.6 shows an SEM photomicrograph of the surface and cross section of the fibres. Drawn fibres had a uniform circular cross section with acceptable uniform surface, the fibres' cross section in the centre could deform into a polygonal shape under pressure. All statistical analysis and presented plots were constructed directly from the raw data using the computer software available.

Trial Number	Birefringence	FWHM (^{o})	Thermal Shrinkage (%)	Tenacity (g/den)	Elongation at break (%)	Modulus (g/den)
1	0.090	0.836	11.9	1.0	91.67	1.66
2	0.097	0.790	14.6	1.3	81.94	1.90
3	0.060	0.705	14.9	0.6	222.92	0.48
4	0.095	0.864	11.5	1.0	79.17	1.69
5	0.088	0.908	14.0	1.1	84.72	1.64
6	0.066	0.511	14.1	0.6	193.75	0.45
7	0.091	0.521	14.0	0.7	183.33	0.81
8	0.066	0.697	09.8	0.7	200	0.47
9	0.106	0.888	14.2	1.3	84.72	1.92
10	0.085	0.670	14.0	0.8	220.83	0.45
11	0.067	0.656	10.3	0.8	183.33	0.45
12	0.061	0.686	14.9	0.8	183.33	0.48
13	0.103	0.997	14.3	1.0	56.94	1.55
14	0.068	0.671	10.2	1.0	241.67	0.50
15	0.082	0.737	13.0	0.7	195.83	0.74
16	0.070	0.868	13.8	0.6	175	0.47
17	0.067	0.118	11.3	0.8	222.92	0.44
18	0.080	1.029	13.5	0.8	195.83	0.54
19	0.088	0.347	14.1	1.1	95.83	1.63
20	0.081	0.605	13.1	0.7	212.5	0.51
21	0.082	0.612	13.0	0.8	187.5	0.48
22	0.103	0.871	14.4	0.9	62.5	2.01
23	0.088	0.619	14.0	1.1	86.11	1.67
24	0.088	0.354	12.5	0.9	77.78	1.71
25	0.084	0.162	12.4	1.1	91.67	1.47
26	0.096	0.127	12.4	1.0	70.83	1.56
27	0.095	0.689	13.7	1.1	75	1.64
28	0.086	0.136	11.7	1.1	100	1.64
29	0.092	0.384	13.1	1.1	77.78	1.69
30	0.107	0.508	13.3	1.2	76.39	2.16
31	0.074	0.479	15.4	0.7	210.42	0.49
32	0.074	0.302	14.5	0.8	193.75	0.45

Table 6.3 Results for the hot drawing experiments for LAAC fibres

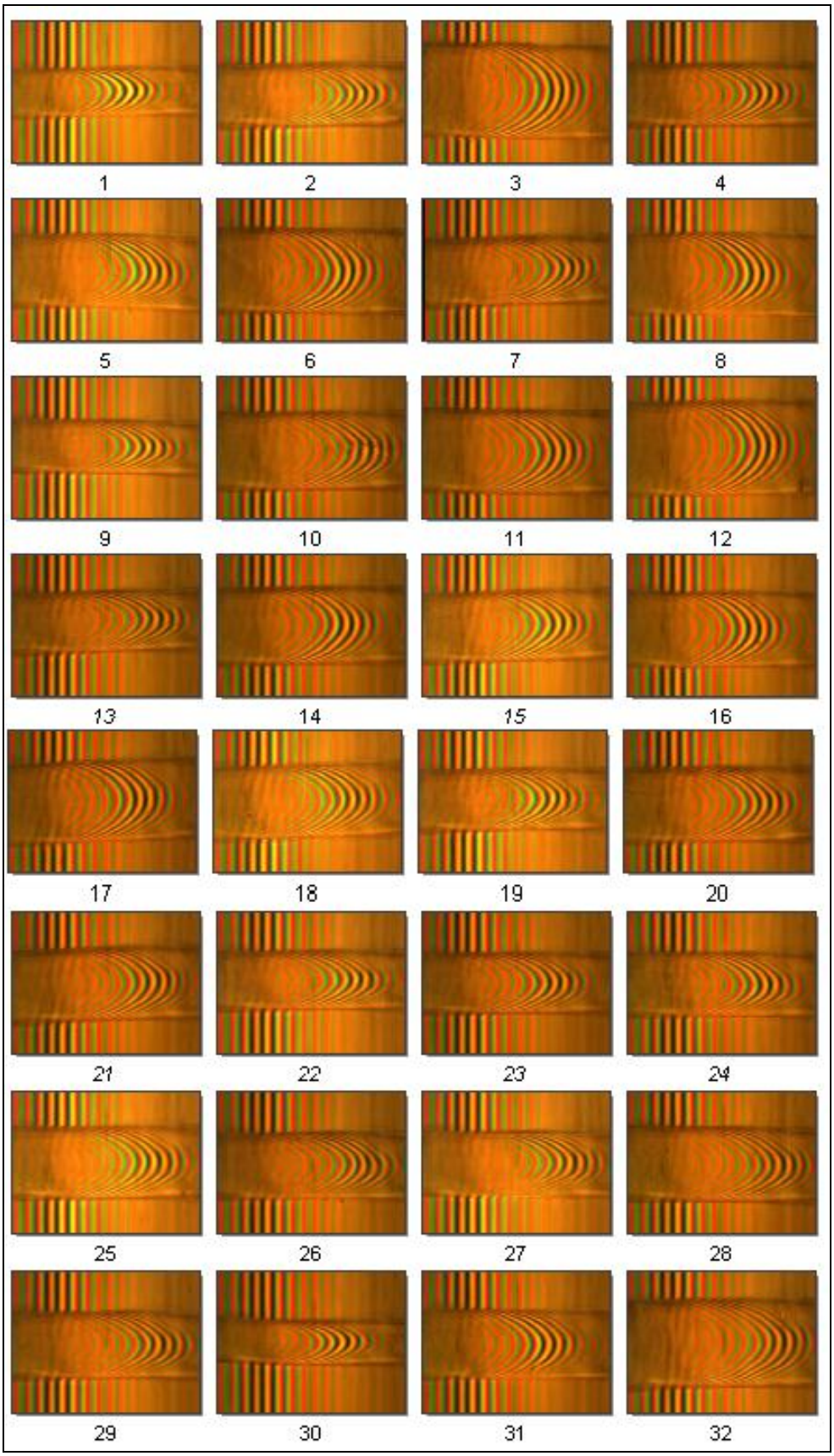

Figure 6.2 The microinterferograms of the drawn LAAC fibres using a Pluta microscope

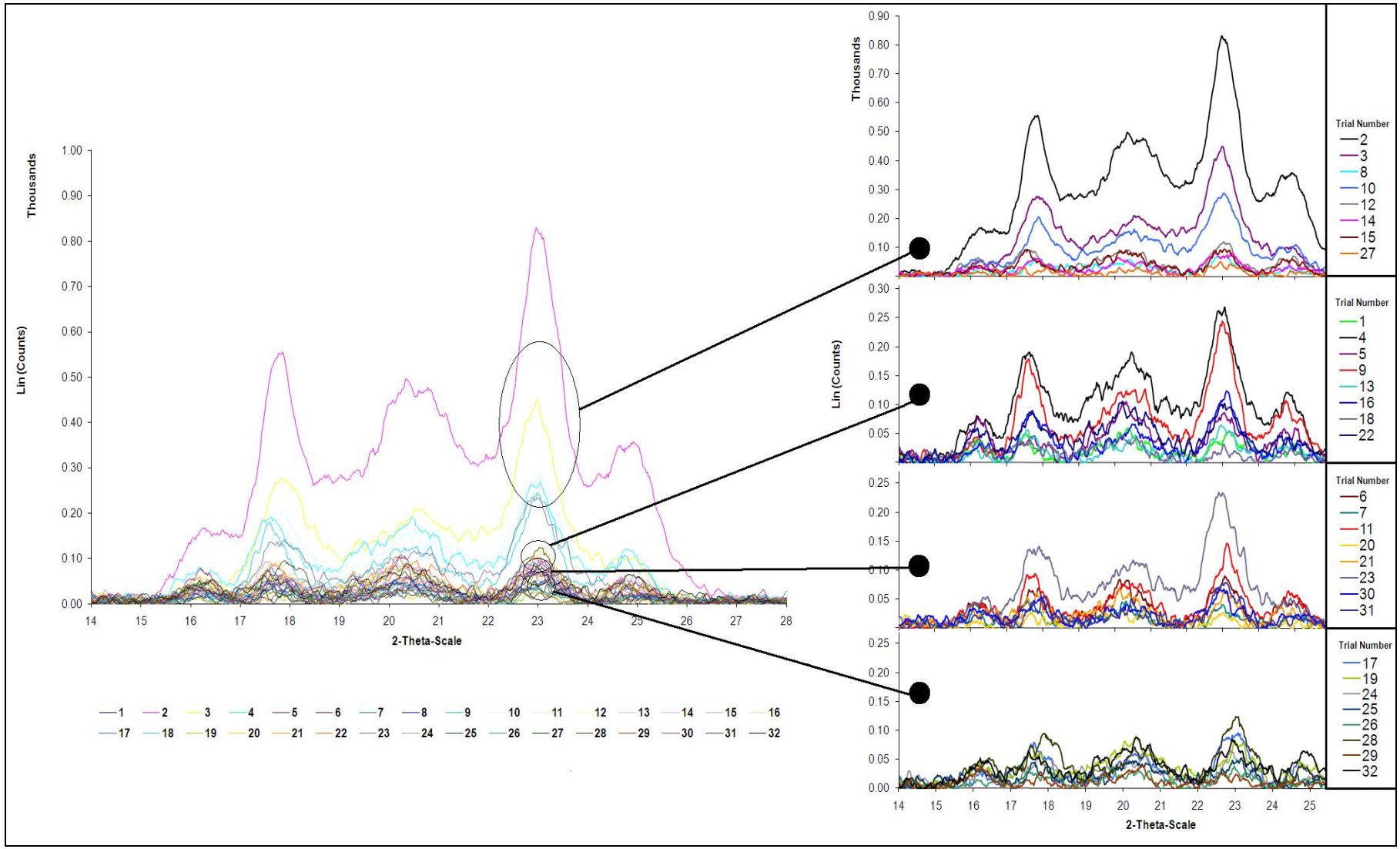

Figure 6.3. WAXS traces of LAAC fibres

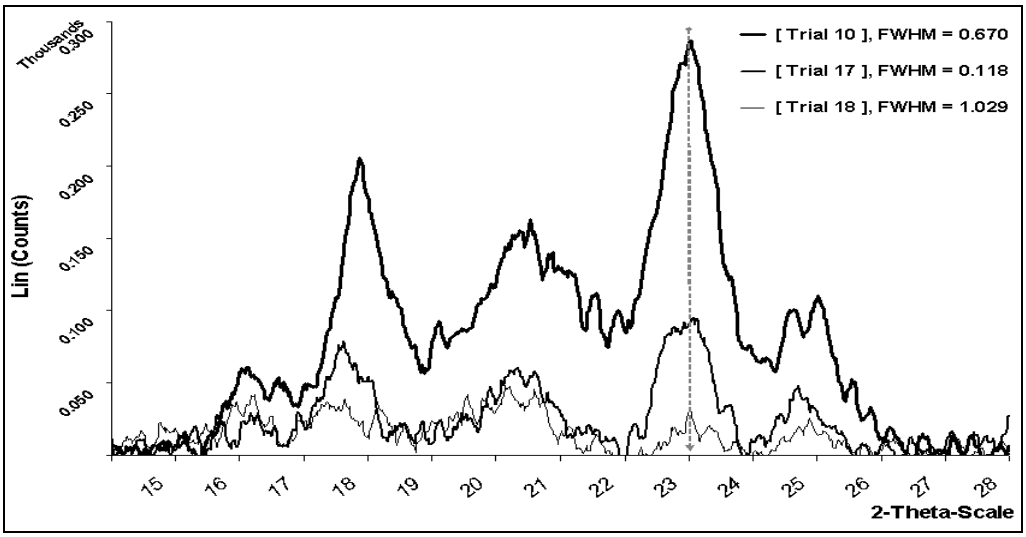

Figure 6.4. WAXS traces of three selected LAAC fibres (Trials 10, 17 and 18)

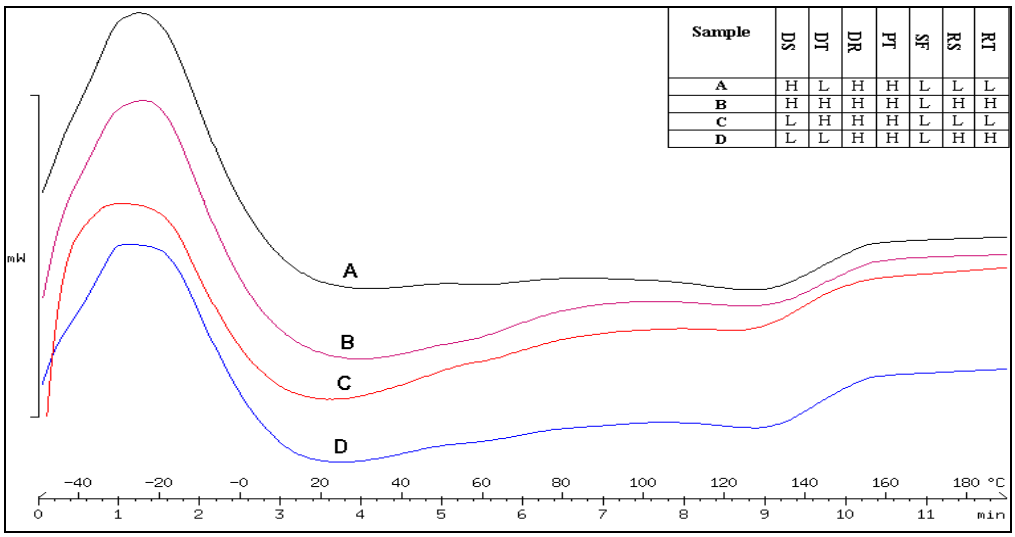

Sample	DS	DT	DR	FT	SF	RS	RT
A	H	L	H	H	L	L	L
B	H	H	H	H	L	H	H
C	L	H	H	H	L	L	L
D	L	L	H	H	L	H	H

Figure 6.5 DSC curves of hot drawn LAAC fibres
(A: trial 13, B: trial 23, C: trial 4 and D: trial 30)

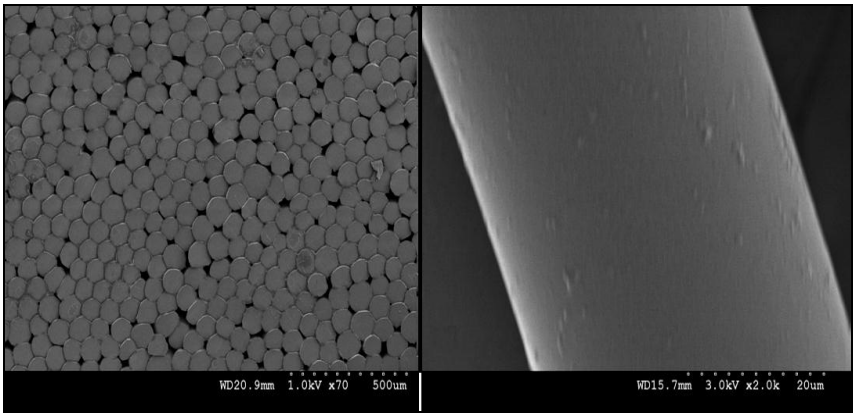

(3:1magnification ratio) (90:1 magnification ratio)

Figure 6.6 SEM photomicrograph of LAAC fibres' surface and cross section.

6.4.2 Statistical Analysis and Discussion

As a two-level experiment, the factor and interaction effects could be determined as the difference between the average responses at the low and the high level of hot drawing process parameters. Pareto charts (Figure 6.7) for birefringence (a), FWHM (b), thermal shrinkage (c), tenacity (d), elongation at break at break (e) and modulus (f) show the significant arrangement of the factors and their interactions in decreasing order. The Pareto chart for birefringence shows that the total draw ratio (DR) and draw temperature (DT) are the most important factors affecting the birefringence, followed by the interactions DS&RT and DT&PT, the plate temperature (PT), the relaxing temperature (RT), followed by the other factors and their interactions. The tension generated from applying a high drawing ratio with a lower relaxing ratio will create high internal stress in the fibre structure and affect the shrinkage properties. The polymer chains move in the direction of drawing to become oriented parallel to the fibre axis. The crystallinity will be increased as a result of shear induction and the fibre properties are improved. The Pareto chart for FWHM shows that the relaxing stage ratio (RS), the interactions DS&DR and DT&RS, spin finish application (SF), drawing temperature (DT), total number of drawing stages (DS), the interaction (DR&SF), relaxing temperature (RT) and the interaction (SF&RS) have a notable effect on FWHM, followed by other factors and interactions. As a second order transition is obtained with high relaxing stage ratio and with lower temperature in the relaxing stage, the chains lose their freedom and elasticity and so become fixed. A Pareto chart of the thermal shrinkage is a useful tool for investigation of the extent to which a fibre has been heat stabilized. It shows that total drawing stages number (DS), the interactions (DS&DT, DR&RS and PT&RT), drawing temperature (DT), relaxing stage ratio (RS), the interactions (DS&DR and DT&RS) and plate temperature (PT) are the most important factors affecting the thermal shrinkage properties of the fibres, followed by other factors and interactions. As mentioned previously, determined factors would affect the tension and the internal stress affecting the orientation and the thermal shrinkage properties. In terms of the mechanical properties of drawn LAAC fibres, the Pareto chart for tenacity shows that drawing ratio and the interactions PT&SF, DS&RT, DT&PT, DS&DR, DT&RS and SF&RS are the most important factors affecting the tenacity, followed by other factors and interactions.

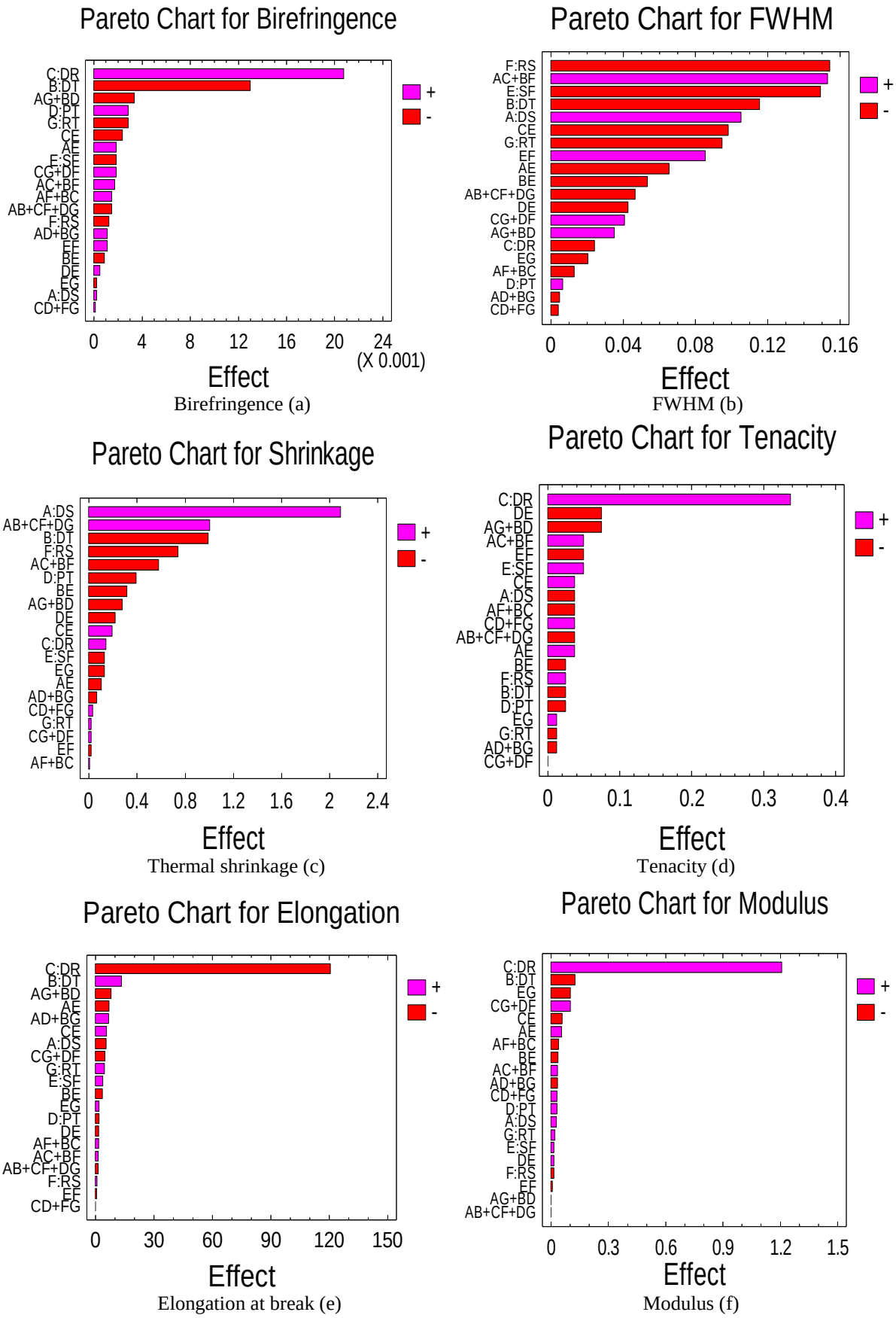

Birefringence (a)

FWHM (b)

Thermal shrinkage (c)

Tenacity (d)

Elongation at break (e)

Modulus (f)

Figure 6.7 Pareto chart for birefringence (a), FWHM (b), thermal shrinkage (c), tenacity (d), elongation at break (e) and modulus (f)

The Pareto chart for elongation at break shows that total draw ratio, drawing temperature and the interactions DS&RT, DT&PT and DS&SF are the most important factors affecting the elongation at break, followed by other factors and interactions. The Pareto chart for modulus shows that total draw ratio, drawing temperature and the interactions SF&RT, DR&RT and PT&RS are the most important factors affecting the modulus, followed by other factors and interactions. There is a clear relationship between the factors affecting the chain orientation and those affecting the elongation at break. Spin finish oil could chemically affect the fibre; but the current study will not deal with that possibility which needs structural and molecular analyses. In the relaxation process and when the relaxing ratio increases, yarn speed decreases, cooling time increases and the thickness of the spin finish layer increases. This relationship could explain the interaction between process conditions and fibre structure; when a higher draw ratio is applied, the speed of the final roller will increase and the spin finish layer thickness on the fibres at constant spin finish pump speed will be affected, which could explain the interaction between the spin finish applicator speed and the draw ratio.

The main effects and interaction plots of the statistical analysis of the effects could give an idea about their effects on studied responses. The factor effect on birefringence between the average responses of the low and high level of the factors was obtained using the design matrix and is presented in Figure 6.8. The main effects of total draw ratio (DR) and draw temperature (DT) were more pronounced on birefringence than those of the other factors, as their lines are longer and their slopes are sharper. For example; birefringence increases either by increasing the draw ratio or by decreasing drawing temperature. Further assessment of the major factors influencing birefringence value would be advised to understand their influence more fully. All the interactions could be simulated, as the plot shows the existence or otherwise of each two factor interaction, as coded in Table 6.1. For example, the interaction between total number of drawing stages (DS) coded as A and drawing temperature (DT) coded as B is presented as AB on the plot. The first factor (A) is presented on the X-axis from low level to high level, while the second factor (B) is shown as two different lines, one for low level coded as (-) and another for high level coded as (+). The nonparallel lines confirm the presence of an intersection. Even though there are noted interactions, DS&DT, DS&DR, DS&SF, DS&RS, DS&RT, DT&PT, DR&SF, PT&RS, PT&RT and SF&RS, their significance needs to be further investigated because of the small angles between the interaction lines; statistical analysis ANOVA is given in next section.

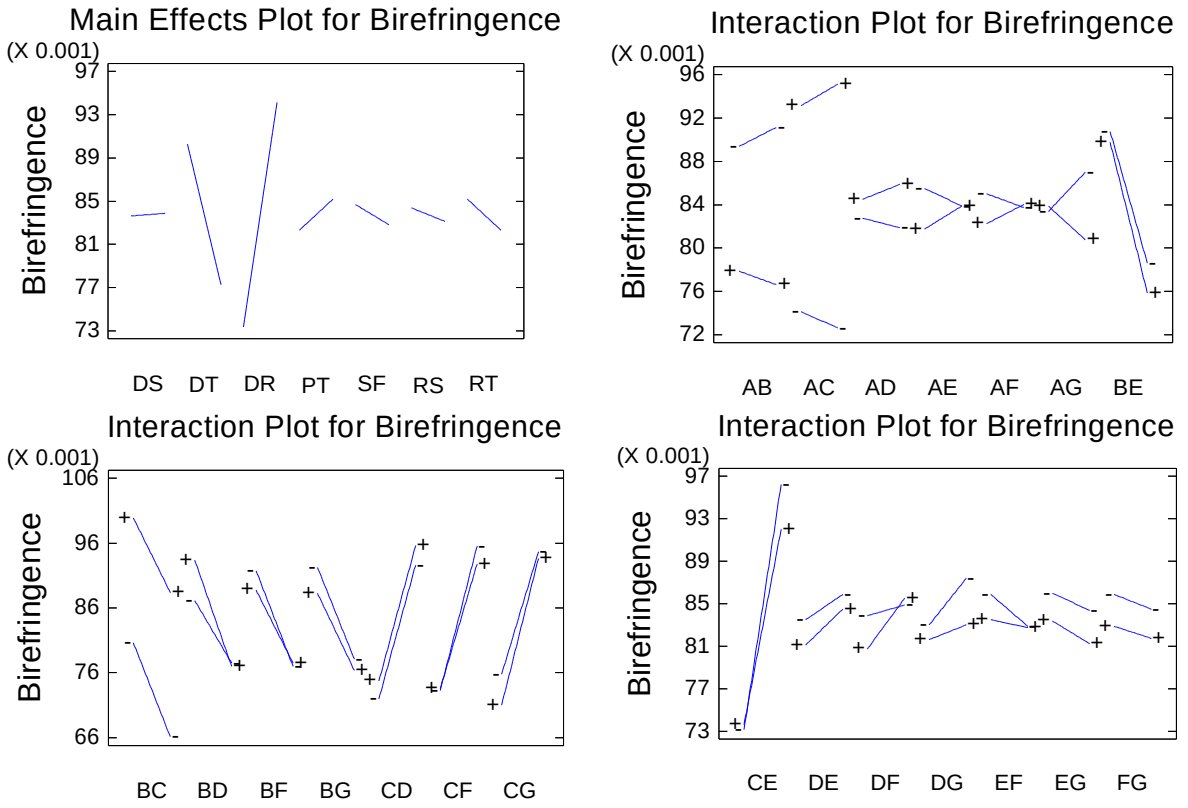

Figure 6.8 Main effect plots and interaction plots for the birefringence

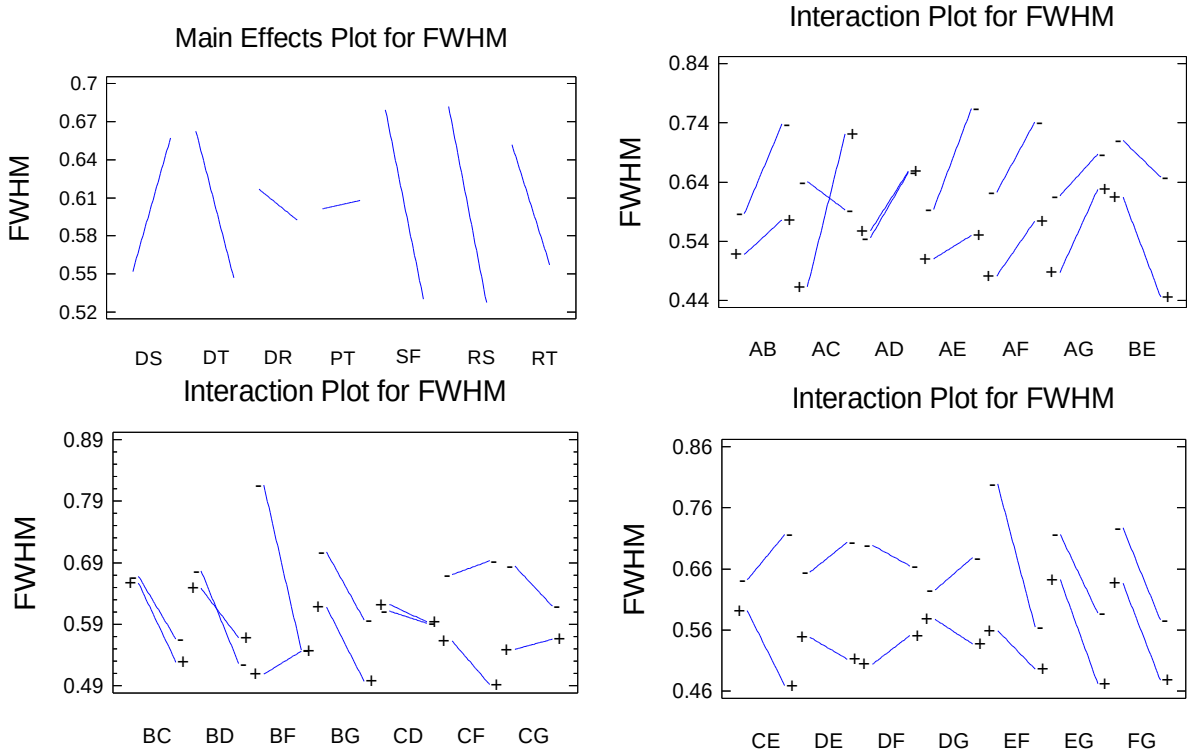

Figure 6.9 Main effect plots and interaction plots for the FWHM

For full-width half-maximum of an x-ray scattering profile (FWHM), the effects of total drawing stages number, drawing temperature, spin finish application, relaxing stage ratio and relaxing temperature were more pronounced than total draw ratio and the plate temperature, as their lines were longer and their slopes sharper than those of the other factors (Figure 6.9). FWHM is increased either by increasing the number of drawing stages and plate temperature or by using the lower level of other factors which affect the FWHM negatively. In other words, increasing the number of drawing stages and plate temperature decreased the degree of crystallographic order of the samples as a result of the stretch force differences.

In Figure 6.10, all the interactions could be simulated, as the plots show the existence or otherwise of the interaction of each of the two factors. The interaction between the number of drawing stages and drawing temperature (Figure 6.10) is presented as AB on the plot. When the high level of the number of drawing stages was paired with the high level of drawing temperature, the maximum thermal shrinkage was obtained. However, there were other noteworthy interactions and their significance needs to be further investigated because of the angles between the interaction lines such as DS&DR, DT&RS, DR&RS, DR&SF and PT&RT. From the main effects plot for shrinkage, the main effects of total number of drawing stages, drawing temperature, relaxing stage ratio and plate temperature were more pronounced than those of the other factors, total draw ratio, spin finish application and relaxing temperature, as their lines were longer and their slopes sharper than those of the other factors. The interactions DS&DT, DR&RS, PT&RT, DS&DR, DT&RS and DT&SF had their effects which will be further investigated using ANOVA analysis. Thermal shrinkage increased either by increasing the number of drawing stages and drawing ratio, or by using the lower level of other factors which affected negatively the thermal shrinkage. When the high number of drawing stages was paired with the high drawing temperature, the maximum thermal shrinkage was obtained. The effects and interaction plots for tenacity (Figure 6.11) show that total draw ratio, PT&SF, DS&RT, DT&PT, DS&DR, DT&RS and SF&RS were the most important factors. From main effects and interaction plots for elongation at break, total draw ratio, drawing temperature, DS&RT, DT&PT and DS&SF were the factors affecting the elongation at break (Figure 6.12). The effects and interaction plots for modulus show that total draw ratio, drawing temperature and the interactions SF&RT, DR&RT and PT&RS affect the modulus (Figure 6.13). In the relaxation stage, the chains could return to their random arrangement depending on the total draw ratio.

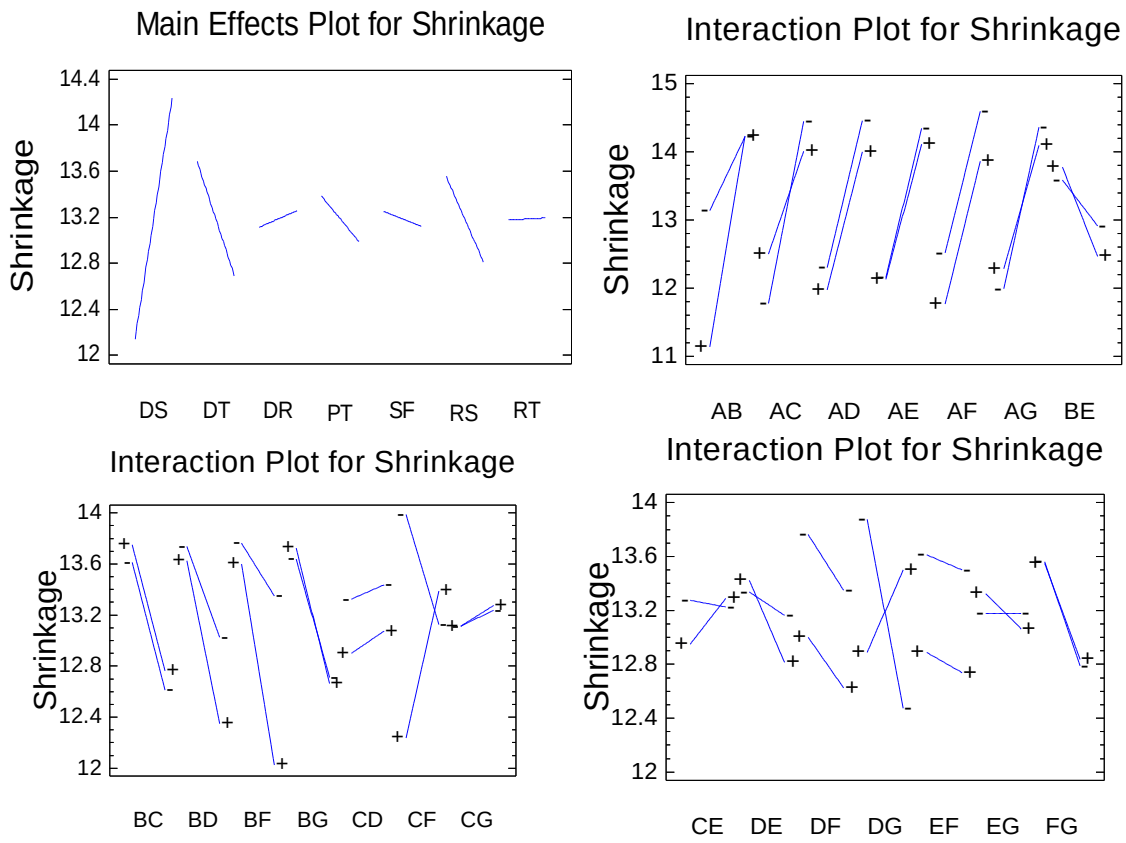

Figure 6.10 Main effect plots and interaction plots for the thermal shrinkage

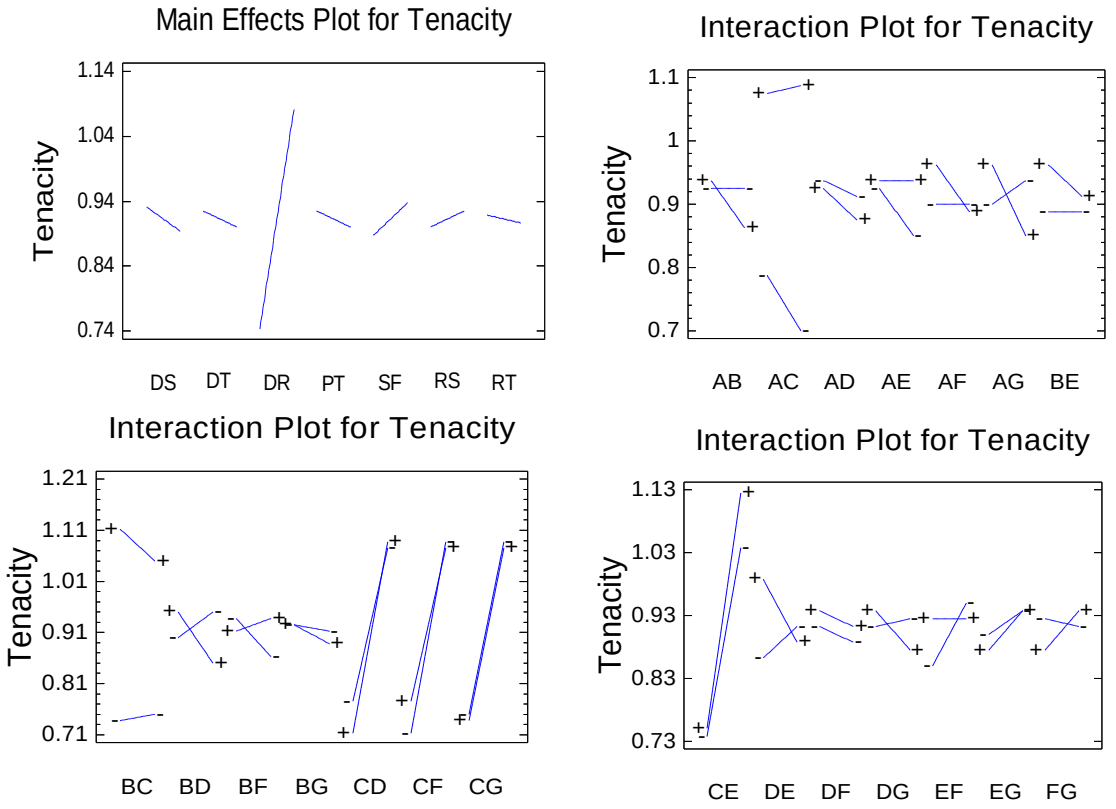

Figure 6.11 Main effect plots and interaction plots for the tenacity

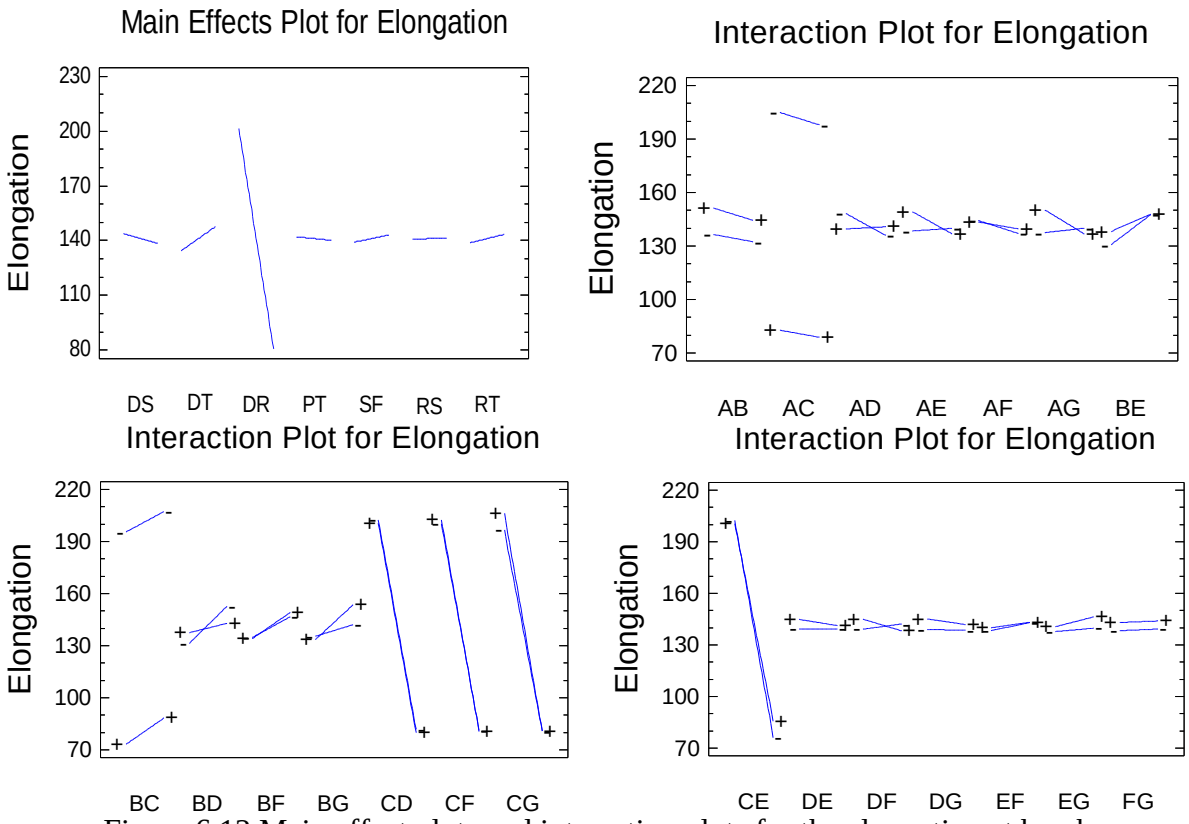

Figure 6.12 Main effect plots and interaction plots for the elongation at break

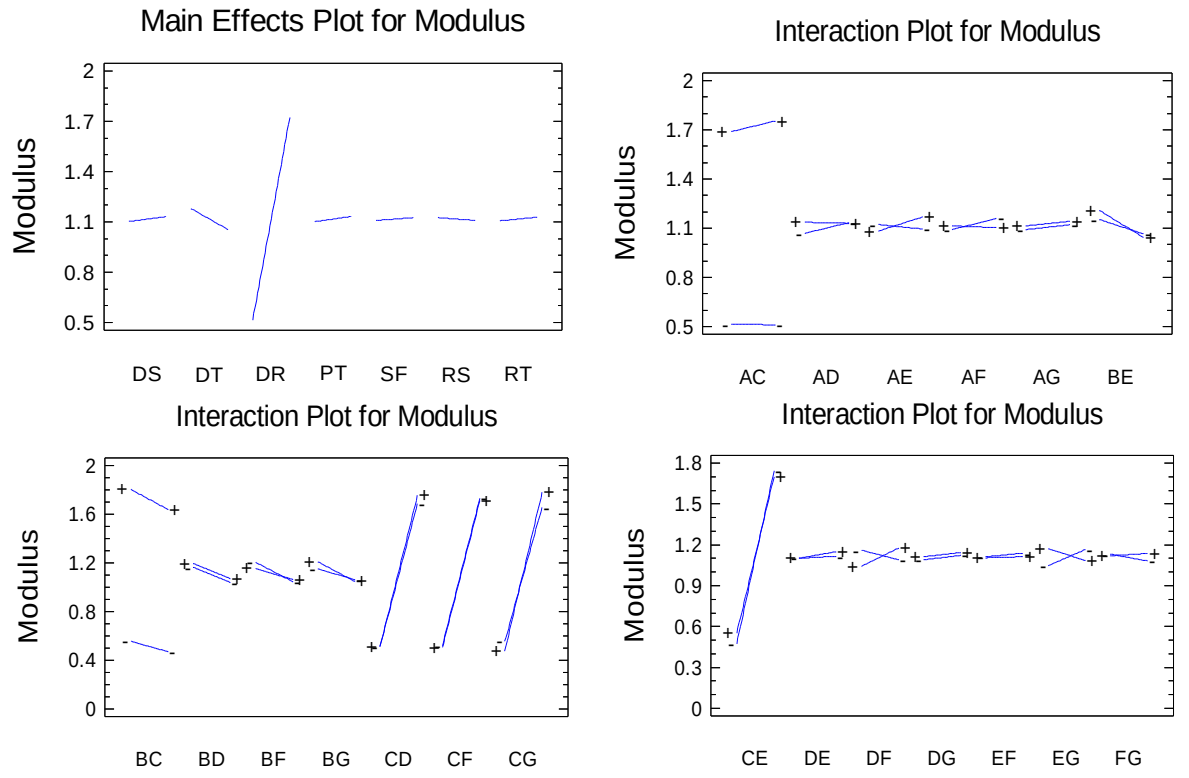

Figure 6.13 Main effect plots and interaction plots for the modulus

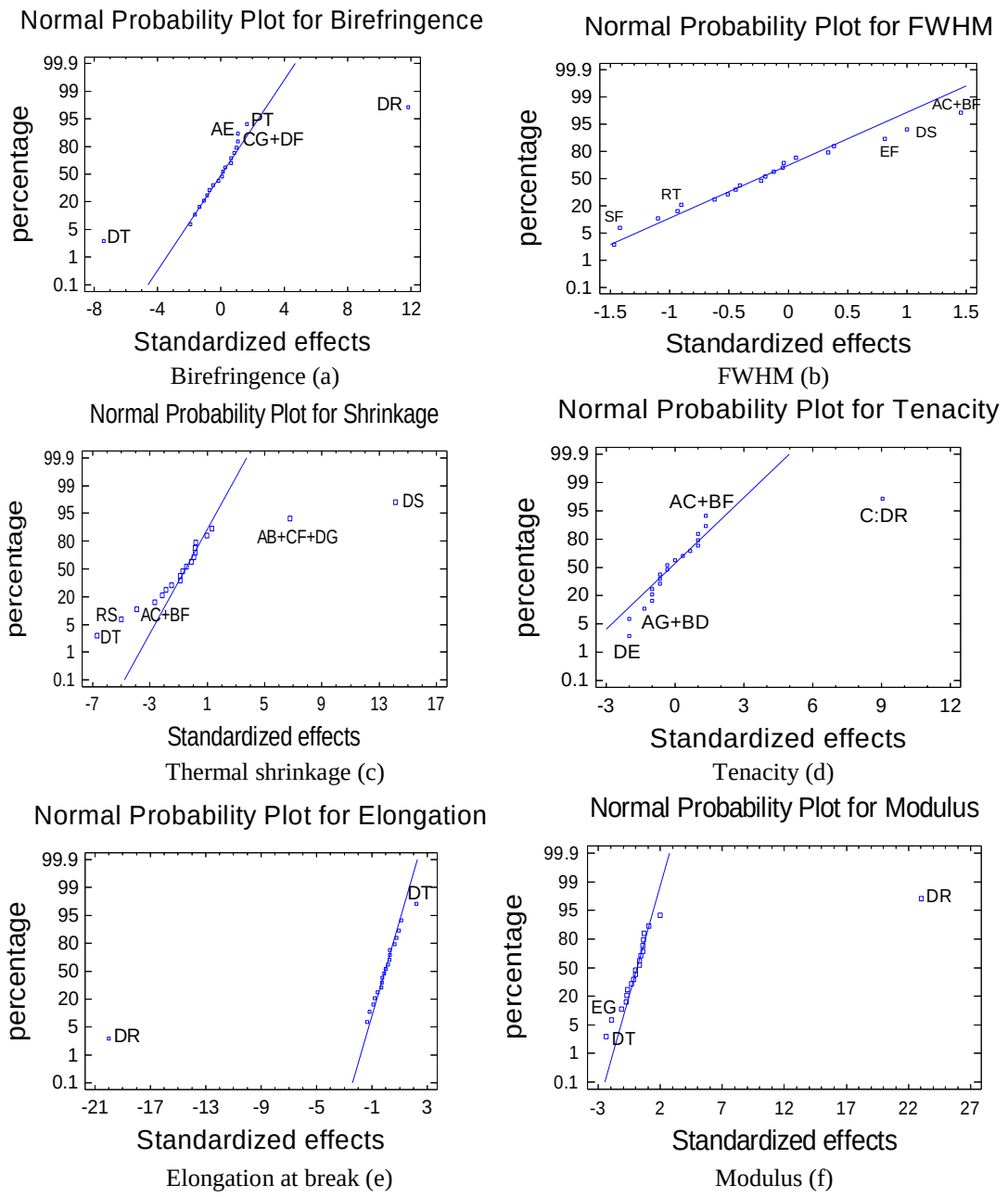

Figure 6.14 Normal Probability Plot for birefringence (a), FWHM (b), thermal shrinkage (c), tenacity (d), elongation at break (e) and modulus (f).

Figure 6.14 displays the normal probability plot of the responses estimated and illustrates further details about the normal distribution for the data. Draw ratio has a positive effect but draw temperature and plate temperature have a negative effect on the birefringence.

The negative effects from the interaction between draw stage and spin finish are less prominent and could be related to the practical relationship between the tension and the oily roller surface on the last roller in the relaxing stage ratio which caused some slippage. In the normal probability plot for FWHM (Figure 6.14, b), the positive effects from the total number of drawing stages (DS), the interactions (DS&DR and DT&RS) and the interaction

(SF&RS) were again prominent. Spin finish application (SF) and relaxing temperature (RT) have negative effects on FWHM. Figure 6.14 (c) displays the normal probability plot for the shrinkage. The positive effects from the total number of drawing stages (DS) and the interactions DS&DT, DR&RS and PT&RT are prominent. Drawing temperature (DT), relaxing stage ratio (RS) and the interactions DS&DR and DT&RS had a negative effect on thermal shrinkage. In terms of mechanical properties, draw ratio had a negative effect on elongation at break and a positive effect on tenacity and modulus.

Draw temperature had either a positive effect on elongation at break or a negative effect on tenacity and modulus. Other factors and interactions had a less important effect on mechanical properties. With one stage, the tension will be very high and the spin finish plays an important role in the filament slippage on the last roller after applied spin finish, in addition to the spin finish in the as-spun samples. Some interactions between factors could be related to the fractional design; These results were analyzed by ANOVA.

6.4.2.1 Analysis of Variance (ANOVA)

Analysis of variance (ANOVA) of the data obtained determined the factor effects in terms of statistical significance. Each factor had a P-value less than 0.05, indicating that the factor was significantly different from zero at the 95.0% confidence level. ANOVA results are listed in Table 5.5; birefringence was significantly affected by draw ratio (P_{DR} = 0.000) and drawing temperature (P_{DT} = 0.000). Note that, even when P_{DR} = P_{DT} = 0.000, the order of the significance was obtained depending on F-Ratio listed, F-Ratio$_{\mathbf{DR}}$ > F-Ratio$_{\mathbf{DT}}$. Even though there were noted interactions between factors, their effects on birefringence were not significant. P-values of the factors affecting FWHM were greater than 0.05; then factors and their interaction did not affect FWHM significantly. The significance of the studied factors affecting the thermal shrinkage will then be the total number of drawing stages (DS)> the interactions DS&DT, DR&RS and PT&RT > drawing temperature (DT)> relaxing stage ratio (RS) > the interactions DS&DR and DT&RS > plate temperature (PT). The interaction DT&SF was on the border line of significance effect. There were no significant effects of the other interactions within the factor range in the experiments.

The ANOVA analysis for mechanical properties shows that draw ratio had a significant effect on tenacity, elongation at break and modulus. Drawing temperature had a significant

effect on elongation at break and modulus as it affected the internal structure of the fibres. According to the statistical analyses, the most effective and significant parameters on mechanical properties are the drawing ratio and the drawing temperature. Other factors and interactions had their effect, but they were limited and less significant; they were overcome by the significance of the drawing ratio and temperature. An error could come from either assignable causes that represent variation resulting from changes in the independent factors, or random causes that signify uncontrolled variation.

Source	P-Value					
	Birefringence	**FWHM**	**Thermal Shrinkage**	**Tenacity**	**Elongation at break**	**Modulus**
DS	0.8891	0.3379	0.0000	0.3365	0.3801	0.5864
DT	0.0000	0.2950	0.0000	0.5166	0.0480	0.0354
DR	0.0000	0.8222	0.3524	0.0000	0.0000	0.0000
PT	0.1291	0.9504	0.0222	0.5166	0.7627	0.5554
SF	0.3075	0.1835	0.3943	0.2072	0.5349	0.7535
RS	0.4904	0.1701	0.0004	0.5166	0.8826	0.7535
RT	0.1291	0.3870	0.9015	0.7439	0.4490	0.6844
DS&DT DR&RS PT&RT	0.4102	0.6655	0.0000	0.3365	0.8166	0.9907
DS&DR DT&RS	0.3393	0.1729	0.0024	0.2072	0.8059	0.5107
DS&PT DT&RT	0.5340	0.9634	0.6514	0.7439	0.2883	0.5107
DS&SF	0.3075	0.5455	0.4879	0.3365	0.2710	0.3010
DS&RS DT&DR	0.4102	0.9043	0.9671	0.3365	0.7842	0.4682
DS&RT DT&PT	0.0803	0.7441	0.0840	0.0696	0.2099	0.9907
DT&SF	0.6273	0.6212	0.0543	0.5166	0.5716	0.4821
DR&PT RS&RT	0.9444	0.9689	0.8367	0.3365	0.9945	0.5403
DR&SF	0.2024	0.3697	0.2173	0.3365	0.3659	0.2813
DR&RT PT&RS	0.3075	0.7061	0.9015	1.0000	0.4332	0.0748
PT&SF	0.7807	0.6924	0.1675	0.0696	0.7735	0.7535
SF&RS	0.5340	0.4329	0.9015	0.2072	0.9050	0.8613
SF&RT	0.8891	0.8485	0.3943	0.7439	0.7627	0.0748

Table 6.4 ANOVA Results identifying the statistical significance of factor effects on the results from analysis of variance (ANOVA) of the data identifying the statistical significance of each factor for birefringence, FWHM, thermal shrinkage, tenacity, elongation at break and modulus

The geometric result of plotting a response variable was as a function of two factors; the interaction appeared with the surface twist. The estimated response surface was based on the assumed regression model. The estimated response surfaces of thermal shrinkage were used to determine the direction and the significance of the interactions, as shown in Figure 6.15 (a). In order to determine the direction of the interactions DS&DT, DR&RS and PT&RT, the geometric result of plotting a response variable was required. There was a twist which confirmed the interaction between total number of drawing stages and drawing temperature. As the surface was flat with no twist found in the surface DR&RS and PT&RT, their determined effects were not significant. This corresponds with the previous statistical analysis results of the interaction plot and ANOVA derived from the experimental data. There was a significant interaction between the number of drawing stages and drawing ratio as there was no twist in the estimated response surface for the insignificant interaction DT&RS. The interaction between DT&SF was borderline and noted twist was found in the surface.

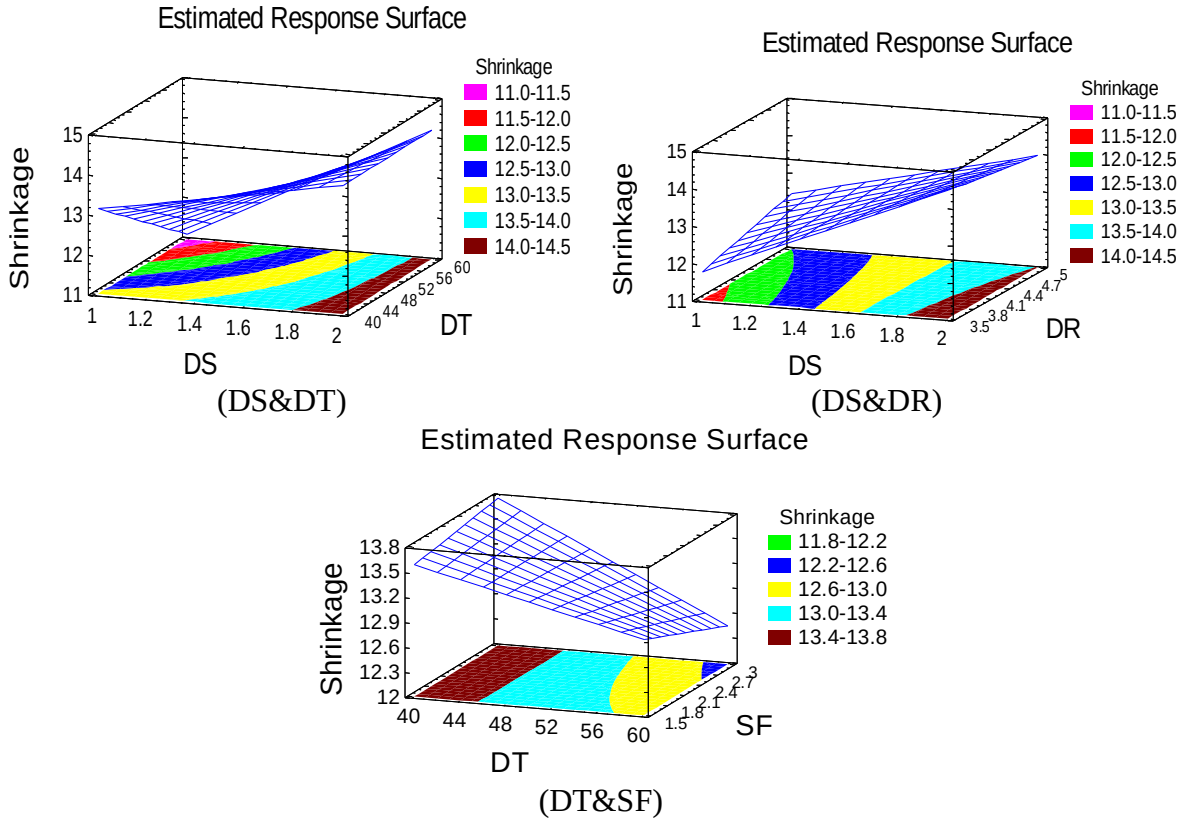

Figure 6.15 The estimated response surface for the interactions (DS&DT, DS&DR and DT&SF) for thermal shrinkage

By increasing the relaxing temperature, increasing the molecular mobility and the decreasing of internal stress could be achieved. Drawing tension is related to the stability of drawing

conditions. It was increased with reduction of drawing temperature or increasing of drawing ratio. In other words, increasing the number of drawing stages and plate temperature decreased the degree of crystallographic order of the samples even they have not significant effects. Alternatively, when a higher draw ratio is applied, the speed of the final roller will increase and the spin finish layer thickness on the fibres at constant spin finish pump speed will be decreased which could explain the interaction between the spin finish and the draw ratio increasing, in terms of cooling time effect. The possible mechanism of the effect of the spin-finish application on the crystallographic order is a heat transfer and cooling effect in the number of drawing stages caused by friction or slippage (stick-slip) in the drawing and relaxing stage.

6.4.2.2 The Regression Equation and Estimation Results

Based on the analysis of the fraction factorial experimental design (L32) results, simplified models based on statistical analysis for studied factors and their interactions were fitted by the regression equations for birefringence, FWHM, thermal shrinkage, tenacity, elongation at break and modulus which have been fitted to the experimental data. Enhanced regression equations forecast the fibre properties in order to achieve the most satisfactory properties in the final desired fibre for different applications. The regression equations in terms of the previous coded values (Table 6.1) are given as follows:

Birefringence = 0.0722292 - 0.00104167*DS - 0.00029375*DT + 0.00841667*DR - 0.000135417*PT + 0.00380556*SF - 0.228125*RS - 0.00013125*RT - 0.00015*DS*DT + 0.00233333*DS*DR + 0.0001125*DS*PT + 0.0025*DS*SF + 0.075*DS*RS - 0.0003375*DS*RT - 0.0000583333*DT*SF + 0.00000833333*DR*PT - 0.00211111*DR*SF + 0.000125*DR*RT + 0.0000333333*PT*SF + 0.0375*SF*RS - 0.0000166667*SF*RT (6.1)

FWHM = 0.892406 + 0.302*DS - 0.0246375*DT + 0.223625*DR + 0.00350938*PT + 0.620903*SF - 33.9859*RS + 0.0118844*RT - 0.0874167*DS*SF - 0.0008625*DT*DR + 0.000175937*DT*PT - 0.0035625*DT*SF + 0.382969*DT*RS - 0.0000246875*DT*RT - 0.0873889*DR*SF - 0.00284583*PT*SF + 0.101719*PT*RS - 0.000233438*PT*RT + 2.85208*SF*RS - 0.00137083*SF*RT - 0.0104688*RS*RT (6.2)

Thermal shrinkage = 11.1573 + 2.40625*DS - 0.152812*DT + 0.704167*DR + 0.0145833*PT + 1.65972*SF - 17.6563*RS + 0.0575*RT + 0.100625*DS*DT - 0.775*DS*DR - 0.006875*DS*PT - 0.141667*DS*SF + 0.3125*DS*RS - 0.028125*DS*RT - 0.02125*DT*SF + 0.00208333*DR*PT + 0.172222*DR*SF + 0.00125*DR*RT - 0.0145833*PT*SF - 0.625*SF*RS - 0.00875*SF*RT (6.3)

Tenacity = -0.4875 + 0.304167*DS + 0.008125*DT - 0.075*DR + 0.00125*PT + 0.208333*SF + 7.1875*RS + 0.00875*RT - 0.00375*DS*DT + 0.0666667*DS*DR - 0.00125*DS*PT + 0.05*DS*SF - 1.875*DS*RS - 0.0075*DS*RT - 0.00166667*DT*SF + 0.0025*DR*PT + 0.0333333*DR*SF + 0.0*DR*RT - 0.005*PT*SF - 1.66667*SF*RS + 0.000833333*SF*RT (6.4)

Elongation at break = 361.045 + 15.4508*DS + 1.413*DT - 78.3267*DR - 0.823583*PT + 7.97278*SF - 48.9375*RS + 2.551*RT - 0.14325*DS*DT + 2.02333*DS*DR + 0.67275*DS*PT - 9.31833*DS*SF + 84.625*DS*RS - 0.803*DS*RT - 0.234417*DT*SF - 0.00283333*DR*PT + 5.05444*DR*SF - 0.327*DR*RT - 0.118583*PT*SF - 24.5417*SF*RS + 0.124417*SF*RT (6.5)

Modulus = -1.61469 - 0.040625*DS - 0.00046875*DT + 0.39875*DR - 0.00497917*PT + 0.555139*SF + 3.23438*RS - 0.0125625*RT - 0.0000625*DS*DT + 0.0475*DS*DR - 0.0035625*DS*PT + 0.0758333*DS*SF - 1.96875*DS*RS - 0.0000625*DS*RT - 0.00254167*DT*SF + 0.00220833*DR*PT - 0.0527778*DR*SF + 0.006875*DR*RT + 0.001125*PT*SF - 0.3125*SF*RS - 0.006875*SF*RT (6.6)

The models evaluated the significance effect of each independent variable to a predicted response depending on the coefficient constant for the linear effects of independent factors and the coefficient constant for the interactions effects, depending on the coefficient constant for the offset term. Figure 6.16 shows the experimental results observed and calculated fitted results plot for birefringence (a), FWHM (b), thermal shrinkage (c), tenacity (d), elongation at break (e) and modulus (f). The experimental results observed were plotted on the Y axis and data for calculated fitted results generated using the last fitted model were plotted on the X axis for each trial. Their Model Standard Error (MSE) values listed in Table 6.5 indicate the dispersion of predicted and observed values around the theoretical fitted line generated using the fitted model for each trial. The pattern of estimated responses was based on the assumed model derived from the experimental observations. The predictive models gave useful results if the draw frame setting based variation, the tension or slippage on the drawing roles and some tension during the preparation of the sample for testing were controlled and taken into account.

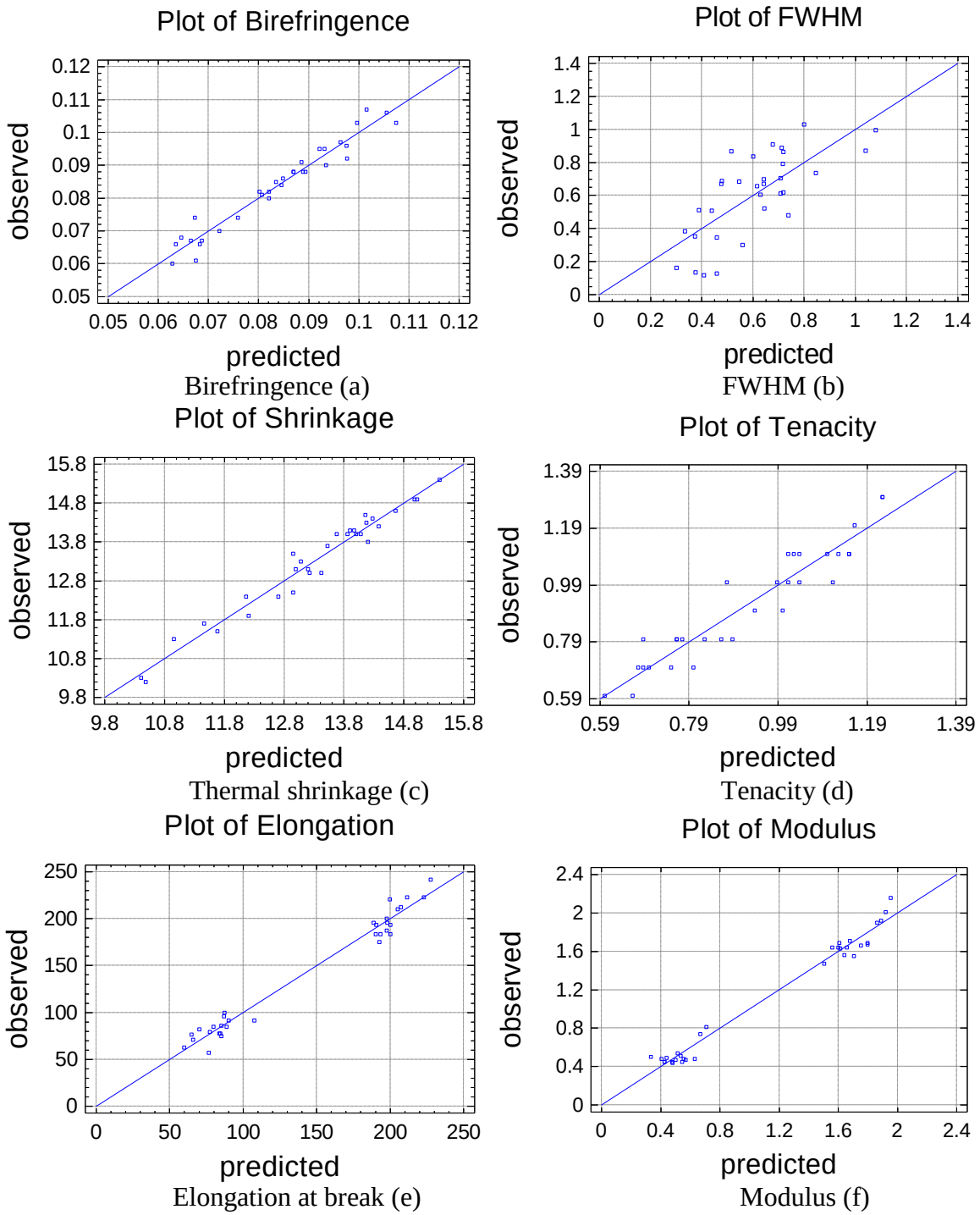

Birefringence (a) FWHM (b)

Thermal shrinkage (c) Tenacity (d)

Elongation at break (e) Modulus (f)

Figure 6.16 Experimental observed results and calculated fitted results plot for birefringence (a), FWHM (b), thermal shrinkage (c), tenacity (d), elongation at break (e) and modulus (f)

6.4.3 Conclusion and Statistical Model for Optimisation

As-spun, biodegradable, linear aliphatic-aromatic co-polyester fibres were drawn at different multi-stage hot drawing conditions. The statistical models covered the number of drawing stages, drawing temperature, total drawing ratio, plate temperature, spin finish application, relaxing stage ratio, relaxing temperature and their interactions. The models specified the combinations of their levels for enhancing properties.

Table 6.5 shows the combination of factor levels over the indicated region which maximize and minimize the responses which are overall orientation (birefringence), crystallographic order (full-width half-maximum of an x-ray scattering profile - FWHM), thermal shrinkage, tenacity, elongation at break and modulus. It also shows theeir Model Standard Error (MSE) values described previously. According to the analyses, the most effective and significant parameters influencing the fibre overall orientation were the drawing ratio and the drawing temperature. Other effects were overcome by the significance of the drawing ratio and drawing temperature. Birefringence or overall orientation was positively affected by drawing ratio and plate temperature and negatively by drawing temperature, the interaction between the number of drawing stages and relaxing temperature, relaxing temperature and the interaction between draw ratio and spin finish. As the relaxation stage ratio increases, the yarn speed decreases and more time is available for the relaxation process. The interactions (DS&DR and DT&RS), spin finish application, the interaction between drawing ratio and spin finish application, relaxing temperature and the interaction between spin finish application and relaxing stage ratio have an effect on FWHM.

There are three noted factors affecting the thermal shrinkage which are the number of drawing stages (affecting the tension), drawing temperature and relaxing stage ratio. Plate temperature and the interactions DS&DT, DR&RS and PT&RT have a notable effect on the thermal shrinkage. The number of drawing stages and relaxation stages and their interactions with temperature would affect the internal tension of the fibre chains which creates strain inside the fibre structure. The strain affects the freedom and the flexibility of the molecules, which in turn affects the shrinkage properties. Mechanical properties are significantly affected by draw ratio and draw temperature, the most effective and significant parameters. Other factors and interactions have their effects but they are limited and less significant as they are covered by the governing factors which are drawing ratio and temperature. Some interactions between factors could be related to the fractional design.

To explain the interaction effect between the analysed factors, some facts should be considered from the scientific point of view: when a higher draw ratio is applied, the speed of the final roller will increase which could explain the effect of the interaction between the spin finish and the draw ratio on cooling time; the internal stress of fibres are decreased in the relaxing stage to allow the new form to stabilize by re-crystallization. The possible mechanism of the effect of the spin-finish application on the crystallographic order is a heat transfer and cooling effect in the number of drawing stages, caused by friction or slippage (stick-slip) in the drawing and relaxing stage. This relationship could help to explain the interaction between process conditions and internal fibre structure.

Response	MSE	Optimum model	The combination of factor levels (↓: Low Level, ↑: High Level)						
			DS	DT	DR	PT	SF	RS	RT
Birefringence ×10^3	0.0024	Maximum	↑	↓	↑	↑	↓	↓	↓
		Minimum	↑	↑	↓	↓	↓	↓	↑
FWHM (^{o})	0.046	Maximum	↑	↓	↑	↑	↓	↓	↑
		Minimum	↓	↑	↑	↑	↑	↑	↑
Thermal Shrinkage (%)	0.254	Maximum	↑	↑	↓	↓	↓	↓	↓
		Minimum	↓	↑	↓	↑	↑	↑	↓
Tenacity (g/den)	0.0358	Maximum	↑	↓	↑	↓	↑	↓	↓
		Minimum	↑	↑	↓	↑	↓	↓	↑
Elongation at break (%)	11.16	Maximum	↓	↑	↓	↓	↑	↓	↑
		Minimum	↑	↓	↑	↓	↓	↓	↑
Modulus (g/den)	0.112	Maximum	↓	↓	↑	↑	↓	↑	↑
		Minimum	↓	↑	↓	↓	↑	↓	↑

Table 6.5 The combinations of factor levels for the effect of multi-stage hot drawing on the properties of linear aliphatic-aromatic co-polyester fibres for birefringence, FWHM, thermal shrinkage, tenacity, elongation at break and modulus
(MSE: Model Standard Error)

Increasing the draw ratio or decreasing drawing temperature plays an important role in stretching the chain inside the fibres, resulting in an improvement in the fibre's overall orientation. With one stage, the tension will be very high and the spin finish plays an important role in the filament slippage on the last roller after the applied spin finish, in addition to the spin finish in the as-spun samples. In the relaxation process, when relaxing stage ratio increases, the yarn speed decreases, the cooling time increases and the spin finish layer's thickness will be increased; the cooling action consequently affects the crystal

structure arrangement. This relationship could explain the interaction between process conditions and fibre structure. The regression equations achieved form a part in a forecasting program designed to optimize the drawing process of selected as-spun fibres. The designed models help processing scientists and technologists in industry to obtain the enhanced properties at suitable conditions related to final product cost and to obtain environmentally friendly, economical and energy saving fibres. LAAC fibres could be used in agricultural, horticultural and other non-traditional textile applications.

6.5 Statistical Modelling of The Effect of Multi-Stage Hot Drawing on Branched Aliphatic-Aromatic Co-Polyester Fibres (BAAC)

6.5.1 Experimental Results

The experiments shown in Table 6.2 were randomly conducted in one block involving control factors and their levels (Table 6.1). The data collected of the thermal shrinkage and mechanical properties for branched AAC fibres were measured and listed in Table 6.6. Figure 6.17 show DSC curves for two selected samples (Trials 18 and 24) produced with different hot drawing conditions; no appreciable changes of relative intensity of the peaks in the endotherm were observed in different samples for the same trial. The fibre did not melt completely below 140^{o}C, as an optimum temperature window for melting was found taking all factors into account. A broad range of melting temperature was observed for the as-spun fibres. The interaction between the thermal and mechanical properties of the BAAC fibres regularly decreases the drawability; as-spun fibres will be broken if they are heated under high drawing ratio. No significant effect was reported in their thermal properties but the mechanical properties will be better with the relaxation stage. Each thermal shrinkage test was carried out using a MK IV Shrinkage-Force Tester; samples were heated for 2 minutes at 60^{o}C under a load cell of 10 g. From the structural point of view and owing to the limitation of funding needed for the X-ray and the polarizing (Pluta) microscope tests in this project, 2 samples (18 and 24) were selected and characterized, comparing the similar factor levels. Typical x-ray diffractometer traces (Figure 6.18) showed five major crystalline diffraction peaks with different FWHM of an x-ray scattering profile observed around 16, 17.5, 20.5, 23 and 24.5 2θ° (the same peaks as previous chapter). The peaks observed at 16, 20.5 and 24.5 2θ° are very wide and weak; the peaks at 17.5 and 23 2θ° are slightly sharper, more intense

and smaller in width. The peak at 23 2θ° was fitted using DIFFRAC plus EVA software to compare the half-height widths. From the results, it was found that with (FWHM $_{LAAC18}$ (1.029 ^{o}) > FWHM $_{LAAC24}$ (0.354^{o}), FWHM $_{BAAC18}$ (0.321 ^{o}) > FWHM $_{BAAC24}$ (0.312 ^{o})), the lower value of FWHM leads to the higher size of the crystallite and the higher degree of crystallographic order and vice versa, as mentioned previously. An increase in structural order was obtained from an increase in the peak intensity, a decrease in the x-ray peak width and a decrease in the background area. Figure 6.19 shows the recorded microinterferograms of the selected samples. The measured values of birefringence were averaged from the repeated measurements: Birefringence $_{BAAC24}$ (0.075) > Birefringence $_{BAAC18}$ (0.061) and Birefringence $_{LAAC24}$ (0.088) > Birefringence $_{LAAC18}$ (0.080). Generally, the results of the BAAC fibres show the same general behaviour noted for those of the LAAC fibres.

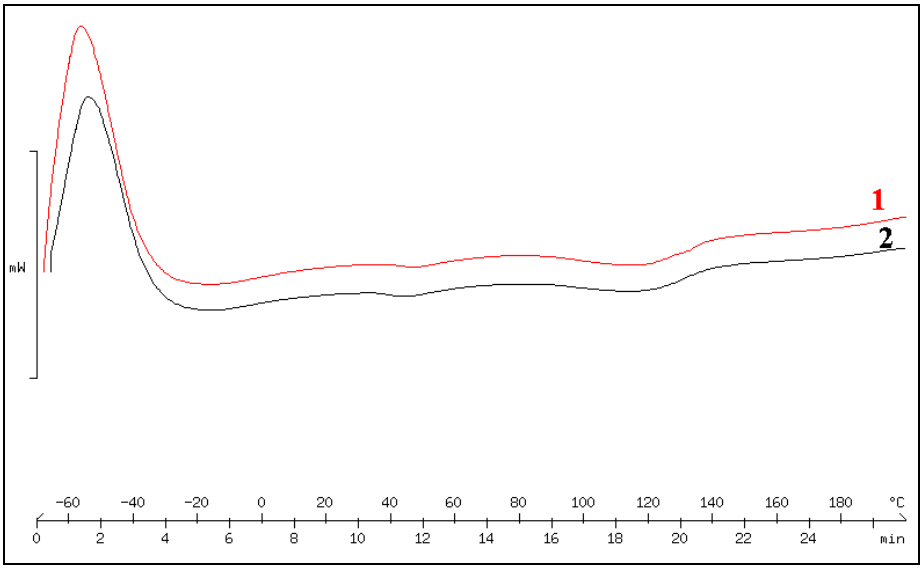

Figure 6.17 DSC curves of hot drawn BAAC fibres
(1: trial 24 and 2: trial 18)

The average data of the measured specimens were calculated: acceptable standard deviations could be related to the draw frame setting based variation which could not be totally controlled, the tension or slippage on the drawing roles, as noted in the drawing study or they could be related to some tension error during the preparation of the sample for testing. The surface and cross section of the fibres were investigated by an SEM photomicrograph (Figure 6.20). After drawing, the outer surface and the cross section photographs show uniformity without any deformation. For future work, fineness of the fibres could be related to the drawing process parameters to find the relationship between them.

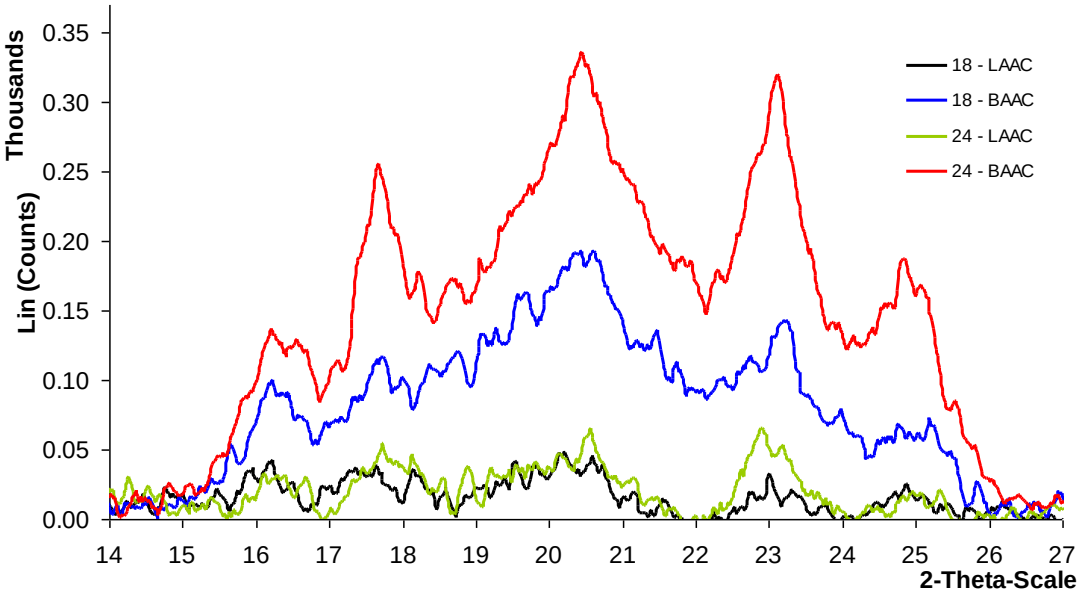

Figure 6.18 WAXS traces of the selected fibres (Trials 18 and 24)

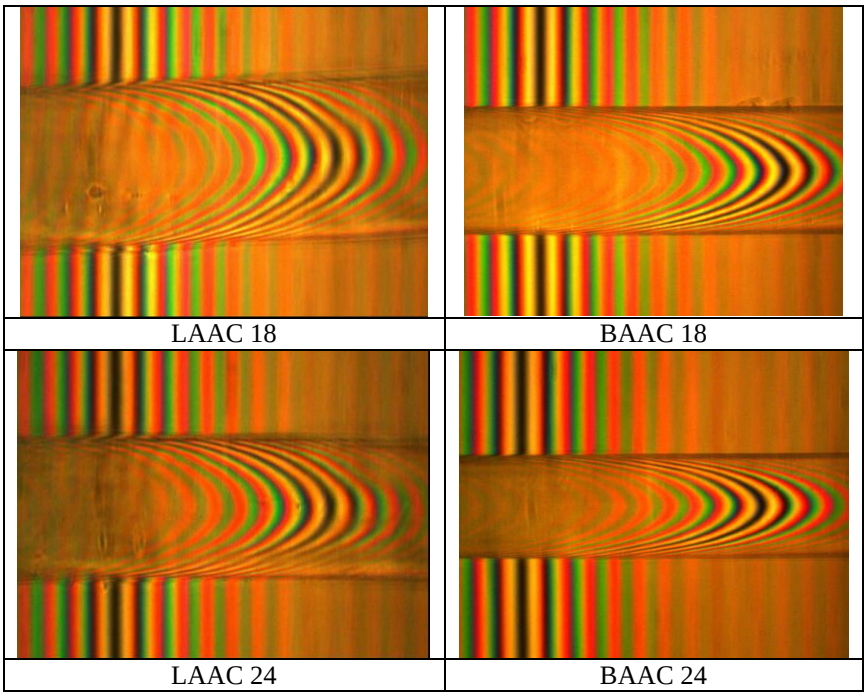

Figure 6.19 The microinterferograms of the selected fibres using a Pluta microscope

Trial Number	Thermal Shrinkage (%)	Tenacity (g/den)	Elongation at break (%)	Modulus (g/den)
1	8.5	1.0	81.25	2.00
2	9.3	1.0	83.33	2.10
3	9.5	1.0	84.72	1.89
4	8.5	1.1	87.50	2.28
5	10.0	1.2	69.44	2.69
6	10.4	1.0	63.89	2.24
7	5.8	0.9	118.75	1.19
8	6.5	0.9	120.83	1.16
9	10.3	1.1	91.67	2.23
10	6.1	1.0	129.17	1.32
11	6.2	0.9	129.17	1.01
12	9.0	1.1	75.00	1.98
13	10.2	1.0	41.67	2.23
14	6.5	0.9	114.58	1.09
15	3.7	0.8	129.17	0.90
16	5.8	0.9	116.67	1.20
17	6.2	1.0	125.00	1.10
18	3.7	0.9	131.25	0.78
19	10.3	1.2	61.11	2.66
20	4.5	0.9	114.58	1.12
21	5.0	0.9	122.92	0.97
22	10.3	1.1	95.83	2.04
23	10.0	1.2	77.08	2.36
24	9.9	1.1	68.75	2.36
25	8.5	1.1	85.42	1.99
26	6.4	1.0	106.25	1.37
27	6.0	1.0	120.83	1.31
28	9.0	1.1	84.72	2.48
29	9.3	1.1	108.33	1.75
30	8.4	1.0	87.50	1.71
31	9.5	1.0	85.42	1.82
32	5.5	0.9	116.67	1.17

Table 6.6. Results for the hot drawing experiments for BAAC fibres

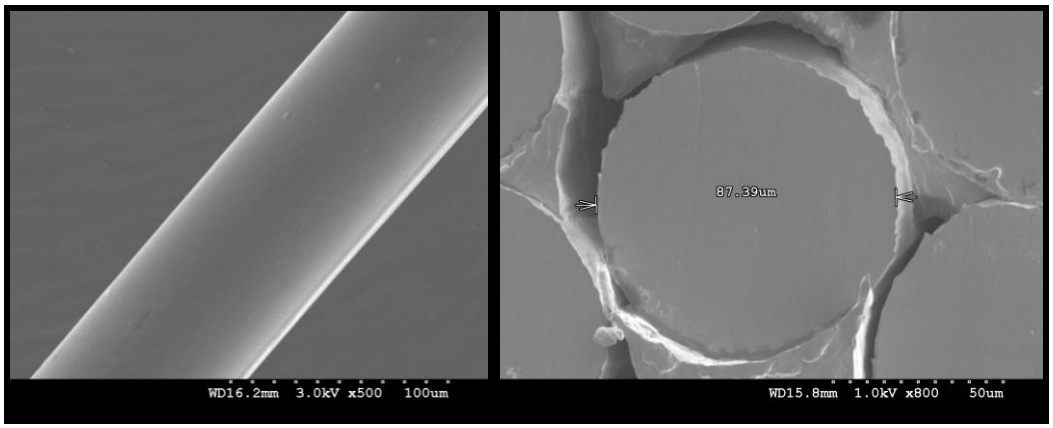

Figure 6.20 SEM photomicrograph of BAAC fibres' surface and cross section.

6.5.2 Statistical Analysis and Discussion

Figure 6.21 shows the Pareto charts for thermal shrinkage (a), tenacity (b), elongation at break (c) and modulus (d) in terms of the significant arrangement of factors and their interactions in decreasing order. The Pareto chart for thermal shrinkage shows that the drawing ratio (DR), the total number of drawing stages (DS), drawing temperature (DT), the interactions (DS&RS and DT&DR), relaxing stage ratio (RS), plate temperature (PT), the interactions (DS&RT and DT&PT) and relaxing temperature (RT) are the most important factors affecting the thermal shrinkage properties of the fibres, followed by other factors and interactions. The determined factors would affect the tension and the internal stress, and then affect the thermal shrinkage properties.

In terms of mechanical properties of drawn BAAC fibres, the Pareto chart for tenacity shows that total draw ratio, drawing temperature, total number of drawing stages and the interactions DS&RT, DT&PT, DS&DT, DR&RS and PT&RT are the most important factors affecting the tenacity, followed by other factors and interactions. The Pareto chart for elongation at break shows that total draw ratio, number of drawing stages, drawing temperature, relaxing stage ratio, DR&SF and DT&SF are the most important factors affecting the elongation at break, followed by other factors and interactions. The Pareto chart for modulus shows that total draw ratio, total number of drawing stages, drawing temperature, relaxing stage ratio, the plate temperature, DS&PT, DT&RT, DR&RT and PT&RS are the most important factors affecting the modulus, followed by other factors and interactions.

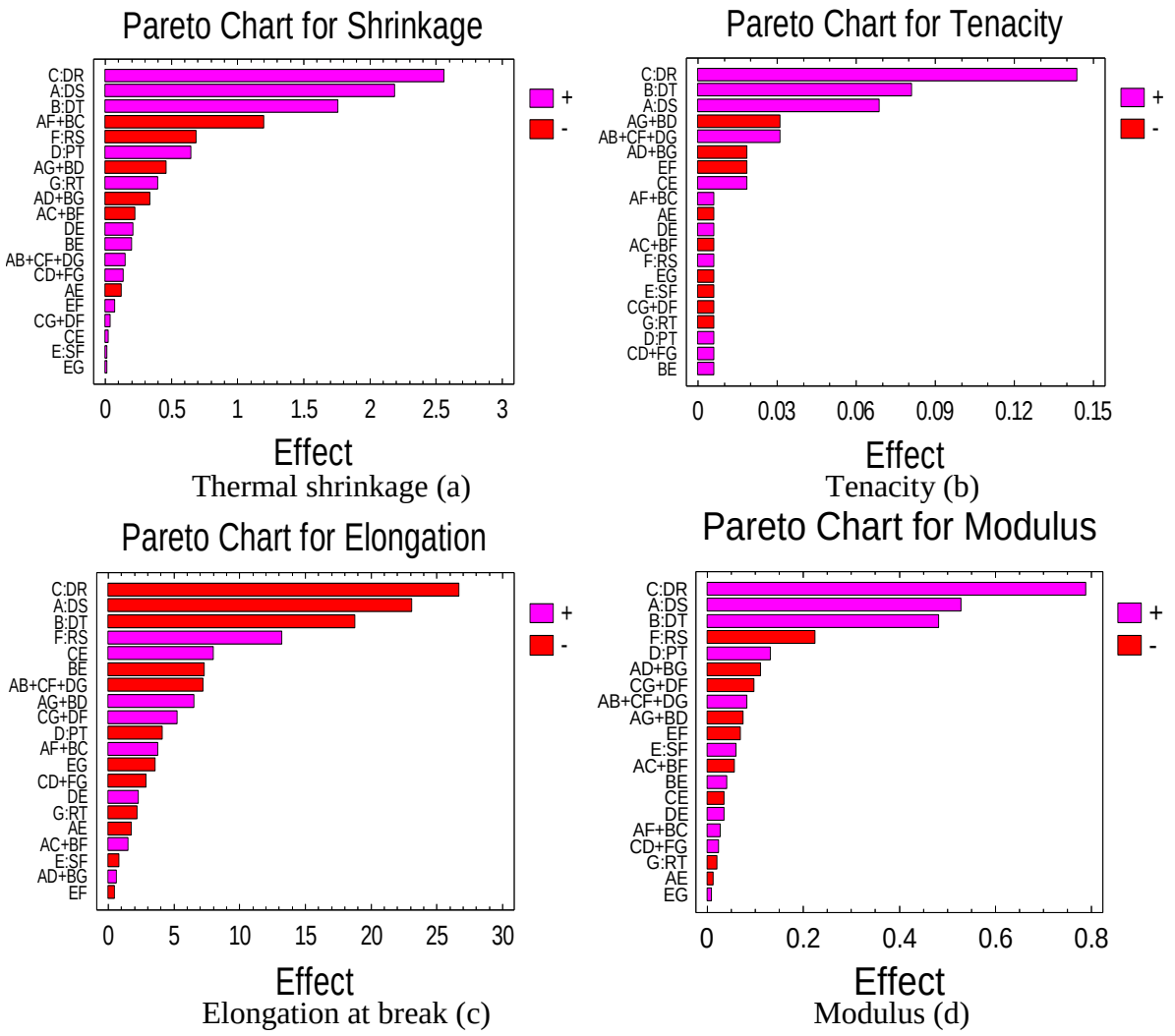

Figure 6.21 The ranked list of significant arrangement effects and interactions for thermal shrinkage (a), tenacity (b), elongation at break (c) and modulus (d) (Pareto chart)

All the interactions could be simulated, as the plot shows the existence or otherwise of interactions between each of the two factors, as coded in Table 6.1. Figure 6.22 shows the main effects and interaction plots of the statistical analysis of the effects caused by the main factors and their interactions on thermal shrinkage. The factor effect on the responses of the low and high level of the factors was obtained using the design matrix. The main effects of all factors except spin finish applicator (SF) were pronounced on shrinkage, as their lines are long and their slopes are sharp. The interactions DT&DR, DS&RS, DS&RT, DS&PT, DT&RT and DT&PT have their effects on thermal shrinkage which will be further investigated using ANOVA analysis. It is advised that the major factors influencing thermal shrinkage value be assessed further to understand their influence more fully.

Main effects and interaction plots for tenacity show that the total number of drawing stages, DT and total draw ratio were the factors affecting the tenacity (Figure 6.23). DS&DT, DR&RS, PT&RT, DS&RT and DT&PT had their effects which need to be further investigated using other methods to identify their significance. Effects and interaction plots for elongation at break show that number of total drawing stages, total draw ratio, drawing temperature, relaxing stage ratio, DS&DT, DR&RS, PT&RT, DT& SF and DR&SF were the factors affecting the elongation at break (Figure 6.24). The main effects of all factors except spin finish applicator (SF) and relaxing temperature (RT) were pronounced on modulus, as their lines were long and their slopes were sharp. The interactions DS&DT, DS&PT, DR&RS, DT&RT, PT&RT, PT&RS and DR&RT affected the modulus, as shown in Figure 6.25, there were investigated statistically using ANOVA to adjust their effects.

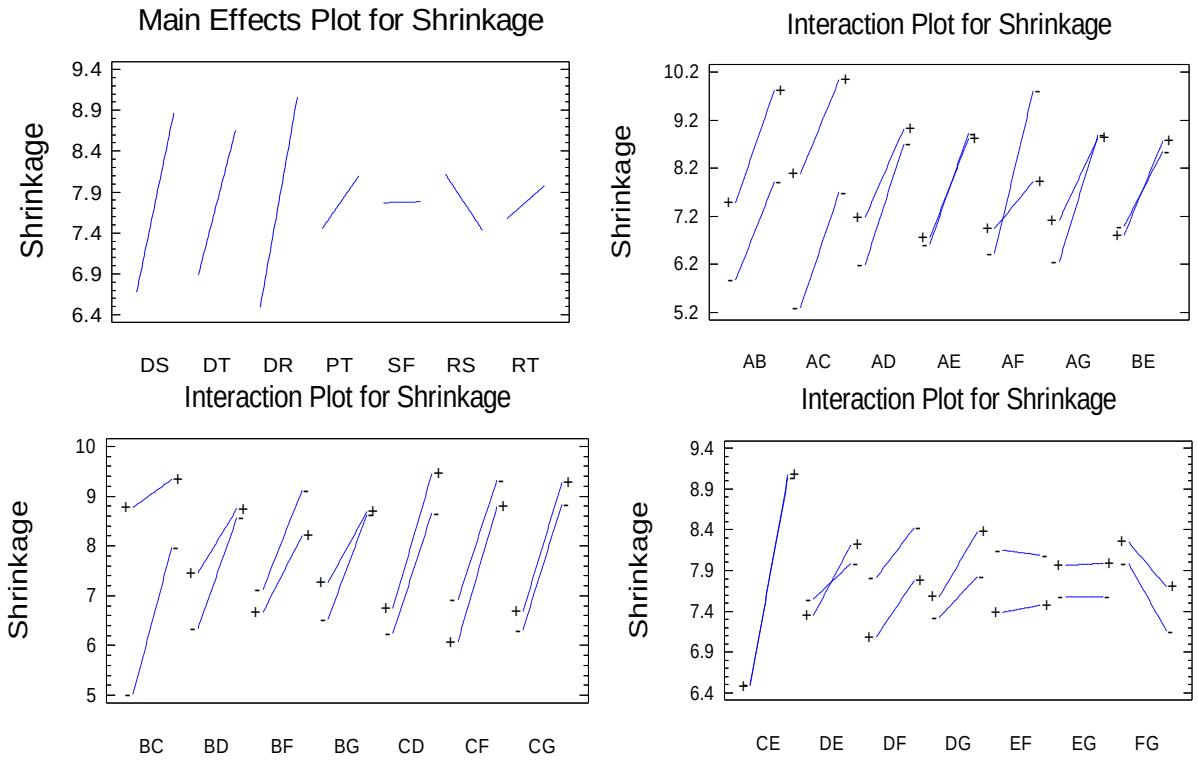

Figure 6.22. Main effect plots and Interaction plots for the thermal shrinkage

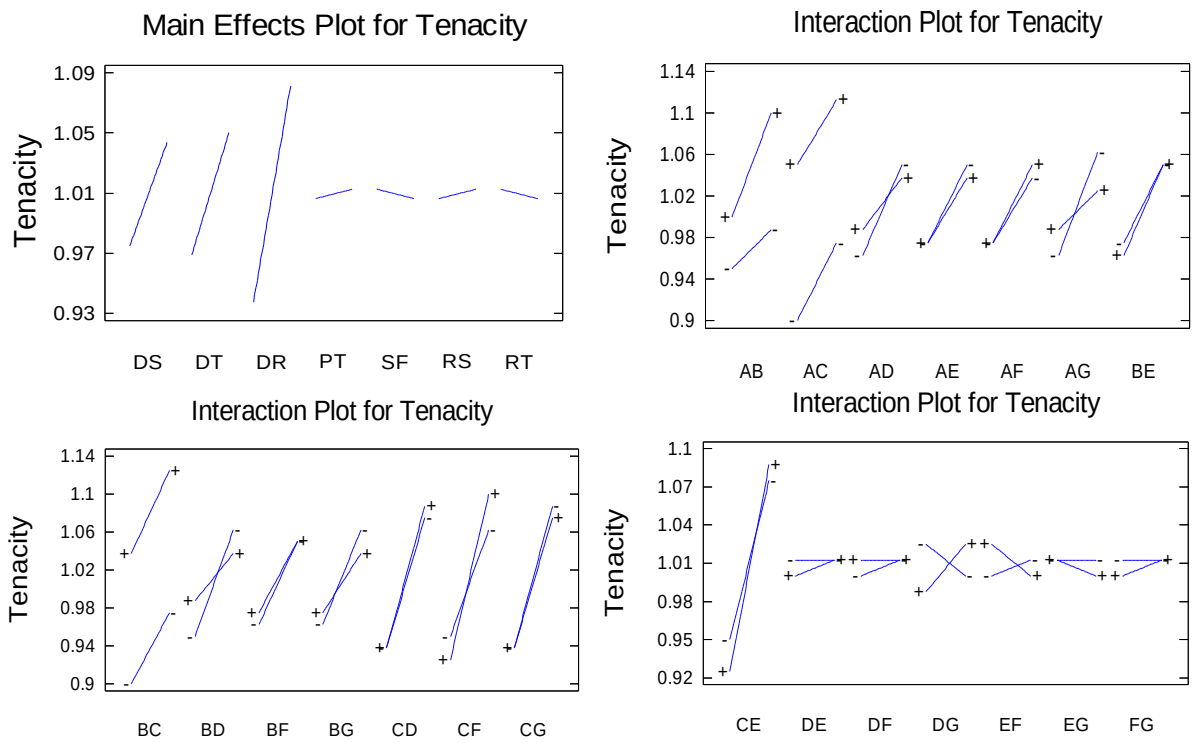

Figure 6.23. Main effect plots and Interaction plots for the tenacity

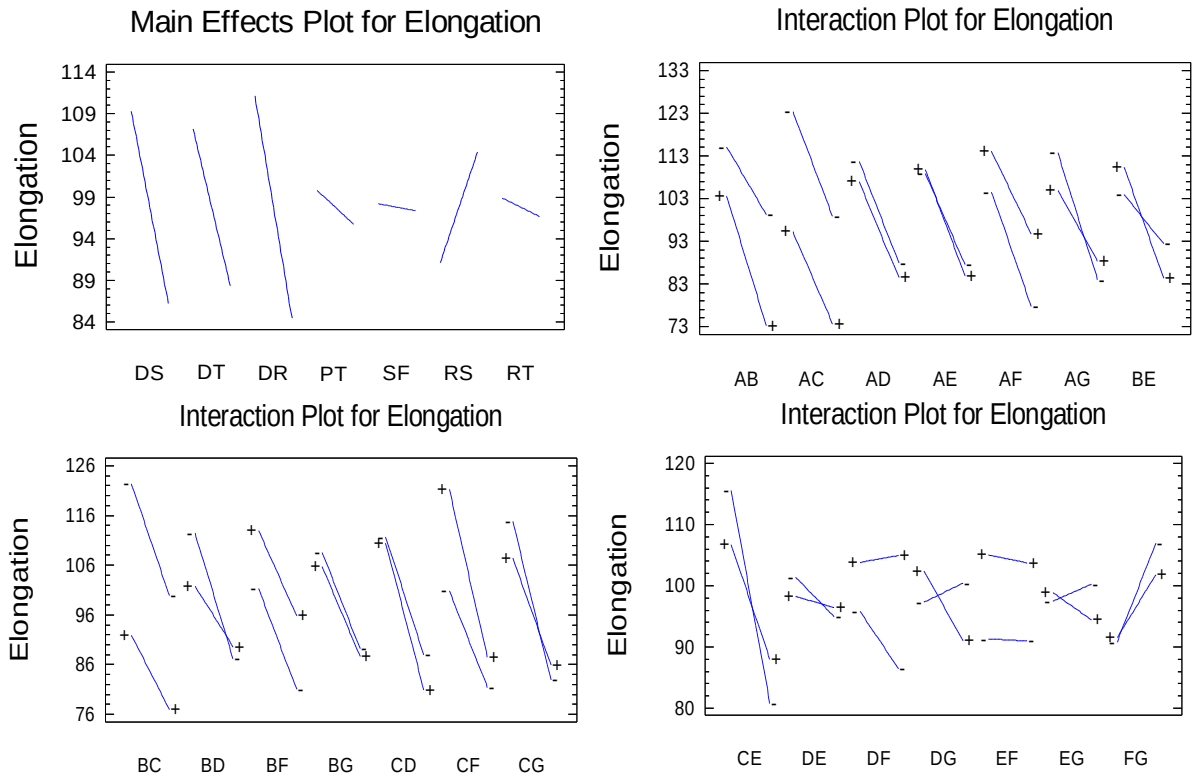

Figure 6.24. Main effect plots and Interaction plots for the elongation at break

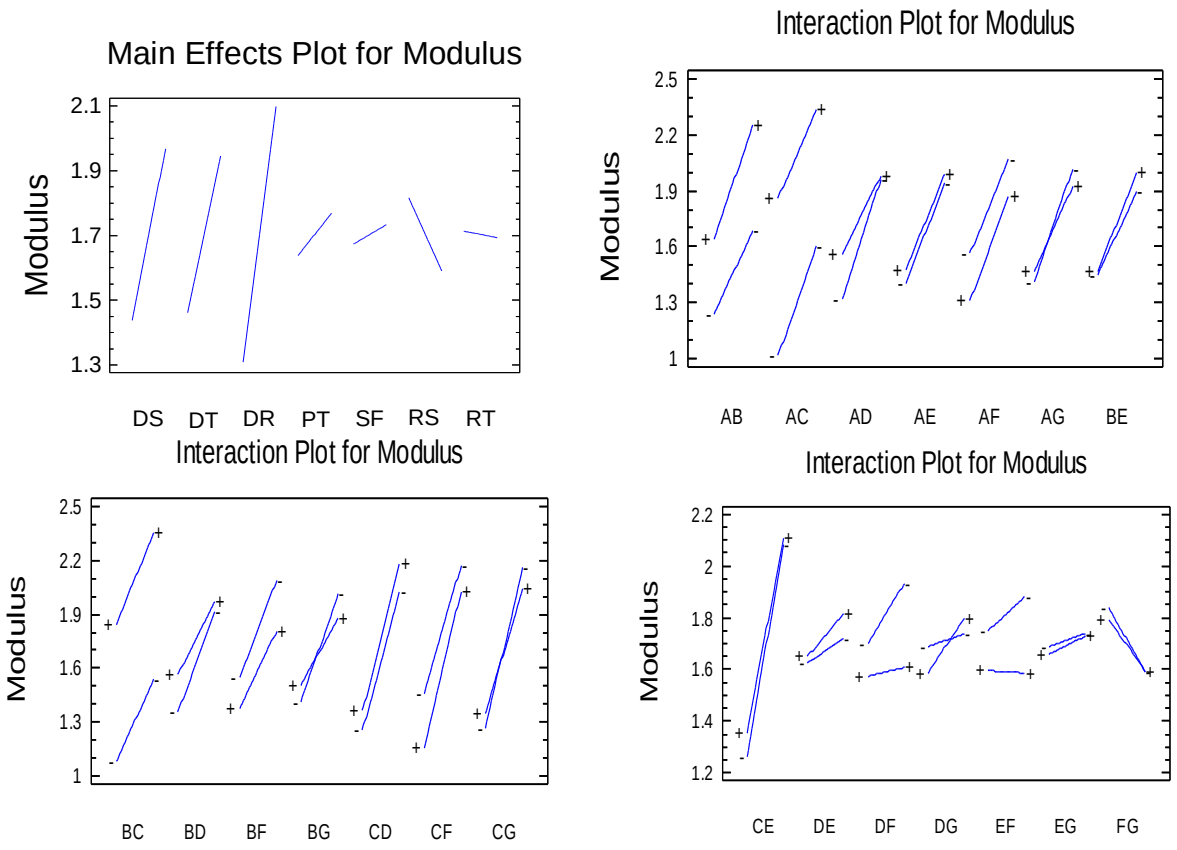

Figure 6.25. Main effect plots and Interaction plots for the modulus

By plotting statistical standardized via percentage order in Figure 6.26, the normal probability plot of the responses estimated illustrates further details about the normal distribution for the data. Draw ratio, draw temperature, plate temperature and draw stage had a positive effect on thermal shrinkage, tenacity and modulus, and a negative effect on elongation at break. Relaxing stage ratio had a positive effect on elongation at break and a negative effect on thermal shrinkage and modulus; relaxing stage ratio had a small effect on tenacity. The interactions DT&DR and DS&RS had a clear effect on thermal shrinkage. The interactions (DS&DT, DR&RS and PT&RT) were prominent and had a positive effect on tenacity. With the one-stage drawing process, the tension is high and the spin finish plays an important role in the filament slippage on the last roller after applying spin finish, in addition to the spin finish added to the as-spun fibres in the extrusion process.

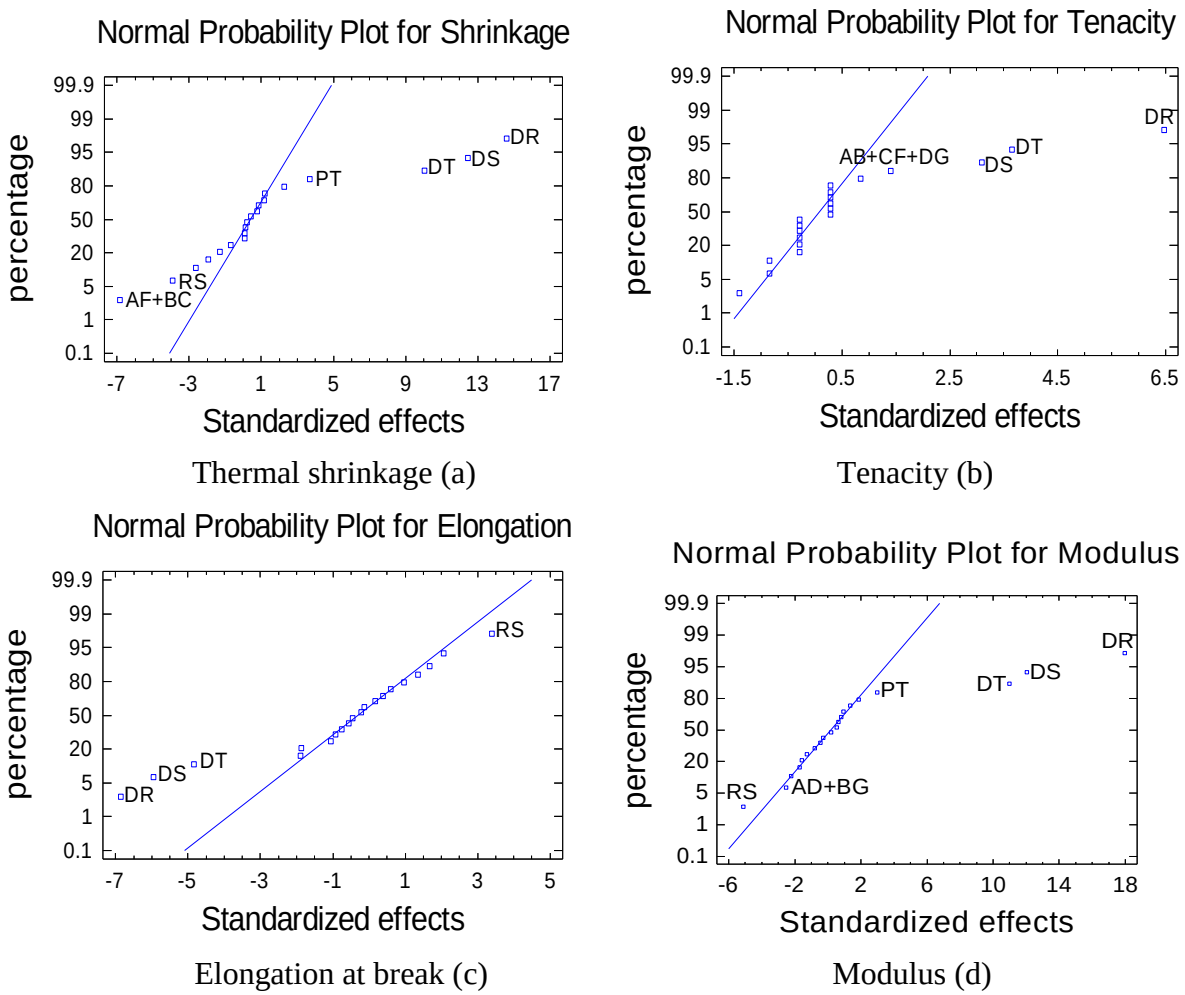

Figure 6.26 Normal Probability Plot for thermal shrinkage (a), tenacity (b), elongation at break (c) and modulus (d).

6.5.2.1 Analysis of Variance (ANOVA)

In order to investigate the factors and their interaction effects, analysis of variance (ANOVA) was used to analyze the data obtained. The ANOVA results are listed in Table 6.7. The significance of the studied factors affecting the thermal shrinkage are the drawing ratio (DR), the total number of drawing stages (DS), drawing temperature (DT), the interactions (DS&RS and DT&DR), relaxing stage ratio (RS), plate temperature (PT), the interactions (DS&RT and DT&PT) and relaxing temperature (RT). ANOVA analysis for mechanical properties shows that the drawing ratio (DR), the total number of drawing stages (DS) and the drawing temperature (DT) had a significant effect on tenacity, elongation at break and modulus. The relaxing stage ratio had a significant effect on elongation at break and modulus

which could relate to its effect on the internal structure of the fibres. The interactions DS&PT, DT&RT, PT&RS and DR&RT had a significant effect on the modulus.

Source	P-Value			
	Thermal Shrinkage	Tenacity	Elongation at break	Modulus
DS	0.0000	0.0102	0.0001	0.0000
DT	0.0000	0.0038	0.0005	0.0000
DR	0.0000	0.0000	0.0000	0.0000
PT	0.0035	0.7837	0.3118	0.0123
SF	0.9445	0.7837	0.8358	0.1991
RS	0.0024	0.7837	0.0059	0.0003
RT	0.0435	0.7837	0.5805	0.6577
DS&DT DR&RS PT&RT	0.4106	0.1872	0.0892	0.0871
DS&DR DT&RS	0.2259	0.7837	0.7037	0.2266
DS&PT DT&RT	0.0805	0.4167	0.8699	0.0278
DS&SF	0.4908	0.7837	0.6564	0.7812
DS&RS DT&DR	0.0000	0.7837	0.3524	0.5440
DS&RT DT&PT	0.0231	0.1872	0.1201	0.1157
DT&SF	0.2783	0.7837	0.0860	0.3678
DR&PT RS&RT	0.4495	0.7837	0.4705	0.5994
DR&SF	0.8892	0.4167	0.0633	0.4423
DR&RT PT&RS	0.8346	0.7837	0.2040	0.0484
PT&SF	0.2510	0.7837	0.5663	0.4423
SF&RS	0.6771	0.4167	0.9044	0.1458
SF&RT	0.9445	0.7837	0.3742	0.8457

Table 6.7 ANOVA Results identifying the statistical significance of factor effects on the results from analysis of variance (ANOVA) of the data identifying the statistical significance of each factor for thermal shrinkage, tenacity, elongation at break and modulus

Some interactions between factors could be related to the fractional design. An error could result from either assignable causes which represent variation caused by changes in the independent factors, or random causes that signify uncontrolled variation. The estimated response surfaces of thermal shrinkage were used to determine the direction and the significance of the interactions, as shown in Figure 6.27. In order to determine the direction

of the interactions DS&RS, DT&DR, DS&RT and DT&PT, the geometric result of plotting a response variable was required. There was a twist which confirms the interactions DS&RS and DS&RT. As the surface was flat with no twist found in the surface represented the interactions DT&DR and DT&PT, their determined effects are not significant. This corresponds with the previous statistical results of the interaction plot derived from the experimental data. Using the same technique, there were significant effects of the interactions DS&PT and DR&RT on the modulus (Figure 6.28). There was no twist in the estimated response surfaces for the insignificant interactions DT&RT and PT&RS.

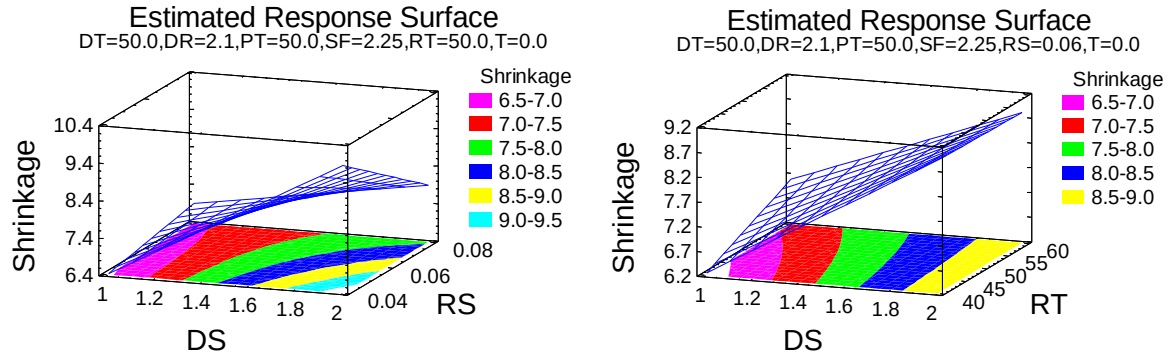

Figure 6.27. The Estimated response surface for the interactions DS&RS and DS&RT for the shrinkage.

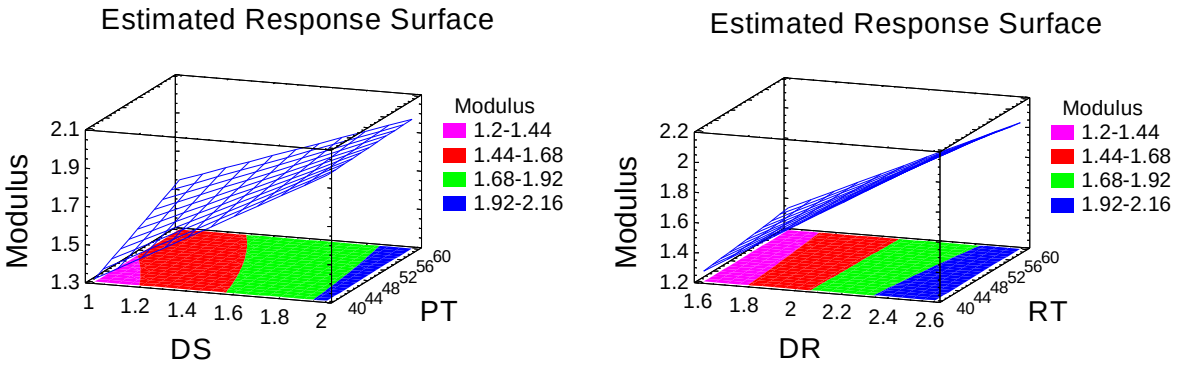

Figure 6.28. The Estimated response surface for the interactions DS&PT and DR&RT for the modulus

6.5.2.2 The Regression Equation and Estimation Results

Based on the analysis of the fraction factorial experimental design results, simplified models based on statistical analysis for studied factors and their interactions were fitted by the

regression equations for thermal shrinkage, tenacity, elongation at break and modulus which were fitted to the experimental data. The regression equations in terms of the previous coded values (Table 6.1) are given as follows:

Thermal shrinkage = -13.6413 + 10.3575*DS + 0.035625*DT + 2.2875*DR + 0.022375*PT - 1.37833*SF + 67.1875*RS + 0.079625*RT + 0.015*DS*DT - 0.45*DS*DR - 0.03375*DS*PT - 0.166667*DS*SF - 60.0*DS*RS - 0.04625*DS*RT + 0.0133333*DT*SF + 0.01375*DR*PT + 0.0333333*DR*SF + 0.00375*DR*RT + 0.0141667*PT*SF + 2.5*SF*RS + 0.000833333*SF*RT (6.7)

Tenacity = 0.301875 + 0.18875*DS - 0.0015625*DT + 0.10625*DR + 0.000875*PT - 0.0275*SF + 1.09375*RS + 0.006625*RT + 0.003125*DS*DT - 0.0125*DS*DR - 0.001875*DS*PT - 0.00833333*DS*SF + 0.3125*DS*RS - 0.003125*DS*RT + 0.000416667*DT*SF + 0.000625*DR*PT + 0.025*DR*SF - 0.000625*DR*RT + 0.000416667*PT*SF - 0.625*SF*RS - 0.000416667*SF*RT (6.8)

Elongation at break = 259.248 - 35.2836*DS + 1.24784*DT - 67.0656*DR - 0.0384*PT + 10.2659*SF + 83.5156*RS - 1.6563*RT - 0.724938*DS*DT + 3.03625*DS*DR + 0.0651875*DS*PT - 2.37083*DS*SF + 188.844*DS*RS + 0.655312*DS*RT - 0.488958*DT*SF - 0.290688*DR*PT + 10.7075*DR*SF + 0.525188*DR*RT + 0.153292*PT*SF - 15.9375*SF*RS - 0.240125*SF*RT (6.9)

Modulus = -3.715 + 1.23875*DS + 0.0055625*DT + 1.43125*DR + 0.0130125*PT + 0.0171667*SF - 2.53125*RS + 0.0294125*RT + 0.00825*DS*DT - 0.1125*DS*DR - 0.011125*DS*PT - 0.0166667*DS*SF + 1.375*DS*RS - 0.0075*DS*RT + 0.00275*DT*SF + 0.002375*DR*PT - 0.0466667*DR*SF - 0.00975*DR*RT + 0.00233333*PT*SF - 2.29167*SF*RS + 0.000583333*SF*RT (6.10)

The models evaluated the significance effect of each independent variable to a predicted response. The regression equations depended on the coefficient constant for the linear effects of independent factors, the coefficient constant for the interactions effects and the coefficient constant for the offset term. The pattern of estimated responses was based on the assumed model derived from the experimental observations. Figure 6.29 shows the experimental observed results and calculated fitted results plot for thermal shrinkage (a), tenacity (b), elongation at break (c) and modulus (d). Their Model Standard Error (MSE) values listed in Table 6.8 indicate the dispersion of predicted and observed values around the theoretical fitted line generated using the fitted model for each trial. The predictive models gave useful results, with small variation for the previously mentioned reasons such as draw frame setting-based variation, the tension or slippage on the drawing roles or some tension while the preparation of the sample for testing.

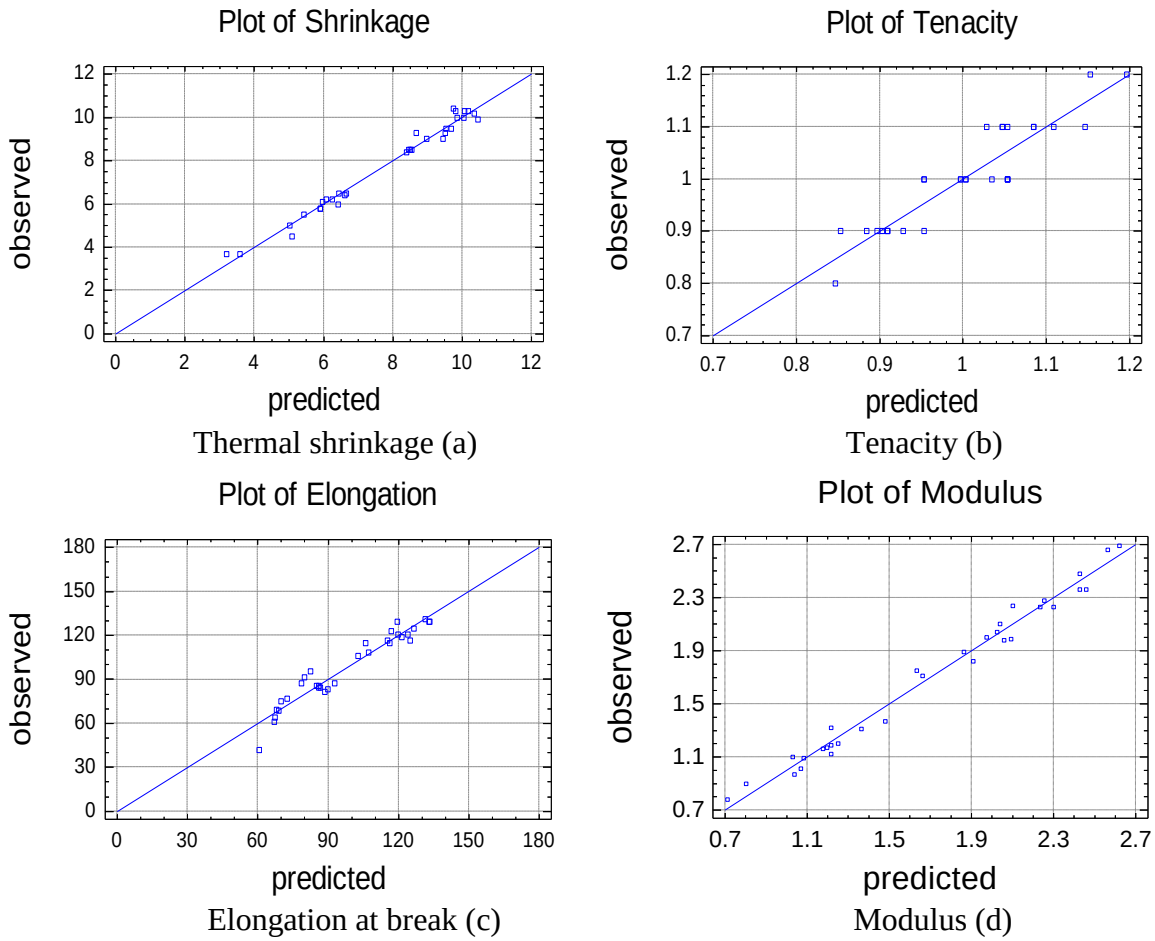

Thermal shrinkage (a) Tenacity (b)

Elongation at break (c) Modulus (d)

Figure 6.29 Experimental observed results and calculated fitted results plot for thermal shrinkage (a), tenacity (b), elongation at break (c) and modulus (d)

6.5.3 Conclusion and Statistical Model for Optimisation

As-spun, biodegradable, branched aliphatic-aromatic co-polyester fibres were drawn at different multi-stage hot drawing conditions. The variation in drawing conditions leads to the enhancement of fibre properties and the investigation sought to explain the main effects and interactions observed. The statistical models covered the number of drawing stages, drawing temperature, total drawing ratio, plate temperature, spin finish application, relaxing stage ratio, relaxing temperature and their interactions. The models specified the combinations of their levels for enhancing properties. The number of drawing stages and relaxation stages and their interactions with temperature would affect the internal tension of the fibre chains which creates strain inside the fibre structure. Some interactions between factors could be related to the fractional design as mentioned in Chapter 2. The strain affects the freedom and the flexibility of the molecules which in turn affects the shrinkage properties. Draw ratio, draw

temperature, plate temperature and draw stage had a positive effect on thermal shrinkage, tenacity and modulus and a negative effect on elongation at break. Relaxing stage ratio had a positive effect on elongation at break and a negative effect on thermal shrinkage and modulus; the relaxing stage ratio had a small effect on tenacity. The interactions DT&DR and DS&RS had a clear effect on thermal shrinkage. The interactions (DS&DT, DR&RS and PT&RT) were prominent and had a positive effect on tenacity. The tension is high in the one stage drawing process and the spin finish plays an important role in the filament slippage on the last roller after applying spin finish, in addition to the spin finish added to the as-spun fibres in the extrusion process. In the relaxation process with relaxing stage ratio increasing, the yarn speed decreased and the cooling time increased and the spin finish layer's thickness is increased. This relationship could explain the interaction between process conditions and fibre structure. Alternatively, when a higher draw ratio is applied, the speed of the final roller increases and the spin finish layer thickness on the fibres at constant spin finish pump speed is affected: which could explain the interaction between the spin finish and the draw ratio, in terms of cooling time effect.

Response	**MSE**	**Optimum model**	**The combination of factor levels (↓: Low Level, ↑: High Level)**						
			DS	**DT**	**DR**	**PT**	**SF**	**RS**	**RT**
Shrinkage (%)	0.379	Maximum	↑	↑	↑	↑	↑	↓	↑
		Minimum	↓	↓	↓	↓	↑	↓	↓
Tenacity (g/den)	0.0182	Maximum	↑	↑	↑	↓	↓	↑	↓
		Minimum	↓	↓	↓	↓	↑	↑	↓
Elongation at break (%)	4.26	Maximum	↓	↓	↓	↓	↑	↑	↓
		Minimum	↑	↑	↑	↑	↓	↓	↓
Modulus (g/den)	0.101	Maximum	↑	↑	↑	↑	↓	↓	↓
		Minimum	↓	↓	↓	↓	↓	↑	↓

Table 6.8 The combinations of factor levels for the effect of multi-stage hot drawing on the properties of BAAC fibres for thermal shrinkage, tenacity, elongation at break and modulus (MSE: Model Standard Error)

Table 6.8 shows the combination of factor levels which maximize and minimize the responses over the indicated region. Other factors and interactions have their effects but they are limited and less significant as they are covered by the governing factors, drawing ratio and temperature. It also shows the Model Standard Error (MSE) values described previously. The achieved models could form a part in a forecasting program designed to optimize the

drawing process of selected as-spun fibres. The models help processing scientists and technologists in industry to obtain the enhanced properties at suitable conditions related to final product cost and to obtain environmentally friendly, economical and energy-saving fibres. BAAC fibres could be used in agricultural, horticultural and other non-traditional textile applications.

6.6 Experimental Design for Multi-Stage Hot Drawing and Twisting of Aliphatic-Aromatic Co-Polyester Fibres

The designed experiment here was used to investigate the influence of twist and hot-drawing processing conditions on the structural and physical properties of LAAC and BAAC fibres. For technical and experimental reasons, the multi-stage hot drawing and twisting processes of as-spun AAC fibres were operated individually. Twist kept the filaments together in continuous filament yarns; filaments were given axial strength and lateral pressure with increasing the twisting. Twisting (two for one twist, ***S*** direction twist) was carried out at room temperature to twist the continuous drawn filaments at a different twist level, with a constant spindle speed of 316 rpm. A new fraction factorial experimental design was applied to discover how the analyses of the previous drawing experiments could be changed as a result of adding twist to the continuous fibres. The investigation of the interaction between the drawing and the twist processes gave more details about the effect of applying twist to the drawn fibres; and how it interacts with the drawing process factors. The eight control parameters for the hot drawing and twisting experiments were the total number of drawing stages (DS), drawing temperature (DT), total drawing ratio (DR), plate temperature (PT), spin finish (SF), relaxing stage ratio between relaxation process rollers (RS) (where speed of the second roller = RS * speed of the first roller), relaxing temperature (RT) and twist level (T). These are listed with their abbreviations in Table 6.9. The two levels of each parameter were separated as far apart as possible from one another.

A fractional factorial design (L32; $\mathbf{2^{8-3}} = \mathbf{2^5} = 32$) was used for the thirty-two screening trials in this experiment, involving eight control parameters and two levels for each parameter, as shown in Table 6.10. The applied matrix was designed using the STATGRAPHICS program and was randomly conducted in one block.

Factor abbreviation	Factor	Level	
		Low	High
A : DS	Total drawing stages number	1	2
B : DT	Drawing temperature (^{O}C)	40	60
C : DR	Total drawing ratio for LAAC	3.5	5.0
	Total drawing ratio for BAAC	1.6	2.6
D : PT	Plate temperature (^{O}C)	40	60
E : SF	Spin finish (rpm)	1.5	3.0
F : RS	Relaxing stage ratio (%)	0.04	0.08
G : RT	Relaxing temperature (^{O}C)	40	60
H:T	Twist level (Turns/inch)	4	8

Table 6.9 Factors and their levels for the hot drawing and twisting experiments

Trial Number	DS	DT	DR	PT	SF	RS	RT	T
1	L	H	H	L	L	L	H	H
2	H	L	H	L	H	L	H	H
3	H	H	L	H	L	L	H	H
4	L	H	H	H	L	L	L	L
5	H	H	H	L	L	H	L	H
6	H	H	L	H	H	L	H	L
7	H	L	L	H	H	H	L	H
8	L	H	L	H	H	H	L	L
9	H	L	H	H	H	L	L	L
10	H	L	L	H	L	H	L	L
11	L	H	L	H	L	H	L	H
12	H	H	L	L	H	L	L	H
13	H	L	H	H	L	L	L	H
14	L	H	L	L	H	H	H	H
15	L	L	L	L	H	L	L	L
16	H	L	L	L	L	H	H	H
17	L	H	L	L	L	H	H	L
18	L	L	L	L	L	L	L	H
19	H	H	H	L	H	H	L	L
20	L	L	L	H	H	L	H	H
21	L	L	L	H	L	L	H	L
22	H	L	H	L	L	L	H	L
23	H	H	H	H	L	H	H	L
24	H	H	H	H	H	H	H	H
25	L	H	H	L	H	L	H	L
26	L	L	H	L	L	H	L	L
27	L	L	H	L	H	H	L	H
28	L	H	H	H	H	L	L	H
29	L	L	H	H	H	H	H	L
30	L	L	H	H	L	H	H	H
31	H	H	L	L	L	L	L	L
32	H	L	L	L	H	H	H	L

Table 6.10 L32 Experimental design array and results for the hot drawing and twisting experiments (L: Low, H: High)

6.7 Statistical Modelling of The Effect of Hot Drawing and Twisting on Linear Aliphatic-Aromatic Co-Polyester Fibres (LAAC)

6.7.1 Experimental Results

According to the design shown in Table 6.10 involving the eight control factors listed in Table 6.9, the experiments were randomly conducted in one block. The thermal shrinkage, mechanical properties and abrasion for LAAC twisted fibres were measured and are listed in Table 6.11. Each thermal shrinkage test was carried out using a MK IV Shrinkage-Force Tester; samples were heated for 2 minutes at 60^{o}C under a load cell of 10 g. The Shirley Yarn Abrasion Tester was used to determine the abrasion resistance of yarns. The data present the average of the measured values for each sample; the small standard deviations are related to the draw frame setting based variation, the tension or slippage on the drawing roles or some measurement error relating to preparing the sample for testing. Figure 6.30 shows a SEM photomicrograph of the surface of twisted LAAC fibres. After drawing and twisting, the outer surface of twisted fibres showed uniformity without any deformation.

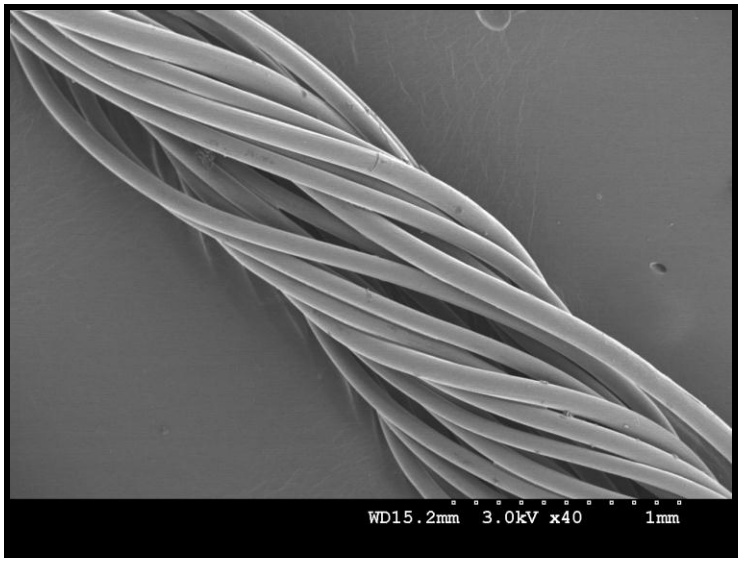

Figure 6.30 SEM photomicrograph of LAAC twisted fibres

Trial Number	Shrinkage (%)	Tenacity (g/den)	Elongation at break (%)	Modulus (g/den)	Abrasion (number of rubs)
1	10.5	1.2	160	0.93	7
2	11.5	1.3	78	1.37	7
3	12.8	0.8	304	0.37	11
4	11.3	1.3	82	1.40	11
5	12.3	1.2	108	1.14	6
6	14.1	0.7	276	0.32	15
7	13.5	0.8	276	0.40	17
8	9.2	0.8	261	0.34	12
9	12.3	1.5	157	1.63	7
10	11.9	0.9	264	0.36	10
11	10.0	0.9	328	0.35	14
12	14.6	0.8	280	0.43	12
13	13.2	1.6	142	1.75	7
14	10.2	0.8	360	0.32	10
15	12.3	0.8	262	0.40	8
16	13.1	0.9	340	0.36	13
17	08.7	0.7	270	0.30	10
18	11.8	0.8	280	0.35	10
19	12.3	1.3	112	1.00	5
20	11.3	0.8	372	0.38	8
21	12.3	0.8	176	0.35	10
22	13.4	1.3	124	1.27	10
23	12.7	1.3	108	1.13	5
24	12.0	1.3	112	1.05	4
25	11.4	1.4	108	1.07	6
26	12.3	1.1	43	1.23	8
27	11.5	1.3	152	0.87	5
28	10.6	1.2	90	0.89	3
29	13.2	1.2	41	1.41	7
30	12.5	1.3	56	1.18	8
31	13.9	0.8	216	0.34	9
32	13.7	0.9	280	0.37	12

Table 6.11 Results for the hot drawing and twisting experiments for LAAC twisted fibres

6.7.2 Statistical Analysis and Discussion

Pareto charts (Figure 6.31 and Figure 6.32) for thermal shrinkage, tenacity, elongation at break, modulus and abrasion show the significant arrangement of factors and their interactions in decreasing order. The Pareto chart for thermal shrinkage shows that the total number of drawing stages (DS), the interactions DS&DT, DR&RS, PT&RT, DS&DR and DT&RS, drawing temperature (DT) and relaxing stage ratio (RS) are the most important

factors affecting the thermal shrinkage properties of the fibres, followed by other factors and interactions. Factors affect the tension and the internal stress affects the thermal shrinkage properties. In terms of mechanical properties of drawn AAC fibres, the Pareto chart for tenacity shows that the drawing ratio (DR), PT&SF, the interactions DS&DT, DR&RS and PT&RT, the total number of drawing stages (DS), drawing temperature (DT), SF&T and PT are the most important factors affecting the tenacity, followed by other factors and interactions. The Pareto chart for elongation at break shows that the drawing ratio (DR), twist level (T) and the interactions (DS&T, DS&DT, DR&RS, PT&RT and DR&T) were the most important factors affecting the elongation at break, followed by other factors and interactions. It is noted that, when the relaxing stage ratio increases, the yarn speed decreases, the cooling time increases and the spin finish layer's thickness is increased. The Pareto chart for modulus shows that total draw ratio, drawing temperature, DS&RS, DT&DR, and DS&T, DR&PT, RS&RT, the plate temperature, total number of drawing stages and relaxing stage ratio were the most important factors affecting the modulus, followed by other factors and interactions. When a higher draw ratio is applied, the speed of the final roller will increase and the spin finish layer thickness on the fibres at constant spin finish pump speed will be affected. At high twist level, the inter-fibre cohesive forces increase, the breaking strength of composite yarns tends to increase and the breaking elongations tend to increase. The Pareto chart for abrasion (Figure 6.32) shows that total draw ratio, DS&DT, DR&RS, PT&RT, DR&SF, DS&SF, RS&T, DS&DR, DT&RS and DR&T were the most important factors affecting the abrasion, followed by other factors and interactions.

The factor effect on thermal shrinkage between the average responses of the low and high level of the factors was obtained using the design matrix and is presented in Figure 6.33, which shows the main effects and interaction plots of the statistical analysis of the effects caused by the main factors and their interactions on responses. The total number of drawing stages (DS), drawing temperature (DT), relaxing stage ratio (RS), the interactions DS&DR, DT&RS, DS&DT, DR&RS and PT&RT have their effects on thermal shrinkage. It is advised that factors influencing thermal shrinkage be assessed further to understand their influence more fully. All the interactions could be simulated, as the plot shows the existence or otherwise of the interaction of each of the two factors, as coded in Table 6.9.

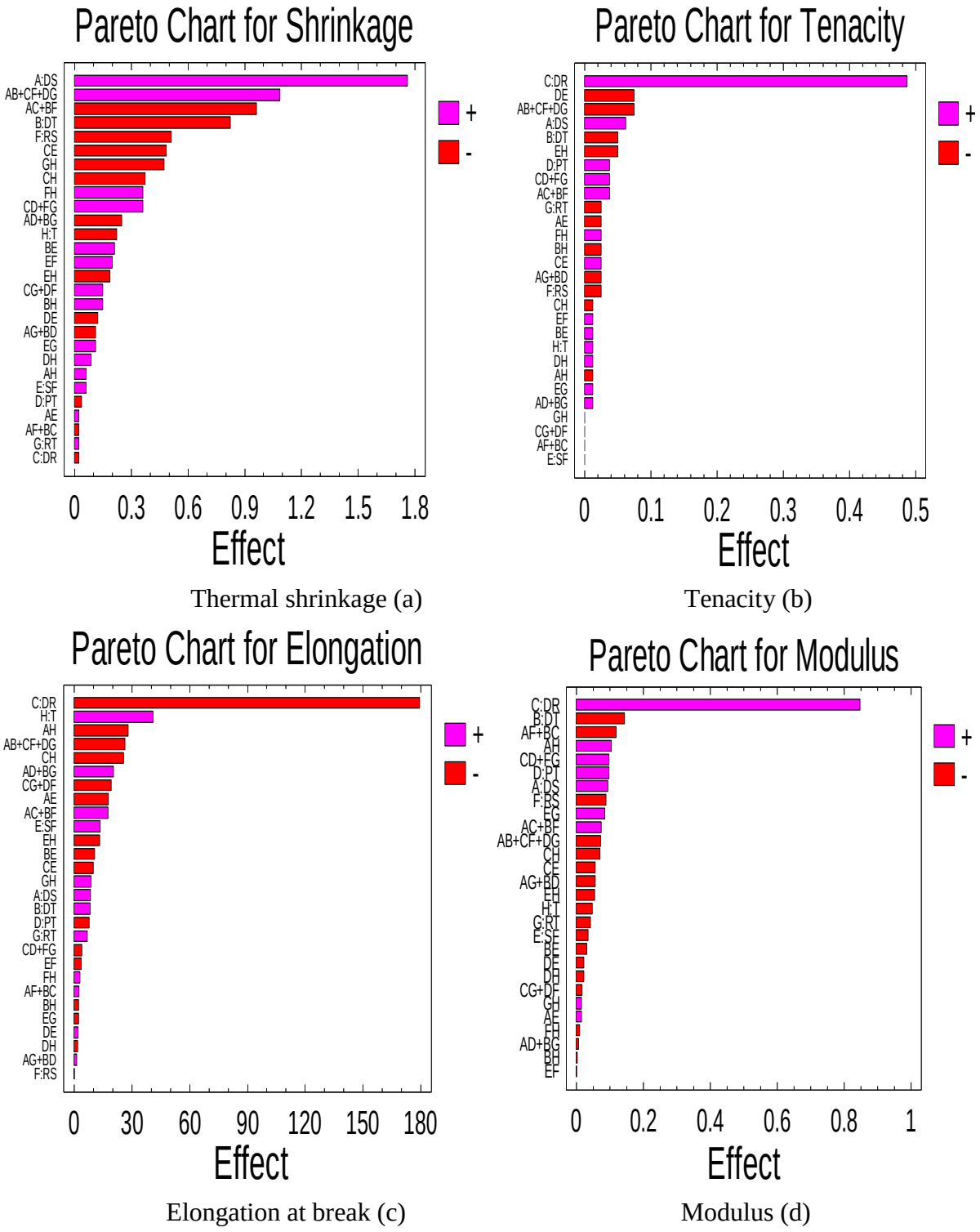

Thermal shrinkage (a)

Tenacity (b)

Elongation at break (c)

Modulus (d)

Figure 6.31 A ranked list of significant arrangement effects and interactions for thermal shrinkage (a), tenacity (b), elongation at break (c) and modulus (d)

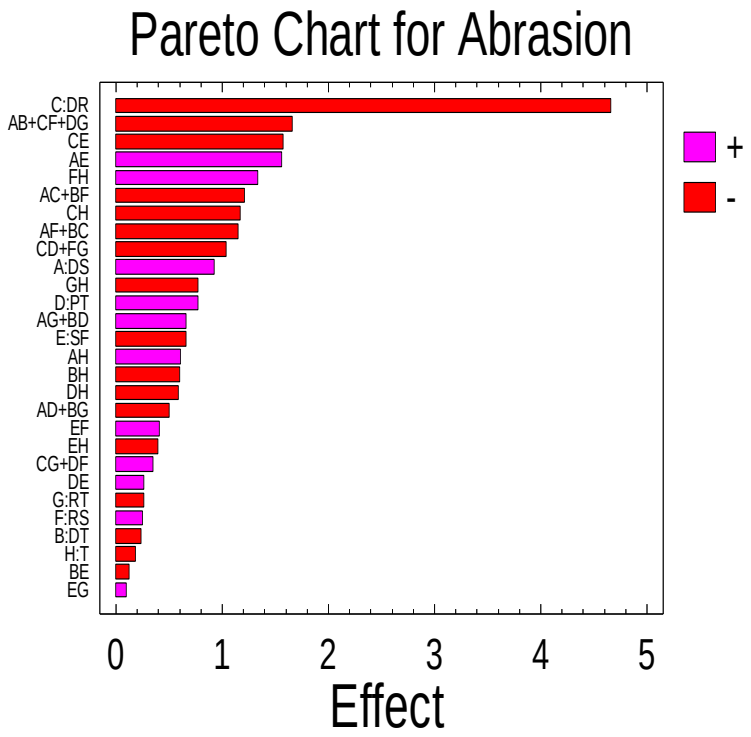

Figure 6.32 Pareto chart for abrasion

The effects and interaction plots for tenacity show that total number of drawing stages, drawing temperature and total draw ratio were the factors affecting the tenacity (Figure 6.34). DS&DT, DT&RS, DT&RS, PT&RT and PT&SF had their effects which need to be further investigated; statistical analysis ANOVA is given in next section. Effects and interaction plots for elongation at break show that total draw ratio, twist level, DS&DR, DS&T, DS&DT, DR&RS, DS&SF, and PT&RT were the factors affecting the elongation at break (Figure 6.35). The main effects of all factors and most of their interactions, especially the draw ratio, were pronounced on modulus (Figure 6.36). The total draw ratio, total number of drawing stages, DS&DT, DR&RS, DR&SF, PT&RT, DS&SF, DS&DR, DT&RS, DR&T and RS&T significantly affect the abrasion (Figure 6.37).

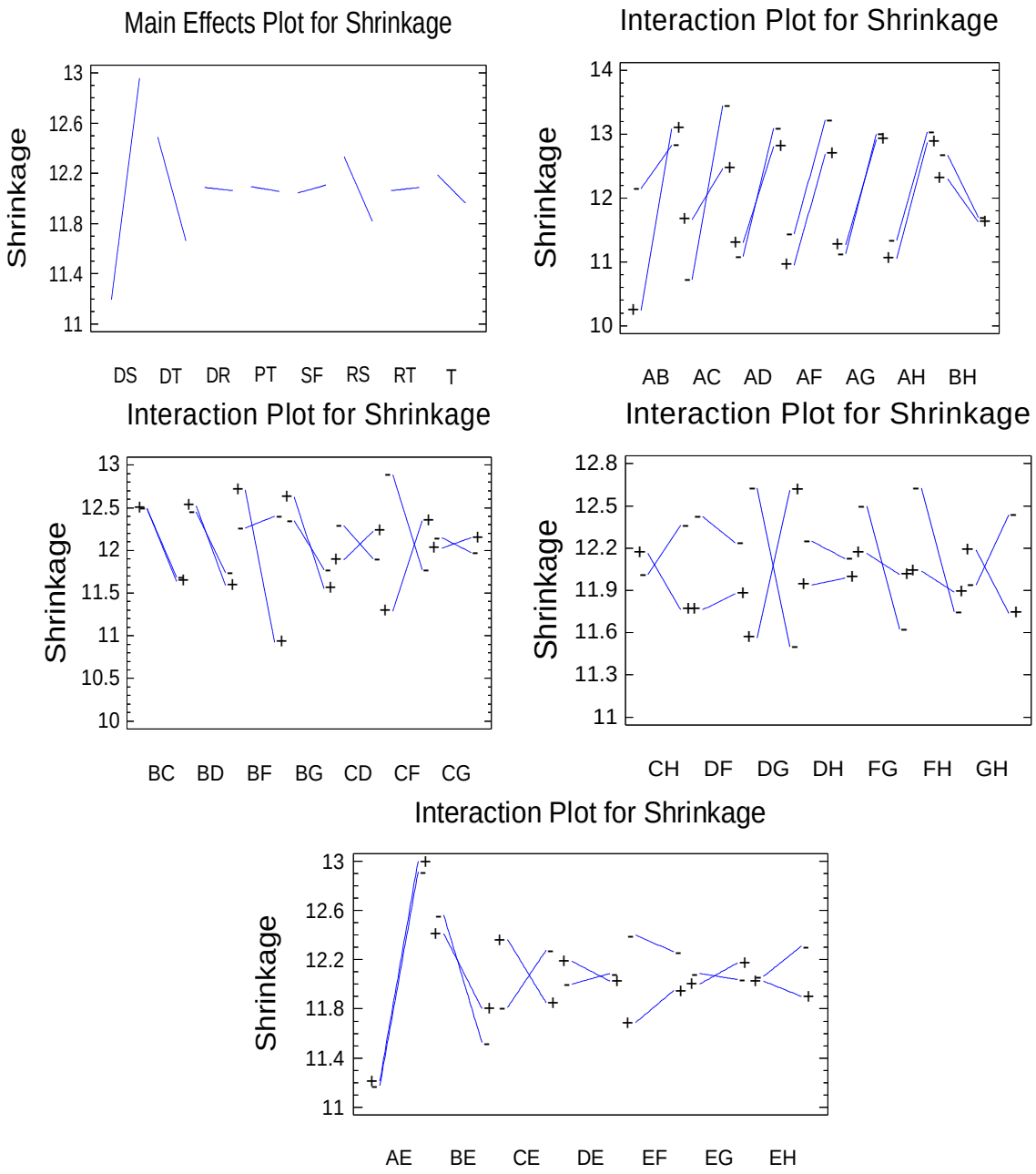

Figure 6.33. Main effect plots and Interaction plots for the thermal shrinkage

Figure 6.38 displays the normal probability plot of the responses estimated and illustrates further details about the normal distribution for the data. Draw ratio had a positive effect on tenacity and modulus and a negative effect on thermal shrinkage, elongation at break and abrasion. Twist level had a positive effect on elongation at break. Draw stage had a positive effect on thermal shrinkage. The interactions (DS&DT, DR&RS and PT&RT) were prominent and had a positive effect on thermal shrinkage and abrasion. DS&DR and DT&RS had a positive effect on abrasion and a negative effect on thermal shrinkage. The effects from

the interaction between draw stage and spin finish could be related to the practical relationship between the tension and the oily roller surface on the last roller in the relaxing stage ratio which caused some slippage. These results were analyzed by ANOVA.

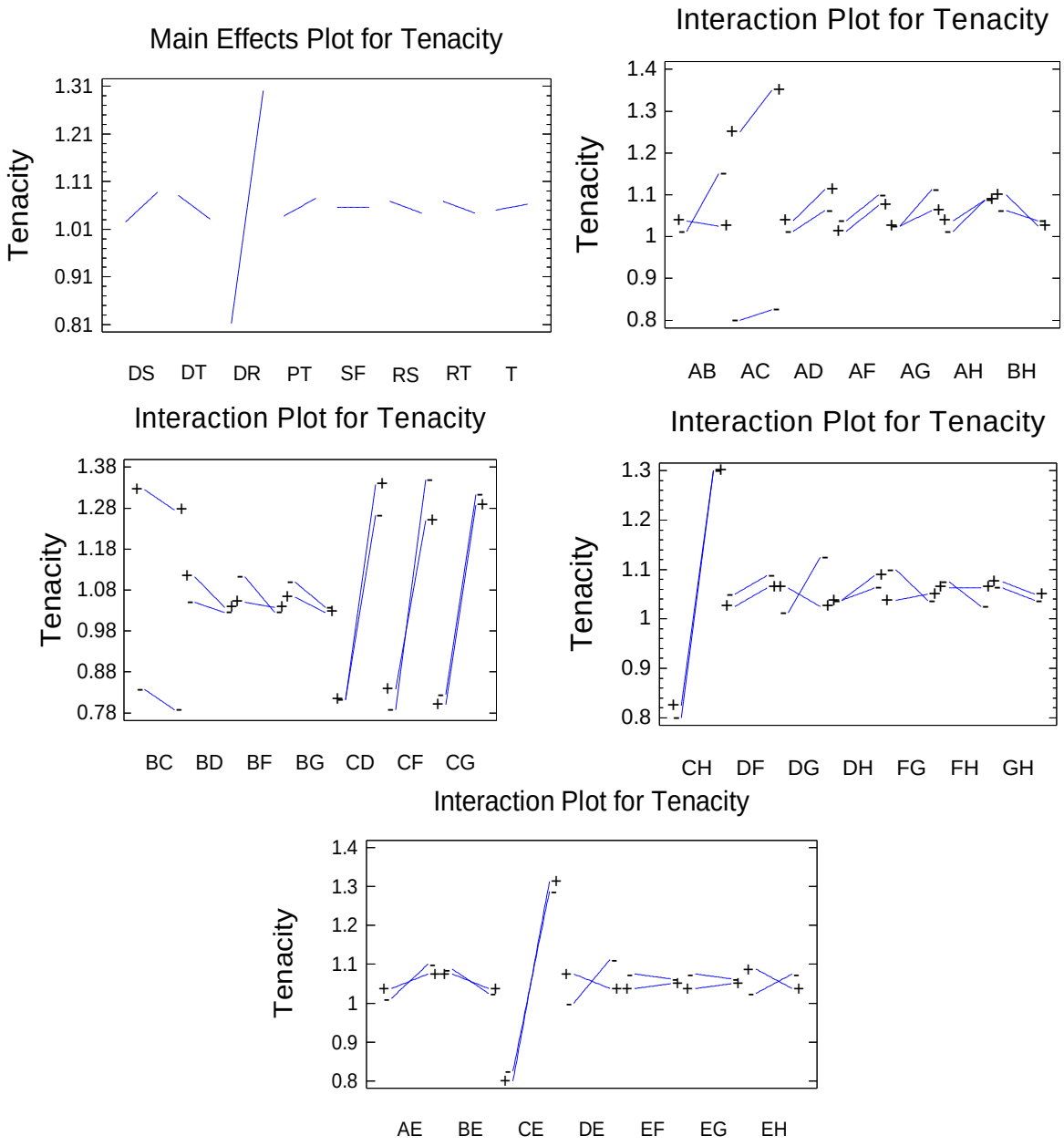

Figure 6.34. Main effect plots and Interaction plots for the tenacity

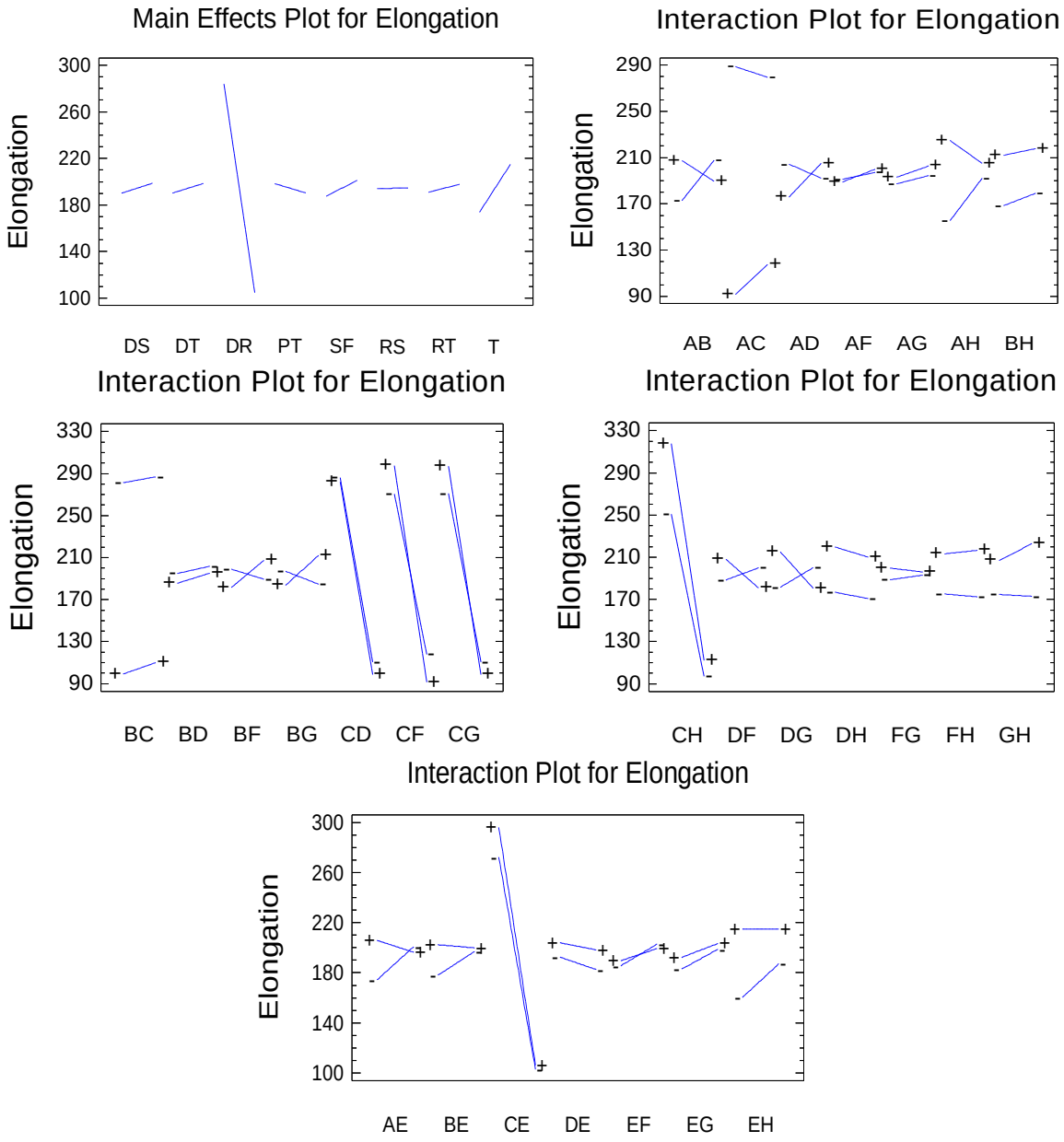

Figure 6.35. Main effect plots and Interaction plots for the elongation at break

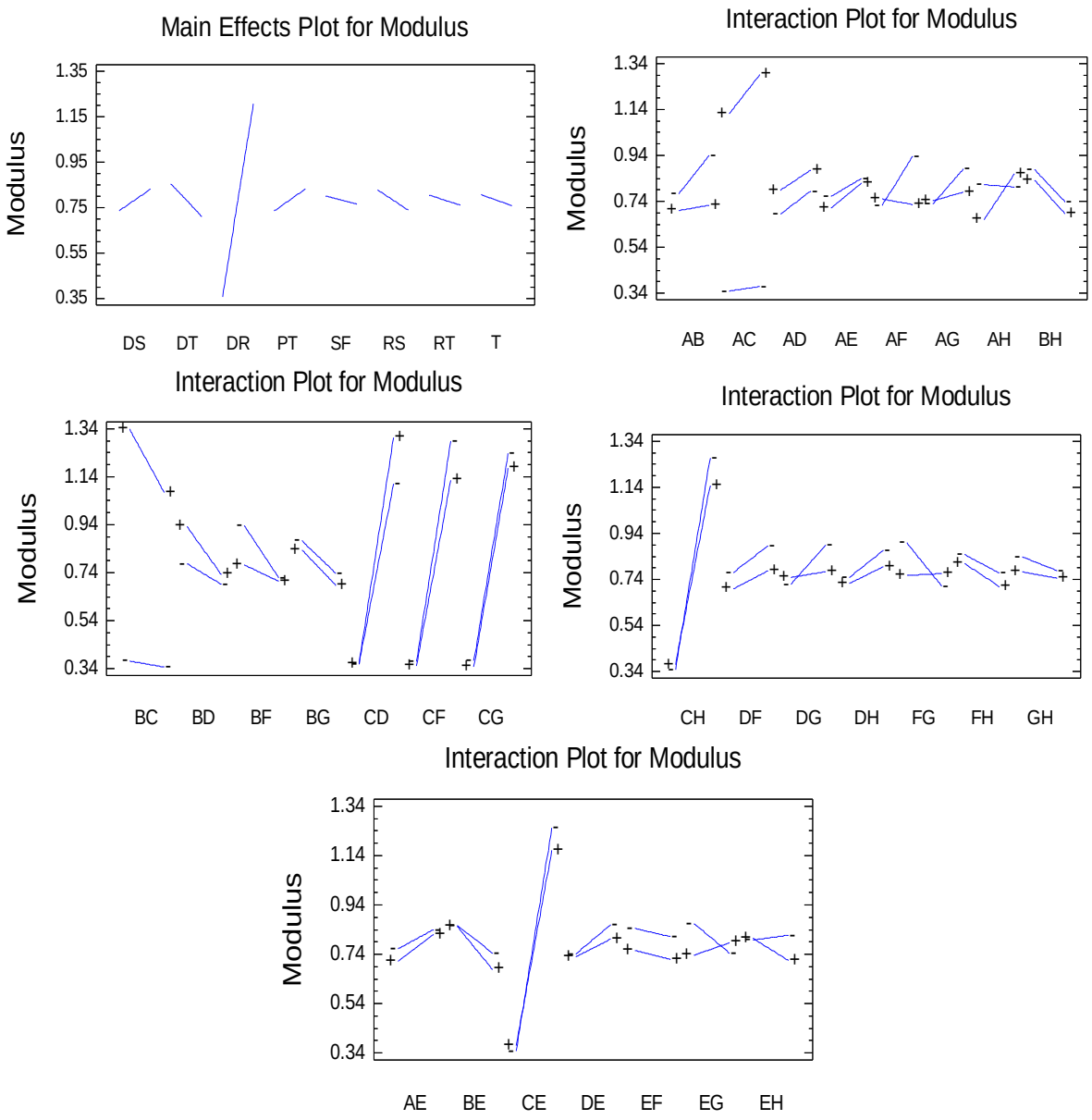

Figure 6.36. Main effect plots and Interaction plots for the modulus

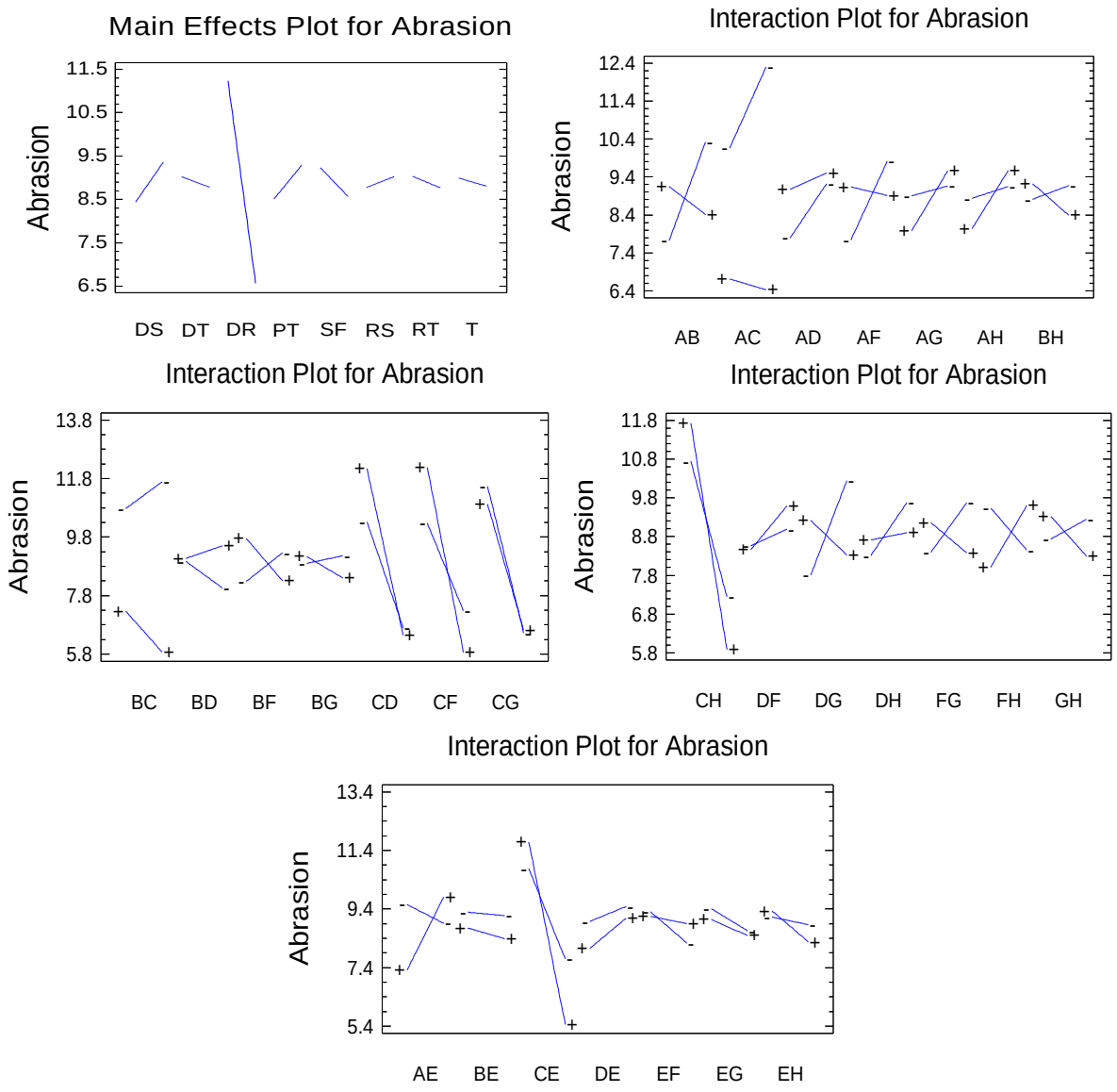

Figure 6.37. Main effect plots and Interaction plots for the abrasion

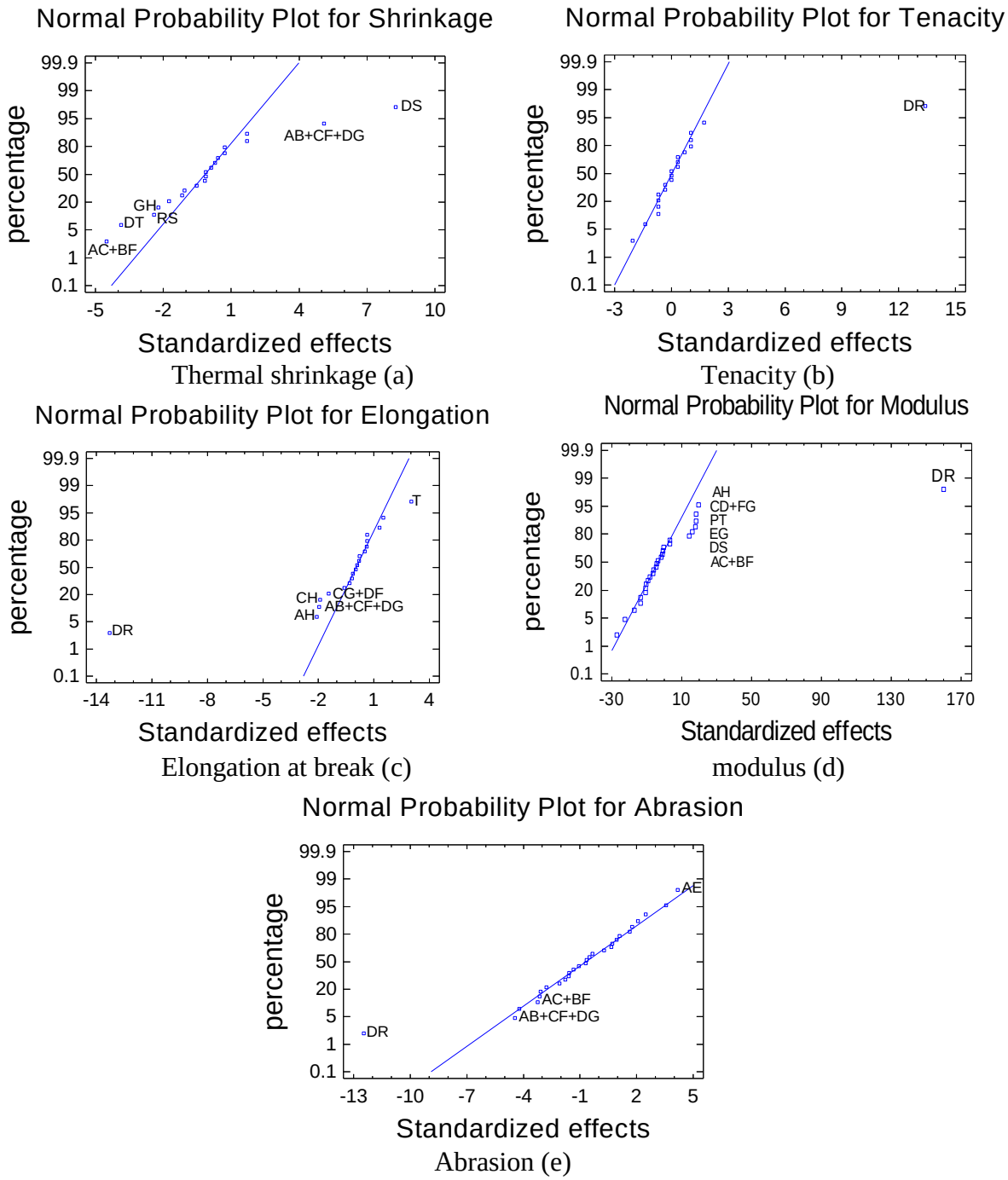

Figure 6.38 Statistical standardized and percentage order values of factors and their interactions for thermal shrinkage (a), tenacity (b), elongation at break (c), modulus (d) and abrasion (e) (Normal Probability Plot)

6.7.2.1 Analysis of Variance (ANOVA)

To determine the factor effects in terms of statistical significance, an analysis of variance (ANOVA) of the obtained data was used. The ANOVA results are listed in Table 6.12; the

significance of the studied factors affecting the thermal shrinkage will then be the total number of drawing stages (DS), (DS&DT, DR&RS, PT&RT), (DS&DR,DT&RS) and drawing temperature DT. The ANOVA analysis for mechanical properties shows that the drawing ratio (DR) had its significant effect on tenacity, elongation at break, modulus and abrasion. All factors had a significant effect on the modulus. The significance of the studied factors affecting the abrasion are DS&DT, DR&RS, PT&RT, DR&SF, DS&SF, RS&T, DS&DR and DT&RS. The interactions DS&RS, DT&DR and DR&T had a borderline significant effect on the abrasion. It could be concluded that some interactions between factors could be related to the fractional design; an error could result from either assignable causes that represent variation because of changes in the independent factors or random causes that signify uncontrolled variation. In order to determine the direction of the interactions (DS&DT, DR&RS, PT&RT) and (DS&DR,DT&RS), the geometric result of plotting a response variable was required. Based on the assumed regression model, the estimated response surfaces of thermal shrinkage were used to determine the direction and the significance of the interactions for thermal shrinkage, as shown in Figure 6.39 (a). There is a twist which confirms the interactions DS&DT and DS&DR. As the surface is flat with no twist found in the surface represented, the determined effects of interactions DT&DR and DT&PT are not significant which corresponds with the previous statistical analysis results of the interaction plot and ANOVA derived from the experimental data. Using the same technique, the interactions DS&DT, DR&SF, DS&SF, RS&T and DS&DR are significant and affect the abrasion as twist found on the surface. There is no twist in the estimated response surfaces for the insignificant interactions DR&RS, PT&RT and DT&RS.

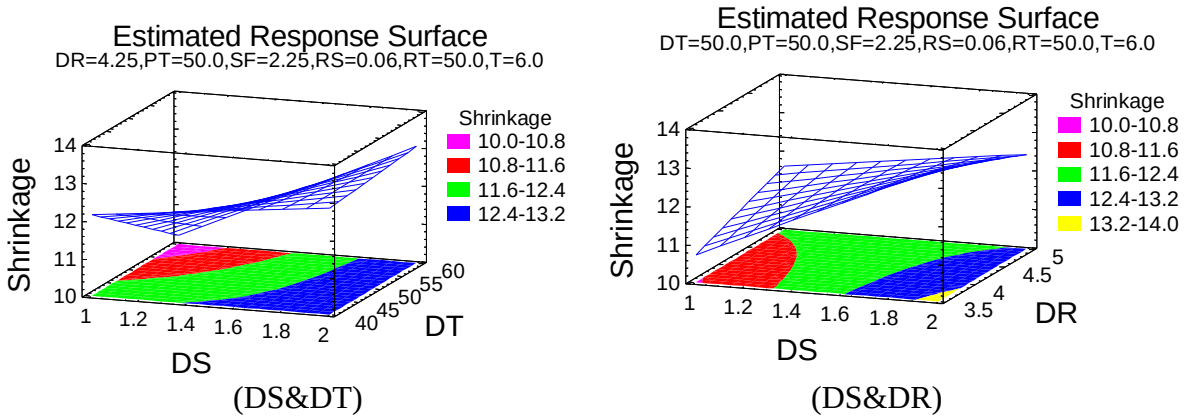

Figure 6.39. The Estimated response surface for the interactions DS&DT and DS&DR for the thermal shrinkage

Source	P-Value				
	Thermal Shrinkage	Tenacity	Elongation at break	Modulus	Abrasion
DS	0.0027	0.2120	0.6851	0.0004	0.0896
DT	0.0225	0.2952	0.6937	0.0001	0.5702
DR	0.9036	0.0011	0.0025	0.0000	0.0011
PT	0.8561	0.4128	0.7051	0.0004	0.1297
SF	0.7638	1.0000	0.5266	0.0071	0.1744
RS	0.0739	0.5720	0.9903	0.0004	0.5514
RT	0.9036	0.5720	0.7372	0.0037	0.5330
T	0.3216	0.7726	0.1195	0.0027	0.6503
DS&DT DR&RS PT&RT	0.0106	0.1540	0.2589	0.0008	0.0211
DS&DR DT&RS	0.0148	0.4128	0.4213	0.0008	0.0477
DS&PT DT&RT	0.2797	0.7726	0.3582	0.3236	0.2733
DS&SF	0.9036	0.5720	0.4156	0.0548	0.0249
DS&RS DT&DR	0.9036	1.0000	0.9005	0.0002	0.0542
DS&RT DT&PT	0.5954	0.5720	0.9485	0.0017	0.1744
DS&T	0.7638	0.7726	0.2340	0.0003	0.1997
DT&SF	0.3448	0.7726	0.6140	0.0087	0.7600
DT&T	0.4874	0.5720	0.9037	0.5305	0.2067
DR&PT RS&RT	0.1524	0.4128	0.8437	0.0004	0.0692
DR&SF	0.0828	0.5720	0.6326	0.0017	0.0244
DR&RT PT&RS	0.4874	1.0000	0.3841	0.0385	0.4180
DR&T	0.1429	0.7726	0.2686	0.0009	0.0515
PT&SF	0.5576	0.1540	0.9165	0.0208	0.5330
PT&T	0.6764	0.7726	0.9293	0.0240	0.2139
SF&RS	0.3698	0.7726	0.8531	0.8288	0.3502
SF&RT	0.5954	0.7726	0.9069	0.0005	0.8063
SF&T	0.3964	0.2952	0.5337	0.0019	0.3629
RS&T	0.1524	0.5720	0.8846	0.1558	0.0373
RT&T	0.0877	1.0000	0.6767	0.0548	0.1297

Table 6.12 ANOVA results identifying the statistical significance of factor effects on the results from analysis of variance (ANOVA) of the data identifying the statistical significance of each factor for thermal shrinkage, tenacity, elongation at break , modulus and abrasion.

6.7.2.2 The Regression Equation and Estimation Results

Based on the analysis of the fraction factorial experimental design results, simplified models based on statistical analysis for studied factors and their interactions were fitted by the regression equations for thermal shrinkage, tenacity, elongation at break, modulus and abrasion which had been fitted to the experimental data. The regression equations in terms of the previous coded values (Table 6.9) are given as follows:

Thermal shrinkage = 11.4812 + 3.40417*DS - 0.25875*DT + 1.925*DR - 0.0614583*PT + 1.14167*SF - 53.125*RS + 0.03*RT + 0.59375*T + 0.10875*DS*DT - 1.28333*DS*DR - 0.025*DS*PT + 0.0333333*DS*SF - 1.25*DS*RS - 0.01125*DS*RT + 0.03125*DS*T + 0.0141667*DT*SF + 0.00375*DT*T + 0.0241667*DR*PT - 0.433333*DR*SF + 0.01*DR*RT - 0.125*DR*T - 0.00833333*PT*SF + 0.0021875*PT*T + 6.66667*SF*RS + 0.0075*SF*RT - 0.0625*SF*T + 4.53125*RS*T - 0.011875*RT*T (6.11)

Tenacity = -0.7 + 0.4*DS + 0.010625*DT + 0.1*DR - 0.00125*PT + 0.197222*SF - 3.4375*RS + 0.000625*RT + 0.0645833*T - 0.0075*DS*DT + 0.05*DS*DR + 0.00125*DS*PT - 0.0333333*DS*SF + 0.0*DS*RS - 0.0025*DS*RT - 0.00625*DS*T + 0.000833333*DT*SF - 0.000625*DT*T + 0.0025*DR*PT + 0.0222222*DR*SF + 0.0*DR*RT - 0.00416667*DR*T - 0.005*PT*SF + 0.0003125*PT*T + 0.416667*SF*RS + 0.000833333*SF*RT - 0.0166667*SF*T + 0.3125*RS*T + 0.0*RT*T (6.12)

Elongation at break = -239.061 + 61.6325*DS + 6.34987*DT - 5.27333*DR - 2.37644*PT + 153.702*SF - 125.0*RS + 4.67777*RT + 70.1651*T - 2.64163*DS*DT + 23.555*DS*DR + 2.05837*DS*PT - 23.8883*DS*SF + 129.188*DS*RS + 0.133375*DS*RT - 14.125*DS*T - 0.711083*DT*SF - 0.0625*DT*T - 0.27225*DR*PT - 8.96333*DR*SF - 1.28892*DR*RT - 8.58333*DR*T + 0.144417*PT*SF - 0.0458125*PT*T - 127.792*SF*RS - 0.161083*SF*RT - 4.44417*SF*T + 37.5*RS*T + 0.21875*RT*T (6.13)

Modulus = -1.78792 + 0.34375*DS + 0.009125*DT + 0.410833*DR - 0.014875*PT + 0.178056*SF + 7.5*RS - 0.0034375*RT + 0.07125*T - 0.00725*DS*DT + 0.1*DS*DR - 0.000625*DS*PT + 0.0216667*DS*SF - 5.9375*DS*RS - 0.00575*DS*RT + 0.0525*DS*T - 0.00216667*DT*SF - 0.00009375*DT*T + 0.0065*DR*PT - 0.0511111*DR*SF - 0.00125*DR*RT - 0.02375*DR*T - 0.00158333*PT*SF - 0.0005625*PT*T - 0.0416667*SF*RS + 0.00566667*SF*RT - 0.0183333*SF*T - 0.125*RS*T + 0.00040625*RT*T (6.14)

Abrasion = -35.9854 + 12.2208*DS + 0.34625*DT + 7.10833*DR + 0.456458*PT + 1.56667*SF - 38.75*RS - 0.110417*RT + 2.90833*T - 0.16625*DS*DT - 1.61667*DS*DR - 0.05*DS*PT + 2.08333*DS*SF - 57.5*DS*RS + 0.06625*DS*RT + 0.30625*DS*T - 0.00833333*DT*SF - 0.015*DT*T - 0.0691667*DR*PT - 1.4*DR*SF + 0.0233333*DR*RT - 0.391667*DR*T + 0.0175*PT*SF - 0.0146875*PT*T + 13.75*SF*RS + 0.00666667*SF*RT - 0.133333*SF*T + 16.7188*RS*T - 0.019375*RT*T (6.15)

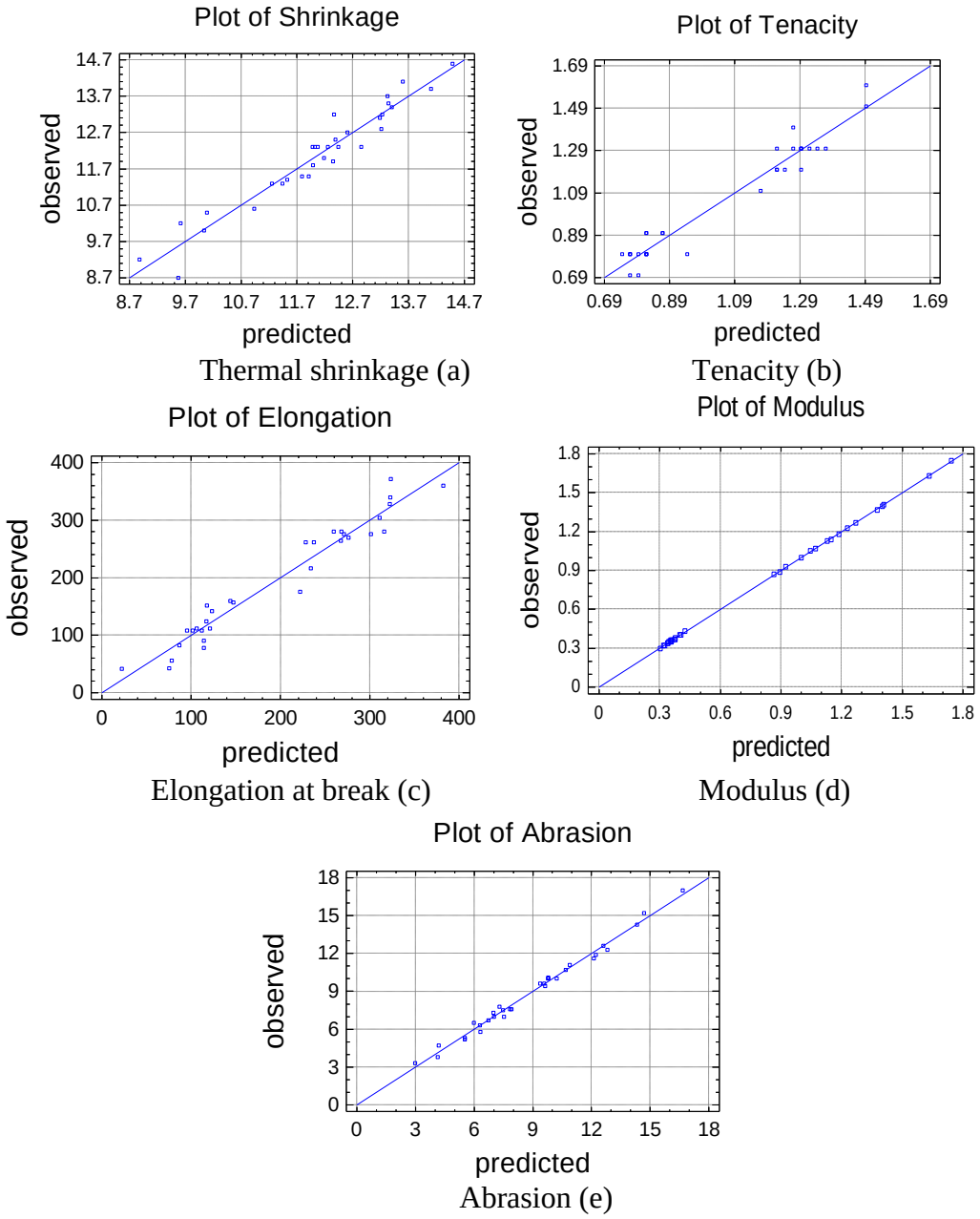

Figure 6.40 Experimental observed results and calculated fitted results plot for thermal shrinkage (a), tenacity (b), elongation at break (c), modulus (d) and abrasion (e)

The models evaluated the significance effect of each independent variable to a predicted response which depended on the coefficient constant for the linear effects of independent factors and the coefficient constant for the interactions effects, depending on the coefficient constant for the offset term. Figure 6.40 shows the experimental observed results and calculated fitted results plot for thermal shrinkage (a), tenacity (b), elongation at break (c), modulus (d) and abrasion (e). Their Model Standard Error (MSE) values listed in Table 6.13 indicate the dispersion of predicted and observed values around the theoretical fitted line

generated using the fitted model for each trial. The predictive models gave useful results with small variation, for previously mentioned reasons such as draw frame setting based variation, the tension or slippage on the drawing roles or some tension during the preparation of the sample for testing.

6.7.3 Conclusion and Statistical Model for Optimisation

As-spun, biodegradable, linear aliphatic-aromatic co-polyester fibres were drawn at different multi-stage hot drawing conditions, then twisted. The statistical models covered the number of drawing stages, drawing temperature, total drawing ratio, plate temperature, spin finish application, relaxing stage ratio, relaxing temperature, twist level and their interactions. The models specified the combinations of their levels for enhancing properties. The effects from the interaction between draw stage and spin finish could be related to the practical relationship between the tension and the oily roller surface on the last roller in the relaxing stage ratio, which caused some slippage. Draw ratio had a positive effect on tenacity and modulus and a negative effect on thermal shrinkage, elongation at break and abrasion.

Response	MSE	Optimum model	The combination of factor levels (↓: Low Level, ↑: High Level)							
			DS	DT	DR	PT	SF	RS	RT	T
Shrinkage (%)	0.245	Maximum	↑	↑	↓	↓	↑	↑	↓	↑
		Minimum	↓	↑	↓	↑	↓	↑	↓	↓
Tenacity (g/den)	0.470	Maximum	↑	↓	↑	↑	↓	↓	↓	↑
		Minimum	↑	↑	↓	↓	↓	↑	↑	↓
Elongation at break (%)	17.86	Maximum	↓	↑	↓	↓	↑	↓	↑	↑
		Minimum	↓	↓	↑	↑	↓	↑	↑	↓
Modulus (g/den)	0.082	Maximum	↑	↓	↑	↑	↓	↓	↓	↑
		Minimum	↑	↑	↓	↓	↓	↑	↑	↓
Abrasion (number of rubs)	0.581	Maximum	↑	↓	↓	↑	↑	↑	↓	↑
		Minimum	↓	↓	↑	↑	↑	↓	↑	↑

Table 6.13 The combinations of factor levels for the effect of multi-stage hot drawing on the properties of LAAC fibres for thermal shrinkage, tenacity, elongation at break, modulus and abrasion.(MSE: Model Standard Error)

Twist level had a positive effect on elongation at break. Draw stage had a positive effect on thermal shrinkage. The interactions DS&DT, DR&RS and PT&RT were prominent and had a positive effect on thermal shrinkage and abrasion. When the relaxing stage ratio increases, the yarn speed decreases, the spin finish layer's thickness is increased which affects the inter-fibre cohesion which enhances in tenacity. DS&DR and DT&RS had a positive effect on abrasion and a negative effect on thermal shrinkage as described previously. Other factors and interactions had their effects but they were limited and less significant as it was covered by the governing factors, drawing ratio and temperature.

To explain some of the interaction effect between the factors analysed; the number of drawing stages and relaxing stage ratio and their interactions with temperature would affect the internal stress. Increasing the draw ratio or decreasing drawing temperature plays an important role in stretching the chain inside the fibres, thus affecting the fibre's elongation. The speed of the final roller will increase, when a higher draw ratio is applied. In the optimization of thermal shrinkage, tenacity, elongation at break and modulus, there are factor levels which maximize and minimize the responses over the region indicated (Table 6.13). Table 6.13 also shows the Model Standard Error (MSE) values described previously. The models help processing scientists and technologists in industry to obtain the enhanced properties at suitable conditions related to final product cost and to obtain environmentally friendly, economical and energy saving fibres. The achieved models could form a part in a forecasting program designed to optimize the drawing process of selected as-spun fibres. Manufactured fibres could be used in agricultural, horticultural and other non-traditional textile applications.

6.8 Statistical Modelling of The Effect of Hot Drawing and Twisting on Branched Aliphatic-Aromatic Co-Polyester Fibres (BAAC)

6.8.1 Experimental Results

According to the design shown in Table 6.10 involving the eight control factors listed in Table 6.9, the experiments were randomly conducted in one block. The thermal shrinkage, mechanical properties and abrasion for BAAC twisted fibres were measured and are listed in Table 6.14. Each thermal shrinkage test was carried out using MK IV Shrinkage-Force Tester; samples were heated for 2 minutes at 60^{o}C under a load cell of 10g. The Shirley Yarn Abrasion Tester was used to determine the abrasion resistance of yarns. Again draw frame setting based variation, the tension or slippage on the drawing roles and variation in the sample testing had an effect on the deviations which may have been raised from them. Figure 6.41 shows an SEM photomicrograph of the surface of twisted BAAC fibres; the outer surface of twisted fibres shows uniformity without any deformation.

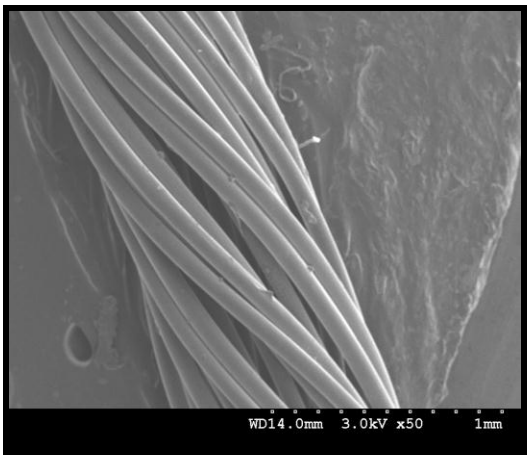

Figure 6.41 SEM photomicrograph of BAAC twisted fibres

Trial Number	Shrinkage (%)	Tenacity (g/den)	Elongation at break (%)	Modulus (g/den)	Abrasion (number of rubs)
1	8.5	0.9	112	0.83	45
2	10.0	0.8	80	1.19	59
3	9.0	0.8	119	0.97	42
4	9.3	1.0	92	1.75	43
5	9.2	0.9	60	0.99	33
6	10.4	0.9	52	1.91	26
7	5.9	0.8	140	0.73	36
8	6.6	0.8	124	0.82	108
9	10.3	0.8	79	1.09	88
10	6.8	0.8	124	0.76	46
11	7.0	0.7	143	0.68	59
12	6.6	0.8	169	0.77	37
13	8.0	0.8	110	0.39	22
14	5.7	0.6	155	0.35	34
15	4.0	0.7	145	0.68	144
16	6.9	0.7	143	0.72	80
17	6.8	0.8	129	0.84	35
18	3.8	0.7	161	0.51	57
19	9.5	0.9	55	2.20	55
20	8.6	0.6	100	0.81	25
21	5.0	0.8	136	0.73	41
22	9.6	1.0	73	1.65	124
23	9.8	0.9	48	1.84	60
24	9.5	0.9	80	1.32	41
25	8.0	0.8	97	0.69	51
26	6.8	0.8	119	0.44	20
27	6.7	0.7	144	0.65	36
28	8.3	0.7	93	0.63	46
29	9.7	0.9	115	1.34	51
30	8.0	0.8	131	0.67	24
31	9.3	0.8	100	1.49	92
32	6.4	0.8	139	1.01	110

Table 6.14 Results for the hot drawing and twisting experiments for BAAC twisted fibres

6.8.2 Statistical Analysis and Discussion

Pareto charts for thermal shrinkage, tenacity, elongation at break, modulus and abrasion show the arrangement of factors and their interactions in decreasing order (Figure 6.42 and Figure 6.43). The Pareto chart for thermal shrinkage shows how the determined factors would affect the tension and the internal stress affecting the thermal shrinkage properties; the drawing ratio (DR), the total number of drawing stages (DS), the drawing temperature (DT), the plate temperature (PT), the relaxing temperature (RT); the interactions (DT&SF, DS&RS,

DT&DR, PT&SF, DS&PT, DT&RT and RT&T are the most important factors affecting the thermal shrinkage properties of the fibres, followed by other factors and interactions. When a higher draw ratio is applied, the speed of the final roller will increase and the spin finish layer thickness on the fibres at constant spin finish pump speed will be affected which could explain the interaction between the spin finish and the draw ratio. The Pareto chart for tenacity shows that the drawing ratio (DR), twist level (T), the total number of drawing stages (DS), DS&SF, SF, SF&RS and the drawing temperature (DT), the interactions DR&SF,DR&RT, PT&RS and DS&T were the most important factors affecting the tenacity, followed by other factors and interactions. The Pareto chart for elongation at break shows that the drawing ratio (DR), total number of drawing stages (DS), twist level (T), draw temperature (DT) , the interactions DR&PT, RS&RT, DS&DR, DT&RS, PT&SF, PT and DT&T were the most important factors affecting the elongation at break, followed by other factors and interactions. The Pareto chart for modulus shows that twist level, total number of drawing stages, drawing temperature, total draw ratio, the interactions DS&PT, DT&RT, DS&DT, DR&RS, PT&RT, DT&T, DS&T, DT&SF and relaxing temperature were the most important factors affecting the modulus, followed by other factors and interactions. The Pareto chart for abrasion shows that twist level, the interactions DS&RT, DT&PT, DR&RT and PT&RS, the plate temperature, SF&RT, DS&SF, SF&T, DS&PT, DT&RT, DS&DR, DT&RS, DS&DT, DR&RS, PT&RT, total draw ratio, DR&PT, RS&RT and drawing temperature were the most important factors affecting the abrasion, followed by other factors and interactions.

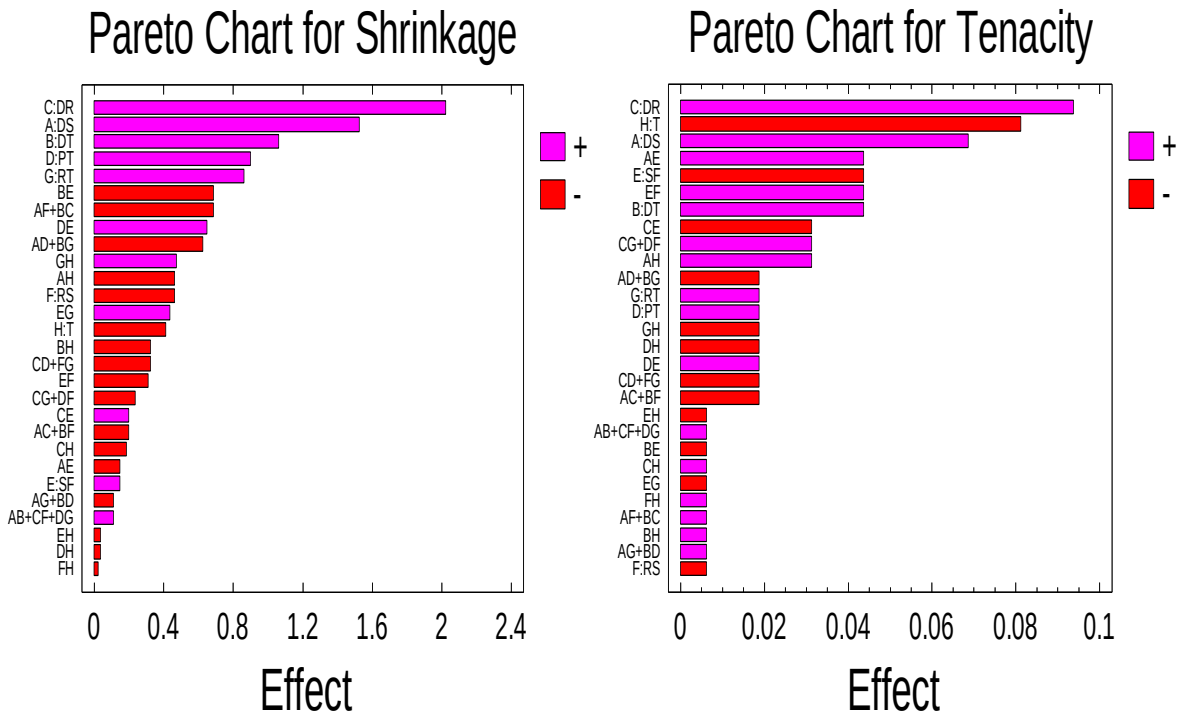

Thermal shrinkage (a)

Tenacity (b)

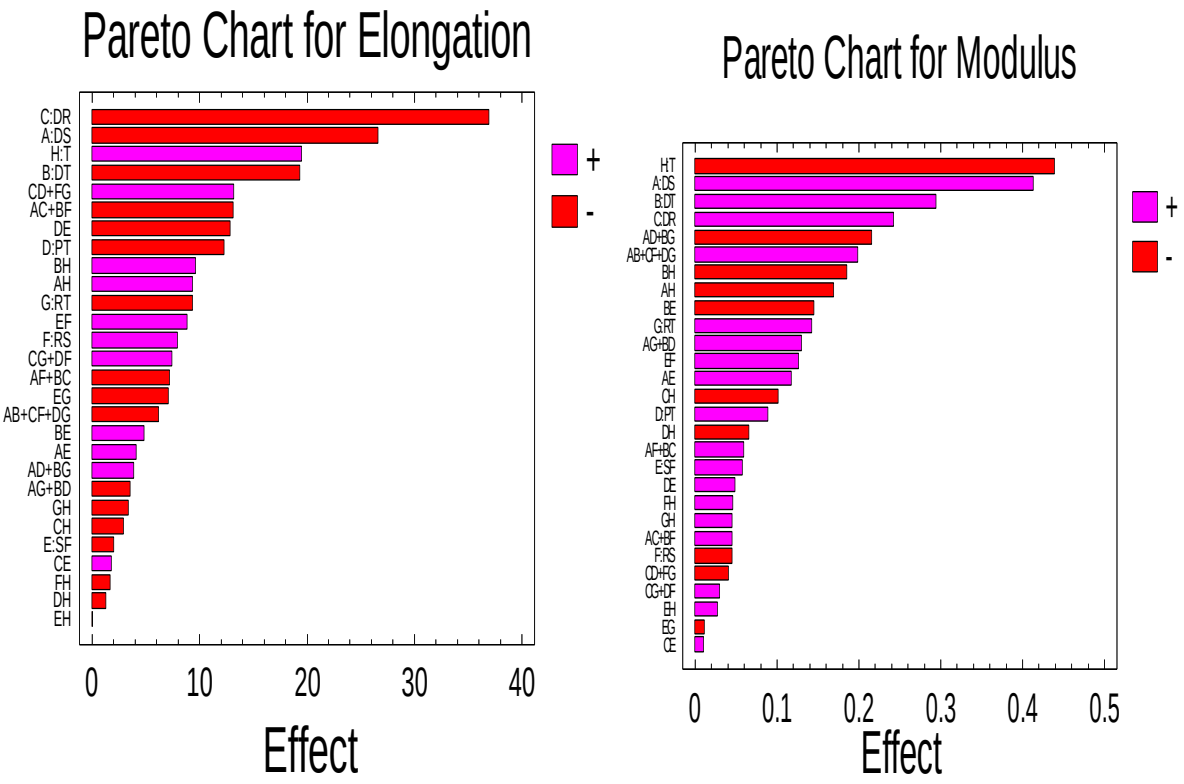

Elongation at break (c)

Modulus (d)

Figure 6.42 A ranked list of significant arrangement effects and interactions for thermal shrinkage (a), tenacity (b), elongation at break (c) and modulus (d) (Pareto chart)

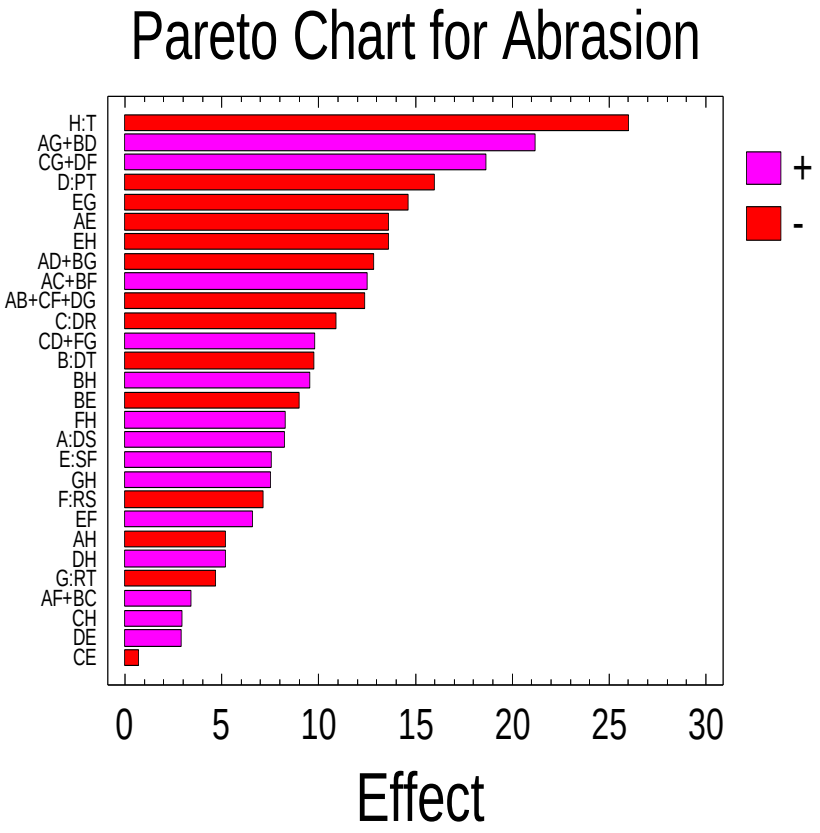

Figure 6.43 A ranked list of significant arrangement effects and interactions for abrasion (Pareto chart)

Figure 6.44 shows the main effects and interaction plots of the statistical analysis of the effects caused by the main factors and their interactions on thermal shrinkage. The factor effect on thermal shrinkage between the average responses of the low and high level of the factors was obtained using the design matrix. The total number of drawing stages (DS), drawing temperature (DT), drawing ratio (DR), plate temperature (PT), relaxing stage ratio (RS), the interactions DT&SF, DS&RS, DT&DR, PT&SF, DS&PT, DT&RT and RT&T had their effects on thermal shrinkage, to be further investigated using ANOVA analysis. It is advised that the major factors influencing thermal shrinkage value be assessed further to understand their influence more fully. All the interactions could be simulated as the plot shows the existence or otherwise of the interaction between each of the two factors, as coded in Table 6.9.

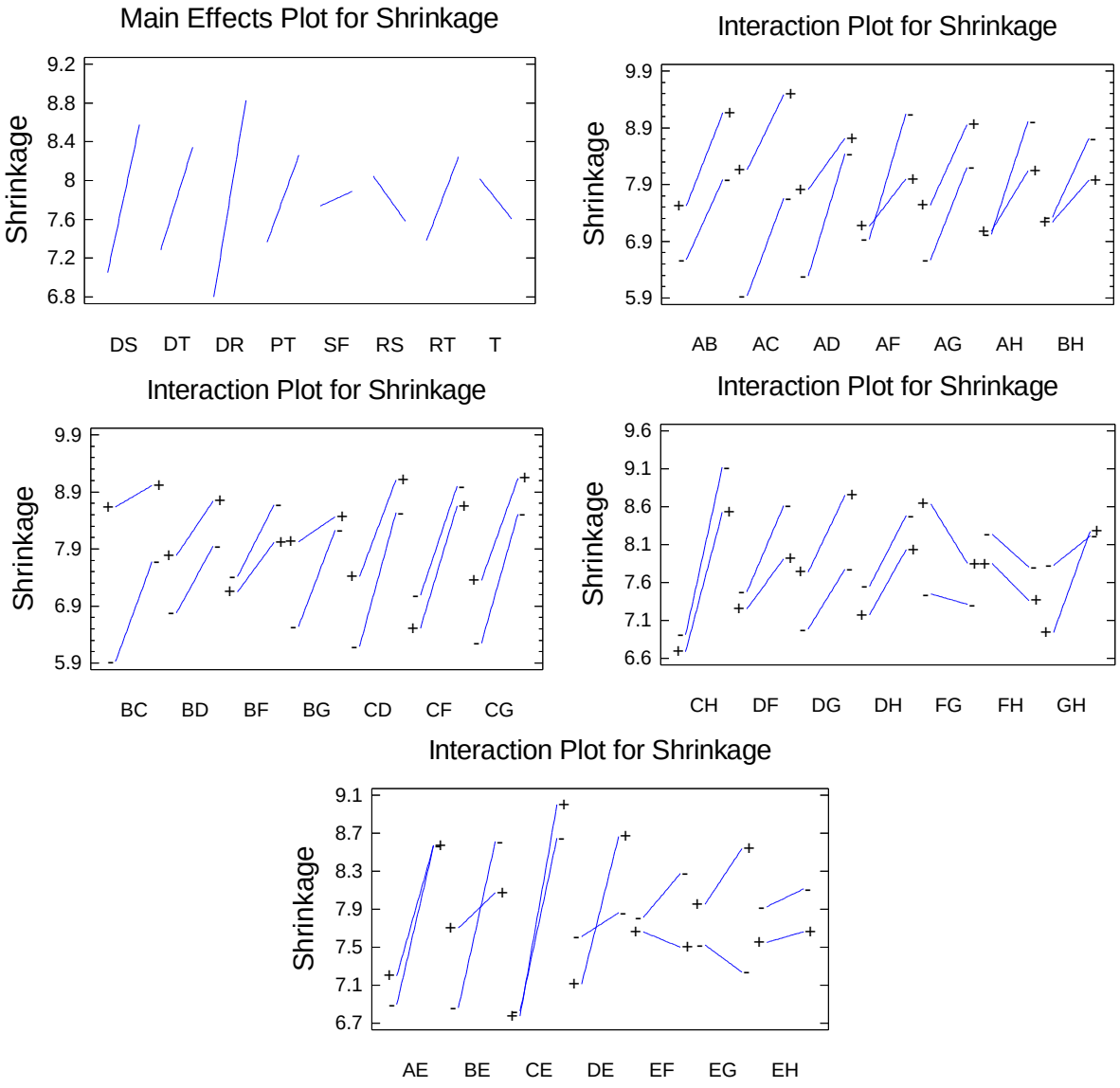

Figure 6.44. Main effect plots and Interaction plots for the thermal shrinkage

Effects and interaction plots for tenacity show that the total number of drawing stages (DS), the drawing temperature (DT) the drawing ratio (DR), spin finish application (SF), twist level (T). DS&SF, SF&RS and DR&SF, DR&RT, PT&RS and DS&T had their effects which need to be further investigated (Figure 6.45); statistical analysis ANOVA is given in next section.

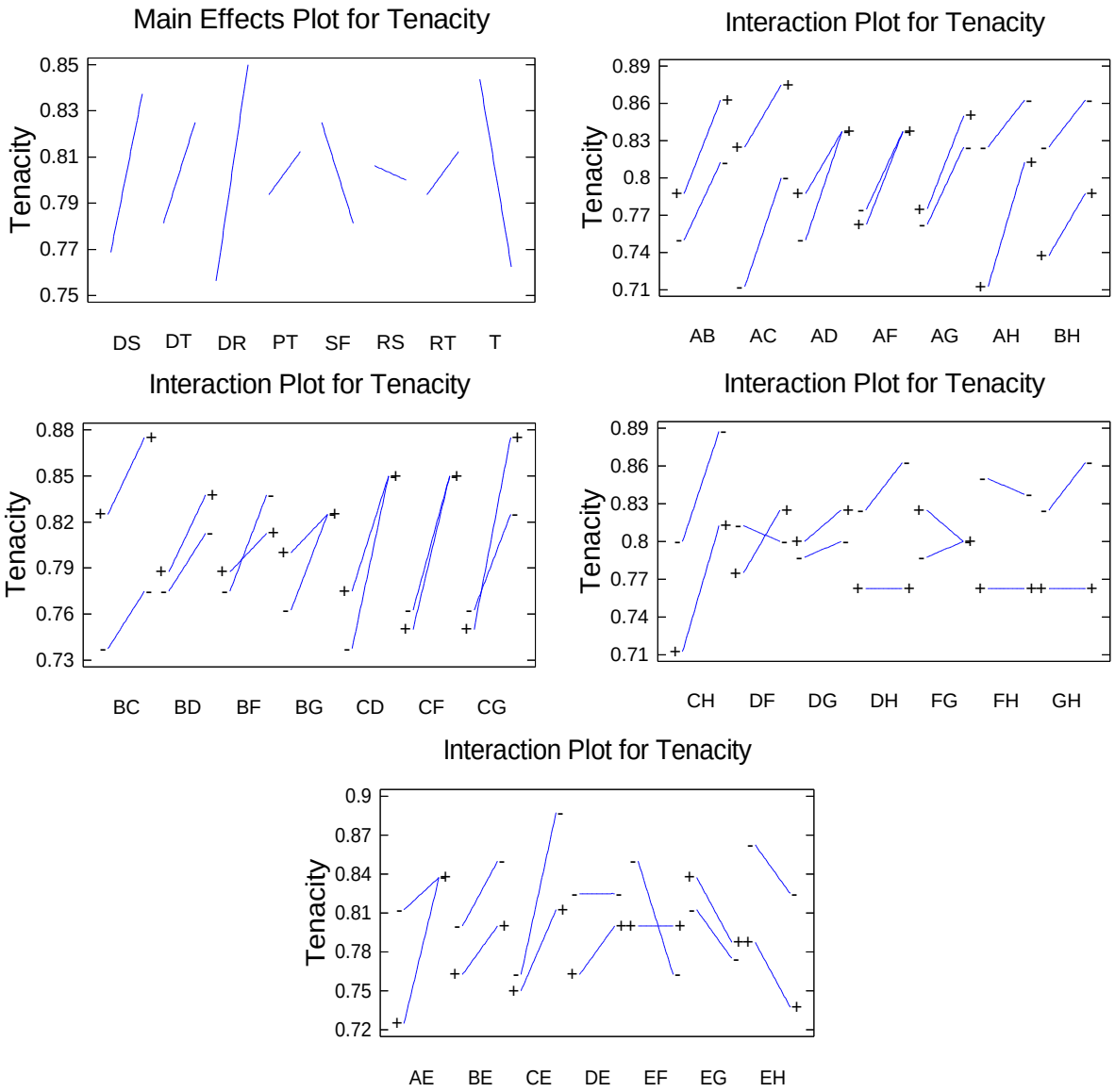

Figure 6.45. Main effect plots and Interaction plots for the tenacity

Effects and interaction plots for elongation at break shows that the total number of drawing stages (DS), the drawing temperature (DT), the drawing ratio (DR), twist level (T) and the interactions DT&RS, PT&RS, RS&RT, PT&SF, SF&RS and SF&RT were the factors affecting the elongation at break (Figure 6.46). Modulus (Figure 6.47) was affected by twist level, total number of drawing stages, drawing temperature, total draw ratio, RT and the interactions DS&PT, DT&RT, DS&DT, DR&RS, PT&RT, DT&T, DS&T and DT&SF. The main effects of all factors and most of their interactions were pronounced. However, relaxing stage ratio and relaxing temperature significantly affected the abrasion (Figure 6.48).

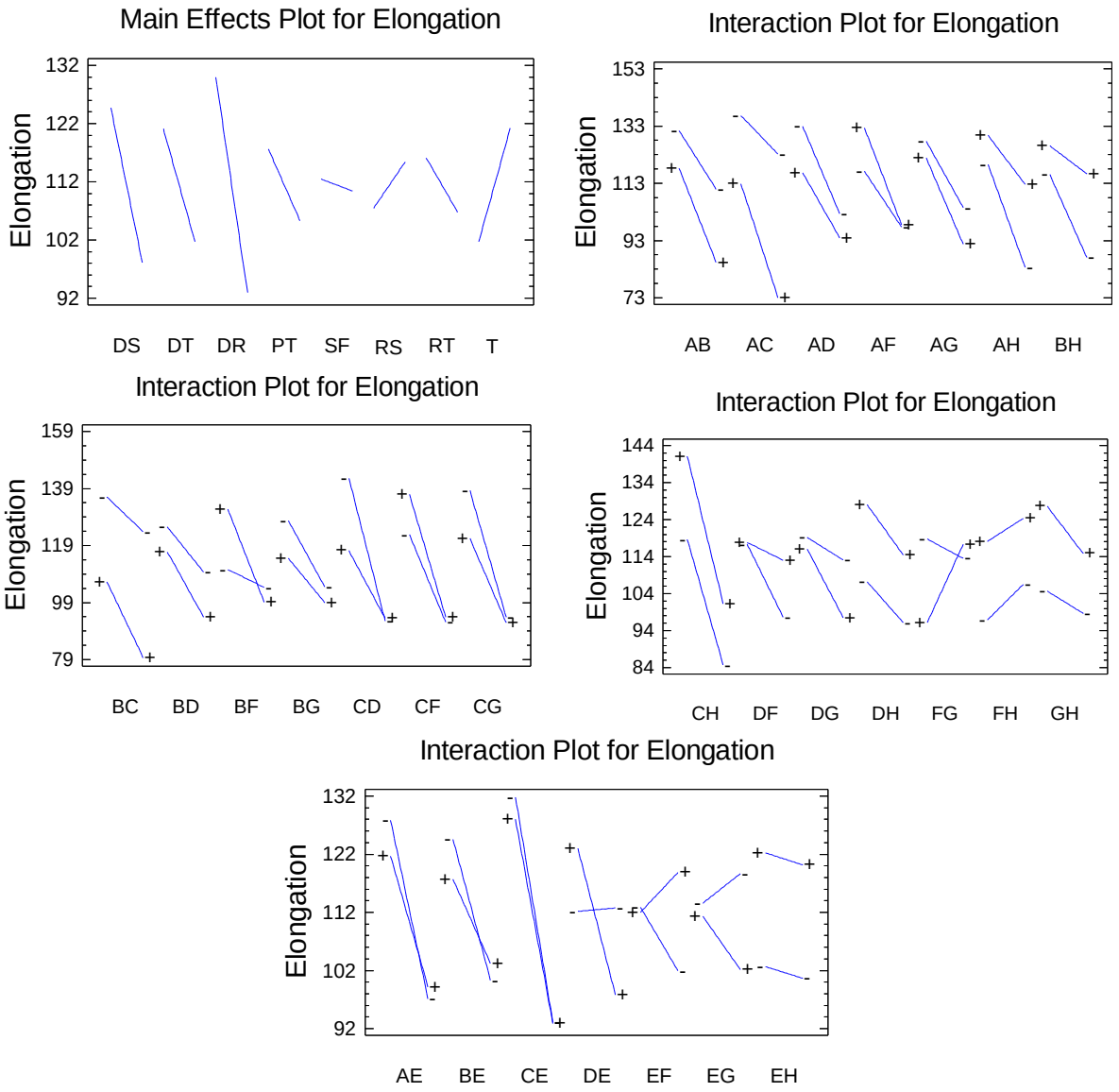

Figure 6.46. Main effect plots and Interaction plots for the elongation at break

Figure 6.49 displays the normal probability plot of the responses estimated, and illustrates further details about the normal distribution for the data. Draw ratio, drawing temperature and the number of drawing stages had a positive effect on thermal shrinkage, tenacity and modulus and a negative effect on elongation at break; draw stage had a positive effect on abrasion affected negatively by drawing ratio. With one stage drawing processes, the tension will be high and the spin finish plays an important role in the filament slippage on the last roller after applied spin finish. Twist affects negatively on modulus and abrasion. Plate temperature, relaxing temperature and the interactions DT&SF and PT&SF were prominent and had a positive effect on thermal shrinkage. These results were analyzed by ANOVA.

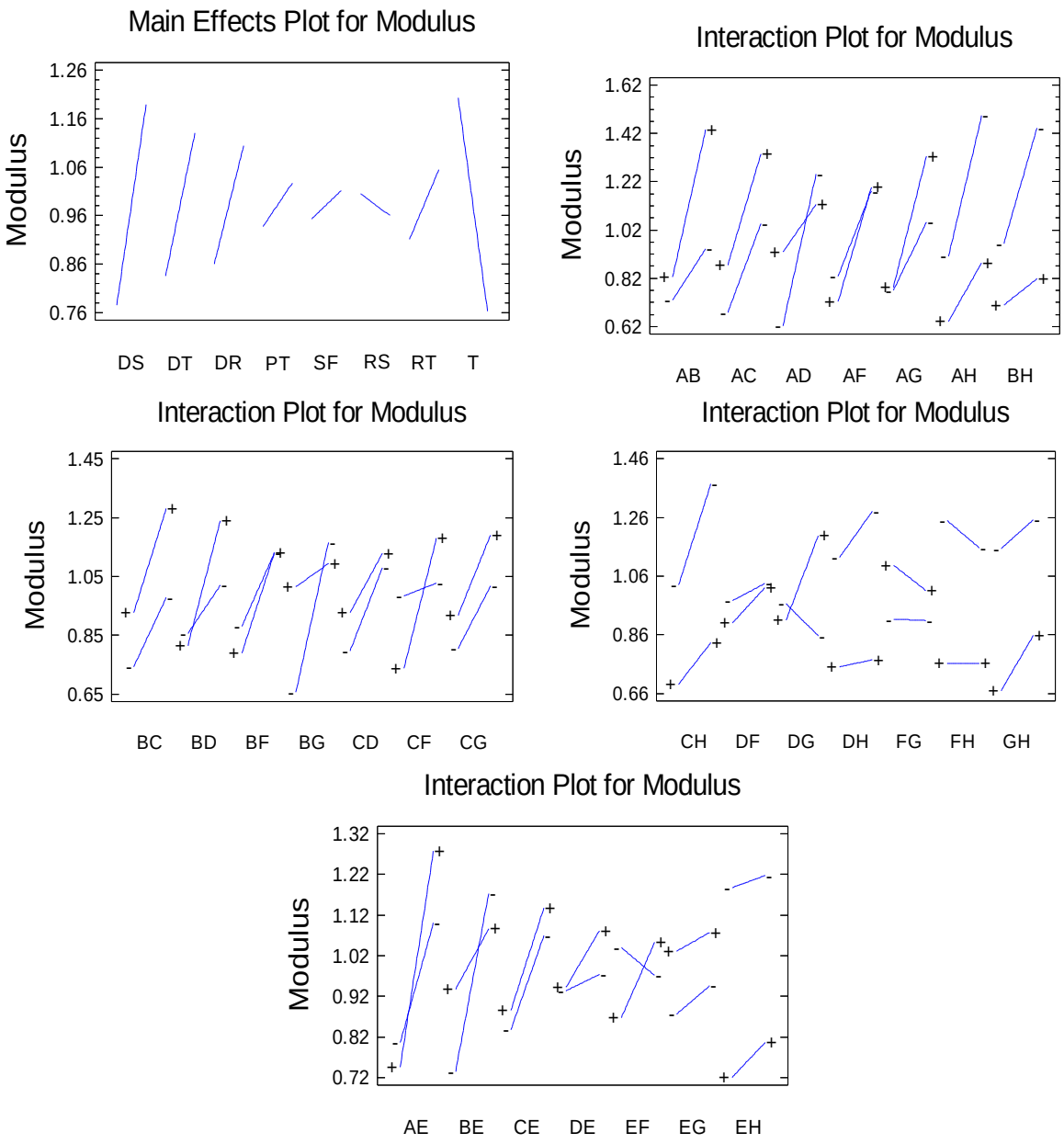

Figure 6.47. Main effect plots and Interaction plots for the modulus

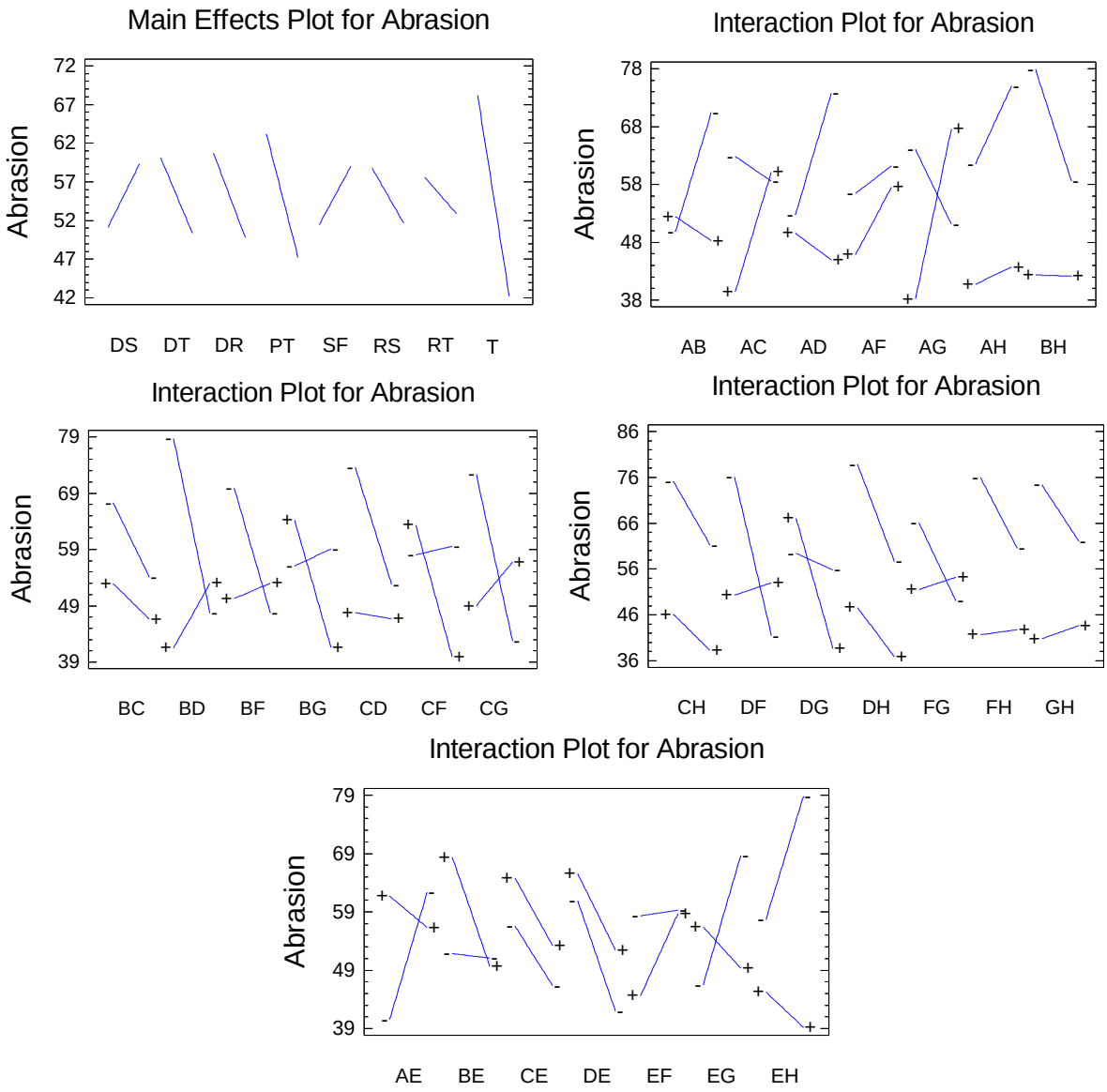

Figure 6.48. Main effect plots and Interaction plots for the abrasion

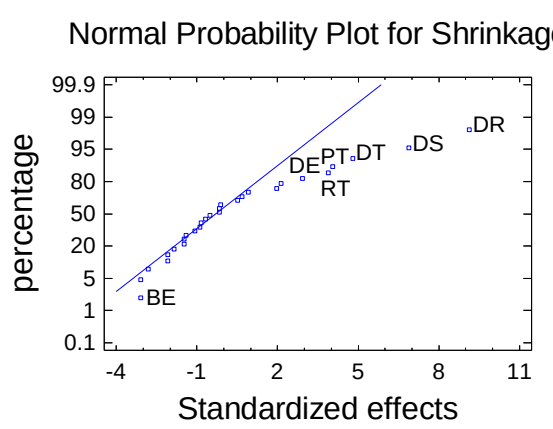

Thermal shrinkage (a)

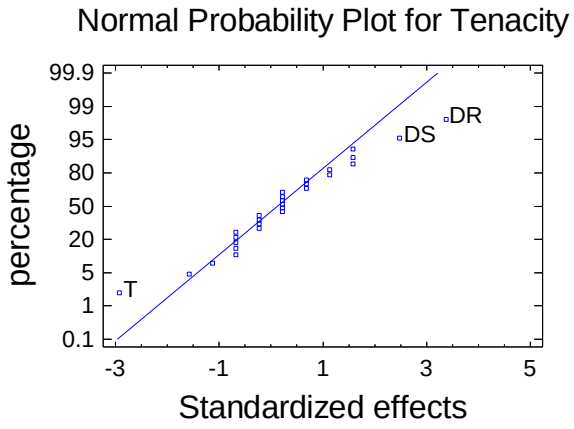

Tenacity (b)

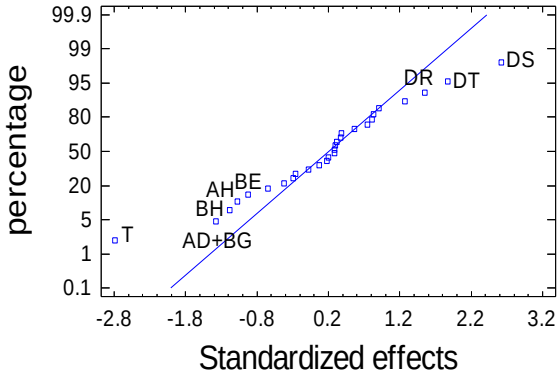

Elongation at break (c)

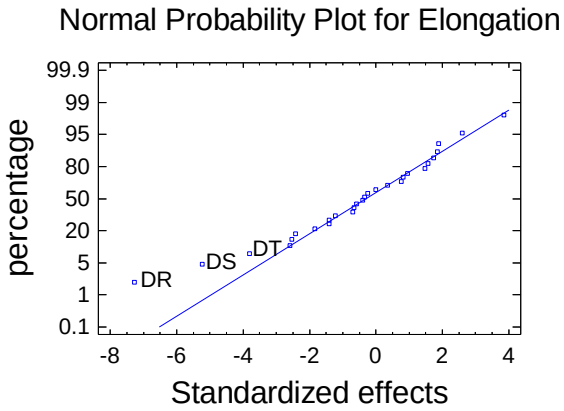

Modulus (d)

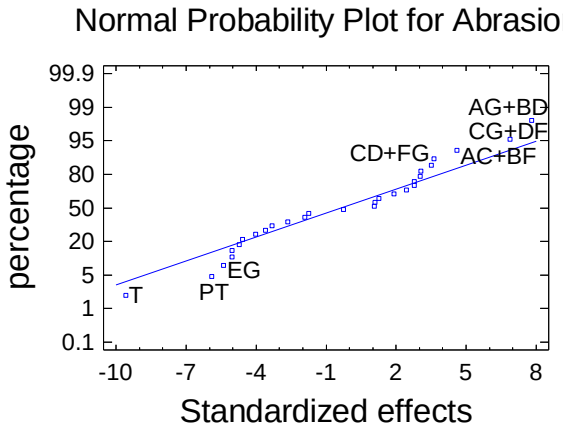

Abrasion (e)

Figure 6.49 Statistical standardized and percentage order values of factors and their interactions for thermal shrinkage (a), tenacity (b), elongation at break (c), modulus (d) and abrasion (e) (Normal Probability Plot).

6.8.2.1 Analysis of Variance (ANOVA)

In order to determine the factor effects in terms of statistical significance, an analysis of variance (ANOVA) of the data obtained was carried out (Table 6.15). Drawing ratio had a significant effect on tenacity, elongation at break, thermal shrinkage and abrasion. Draw temperature had a significant effect on elongation at break, thermal shrinkage and abrasion. Draw stage had a significant effect on elongation at break and thermal shrinkage. The effect of the number of drawing stages is on the borderline of significance for abrasion.

Draw ratio had a significant effect on thermal shrinkage, tenacity, elongation at break and abrasion. Plate temperature had significant effect on thermal shrinkage and abrasion. Relaxing temperature had significant effect on thermal shrinkage as it helped in releasing the internal stress. Twist level had significant effect on elongation at break and also on tension and abrasion. There were significant interactions between spin finish and total number of drawing stages, drawing temperature, relaxing temperature or twist level which significantly affected abrasion. The interaction between draw temperature and spin finish application effect on thermal shrinkage was on the borderline of significance. Other interactions include the significant effects of their factors on abrasion; their estimated response surfaces were investigated.

The geometric result of plotting a response variable is as a function of two factors and the interaction appears with the surface twist. The estimated response surface was based on the assumed regression models. The estimated response surfaces of abrasion were used to determine the direction and the significance of the interactions, as shown in Figure 6.50.

In order to determine the direction of the interactions DS&DT, DR&RS, PT&RT, DS&DR and DT&RS; the geometric result of plotting a response variable was required. There was a twist which confirms the interactions DS&DT and DS&DR only. As the surface was flat with no twist found on the surface represented, the determined effects of interactions DR&RS, PT&RT and DT&RS are not significant on abrasion which corresponds with the previous statistical analysis results of the interaction plot and ANOVA derived from the experimental data. Using the same technique, there were significant interactions from DS&PT, DR&SF, DS&RT, DT&SF, DT&T, DR&PT, DR&RT, SF&RT and SF&T which significantly affected the abrasion, as twist was found in the surface. There was no twist in the estimated response surfaces for the other insignificant interactions.

Source	P-Value				
	Thermal Shrinkage	Tenacity	Elongation at break	Modulus	Abrasion
DS	0.0063	0.0892	0.0135	0.0785	0.0561
DT	0.0173	0.2126	0.0317	0.1580	0.0367
DR	0.0028	0.0430	0.0054	0.2199	0.0276
PT	0.0270	0.5472	0.0943	0.6096	0.0098
SF	0.5474	0.2126	0.7148	0.7362	0.0686
RS	0.1284	0.8361	0.2153	0.7906	0.0777
RT	0.0302	0.5472	0.1623	0.4299	0.1811
T	0.1599	0.0609	0.0310	0.0682	0.0024
DS&DT DR&RS PT&RT	0.6470	0.8361	0.3091	0.2944	0.0196
DS&DR DT&RS	0.4338	0.5472	0.0816	0.7906	0.0192
DS&PT DT&RT	0.0669	0.5472	0.5013	0.2639	0.0178
DS&SF	0.5474	0.2126	0.4764	0.5072	0.0152
DS&RS DT&DR	0.0533	0.8361	0.2511	0.7309	0.2951
DS&RT DT&PT	0.6470	0.8361	0.5360	0.4672	0.0044
DS&T	0.1284	0.3416	0.1623	0.3604	0.1500
DT&SF	0.0533	0.8361	0.4083	0.4228	0.0450
DT&T	0.2392	0.8361	0.1546	0.3230	0.0388
DR&PT RS&RT	0.2392	0.5472	0.0805	0.8129	0.0362
DR&SF	0.4338	0.3416	0.7477	0.9504	0.8082
DR&RT PT&RS	0.3629	0.3416	0.2386	0.8581	0.0063
DR&T	0.4601	0.8361	0.6012	0.5633	0.3537
PT&SF	0.0610	0.5472	0.0852	0.7741	0.3624
PT&T	0.8765	0.5472	0.8158	0.7046	0.1514
SF&RS	0.2537	0.2126	0.1791	0.4789	0.0928
SF&RT	0.1432	0.8361	0.2555	0.9446	0.0125
SF&T	0.8765	0.8361	0.9938	0.8695	0.0152
RS&T	0.9174	0.8361	0.7589	0.7851	0.0551
RT&T	0.1217	0.5472	0.5543	0.7906	0.0689

Table 6.15 ANOVA results identifying the statistical significance of factor effects on the results from analysis of variance (ANOVA) of the data identifying the statistical significance of each factor for thermal shrinkage, tenacity, elongation at break, modulus and abrasion.

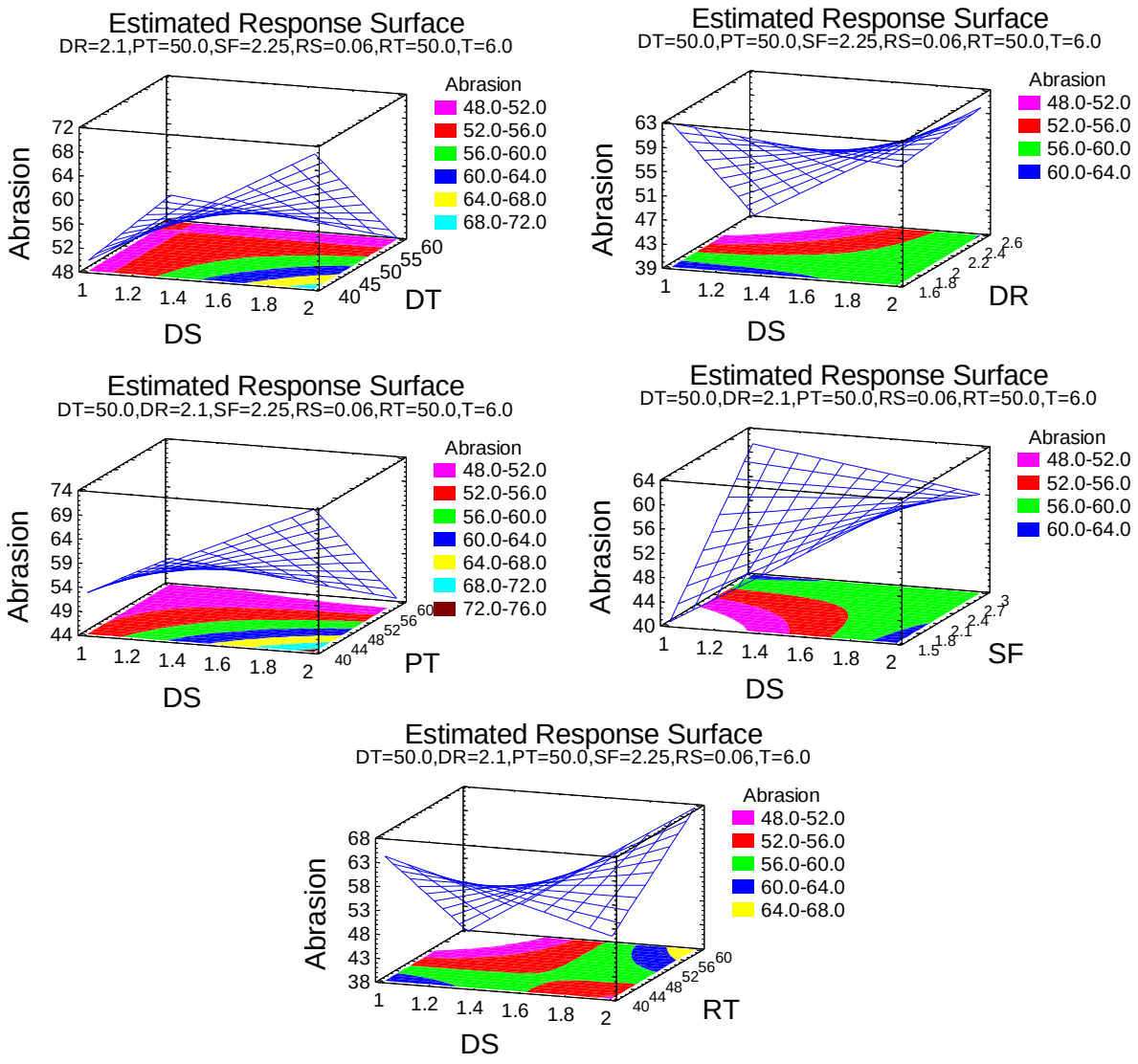

Figure 6.50 (a). The Estimated response surface for the interactions for the abrasion

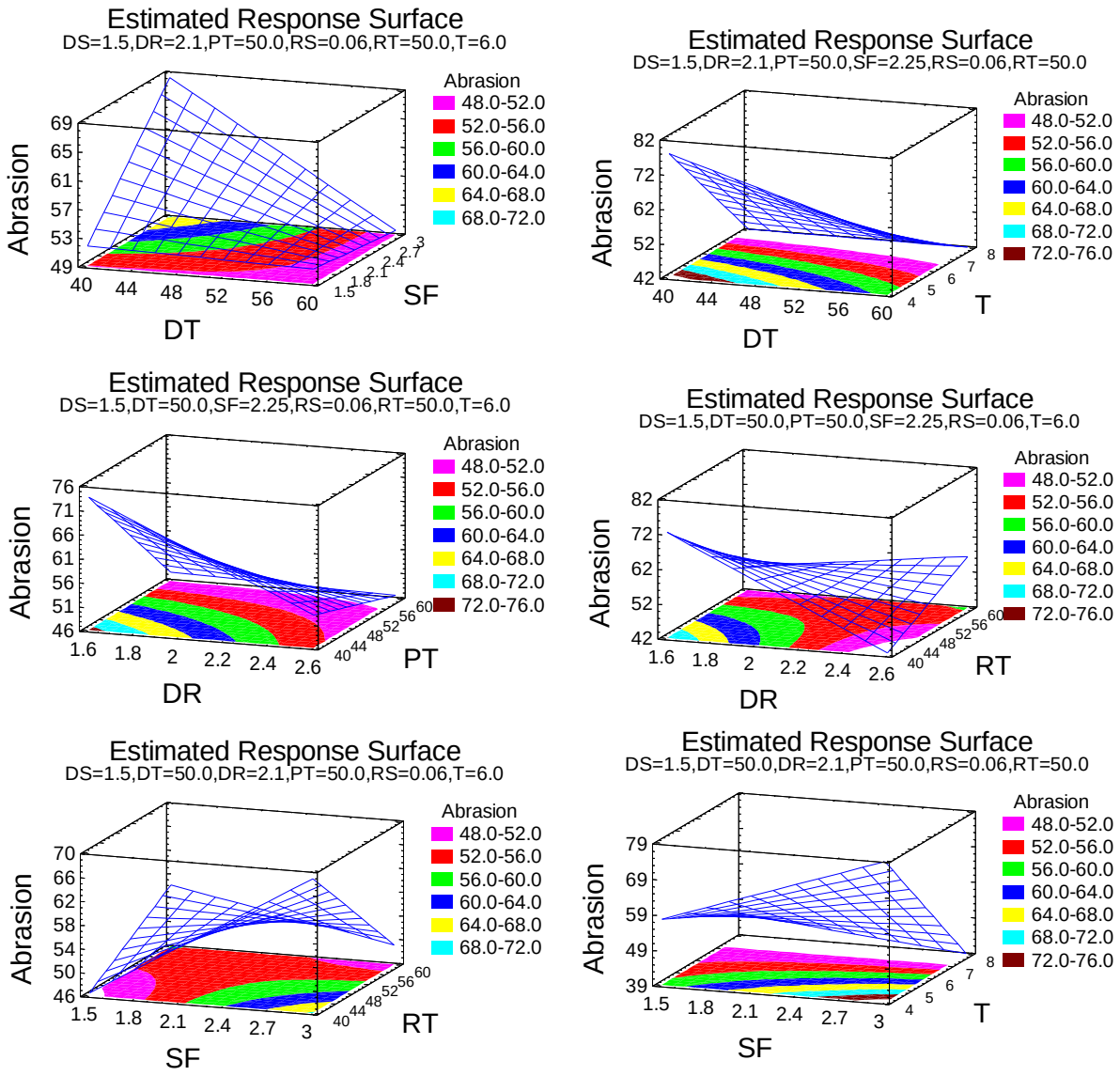

Figure 6.50 (b). The Estimated response surface for the interactions for the abrasion

6.8.2.2 The regression Equation and Estimation Results

Based on the analysis of the fraction factorial experimental design results, simplified models based on statistical analysis for studied factors and their interactions were fitted by the regression equations for thermal shrinkage, tenacity, elongation at break, modulus and abrasion. The regression equations in terms of the previous coded values (Table 6.9) are given as follows:

Thermal shrinkage = -20.1713 + 9.39*DS + 0.188125*DT + 5.4*DR + 0.115125*PT - 0.793333*SF + 65.3125*RS - 0.027*RT + 0.346875*T + 0.01125*DS*DT - 0.4*DS*DR - 0.0625*DS*PT - 0.2*DS*SF - 34.375*DS*RS - 0.01125*DS*RT - 0.23125*DS*T - 0.0458333*DT*SF - 0.008125*DT*T - 0.0325*DR*PT + 0.266667*DR*SF - 0.02375*DR*RT - 0.09375*DR*T + 0.0433333*PT*SF - 0.0009375*PT*T - 10.4167*SF*RS + 0.0291667*SF*RT - 0.0125*SF*T - 0.3125*RS*T + 0.011875*RT*T (6.16)

Tenacity = 0.680625 - 0.065*DS + 0.00125*DT + 0.1625*DR + 0.0076875*PT - 0.125*SF - 4.375*RS - 0.0028125*RT - 0.01125*T + 0.000625*DS*DT - 0.0375*DS*DR - 0.001875*DS*PT + 0.0583333*DS*SF + 0.3125*DS*RS + 0.000625*DS*RT + 0.015625*DS*T - 0.000416667*DT*SF + 0.00015625*DT*T - 0.001875*DR*PT - 0.0416667*DR*SF + 0.003125*DR*RT + 0.003125*DR*T + 0.00125*PT*SF - 0.00046875*PT*T + 1.45833*SF*RS - 0.000416667*SF*RT - 0.00208333*SF*T + 0.078125*RS*T - 0.00046875*RT*T (6.17)

Elongation at break = 360.396 + 39.0095*DS - 2.21256*DT - 97.4037*DR - 1.84427*PT + 18.124*SF + 202.156*RS + 0.0712438*RT - 3.92531*T - 0.620812*DS*DT - 26.2513*DS*DR + 0.387437*DS*PT + 5.50083*DS*SF - 360.469*DS*RS - 0.354187*DS*RT + 4.68719*DS*T + 0.324958*DT*SF + 0.240641*DT*T + 1.32081*DR*PT + 2.38917*DR*SF + 0.745688*DR*RT - 1.47969*DR*T - 0.858375*PT*SF - 0.0322969*PT*T + 295.854*SF*RS - 0.474958*SF*RT - 0.014375*SF*T - 21.3516*RS*T - 0.0843281*RT*T (6.18)

Modulus = -1.76706 - 0.37475*DS + 0.0345*DT + 0.43*DR + 0.0477812*PT - 0.176833*SF - 18.625*RS - 0.0239312*RT + 0.324938*T + 0.0199375*DS*DT + 0.09125*DS*DR - 0.0215625*DS*PT + 0.1575*DS*SF + 2.96875*DS*RS + 0.0130625*DS*RT - 0.0846875*DS*T - 0.00970833*DT*SF - 0.00464063*DT*T - 0.0040625*DR*PT + 0.0141667*DR*SF + 0.0030625*DR*RT - 0.0509375*DR*T + 0.00329167*PT*SF - 0.00164063*PT*T + 4.22917*SF*RS - 0.000791667*SF*RT + 0.009375*SF*T + 0.585937*RS*T + 0.00114062*RT*T (6.19)

Abrasion = 490.102 + 22.18*DS + 1.29*DT - 197.612*DR - 2.14944*PT + 117.483*SF - 1553.75*RS - 6.27169*RT - 29.5781*T - 1.24063*DS*DT + 25.0125*DS*DR - 1.28438*DS*PT - 18.175*DS*SF + 171.562*DS*RS + 2.12062*DS*RT - 2.60938*DS*T - 0.600417*DT*SF + 0.238906*DT*T + 0.981875*DR*PT - 0.958333*DR*SF + 1.86687*DR*RT + 1.48437*DR*T + 0.19375*PT*SF + 0.129844*PT*T + 220.208*SF*RS - 0.97625*SF*RT - 4.53958*SF*T + 103.672*RS*T + 0.188594*RT*T (6.20)

Figure 6.51 shows the experimental observed results and calculated fitted results plot for thermal shrinkage (a), tenacity (b), elongation at break (c), modulus (d) and abrasion (e). The pattern of estimated responses was based on the assumed model derived from the experimental observations. Their Model Standard Error (MSE) values listed in Table 6.16 indicate the dispersion of predicted and observed values around the theoretical fitted line generated using the fitted model for each trial.

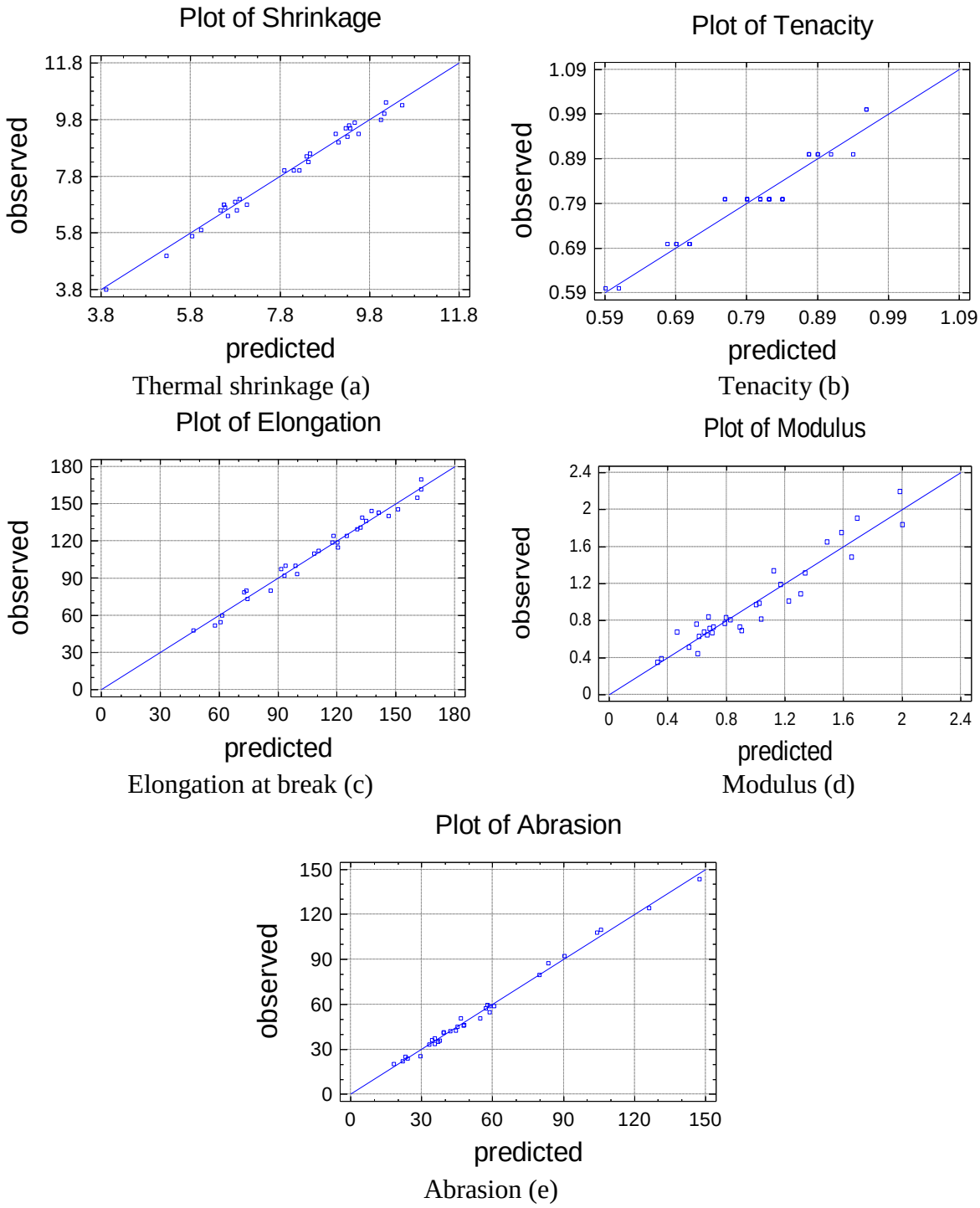

Figure 6.51 Experimental observed results and calculated fitted results plot for thermal shrinkage (a), tenacity (b), elongation at break (c), modulus (d) and abrasion (e).

6.8.3 Conclusion and Statistical Model for Optimisation

The main goal from drawing optimization was to model the drawing and twisting processes with regard to the processing conditions and the structure and properties of the twisted fibres. As-spun, biodegradable, branched aliphatic-aromatic co-polyester fibres were drawn at different multi-stage hot drawing conditions, then twisted. The statistical models covered the number of drawing stages, drawing temperature, total drawing ratio, plate temperature, spin finish application, relaxing stage ratio, relaxing temperature, twist level and their interactions.

Response	MSE	Optimum model	The combination of factor levels (↓: Low Level, ↑: High Level)							
			DS	DT	DR	PT	SF	RS	RT	T
Tenacity (g/den)	0.017	Maximum	↑	↑	↑	↓	↓	↓	↑	↓
		Minimum	↓	↓	↓	↓	↑	↓	↑	↑
Elongation at break (%)	5.875	Maximum	↓	↓	↓	↓	↑	↑	↓	↑
		Minimum	↑	↑	↑	↓	↓	↑	↓	↓
Modulus (g/den)	0.084	Maximum	↑	↑	↑	↓	↑	↑	↑	↓
		Minimum	↓	↑	↓	↓	↑	↓	↓	↑
Thermal Shrinkage (%)	0.318	Maximum	↑	↑	↑	↑	↑	↓	↑	↓
		Minimum	↓	↓	↓	↓	↑	↑	↓	↓
Abrasion (number of rubs)	5.49	Maximum	↓	↓	↓	↓	↑	↓	↓	↓
		Minimum	↓	↓	↑	↓	↓	↑	↓	↑

Table 6.16 The combinations of factor levels for the effect of multi-stage hot drawing on the properties of BAAC fibres for thermal shrinkage, tenacity, elongation at break, modulus and abrasion. (MSE: Model Standard Error)

Statistical models specified the combinations of their levels for enhancing properties. Draw ratio, drawing temperature and the number of drawing stages had a positive effect on thermal shrinkage, tenacity and modulus and a negative effect on elongation at break; draw stage had a positive effect on abrasion, affected negatively by the drawing ratio. With one stage drawing processes, the tension will be very high and the spin finish plays an important role in the filament slippage on the last roller after applied spin finish. Twist negatively affects modulus and abrasion. Plate temperature, relaxing temperature and the interactions DT&SF and PT&SF were prominent and had a positive effect on thermal shrinkage. Other factors and interactions had their effects but they were limited and less significant as it was covered by

the governing factors, drawing ratio and temperature. In the optimization of thermal shrinkage, tenacity, elongation at break and modulus, Table 6.16 shows the combination of factor levels which maximize and minimize the responses over the region indicated, in addition to their MSE values. The models will help processing scientists and technologists in industry to obtain the enhanced properties at suitable conditions related to final product cost, and to obtain environmentally friendly, economical and energy saving fibres. The achieved models could play a part in a forecasting program designed to optimize the drawing process of selected as-spun fibres. AAC fibres could be used in agricultural, horticultural and other non-traditional textile applications.

6.9 General Conclusion

In this chapter, modelling of the effects of multi-stage hot drawing and twist processes' conditions on thermal and physical properties of linear (LAAC) and branched (BAAC) aliphatic-aromatic co-polyester fibres was statistically investigated and characterized. The additional effect gained from adding twisting to the continuous drawn filament was investigated in terms of the interaction processes. A statistical experimental design was used as a function of process parameters using statistical factorial methods. As a two-level experiment, factor effects and interaction effects could be determined as the difference between the average responses at the low and the high level of hot drawing process parameters. The statistical models covered the number of drawing stages, drawing temperature, total drawing ratio, plate temperature, spin finish application, relaxing stage ratio, relaxing temperature, twisting level and their interactions. In terms of hot drawing processes, fibres could have improved mechanical properties after hot drawing. Adding the annealing effect (the hot relaxation) after hot drawing forms an additional, continuous step for the hot drawing process; which decrease the internal stress and improve the internal structure. This step will affect the contemporary fast process and could add heat shock to the internal structure, if it is applied at high temperature and over a short time. Some applications need special mechanical properties without additional treatment processes. In such cases, the hot drawing process could be an economical process to obtain the fibres which have the high stability of AAC fibres when it is connected to the relaxing stage. Aliphatic aromatic copolyesters' filament, single and simple yarns are assemblies of continuous filament. When

filaments are twisted together, each individual filament runs through the entire length of flat yarn (not texturized). AAC continuous filament yarns could be texturized, in order to produce fabrics with spun-yarn aesthetics. A general conclusion could be summarized as follows:

1. **When as-spun, biodegradable, linear aliphatic-aromatic co-polyester fibres are hot drawn**: Draw ratio has a positive effect, but draw temperature and plate temperature have an important negative effect on the birefringence. The negative effects from the interaction between draw stage and spin finish were less prominent and could be related to the practical relationship between the tension and the oily roller surface on the second roller in the relaxing stage which caused some slippage. In the normal probability plot for FWHM, the positive effects from the number of drawing stages, the interactions (DS&DR and DT&RS) and the interaction (SF&RS) were prominent. Spin finish application and relaxing temperature had negative effects on FWHM. The positive effects from the number of drawing stages, the interactions (DS&DT, DR&RS and PT&RT) were prominent. Drawing temperature, relaxing stage ratio and the interactions (DS&DR and DT&RS) had a negative effect on thermal shrinkage. In terms of mechanical properties, draw ratio had a negative effect on elongation at break and a positive effect on tenacity and modulus. Draw temperature had either a positive effect on elongation at break or a negative effect on tenacity and modulus; that could be connected to the results of the overall orientation presented previously.

2. **When as-spun, biodegradable, branched aliphatic-aromatic co-polyester fibres are hot drawn**: Draw ratio, draw temperature, plate temperature and draw stage had a positive effect on thermal shrinkage, tenacity and modulus and a negative effect on elongation at break. Relaxing stage ratio had a positive effect on elongation at break and a negative effect on thermal shrinkage and modulus; relaxing stage ratio had a small effect on tenacity. The interactions DT&DR and DS&RS had a clear effect on thermal shrinkage. The interactions (DS&DT, DR&RS and PT&RT) were prominent and had a positive effect on tenacity.

3. **For further investigation and by comparing of the analysed results of hot drawing process of the LAAC and BAAC as-spun, Table 6.17** summarizes points 1 and 2 and makes it easy to identify the differences which could be raised, depending on polymer grade (linear or branched). When the higher draw ratio was applied with one-drawing stages, the time of contact of the filaments with the second roller surface was decreased,

leading to a difference in the softening ratio from those of other conditions. The high drawing temperature made the chains more mobile and flexible, which reduced the internal stress, see Table 6.17. The relaxing stage helps the fibre chain to relax and stabilize. The higher draw ratio led to a higher degree of molecular orientation and higher fibre tenacity with lower extensibility and thus the fibre could be stiffer. A low relaxing ratio will give less opportunity for loss of heat before filaments go to the winder, which will add another effect of relaxing process time. The relaxation ratio could increase slightly because of the increase in relaxation temperature because the fibre will be more flexible. Drawing temperature affects the occurred crystallization because of its influence on the number of nuclei present; it helps in improving the internal structure and chain mobility.

Source	Thermal Shrinkage		Tenacity		Elongation at break		Modulus	
	LAAC	BAAC	LAAC	BAAC	LAAC	BAAC	LAAC	BAAC
DS	▲	▲	—	▲	—	▲	—	▲
DT	▲	▲	—	▲	▲	▲	▲	▲
DR	—	▲	▲	▲	▲	▲	▲	▲
PT	▲	▲	—	—	—	—	—	▲
SF	—	—	—	—	—	—	—	—
RS	▲	▲	—	—	—	▲	—	▲
RT	—	▲	—	—	—	—	—	—
DS&DT	▲	—	—	—	—	—	—	—
DS&DR	▲	—	—	—	—	—	—	—
DS&PT	—	—	—	—	—	—	—	▲
DS&RS	—	▲	—	—	—	—	—	—
DS&RT	—	▲	—	—	—	—	—	—
DR&RT	—	—	—	—	—	—	—	▲

Table 6.17 The combinations of the factor effect of multi-stage hot drawing on the properties of AACs fibres (▲: Significant, —: Not Significant)

4. **When drawn, biodegradable, linear aliphatic-aromatic co-polyester fibres are twisted:** Draw ratio had a positive effect on tenacity and modulus and a negative effect on thermal shrinkage, elongation at break and abrasion. Twist level had a positive effect on elongation at break. Draw stage had a positive effect on thermal shrinkage. The interactions (DS&DT, DR&RS and PT&RT) were prominent and had a positive effect on thermal shrinkage and abrasion. The interactions DS&DR and DT&RS had a positive effect on

abrasion and a negative effect on thermal shrinkage. From Table 6.18, it can be seen that applying twist does not affect significantly thermal shrinkage itself as found in the previous results. By connecting the twist process to the drawing process, the effects of plate temperature, relaxing stage ratio, the interaction between the number of drawing stages and both of drawing ratio and drawing temperature on thermal shrinkage were decreased. Applying twist did not have a significant effect on the factors' significance on tenacity. Adding twist to the drawn fibres decreases the effect of the roller temperature of drawing process on elongation at break; the fibres with higher twist will have additional extension ratio than the untwisted fibres. By connecting the twist process to the drawing process, the effect of the interaction between the number of drawing stages and both of drawing ratio and drawing temperature effects on modulus was decreased. All the factors had a significant effect on modulus, which varied depending on other factor conditions; twist helps fibres to support each other and increase the friction between the fibres.

Source	Thermal Shrinkage		Tenacity		Elongation at break		Modulus	
	D	T	D	T	D	T	D	T
DS	▲	▲	—	—	—	—	—	▲
DT	▲	▲	—	—	▲	—	▲	▲
DR	—	—	▲	▲	▲	▲	▲	▲
PT	▲	—	—	—	—	—	—	▲
SF	—	—	—	—	—	—	—	▲
RS	▲	—	—	—	—	—	—	▲
RT	—	—	—	—	—	—	—	▲
T	/	—	/	—	/	—	/	▲
DS&DT	▲	—	—	—	—	—	▲	—
DS&DR	▲	—	—	—	—	—	▲	—

Table 6.18 The combinations of the effect of multi-stage hot drawing factors before and after applying twist on the properties of LAAC fibres (▲: Significant, —: Not Significant, /: Not applied, **D**: drawing only, **T**: drawing and twisting)

5. **When drawn, biodegradable, branched aliphatic-aromatic co-polyester fibres are twisted:** Draw ratio, drawing temperature and the number of drawing stages had a positive effect on thermal shrinkage, tenacity and modulus and a negative effect on elongation at break; the draw stage had a negative effect on abrasion positively affected by the drawing ratio. With one stage drawing processes, the tension will be very high and the spin finish plays an important role in the filament slippage on the last roller after applied spin finish. Twist affected negatively on modulus and positively on abrasion. Plate

temperature, relaxing temperature and the interactions (DT&SF and PT&SF) were prominent and had a positive effect on thermal shrinkage. From Table 6.19, it can be seen that applying twist did not have a significant effect on thermal shrinkage itself.

Source	Thermal Shrinkage		Tenacity		Elongation at break		Modulus	
	D	T	D	T	D	T	D	T
DS	▲	▲	▲	—	▲	▲	▲	—
DT	▲	▲	▲	—	▲	▲	▲	—
DR	▲	▲	▲	▲	▲	▲	▲	—
PT	▲	▲	—	—	—	—	▲	—
SF	—	—	—	—	—	—	—	—
RS	▲	—	—	—	▲	—	▲	—
RT	▲	▲	—	—	—	—	—	—
T	/	—	/	—	/	—	/	▲
DS&PT	—	—	—	—	—	—	▲	—
DS&RS	▲	—	—	—	—	—	—	—
DS&RT	▲	—	—	—	—	—	—	—
DR&RT	—	—	—	—	—	—	▲	—

Table 6.19 The combinations of the effect of multi-stage hot drawing factors before and after applying twist on the properties of BAAC fibres (▲: Significant, —: Not Significant, /: Not applied, **D**: drawing only, **T**: drawing and twisting)

6. By connecting the twist process to the drawing process, the effects of relaxing stage ratio, the interaction between the number of drawing stages and both the relaxing stage ratio and relaxing temperature effects on thermal shrinkage were minimized. That could be related to increasing the friction between the fibres and the effect added to the twisted yarn structure and properties. Applying twist does not have a significant effect on the factors' significance on tenacity. Twist eliminated the effect of the roller temperature and the number of drawing stages of drawing process on tenacity. Twist eliminated the effect of the relaxing stage ratio of drawing process on elongation at break. By connecting the twist process to the drawing process, the effect of the twist level overcame all other factors and the effect of their interactions on modulus; which increase the friction between the fibres and improve the yarn strength.

For further investigation and by comparing the results of applying twist to both LAAC and BAAC drawn fibres in Table 6.20, it could be concluded that there is a recognized effect of the number of drawing stages and drawing temperature on thermal shrinkage of LAAC and BAAC twisted fibres. According to the analyses, other factors and interactions had less effects as they were covered by the influencing factors.

Source	Thermal Shrinkage		Tenacity		Elongation at break		Modulus		Abrasion	
	LAAC	BAAC	LAAC	BAAC	LAAC	BAAC	LAAC	BAAC	LAAC	BAAC
DS	▲	▲	—	—	—	▲	▲	—	—	—
DT	▲	▲	—	—	—	▲	▲	—	—	▲
DR	—	▲	▲	▲	▲	▲	▲	—	—	▲
PT	—	▲	—	—	—	—	▲	—	—	▲
SF	—	—	—	—	—	—	▲	—	—	—
RS	—	—	—	—	—	—	▲	—	—	—
RT	—	▲	—	—	—	—	▲	—	—	—
T	—	—	—	—	—	—	▲	▲	—	▲
DS&DT	▲	—	—	—	—	—	▲	—	▲	▲
DS&DR	▲	—	—	—	—	—	▲	—	▲	▲
DS&PT	—	—	—	—	—	—	—	—	—	▲
DS&SF	—	—	—	—	—	—	—	—	▲	▲
DS&RT	—	—	—	—	—	—	▲	—	—	▲
DT&SF	—	—	—	—	—	—	▲	—	—	▲
DT&T	—	—	—	—	—	—	—	—	—	▲
DR&PT	—	—	—	—	—	—	▲	—	—	▲
DR&SF	—	—	—	—	—	—	▲	—	▲	—
DR&RT	—	—	—	—	—	—	▲	—	—	▲
SF&RT	—	—	—	—	—	—	▲	—	—	▲
SF&T	—	—	—	—	—	—	▲	—	—	▲
RS&T	—	—	—	—	—	—	—	—	▲	—

Table 6.20 The combinations of the factor effect of multi-stage hot drawing and twisting on the properties of AACs fibres (▲: Significant, —: Not Significant)

The interaction between the number of drawing stages and drawing temperature and the interaction between the number of drawing stages and drawing ratio had a significant effect on thermal shrinkage of LAAC twisted fibres. Drawing ratio, plate temperature and relaxing temperature had a significant effect on thermal shrinkage of BAAC twisted fibres. Drawing ratio had a significant effect on tenacity and elongation at break of both LAAC and BAAC twisted fibres. There was a recognized effect of the number of drawing stages and drawing temperature on elongation at break of BAAC twisted fibres. Alternatively, the significant effect of twist level number of twisted BAAC fibres overcame the effect of other factors on modulus. The interactions (DS&DT, DS&DR and DS&SF) had a significant effect on abrasion of LAAC and BAAC twisted fibres. The interactions (DR&SF and RS&T) had a significant effect on abrasion of LAAC twisted fibres. Abrasion of BAAC twisted fibres was significantly affected by drawing temperature, plate temperature, drawing ratio, twist level and the interactions (DS&PT, DS&RT, DT&SF, DT&T, DR&PT, DR&RT, SF&RT and

SF&T). Abrasion-resistance as a fibre property gave an idea about the wear in the actual fibre use. The increase of twist increased the cohesion between the fibres, surface contact and the stiffness of yarn which might have reduced abrasion resistance. This is in agreement with the literature as the high twist level does not allow the yarn to flatten or distort under pressure when being abraded [172]. Drawing and adding twist to yarn could cause deformation of the fibres resulting in the change of yarn cross section and friction among fibres in the yarn. Thoretically, fibres in the centre could deform into a polygonal shape under tension.

The interaction between draw stage and spin finish could be related to the practical relationship between the tension and the oily roller surface on the last roller in the relaxing stage; the high tension could cause some slippage. Drawing tension is a function of drawing; the stability of the process is affected by a reduction of drawing temperature or an increase of drawing ratio. The actual draw ratio was less than the nominal draw ratio because the draw line shrank when tension was removed; yarn should not slip during drawing under high tension (high draw ratio). In one stage drawing experiments and in addition to the spin finish applied to the as-spun fibres during extrusion process, the tension will be very high and the spin finish plays a central role in the filament slippage on the last roller after applied spin finish. A variation in the result could come from either assignable causes that represent variation caused by changes in the independent factors, or random causes that signify uncontrolled variation. The optimization of thermal shrinkage, tenacity, elongation at break and modulus showed the combination of factor levels which maximized and minimized the responses over the indicated region.

The achieved models could form a source code in a forecasting program designed to optimize the drawing process of selected as-spun fibres, see **section 5.9**. Results and statistical analysis indicated a combination of factor levels which controlled the production processes of environmentally friendly, biodegradable fibre. The achieved models specified the combinations of their levels for responses and will form a part in a forecasting program designed to optimize the drawing process of selected as-spun fibres, see Appendices **E** and **F**. The achieved mathematical models will help processing experimentalists and technologists in industry to obtain the enhanced properties at suitable conditions related to final product cost, and to obtain environmentally friendly, economical and energy saving fibres. AACs fibres, yarns and textiles could be used in agricultural, horticultural and more of non-traditional textile applications. Optimization allows the production of a range of different properties from the same sample to suit different purposes.

CHAPTER 7 - STATISTICAL MODELLING OF THE EFFECT OF COLD DRAWING AND TWISTING ON LINEAR AND BRANCHED ALIPHATIC-AROMATIC CO-POLYESTER FIBRES

7.1 Introduction

Textile scientists, researchers and commercial companies are striving to be important players in the race to manufacture environmentally friendly products, and to be in an advanced stage in the waste management of synthetic products. Some fibres could have excellent mechanical properties after cold drawing, which does not mean they will have the best structural properties required for further treatment processes. AACs are made from petroleum with stable physical and chemical properties, with comparable cost to the other thermoplastic polymers. Some applications need special mechanical properties without additional treatment processes; in such cases the cold drawing process could be an economical process to obtain the compatible fibres. The temperature affects the contemporary fast process and could add heat shock to the internal structure, if it is applied at high temperature and over a short time.

To separate the effect of temperature and the remaining factors in the hot drawing process, modelling of cold drawing is needed. As-spun fibres having been drawn unheated to eliminate the temperature effect and interactions. This chapter will study the real effects of the other factors which have significant effects on the fibres' properties. Modelling of the effects of multi-stage cold drawing and the conditions of twisting processes on thermal and physical properties of linear (LAAC) and branched (BAAC) aliphatic-aromatic co-polyester fibres were statistically investigated and characterized. Usually the relaxation zone is located before the winding of the fibres, where the fibres are allowed to relax to a predetermined degree or to a desired tension [199]. The relaxation stage after cold drawing forms an additional continuous step for the cold drawing process to add more economic aspects of the operation. In addition to adding an advantage to the thermal stability of the fibres, the relaxation stage, a kind of pre-shrinkage, is a method used to prevent fibre shrinkage in the fibre's final use. As the relaxation and annealing is a time-consuming process, multiple roller systems could prolong the travelling distance.

In this chapter, a fractional factorial statistical experimental design was used as a function of the process parameters, using statistical factorial methods. The aliphatic-aromatic co-

polyester fibres were spun, cold drawn, twisted, characterised and analysed using a fractional factorial design as a function of the process parameters using appropriate statistical methods to model the effects of the process parameters. As a two-level experiment, factor effects and interaction effects could be determined as the difference between the average responses at the low and high levels of the cold drawing process parameters. Two general lines were used in this chapter to produce multifilament, single and simple untwisted or twisted yarns: first, for untwisted yarns, modelling the effect of the multi-stage cold drawing process on the thermal and mechanical properties of both drawn linear (LAAC) and branched (BAAC) aliphatic-aromatic co-polyester fibres were statistically investigated and characterized; secondly, for twisted yarns, selected continuous drawn filaments were gently twisted. Modelling the effects of multi-stage cold drawing and twisting process conditions on the thermal and mechanical properties of drawn linear (LAAC) and branched (BAAC) aliphatic-aromatic co-polyester fibres were statistically analysed and characterized. The additional effect gained from adding twisting to the continuous drawn filament was investigated in terms of process interactions. Results and statistical analysis help to model a combination of factor levels which controls the production processes of environmentally friendly, biodegradable fibres. The combination of factor levels which maximize and minimize the responses over the indicated region is obtained. Useful results have been achieved and a new forecasting data source has been set for optimizing the drawing process.

7.2 Preparation of As-Spun AAC Fibres for Cold Drawing Without/With Twisting

The same sample of as-spun AACs fibres was extruded via melt-spinning using the Lab-Spin machine for cold drawing without / with twisting. For technical and experimental reasons, the spinning and multi-stage cold drawing processes of as-spun AAC fibres were operated individually. The specially designed spinneret of 30 holes was used. Temperature profile and spinning conditions were selected based on statistical experimental analysis and the results of the spinning study (Chapter 5). For LAAC fibres made of Solanyl flexibility component, the six heating zones in the extrusion machine profile were 115, 120, 125, 130, 140 and 140^{o}C. The metering pump was fixed at 12 rpm at pre pump pressure of 1000 psi. The air cooling quench speed percentage was set at 73%. The spin finish application speed was set at 0.3 rpm. The godets and the Leesona winder were set at a speed of 50 m min^{-1}. For BAAC fibres

made of Ecoflex, the six heating zones in the extrusion machine profile were 120, 125, 135, 140, 150 and 150^{o}C. The metering pump was fixed at 8 rpm at a pre pump pressure of 1000 psi. The air cooling quench speed percentage was set at 35%. The spin finish application speed was set at 0.3 rpm. Godets and the Leesona winder were set at a speed of 50 m min^{-1}. The godets and the Leesona winders were controlled independently by DC motors; all speeds were confirmed by the laser digital tachometer. The drawability value of the as-spun fibres played an important role in identifying the levels of the cold drawing parameters in the fraction factorial experimental design matrix. The as-spun fibres' drawability value played an important role in identifying of the levels of cold drawing parameters in the fraction factorial experimental design matrix. As-spun aliphatic-aromatic co-polyester (AACs) fibres were drawn under a full factorial design as a function of cold drawing conditions using appropriate experimental and statistical methods. The cold drawing conditions and properties of the fibres were characterized and statistically modelled; the regression model generated forms part of a forecasting program for environmentally friendly biodegradable fibre production. After results analysis, a forecasting model was achieved to optimize the cold drawing of as-spun linear aliphatic-aromatic co-polyester (AAC) fibres. Useful results have been achieved and a new forecasting model has been set for optimizing the drawing process. From the results and analysis, a combination of factor levels has been designed to control the forecasting process.

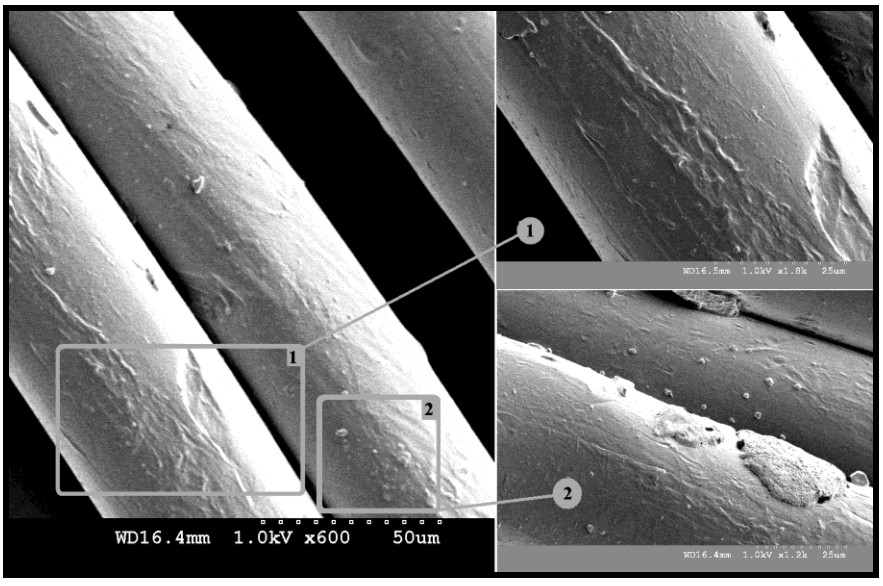

Figure 7.1 SEM photomicrograph of LAAC fibres' surface

With the higher level of draw ratio, there is positive clamping of the threadline around the pair of rollers. Some residues rarely were found on the fibre surface after processing (Figure 7.1); with a dirty roller or faulty guide, small marks could be found on the fibre surface as a result of high friction (1). Fibres in some parts could have an oily appearance and could be associated with the spin finish applied to the fibre (2), or they could be an exudate coming to the surface, indicating that the original structure is not a homogeneous mixture. That could happen, if there are solid particles or higher melting point material inside the mix which will not make a homogeneous mixture.

7.3 Experimental Design for Cold Drawing of Aliphatic-Aromatic Co-Polyester Fibres

To investigate the influence of cold-drawing process conditions on the structural and physical properties of LAAC and BAAC fibres, a fraction factorial experimental design (L32) with random order was used. Cold drawing was carried out on the ESL draw frame described in Chapter 3. The four control parameters for the cold drawing experiments were the number of drawing stages (DS), total drawing ratio (DR), spin finish (SF) and relaxing stage ratio between relaxation process rollers at 40 ^{o}C (RS), where speed of the second roller = RS * speed of the first roller. The total drawing ratio (DR = DR1*DR2=V2/V1 *V3/V2 = V3/V1) used in the optimization represents the ratio between the speed of the second roller (V3) of the second stage to the speed of the first roller of the first stage (V1 = 35 m min^{-1}). The speed of the second roller of the first stage equals the speed of the first roller of the second stage, V2. The draw ratio of first stage (DR1:V2/V1) is larger than that of the second stage (DR2:V3/V2); DR1 to DR2 ratio is 2 to 1. The relaxing stage helps with the fibre's deformability; it adds additional annealing actions to the drawn fibres before it is wound on the bobbin. The two levels of each parameter were separated as far apart as possible from one another. The factors are listed with their abbreviations in Table 7.1. Some time replication of the experiments was applied to delete the experiment error or the effect of a factor in the experiment by using the sample mean [127].

Factor abbreviation	Factor name	Level	
		Low L	High H
DS	Total number of drawing stages	1	2
DR	Total drawing ratio for LAAC	4.5	6
	Total drawing ratio for BAAC	1.6	2.6
SF	Spin finish application (rpm, 0.292 cc/rev)	1.5	3.0
RS	Relaxing stage ratio (4 %)	0: Without	1: With

Table 7.1 Factors and their levels for the cold drawing experiment.

Trial Number	The number of drawing stages DS	Drawing Ratio DR	Spin Finish SF	Relaxing stage ratio RS
1	H	H	H	L
2	H	H	H	H
3	H	H	L	H
4	L	H	H	H
5	L	H	H	L
6	L	H	L	H
7	H	H	H	L
8	H	L	L	L
9	L	L	H	H
10	L	L	L	L
11	L	L	H	L
12	H	L	H	L
13	L	H	H	H
14	H	H	L	L
15	L	L	H	L
16	H	L	L	H
17	L	H	L	L
18	L	L	L	H
19	L	H	L	L
20	L	L	L	L
21	L	L	H	H
22	H	H	H	H
23	H	L	L	H
24	L	H	H	L
25	H	H	L	L
26	L	H	L	H
27	H	L	L	L
28	H	H	L	H
29	L	L	L	H
30	H	L	H	H
31	H	L	H	L
32	H	L	H	H

Table 7.2 L32 Experimental design array and results for the multi-stage cold drawing experiment (L: Low, H: High)

As a function of cold-drawing conditions, a full factorial design was used for the thirty-two screening trials in one block, involving four control parameters and two levels for each parameter, as shown in Table 7.2, designed using the STATGRAPHICS program. The major tools of statistical analysis include Pareto charts, effects and interaction plots, Daniel's plots and Analysis of Variance. All statistical analysis and presented plots were constructed directly from the raw data using the computer software available. Determined factors would affect the tension and the internal stress would affect the structural and physical properties. The relationship between the annealing temperature and the temperature at which the crystals were grown and oriented affects the morphology of fibres; annealing under tension does not permit a large decrease of mechanical properties and gives dimensional stability, unless the temperature is too high [199]. In the relaxation process and when the relaxing stage ratio increases, the yarn speed decreases and the relaxation time increases. Drawing tension is a function of drawing; the stability of the process is affected by reduction or an increase of drawing ratio. Some variations could be related to the actual draw ratio which is less than the nominal draw ratio. In case of non-linear, viscoelastic behaviour and necking effects, the velocity is neither steady nor uniform and there is a kinematics problem of continuous drawing [159]. Orientation could be improved and molecules in the amorphous regions are extended [161].

7.4 Statistical Modelling of The Effect of Cold Drawing on Linear Aliphatic-Aromatic Co-Polyester Fibres (LAAC)

7.4.1 Experimental Results

The experiments were randomly conducted in one block according to the design shown in Table 7.2, involving four control factors and their levels, as listed in Table 7.1. The thermal shrinkage and mechanical properties for fibres were measured and the data listed in Table 7.3. The results were averaged for five measurements for each sample represented by the random order number in the first column in the designed matrix.

Each thermal shrinkage test was carried out using a MK IV Shrinkage-Force Tester; samples were heated for 2 minutes at 60^{o}C under a load cell of 10g, during thermal shrinkage testing.

DSC curves for two selected samples were produced with different cold drawing conditions for trials 4 and 5 (see Figure 7.2). According to the DSC results, the fibre does not melt completely below 120 °C, as an optimum temperature window was found, taking all factors into account. A broad range of melting temperature (about 100-135°C) was observed for the fibres. No appreciable changes of relative intensity of the peaks in the endotherm were observed in different samples for the same trial. No significant effect has been reported in their thermal properties but a notable effect has been reported in the mechanical properties.

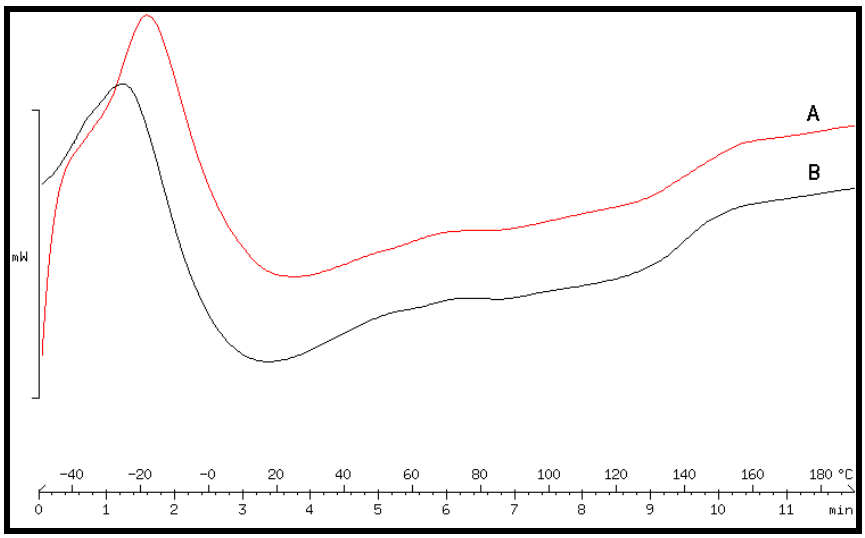

Figure 7.2 DSC curves of cold drawn LAAC fibres
(A: trial 5 and B: trial 4)

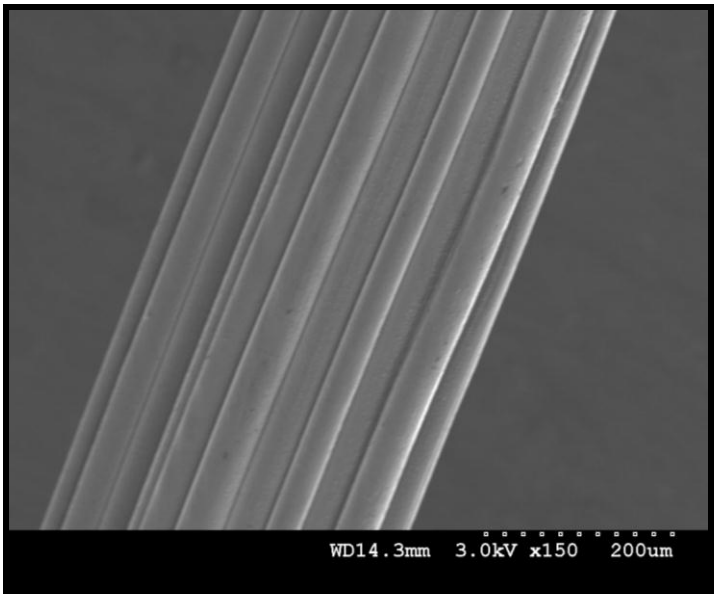

Figure 7.3 SEM photomicrograph of LAAC fibres' surface

Trial Number	Thermal shrinkage (%)	Tenacity (g/den)	Elongation at Break (%)	Modulus (g/den)
1	13.3	0.9	118.1	0.71
2	13.5	1.2	94.4	0.95
3	13.0	1.0	137.5	0.67
4	11.7	1.6	25.0	2.74
5	12.7	1.4	33.3	2.57
6	13.0	1.4	35.4	2.44
7	12.0	0.9	115.3	0.74
8	13.2	1.0	105.6	0.63
9	13.5	1.3	89.6	1.32
10	13.5	1.0	89.6	1.02
11	13.3	1.2	88.9	1.23
12	13.5	0.9	140.3	0.66
13	11.8	1.7	35.4	2.18
14	13.2	1.0	133.3	0.78
15	13.3	1.2	81.3	1.14
16	12.5	1.0	140.3	0.69
17	12.8	1.5	30.6	2.69
18	13.2	1.2	76.4	0.91
19	12.7	1.5	34.7	2.37
20	13.7	1.0	89.6	1.06
21	13.3	1.3	84.7	1.22
22	13.5	1.2	81.3	0.94
23	12.5	1.0	147.9	0.64
24	12.8	1.4	52.8	2.39
25	13.1	1.0	136.1	0.81
26	12.8	1.4	50.0	2.21
27	13.2	1.0	108.3	0.66
28	13.0	1.0	140.3	0.66
29	13.2	1.2	79.2	1.27
30	13.5	1.0	150.0	0.80
31	13.5	0.9	133.3	0.68
32	13.5	1.0	147.9	0.77

Table 7.3 Results for the cold drawing experiment (LAAC)

The mechanical properties will be better with the relaxation stage, as it helps in decreasing internal stress in the fibre. Results analysis helps in the evaluation of the effect between drawn fibre structure and the thermal shrinkage to enhance better fully drawn fibres in the practical stage. Figure 7.3 shows an SEM photomicrograph of the surface of the fibres; drawn fibres had a uniform circular cross section with acceptable uniform surface. The uniformity determines the fibre quality and could be affected in case of slippage or fibre on

the rollers under high tension. The data of the measured specimens have small standard deviations related to draw frame setting based variation, the tension or slippage on the drawing roles, or some tension while the preparation of the sample for testing. All statistical analysis and presented plots were constructed directly from the raw data using the computer software available.

7.4.2 Statistical Analysis and Discussion

The Pareto charts (Figure 7.4) for thermal shrinkage (a), tenacity (b), elongation at break at break (c) and modulus (d) show the significant arrangement of factors and their interactions in decreasing order. The Pareto chart for thermal shrinkage shows that the drawing ratio (DR), the interactions DS&DR, DS&SF and DR&SF, the number of drawing stages (DS) and relaxing stage ratio (RS) are the most important factors affecting the thermal shrinkage properties of the fibres, followed by other factors and interactions. In terms of mechanical properties of drawn LAAC fibres, the Pareto chart for tenacity shows that the total number of drawing stages, total drawing ratio, relaxing stage ratio, spin finish application and the interactions DS&DR, SF&RS and DS&SF are the most important factors affecting the tenacity, followed by other factors and interactions. The Pareto chart for elongation at break shows that the total number of drawing stages, total drawing ratio and the interactions DS&DR, DR&SF, SF&RS, DR&RS, DS&RS and DS&SF are the most important factors affecting the elongation at break, followed by other factors and interactions. The Pareto chart for modulus shows that the total number of drawing stages, total drawing ratio, spin finish application and the interactions DS&DR, SF&RS and DR&RS are the most important factors affecting the modulus, followed by other factors and interactions.

The relaxation stage could help the chains return to their random arrangement which depends on the total draw ratio and relaxing ratio. Alternatively, when a higher draw ratio is applied, the speed of the final roller will increase and the spin finish layer thickness on the fibres at constant spin finish pump speed will be affected. This could explain the interaction between the spin finish and the draw ratio or relaxing stage ratio. As the yarn speed decreases, the relaxing time increases and the thickness of the spin finish layer increases and this relationship could explain the interaction between other conditions and fibre structure.

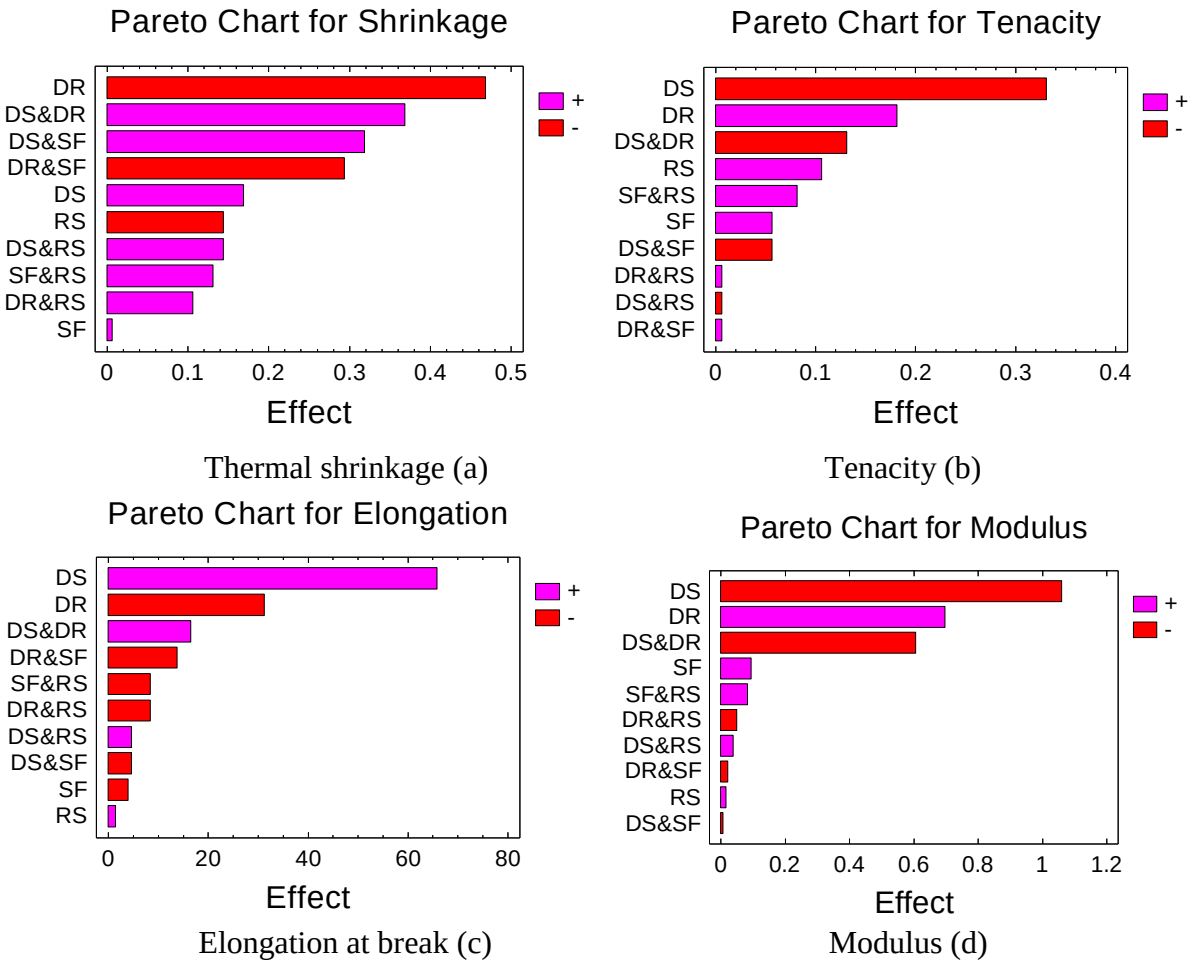

Figure 7.4 A ranked list of significant arrangement effects and interactions for thermal shrinkage (a), tenacity (b), elongation at break (c) and modulus (d) (Pareto chart)

Figure 7.5 and Figure 7.6 show the main effects and interaction plots of the statistical analysis of the effects caused by the main factors and their interactions on studied responses. The factor effect on responses between the average responses of the low and high levels of the factors is obtained using the design matrix; all the interactions could be simulated as the plots show the existence or otherwise of the interaction between each two factors. From the main effects plot for shrinkage, the main effects of the number of drawing stages and total drawing ratio are more pronounced than the other factors, spin finish application and relaxing stage ratio, as their lines are longer and their slopes are sharper than those of the other factors. The interactions DS&DR, DS&SF and DR&SF have their effects which will be further investigated using ANOVA analysis. Thermal shrinkage increases either by increasing the number of drawing stages or by using the lower level of drawing ratio and relaxing stage ratio which negatively affect the thermal shrinkage. For example, the

interaction between the number of drawing stages (DS) and the total drawing ratio (DR) is presented as DS&DR on the plot. The first factor (DS) is presented on the X-axis from low level to high level, the second factor (DR) shows as two different lines. The nonparallel lines confirm the presence of interaction; it is a useful method to render the interaction relatively easy to understand. When the one drawing stage is paired with the high level of total drawing ratio, the maximum thermal shrinkage is obtained and via versa. Effects and interaction plots for tenacity show that total number to drawing stages, total drawing ratio, relaxing stage ratio, spin finish application and the interactions DS&DR, SF&RS and DS&SF are the notable factors affecting the tenacity. Effects and interaction plots for elongation at break shows that the total number of drawing stages, total drawing ratio and the interactions DS&DR, DS&SF, DR&RS and SF&RS are the factors affecting the elongation at break.

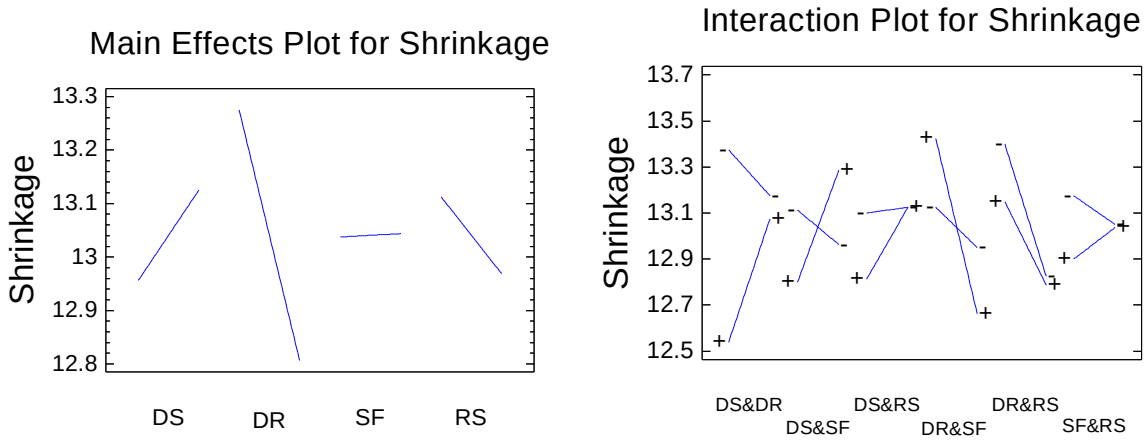

(Thermal shrinkage)

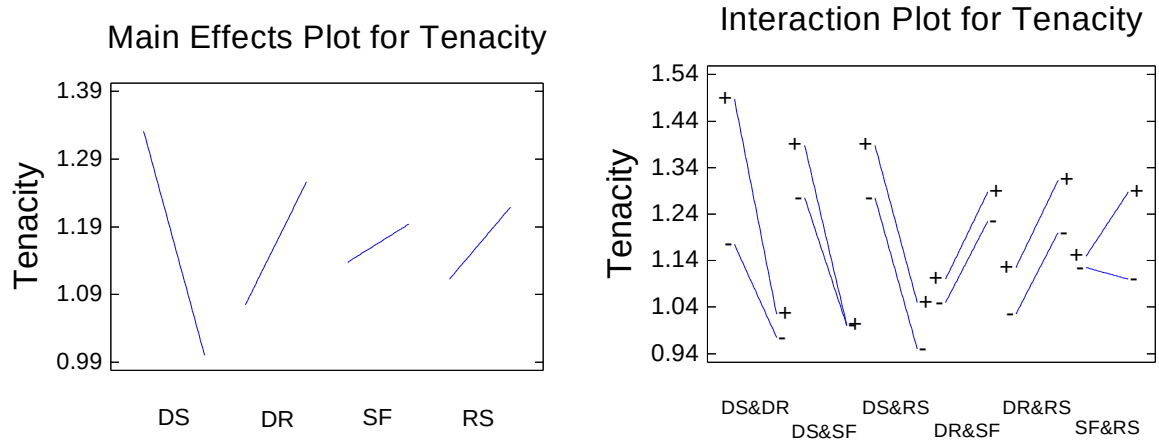

(Tenacity)

Figure 7.5 Main effect plots and interaction plots for the thermal shrinkage and tenacity

Main effects and interaction plots for modulus show that the total number of drawing stages, total drawing ratio and the interactions DS&DR and SF&RS have a notable effect on the modulus. By calculating statistical standardized and percentage order values for factors and their interaction to give more details whether the factor's effect is important or unimportant.

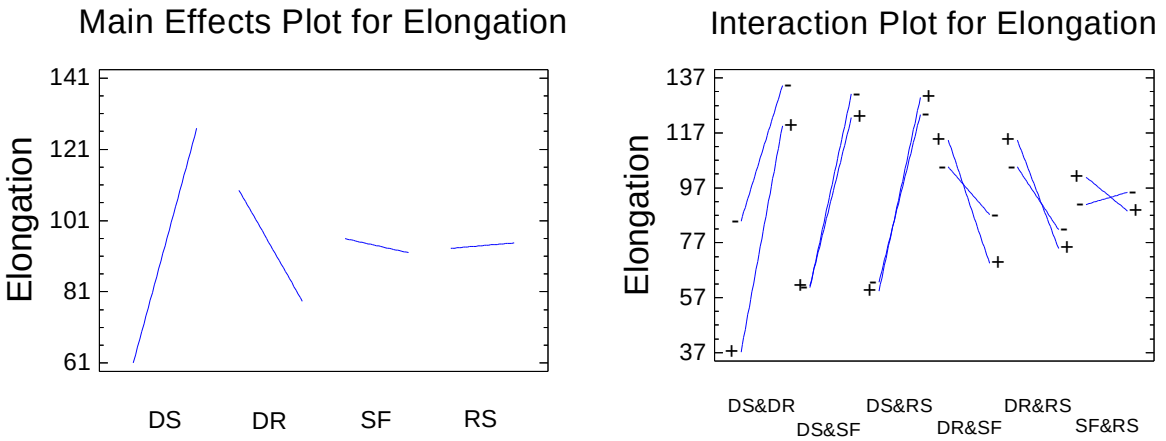

(Elongation at break)

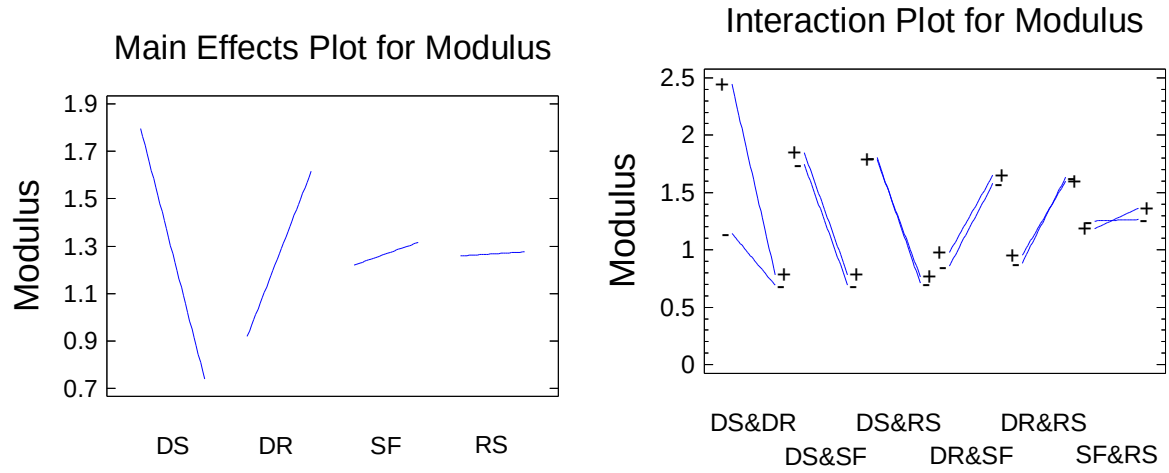

(Modulus)

Figure 7.6 Main effect plots and interaction plots for the elongation at break and modulus

Figure 7.7 displays the normal probability plot of the estimated responses and illustrates further details of the normal distribution for the data. Total draw ratio, the number of drawing stages and the interactions DS&DR, DS&SF and DR&SF have a positive effect on thermal shrinkage. In terms of mechanical properties, draw ratio has a negative effect on elongation at break and a positive effect on tenacity and modulus. Drawing stage number and its interaction with draw ratio have a positive effect on elongation at break and a negative effect on tenacity and modulus. Other factors and interactions had a less important effects on

mechanical properties. If the tension is very high, the spin finish plays an important role in the filament slippage on the last roller after applied spin finish in the one-stage drawing process; in addition to the effect of spin finish added the as-spun fibres during extrusion process. The interaction between total draw ratio and the spin finish application affects thermal shrinkage and elongation at break. With one draw stage and no relaxing stage, the tension is increased and the effect of slippage on the oily surface appears as an action of the interaction between the spin finish application and draw stages number which affects the tenacity.

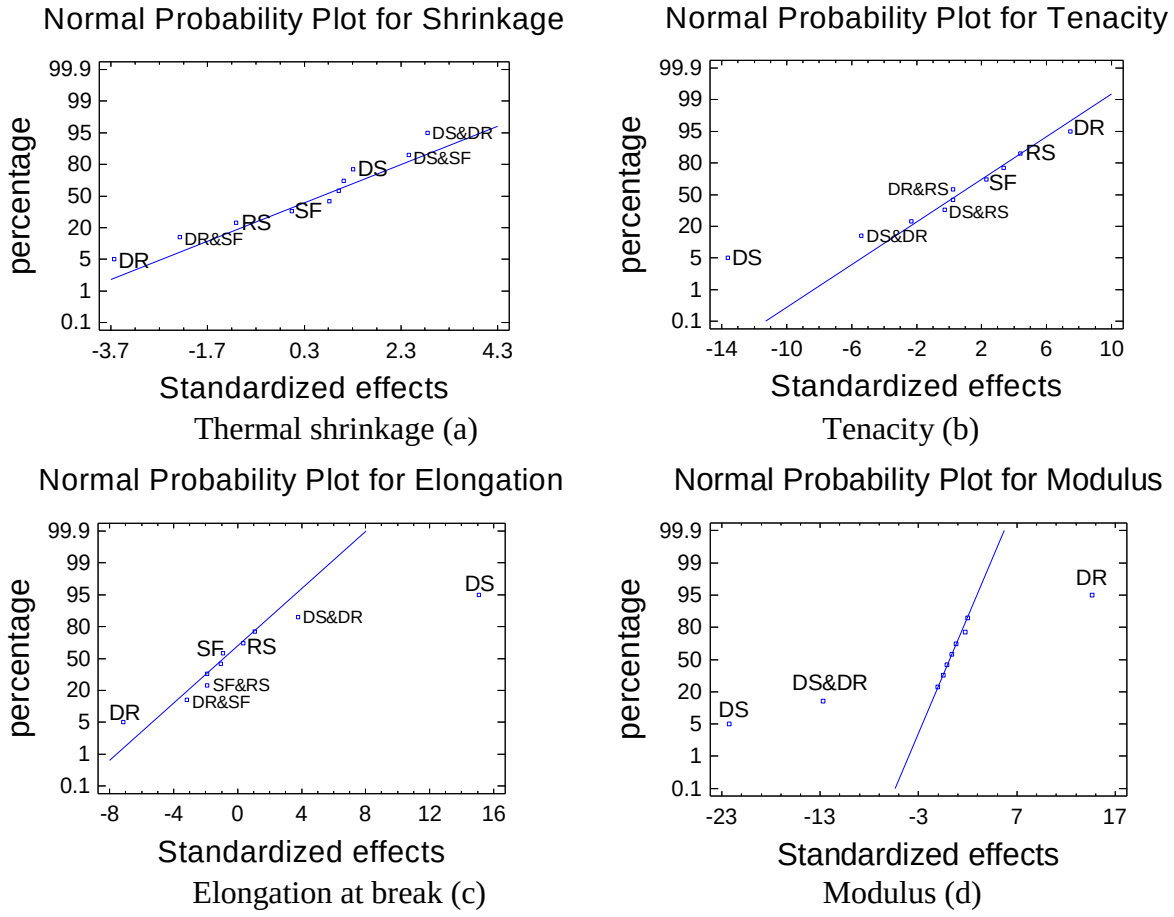

Figure 7.7 Statistical standardized and percentage order values of factors and their interactions for thermal shrinkage (a), tenacity (b), elongation at break (c) and modulus (d) (Normal Probability Plot)

7.4.2.1 Analysis of Variance (ANOVA)

Analysis of variance (ANOVA) of the obtained data determines the factor effects in terms of statistical significance. ANOVA results are listed in Table 7.4; the significance of the studied factors affecting the thermal shrinkage will then be the total drawing ratio and the interactions DS&DR, DS&SF and DR&SF. ANOVA analysis for mechanical properties shows that draw ratio, draw stage and their interaction have a significant effect on tenacity, elongation at break and modulus. Spin finish application, drawing ratio and their interaction have a significant effect on tenacity. As the tension is increased by a lower draw stage and high draw ratio, the effect of slippage on the oily surface appears, adding an interaction between the spin finish application and draw stages number which affects the mechanical properties. Spin finish application interaction with total draw stages number affect significantly on tenacity and thermal shrinkage, spin finish application interaction with draw ratio affect elongation and thermal shrinkage significantly.

Source	P-Value			
	Thermal shrinkage	**Tenacity**	**Elongation at Break**	**Modulus**
DS	0.2054	0.0000	0.0000	0.0000
DR	0.0016	0.0000	0.0000	0.0000
SF	0.9619	0.0307	0.3760	0.0576
RS	0.2782	0.0003	0.7325	0.7266
DS&DR	0.0095	0.0000	0.0011	0.0000
DS&SF	0.0222	0.0307	0.3003	0.8866
DS&RS	0.2782	0.7994	0.2991	0.4176
DR&SF	0.0335	0.7994	0.0046	0.6507
DR&RS	0.4199	0.7994	0.0688	0.2998
SF&RS	0.3210	0.0031	0.0685	0.0955

Table 7.4 ANOVA Results identifying the statistical significance of factor effects on the results from analysis of variance (ANOVA) of the data identifying the statistical significance of each factor for thermal shrinkage, tenacity, elongation at break and modulus

Other factors and interactions have their effects but they are limited and less significant. The significance of the total drawing ratio and draw stages number overcome other effects when they are at a low level. An error could come from either assignable causes that represent variation resulting from changes in the independent factors, or random causes that signify

uncontrolled variation. The geometric result of plotting a response variable is as a function of two factors; the interaction appears with the surface twist. The estimated response surface is based on the assumed regression model. The estimated response surfaces are used to determine the direction and the significance of the interactions.

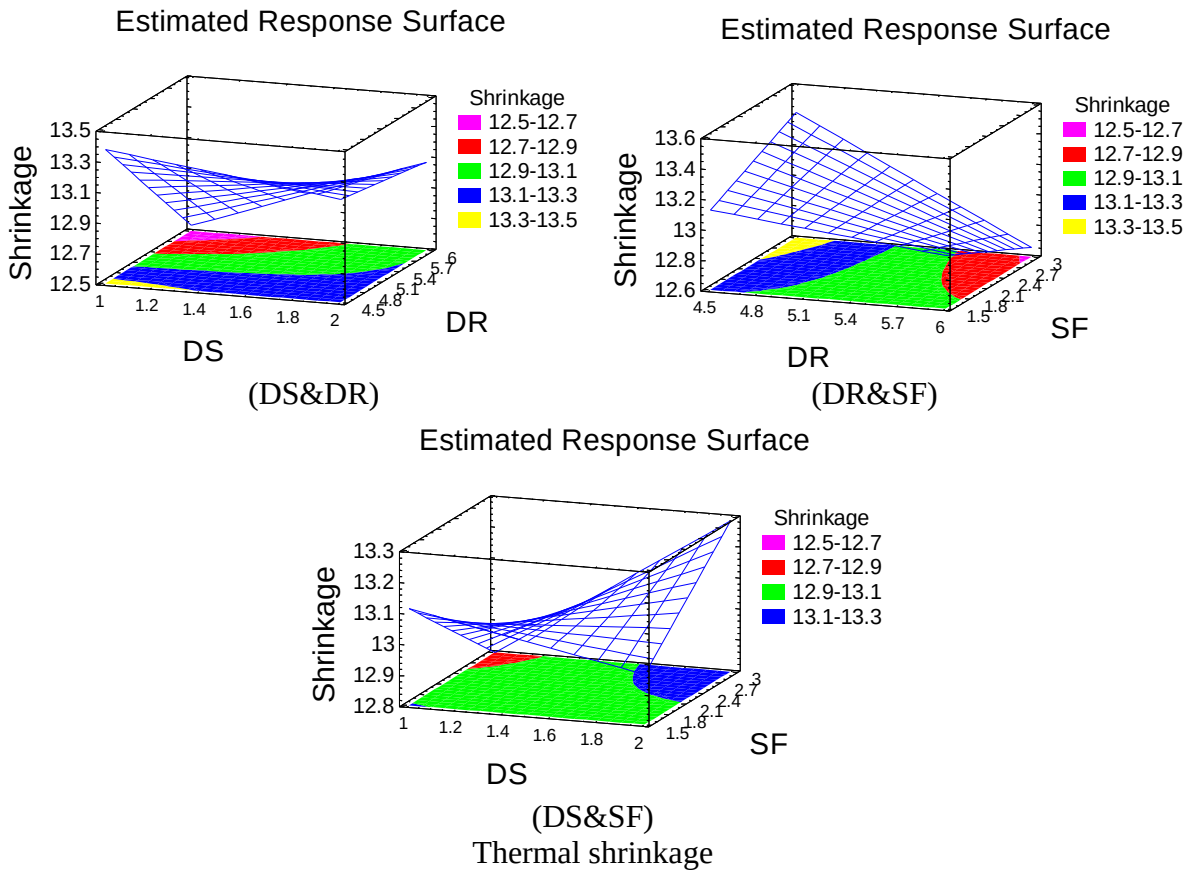

Thermal shrinkage

Figure 7.8 The estimated response surface for the interactions for thermal shrinkage

In Figure 7.8, there are three axes presents the surface of interaction DS&DR; the first factor (DS) is on the X-axis with low and high levels, the second factor (DR) is on the Y-axis with low and high levels and the Z-axis shows the averages of the estimated thermal shrinkage. There is a twist which confirms the interaction effect on thermal shrinkage (DS&DR, DR&SF and DS&SF), tenacity (DS&DR, DS&SF and SF&RS), elongation at break (DS&DR and DR&SF) and modulus (DS&DR); a noted twist was found in each surface. This corresponds with the previous statistical analysis results of the interaction plot and ANOVA derived from the experimental data.

7.4.2.2 The Regression Equation and Estimation Results

Based on the analysis of the fraction factorial experimental design (L32) results, simplified models based on statistical analysis for studied factors and their interactions were fitted by the regression equations for thermal shrinkage, tenacity, elongation at break and modulus, which have been fitted to the experimental data. Enhanced regression equations forecast the fibre properties in order to achieve the most satisfactory properties in the final desired fibre for different applications. The regression equations in terms of the previous coded values (Table 7.1) are given as below:

Thermal shrinkage = 17.4969 - 3.5125*DS - 0.533333*DR + 0.65*SF - 1.7125*RS + 0.491667*DS*DR + 0.425*DS*SF + 0.2875*DS*RS - 0.261111*DR*SF + 0.141667*DR*RS + 0.175*SF*RS (7.1)

Tenacity = -0.540625 + 0.7625*DS + 0.366667*DR + 0.0666667*SF - 0.1625*RS - 0.175*DS*DR - 0.075*DS*SF - 0.0125*DS*RS + 0.00555556*DR*SF + 0.00833333*DR*RS + 0.108333*SF*RS (7.2)

Elongation at Break = 82.3 - 40.75*DS - 20.65*DR + 76.8083*SF + 71.35*RS + 22.0667*DS*DR - 6.18333*DS*SF + 9.3*DS*RS - 12.3*DR*SF - 11.1667*DR*RS - 11.1833*SF*RS (7.3)

Modulus =-6.34594 + 3.16*DS + 1.75333*DR + 0.124167*SF + 0.00375*RS - 0.8075*DS*DR - 0.00916667*DS*SF + 0.07875*DS*RS - 0.0194444*DR*SF - 0.0675*DR*RS + 0.110833*SF*RS (7.4)

Figure 7.9 shows the experimental observed results and calculated fitted results plot for thermal shrinkage (a), tenacity (b), elongation at break (c) and modulus (d). Their Model Standard Error (MSE) values listed in Table 7.5 indicate the dispersion of predicted and observed values around the theoretical fitted line generated using the fitted model for each trial. The models evaluate the significance effect of each independent variable to a predicted response, depending on the coefficient constant for the linear effects of independent factors and the coefficient constant for the interaction effects, depending on the coefficient constant for the offset term. Experimentally observed results were plotted on the Y axis and data for calculated fitted results generated using the last fitted model were plotted on the X axis for each trial. The pattern of estimated responses is based on the assumed model derived from the experimental observations. The predictive models gave useful results if draw frame

setting based variation, the tension or slippage on the drawing roles and some tension during the preparation of the sample for testing have been controlled and taken into account.

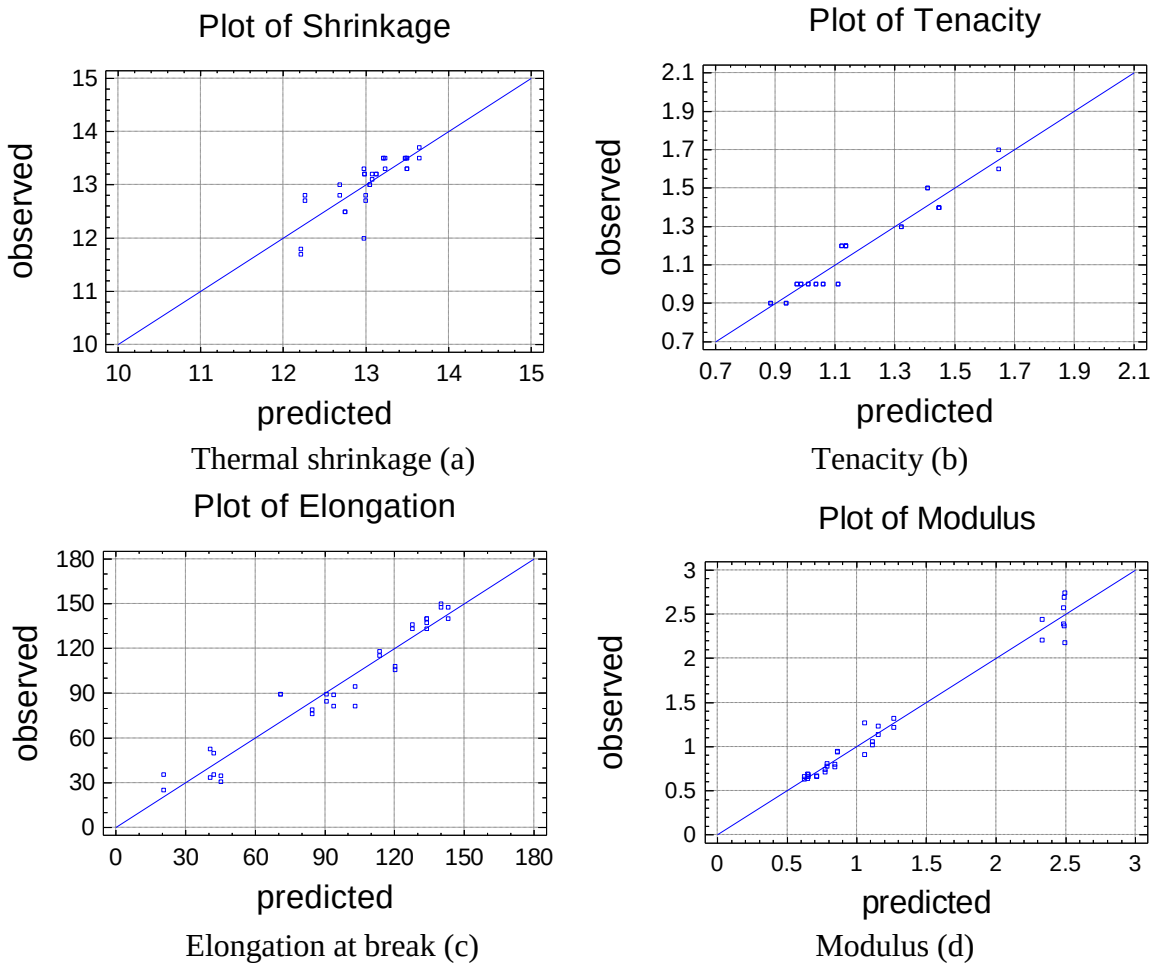

Figure 7.9 Experimental observed results and calculated fitted results plot for thermal shrinkage (a), tenacity (b), elongation at break (c) and modulus (d)

7.4.3 Conclusion and Statistical Model for Optimisation

As-spun, biodegradable, linear aliphatic-aromatic co-polyester fibres were drawn at different multi-stage cold drawing conditions. The statistical models cover the number of drawing stages, total drawing ratio, spin finish application, relaxing stage ratio and their interactions; models specify the combinations of their levels for enhancing studies responses. In order to optimize thermal shrinkage, tenacity, elongation at break and modulus, Table 7.5 shows the combination of factor levels which maximize and minimize the responses over the indicated

region and their MSE values described previously. The designed models will help processing scientists and technologists in industry to obtain the enhanced properties at suitable conditions related to final product cost and to obtain environmentally friendly, economical and energy saving fibres.

Response	MSE	Optimum model	The combination of factor levels (↓: Low Level, ↑: High Level)			
			DS	DR	SF	RS
Thermal Shrinkage (%)	0.0894	Maximum	↓	↓	↓	↓
		Minimum	↓	↑	↑	↑
Tenacity (g/den)	0.039	Maximum	↓	↑	↑	↑
		Minimum	↑	↓	↑	↓
Elongation at Break (%)	7.171	Maximum	↑	↓	↓	↑
		Minimum	↓	↑	↑	↑
Modulus (g/den)	0.128	Maximum	↓	↑	↑	↑
		Minimum	↑	↓	↓	↓

Table 7.5 The combinations of factor levels for the effect of multi-stage cold drawing on the properties of LAAC fibres for thermal shrinkage, tenacity, elongation at break and modulus. (MSE: Model Standard Error)

In conclusion, the draw ratio, the interaction between the number of drawing stages and drawing ratio and the interaction between spin finish application and both of the number of drawing stages and drawing ratio have a positive effect on thermal shrinkage, In terms of mechanical properties, draw ratio has a negative effect on elongation at break and a positive effect on tenacity and modulus. Draw stage and its interaction with draw ratio have a positive effect on elongation at break and a negative effect on tenacity and modulus. The interaction between draw ratio and the spin finish application have an effect on the internal stress and also on thermal shrinkage and elongation. Other factors and interactions have their limited effects which are covered by the governing factors, drawing ratio and temperature. Drawing tension is related to the stability of drawing conditions; it was increased with the increasing of the drawing ratio. From a physical point of view, adding the relaxing stage decreases of internal stress. When a higher draw ratio is applied, the speed of the final roller increases and the spin finish layer thickness on the fibres at constant spin finish pump speed will be affected. This could explain the interaction between the spin finish and the draw ratio, in terms of relaxing ratio effect or slippage in the drawing and relaxing stage. In the relaxation

process, when relaxing stage ratio increases, the yarn speed decreases, the relaxation time increases and the spin finish layer's thickness will be increased. This relationship could explain the interaction between process conditions and fibre structure. The tension will be high with one stage or high draw ratio and the spin finish plays an important role in the filament slippage on the last roller after applied spin finish at constant spin finish pump speed. The regression equations achieved could form a part in a forecasting program designed to optimize the drawing process of selected as-spun fibres. Drawn LAAC fibres could be used in agricultural, horticultural and other non-traditional textile applications.

7.5 Statistical Modelling of The Effect of Cold Drawing on Branched Aliphatic-Aromatic Co-Polyester Fibres (BAAC)

7.5.1 Experimental Results

The experiments were randomly conducted in one block according to the design shown in Table 7.2 and involved control factors and their levels as listed in Table 7.1. The collected data of the thermal shrinkage and mechanical properties for fibres were measured and are listed in Table 7.6. The average data of the measured specimens were calculated; small standard deviations could be related to draw frame setting based variation which could not be totally controlled, the tension or slippage on the drawing roles as was been noted in drawing study or could be related to some tension error while preparing the sample for testing. Each thermal shrinkage test was carried out using a MK IV Shrinkage-Force Tester; samples were heated for 2 minutes at 60^{o}C under a load cell of 10 g.

Figure 7.10 shows the DSC curve for trial 5 produced with cold drawing. No appreciable changes of relative intensity of the peaks in the endotherm were observed in different samples for same trial. No significant effect was reported in their thermal properties but the mechanical properties will be better with the relaxation stage. A broad range of melting temperature was observed for the fibres; the fibre did not melt completely below 140 ^{o}C, as an optimum temperature window was found taking all factors into account. In Figure 7.11, the SEM photomicrograph of BAAC fibre shows the fibre's surface.

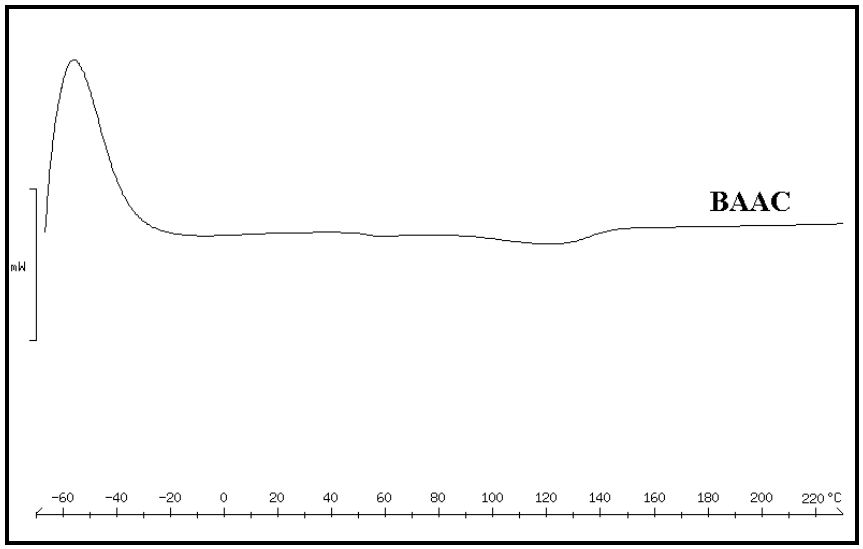

Figure 7.10 DSC curve of cold drawn BAAC fibres - Trial 5

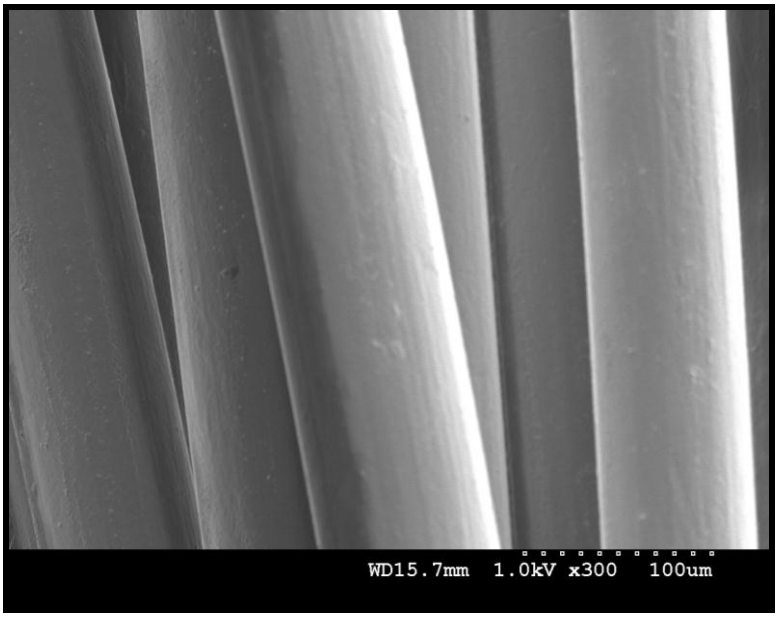

Figure 7.11 SEM photomicrograph of BAAC fibres' surface

Trial Number	Thermal shrinkage (%)	Tenacity (g/den)	Elongation at Break (%)	Modulus (g/den)
1	8.7	1.1	104.2	1.55
2	8.2	1.1	118.8	1.42
3	9.2	1.0	93.8	1.66
4	5.6	1.0	120.8	1.10
5	5.7	1.0	114.6	1.15
6	5.5	1.0	122.9	1.07
7	8.7	1.1	104.2	1.55
8	6.9	1.0	120.8	1.14
9	6.3	0.9	137.5	1.08
10	6.3	0.8	110.4	1.05
11	5.3	0.9	112.5	0.98
12	4.8	0.9	122.9	1.00
13	5.6	1.0	110.4	1.10
14	8.2	1.1	95.8	1.90
15	5.3	0.9	112.5	0.98
16	7.7	0.8	97.9	1.33
17	5.8	0.9	106.3	1.05
18	4.0	0.9	147.9	0.75
19	5.5	1.0	108.3	1.18
20	6.3	0.8	110.4	1.05
21	6.3	0.9	137.5	1.08
22	9.2	1.0	93.8	1.66
23	7.7	0.8	97.9	1.33
24	6.8	0.9	114.6	1.15
25	8.2	1.1	95.8	1.90
26	5.5	1.0	122.9	1.07
27	6.9	1.0	120.8	1.14
28	8.2	1.1	118.8	1.42
29	4.0	0.9	147.9	0.75
30	4.3	0.9	147.9	0.92
31	4.8	0.9	122.9	1.00
32	4.3	0.9	147.9	0.92

Table 7.6 Results for the cold drawing experiment (BAAC)

7.5.2 Statistical Analysis and Discussion

In Figure 7.12, The Pareto charts for thermal shrinkage (a), tenacity (b), elongation at break (c) and modulus (d) show the significant arrangement of factors and their interactions in decreasing order. The Pareto chart for thermal shrinkage shows that the total number of drawing stages (DS), the drawing ratio (DR), spin finish application (SF) and the interactions DS&DR, DS&SF, DR&SF and DS&RS are the most important factors affecting the thermal shrinkage properties of the fibres, followed by other factors and interactions. In terms of mechanical properties, the Pareto chart for tenacity shows that total drawing ratio, the total number of drawing stages, the interactions DS&RS, DS&DR, DS&SF, spin finish application and relaxing stage ratio are the most important factors affecting the tenacity, followed by other factors and interactions. Determined factors would affect the tension and the internal stress and then affect the thermal shrinkage properties. The Pareto chart for elongation at break shows that total drawing ratio, relaxing stage ratio, the total number of drawing stages, spin finish application, the interactions DS&SF, DS&RS, DR&SF, DR&RS and DS&DR are the most important factors affecting the elongation at break, followed by other factors and interactions. The Pareto chart for modulus shows that total drawing ratio, the total number of drawing stages, spin finish application, relaxing stage ratio and the interactions DS&DR, DS&SF, SF&RS and DR&RS are the most important factors affecting the modulus, followed by other factors and interactions. As noted previously with LAAC and by taking into account the branching in the BAAC structure, with the one stage drawing process and relaxing stage, the tension will be high and the spin finish plays an important role in the filament slippage on the last roller after applying spin finish. Technically then, the relaxation time and the thickness of the spin finish layer will be increased.

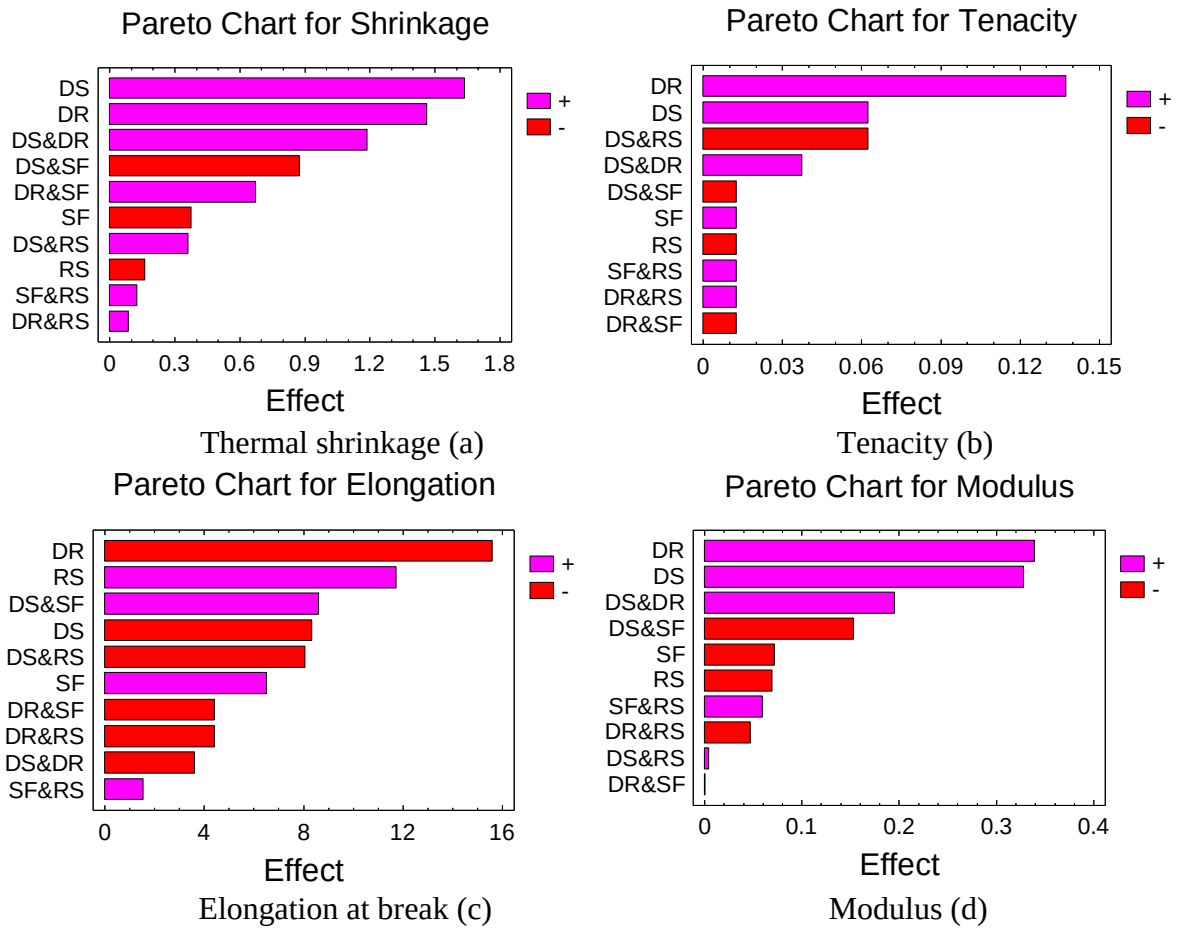

Figure 7.12 A ranked list of significant arrangement effects and interactions for thermal shrinkage (a), tenacity (b), elongation at break (c) and modulus (d) (Pareto chart)

Figure 7.13 and Figure 7.14 show the main effects and interaction plots of the statistical analysis of the effects caused by the main factors and their interactions on responses. The main effects of draw ratio and draw stage are significant on shrinkage, as their lines are long and their slopes are sharp. The interactions DS&DR, DS&SF, DR&SF and DS&RS affect thermal shrinkage which will be further investigated statistically using ANOVA analysis. It is advised that the major factors influencing thermal shrinkage value be assessed further to understand their influence more fully. Effects and interaction plots for tenacity show that total drawing ratio, the total number of drawing stages and the interactions DS&RS and DS&DR are the factors affecting tenacity. Other interactions have their effects which need to be further investigated using other methods to identify their significance. Effects and interaction plots for elongation at break show that total drawing ratio, relaxing stage ratio, the total number of drawing stages and the interactions (DS&SF and DS&RS) are the factors

affecting the elongation at break. The interactions DR&SF, DR&RS and DS&DR affect the elongation and need to be investigated later, as their line angles are small.

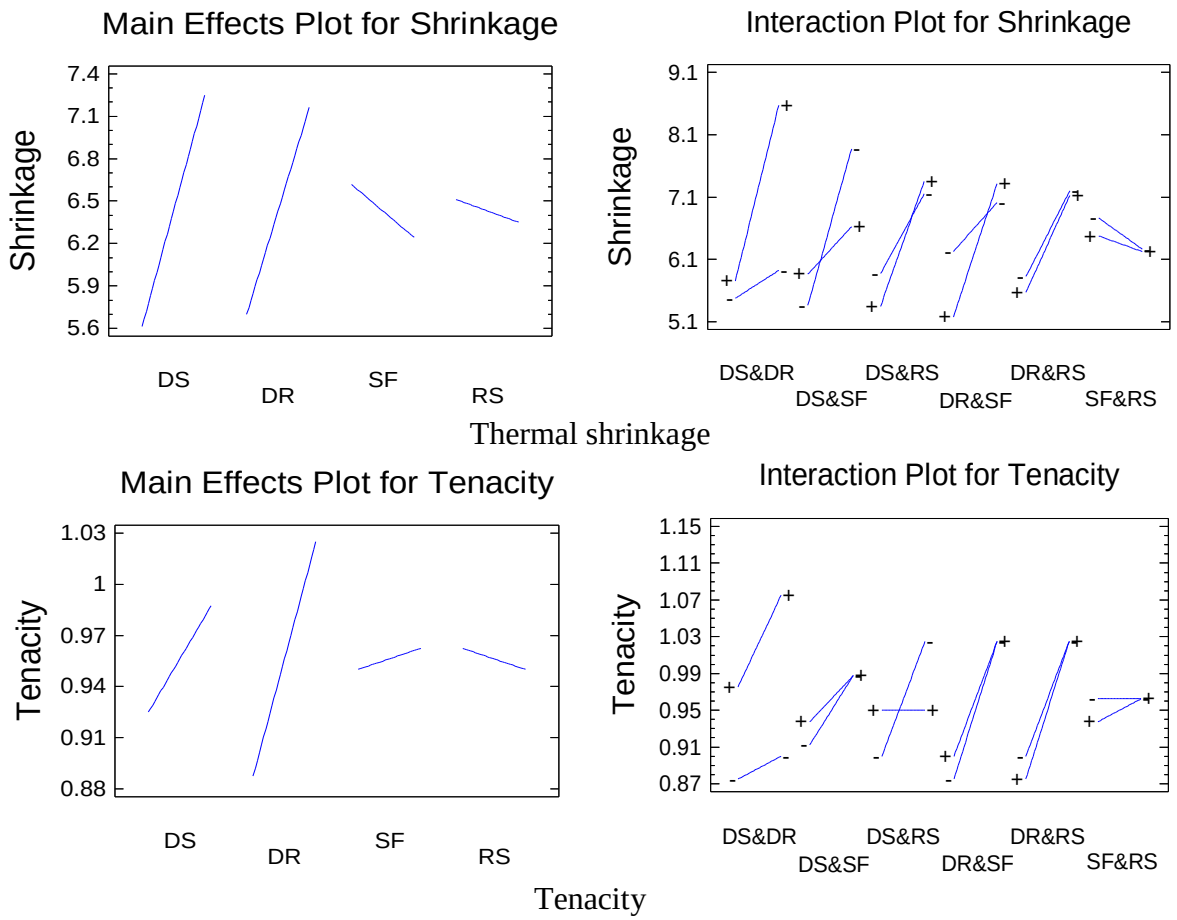

Figure 7.13 Main effect plots and interaction plots for the thermal shrinkage and tenacity

The main effects of draw stage (DS) and draw ratio (DR) are pronounced on modulus, as their lines are long and their slopes are sharp. When a higher draw ratio was applied, the speed of the final roller increased and the spin finish layer thickness on the fibres at constant spin finish pump speed was affected. The interactions DS&DR, DS&SF and SF&RS affect the modulus and will be investigated statistically using ANOVA to adjust their effects. When a higher draw ratio is applied, the speed of the final roller increases and the fibres will deform in the relaxation stage to allow the new form to stabilize by reducing the tension. Again, the technical-physical relationship could explain the interaction between relaxing stage process conditions and fibre structure and statistically could explain the interaction between the spin finish and the draw ratio.

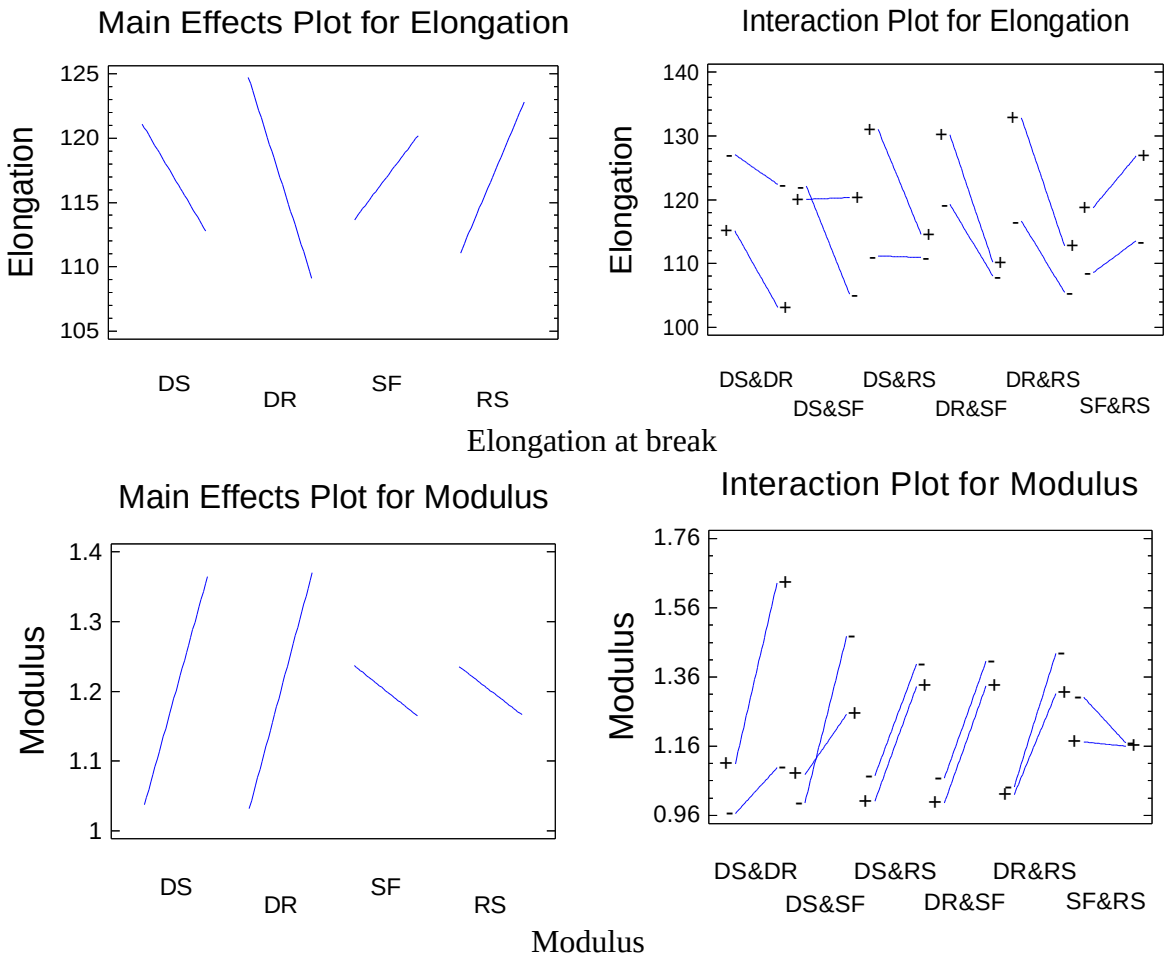

Figure 7.14 Main effect plots and interaction plots for the elongation at break and modulus

Figure 7.15 displays the normal probability plot of the responses estimated and illustrates further details about the normal distribution for the data. More details relating to whether the factor's effect is important or unimportant could be obtained by plotting statistical standardized via percentage order. Draw ratio and draw stage have a positive effect on thermal shrinkage, tenacity, modulus and elongation at break. Relaxing stage ratio has a negative effect on thermal shrinkage, tenacity, modulus and a positive effect on elongation at break. The interaction between drawing stage and total drawing ratio has a positive effect on thermal shrinkage, tenacity, modulus and a negative effect on elongation at break. The interaction between drawing stage and spin finish application has a negative effect on thermal shrinkage, tenacity, modulus and a positive effect on elongation at break. The interaction between total draw ratio and spin finish application positively affects thermal shrinkage. The interaction between draw stage and spin finish could be related to the practical relationship between the tension and the oily roller surface on the last roller in the

relaxing stage, which causes some slippage and cooling action in the relaxation process. In one-stage drawing experiments, the tension will be high and the spin finish plays a central role in the filament slippage on the last roller after applied spin finish, in addition to the spin finish in the as-spun samples. These results were analyzed by ANOVA.

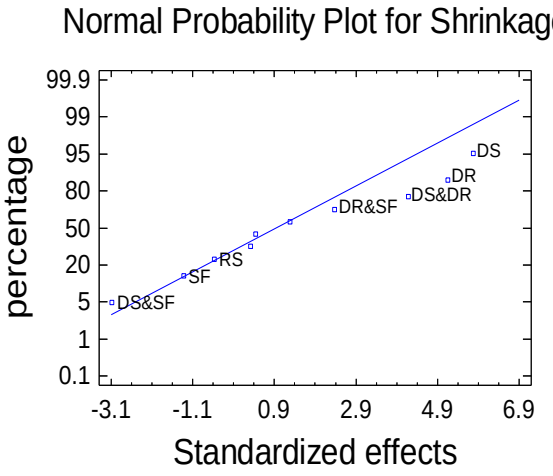

Thermal shrinkage (a)

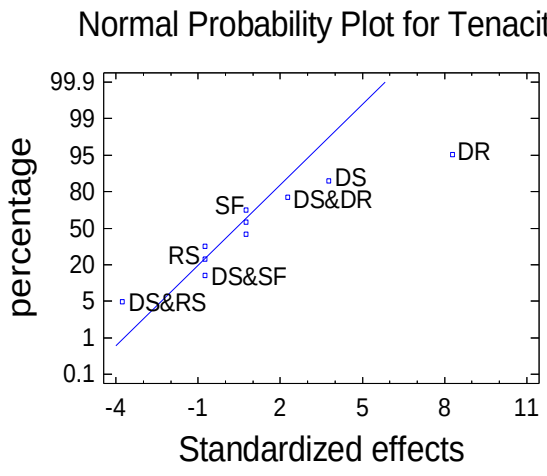

Tenacity (b)

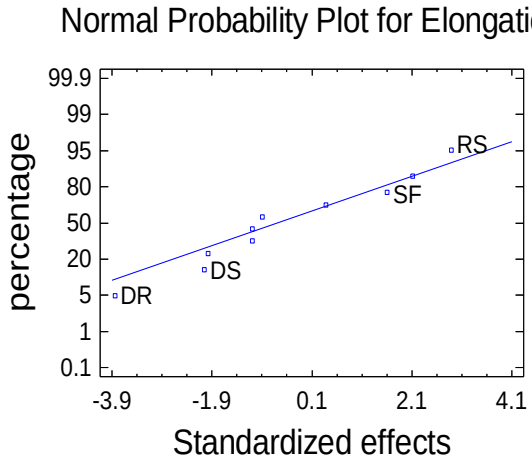

Elongation at break (c)

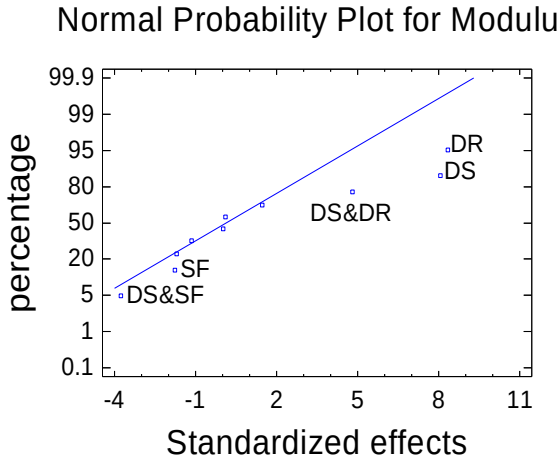

Modulus (d)

Figure 7.15 Statistical standardized and percentage order values of factors and their interactions for thermal shrinkage (a), tenacity (b), elongation at break (c) and modulus (d) (Normal Probability Plot).

7.5.2.1 Analysis of Variance (ANOVA)

Analysis of variance (ANOVA) of the data obtained identifies the factors and their interaction effects in terms of statistical significance. ANOVA results are listed in Table 7.7; the significance of the studied factors affecting the thermal shrinkage will then be the total drawing ratio, the number of drawing stages, the interactions DS&DR, DS&SF and DR&SF. There are no significant effects of the other interactions within the ranges of the parameters in the experiments. For mechanical properties, ANOVA shows that the total drawing ratio and the number of drawing stages have a significant effect on tenacity, elongation at break and modulus. Relaxing stage ratio has significant effect on elongation at break, as it could relate to its effect on the internal structure of the fibres. The interaction between the draw stage and the total draw ratio has a significant effect on the tenacity and the modulus. The interaction between draw stage and spin finish application has a significant effect on the modulus and the elongation at break. The interaction draw stage and relaxation has a significant effect on the tenacity. The processing time and cooling in relaxation stage will be affected.

Source	P-Value			
	Thermal shrinkage	Tenacity	Elongation at Break	Modulus
DS	0.000	0.001	0.053	0.000
DR	0.000	0.000	0.001	0.000
SF	0.200	0.459	0.123	0.092
RS	0.573	0.459	0.009	0.103
DS&DR	0.000	0.035	0.382	0.000
DS&SF	0.0056	0.459	0.046	0.001
DS&RS	0.215	0.001	0.060	0.915
DR&SF	0.027	0.459	0.288	0.988
DR&RS	0.761	0.459	0.288	0.262
SF&RS	0.664	0.459	0.706	0.159

Table 7.7 ANOVA results identifying the statistical significance of each factor for thermal shrinkage, tenacity, elongation at break and modulus

To understand the interaction between process conditions and fibre structure, when a higher draw ratio is applied, the speed of the final roller increases and the spin finish layer thickness on the fibres at constant spin finish pump speed will be affected. The estimated response surfaces are used to determine the direction and the significance of the interactions.

7.5.2.2 The Regression Equation and Estimation Results

Based on the analysis of the fraction factorial experimental design (L32) results, simplified models based on statistical analysis for studied factors and their interactions were fitted by the regression equations for thermal shrinkage, tenacity, elongation at break and modulus, which were fitted to the experimental data. The regression equations in terms of the previous coded values (Table 7.1) are given as follows:

Thermal shrinkage = 10.2588 - 1.0875*DS - 4.2125*DR - 0.473333*SF - 1.9925*RS + 2.375*DS*DR - 1.16667*DS*SF + 0.725*DS*RS + 0.9*DR*SF + 0.175*DR*RS + 0.166667*SF*RS (7.5)

Tenacity = 0.61375 + 0.005*DS + 0.05*DR + 0.06*SF + 0.085*RS + 0.075*DS*DR - 0.0166667*DS*SF - 0.125*DS*RS - 0.0166667*DR*SF + 0.025*DR*RS + 0.0166667*SF*RS (7.6)

Elongation at Break = 115.465 - 10.85*DS + 12.975*DR - 1.49333*SF + 49.81*RS - 7.25*DS*DR + 11.4667*DS*SF - 16.1*DS*RS - 5.9*DR*SF - 8.85*DR*RS + 2.06667*SF*RS (7.7)

Modulus = 0.683063 - 0.0385*DS - 0.2025*DR + 0.217*SF - 0.06375*RS + 0.39125*DS*DR - 0.204167*DS*SF + 0.00875*DS*RS + 0.000833333*DR*SF - 0.09375*DR*RS + 0.0791667*SF*RS (7.8)

Figure 7.16 shows the experimental observed results and calculated fitted results plot for thermal shrinkage (a), tenacity (b), elongation at break (c) and modulus (d). The model evaluates the significance effect of each independent variable to a predicted response, depending on the coefficient constant for the linear effects of independent factors and the coefficient constant for the interactions effects, depending on the coefficient constant for the offset term. The pattern of estimated responses is based on the assumed model derived from the experimental observations. Their Model Standard Error (MSE) values listed in Table 7.8 indicate the dispersion of predicted and observed values around the theoretical fitted line generated using the fitted model for each trial. The predictive models gave useful results (Figure 7.16) with small variation for previously described reasons, such as draw frame setting based variation, the tension or slippage on the drawing roles or some tension while preparing the sample for testing.

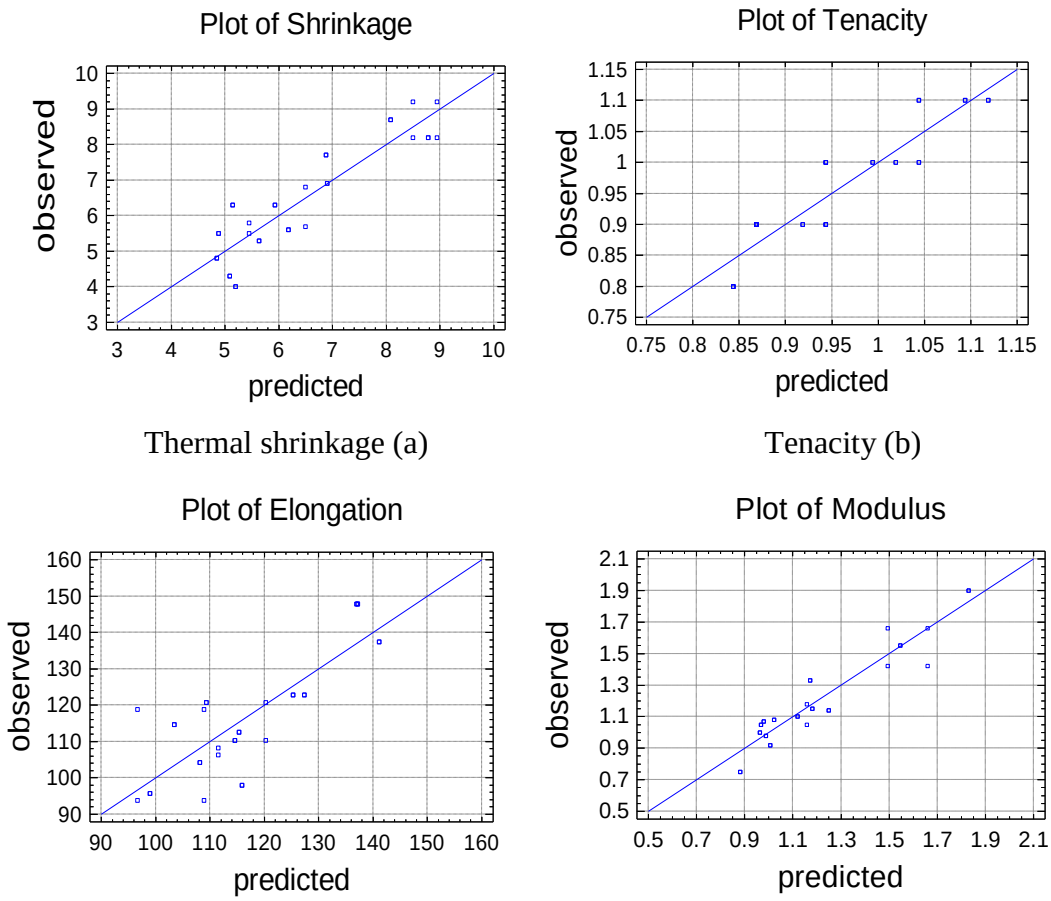

Thermal shrinkage (a)

Tenacity (b)

Elongation at break (c)

Modulus (d)

Figure 7.16. Experimental observed results and calculated fitted results plot for thermal shrinkage (a), tenacity (b), elongation at break (c) and modulus (d)

7.5.3 Conclusion and Statistical Model for Optimisation

As-spun, biodegradable, branched aliphatic-aromatic co-polyester fibres were drawn at different multi-stage cold drawing conditions. The statistical models cover the total number of drawing stages DS, total drawing ratio DR, spin finish application SF, relaxing stage ratio RS and their interactions. Draw ratio and draw stage have a positive effect on thermal shrinkage, tenacity, modulus and elongation at break. Relaxing stage ratio has a negative effect on thermal shrinkage, tenacity, modulus and a positive effect on elongation at break. The interaction between draw stage and draw ratio has a positive effect on thermal shrinkage, tenacity, modulus and a negative effect on elongation at break. The interaction between the number of drawing stages and spin finish application has a negative effect on thermal

shrinkage, tenacity, modulus and a positive effect on elongation at break. The interaction between draw ratio and spin finish application positively affect thermal shrinkage. Other factors and interactions have their effects but they are limited and less significant as they are covered by the governing factors, drawing ratio and temperature. In one-stage drawing experiments and in addition to the spin finish applied to the as-spun fibres during extrusion process, the tension will be high and the spin finish plays a central role in the filament slippage on the last roller after applied spin finish; the high tension could cause some slippage and small variation in the results. A variation in the results could come from either assignable causes that represent variation resulting from changes in the independent factors, or random causes that signify uncontrolled variation. In Table 7.8, the optimization of thermal shrinkage, tenacity, elongation at break and modulus shows the combination of factor levels which maximize and minimize the responses over the region indicated, in addion to their MSE values described later. The achieved models specify the combinations of their levels for responses and will form a part in a forecasting program designed to optimize the drawing process of selected as-spun fibres. The models help processing scientists and technologists in industry to obtain the enhanced properties at suitable conditions related to final product cost and to obtain environmentally friendly, economical and energy-saving fibres.

Response	**MSE**	**Optimum model**	**The combination of factor levels (↓: Low Level, ↑: High Level)**			
			DS	DR	SF	RS
Thermal Shrinkage (%)	0.276	Maximum	↑	↑	↓	↑
		Minimum	↑	↓	↑	↓
Tenacity (g/den)	0.0167	Maximum	↑	↑	↓	↓
		Minimum	↓	↓	↓	↓
Elongation at Break (%)	2.88	Maximum	↓	↓	↑	↑
		Minimum	↑	↑	↓	↑
Modulus (g/den)	0.167	Maximum	↑	↑	↓	↓
		Minimum	↓	↓	↓	↑

Table 7.8 The combinations of factor levels for the effect of multi-stage cold drawing on the properties of BAAC fibres for thermal shrinkage, tenacity, elongation at break and modulus. (MSE: Model Standard Error)

7.6 Experimental Design for Cold Drawing and Twisting of AAC Fibres

The investigation of the interaction between the drawing and the twist processes gave more details about the effect of applying twist to the drawn fibres and how it interacts with the drawing process factors. To investigate the influence of twist and cold-drawing conditions on the properties of LAAC and BAAC fibres, a new, full factorial experimental design was applied to discover how the analyses of the previous drawing experiments could be changed as a result of adding twist to the continuous fibres. For technical and experimental reasons, the multi-stage hot drawing and twisting processes of as-spun AAC fibres were operated individually. The five control parameters for the cold drawing and twisting experiments are the number of drawing stages (DS), total drawing ratio (DR), spin finish (SF), relaxing stage ratio between relaxation process rollers at 40 ^{o}C (RS) (where speed of the second roller = RS * speed of the first roller) and twist level (T). The two levels of each parameter were separated as far apart as possible from one another. Twisting was carried out at room temperature to twist the continuous drawn filaments at a different twist level. Twist keeps the filaments together in continuous filament yarns; filaments are given axial strength and lateral pressure when increasing the twisting.

These are listed with their abbreviations and levels in Table 7.9. A full factorial design (L32; 2^5 = 32) was used for the thirty-two screening trials in this experiment, as shown in Table 7.10. The experiments were randomly conducted in one block. The friction between the fibres after applying the twist is affected by the higher draw ratio applied; the speed of the final roller increases and the spin finish layer thickness on the fibres at constant spin finish pump speed will be affected. That could explain the interaction between the spin finish, the draw ratio and twist level in terms of fibre to fibre friction during force application. The high twist level does not allow the yarn to flatten or distort under pressure when being abraded [172]. Drawing and high twist could cause deformation in the fibre shape; fibres in the centre could deform into a polygonal shape under tension.

Factor abbreviation	Factor name	Level	
		Low L	High H
DS	Total number of drawing stages	1	2
DR	Total drawing ratio for LAAC	4.5	6
	Total drawing ratio for BAAC	1.6	2.6
SF	Spin finish application (rpm)	1.5	3.0
RS	Relaxing stage ratio (4%)	0: Without	1: With
T	Twist level (Turns/inch)	4	8

Table 7.9 Factors and their levels for the cold drawing and twisting experiment

Trial Number	The number of drawing stages DS	Drawing Ratio DR	Spin Finish SF	Relaxing stage ratio RS	Twist T
1	H	H	H	L	L
2	H	H	H	H	L
3	H	H	L	H	H
4	L	H	H	H	H
5	L	H	H	L	H
6	L	H	L	H	L
7	H	H	H	L	H
8	H	L	L	L	H
9	L	L	H	H	H
10	L	L	L	L	L
11	L	L	H	L	L
12	H	L	H	L	L
13	L	H	H	H	L
14	H	H	L	L	L
15	L	L	H	L	H
16	H	L	L	H	L
17	L	H	L	L	H
18	L	L	L	H	H
19	L	H	L	L	L
20	L	L	L	L	H
21	L	L	H	H	L
22	H	H	H	H	H
23	H	L	L	H	H
24	L	H	H	L	L
25	H	H	L	L	H
26	L	H	L	H	H
27	H	L	L	L	L
28	H	H	L	H	L
29	L	L	L	H	L
30	H	L	H	H	H
31	H	L	H	L	H
32	H	L	H	H	L

Table 7.10 L32 Experimental design array and results for the cold drawing and twisting experiment (for LAAC and BAAC fibres).

7.7 Statistical Modelling of The Effect of Cold Drawing and Twisting on Linear Aliphatic-Aromatic Co-Polyester Fibres (LAAC)

7.7.1 Experimental Results

The experiments were randomly conducted in one block according to the design shown in Table 7.10. Each thermal shrinkage test was carried out using a MK IV Shrinkage-Force Tester; samples were heated for 2 minutes at 60^{o}C under a load cell of 10 g. The Shirley Yarn Abrasion Tester was used to determine the abrasion resistance of yarns. The data present the average of the measured values for each sample; the small standard deviations are related to the draw frame setting based variation, the tension or slippage on the drawing roles or some measurement error relating to preparing the sample for testing. The thermal shrinkage, mechanical properties and abrasion for fibres were measured and listed in Table 7.11. The data present the average of the measured values for each sample; they have small standard deviations as a result of draw frame setting based variation, the tension or slippage on the drawing roles or some measurement error relating to preparing the sample for testing. Figure 7.17 shows the SEM photomicrograph of LAAC twisted fibres' surface; no deformation was noted in the surface as a result of twist effect.

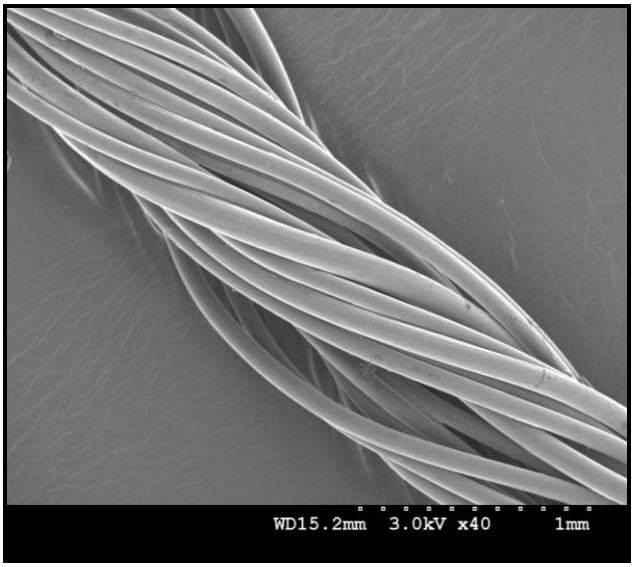

Figure 7.17 SEM photomicrograph of LAAC twisted fibres' surface

Trial Number	Thermal shrinkage (%)	Tenacity (g/den)	Elongation at Break (%)	Modulus (g/den)	Abrasion (number of rubs)
1	13.2	0.8	146.0	0.52	15
2	12.5	1.0	140.0	0.56	12
3	12.8	0.8	136.0	0.57	11
4	11.7	1.4	37.3	1.76	4
5	12.4	1.3	26.7	1.99	5
6	12.6	1.3	49.0	1.98	7
7	12.2	0.9	116.0	0.76	5
8	12.6	0.8	124.0	0.60	11
9	13.7	1.0	65.3	1.04	8
10	13.5	1.0	106.7	0.88	8
11	13.4	1.0	98.0	0.76	12
12	12.7	1.0	28.0	1.47	5
13	12.4	1.4	38.0	2.18	4
14	13.1	0.9	186.0	0.53	7
15	12.8	1.1	104.0	0.98	7
16	12.2	0.9	168.0	0.59	11
17	12.6	1.3	30.0	1.88	4
18	12.5	1.0	98.0	0.94	6
19	12.6	0.9	112.0	0.54	6
20	12.7	1.0	100.0	0.90	6
21	12.9	1.1	94.0	0.98	11
22	12.9	1.0	128.0	0.66	10
23	12.7	0.9	168.0	0.56	9
24	12.8	1.4	35.0	2.17	6
25	13.2	0.9	129.3	0.64	7
26	11.9	1.3	34.7	1.41	5
27	12.2	1.1	148.0	0.69	6
28	12.2	0.8	164.0	0.59	10
29	13.2	1.1	108.0	1.05	8
30	13.2	0.7	162.7	0.56	7
31	12.8	0.8	196.0	0.58	7
32	13.0	0.8	182.7	0.53	12

Table 7.11 Results for the cold drawing and twisting experiment (LAAC)

7.7.2 Statistical Analysis and Discussion

In Figure 7.18, the Pareto charts for thermal shrinkage (a), tenacity (b), elongation at break (c), modulus (d) and abrasion (e) show the significant arrangement of factors and their interactions in decreasing order. The Pareto chart for thermal shrinkage shows that the total drawing ratio, relaxing stage ratio, spin finish application, the interactions DR&RS, RS&T,

RS&SF, DS&DR, DS&T and SF&RS are the most important factors affecting the thermal shrinkage properties of the fibres, followed by other factors and interactions. In terms of mechanical properties, the Pareto chart for tenacity shows that the total number of drawing stages, total drawing ratio, twist level, spin finish application and the interactions DS&DR, DR&T, DS&RS, DR&RS, DS&T and SF&RS are the most important factors affecting the tenacity, followed by other factors and interactions.

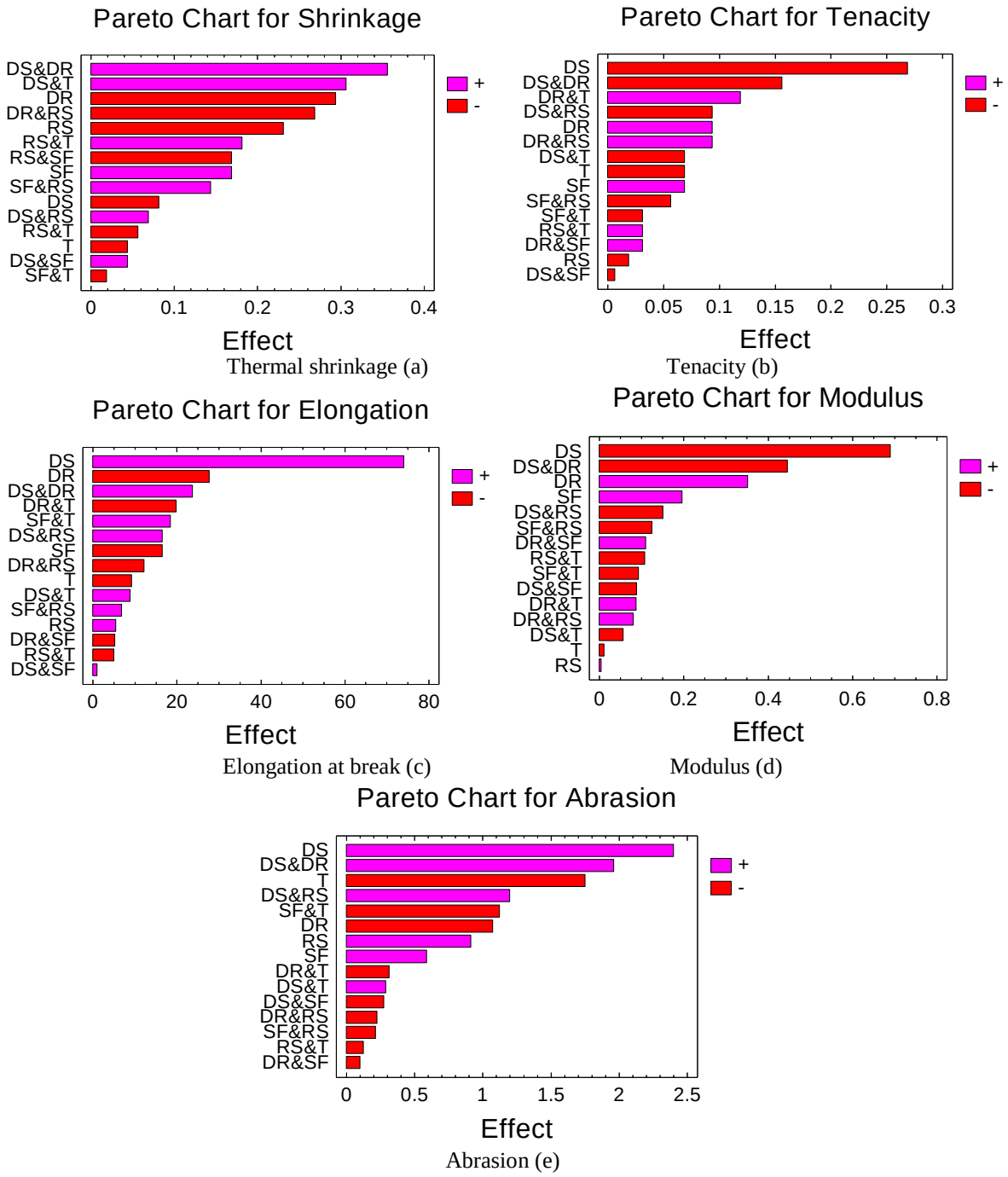

Thermal shrinkage (a)

Tenacity (b)

Elongation at break (c)

Modulus (d)

Abrasion (e)

Figure 7.18 A ranked list of significant arrangement effects and interactions for thermal shrinkage (a), tenacity (b), elongation at break (c), modulus (d) and abrasion (e) (Pareto chart)

The Pareto chart for elongation at break shows that the total number of drawing stages, total drawing ratio, spin finish application, twist level the interactions, DS&DR, DR&T, SF&T, DS&RS, DR&RS and DS&T are the most important factors affecting the elongation at break, followed by other factors and interactions. The Pareto chart for modulus shows that the total number of drawing stages, total drawing ratio, spin finish application and the interactions DS&DR, DS&RS, SF&RS, DR&SF, RS&T and SF&T are the most important factors affecting the modulus, followed by other factors and interactions. When a higher draw ratio is applied, the speed of the final roller increases and the spin finish layer thickness on the fibres at constant spin finish pump speed will be affected, which could explain the interaction between the spin finish and the other factors. The friction between the oily fibres is affected after twist which has a notable effect on the related properties.

The Pareto chart for abrasion shows that the total number of drawing stages, twist level, total drawing ratio, relaxing stage, spin finish application and the interactions DS&DR, DS&RS, SF&T, DR&T and DS&T are the most important factors affecting the abrasion, followed by other factors and interactions. It could be noted that, when low draw ratio is applied with the relaxing stage, the yarn speed decreases, the cooling time increases and the spin finish layer's thickness will be increased.

Figure 7.19 and Figure 7.20 show the main effects and interaction plots of the statistical analysis of the effects caused by the main factors and their interactions on responses. The factor effect on the average responses of the low and high level of the factors was obtained using the design matrix and presented. All the interactions could be simulated, as the plot shows the existence or otherwise of the interaction of each of the two factors. The total drawing ratio, spin finish application, relaxing stage, twist level and the interactions DS&DR, DR&SF, DS&T, DR&RS, RS&T and SF&RS have their effects on thermal shrinkage. Effects and interaction plots for tenacity show that the total number of drawing stages and total drawing ratio are the factors affecting the tenacity. The interactions DS&DR, DR&T, DR&SF, DR&RS, DS&T and DS&RS and DS&SF have their effects which need to be further investigated using other methods to identify their significance.

Effects and interaction plots for elongation at break show that the total number of drawing stages, total drawing ratio and the interactions DS&DR, DR&T, SF&T, DS&RS and DR&RS are the factors affecting the elongation at break. The main effects of all factors and their interactions pronounced on modulus are the total number of drawing stages, total drawing ratio and the interactions DS&DR, DS&RS, SF&RS, DR&SF, RS&T and SF&T. The total

number of drawing stages, the total drawing ratio, the twist level and the interactions DS&DR, DS&RS, SF&T and DR&T affect the abrasion and their effects need to be analysed statistically. It is advised that factors influencing responses be assessed further to understand their influence more fully.

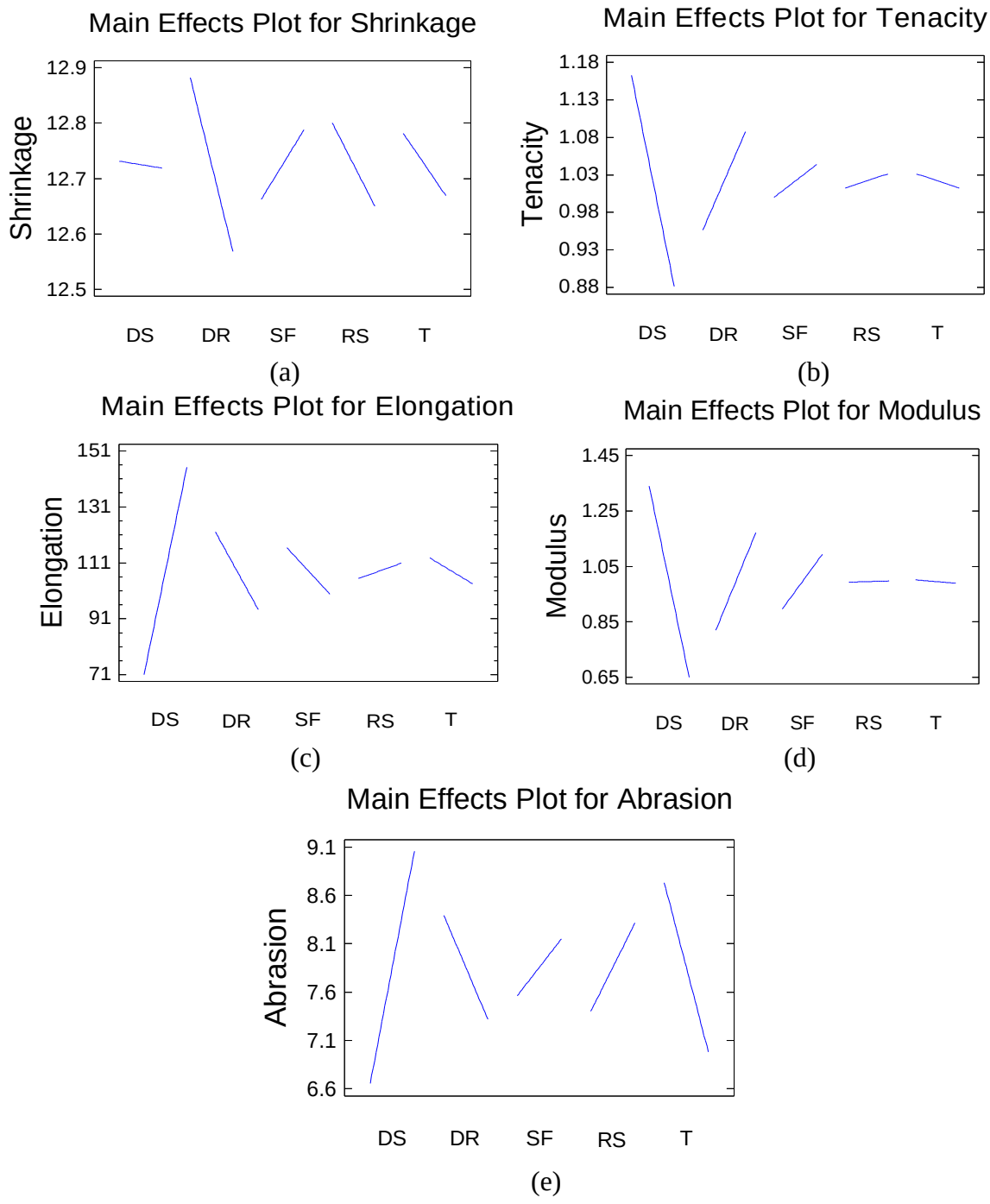

Figure 7.19 Main effect plots for the thermal shrinkage (a), tenacity (b), elongation at break (c), modulus (d) and abrasion (e)

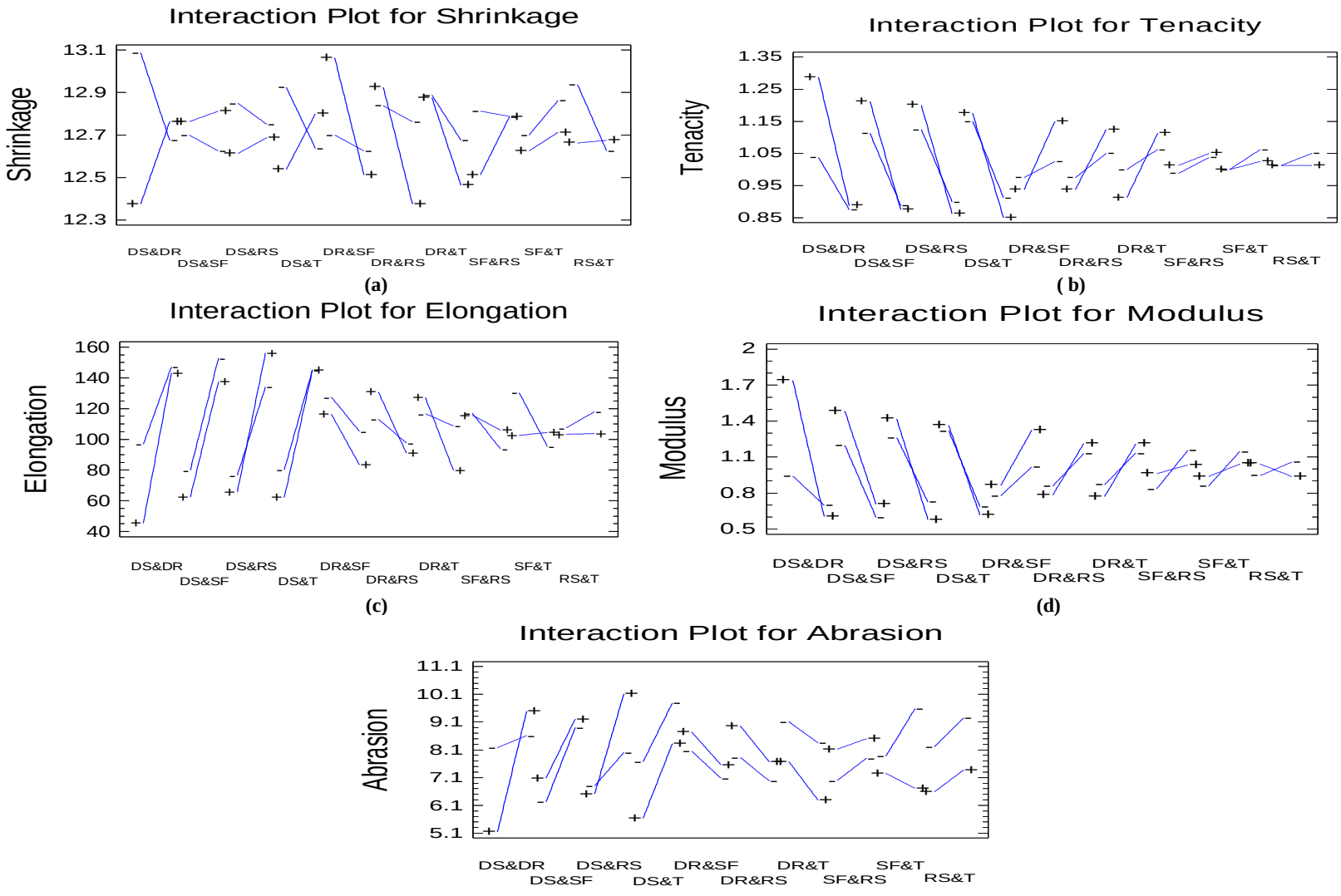

Figure 7.20 The interaction plots for the thermal shrinkage (a), tenacity (b), elongation at break (c), modulus (d) and abrasion (e)

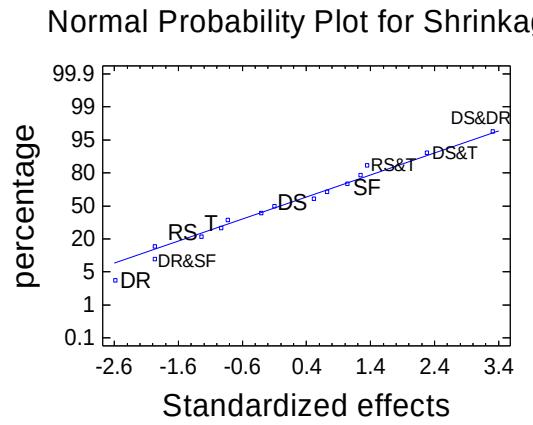

Thermal shrinkage (a)

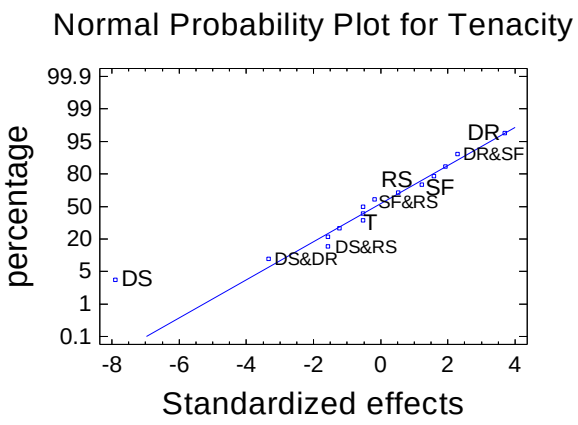

Tenacity (b)

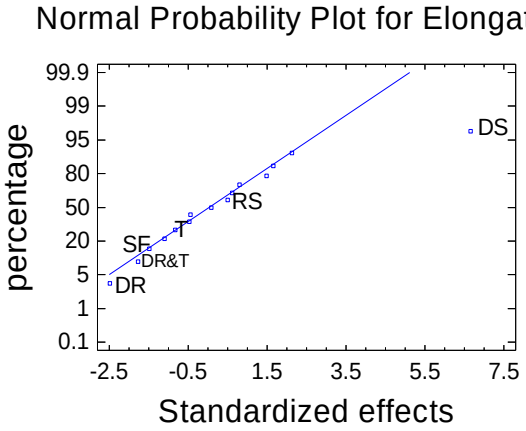

Elongation at break (c)

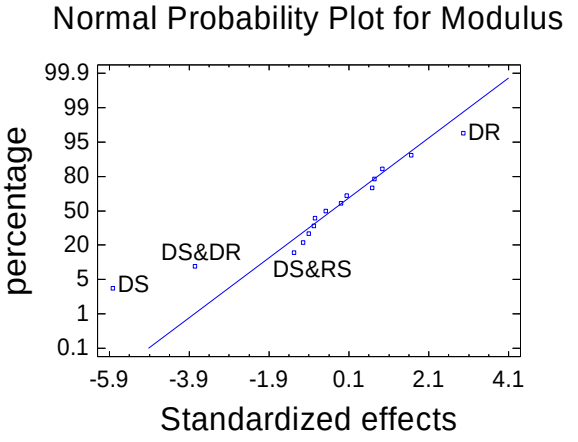

Modulus (d)

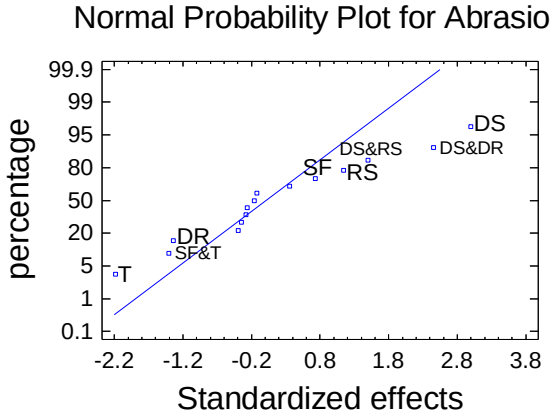

Abrasion (e)

Figure 7.21 Statistical standardized and percentage order values (Normal Probability Plot) of factors and their interactions for thermal shrinkage (a), tenacity (b), elongation at break (c), modulus (d) and abrasion (e)

Figure 7.21 displays the normal probability plot of the responses estimated. Draw ratio has a positive effect on tenacity and modulus and a negative effect on thermal shrinkage, elongation at break and abrasion. Twist level has a negative effect on all responses. Draw

stage has a positive effect on elongation at break and abrasion and a negative effect on thermal shrinkage, tenacity and modulus. The interaction between draw stage and drawing ratio has a positive effect on thermal shrinkage, elongation at break and abrasion and a negative effect on tenacity and modulus. When the tension is high and after applying spin finish, the spin finish plays a major role in the filament slippage on the last roller during processing and reduces the friction between the fibres during the testing which adds an additional interaction effect caused by the spin finish's relationship with other parameters.

7.7.2.1 Analysis of Variance (ANOVA)

To determine the factor effects in terms of statistical significance, analysis of variance (ANOVA) of the obtained data was conducted. ANOVA results are listed in Table 7.12; the significance of the studied factors affecting the thermal shrinkage are then total draw ratio and the interactions DS&DR and DS&T.

Source	P-Value				
	Thermal shrinkage	**Tenacity**	**Elongation at Break**	**Modulus**	**Abrasion**
DS	0.9189	0.0000	0.0000	0.0000	0.0085
DR	0.0199	0.0020	0.0243	0.0090	0.1981
SF	0.3163	0.2372	0.1580	0.1158	0.4737
RS	0.2323	0.6059	0.6282	0.9710	0.2712
T	0.3657	0.6059	0.4204	0.9214	0.0441
DS&DR	0.0044	0.0042	0.0493	0.0017	0.0261
DS&SF	0.6121	0.1340	0.9287	0.4675	0.7357
DS&RS	0.4794	0.1340	0.1577	0.2215	0.1534
DS&T	0.0369	0.2372	0.4373	0.6375	0.7242
DR&SF	0.0669	0.0366	0.6438	0.3641	0.9022
DR&RS	0.0669	0.1340	0.2877	0.5057	0.7823
DR&T	0.4201	0.0716	0.0947	0.4738	0.7015
SF&RS	0.2323	0.8630	0.5508	0.3092	0.7941
SF&T	0.7603	0.6059	0.1162	0.4431	0.1791
RS&T	0.1974	0.6059	0.6595	0.3747	0.8779

Table 7.12 ANOVA Results identifying the statistical significance of factors' effects on the results from analysis of variance (ANOVA) of the thermal shrinkage, tenacity, elongation at break, modulus and abrasion.

ANOVA analysis for mechanical properties shows that the drawing ratio, the number of drawing stages and their interaction have their significant effect on tenacity, elongation at break and modulus. The interaction between total draw ratio and spin finish application has a significant effect on tenacity. In terms of abrasion analysis, draw stage, twist level and the interaction between draw stage number and total draw ratio DS&DR have a significant effect and should be considered in process analyses which is related to the tension applied on the fibres during processing time which will add additional internal strain inside the fibres.

7.7.2.2 The regression Equation and Estimation Results

Based on the analysis of the fraction factorial experimental design (L32) results, simplified models based on statistical analysis for studied factors and their interactions were fitted by the regression equations for thermal shrinkage, tenacity, elongation at break, modulus and abrasion. The regression equations in terms of the previous coded values (Table 7.9) are as follows:

Thermal shrinkage = 15.6687 - 3.9125*DS - 0.175*DR + 1.04167*SF + 0.3125*RS - 0.071875*T + 0.533333*DS*DR + 0.0833333*DS*SF + 0.175*DS*RS + 0.1375*DS*T - 0.211111*DR*SF - 0.316667*DR*RS - 0.0333333*DR*T + 0.2*SF*RS - 0.0125*SF*T + 0.08125*RS*T (7.9)

Tenacity = 0.80625 + 0.90625*DS - 0.0125*DR - 0.195833*SF - 0.13125*RS - 0.0734375*T - 0.158333*DS*DR - 0.075*DS*SF - 0.1125*DS*RS - 0.021875*DS*T + 0.0722222*DR*SF + 0.075*DR*RS + 0.0229167*DR*T - 0.00833333*SF*RS - 0.00625*SF*T - 0.009375*RS*T (7.10)

Elongation at Break = 228.006 - 137.95*DS - 7.63333*DR - 30.05*SF + 36.35*RS + 13.0438*T + 31.6*DS*DR + 1.35*DS*SF + 33.025*DS*RS + 4.4375*DS*T - 4.66667*DR*SF - 16.3333*DR*RS - 6.59583*DR*T + 9.05*SF*RS + 6.16667*SF*T - 2.5*RS*T (7.11)

Modulus = -3.45125 + 3.01562*DS + 0.677083*DR + 0.0604167*SF + 0.589375*RS - 0.0154688*T - 0.594167*DS*DR - 0.1175*DS*SF - 0.30125*DS*RS - 0.0284375*DS*T + 0.0983333*DR*SF + 0.1075*DR*RS + 0.0289583*DR*T - 0.165833*SF*RS - 0.0310417*SF*T - 0.0540625*RS*T (7.12)

Abrasion = 21.0813 - 12.575*DS - 3.66667*DR + 3.8*SF - 0.1*RS + 0.76875*T + 2.61667*DS*DR - 0.366667*DS*SF + 2.4*DS*RS + 0.14375*DS*T - 0.0888889*DR*SF - 0.3*DR*RS - 0.104167*DR*T - 0.283333*SF*RS - 0.375*SF*T - 0.0625*RS*T (7.13)

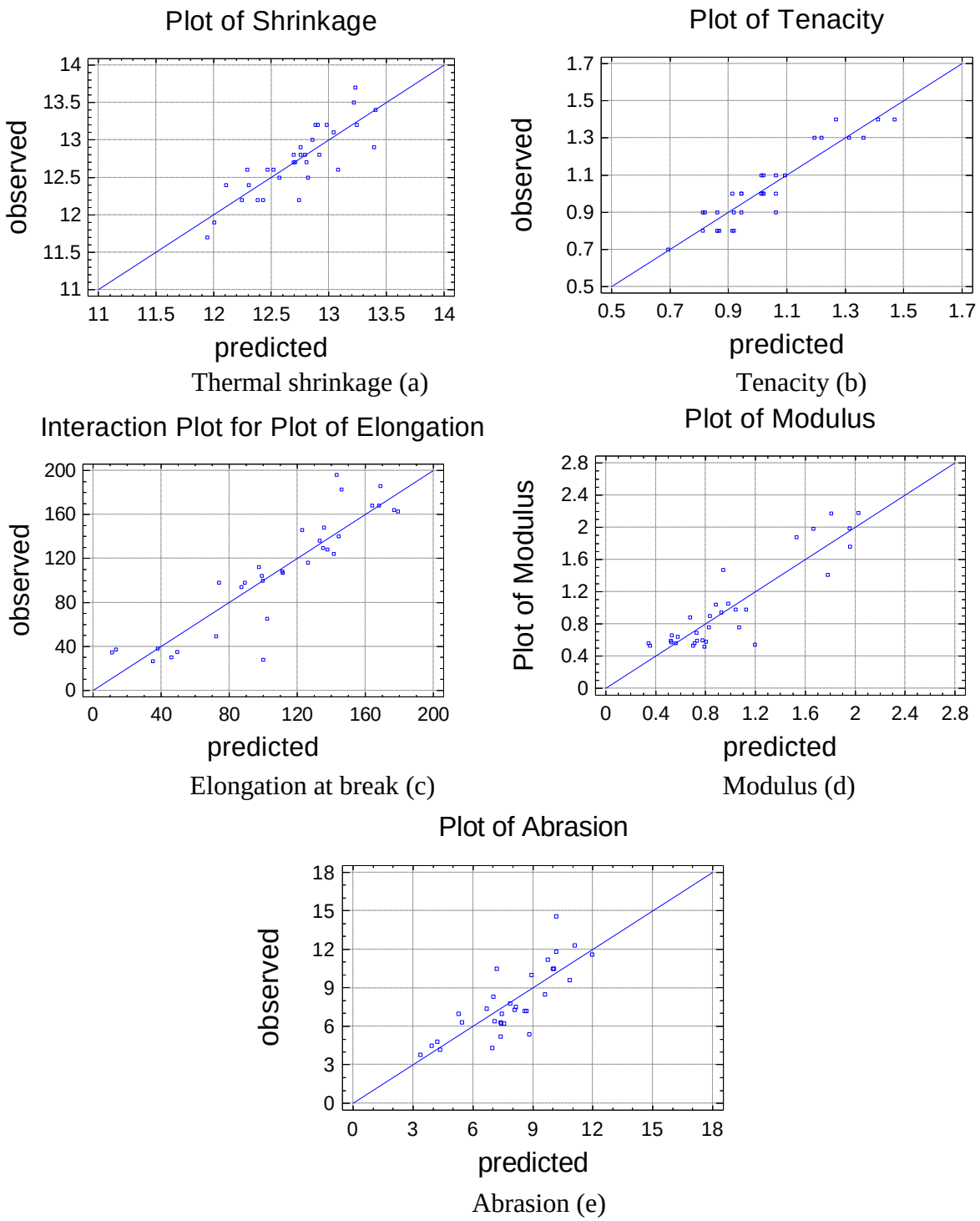

Figure 7.22 Experimental observed results and calculated fitted results plot for thermal shrinkage (a), tenacity (b), elongation at break (c), modulus (d) and abrasion (e).

Figure 7.22 shows the experimental observed results and calculated fitted results plot for thermal shrinkage (a), tenacity (b), elongation at break (c), modulus (d) and abrasion (e). Their Model Standard Error (MSE) values listed in Table 7.13 indicate the dispersion of

predicted and observed values around the theoretical fitted line generated using the fitted model for each trial. The model evaluates the significance effect of each independent variable to predict the response, depending on the coefficient constant for the linear effects of independent factors and the coefficient constant for the interaction effects, depending on the coefficient constant for the offset term. The predictive models gave useful results with small variation for previously described reasons such as draw frame setting based variation, the tension or slippage on the drawing roles or some tension while preparing the sample for testing. The pattern of estimated responses is based on the assumed model derived from the experimental observations.

7.7.3 Conclusion and Statistical Model for Optimisation

As-spun, biodegradable, linear aliphatic-aromatic co-polyester fibres were drawn and twisted at different multi-stage cold drawing and twisting conditions. The statistical model covers the number of drawing stages, total drawing ratio, spin finish application, relaxing stage ratio, twist level and their interactions. Regression models specify the combinations of the factor levels for enhancing the enhanced properties. Twist level has a negative effect on all responses. Draw stage has a positive effect on elongation at break and abrasion and a negative effect on thermal shrinkage, tenacity and modulus. The interaction between draw stage and drawing ratio has a positive effect on thermal shrinkage, elongation at break and abrasion and a negative effect on tenacity and modulus. Other factors and interactions have their effects but they are limited and less significant as they are covered by the governing factors, drawing ratio and temperature. The interaction between draw stage and spin finish could be related to the relationship between the tension in the last roller in the relaxing stage. The possible mechanism of the effect of the spin-finish application is caused by fibre friction or slippage in the drawing and relaxing stage. The models help processing scientists and technologists in industry to obtain the enhanced thermal shrinkage, tenacity, elongation at break, modulus and abrasion at suitable conditions related to final product cost and to obtain environmentally friendly, economical, energy-saving fibres. LAAC twisted yarns could be used in agricultural, horticultural and more non-traditional textile applications.

In Table 7.13, the optimization of thermal shrinkage, tenacity, elongation at break, modulus and abrasion shows the combination of factor levels which maximize and minimize the responses over the indicated region, and their MSE values described previously. The achieved models will form a source code in a forecasting program designed to optimize the drawing process of selected as-spun fibres.

Response	MSE	Optimum model	The combination of factor levels (↓: Low Level, ↑: High Level)				
			DS	DR	SF	RS	T
Thermal Shrinkage (%)	0.084	Maximum	↓	↓	↑	↓	↓
		Minimum	↓	↑	↑	↑	↑
Tenacity (g/den)	0.0416	Maximum	↓	↑	↑	↑	↑
		Minimum	↑	↓	↑	↑	↑
Elongation at Break (%)	9.22	Maximum	↑	↓	↑	↑	↑
		Minimum	↓	↑	↓	↑	↑
Modulus (g/den)	0.097	Maximum	↓	↑	↑	↑	↓
		Minimum	↑	↓	↑	↑	↑
Abrasion (number of rubs)	0.478	Maximum	↑	↑	↑	↑	↓
		Minimum	↓	↑	↑	↑	↑

Table 7.13 The combinations of factor levels for the effect of multi-stage cold drawing on the properties of LAAC fibres for thermal shrinkage, tenacity, elongation at break, modulus and abrasion.(MSE: Model Standard Error)

7.8 Statistical Modelling of The Effect of Cold Drawing and Twisting on Branched Aliphatic-Aromatic Co-Polyester Fibres (BAAC)

7.8.1 Experimental Results

According to the design shown in Table 7.10 involving control factors and their levels as listed in Table 7.9, the experiments were randomly conducted in one block. Each thermal shrinkage test was carried out using a MK IV Shrinkage-Force Tester; samples were heated for 2 minutes at 60^{o}C under a load cell of 10g. The Shirley Yarn Abrasion Tester was used to determine the abrasion resistance of yarns. The thermal shrinkage, mechanical properties and abrasion for BAAC fibres were measured and are listed in Table 7.14.

Again, draw frame setting based variation, the tension or slippage on the drawing roles and variation in the sample testing had an effect on the deviations which may have been related to them. The SEM photomicrograph of BAAC twisted fibres (Figure 7.23) shows the surface of the twisted fibres.

Trial Number	Thermal shrinkage (%)	Tenacity (g/den)	Elongation at Break (%)	Modulus (g/den)	Abrasion (number of rubs)
1	9.2	0.8	92	0.45	23
2	7.5	0.8	112	0.60	28
3	9.8	0.9	112	1.09	35
4	5.6	0.7	134	0.78	26
5	5.3	0.7	144	0.33	20
6	6.3	0.8	124	0.79	34
7	9.3	0.7	072	1.53	105
8	5.7	0.7	094	0.26	30
9	4.0	0.7	156	0.35	34
10	6.3	0.8	124	0.81	91
11	6.3	0.8	124	0.85	34
12	6.8	0.8	116	1.07	134
13	6.9	0.8	130	0.89	119
14	11	0.8	50.7	1.28	182
15	5.6	0.7	114	0.92	55
16	7.5	0.8	094	1.12	82
17	4.9	0.7	138	0.37	30
18	4.5	0.7	134	0.66	62
19	7.9	0.9	124	1.09	146
20	4.0	0.7	134	0.43	36
21	8.5	0.8	108	1.10	72
22	8.2	0.9	126	0.31	31
23	5.9	0.8	130	0.37	27
24	6.7	0.8	124	0.51	29
25	10	0.8	102	0.91	91
26	4.5	0.7	160	0.26	24
27	8.0	0.9	116	1.05	31
28	9.7	0.9	074	1.32	71
29	4.1	0.6	136	0.62	113
30	4.8	0.8	132	0.44	29
31	6.7	0.8	124	0.73	21
32	5.9	0.8	126	0.65	50

Table 7.14 Results for the cold drawing and twisting experiment (BAAC)

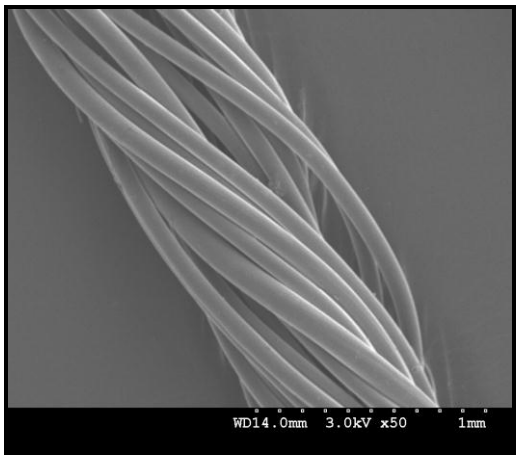

Figure 7.23. SEM photomicrograph of the surface of BAAC twisted fibres

7.8.2 Statistical Analysis and Discussion

In Figure 7.24, the Pareto charts for thermal shrinkage (a), tenacity (b), elongation at break (c), modulus (d) and abrasion (e) show the significant arrangement of factors and their interactions in decreasing order. The Pareto chart for thermal shrinkage shows that the determined factors would affect the tension and the internal stress affecting the thermal shrinkage properties, relaxing stage ratio, drawing stage number, total drawing ratio, twist level and the interactions DS&DR, DS&SF, DS&T, DR&SF, DS&RS and DR&T are the most important factors affecting the thermal shrinkage properties of the fibres, followed by other factors and interactions. In terms of mechanical properties, the Pareto chart for tenacity shows that the total number of drawing stages, twist level, total drawing ratio and the interactions DS&RS, RS&T, DS&T, DR&SF, DR&RS, SF&RS and DS&SF are the most important factors affecting the tenacity, followed by other factors and interactions.

The Pareto chart for elongation at break shows that the total number of drawing stages, twist level, relaxing stage, total drawing ratio, spin finfish application and the interactions DS&DR, DS&SF, RS&T, SF&T, DR&T and DS&RS are the most important factors affecting the elongation at break, followed by other factors and interactions. The Pareto chart for modulus shows that twist level, the total number of drawing stages, relaxing stage and the interactions SF&T, DS&DR, DR&SF, DS&SF, DR&T, DS&RS, SF&RS and RS&T are the most important factors affecting the modulus, followed by other factors and interactions. The Pareto chart for abrasion shows that twist level, spin finfish application, relaxing stage number, total drawing ratio and the interactions DS&RS, DR&RS, SF&T, DS&DR, DR&SF,

SF&RS and DS&T are the most important factors affecting the abrasion, followed by other factors and interactions. The interaction between the spin finish and other factors must be noted, as described previously.

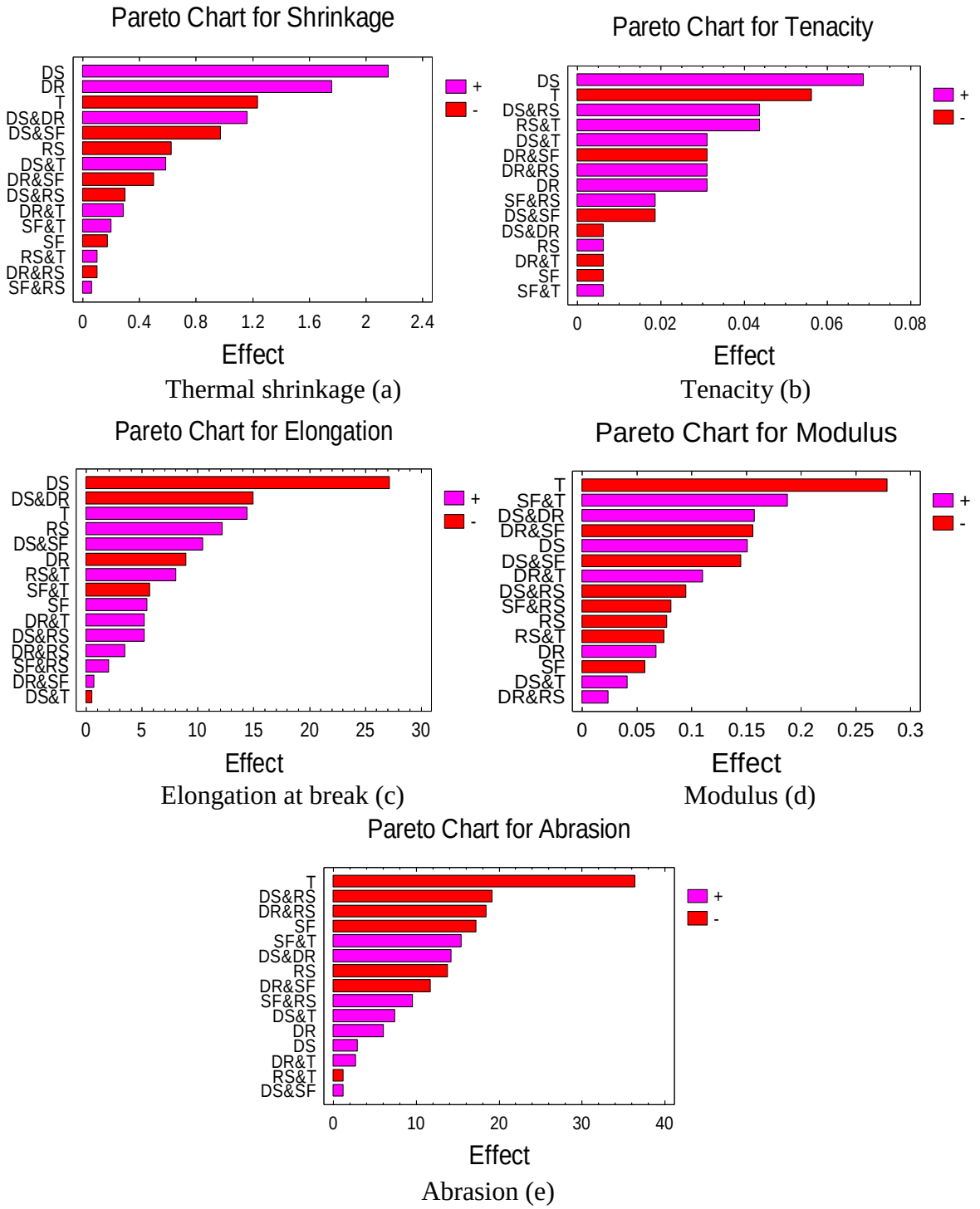

Figure 7.24 A ranked list of significant arrangement effects and interactions for thermal shrinkage (a), tenacity (b), elongation at break (c), modulus (d) and abrasion (e) (Pareto chart)

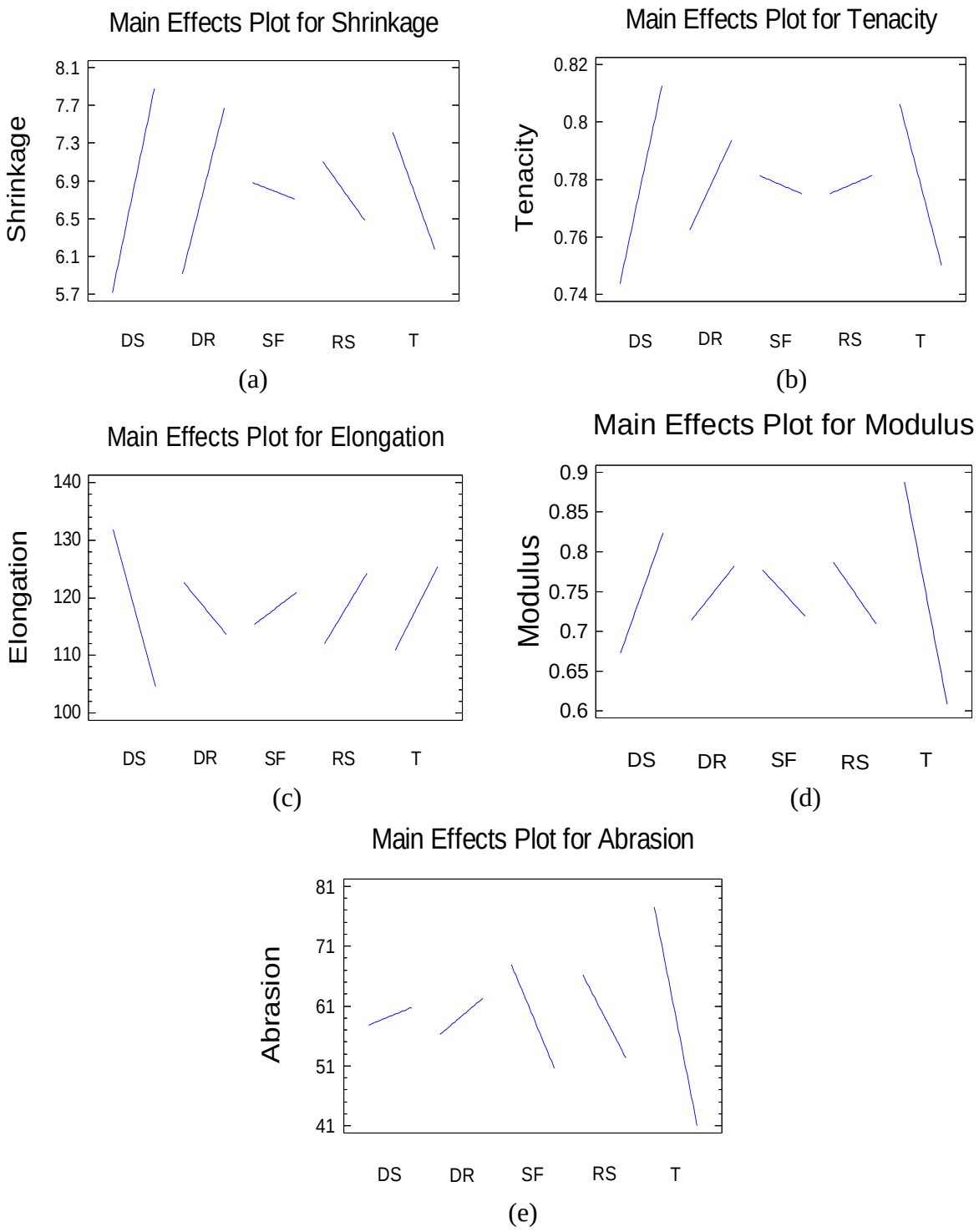

Figure 7.25 Main effect plots for the thermal shrinkage (a), tenacity (b), elongation at break (c), modulus (d) and abrasion (e).

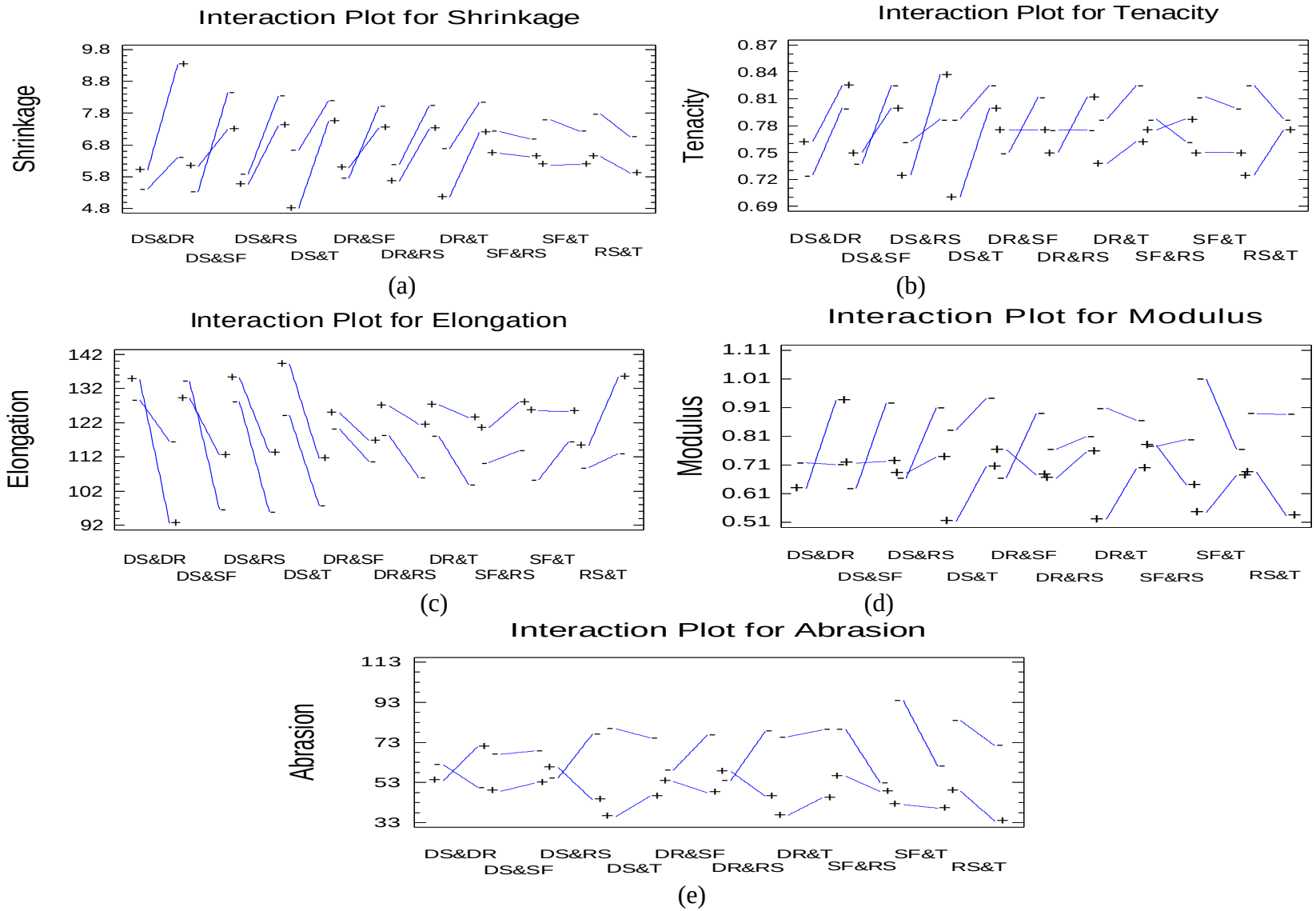

Figure 7.26 The interaction plots for the thermal shrinkage (a), tenacity (b), elongation at break (c), modulus (d) and abrasion (e).

Figure 7.25 and Figure 7.26 show the main effects and interaction plots of the statistical analysis of the effects caused by the main factors and their interactions on responses. The factor effect on the average responses of the low and high level of the factors was obtained using the design matrix and presented. The total number of drawing stages, total drawing ratio, twist level, relaxing stage and the interactions DS&DR, DS&SF, DS&T and DR&SF have their effects on thermal shrinkage which will be further investigated using ANOVA analysis to understand their influence more fully. Effects and interaction plots for tenacity show that the total number of drawing stages, total drawing ratio, twist level and the interactions DS&RS, RS&T, DS&T, DR&SF, DR&RS, SF&RS and DS&SF have their effects which need to be further investigated. Statistical analysis by ANOVA is given in the next section. The main effects and interaction plots for elongation at break show that the total number of drawing stages, twist level, relaxing stage and the interactions DS&DR, DS&SF, RS&T and SF&T are the factors affecting the elongation at break. Modulus is affected by twist level, the total number of drawing stages and the interactions SF&T, DS&DR, DR&SF, DS&SF, DR&T, DS&RS and SF&RS. Abrasion is affected by twist level, spin finish application, relaxing stage and the interactions DS&RS, DR&RS, SF&T, DS&DR and DR&SF. With one-stage drawing processes, the tension will be high and the spin finish plays an important role in the filament slippage on the last roller after applied spin finish. All the interactions could be simulated, as the plot shows the existence or otherwise of interaction between each of the two factors.

Figure 7.27 displays the normal probability plot of the responses estimated and illustrates further details about the normal distribution for the data. Draw stage has a positive effect on thermal shrinkage, tenacity, modulus and abrasion and a negative effect on elongation at break. Twist level has a negative effect on thermal shrinkage, tenacity, modulus and abrasion and a positive effect on elongation at break. The interactions RS&T and DS&RS positively affect tenacity. Relaxation stage and the interaction between drawing stage number and spin finish application positively affect elongation and thermal shrinkage negatively; These results were analyzed by ANOVA.

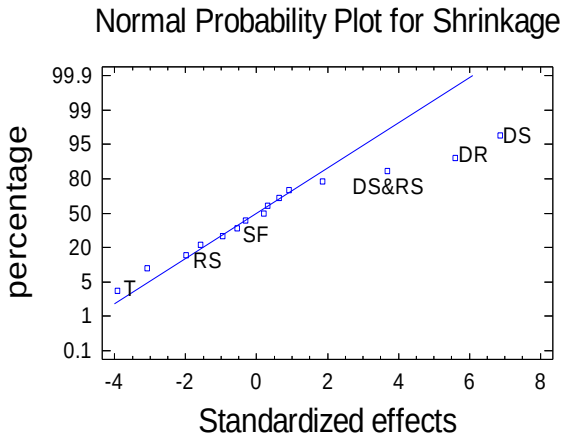

Thermal shrinkage (a)

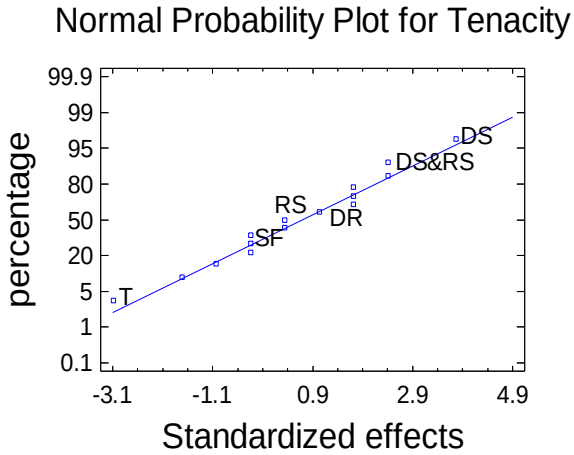

Tenacity (b)

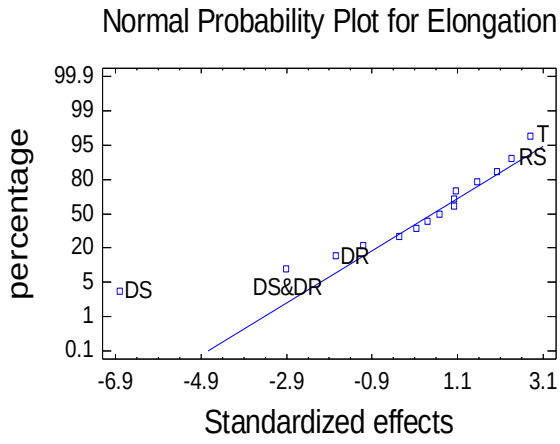

Elongation at break (c)

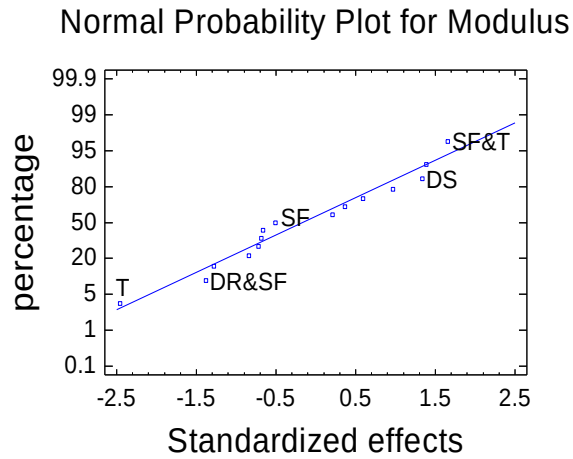

Modulus (d)

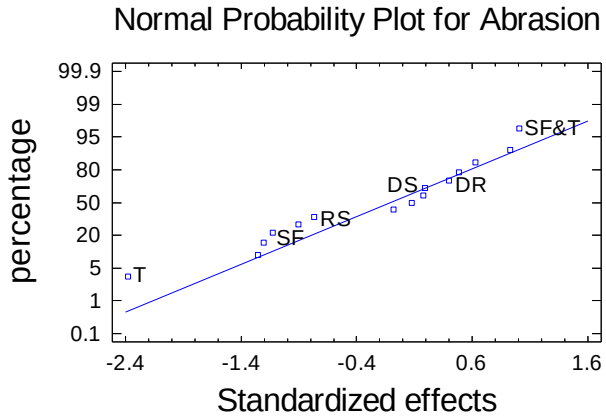

Abrasion (e)

Figure 7.27 Statistical standardized and percentage order values of factors and their interactions for thermal shrinkage (a), tenacity (b), elongation at break (c), modulus (d) and abrasion (e)

7.8.2.1 Analysis of Variance (ANOVA)

In order to determine the factor effects in terms of statistical significance, analysis of variance (ANOVA) of the obtained data was conducted. ANOVA results are listed in Table 7.15; drawing ratio has significant effect on tenacity, elongation at break, thermal shrinkage and abrasion. Draw stage has a significant effect on thermal shrinkage, tenacity and elongation at break. Twist has significant effect on thermal shrinkage, tenacity, elongation at break, modulus and abrasion. The interactions DS&RS and RS&T have a significant effect on tenacity. The interaction DS&DR significantly affects elongation at break and thermal shrinkage. Relaxing stage ratio and the interaction DS&SF significantly affect thermal shrinkage. Other interactions include their factors' significant effects on abrasion; their estimated response surfaces will be investigated.

Source	P-Value				
	Thermal shrinkage	**Tenacity**	**Elongation at Break**	**Modulus**	**Abrasion**
DS	0.0000	0.0017	0.0001	0.2010	0.8505
DR	0.0000	0.1056	0.1009	0.5601	0.6975
SF	0.5866	0.7361	0.3047	0.6191	0.2765
RS	0.0649	0.7361	0.0305	0.5042	0.3795
T	0.0012	0.0071	0.0126	0.0258	0.0300
DS&DR	0.0020	0.7361	0.0103	0.1840	0.3662
DS&SF	0.0070	0.3188	0.0591	0.2193	0.9382
DS&RS	0.3555	0.0289	0.3266	0.4146	0.2275
DS&T	0.0809	0.1056	0.9171	0.7208	0.6344
DR&SF	0.1323	0.1056	0.8925	0.1873	0.4540
DR&RS	0.7552	0.1056	0.5113	0.8368	0.2447
DR&T	0.3754	0.7361	0.3266	0.3466	0.8625
SF&RS	0.8454	0.3188	0.6964	0.4841	0.5396
SF&T	0.5348	0.7361	0.2838	0.1178	0.3272
RS&T	0.7552	0.0289	0.1375	0.5179	0.9375

Table 7.15 ANOVA results identifying the statistical significance of factor effects on the results from analysis of variance (ANOVA) of the data identifying the statistical significance of each factor for thermal shrinkage, tenacity, elongation at break, modulus and abrasion.

7.8.2.2 The regression Equation and Estimation Results

Based on the analysis of the fraction factorial experimental design (L32) results, simplified models based on statistical analysis for studied factors and their interactions were fitted by the regression equations for thermal shrinkage, tenacity, elongation at break, modulus and abrasion which were fitted to the experimental data. The pattern of estimated responses was based on the assumed model derived from the experimental observations; an error could come from either assignable causes that represent variation resulting from changes in the independent factors, or random causes that signify uncontrolled variation. The models evaluate the significance effect of each independent variable to a predicted response, depending on the coefficient constant for the linear effects of independent factors and the coefficient constant for the interaction effects, depending on the coefficient constant for the offset terms. The regression equations in terms of the previous coded values (Table 7.9) are given as follows:

Thermal shrinkage = 7.005 - 1.2575*DS - 0.9875*DR + 2.79167*SF + 0.2075*RS - 1.22687*T + 2.325*DS*DR - 1.3*DS*SF - 0.6*DS*RS + 0.29375*DS*T - 0.666667*DR*SF - 0.2*DR*RS + 0.14375*DR*T + 0.0833333*SF*RS + 0.0666667*SF*T + 0.05*RS*T (7.14)

Tenacity = 0.73375 + 0.01375*DS + 0.13125*DR + 0.0958333*SF - 0.44375*RS - 0.0465625*T - 0.0125*DS*DR - 0.025*DS*SF + 0.0875*DS*RS + 0.015625*DS*T - 0.0416667*DR*SF + 0.0625*DR*RS - 0.003125*DR*T + 0.025*SF*RS + 0.00208333*SF*T + 0.021875*RS*T (7.15)

Elongation at Break = 133.944 + 0.66625*DS + 14.7188*DR - 9.2025*SF - 48.1912*RS + 0.824063*T - 29.9125*DS*DR + 13.9417*DS*SF + 10.4125*DS*RS - 0.271875*DS*T + 0.941667*DR*SF + 6.9125*DR*RS + 2.60312*DR*T + 2.725*SF*RS - 1.90208*SF*T + 4.02188*RS*T (7.16)

Modulus = 1.67338 - 0.104*DS - 0.29*DR + 0.368333*SF + 0.5765*RS - 0.338*T + 0.315*DS*DR - 0.193333*DS*SF - 0.19*DS*RS + 0.020625*DS*T - 0.208333*DR*SF + 0.0475*DR*RS + 0.055*DR*T - 0.108333*SF*RS + 0.0625*SF*T - 0.0375*RS*T (7.17)

Abrasion = 215.635 - 63.5087*DS + 8.99375*DR - 18.3592*SF + 96.2838*RS - 28.8034*T + 28.4625*DS*DR + 1.60833*DS*SF - 38.4125*DS*RS + 3.70937*DS*T - 15.6583*DR*SF - 36.9625*DR*RS + 1.34688*DR*T + 12.7917*SF*RS + 5.15625*SF*T - 0.609375*RS*T (7.18)

Figure 7.28 shows the experimental observed results and calculated fitted results plot for thermal shrinkage (a), tenacity (b), elongation at break (c), modulus (d) and abrasion (e). Their Model Standard Error (MSE) values listed in Table 7.16 indicate the dispersion of predicted and observed values around the theoretical fitted line generated using the fitted

model for each trial. The predictive models gave useful results with small variation for previously described reasons, such as draw frame setting based variation, the tension or slippage on the drawing roles or some tension while preparing the sample for testing.

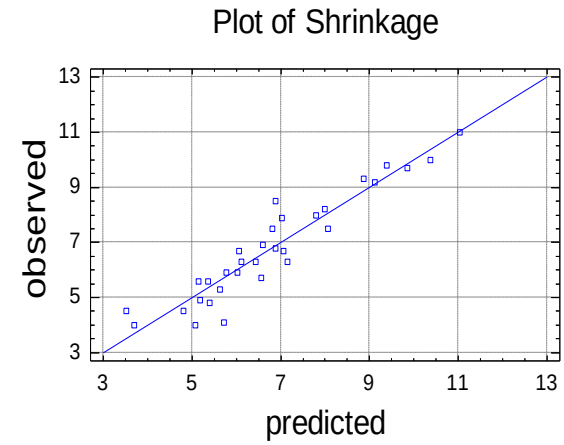

Thermal shrinkage (a)

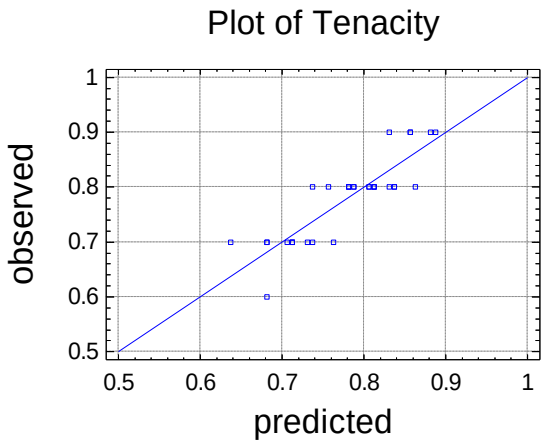

Tenacity (b)

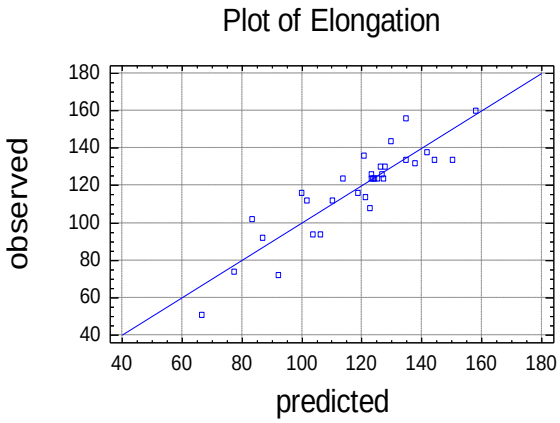

Elongation at break (c)

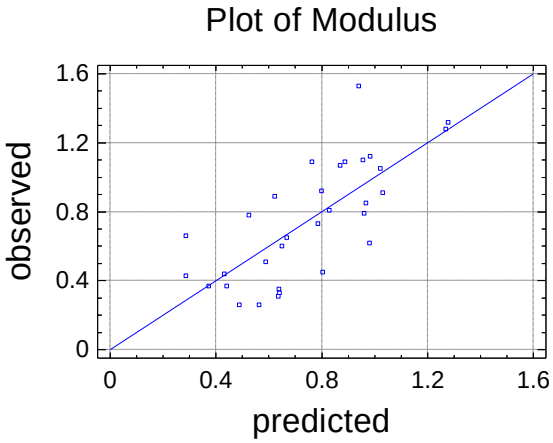

Modulus (d)

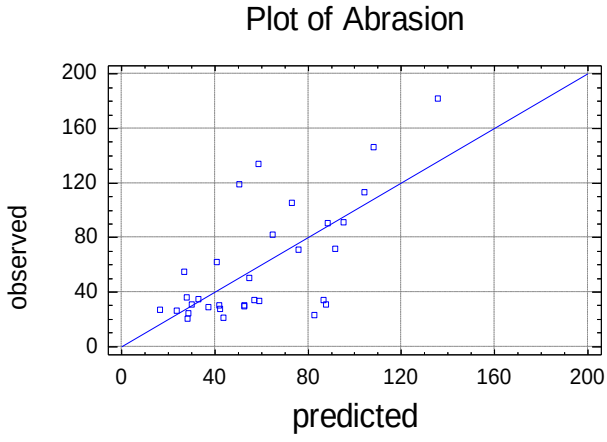

Abrasion (e)

Figure 7.28 Experimental observed results and calculated fitted results plot for thermal shrinkage (a), tenacity (b), elongation at break (c), modulus (d) and abrasion (e)

7.8.3 Conclusion and Statistical Model for Optimisation

As-spun, biodegradable, branched aliphatic-aromatic co-polyester fibres were drawn at different multi-stage cold drawing conditions. The statistical model covers the number of drawing stages, total drawing ratio, spin finish application, relaxing stage ratio, twist level and their interactions; models specify the combinations of the factors' levels for enhancing properties. Draw stage has a positive effect on thermal shrinkage, tenacity, modulus and abrasion and a negative effect on elongation at break. Twist level has a negative effect on thermal shrinkage, tenacity, modulus and abrasion and a positive effect on elongation at break. The interaction between the relaxing stage ratio and twist level or the number of drawing stages positively affects tenacity. Relaxation stage and the interaction between the number of drawing stages and spin finish application positively affect elongation and negatively affect thermal shrinkage. Other factors and interactions have their effects but they are limited and less significant as they are covered by the governing factors, drawing ratio and temperature. The effects from the interaction between draw stage and spin finish could be related to the practical relationship between the tension and the oily roller surface on the last roller in the relaxing stage, which causes some slippage. The optimization allows the production of a range of different properties from the same sample to suit different purposes.

Response	MSE	Optimum model	The combination of factor levels (↓: Low Level, ↑: High Level)				
			DS	DR	SF	RS	T
Thermal Shrinkage (%)	0.341	Maximum	↑	↑	↓	↓	↓
		Minimum	↓	↓	↓	↑	↑
Tenacity (g/den)	0.013	Maximum	↑	↑	↓	↑	↑
		Minimum	↓	↓	↓	↑	↑
Elongation at Break (%)	4.15	Maximum	↓	↑	↓	↑	↑
		Minimum	↑	↑	↓	↓	↓
Modulus (g/den)	0.061	Maximum	↑	↑	↓	↑	↓
		Minimum	↓	↓	↓	↓	↑
Abrasion (number of rubs)	7.54	Maximum	↑	↑	↓	↓	↓
		Minimum	↑	↓	↓	↑	↑

Table 7.16 The combinations of factor levels for the effect of multi-stage cold drawing on the properties of BAAC fibres for thermal shrinkage, tenacity, elongation at break, modulus and abrasion. (MSE: Model Standard Error)

Table 7.16 shows the combination of factor levels which maximize and minimize the responses over the region indicated. The achieved models could play a part in a forecasting program designed to optimize the drawing process of selected as-spun fibres. it also shows MSE values described previously. BAAC twisted yarns could be used in agricultural, horticultural and other non-traditional textile applications. The achieved model will form a part in a forecasting program designed to optimize the drawing process of selected as-spun fibres. The models will help processing scientists and technologists in industry to obtain the enhanced properties at suitable conditions related to final product cost and to obtain environmentally friendly, economical and energy-saving fibres.

7.9 Forecasting Program Based on the Texas Instrument TI-83

The programming stage is the most important stage in this research for developing a forecasting application depending on previous results and their optimization for this chapter and the obtained regression formulas in Chapter 6.

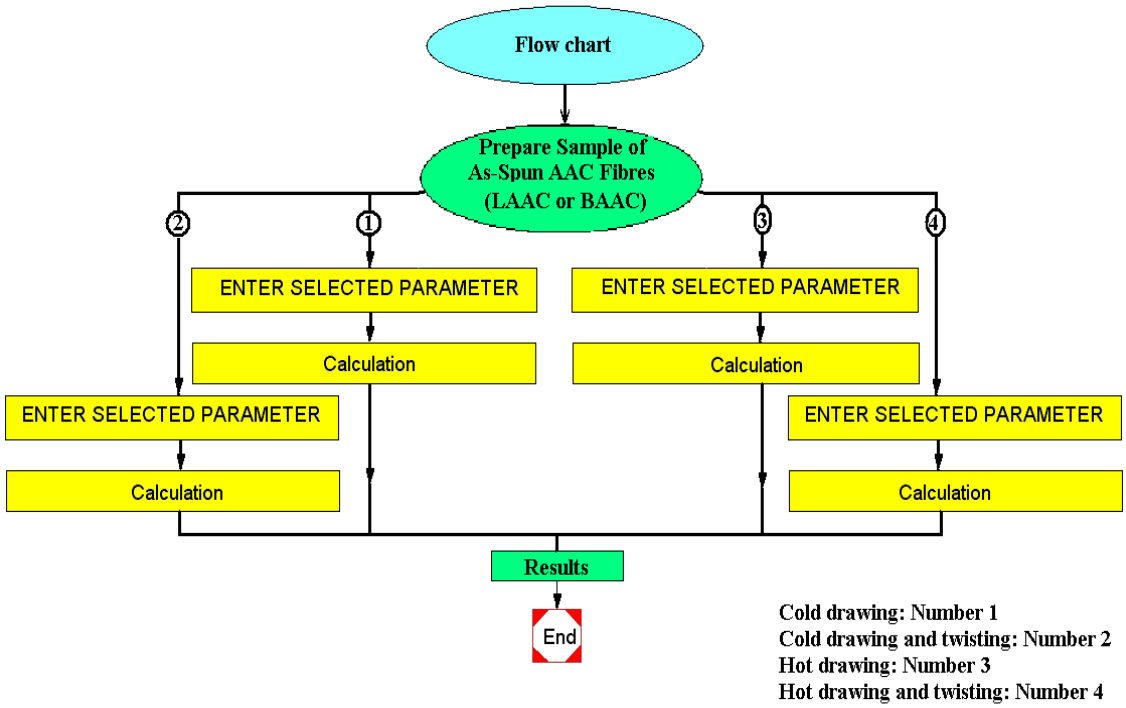

Figure 7.29 Schematic program process

Different samples of the same as-spun aliphatic-aromatic co-polyester fibres were drawn within the studied range to determine the parameters and their interaction effects and to test the forecasting regression equations. The program includes the mathematical models which estimate the studied responses, depending on the modelling and controlling of the processes. In the programming process, the relationship between key inputs (factors) and performance measures (responses) using factorial statistical experimental design technology is reported; the schematic program process for Texas Instrument is listed in
Figure 5.57. This application provides a basis for identifying the relationship between process-input and process-output data; it is based on and limited by the regions of the factors studied between the factors' levels. The programs for Texas instrument are outlined in Appendices **E** and **F**. The estimates are sufficiently accurate for practical application; the simulation results for the selected as-spun fibres are in agreement with available data within acceptable variation.

7.10 General Conclusion

In the present chapter, modelling of the effects of multi-stage cold drawing and twist processes' conditions on thermal and physical properties of linear (LAAC) and branched (BAAC) aliphatic-aromatic co-polyester fibres was statistically investigated and characterized. To separate the effect of temperature and the remaining factors in the hot drawing process, modelling of cold drawing was needed. The additional effect gained from adding twisting to the continuous drawn filament was investigated in terms of the interaction processes. In terms of cold drawing process, fibres could have improved mechanical properties after cold drawing. Drawing orients crystallites in the direction of the stretch; the modulus in that direction is increased and elongation at break is decreased. That does not mean they will have the best structural properties required for further treatment processes. Adding the annealing effect (the hot relaxation) after cold drawing forms an additional continuous step for the cold drawing process. This stage affects the contemporary fast process and could add heat shock to the internal structure, if it is applied at high temperature and over a short time. In addition to the fraction effect, spin finish adds a cooling effect in this stage and overcomes other interaction with the factors controlling the speed and then the spin finish oil layer thickness on the coated fibres. Some applications need special

mechanical properties without additional treatment processes; in such cases, the cold drawing process could be an economical process to obtain the compatible fibres which have the high stability of AAC fibres. A full statistical experimental design was used as a function of process parameters using statistical factorial methods. As a two-level experiment, factor and interaction effects could be determined as the difference between the average responses at the low and the high level of cold drawing process parameters. A general conclusion could be summarized as follows:

1. **When as-spun, biodegradable, linear aliphatic-aromatic co-polyester fibres are cold drawn**: The draw ratio, the interaction between the number of drawing stages and drawing ratio and the interaction between spin finish application and both of the number of drawing stages and drawing ratio have a positive effect on thermal shrinkage. Draw ratio has a negative effect on elongation at break and a positive effect on tenacity and modulus. Draw stage and its interaction with draw ratio have a positive effect on elongation at break and a negative effect on tenacity and modulus. The negative effects from the interaction between draw stage and spin finish were less prominent and could be related to the practical relationship between the tension and the oily roller surface on the last roller in the relaxing stage which caused some slippage affecting the internal stress and also on thermal shrinkage and elongation.
2. **When as-spun, biodegradable, branched aliphatic-aromatic co-polyester fibres are cold drawn**: Draw ratio and draw stage have a positive effect on thermal shrinkage, tenacity, modulus and elongation at break. Relaxing stage ratio has a negative effect on thermal shrinkage, tenacity, modulus and a positive effect on elongation at break. The interaction between draw stage and draw ratio has a positive effect on thermal shrinkage, tenacity, modulus and a negative effect on elongation at break.
3. **For further investigation and by comparing of the results of drawing the LAAC and BAAC as-spun fibres in Table 7.17**, the table below summarizes points 1 and 2 and makes it easy to identify the differences which could arise, depending on polymer grade, linear or branched. When the high draw ratio was applied without the relaxing stage, the time of contact of the filaments with the spin finish guide decreased. If the relaxing ratio is low, that will give less opportunity for loss of heat before filaments go to the winder and add another effect of relaxing process time. With no relaxation under heat, a difference in the softening ratio from those of other conditions could be found; the relaxing stage helps the fibre chain to relax and stabilize. As was found in the hot

drawing process, the higher draw ratio led to a higher degree of molecular orientation and higher fibre tenacity with lower extensibility and then the fibre could be stiffer and that will be noted later when twist is applied and an abrasion test is discussed.

Source	Thermal shrinkage		Tenacity		Elongation at Break		Modulus	
	LAAC	BAAC	LAAC	BAAC	LAAC	BAAC	LAAC	BAAC
DS	—	▲	▲	▲	▲	▲	▲	▲
DR	▲	▲	▲	▲	▲	▲	▲	▲
SF	—	—	▲	—	—	—	—	—
RS	—	—	▲	—	—	▲	—	—
DS&DR	▲	▲	▲	▲	▲	—	▲	▲
DS&SF	▲	▲	▲	—	—	▲	—	▲
DS&RS	—	—	—	▲	—	—	—	—
DR&SF	▲	▲	—	—	▲	—	—	—
SF&RS	—	—	▲	—	—	—	—	—

Table 7.17 The combinations of the factor effect of multi-stage cold drawing on the properties of AACs fibres (▲: Significant, —: Not Significant)

Source	Thermal shrinkage		Tenacity		Elongation at Break		Modulus	
	D	T	D	T	D	T	D	T
DS	—	—	▲	▲	▲	▲	▲	▲
DR	▲	▲	▲	▲	▲	▲	▲	▲
SF	—	—	▲	—	—	—	—	—
RS	—	—	▲	—	—	—	—	—
T	/	—	/	—	/	—	/	—
DS&DR	▲	▲	▲	▲	▲	▲	▲	▲
DS&SF	▲	▲	▲	—	—	—	—	—
DR&SF	▲	—	—	▲	▲	—	—	—
SF&RS	—	—	▲	—	—	—	—	—
DS&T	/	▲	/	—	/	—	/	—

Table 7.18 The combinations of the effect of multi-stage cold drawing factors before and after applying twist on the properties of LAAC fibres (▲: Significant, —: Not Significant, /: Not applied, **D**: drawing only, **T**: drawing and twisting)

4. **When drawn, biodegradable, linear aliphatic-aromatic co-polyester fibres are twisted:** Draw stage has a positive effect on elongation at break and abrasion and a negative effect on thermal shrinkage, tenacity and modulus. The interaction between draw stage and drawing ratio has a positive effect on thermal shrinkage, elongation at break and abrasion and a negative effect on tenacity and modulus.

Twist level has no individual effect but its interaction with the number of drawing stages affecting the internal stress when high twist level is applied without relaxing stage. Twist level decreases the impact of the effect of the interaction between drawing ratio and spin finish on thermal shrinkage. Twist decreases the effect of the interaction between the spin finish application and total number of drawing stages of the drawing process on tenacity; twist level value increases the effect of the interaction between the spin finish application and the draw ratio on tenacity and elongation at break. The effect of other factors and their interactions seem to be the same, as the soft twist process was added to the process. Twisting provides lateral cohesion of filaments which helps in fabric manufacturing, in addition to the increase of the strength of twisted fibres compared with untwisted fibres. The radial position of the filaments improves the strength of the yarn as a result of the interaction effect. From Table 7.18, it can be seen that applying twist does not significantly affect tenacity but it decreases the effect of spin finish application and the relaxing stage of the drawing process and their interaction.

5. **When drawn, biodegradable, branched aliphatic-aromatic co-polyester fibres are twisted:** Draw stage has a positive effect on thermal shrinkage, tenacity, modulus and abrasion and a negative effect on elongation at break. Twist level has a negative effect on thermal shrinkage, tenacity, modulus and abrasion and a positive effect on elongation at break. The interaction between the relaxing stage ratio and twist level or the number of drawing stages positively affects tenacity. Relaxation stage and the interaction between the number of drawing stages and spin finish application positively affect elongation and negatively on thermal shrinkage. From Table 7.19, it can be seen that applying twist significantly affects thermal shrinkage, tenacity, elongation at break and modulus.

Twist level decreases the effect of the effect of the interaction between drawing ratio and spin finish on thermal shrinkage. Twist level decreases the impact of the effect of the drawing ratio on mechanical properties. Twist level decreases the effect of the number of drawing stages on modulus. Twist level decreases the effect of interaction between the number of drawing stages and the draw ratio on tenacity and modulus and increases the elongation at break. Twist level decreases the effect of interaction between the number of drawing stages and the spin finish on elongation at break and modulus. The twist level value interaction with the relaxing stage ratio has a significant effect on the tenacity. The effect of

other factors and their interactions appeared to be the same as the soft twist process was added to the process.

Source	Thermal shrinkage		Tenacity		Elongation at Break		Modulus	
	D	T	D	T	D	T	D	T
DS	▲	▲	▲	▲	▲	▲	▲	—
DR	▲	▲	▲	—	▲	—	▲	—
SF	—	—	—	—	—	—	—	—
RS	—	—	—	—	▲	▲	—	—
T	/	▲	/	▲	/	▲	/	▲
DS&DR	▲	▲	▲	—	—	▲	▲	—
DS&SF	▲	▲	—	—	▲	—	▲	—
DS&RS	—	—	▲	▲	—	—	—	—
DR&SF	▲	—	—	—	—	—	—	—
RS &T	/	—	/	▲	/	—	/	—

Table 7.19 The combinations of the effect of multi-stage cold drawing factors before and after applying twist on the properties of BAAC fibres (▲: Significant, —: Not Significant, /: Not applied, **D**: drawing only, **T**: drawing and twisting)

6. **For further investigation and by comparing the results of applying twist to both LAAC and BAAC drawn fibres in Table 7.20**, it could be concluded that there is recognized effect of the number of drawing stages and twist on thermal shrinkage of BAAC twisted fibres; their interaction has a significant effect on thermal shrinkage of LAAC twisted fibres. Draw ratio and its interaction with the number of drawing stages have a significant effect on thermal shrinkage of both LAAC and BAAC twisted fibres. The number of drawing stages, twist level value and their interactions with relaxing stage ratio have a significant effect on tenacity of BAAC twisted fibres. Draw stages number, drawing ratio, their interaction and the interaction between draw ratio and spin finish application have a significant effect on the tenacity of LAAC twisted fibres. Draw stages number, drawing ratio and their interaction have a significant effect on elongation at break and modulus of LAAC twisted fibres. Draw stages number, relaxing stage ratio, twist level value and the interaction between draw stage and draw ratio have a significant effect on elongation at break of BAAC twisted fibres.

The significant effect of twist level number of twisted BAAC fibres overcomes the effect of other factors on modulus and abrasion. Draw stages number, twist level value and the interaction between draw stage and draw ratio have a significant effect on abrasion of twisted

LAAC fibres. Abrasion-resistance as a fibre property gave an indication about the wear in the actual fibre use. The increase of twist increased the cohesion between the fibres and the stiffness of yarn, which might have reduced abrasion resistance. Theoretically, thermal shrinkage without the dimensional restraint annealing process will decrease with increasing draw ratio and annealing temperature but will decrease with an increase in the drawing temperature. Thermal shrinkage in the dimensional restraint annealing process will affect the fibre structure and will be different with regard to the material properties [224].

Source	Thermal shrinkage		Tenacity		Elongation at Break		Modulus		Abrasion	
	LAAC	BAAC	LAAC	BAAC	LAAC	BAAC	LAAC	BAAC	LAAC	BAAC
DS	—	▲	▲	▲	▲	▲	▲	—	▲	—
DR	▲	▲	▲	—	▲	—	▲	—	—	—
SF	—	—	—	—	—	—	—	—	—	—
RS	—	—	—	—	—	▲	—	—	—	—
T	—	▲	—	▲	—	▲	—	▲	▲	▲
DS&DR	▲	▲	▲	—	▲	▲	▲	—	▲	—
DS&RS	—	—	—	▲	—	—	—	—	—	—
DS&T	▲	—	—	—	—	—	—	—	—	—
DR&SF	—	—	▲	—	—	—	—	—	—	—
RS&T	—	—	—	▲	—	—	—	—	—	—

Table 7.20 The combinations of the factor effect of multi-stage cold drawing and twisting on the properties of AACs fibres (▲: Significant, —: Not Significant)

Drawing tension is a function of drawing; the stability of the process is affected by a reduction of drawing temperature or an increase of drawing ratio. The actual draw ratio was less than the nominal draw ratio, because the draw line shrank when tension was removed; yarn should not slip during drawing. In one-stage drawing experiments and in addition to the spin finish applied to the as-spun fibres during extrusion process, the tension will be high and the spin finish plays a central role in the filament slippage on the last roller after applied spin finish, in addition to its interaction with twist level and surface friction. The mathematical models achieved will help processing experimentalists and technologists in industry to obtain the enhanced properties at suitable conditions related to final product cost and to obtain environmentally friendly, economical and energy saving fibres. AAC fibres, yarns and textiles could be used in agricultural, horticultural and more non-traditional textile applications.

CHAPTER 8 - CONCLUSIONS AND FUTURE WORK

8.1 Overall Conclusion

This research offers economical biodegradable fibres for use in disposable textiles setting new horizons of textile industries; the statistical method used and designed program will help in the optimization, planning and organizing of both processing cost and the fibre properties. The statistical forecasting programs based on the regression models obtained, resulting in the fast and accurate practices of the process energy reduction to get the required fibres over the indicated region; it covers the identified, significant parameters of the main and interaction processes and specifies the combinations of setting values for enhancing response.

An understanding of the interactive relationships between the parameters is very important when managing the melt spinning process through the fibre quality. From previous investigations, the following conclusion has been drawn:

- Although aliphatic-aromatic co-polyester is an oil-based polymer, it is biodegradable and therefore has minimal environmental effects when sent to landfill where it degrades naturally with no toxic by-products as a new generation of smart materials. The biodegradable fibres processed at low temperature have a positive environmental impact and reduction in the carbon footprint; the process parameters affect the properties, productivity and product cost.
- Fibres and fabrics could be produced from AACs after optimizing and finding the suitable conditions for the enhanced product properties. The AAC fibres produced are biodegradable and less complex than natural fibres. AAC fibres could be mixed with other fibres to make stable yarns, non-woven, woven and knitted fabrics.
- The torque value required for the extrusion process decreases with an increase in the temperature profile and through extrusion time; it depends scientifically on the temperature profile and the polymer grade. The metering zone temperature and die head or extrusion temperature exhibit little effect on torque; their effects on the viscosity leads to a decrease in the torque needed to run the screw because the die head pressure decreasing.

- In the optimization of processability and spinability, as-spun linear aliphatic-aromatic co-polyester fibres were spun under a fractional factorial design as a function of the extrusion temperature profile and polymer grade, using appropriate statistical methods. The overall orientation and the crystallographic order of as-spun fibres are affected by the polymer grade and the extrusion temperature. It has been noted that the extrusion temperature, the polymer grade and their interaction are the most significant factors affecting the mechanical properties and spinning productivity. The fibres spun at relatively low temperature had more highly oriented structure than those at high temperature.

  An additional statistical analysis of the heat setting effect on the thermal shrinkage and mechanical properties of drawn LAAC fibres has been optimized; which helps in the treatment, finishing and method of use of the produced fibres. Regarding the heat setting effects on the internal structure of the fibres, temperature positively affects the elongation at break and thermal shrinkage and negatively the tenacity and the modulus of the fibres. Tension load negatively affects the thermal shrinkage and positively the tenacity and the modulus of the fibres. The insignificant effect of tension load was identified on elongation at break and the effect of heat setting time was identified on all responses. The LAAC fibres made of the low melt flow index have more stabilized structure and mechanical properties than those made of the higher melt flow index grade.
- Variation in spinning conditions leads to a better insight into the relationship between melt spinning process conditions and the fibre properties produced. Different samples of as-spun linear aliphatic-aromatic co-polyester (the lower melt flow index grade - Solanyl flexibility component) and branched aliphatic-aromatic co-polyester (Ecoflex F BX 7011) were spun at different melt spinning conditions to determine their effects.
- **For as-spun LAAC fibre modelling:**

  An investigation of the thermo-graphic measurement results showed that the combination between the metering pump speed and the high spinning temperature in filaments extrusion leads to small reduction in the filament diameter and then the heat content and vice versa. There is a clear relationship between spin draw ratio and the improvement of the overall orientation of the fibres which has a significant effect on the drawability.

  Temperature has a significant effect on the spin draw ratio and drawability, which are related to the extrusion rate and spin line tension. Spinning temperature and metering pump speed are the most important factors affecting the die head pressure; a decrease of

spinning temperature leads to higher viscosity, higher flow resistance through the spinneret's nozzle and high die head pressure. The metering pump speed and the interaction between the spinning temperature and the quench air cooling speed seem to have an effect on crystallographic order. Cooling time is affected by extrusion rate, fibre cross-section and air cooling temperature. Metering pump speed, spinning temperature, winding speed and quench air cooling speed are the most important factors affecting the temperature average of the filaments in the cooling window. Melt extrusion temperature, metering pump speed, winding speed and the interaction between the metering pump and the winding speeds are the most important factors affecting the diameter. Extrusion temperature, winding speed and metering pump speed are the most important factors affecting the mechanical properties and thermal shrinkage.

- **For as-spun BAAC fibre modelling:**

  A decrease of spinning temperature leads to higher viscosity and higher flow resistance through the spinneret's nozzle and high die head pressure which should be taken into account in the BAAC production stage. From an investigation of the thermo-graphic measurement results, it is clear that the combination between the higher metering pump speed and the high spinning temperature in filaments extrusion leads to high level in the filament heating content. The spin draw ratio is significantly affected by winding speed, metering pump speed, spinning temperature and the interactions between them. The winding speed affects the spin draw ratio and tension on material from the spinneret through the cooling and solidification stages. Metering pump speed plays an interactive role with winding speed in the relationship between the extrusion speed and the collecting at different speeds. Spinning temperature and metering pump speed have a significant effect on die head pressure while low spinning temperature leads to high die head pressure. The air quench cooling ratio is affected by throughput rate, yarn cross section and air cooling temperature. The filament temperature average in the cooling window is significantly affected by metering pump speed, spinning temperature, winding speed, quench air speed and the interactions between quench air speed, spinning temperature and metering pump speed. The diameter is positively affected by metering pump speed and the interaction between the spinning temperature and the winding speed and negatively affected by winding speed and its interaction with the metering pump speed. Tenacity is positively affected by winding speed and spinning temperature speed and negatively by the metering pump speed. Together with the negative effects of

spinning temperature and winding speed, metering pump speed and its interaction with winding speed positively affect the elongation at break. It is significant that winding speed has a positive effect and metering pump speed has a negative effect on the modulus. The thermal shrinkage is positively affected by winding speed, spinning temperature, the interaction between winding speed and metering pump speed and the spin finish application and negatively affected by increasing metering pump speed.

- **For blend ratio modelling:**

  The three grades of aliphatic aromatic copolyester were used in this investigation: linear grades (LAAC1/low MFI and LAAC2/high MFI) and branched grade (BAAC).

  For as-spun fibre, the BAAC blend ratio positively affects the count, tension and die-head pressure. LAAC2 blend ratio negatively affects the count, tension and die-head pressure. The LAAC1 blend ratio has a small effect on the count, tension and die-head pressure. The count, tension and die head pressure are affected by rheology and density of the polymer which explains the significant effect of the branched grade on those properties. The BAAC blend ratio positively affects the tenacity and the modulus and negatively affects the elongation at break, with a small effect on thermal shrinkage. The LAAC2 blend ratio negatively affects the tenacity, modulus and thermal shrinkage. It positively affects elongation at break. The LAAC1 blend ratio has a small negative effect on the tenacity and modulus. It positively affects the elongation at break, with small effect on thermal shrinkage.

  For drawn fibres, the BAAC blend ratio positively affects the count and negatively the thermal shrinkage properties of the fibres. The LAAC2 blend ratio negatively affects the count and positively the thermal shrinkage properties. The LAAC1 blend ratio has a small effect. The BAAC blend ratio positively affects the tenacity and the modulus and it negatively affects elongation at break. The LAAC2 blend ratio negatively affects the tenacity and modulus. It has a positive effect on elongation at break. The LAAC1 blend ratio has a negative effect on the elongation at break. It has a small effect on tenacity and modulus.

- The programming stage using a visual basic program is very important for developing a forecasting application, depending on the previous multiple regression analysis and forecasting mathematical models. The program includes the mathematical models which estimate the studied responses to realize the full potential of the simulator for identifying

the relationship between process-input and process-output data. It provides a communication environment between the industrial application and research results.

The program saves the processing cost required for enhanced fibres, depending on the process conditions selected by the user. For the non-statistician, the Texas instrument covers the need for a fast and accurate technique to calculate without the need for further statistical background and computing equipment (Appendices B, C, D, E and F).

A set of processing conditions was selected for each of the ranges studied to evaluate the forecasting regression equations obtained. The simulation results are in agreement with available data within useful results for physical properties and small variation for structural related properties.

- Modelling of the effects of multi-stage hot drawing and twist process conditions on the thermal and physical properties of linear and branched aliphatic-aromatic co-polyester fibres was statistically investigated and characterized.

  When as-spun, biodegradable, linear aliphatic-aromatic co-polyester fibres are hot drawn, the total draw ratio has a positive effect but draw temperature and plate temperature have a negative but important effect on the birefringence. Spin finish application and relaxing temperature had negative effects on FWHM. The positive effects from the number of drawing stages, the interactions (DS&DT, DR&RS and PT&RT) were drawing temperature, relaxing stage ratio while the interactions (DS&DR and DT&RS) had a negative effect on thermal shrinkage. In terms of mechanical properties, draw ratio had a negative effect on elongation at break and a positive effect on tenacity and modulus. Draw temperature had either a positive effect on elongation at break or a negative effect on tenacity and modulus.

  When as-spun, biodegradable, branched aliphatic-aromatic co-polyester fibres are hot drawn, the total raw ratio, draw temperature, plate temperature and draw stage had a positive effect on thermal shrinkage, tenacity and modulus and a negative effect on elongation at break. Relaxing stage ratio had a positive effect on elongation at break and a negative effect on thermal shrinkage and modulus; relaxing stage ratio had a small effect on tenacity. The interactions DT&DR and DS&RS had a clear effect on thermal shrinkage. The interactions (DS&DT, DR&RS and PT&RT) were significant and had a positive effect on tenacity.

  When drawn biodegradable linear aliphatic-aromatic co-polyester fibres were twisted, the twist level had a positive effect on elongation at break. The total raw ratio had a positive

effect on tenacity and modulus and a negative effect on thermal shrinkage, elongation at break and abrasion. Draw stage had a positive effect on thermal shrinkage. The interactions (DS&DT, DR&RS and PT&RT) were prominent and had a positive effect on thermal shrinkage and abrasion. DS&DR and DT&RS had a positive effect on abrasion and a negative effect on thermal shrinkage. By connecting the twist process to the drawing process, the effect of plate temperature, relaxing stage ratio, the interaction between the number of drawing stages and both of drawing ratio and drawing temperature on thermal shrinkage effects were decreased. Twist decreases the effect of the roller temperature of the drawing process on elongation at break. By connecting the twist process to the drawing process, the effect of the interaction between the number of drawing stages and both the drawing ratio and drawing temperature effects on modulus was decreased; all the factors had a significant effect on modulus, which varied depending on other factor conditions.

When drawn biodegradable branched aliphatic-aromatic co-polyester fibres are twisted, the lower draw stage had a negative effect on abrasion which is positively affected by the lower drawing ratio, as expected. The total draw ratio, drawing temperature and the number of drawing stages had a positive effect on thermal shrinkage, tenacity and modulus and a negative effect on elongation at break. With one stage drawing processes, the tension will be high and the spin finish plays an important role in the slippage of the filaments on the last roller after spin finish application. Twist had a negative effect on modulus and abrasion. Plate temperature, relaxing temperature and the interactions (DT&SF and PT&SF) were prominent and had a positive effect on thermal shrinkage. It can be seen that applying twist did not have a significant effect on thermal shrinkage. By connecting the twist process to the drawing process, the effect of relaxing stage ratio, the interaction between the number of drawing stages and both the relaxing stage ratio and relaxing temperature effects on thermal shrinkage were decreased. Twist eliminated the effect of the roller temperature and the number of drawing stages of drawing process on tenacity and the effect of the relaxing stage ratio of drawing process on elongation at break. By connecting the twist process to the drawing process, the effect of the twist level overcame all other factors and the effect of their interactions on modulus.

- To separate the effect of temperature and the remaining factors in the hot drawing process, modelling of cold drawing of linear and branched aliphatic-aromatic co-

polyester fibres is needed. The additional effect gained from adding twisting to the continuous drawn filament was investigated in terms of the interaction processes.

When as-spun, biodegradable, linear aliphatic-aromatic co-polyester fibres are cold drawn, the total draw ratio, the interaction between the number of drawing stages and drawing ratio and the interaction between spin finish application and both the number of drawing stages and drawing ratio have a positive effect on thermal shrinkage. The total draw ratio has a negative effect on elongation at break and a positive effect on tenacity and modulus. Draw stage and its interaction with draw ratio have a positive effect on elongation at break and a negative effect on tenacity and modulus. The negative effects from the interaction between draw stage and spin finish were less prominent and could be related to the practical relationship between the tension and the oily roller surface on the last roller in the relaxing stage.

When as-spun, biodegradable, branched aliphatic-aromatic co-polyester fibres are cold drawn, the relaxing stage ratio has a negative effect on thermal shrinkage, tenacity, modulus and a positive effect on elongation at break. The total draw ratio and draw stage have a positive effect on thermal shrinkage, tenacity, modulus and a negative effect on elongation at break. The interaction between draw stage and draw ratio has a positive effect on thermal shrinkage, tenacity, modulus and a negative effect on elongation at break.

When drawn biodegradable linear aliphatic-aromatic co-polyester fibres are twisted, the interaction between draw stage and drawing ratio has a positive effect on thermal shrinkage, elongation at break and abrasion and a negative effect on tenacity and modulus. The total draw stage has a positive effect on elongation at break and abrasion and a negative effect on thermal shrinkage, tenacity and modulus. Applying twist does not significantly affect thermal shrinkage but could play a role in its interaction with the number of drawing stages affecting the internal stress. Twist level decreases the effect of the interaction between drawing ratio and spin finish on thermal shrinkage. Applying twist decreases the effects of spin finish application, the relaxing stage of the drawing process and the interaction between the spin finish application and total number of drawing stages of drawing process on tenacity; twist level value increases the effect of the interaction between the spin finish application and the draw ratio on tenacity and elongation at break.

When drawn, biodegradable, branched, aliphatic-aromatic co-polyester fibres are drawn, the relaxation stage and the interaction between the total number of drawing stages and spin finish application positively affect elongation and negatively thermal shrinkage. The total number of draw stages has a positive effect on thermal shrinkage, tenacity, modulus and abrasion and a negative effect on elongation at break. Twist level has a negative effect on thermal shrinkage, tenacity, modulus and abrasion and a positive effect on elongation at break. The interaction between the relaxing stage ratio and twist level or the number of drawing stages positively affects tenacity; there seems to be little or no effect of other parameters. Twist level decreases the effect of the interaction between drawing ratio and spin finish on thermal shrinkage and the effect of the drawing ratio on mechanical properties. Twist level decreases the effect of the number of drawing stages on modulus and the effect of the interaction between the number of drawing stages and the draw ratio on tenacity and modulus and increases this effect on the elongation at break. Twist level decreases the effect of the interaction between the number of drawing stages and the spin finish on elongation at break and modulus. The AAC textiles could be used for different applications, as an alternative to commercial chemical fibres at reasonable cost, leaving no environmental footprint.

- After drawing and twisting process modelling, the programming stage is the next most important stage for developing a forecasting application, depending on results and their optimization from Chapter 6 and Chapter 7. The forecasting TI-83 instrument programs are outlined in Appendices VI and VII. They allow a fast simulation to describe the behaviour of a factor-response relationship. The equations achieved could form a source code in a forecasting program designed to optimize the drawing process of selected as-spun fibres. Different samples were drawn within the studied range to determine the parameters and their interaction effects and to test the forecasting regression equations. The simulation results are in agreement with the data obtained within acceptable variation.
- The fibres obtained can be used as the total fibre content in the fabric in disposable use in medical, agricultural, horticultural and other non-traditional fibres and in fabric applications such as seed mats, erosions and seasonal weed control ground covers and other non-traditional fibres and fabric applications.

With low melting point temperature of the fibres, high-speed bonding in fabrication processes can be improved. A continuous filament yarn can be used as produced or texturized for use in a variety of applications and it can be a mixture of two or more different types of filaments; it can be used as a filling yarn (weft) in some woven fabrics which take the biodegradability property from these fibres and the strength properties from warp yarns such as polyester and nylon. This work will be helpful to major experimentalists and technologists in polymer processing fields using biodegradable polymers in terms of process engineering to meet the needs of industry. Practically, the statistical approach used could be applied in other plastic industries, which will help to analyse the extrusion temperature profile and machine settings required, which in turn will help in reducing energy bills for the same product production. When the economical size experiment is statically analysed and forecasting model is designed, high energy savings will be obtained, depending on the material, machine, energy saving product design and production time. A forecasting software application could be connected to the production process, which would confirm the sustainable change achieved in the production process. Such a program will help in finding the input values which will achieve the outcome.

8.2 Future Work

The statistical simulation will help processing scientists and technologists in industry to obtain the enhanced properties at suitable conditions related to final product cost and to obtain environmentally friendly, economical, energy-saving textiles. The statistical experimental design approach identifies the process parameters as a result of the controlled relationship during the process. Further research and development could be conducted for many applications where the long life time of textiles is not issue:

- After determining the significant factors which will help lower the number of total factors in spinning and drawing processes, a continuous process (spinning and drawing) be investigated. For commercial application, the combination between the melt spinning and the multi-stage drawing process before twisting provides a better focus on fibre manufacturing and could find the best conditions to produce fibres at higher speeds. Neural network theory could be matched to improve the result quantitatively.
- The study was limited to only two-parameter interactions, since interactions of more than two parameters are not useful in practice. After select the significant factors only, the three parameters interaction or more levels could be applied in further study.
- Related to the thermal study, quench air temperature could be investigated by using the thermo-graphic measurement theory.
- To eliminate the kinking and snarling tendency of yarns, further research is needed to study the effect of the last treatment processes on the physical and structural properties of produced yarns and more research could be found on synthetic yarns [225-227]. Improving the relaxing stage would reduce the fibre shrinkage, after drawing the fibres on draw frame, in either hot or cold conditions.
- Further study about the filament fineness and surface area which play a vital role in deciding the comfort characteristics of the fabric, as also moisture management finish treatment should be done. The effect of fineness could essentially be regarded as an effect of changing filament diameter.
- Further research could be done on weavability; the produced fibres were woven using a simple hand loom to produce small samples. Light optical microscopy images of the fabric and 2D weft cross section (non-destructively reconstructed slice) using the SkyScan 1174 System are presented in Figure 8.1 (a,b). Figure 8.1 (c) shows the X-ray image through the drawn fibres, giving details about its structure. To test the knit-ability

of produced fibres, these were knitted using the silver reed standard gauge knitting machine to produce different designs. Figure 8.2 shows the optical camera image of knitted fabrics. For more details about the behaviour of the manufactured fibres through fabrication, fabrics were microscopically analyzed. Figure 8.3 shows light optical microscopy images of the knitted AAC fabric, an X-ray image through the sample, a 2D cross section (non-destructively reconstructed slice), 3D visualization of the sample microstructure and standard SEM image. Fabrics could be degraded under the right conditions and may be bonded to various components.

- Further work could be done on finished AAC fibres which are potential candidates for making continuous or staple fibres for knitted and woven fabrics. The degree of elasticity may be adjusted by varying filament production conditions. Coloured yarns are produced by adding a provided biodegradable dye.
- Further research could be done to produce fibres from the AAC blend with starch-based polymer. Regarding the research on starch based polymer (Solanyl rigidity component) [228], the increasing of the starch ratio involves a plastifying agent lowering the glass transition temperature of starch and melting of the mixture because of the introduction of mechanical and heat energy to improve the fibre properties (Figure 8.4).
- The results obtained could forecast how variation in starch ratio affects the surface of the fibres, as well as the varying levels of mechanical properties. The selection of starch based polymer depends upon some points [59] such as non-toxic material with non-toxic degradation and mechanical and rheological properties and economic reasons and the ability of the degradation control via polymer manufacturing and processability. As an increase in temperature causes an increase in the mobility of starch granules and melting of the crystalline structures [28], the melt viscosity of starch polymers [156] reduces by the increasing of the temperature, which could help in achieving improved properties. Blends made from different starches [32] will have different properties, depending on the ratio of the branched polymer fractions to linear polymer fractions in the blends.

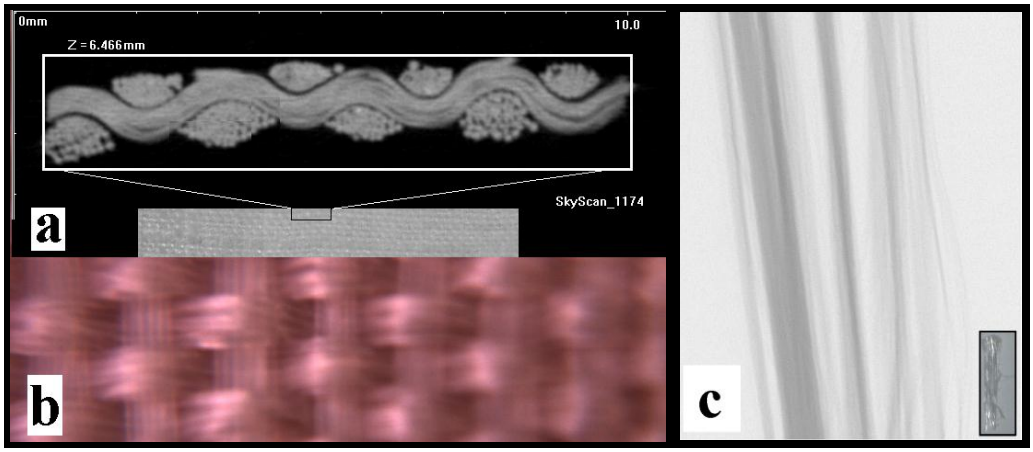

Figure 8.1

(a) Light optical microscopy image of the fabric, (b) 2D weft cross section (c) X-ray camera shadow image through the fibres

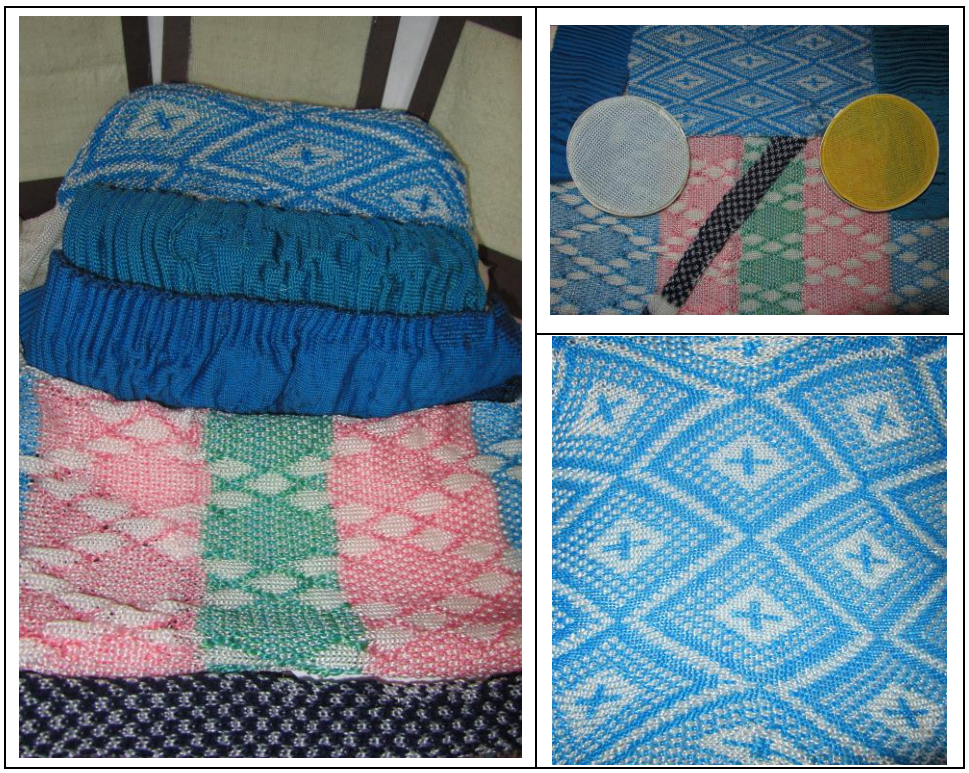

Figure 8.2. Optical images of the knitted designs

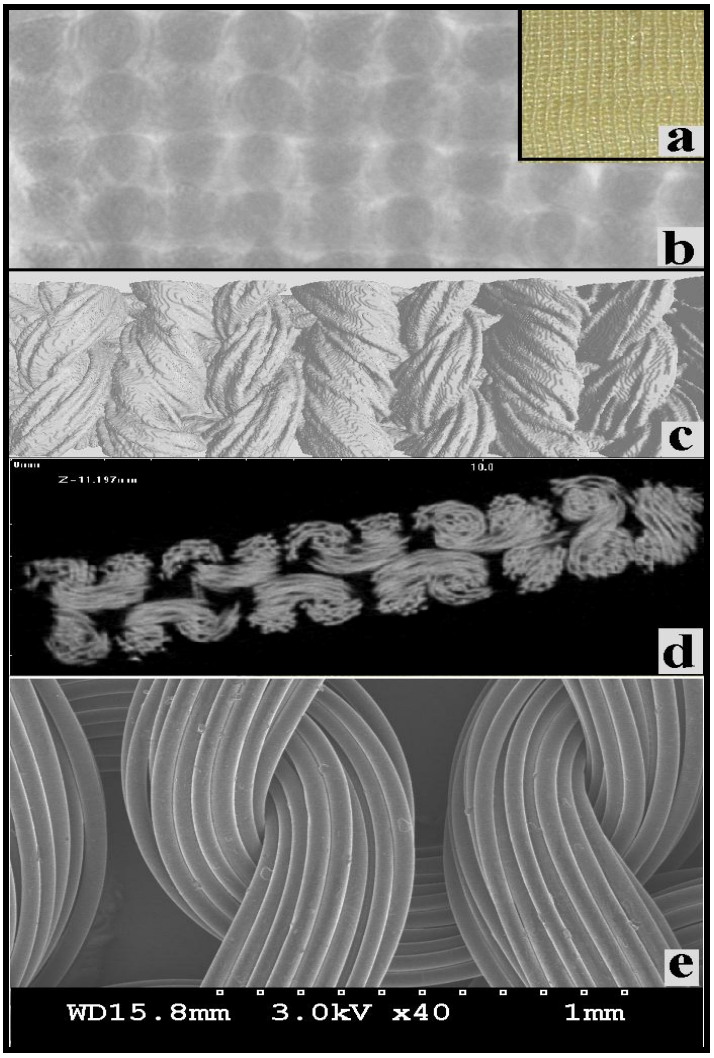

Figure 8.3. Analysis of knitted fabrics

(a) Light optical microscopy image of the fabric
(b) X-ray image through the sample (SkyScan 1174 System)
(c) 2D cross section (SkyScan 1174 System)
(d) 3D visualization of the fabric microstructure (SkyScan 1174 System)
(e) Standard SEM image

- Produce hollow fibres which take advantage of low thickness effects on fibre biodegradability and suggest a new method to colour the material as oil-based fibres.
- Suggest a new method for adding an agent or by cross-linking methods to improve the physical and chemical properties, while balancing the improvement of mechanical properties and the biodegradability.

- Additional biodegradability testing is required to establish how different processing conditions could affect the biodegradation. The general rule for biopolymers, as established by biodegradable plastics researchers, is ‘If nature makes it, nature will degrade it’. As knitted or woven structure has the advantage of providing the surface area for the degradation action before or after shrinkage, control of the yarn and fabric biodegradability could be done using factorial experimental design.

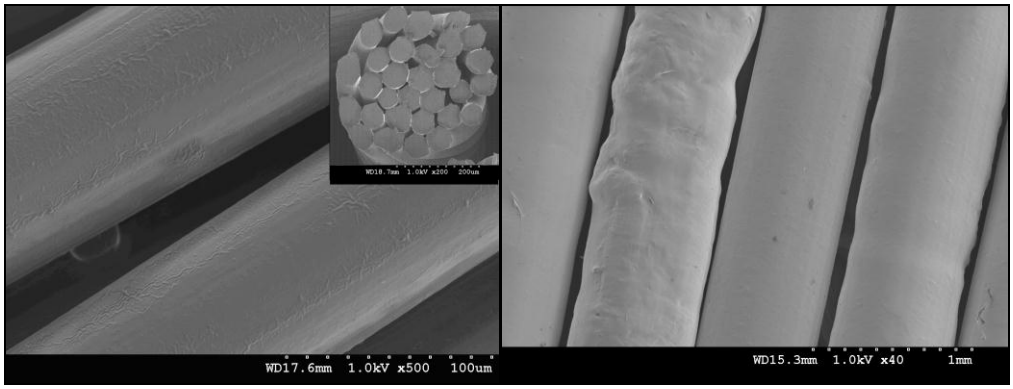

(5%) (10%)

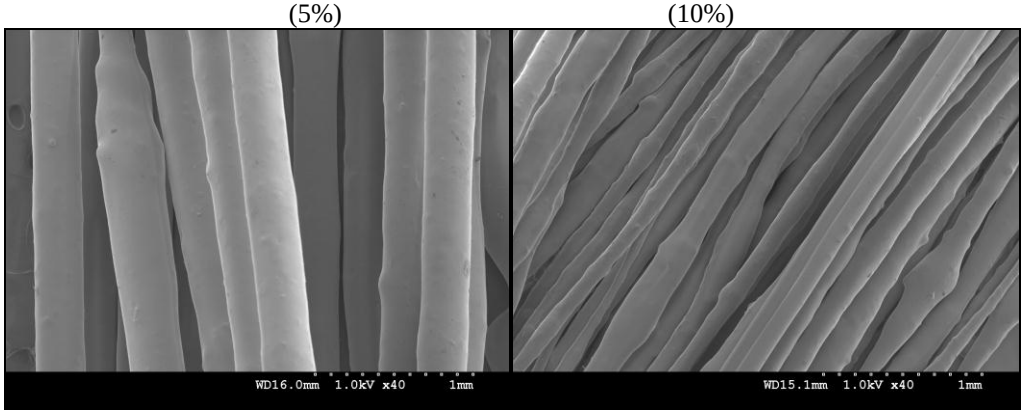

(25%) (40%)

Figure 8.4. Standard SEM image of starch-based fibre (Starch %)

APPENDICES

1. **APPENDIX A**
2. **APPENDIX B**
3. **APPENDIX C**
4. **APPENDIX D**
5. **APPENDIX E**
6. **APPENDIX F**

APPENDIX A

The C++ source code

```
//Melt spinning .cpp : main project file.
#include "stdafx.h"
#include<iostream>
using namespace System;
int main()
{       double
G,T,M,Q,S,W,C,D,D1,D2,F,t,E,m,s,s1,s2;
        cout<<"WELCOME TO AAC
EXTRUDED FIBRES
CALCULATER"<<"\n"<<"\n";
        cout<<"PLEASE SELECT YOUR
GRADE, Inter 1 for Linear AAC and 2 for
Branched AAC"<<"\n"<<"\n";
        cin>>G;
        if (G==1)
        {cout<<"PLEASE ENTER YOUR
SELECTED PARAMETERE"<<"\n"<<"\n";
        cout<<"PLEASE ENTER
TEMPERATURE BETWEEN 130 AND 145
celsius degree"<<"\n";
        cin>>T;
        while (T>145||T<130)
        {cout<<"PLEASE ENTER
TEMPERATURE BETWEEN 130 AND 145
celsius degree"<<"\n";
        cin>>T;}
        cout<<"PLEASE ENTER
METERING PUMP SPEED BETWEEN 6
AND 12 rpm"<<"\n";
        cin>>M;
        while (M>12||M<6)
        {cout<<"PLEASE ENTER
METERING PUMP SPEED BETWEEN 6
AND 12 rpm"<<"\n";
        cin>>M;}
        cout<<"PLEASE ENTER QUINCH
AIR VALUE BETWEEN 35 AND 50
%"<<"\n";
        cin>>Q;
        while (Q>50||Q<35)
        {cout<<"PLEASE ENTER QUINCH
AIR VALUE BETWEEN 35 AND 50
%"<<"\n";
        cin>>Q;}
        cout<<"PLEASE ENTER SPIN
FINISH VALUE BETWEEN 0.35 AND 0.5
rpm"<<"\n";
        cin>>S;
        while (S>0.5||S<0.35)
        {cout<<"PLEASE ENTER SPIN
FINISH VALUE BETWEEN 0.35 AND 0.5
rpm"<<"\n";
        cin>>S;}
        cout<<"PLEASE ENTER WINDING
SPEED VALUE BETWEEN 50 AND 100
m/min"<<"\n";
        cin>>W;
        while (W>100||W<50)
        {cout<<"PLEASE ENTER
WINDING SPEED VALUE BETWEEN 50
AND 100 m/min"<<"\n";
        cin>>W;}
        (Equations 5.1-5.12 and 5.17-5.25)
        Count= C
        Die Head Pressure= D
        Diameter= D1
        Drawability= D2
        Spin Draw Ratio= s1
        Shrinkage= s
        Tenacity= t
        Elongation= E
        Modulus= m
        Full-Width Half-Maximum = F
        Birefringence*1000= s2
          cout<<"Count="<<C<<"
denier"<<"\n";
        cout<<"Die Head Pressure="<<D<<"
DPI"<<"\n";
        cout<<"Diameter="<<D1<<"
micron"<<"\n";
        cout<<"Drawability="<<D2<<"\n";
        cout<<"Spin Draw
Ratio="<<s1<<"\n";
        cout<<"Shrinkage="<<s<<"
%"<<"\n";
        cout<<"Tenacity="<<t<<"
g\den"<<"\n";
        cout<<"Elongation="<<E<<"
%"<<"\n";
        cout<<"Modulus="<<m<<"
g/den"<<"\n";
        cout<<"Full-Width Half-Maximum
="<<F<<" degree"<<"\n";

cout<<"Birefringence*1000="<<s2<<"
degree"<<"\n";
        cout<<"Thank you from
Basel"<<"\n";}
        else
```

```
        {cout<<"PLEASE ENTER YOUR
SELECTED PARAMETERE"<<"\n"<<"\n";
        cout<<"PLEASE ENTER
TEMPERATURE BETWEEN 145 AND 160
celsius degree"<<"\n";
        cin>>T;
        while (T>160||T<145)
        {cout<<"PLEASE ENTER
TEMPERATURE BETWEEN 145 AND 160
celsius degree"<<"\n";
        cin>>T;}
        cout<<"PLEASE ENTER
METERING PUMP SPEED BETWEEN 6
AND 12 rpm"<<"\n";
        cin>>M;
        while (M>12||M<6)
        {cout<<"PLEASE ENTER
METERING PUMP SPEED BETWEEN 6
AND 12 rpm"<<"\n";
        cin>>M;}
        cout<<"PLEASE ENTER QUINCH
AIR VALUE BETWEEN 35 AND 50
%"<<"\n";
        cin>>Q;
        while (Q>50||Q<35)
        {cout<<"PLEASE ENTER QUINCH
AIR VALUE BETWEEN 35 AND 50
%"<<"\n";
        cin>>Q;}
        cout<<"PLEASE ENTER SPIN
FINISH VALUE BETWEEN 0.35 AND 0.5
rpm"<<"\n";
        cin>>S;
        while (S>0.5||S<0.35)

{cout<<"PLEASE ENTER SPIN FINISH
VALUE BETWEEN 0.35 AND 0.5
rpm"<<"\n";
        cin>>S;}
        cout<<"PLEASE ENTER WINDING
SPEED VALUE BETWEEN 50 AND 100
m/min"<<"\n";
        cin>>W;
        while (W>100||W<50)
        {cout<<"PLEASE ENTER
WINDING SPEED VALUE BETWEEN 50
AND 100 m/min"<<"\n";
        cin>>W;}
```

((See Equations. *5.1-5.12* & *5.17-5.25*))

```
        Count= C
        Die Head Pressure= D
        Diameter= D1
        Drawability= D2
        Spin Draw Ratio= s1
        Shrinkage= s
        Tenacity= t
        Elongation= E
        Modulus= m
         cout<<"Count="<<C<<"
denier"<<"\n";
        cout<<"Die Head Pressure="<<D<<"
DPI"<<"\n";
        cout<<"Diameter="<<D1<<"
micron"<<"\n";
        cout<<"Drawability="<<D2<<"\n";
        cout<<"Spin Draw
Ratio="<<s1<<"\n";
        cout<<"Shrinkage="<<s<<"
%"<<"\n";
        cout<<"Tenacity="<<t<<"
g\den"<<"\n";
        cout<<"Elongation="<<E<<"
%"<<"\n";
        cout<<"Modulus="<<m<<"
g/den"<<"\n";
        cout<<"Thank you from
Basel"<<"\n";}
        cout<<"Thank you from
Basel"<<"\n";}

        return 0;}
```

APPENDIX B

Program 01 (Melt spinning of LAAC as-spun fibres)

```
:Disp "---------- "
:Disp "     FIBRES"
:Disp "   CALCULATOR"
:Disp "----------"
:Disp " Polymer Grade"
:Disp " is linear AAC"
:Disp "----------"
:Pause
:Disp ""
:Disp "----------"
:Disp ""
:Disp "Enter  Spinning"
:Disp "  Temperature "
:Disp " Value between"
:Disp "  130 and 145"
:Disp ""
:Input "Temperature=",T
:While T<130 or T>145
:Disp ""
:Disp "----------"
:Disp "-----Sorry-----"
:Disp "Enter  Spinning"
:Disp "  Temperature "
:Disp " Value between"
:Disp "  130 and 145"
:Disp "    only"
:Input "Temperature=",T
:End
:Disp ""
:Disp "----------"
:Disp ""
:Disp "Enter Metering "
:Disp "  Pump Speed"
:Disp " Value between"
:Disp "   6 and 12"
:Disp ""
:Input "Pump Speed=",M
:While M<6 or M>12
Disp ""
:Disp "----------"
:Disp "-----Sorry-----"
:Disp "Enter Metering "
:Disp "  Pump Speed"
:Disp " Value between"
:Disp "   6 and 12"
:Disp "    only"
:Input "Pump Speed=",M
:End
:Disp ""
:Disp "----------"
:Disp "Enter  Quench"
:Disp "  Air Speed"
:Disp "Value between"
:Disp "  35 and 50"
:Disp ""
:Disp " Quench-Air"
:Input " Speed=",Q
:While Q<35 or Q>50
:Disp ""
:Disp "-----Sorry-----"
:Disp "Enter  Quench"
:Disp "  Air Speed"
:Disp "Value between"
:Disp "  35 and 50"
:Disp "   only"
:Disp " Quench-Air"
:Input " Speed=",Q
:End
:Disp ""
:Disp "----------"
:Disp "   Enter Spin "
:Disp "  Finish Speed"
:Disp " Value  between"
:Disp "  0.35 and 0.50"
:Disp ""
:Disp "   Spin-Finish"
:Input "    Speed=",S
:While S<0.35 or S>0.50
:Disp ""
:Disp "----------"
:Disp "-----Sorry-----"
:Disp " Enter Spin "
:Disp "Finish Speed"
:Disp "Value between"
:Disp "0.35 and 0.50"
:Disp "    only"
:Disp " Spin-Finish"
:Input "  Speed=",S
:End
:Disp ""
:Disp "----------"
:Disp ""
:Disp "Enter Winding "
:Disp " Speed Value"
:Disp "   between"
:Disp " 50 and 100"
:Disp ""
:Input "Winding Speed=",W
:While W<50 or W>100
:Disp ""
:Disp "----------"
:Disp "-----Sorry-----"
:Disp "Enter Winding "
:Disp " Speed Value"
:Disp "   between"
:Disp " 50 and 100"
:Disp "    only"
:Input "Winding Speed=",W
:End
:Disp "----------"
:Disp ""
.
.
```

Equations 5.1-5.12

```
.
.
:Disp "*****--1--*****"
:Disp ""
:Disp "Count="
:Disp C
:Disp "         denier"
:Pause
:Disp "----------"
:Disp ""
:Disp "*****--2--*****"
:Disp "Die Head"
:Disp "Pressure="
:Disp D
:Disp "           DPI"
:Pause
:Disp "----------"
:Disp ""
:Disp "*****--3--*****"
:Disp ""
:Disp "Diameter="
:Disp P
:Disp "         micron"
:Pause
:Disp "----------"
:Disp ""
:Disp "*****--4--*****"
:Disp ""
:Disp "Drawability="
:Disp K
:Disp ""
:Pause
:Disp "----------"
:Disp ""
:Disp "*****--5--*****"
:Disp ""
:Disp "Spin Draw Ratio="
:Disp R
```

```
:Disp ""
:Pause
:Disp "----------------"
:Disp ""
:Disp "*****--6--*****"
:Disp ""
:Disp "Shrinkage="
:Disp Y
:Disp "           %"
:Pause
:Disp "----------------"
:Disp ""
:Disp "*****--7--*****"
:Disp ""
:Disp "Tenacity="
:Disp Z
:Disp "          g/den"
:Pause
:Disp "----------------"
:Disp ""
:Disp "*****--8--*****"
:Disp ""
:Disp "Elongation="
:Disp E
:Disp "           %"
:Pause
:Disp "----------------"
:Disp ""
:Disp "*****--9--*****"
:Disp ""
:Disp "Modulus="
:Disp N
:Disp "          g/den"
```

```
:Pause
:Disp "----------------"
:Disp ""
:Disp "*****--10--*****"
:Disp ""
:Disp "Full-Width"
:Disp "Half-Maximum="
:Disp F
:Disp "         degree"
:Pause
:Disp "----------------"
:Disp ""
:Disp "*****--11--*****"
:Disp ""
:Disp "Birefringence"
:Disp "*1000="
:Disp U
:Disp ""
:Pause
:Disp "----------------"
:Disp ""
:Disp "*****--12--*****"
:Disp "  Filament"
:Disp " Temperature "
:Disp "  at 25 mm "
:Disp "from Spinneret="
:Disp O
:Disp " Celsius degree"
:Pause
:Disp "----------------"
:Disp ""
:Disp "*****--13--*****"
:Disp "  Filament"
:Disp " Temperature "
```

```
:Disp "  at 80 mm "
:Disp "from Spinneret="
:Disp I
:Disp " Celsius degree"
:Pause
:Disp "----------------"
:Disp ""
:Disp "*****--14--*****"
:Disp "  Filament"
:Disp " Temperature "
:Disp "  at 170 mm "
:Disp "from Spinneret="
:Disp X
:Disp " Celsius degree"
:Pause
:Disp "----------------"
:Disp ""
:Disp "*****--15--*****"
:Disp "  Filament"
:Disp " Temperature "
:Disp "  at 285 mm "
:Disp "from Spinneret="
:Disp B
:Disp " Celsius degree"
:Pause
:Pause
:Disp "Designed by"
:Disp ""
:Disp "Basel Younes"
:Disp "Heriot  Watt"
:Disp " University"
:Disp "    2011"
```

APPENDIX C

Program 02 (Melt spinning of BAAC as-spun fibres)

```
:Disp "---------------- "
:Disp "     FIBRES"
:Disp "   CALCULATOR"
:Disp "----------------"
:Disp " Polymer Grade"
:Disp "is Branched AAC"
:Disp "----------------"
:Pause
:Disp ""
:Disp "----------------"
:Disp ""
:Disp "Enter  Spinning"
:Disp "  Temperature "
:Disp " Value between"
:Disp "  145 and 160"
:Disp ""
:Input "Temperature=",T
:While T<145 or T>160
:Disp ""
:Disp "---------------"
:Disp "-----Sorry-----"
:Disp "Enter  Spinning"
:Disp "  Temperature "
:Disp " Value between"
:Disp "  145 and 160"
:Disp "    only"
:Input "Temperature=",T
:End
:Disp ""
:Disp "----------------"
:Disp ""
:Disp "Enter Metering "
:Disp "  Pump Speed"
:Disp " Value between"
:Disp "   6 and 12"
:Disp ""
:Input "Pump Speed=",M
:While M<6 or M>12
Disp ""
:Disp "---------------"
:Disp "-----Sorry-----"
:Disp "Enter Metering "
:Disp "  Pump Speed"
:Disp " Value between"
:Disp "   6 and 12"
:Disp "    only"
:Input "Pump Speed=",M
:End
:Disp ""
:Disp "----------------"
:Disp "Enter  Quench"
:Disp "  Air Speed"
:Disp "Value between"
:Disp "  35 and 50"
:Disp ""
:Disp " Quench-Air"
:Input  Speed=",Q
:While Q<35 or Q>50
:Disp ""
:Disp "-----Sorry-----"
:Disp "Enter  Quench"
:Disp "  Air Speed"
:Disp "Value between"
:Disp "  35 and 50"
:Disp "   only"
:Disp " Quench-Air"
:Input " Speed=",Q
:End
:Disp ""
:Disp "----------------"
:Disp "   Enter Spin "
:Disp "  Finish Speed"
:Disp " Value  between"
:Disp "  0.35 and 0.50"
:Disp ""
:Disp "   Spin-Finish"
:Input "    Speed=",S
:While S<0.35 or S>0.50
:Disp ""
:Disp "---------------"
:Disp "-----Sorry-----"
:Disp " Enter Spin "
:Disp "Finish Speed"
:Disp "Value between"
:Disp "0.35 and 0.50"
:Disp "    only"
:Disp " Spin-Finish"
:Input "  Speed=",S
:End
:Disp ""
:Disp "----------------"
:Disp ""
:Disp "Enter Winding "
:Disp " Speed Value"
:Disp "   between"
:Disp " 50 and 100"
:Disp ""
:Input "Winding Speed=",W
:While W<50 or W>100
:Disp ""
:Disp "---------------"
:Disp "-----Sorry-----"
:Disp "Enter Winding "
:Disp " Speed Value"
:Disp "   between"
:Disp " 50 and 100"
:Disp "    only"
:Input "Winding Speed=",W
:End
:Disp "----------------"
:Disp ""
.
.
```

Equations 5.17-5.25

```
.
.

:Disp "*****--1--*****"
:Disp ""
:Disp "Count="
:Disp C
:Disp "         denier"
:Pause
:Disp "----------------"
:Disp ""
:Disp "*****--2--*****"
:Disp "Die Head"
:Disp "Pressure="
:Disp D
:Disp "            DPI"
:Pause
:Disp "----------------"
:Disp ""
:Disp "*****--3--*****"
:Disp ""
:Disp "Diameter="
:Disp P
:Disp "         micron"
:Pause
:Disp "----------------"
:Disp ""
:Disp "*****--4--*****"
:Disp ""
:Disp "Spin Draw Ratio="
:Disp R
:Disp ""
:Pause
:Disp "----------------"
:Disp ""
:Disp "*****--5--*****"
:Disp ""
:Disp "Shrinkage="
```

```
:Disp Y
:Disp "            %"
:Pause
:Disp "----------------"
:Disp ""
:Disp "*****--6--*****"
:Disp ""
:Disp "Tenacity="
:Disp Z
:Disp "          g/den"
:Pause
:Disp "----------------"
:Disp ""
:Disp "*****--7--*****"
:Disp ""
:Disp "Elongation="
:Disp E
:Disp "            %"
:Pause
:Disp "----------------"
:Disp ""
:Disp "*****--8--*****"
:Disp ""
:Disp "Modulus="
:Disp N
:Disp "          g/den"
```

```
:Pause
:Disp "----------------"
:Disp ""
:Disp "*****--9--*****"
:Disp "  Filament"
:Disp " Temperature "
:Disp "  at 25 mm "
:Disp "from Spinneret="
:Disp O
:Disp " Celsius degree"
:Pause
:Disp "----------------"
:Disp ""
:Disp "*****--10--*****"
:Disp "  Filament"
:Disp " Temperature "
:Disp "  at 80 mm "
:Disp "from Spinneret="
:Disp I
:Disp " Celsius degree"
:Pause
:Disp "----------------"
:Disp ""
:Disp "*****--11--*****"
```

```
:Disp "  Filament"
:Disp " Temperature "
:Disp "  at 170 mm "
:Disp "from Spinneret="
:Disp X
:Disp " Celsius degree"
:Pause
:Disp "----------------"
:Disp ""
:Disp "*****--12--*****"
:Disp "  Filament"
:Disp " Temperature "
:Disp "  at 285 mm "
:Disp "from Spinneret="
:Disp B
:Disp " Celsius degree"
:Pause
:Pause
:Disp "Designed by"
:Disp ""
:Disp "Basel Younes"
:Disp "Heriot  Watt"
:Disp " University"
:Disp "    2011"
```

APPENDIX D

Program 04 (Melt spinning of AACs (blending) as-spun fibres)

```
:Disp "----------------"
:Disp "    FIBRES"
:Disp "  CALCULATOR "
:Disp "     From   "
:Disp "  AACs Blends"
:Disp "----------------"
:Pause
:Disp " Polymer Grades"
:Disp "is Linear AAC1"
:Disp " MFI, 6 g/min"
:Disp " Linear AAC2"
:Disp " MFI, 12 g/min "
:Disp " Branched AAC3"
:Disp " MFI, 5.5 g/min "
:Pause
:Disp "----------------"
:Disp "   Enter AAC1"
:Disp " Blending Ratio "
:Disp "    between"
:Disp " 0.00 and 0.50"
:Input "Blending Ratio
=",A
:While A<0 or A>0.50
:Disp "---------------"
:Disp "-----Sorry-----"
:Disp "  Enter  AAC1"
:Disp " Blending Ratio "
:Disp "    between"
:Disp " 0.00 and 0.50"
:Disp "    only"
:Input "Blending Ratio
=",A
:End
:Disp "----------------"
:Disp "   Enter AAC3"
:Disp " Blending Ratio "
:Disp "    between"
:Disp " 0.00 and 0.50"
:Disp ""
:Input "Blending Ratio
=",B
:While B<0.00 or B>0.50
Disp ""
:Disp "---------------"
:Disp "-----Sorry-----"
:Disp "   Enter AAC3"
:Disp " Blending Ratio "
:Disp "    between"
:Disp " 0.00 and 0.50"
:Disp ""
:Input "Blending Ratio
=",B
:End
:A+B→H
:1-H→C
:Disp ""
:Disp "----------------"
:Disp "Add  "
:Disp C
:Disp "        of AAC2"
:Disp " to the Blends"
:Disp ""
:Pause
:Disp ""
:Disp "----------------"
:Disp "Set Spinning"
:Disp "Temperature "
:Disp "Value at 145 "
:Disp "  Celsius degree"
:Disp ""
:Pause
:Disp "----------------"
:Disp "  Set Metering "
:Disp "Pump Speed Value"
:Disp "  at 10 rpm"
:Pause
:Disp "----------------"
:Disp " Set Quench Air"
:Disp "  Speed Value"
:Disp "   at 50 %"
:Disp " "
:Pause
:Disp "----------------"
:Disp "Set Spin Finish "
:Disp "  Speed Value"
:Disp "  at 0.35 rpm"
:Disp ""
:Disp ""
:Pause
:Disp "----------------"
:Disp "  Set Drawing"
:Disp "  Temperature "
:Disp "  Value at 40"
:Disp " Celsius degree"
:Disp ""
:Pause
:Disp ""
:Disp "----------------"
:Disp "  Set Drawing"
:Disp "  Ratio Value "
:Disp "    at 1.5"
:Disp ""
:Pause
:Disp "----------------"
:Disp "  Set Winding "
:Disp "  Speed Value"
:Disp "  at 100 m/min"
:Disp ""
:Disp ""
:Pause
:Disp ""
:Disp "----------------"
:1330.8+100.533*A+876.4
*B→C
:0.274074-
0.0444444*A+0.488889*B
→Z
:471.767-200.133*A-
269.156*B→E
:1.25556+0.2*A+0.733333
*B→N
:1.2*A+4.46667*B-
0.55→Y
:Disp "----------------"
:Disp "*****--1--*****"
:Disp "Count="
:Disp C
:Disp "          denier"
:Pause
:Disp "----------------"
:Disp "*****--2--*****"
:Disp ""
:Disp "Shrinkage="
:Disp Y
:Disp "            %"
:Pause
:Disp "----------------"
:Disp "*****--7--*****"
:Disp "Tenacity="
:Disp Z
:Disp "          g/den"
:Pause
:Disp "----------------"
:Disp "*****--8--*****"
:Disp ""
:Disp "Elongation="
:Disp E
:Disp "            %"
:Pause
:Disp "----------------"
:Disp "*****--9--*****"
:Disp ""
:Disp "Modulus="
:Disp N
:Disp "    g/den"
:Pause
:Disp "Designed by"
:Disp "Basel Younes"
:Disp "Heriot  Watt
University "
:Disp "    2011
```

APPENDIX E

Code listing for the drawing-twisting analyser for as-spun LAAC fibres

```
:Disp "  "
:Disp "----------------"
:Disp "Drawing-Twisting"
:Disp "    Analyser "
:Disp "  for  as-spun"
:Disp "   AAC Fibres"
:Disp "----------------"
:Pause
:Disp "----------------"
:Disp "Prepare Samples"
:Disp "       of "
:Disp " Linear As-Spun "
:Disp "   AAC Fibres"
:Disp "----------------"
:Pause
:Disp "----------------"
:Disp " Set  Spinning"
:Disp "  Temperature "
:Disp "  profile  at  "
:Disp "  115-120-125-"
:Disp "  130-140-140"
:Disp " Celsius degree"
:Pause
:Disp "----------------"
:Disp "  Set Metering "
:Disp "Pump Speed Value"
:Disp "   at 12 rpm"
:Disp "----------------"
:Pause
:Disp ""
:Disp "----------------"
:Disp " Set Quench Air"
:Disp "  Speed Value"
:Disp "   at 73 %"
:Disp "----------------"
:Pause
:Disp ""
:Disp "----------------"
:Disp "Set Spin Finish "
:Disp "  Speed Value"
:Disp "  at 0.3 rpm"
:Disp "----------------"
:Pause
:Disp ""
:Disp "----------------"
:Disp "  Set Winding "
:Disp "  Speed Value"
:Disp "  at 50 m/min"
:Disp "----------------"
:Pause
:Disp ""
:Disp "----------------"
:Disp "----------------"
:Disp "For cold drawing"
:Disp " Enter Number 1"
:Disp "For cold drawing"
:Disp "  and twisting"
:Disp " Enter Number 2"
:Disp "----------------"
:Pause
:Disp "----------------"
:Disp "For hot drawing"
:Disp " Enter Number 3"
:Disp "For hot drawing"
:Disp "  and twisting"
:Disp " Enter Number 4"
:Disp "----------------"
:Input " =",Q
:While Q<1 or Q>4
:Disp "----------------"
:Disp "For cold drawing"
:Disp " Enter Number 1"
:Disp "For cold drawing"
:Disp "  and twisting"
:Disp " Enter Number 2"
:Disp "----------------"
:Pause
:Disp "----------------"
:Disp "For hot drawing"
:Disp " Enter Number 3"
:Disp "For hot drawing"
:Disp "  and twisting"
:Disp " Enter Number 4"
:Disp "----------------"
:Input " =",Q
:End
If Q=1
Then
:Disp ""
:Disp "  COLD DRAWING"
:Disp "----------------"
:Disp " Enter  Drawing"
:Disp "   Stage Value "
:Disp "between 1 and 2"
:Disp "----------------"
:Input "Stage=",A
:While A<1 or A>2
:Disp ""
:Disp "----------------"
:Disp "-----Sorry-----"
:Disp " Enter  Drawing"
:Disp "   Stage Value "
:Disp "between 1and 2"
:Disp "    only"
:Disp "----------------"
:Input "Stage=",A
:End
:Disp "----------------"
:Disp "     Enter  "
:Disp " Drawing Ratio "
:Disp " Value between"
:Disp "  4.5 and 6.0"
:Disp "----------------"
:Input " Ratio =",C
:While C<4.5 or C>6.0
:Disp "-----Sorry-----"
:Disp "     Enter  "
:Disp " Drawing Ratio "
:Disp " Value between"
:Disp "  4.5 and 6.0"
:Disp "      only"
:Disp "----------------"
:Input " Ratio =",C
:End
:Disp "----------------"
:Disp "  Enter  Spin "
:Disp " Finish  Value"
:Disp "    between"
:Disp "  1.5 and 3.0"
:Disp "----------------"
:Input " Spin Finish =",E
:While E<1.5 or E>3.0
:Disp "-----Sorry-----"
:Disp "  Enter  Spin "
:Disp " Finish  Value"
:Disp "    between"
:Disp "  1.5 and 3.0"
:Disp "    only"
:Disp "----------------"
:Input " Spin Finish =",E
:End
:Disp "----------------"
:Disp "   Relaxation stage "
:Disp "      Enter  "
:Disp "     0 or 1"
:Disp "----------------"
:Input "Stage=",F
:While F<0 or F>1
:Disp ""
:Disp "-----Sorry-----"
:Disp "   Relaxation stage "
:Disp "    "
:Disp "      Enter  "
:Disp "     0 or 1"
:Disp "    only"
:Disp "----------------"
:Input "Stage=",F
:End
:Disp "----------------"
```

Equations (7.1 – 7.4)

```
:Disp "*****--1--*****"
:Disp ""
:Disp "Count="
:Disp I
:Disp "          denier"
:Disp "----------------"
:Pause
:Disp ""
:Disp "*****--2--*****"
:Disp "Shrinkage="
:Disp M
:Disp "             %"
:Disp "----------------"
:Pause
:Disp "*****--3--*****"
:Disp ""
:Disp "Tenacity="
:Disp J
```

```
:Disp "          g/den"
:Disp "----------------"
:Pause
:Disp "*****--4--*****"
:Disp "Elongation="
:Disp K
:Disp "            %"
:Disp "----------------"
:Pause
:Disp "*****--5--*****"
:Disp "Modulus="
:Disp L
:Disp "          g/den"
:Disp "----------------"
:Pause
End
If Q=2
Then
:Disp "  COLD DRAWING"
:Disp "   + TWISTING"
:Disp "----------------"
:Disp " Enter  Drawing"
:Disp "   Stage Value "
:Disp "between 1 and 2"
:Disp "----------------"
:Input "Stage=",A
:While A<1 or A>2
:Disp "----------------"
:Disp "-----Sorry-----"
:Disp " Enter  Drawing"
:Disp "   Stage Value "
:Disp "between 1and 2"
:Disp "    only"
:Disp "----------------"
:Input "Stage=",A
:End
:Disp "----------------"
:Disp "     Enter  "
:Disp " Drawing Ratio "
:Disp " Value between"
:Disp "  4.5 and 6.0"
:Disp "----------------"
:Input " Ratio =",C
:While C<4.5 or C>6.0
:Disp "-----Sorry-----"
:Disp "     Enter  "
:Disp " Drawing Ratio "
:Disp " Value between"
:Disp "  4.5 and 6.0"
:Disp "      only"
:Disp "----------------"
:Input " Ratio =",C
:End
:Disp "----------------"
:Disp "  Enter  Spin "
:Disp " Finish  Value"
:Disp "    between"
:Disp "  1.5 and 3.0"
:Disp "----------------"
:Input " Spin Finish =",E
:While E<1.5 or E>3.0
:Disp "-----Sorry-----"
:Disp "  Enter  Spin "
:Disp " Finish  Value"
:Disp "    between"
:Disp "  1.5 and 3.0"
:Disp "    only"
:Disp "----------------"
:Input " Spin Finish =",E
:End
:Disp "----------------"
:Disp "   Relaxation stage "
:Disp "      Enter  "
:Disp "     0 or 1"
:Disp "----------------"
:Input "Stage=",F
:While F<0 or F>1
:Disp "-----Sorry-----"
:Disp "   Relaxation stage "
:Disp "      Enter  "
:Disp "     0 or 1"
:Disp "    only"
:Disp "----------------"
:Input "Stage=",F
:End
:Disp "----------------"
:Disp "  Enter  Twist "
:Disp "     Value    "
:Disp "    between"
:Disp "    4 and 8"
:Disp "----------------"
:Disp " "
:Input " Twist =",H
:While H<4 or H>8
:Disp "-----Sorry-----"
:Disp "  Enter  Twist "
:Disp "     Value    "
:Disp "    between"
:Disp "    4 and 8"
:Disp "   only"
:Disp "----------------"
:Input " Twist =",H
:End
:Disp "----------------"
```

Equations (7.9 – 7.13)

```
:Disp "*****--1--*****"
:Disp ""
:Disp "Count="
:Disp I
:Disp "          denier"
:Disp "----------------"
:Pause
:Disp "*****--2--*****"
:Disp "Shrinkage="
:Disp M
:Disp "            %"
:Disp "----------------"
:Pause
:Disp "*****--3--*****"
:Disp "Tenacity="
:Disp J
:Disp "          g/den"
:Disp "----------------"
:Pause
:Disp "*****--4--*****"
:Disp "Elongation="
:Disp K
:Disp "            %"
:Disp "----------------"
:Pause
:Disp "*****--5--*****"
:Disp "Modulus="
:Disp L
:Disp "          g/den"
:Disp "----------------"
:Pause
:Disp "*****--6--*****"
:Disp "Abrasion="
:Disp N
:Disp "          rotation "
:Disp "----------------"
:Pause
End
If Q=3
Then
:Disp "  HOT DRAWING"
:Disp "----------------"
:Disp " Enter  Drawing"
:Disp "   Stage Value "
:Disp "between 1 and 2"
:Disp "----------------"
:Input "Stage=",A
:While A<1 or A>2
:Disp "----------------"
:Disp "-----Sorry-----"
:Disp " Enter  Drawing"
:Disp "   Stage Value "
:Disp "between 1and 2"
:Disp "    only"
:Disp "----------------"
:Input "Stage=",A
:End
:Disp "----------------"
:Disp " Enter Drawing "
:Disp "  Temperature "
:Disp " Value between"
:Disp "   40 and 60"
:Disp "----------------"
:Input " Temperature =",B
:While B<40 or B>60
:Disp "-----Sorry-----"
:Disp " Enter Drawing "
:Disp "  Temperature "
:Disp " Value between"
:Disp "   40 and 60"
:Disp "      only"
:Disp "----------------"
:Input " Temperature =",B
:End
:Disp "----------------"
:Disp "     Enter  "
:Disp " Drawing  ratio "
:Disp " Value between"
:Disp "  3.5 and 5.0"
:Disp "----------------"
:Input " Ratio =",C
:While C<3.5 or C>5.0
:Disp "-----Sorry-----"
:Disp "     Enter  "
```

```
:Disp " Drawing Ratio "
:Disp " Value between"
:Disp "  3.5 and 5.0"
:Disp "      only"
:Disp "----------------"
:Input " Ratio =",C
:End
:Disp "----------------"
:Disp "  Enter Plate "
:Disp "  Temperature "
:Disp " Value between"
:Disp "   40 and 60"
:Disp "----------------"
:Input " Temperature =",D
:While D<40 or D>60
:Disp "-----Sorry-----"
:Disp "  Enter Plate "
:Disp "  Temperature "
:Disp " Value between"
:Disp "   40 and 60"
:Disp "      only"
:Disp "----------------"
:Input " Temperature =",D
:End
:Disp "----------------"
:Disp "  Enter  Spin "
:Disp " Finish  Value"
:Disp "    between"
:Disp "  1.5 and 3.0"
:Disp "----------------"
:Input " Spin Finish =",E
:While E<1.5 or E>3.0
:Disp "-----Sorry-----"
:Disp "  Enter  Spin "
:Disp " Finish  Value"
:Disp "    between"
:Disp "  1.5 and 3.0"
:Disp "    only"
:Disp "----------------"
:Input " Spin Finish =",E
:End
:Disp "----------------"
:Disp "  Enter  Relax "
:Disp "  Stage  Value "
:Disp "     between"
:Disp " 0.04 and  0.08"
:Disp "----------------"
:Input "Stage=",F
:While F<0.04 or F>0.08
:Disp "-----Sorry-----"
:Disp "  Enter  Relax "
:Disp "  Stage  Value "
:Disp "     between"
:Disp " 0.04 and  0.08"
:Disp "    only"
:Disp "----------------"
:Input "Stage=",F
:End
:Disp ""
:Disp "----------------"
:Disp "  Enter Relax "
:Disp "  Temperature "
:Disp " Value between"
:Disp "   40 and 60"
:Disp "----------------"
:Input " Temperature =",G
:While G<40 or G>60
:Disp ""
:Disp "-----Sorry-----"
:Disp "  Enter Relax "
:Disp "  Temperature "
:Disp " Value between"
:Disp "   40 and 60"
:Disp "    only"
:Disp "----------------"
:Input " Temperature =",G
:End
:Disp ""
:Disp "----------------"
:Disp ""
```

Equations (6.1 – 6.6)

```
.:Disp "*****--1--*****"
:Disp ""
:Disp "Count="
:Disp I
:Disp "         denier"
:Disp "----------------"
:Pause
:Disp ""
:Disp "*****--2--*****"
:Disp ""
:Disp "Shrinkage="
:Disp M
:Disp "           %"
:Disp "----------------"
:Pause
:Disp ""
:Disp "*****--3--*****"
:Disp ""
:Disp "Tenacity="
:Disp J
:Disp "          g/den"
:Disp "----------------"
:Pause
:Disp ""
:Disp "*****--4--*****"
:Disp ""
:Disp "Elongation="
:Disp K
:Disp "           %"
:Disp "----------------"
:Pause
:Disp ""
:Disp "*****--5--*****"
:Disp ""
:Disp "Modulus="
:Disp L
:Disp "          g/den"
:Disp "----------------"
:Pause
:Disp ""
:Disp "*****--6--*****"
:Disp ""
:Disp "Birefringence"
:Disp "*1000="
:Disp P
:Disp ""
:Disp "----------------"
:Pause
:Disp ""
:Disp "*****--7--*****"
:Disp ""
:Disp "Full-Width"
:Disp "Half-Maximum="
:Disp O
:Disp "          degree"
:Disp "----------------"
:Pause
:Disp ""
End
If Q=4
Then
:Disp "  HOT DRAWING"
:Disp "  + TWISTING"
:Disp "----------------"
:Disp " Enter  Drawing"
:Disp "   Stage Value "
:Disp "between 1 and 2"
:Disp "----------------"
:Input "Stage=",A
:While A<1 or A>2
:Disp ""
:Disp "----------------"
:Disp "-----Sorry-----"
:Disp " Enter  Drawing"
:Disp "   Stage Value "
:Disp "between 1and 2"
:Disp "    only"
:Disp "----------------"
:Input "Stage=",A
:End
:Disp ""
:Disp "----------------"
:Disp " Enter Drawing "
:Disp "  Temperature "
:Disp " Value between"
:Disp "   40 and 60"
:Disp "----------------"
:Input " Temperature =",B
:While B<40 or B>60
Disp ""
:Disp "-----Sorry-----"
:Disp " Enter Drawing "
:Disp "  Temperature "
:Disp " Value between"
:Disp "   40 and 60"
:Disp "      only"
:Disp "----------------"
:Input " Temperature =",B
:End
:Disp ""
:Disp "----------------"
:Disp "     Enter  "
:Disp " Drawing Ratio "
:Disp " Value between"
:Disp "  3.5 and 5.0"
:Disp "----------------"
```

```
:Input " Ratio =",C
:While C<3.5 or C>5.0
:Disp ""
:Disp "-----Sorry-----"
:Disp "     Enter  "
:Disp " Drawing Ratio "
:Disp " Value between"
:Disp "  3.5 and 5.0"
:Disp "      only"
:Disp "----------------"
:Input " Ratio =",C
:Disp "  "
:End
:Disp ""
:Disp "----------------"
:Disp "  Enter Plate "
:Disp "  Temperature "
:Disp " Value between"
:Disp "   40 and 60"
:Disp "----------------"
:Disp "  "
:Input " Temperature =",D
:While D<40 or D>60
:Disp ""
:Disp "-----Sorry-----"
:Disp "  Enter Plate "
:Disp "  Temperature "
:Disp " Value between"
:Disp "   40 and 60"
:Disp "      only"
:Disp "----------------"
:Input " Temperature =",D
:End
:Disp ""
:Disp "----------------"
:Disp "  Enter  Spin "
:Disp " Finish  Value"
:Disp "    between"
:Disp "  1.5 and 3.0"
:Disp "----------------"
:Input " Spin Finish =",E
:While E<1.5 or E>3.0
:Disp ""
:Disp "-----Sorry-----"
:Disp "  Enter  Spin "
:Disp " Finish  Value"
:Disp "    between"
:Disp "  1.5 and 3.0"
:Disp "    only"
:Disp "----------------"
:Input " Spin Finish =",E
:End
:Disp "----------------"
:Disp "  Enter  Relax "
:Disp "  Stage  Value "
:Disp "     between"
:Disp " 0.04 and  0.08"
:Disp "----------------"
:Disp ""
:Input "Stage=",F
```

```
:While F<0.04 or F>0.08
:Disp ""
:Disp "-----Sorry-----"
:Disp "  Enter  Relax "
:Disp "  Stage  Value "
:Disp "     between"
:Disp " 0.04 and  0.08"
:Disp "    only"
:Disp "----------------"
:Input "Stage=",F
:End
:Disp ""
:Disp "----------------"
:Disp "  Enter Relax "
:Disp "  Temperature "
:Disp " Value between"
:Disp "   40 and 60"
:Disp "----------------"
:Disp ""
:Input " Temperature =",G
:While G<40 or G>60
:Disp ""
:Disp "-----Sorry-----"
:Disp "  Enter Relax "
:Disp "  Temperature "
:Disp " Value between"
:Disp "   40 and 60"
:Disp "    only"
:Disp "----------------"
:Input " Temperature =",G
:End
:Disp ""
:Disp "----------------"
:Disp "  Enter  Twist "
:Disp "     Value    "
:Disp "    between"
:Disp "    4 and 8"
:Disp "----------------"
:Input " Twist =",H
:While H<4 or H>8
:Disp ""
:Disp "-----Sorry-----"
:Disp "  Enter  Twist "
:Disp "     Value    "
:Disp "    between"
:Disp "    4 and 8"
:Disp "   only"
:Disp "----------------"
:Input " Twist =",H
:Disp "  "
:End
:Disp "----------------"
:Disp ""
```

Equations (6.11 – 6.15)

```
.:Disp "*****--1--*****"
:Disp ""
:Disp "Count="
:Disp I
:Disp "          denier"
:Disp "----------------"
:Pause
:Disp ""
:Disp "*****--2--*****"
:Disp ""
:Disp "Shrinkage="
:Disp M
:Disp "            %"
:Disp "----------------"
:Pause
:Disp ""
:Disp "*****--3--*****"
:Disp ""
:Disp "Tenacity="
:Disp J
:Disp "           g/den"
:Disp "----------------"
:Pause
:Disp ""
:Disp "*****--4--
*****"
:Disp ""
:Disp "Elongation="
:Disp K
:Disp "              %"
:Disp "----------------"
:Pause
:Disp ""
:Disp "*****--5--
*****"
:Disp ""
:Disp "Modulus="
:Disp L
:Disp "           g/den"
:Disp "----------------"
:Pause
:Disp ""
:Disp "*****--6--
*****"
:Disp "Abrasion="
:Disp N
:Disp "          rotation "
:Disp "----------------"
:Pause
:Disp ""
End
:Disp "Designed by"
:Disp "Basel Younes"
:Disp "Heriot-Watt"
:Disp " University"
:Disp "    2011"
```

APPENDIX F

Code listing for the drawing-twisting analyser for as-spun BAAC fibres

```
:Disp "  "
:Disp "----------------"
:Disp "Drawing-
Twisting"
:Disp "    Analyser "
:Disp "  for  as-spun"
:Disp "   AAC Fibres"
:Disp "----------------"
:Pause
:Disp "----------------"
:Disp "Prepare Samples"
:Disp "       of "
:Disp "Branched As-
Spun"
:Disp "   AAC Fibres"
:Disp "----------------"
:Pause
:Disp "----------------"
:Disp " Set  Spinning"
:Disp "  Temperature "
:Disp "  profile  at  "
:Disp "  120-125-135-"
:Disp "  140-150-150"
:Disp " Celsius degree"
:Pause
:Disp "----------------"
:Disp "  Set Metering "
:Disp "Pump Speed
Value"
:Disp "   at 8 rpm"
:Disp "----------------"
:Pause
:Disp "----------------"
:Disp " Set Quench Air"
:Disp "  Speed Value"
:Disp "   at 35 %"
:Disp " "
:Disp "----------------"
:Pause
:Disp "----------------"
:Disp "Set Spin Finish "
:Disp "  Speed Value"
:Disp "  at 0.3 rpm"
:Disp "----------------"
:Pause
:Disp "----------------"
:Disp "  Set Winding "
:Disp "  Speed Value"
:Disp "  at 50 m/min"
:Disp "----------------"
:Pause
:Disp "----------------"
:Disp "----------------"
:Disp "For cold
drawing"
:Disp " Enter Number 1"
:Disp "For cold
drawing"
:Disp "  and twisting"
:Disp " Enter Number 2"
:Disp "----------------"
:Pause
:Disp "----------------"
:Disp "For hot drawing"
:Disp " Enter Number 3"
:Disp "For hot drawing"
:Disp "  and twisting"
:Disp " Enter Number 4"
:Disp "----------------"
:Input " =",Q
:While Q<1 or Q>4
:Disp "----------------"
:Disp "For cold
drawing"
:Disp " Enter Number 1"
:Disp "For cold
drawing"
:Disp "  and twisting"
:Disp " Enter Number 2"
:Disp "----------------"
:Pause
:Disp "----------------"
:Disp "For hot drawing"
:Disp " Enter Number 3"
:Disp "For hot drawing"
:Disp "  and twisting"
:Disp " Enter Number 4"
:Disp "----------------"
:Input " =",Q
:End
If Q=1
Then
:Disp "  COLD
DRAWING"
:Disp "----------------"
:Disp " Enter  Drawing"
:Disp "   Stage Value "
:Disp "between 1 and 2"
:Disp "----------------"
:Input "Stage=",A
:While A<1 or A>2
:Disp "----------------"
:Disp "-----Sorry-----"
:Disp " Enter  Drawing"
:Disp "   Stage Value "
:Disp "between 1and 2"
:Disp "    only"
:Disp "----------------"
:Input "Stage=",A
:End
:Disp "----------------"
:Disp "     Enter  "
:Disp " Drawing Ratio "
:Disp " Value between"
:Disp "  1.6 and 2.6"
:Disp "----------------"
:Input " Ratio =",C
:While C<1.6 or C>2.6
:Disp "-----Sorry-----"
:Disp "     Enter  "
:Disp " Drawing Ratio "
:Disp " Value between"
:Disp "  1.6 and 2.6"
:Disp "      only"
:Disp "----------------"
:Input " Ratio =",C
:Disp "  "
:End
:Disp "----------------"
:Disp "  Enter  Spin "
:Disp " Finish  Value"
:Disp "    between"
:Disp "  1.5 and 3.0"
:Disp "----------------"
:Input " Spin Finish =",E
:While E<1.5 or E>3.0
:Disp ""
:Disp "-----Sorry-----"
:Disp "  Enter  Spin "
:Disp " Finish  Value"
:Disp "    between"
:Disp "  1.5 and 3.0"
:Disp "    only"
:Disp "----------------"
:Input " Spin Finish =",E
:End
:Disp "----------------"
:Disp "   Relaxation
stage "
```

```
:Disp "      Enter  "
:Disp "     0 or 1"
:Disp "----------------"
:Input "Stage=",F
:While F<0 or F>1
:Disp ""
:Disp "-----Sorry-----"
:Disp "   Relaxation
stage "
:Disp "    "
:Disp "      Enter  "
:Disp "     0 or 1"
:Disp "    only"
:Disp "----------------"
:Input "Stage=",F
:End
:Disp "----------------"
```

Equations (7.5-7.8)

```
:Disp "*****--1--
*****"
:Disp "Count="
:Disp I
:Disp "          denier"
:Disp "----------------"
:Pause
:Disp "*****--2--
*****"
:Disp "Shrinkage="
:Disp M
:Disp "            %"
:Disp "----------------"
:Pause
:Disp "*****--3--
*****"
:Disp "Tenacity="
:Disp J
:Disp "          g/den"
:Disp "----------------"
:Pause
:Disp "*****--4--
*****"
:Disp "Elongation="
:Disp K
:Disp "            %"
:Disp "----------------"
:Pause
:Disp "*****--5--
*****"
:Disp ""
:Disp "Modulus="
:Disp L
:Disp "          g/den"
:Disp "----------------"
:Pause
:Disp ""
End
If Q=2
Then
:Disp "  COLD
DRAWING"
:Disp "   + TWISTING"
:Disp "----------------"
:Disp " Enter  Drawing"
:Disp "   Stage Value "
:Disp "between 1 and 2"
:Disp "----------------"
:Input "Stage=",A
:While A<1 or A>2
:Disp "----------------"
:Disp "-----Sorry-----"
:Disp " Enter  Drawing"
:Disp "   Stage Value "
:Disp "between 1and 2"
:Disp "    only"
:Disp "----------------"
:Input "Stage=",A
:End
:Disp "----------------"
:Disp "     Enter  "
:Disp " Drawing Ratio "
:Disp " Value between"
:Disp "  1.6 and 2.6"
:Disp "----------------"
:Input " Ratio =",C
:While C<1.6 or C>2.6
:Disp "-----Sorry-----"
:Disp "     Enter  "
:Disp " Drawing Ratio "
:Disp " Value between"
:Disp "  1.6 and 2.6"
:Disp "      only"
:Disp "----------------"
:Input " Ratio =",C
:End
:Disp "----------------"
:Disp "  Enter  Spin "
:Disp " Finish  Value"
:Disp "    between"
:Disp "  1.5 and 3.0"
:Disp "----------------"
:Input " Spin Finish =",E
:While E<1.5 or E>3.0
:Disp ""
:Disp "-----Sorry-----"
:Disp "  Enter  Spin "
:Disp " Finish  Value"
:Disp "    between"
:Disp "  1.5 and 3.0"
:Disp "    only"
:Disp "----------------"
:Input " Spin Finish =",E
:End
:Disp "----------------"
:Disp "   Relaxation
stage "
:Disp "      Enter  "
:Disp "     0 or 1"
:Disp "----------------"
:Input "Stage=",F
:While F<0 or F>1
:Disp ""
:Disp "-----Sorry-----"
:Disp "   Relaxation
stage "
:Disp "      Enter  "
:Disp "     0 or 1"
:Disp "    only"
:Disp "----------------"
:Input "Stage=",F
:End
:Disp "----------------"
:Disp "  Enter  Twist "
:Disp "     Value    "
:Disp "    between"
:Disp "    4 and 8"
:Disp "----------------"
:Input " Twist =",H
:While H<4 or H>8
:Disp "-----Sorry-----"
:Disp "  Enter  Twist "
:Disp "     Value    "
:Disp "    between"
:Disp "    4 and 8"
:Disp "   only"
:Disp "----------------"
:Input " Twist =",H
:End
:Disp "----------------"
```

Equations (7.14-7.18)

```
:Disp "*****--1--
*****"
:Disp "Count="
:Disp I
:Disp "          denier"
:Disp "----------------"
:Pause
```

```
:Disp "*****--2--
*****"
:Disp "Shrinkage="
:Disp M
:Disp "            %"
:Disp "----------------"
:Pause
:Disp "*****--3--
*****"
:Disp "Tenacity="
:Disp J
:Disp "          g/den"
:Disp "----------------"
:Pause
:Disp "*****--4--
*****"
:Disp ""
:Disp "Elongation="
:Disp K
:Disp "            %"
:Disp "----------------"
:Pause
:Disp ""
:Disp "*****--5--
*****"
:Disp "Modulus="
:Disp L
:Disp "          g/den"
:Disp "----------------"
:Pause
:Disp "*****--6--
*****"
:Disp "Abrasion="
:Disp N
:Disp "         rotation "
:Disp "----------------"
:Pause
:End
If Q=3
Then
:Disp "  HOT
DRAWING"
:Disp "----------------"
:Disp " Enter  Drawing"
:Disp "   Stage Value "
:Disp "between 1 and 2"
:Disp "----------------"
:Input "Stage=",A
:While A<1 or A>2
:Disp "----------------"
:Disp "-----Sorry-----"
:Disp " Enter  Drawing"
:Disp "   Stage Value "
:Disp "between 1and 2"
:Disp "    only"
:Disp "----------------"
:Input "Stage=",A
:End
:Disp "----------------"
:Disp " Enter Drawing "
:Disp "  Temperature "
:Disp " Value between"
:Disp "   40 and 60"
:Disp "----------------"
:Input " Temperature
=",B
:While B<40 or B>60
Disp ""
:Disp "-----Sorry-----"
:Disp " Enter Drawing "
:Disp "  Temperature "
:Disp " Value between"
:Disp "   40 and 60"
:Disp "      only"
:Disp "----------------"
:Input " Temperature
=",B
:End
:Disp "----------------"
:Disp "     Enter  "
:Disp " Drawing Ratio "
:Disp " Value between"
Disp "  1.6 and 2.6"
:Disp "----------------"
:Input " Ratio =",C
:While C<1.6 or C>2.6
:Disp "-----Sorry-----"
:Disp "     Enter  "
:Disp " Drawing Ratio "
:Disp " Value between"
:Disp "  1.6 and 2.6"
:Disp "      only"
:Disp "----------------"
:Input " Ratio =",C
:End
:Disp "----------------"
:Disp "  Enter Plate "
:Disp "  Temperature "
:Disp " Value between"
:Disp "   40 and 60"
:Disp "----------------"
:Disp "  "
:Input " Temperature
=",D
:While D<40 or D>60
:Disp ""
:Disp "-----Sorry-----"
:Disp "  Enter Plate "
:Disp "  Temperature "
:Disp " Value between"
:Disp "   40 and 60"
:Disp "      only"
:Disp "----------------"
:Input " Temperature
=",D
:End
:Disp "----------------"
:Disp "  Enter  Spin "
:Disp " Finish  Value"
:Disp "    between"
:Disp "  1.5 and 3.0"
:Disp "----------------"
:Input " Spin Finish =",E
:While E<1.5 or E>3.0
:Disp "-----Sorry-----"
:Disp "  Enter  Spin "
:Disp " Finish  Value"
:Disp "    between"
:Disp "  1.5 and 3.0"
:Disp "    only"
:Disp "----------------"
:Input " Spin Finish =",E
:End
:Disp "----------------"
:Disp "  Enter  Relax "
:Disp "  Stage  Value "
:Disp "     between"
:Disp " 0.04 and  0.08"
:Disp "----------------"
:Input "Stage=",F
:While F<0.04 or
F>0.08
:Disp "-----Sorry-----"
:Disp "  Enter  Relax "
:Disp "  Stage  Value "
:Disp "     between"
:Disp " 0.04 and  0.08"
:Disp "    only"
:Disp "----------------"
:Input "Stage=",F
:End
:Disp "----------------"
:Disp "  Enter Relax "
:Disp "  Temperature "
:Disp " Value between"
:Disp "   40 and 60"
:Disp "----------------"
:Input " Temperature
=",G
```

```
:While G<40 or G>60
:Disp "-----Sorry-----"
:Disp "  Enter Relax "
:Disp "  Temperature "
:Disp " Value between"
:Disp "   40 and 60"
:Disp "    only"
:Disp "----------------"
:Input " Temperature
=",G
:End
:Disp "----------------"
```

Equations (6.7-6.10)

```
:Disp "*****--1--
*****"
:Disp "Count="
:Disp I
:Disp "         denier"
:Disp "----------------"
:Pause
:Disp "*****--2--
*****"
:Disp ""
:Disp "Shrinkage="
:Disp M
:Disp "            %"
:Disp "----------------"
:Pause
:Disp "*****--3--
*****"
:Disp "Tenacity="
:Disp J
:Disp "          g/den"
:Disp "----------------"
:Pause
:Disp ""
:Disp "*****--4--
*****"
:Disp ""
:Disp "Elongation="
:Disp K
:Disp "            %"
:Disp "----------------"
:Pause
:Disp ""
:Disp "*****--5--
*****"
:Disp ""
:Disp "Modulus="
:Disp L
:Disp "          g/den"
:Disp "----------------"
```

```
:Pause
:Disp ""
End
If Q=4
Then
:Disp "  HOT
DRAWING"
:Disp "  + TWISTING"
:Disp "----------------"
:Disp " Enter  Drawing"
:Disp "   Stage Value "
:Disp "between 1 and 2"
:Disp "----------------"
:Input "Stage=",A
:While A<1 or A>2
:Disp ""
:Disp "----------------"
:Disp "-----Sorry-----"
:Disp " Enter  Drawing"
:Disp "   Stage Value "
:Disp "between 1and 2"
:Disp "    only"
:Disp "----------------"
:Input "Stage=",A
:End
:Disp "----------------"
:Disp " Enter Drawing "
:Disp "  Temperature "
:Disp " Value between"
:Disp "   40 and 60"
:Disp "----------------"
:Input " Temperature
=",B
:While B<40 or B>60
Disp ""
:Disp "-----Sorry-----"
:Disp " Enter Drawing "
:Disp "  Temperature "
:Disp " Value between"
:Disp "   40 and 60"
:Disp "      only"
:Disp "----------------"
:Input " Temperature
=",B
:End
:Disp ""
:Disp "----------------"
:Disp "     Enter  "
:Disp " Drawing Ratio "
:Disp " Value between"
:Disp "  1.6 and 2.6"
:Disp "----------------"
:Input " Ratio =",C
```

```
:While C<1.6 or C>2.6
:Disp ""
:Disp "-----Sorry-----"
:Disp "     Enter  "
:Disp " Drawing Ratio "
:Disp " Value between"
:Disp "  1.6 and 2.6"
:Disp "      only"
:Disp "----------------"
:Input " Ratio =",C
:Disp "  "
:End
:Disp ""
:Disp "----------------"
:Disp "  Enter Plate "
:Disp "  Temperature "
:Disp " Value between"
:Disp "   40 and 60"
:Disp "----------------"
:Input " Temperature
=",D
:While D<40 or D>60
:Disp "-----Sorry-----"
:Disp "  Enter Plate "
:Disp "  Temperature "
:Disp " Value between"
:Disp "   40 and 60"
:Disp "      only"
:Disp "----------------"
:Input " Temperature
=",D
:End
:Disp "----------------"
:Disp "  Enter  Spin "
:Disp " Finish  Value"
:Disp "    between"
:Disp "  1.5 and 3.0"
:Disp "----------------"
:Input " Spin Finish =",E
:While E<1.5 or E>3.0
:Disp ""
:Disp "-----Sorry-----"
:Disp "  Enter  Spin "
:Disp " Finish  Value"
:Disp "    between"
:Disp "  1.5 and 3.0"
:Disp "    only"
:Disp "----------------"
:Input " Spin Finish =",E
:End
:Disp "----------------"
:Disp "  Enter  Relax "
:Disp "  Stage  Value "
```

```
:Disp "     between"
:Disp " 0.04 and  0.08"
:Disp "----------------"
:Disp ""
:Input "Stage=",F
:While F<0.04 or
F>0.08
:Disp ""
:Disp "-----Sorry-----"
:Disp "  Enter  Relax "
:Disp "  Stage  Value "
:Disp "     between"
:Disp " 0.04 and  0.08"
:Disp "    only"
:Disp "----------------"
:Input "Stage=",F
:End
:Disp ""
:Disp "----------------"
:Disp "  Enter Relax "
:Disp "  Temperature "
:Disp " Value between"
:Disp "   40 and 60"
:Disp "----------------"
:Disp ""
:Input " Temperature
=",G
:While G<40 or G>60
:Disp ""
:Disp "-----Sorry-----"
:Disp "  Enter Relax "
:Disp "  Temperature "
:Disp " Value between"
:Disp "   40 and 60"
:Disp "    only"
:Disp "----------------"
:Input " Temperature
=",G
:End
:Disp "----------------"
:Disp "  Enter  Twist "
```

```
:Disp "     Value    "
:Disp "    between"
:Disp "    4 and 8"
:Disp "----------------"
:Disp " "
:Input " Twist =",H
:While H<4 or H>8
:Disp ""
:Disp "-----Sorry-----"
:Disp "  Enter  Twist "
:Disp "     Value    "
:Disp "    between"
:Disp "    4 and 8"
:Disp "   only"
:Disp "----------------"
:Input " Twist =",H
:Disp "  "
:End
:Disp ""
:Disp "----------------"
:Disp ""
```

Equations (6.16-6.20)

```
:Disp "*****--1--
*****"
:Disp ""
:Disp "Count="
:Disp I
:Disp "          denier"
:Disp "----------------"
:Pause
:Disp ""
:Disp "*****--2--
*****"
:Disp ""
:Disp "Shrinkage="
:Disp M
:Disp "            %"
:Disp "----------------"
:Pause
:Disp ""
```

```
:Disp "*****--3--
*****"
:Disp ""
:Disp "Tenacity="
:Disp J
:Disp "           g/den"
:Disp "----------------"
:Pause
:Disp ""
:Disp "*****--4--
*****"
:Disp ""
:Disp "Elongation="
:Disp K
:Disp "            %"
:Disp "----------------"
:Pause
:Disp "*****--5--
*****"
:Disp ""
:Disp "Modulus="
:Disp L
:Disp "           g/den"
:Disp "----------------"
:Pause
:Disp ""
:Disp "*****--6--
*****"
:Disp ""
:Disp "Abrasion="
:Disp N
:Disp "          rotation "
:Disp "----------------"
:Pause
End
:Disp "Designed by"
:Disp ""
:Disp "Basel Younes"
:Disp "Heriot  Watt"
:Disp " University"
:Disp "    2011"
```

REFERENCES

[1] J. W. S. Hearle, "The New Revolution in Textile Technology " Phys Techno, 16 (1985), 269-281.

[2] R. Chandra and R. Rustgi, Biodegradable Biopolymers, Elsevier Science Ltd, Great Britain, 1998.

[3] M. I. Tobler-Rohr, Handbook of Sustainable Textile Production, Woodhead Publishing Limited, UK, 2011.

[4] W. Callister, Materials Science and Engineering: An Introduction, John Wiley and Sons, New York, 1999.

[5] Y. Wang, Recycling in Textiles, Woodhead Publishing Ltd, England, 2006.

[6] A. F. Baldissera, C. E. S. Valério, N. R. d. S. Basso, F. Guaragna, and S. Einloft, "Synthesis and NMR Characterization of Aliphatic- aronatic Copolyester by Reaction of Poly(Ethylene Terephthalate) postconsumer and Poly(Ethylene Adipate)," Quim. Nova, 28:2 (2005), 188-191.

[7] B. Guduri, H. Semosa, and Y. Z. Mengb, Green composites from Woven Flax Fiber and Bio-copolyester, International Conference on Composite Materials (17) Edinburgh, UK, 27-31 July, 2009.

[8] C.-S. Wu, "Characterization of cellulose acetate-reinforced aliphatic–aromatic copolyester composites," Carbohydrate Polymers, 87 (2012), 1249- 1256.

[9] K. Oksman, M. Skrifvars, and J.-F. Selin, "Natural fibres as reinforcement in polylactic acid (PLA) composites," Composites Science and Technology, 63 (2003), 1317-1324.

[10] T. J. Keener, R. K. Stuart, and T. K. Brown, "Maleated coupling agents for natural fibre composites," Composites. Part A, Applied science and manufacturing 35 (2004), 357-362.

[11] D. P. lackett, T. L. Andersen, W. B. Pedersen, and L. Nielsen, "Biodegradable composites based on polylactide and jute fibres," Composites Science and Technology, 63:9 (2003), 1287-1296.

[12] K. Okubo and T. Fujii, "Eco-composites using bamboo and other natural fibers and their mechanical properties," In: Proceedings of the international workshop on ‘‘Green’’ composites (2002), 17-21.

[13] S. Luo and A. N. Netravali, "Interfacial and mechanical properties of environment-friendly green composites made from pineapple fibers and poly(hydroxybutyrate-co-valerate) resin," Journal of Materials Science, 34 (1999), 3709-3719.

[14] T. Nishino, K. Hirao, M. Kotera, K. Nakamae, and H. Inagaki, "Kenaf reinforced biodegradable composite," Composites Science and Technology, 63:9 (2003), 1281-1286.

[15] P. J. Herrera-Franco and A. Valadez-Gonza´lez, "Mechanical properties of continuous natural fibre-reinforced polymer composites," Composites Part A: Applied Science and Manufacturing, 35:3 (2004), 339-345.

[16] C.-S. Wu, "Process, Characterization and Biodegradability of Aliphatic Aromatic Polyester/Sisal Fiber Composites," Journal of Polymers and the Environment 3:19 (2011), 706-713.

[17] A. K. Mohanty, A. Wibowo, M. Misra, and L. T. Drzal, "Effect of process engineering on the performance of natural fiber reinforced cellulose acetate biocomposites," Composites Part A: Applied Science and Manufacturing, 35:3 (2004), 363-370.

[18] S. Ochi, "Development of high strength biodegradable composites using Manila hemp fiber and starch-based biodegradable resin," Composites Part A: Applied Science and Manufacturing, 37:11 (2006), 1879-1883.

[19] R. Smith, Biodegradable Polymers for Industrial Applications, Woodhead Publishing Limited, England, 2005.

[20] A. Steinbüchel, Biopolymers Vol. 10: General Aspects and Special Applications Vol. 10, Wiley-VCH, Germany, 2003.

[21] M. Kolybaba, L. G. Tabil, S. Panigrahi, W. J. Crerar, T. Powell, and B. Wang, Biodegradable Polymers: Past, Present, and Future, ASAE Paper Number: RRV03-0007, ASAE/CSAE North Central Intersectional Meeting, October 3-4, Fargo, North Dakota, 2003.

[22] "Standard guide for assessing the compostability of environmentally degradable plastics, D 6002-96," American Society for Testing and Materials, Washington, D.C. (1996).

[23] H. Sawada, "ISO standard activities in standardization of biodegradability of plastics-development of test methods and definitions," Polymer degradation and Stability, 59 (1998), 365-370.
[24] M. P. Pavlov, J. F. Mano, N. M. Neves, and R. L. Reis, "Fibres and 3D mesh scaffolds from Biodegradable starch based blends: production and characterization," Macromolecular bioscience 4 (2004), 776-784
[25] Y. Chen, R. Wombacher, J. H. Wendorff, J. Visjager, P. Smith, and A. Greiner, "Design, Synthesis, and Properties of New Biodegradable Aromatic/Aliphatic Liquid Crystalline Copolyesters," Biomacromolecules, 4:4 (2003), 974 -980.
[26] L. Han, G. Zhu, W. Zhang, and W. Chen, "Composition, Thermal Properties, and Biodegradability of a New Biodegradable Aliphatic/Aromatic Copolyester," Journal of applied polymer science, 113:2 (2009), 1298-1306.
[27] L. Averous, "Biodegradable multiphase systems based on plasticized starch: a review," Journal of Macromolecular Science - Polymer Reviews, 44:3 (2004), 231-274.
[28] M. Crank, M. Patel, F. Marscheider-Weidemann, J. Schleich, B. Hüsing, and G. Angerer, "Techno-economic Feasibility of Large-scale Production of Bio-based Polymers in Europe (PRO-BIP)-Final Report " Utrecht University& Fraunhofer ISI,Spain (2004).
[29] W. Holding, Biodegradable Polymer Supply Chains: Implications and Opportunities for Australian Agriculture, Rural Industries Research and Development Corporation, Australia 2004.
[30] Monsanto, "Biopolymers to Give Cotton Fibers Synthetic-Like Qualities," Monsanto company, U.S.A, 2003.
[31] B. J. McCarthy, Textiles for Hygiene and Infection Control, Woodhead Publishing Limited, UK, 2011.
[32] S. Kalambur and S. S. H. Rizvi, "Biodegradable and Functionally Superior Starch-Polyester Nanocomposites from Reactive Extrusion," Journal of Applied Polymer Science, 96:4 (2005), 1072 - 1082.
[33] M. Crank, M. Patel, F. Marscheider-Weidemann, J. Schleich, B. Hüsing, G. Angerer, and O. Wolf, "Techno-economic Feasibility of Large-scale Production of Bio-based Polymers in Europe: Technical Report EUR 22103 EN," European Science and Technology Observatory, European Communities (2005).
[34] E. Takiyama and T. Fujimaki, Biodegradable Plastics and Polymers, Elsevier, Amsterdam, 1994.
[35] Nolan-ITU, "Environment Australia:Biodegradable Plastics- Development and Environmental Impacts," Nolan-ITU, East Kew, Victoria (2002).
[36] P. Prowans, M. E. Fray, and J. Slonecki, "Biocompatibility studies of new multiblock poly(ester-ester)s composed of poly(butylene terephthalate) and dimerized fatty acid," Biomaterials, 23:14 (2002), 2973-2978.
[37] M. Renke-Gluszko and M. E. Fray, "The effect of simulated body fluid on the mechanical properties of multiblock poly(aliphatic/aromatic-ester) copolymers," Biomaterials, 25:21 (2004), 5191-5198.
[38] L. Fumin, W. A. Haile, M. E. Tincher, and W. S. Harris, "Bio-Degradable Copolyester Nonwoven Fabric," European Patent EP1330350 (2003).
[39] J. H. Wang and H. Aimin, "Biodegradable Aliphatic-Aromatic Copolyester for use in Nonwoven Webs," 2008).
[40] F. LU, W. Ahaile, M. Etincher, and S. H. Wiley, "Bio-degradable Copolyester Nonwoven Fabric," 2002).
[41] M. Râpă, M. E. Popa, P. Cinelli, A. Lazzeri, R. Burnichi, A. Mitelut, and E. Grosu, "Biodegradable alternative to plastics for agriculture application," ACRomanian Biotechnological Letters, 16:.6 (2011).
[42] K. Ganesh, A. H. Alp, and G. R. Russell, "Biodegradable Aliphatic-Aromatic Copolyesters, Methods of Manufacture, and Articles Thereof " 03/24/2011).
[43] Eastman polymers for fibres, Eastman chemical company, USA, 2002.
[44] C. Bastioli, Handbook of Biodegradable Polymers, Rabra Technology, Shawbury, UK, 2005.
[45] G. K. Hoeschele, "Thermostabile Polyester-Block-Copolymere," US Patent 3 954 689 (1976).

[46] Y. Chen, L. Tan, L. Chen, Y. Yang, and X. Wang, "Study on Biodegradable Aromatic/Aliphatic Copolyester," Brazilian Journal of Chemical Engineering, 25:2 (2008), 321 - 335.
[47] W. Xiao-Hui, S. Jun, C. Ying, F. Zhi-Feng, and S. Yan, "Study on Structure and Crystallinity of a New Biodegradable Aliphatic-Aromatic Copolyester," Petrochemical Research, 13:4 (2011), 64-69.
[48] S. S. Park, S. H. Chae, and S. S. Im, "Transesterification and crystallization behavior of poly (butylene succinate)/poly(butylene terephthalate) block copolymers," Journal of Polymer Science, Part A: Polymer Chemistry 36:1 (1998), 147-156
[49] R. A. Hayes, "Aliphatic-aromatic copolyesters," US Patent 6485819 (2002).
[50] P. Pan and Y. Inoue, "Polymorphism and isomorphism in biodegradable polyesters," Progress in Polymer Science:34 (2009), 605-640.
[51] H. C. Ki and O. O. Park, "Synthesis, characterization and biodegradability of the biodegradable aliphatic–aromatic random copolyesters," Polymer, 42 (2001), 1849-1861.
[52] Y. Tokiwa, T. Suzoki, and J. Appl, "Hydrolysis of copolyesters containing aromatic and aliphatic ester blocks by lipase," Journal of Applied Polymer Science, 26:2 (1981), 441-448.
[53] H.-J. Jin, B.-Y. Lee, M.-N. Kim, and J.-S. Yoon, "Thermal and mechanical properties of mandelic acid-copolymerized poly(butylene succinate) and poly(ethylene adipate)," Journal of Polymer Science, Part B: Polymer Physics, 38 (2000), 1504-1511.
[54] U. Witt, R.-J. Muller, and W.-D. Deckwer, "New biodegradable polyester-copolyesters from commodity chemicals with favorable use properties," Journal of Polymers and the Environment, 3:4 (1995), 215-223.
[55] H. J. Kang and S. S. Park, "Characterization and Biodegradability of Poly(butylene adipate-co-succinate)/Poly(butylene terephthalate) Copolyester," Journal of Applied Polymer Science, 72:4 (1999), 593-608.
[56] E. S. Stevens, Green Plastics, Plastics and the Environment Princeton University Press, USA, 2001.
[57] Y.-M. Suna and C.-S. Wang, "Preparation and characterization of poly(ethylene-1,4-cyclohexanedimethylene arylate)," European Polymer Journal, 35 (1999), 1087-1096.
[58] P. Bajaj, "Aliphatic-Aromatic Copolyester Fibers, Part I. Effect of Bisphenols on Structure and Mechanical Properties " Textile Research Journal, 51:11 (1981), 696-703.
[59] W. Amass, A. Amass, and B. Tighe, "A review of biodegradable polymers," Polymer international, 47 (1998), 89-144.
[60] A. Cao, K.-i. Kasuya, H. Abe, Y. Doi, and Y. Inoue, "Studies on comonomer compositional distribution of the bacterial poly(3-hydroxybutyric acid-co-3-hydroxypropionic acid)s and crystal and thermal characteristics of their fractionated component copolyesters " Polymer, 39 20 (1998), 4801-4816.
[61] Y. Chen, Y. Yang, J. Su, L. Tan, and Y. Wang, "Preparation and characterization of aliphatic/aromatic copolyesters based on bisphenol-A terephthalate, hexylene terephthalate and lactide mioties," Reactive & Functional Polymers, 67 (2007), 396-407.
[62] F. Li, X. Xu, Q. Li, Y. Li, H. Zhang, J. Yu, and A. Cao, "Thermal degradation and their kinetics of biodegradable poly(butylene succinate-co-butylene terephthate)s under nitrogen and air atmospheres," Polymer Degradation and Stability, 91 (2006), 1685 -1693.
[63] L.-M. Deng, Y.-Z. Wang, K.-K. Yang, X.-L. Wang, Q. Zhou, and S.-D. Ding, "A new biodegradable copolyester poly(butylene succinate-co-ethylene succinate-co-ethylene terephthalate) " Acta Materialia, 52:20 (2004), 5871-5878.
[64] S. S. Park and H. J. Kang, "Sequence distribution and crystallization behavior on block copolyesters of poly(butylene glutarate-co-adipate-co-succinate) ternary random copolyester and poly(butylene terephthalate)," Polymer Journal 31:3 (1999), 238-245.
[65] I. Kleeberg, C. Hetz, R. M. Kroppenstedt, R.-J. Müller, and W.-D. Deckwer, "Biodegradation of Aliphatic-Aromatic Copolyesters by Thermomonospora fusca and Other Thermophilic Compost Isolates," Appl Environ Microbiol, 64:5 (1998), 1731-1735.
[66] N. C. Hoppens, T. W. Hudnall, A. Foster, and C. J. Booth, "Aliphatic-aromatic copolyesters derived from 2,2,4,4-tetramethyl-1,3-cyclobutanediol," Journal of Polymer Science, Part A: Polymer Chemistry, 42:14 (2004), 3473-3478
[67] M. Erceg, T. Kovacic, and I. Klaric, "Dynamic thermogravimetric degradation of poly(3-hydroxybutyrate)/aliphaticearomatic copolyester blends," Polymer Degradation and Stability, 90 (2005), 86-94.

[68] X. Q. Shi, K. Aimi, H. Ito, S. Ando, and T. Kikutani, "Characterization on mixed-crystal structure of poly(butylene terephthalate/succinate/adipate) biodegradable copolymer fibers," Polymer, 46 (2005), 751-760.
[69] M. Rolf-Joachim, K. Ilona, and D. Wolf-Dieter, "Biodegradation of polyesters containing aromatic constituents," Journal of biotechnology, 86:2 (2001), 87-95.
[70] U. Witt, M. Yamamoto, U. Seeliger, R.-J. Muller, and V. Warzelhan, " Biodegradable polymeric materials – not the origin but the chemical structure determines biodegradability " Angew chem. Int Ed 38:10 (1999), 1438-1442.
[71] S. H. Lee, S. W. Lim, and K. H. Lee, "Properties of potentially biodegradable copolyesters of (succinic acid-1,4-butanediol)/(dimethyl terephthalate-1,4-butanediol)," polymer international, 48 (1999), 861-867.
[72] M. Okada, "Chemical syntheses of biodegradable polymers," Progress in Polymer Science, 27 (2001), 87-133.
[73] U. Witt, R. J. Müller, and W. D. Deckwer, "Biodegradation behavior and material properties of aliphatic/aromatic polyesters of commercial importance," Journal of Environmental Polymer Degradation and Stability, 5:2 (1997), 81-89.
[74] Y. H. Park and C. G. Cho, "Synthesis and characterization of poly((butylene succinate)-co-(butylene terephthalate))-b-poly(tetramethylene glycol) segmented block copolymer," Journal of Applied Polymer Science, 79:11 (2001), 2067-2075.
[75] B. L. Seala, T. C. Oterob, and A. Panitch, "Polymeric biomaterials for tissue and organ regeneration," Materials Science and Engineering, 34:4-5 (2001), 147-230.
[76] Z. Gana, K. Kuwabaraa, M. Yamamotob, H. Abea, and Y. Doia, "Solid-state structures and thermal properties of aliphatic–aromatic poly(butylene adipate-co-butylene terephthalate) copolyesters," Polymer Degradation and Stability, 83 (2004), 289-300.
[77] U. Witt, T. Einig, M. Yamamoto, I. Kleeberg, W.-D. Deckwer, and R.-J. Müller, "Biodegradation of aliphatic–aromatic copolyesters: evaluation of the final biodegradability and ecotoxicological impact of degradation intermediates," Chemosphere, 44:2 (2001), 289-299.
[78] A. K. Mohanty, M. Misra, and L. T. Drzal, Natural Fibers, Biopolymers and Biocomposites Taylor & Francis-CRC Press, USA, 2005.
[79] H. Rong and G. S. Bhat, "Preparation and Properties Of Cotton-Eastar Nonwovens," International Nonwovens Journal, 12:2 (2003), 53-57.
[80] G. S. Bhat and R. Haoming, "Effect of Binder Fibres on Processing and Properties of Thermal Bonded Cotton-Based Non-woven," International Nonwovens Technical Conference, USA (2002).
[81] H. Rong, R. V. Leon, and G. S. Bhat, "Statistical Analysis of the Effect of Processing Conditions on the Strength of Thermal Point-Bonded Cotton-Based Nonwovens," Textile Research Journal, 75:1 (2005), 35-38.
[82] G. Bhat, M. G. Kamath, D. Mueller, D. V. Parikh, and M. McLean, "Cotton-Based Composites for Automotive Applications," Global Plastics Environmental Conference, Michigan (2004).
[83] K. Twarowska-Schmidt, "Evaluation of the Suitability of Some Biodegradable Polymers for the Forming of Fibres," Fibres & Textiles in Eastern Europe, 12:46 (2004), 15-18.
[84] K. Twarowska-Schmidt and M. Ratajska, "Biodegradability of Non-Wovens Made of Aliphatic-Aromatic Polyester," FIBRES & TEXTILES in Eastern Europe, 13:1 (2005), 71-74.
[85] E. B. Bond, J.-P. M. Autran, L. N. Mackey, I. Noda, and H. O. D'donnell, "United state patent, US 6.890.872, B2, Fibre comprising starch and biodegradable polymers," 2005).
[86] Q. Fang and M. A. Hanna, "Preparation and Characterization of Biodegradable Copolyester–Starch Based Foams," Bio-resource Technology, 78:2 (2001), 115-122.
[87] ASTM, "D 5338, Test Method for Determining Aerobic Biodegradation of Plastic Material under Controlled Compositing Conditions," (1998).
[88] J. Sami, "Processing of the 4th Conference on Biogically Degradable Mterials," Presentation, Germany (1999).
[89] G. Biresaw and C. J. Carriere, "Compatibility and mechanical properties of blends of polystyrene with biodegradable polyesters," Composites: Part A, 35 (2004), 313-320.

[90] G. Kale, T. Kijchavengkul, R. Auras, M. Rubino, S. E. Selke, and S. P. Singh, "Compostability of bioplastic packaging materials: an overview," Macromol. Biosci, 7 (2007), 255-277.
[91] J. C. Huang, A. S. Shetty, and M. S. Wang, "Biodegradable plastics: A review," Advances in Polymer Technology, 10:1 (1990), 23-30.
[92] U. Witt, R.-J. Müller, and W.-D. Deckwer, "Studies on sequence distribution of aliphatic/aromatic copolyesters by high-resolution C nuclear magnetic resonance spectroscopy for evaluation of biodegradability," Makromol Chem Phys, 197 (1996), 1525-1535.
[93] R. J. Muller, U. Witt, E. Rantze, and W. D. Deckwer, "Architecture of biodegradable copolyestyers containing aromatic constituents," Polymer Degradation and Stability 59 (1998), 203-208.
[94] V. Massardier-Nageotte, C. Pestre, T. Cruard-Pradet, and R. Bayard, "Aerobic and anaerobic biodegradability of polymer films and physico-chemical characterization," Polymer Degradation and Stability, 91 (2006), 620-627.
[95] Y. Yokota and H. Marechal, "Processability of biodegradable poly(butylene) succinate and its derivates. A case study," In Biopolymer conference, Wurzbburg, Germany (1999).
[96] T. Fujimaki, "Processability and properties of aliphatic polyesters 'Bionolle', synthesized by polycondensation reaction," Polymer Degradation and Stability, 59 (1998), 209-214.
[97] M. I. Santos, S. Fuchs, M. E. Gomes, and R. E. Unger, "Response of micro- and macrovascular endothelial cells to starch-based fiber meshes for bone tissue engineering," Biomaterials, 28 (2007), 240-248.
[98] H. Yoshimoto, Y. M. Shin, H. Terai, and J. P. Vacanti, "A biodegradable nanofiber scaffold by electrospinning and its potential for bone tissue engineering," Biomaterials, 24 (2003), 2077-2082.
[99] M. Wollerdorfer and H. Bader, "Influence of Natural Fibres on The Mechanical Properties of Biodegradable Polymers," Industrial Crops and Products, 8 (1998), 105–112.
[100] A. Dufresne and M. R. Vignon, "Improvement of Starch Film Performances Using Cellulose Microfibrils," Macromolecules, 31 (1998), 2963-2966.
[101] L. Averous, C. Frigant, and L. Moro, "Plasticized Starch Cellulose Interactions in Polysaccharide Composites," Polymer, 42 (2001), 6565–6572.
[102] A. J. F. Carvalho, A. A. S. Curvelo, and J. A. M. Agnelli, "Wood pulp reinforced thermoplastic starch composites," Int J Polymer Mater, 51 (2002), 647-660.
[103] E. B. Bond, J. P. M. Autrn, L. N. Mackey, I. Noda, and H. J. Odonnell, "WO 02/090630 A1, Multi-component fibres comprising starch and biodegradable polymer," 2002).
[104] B. E. Bryan, A. J. P. Marie, M. L. Neil, N. Isao, and H. J. Odonnell, "WO 02/090629 A1, Fibres comprising starch and biodegradable polymers," 2002).
[105] S. V. Artamonova and N. M. Demina, "New starch based textile onlining agent for glass fibres," Fibre chemistry 29 (1997), 68-70.
[106] Q. Wang, N. Zhang, X. Hu, J. Yang, and Y. Du, "Chitosan/starch fibers and their properties for drug controlled release," European Journal of Pharmaceutics and Biopharmaceutics (2007), Article in Press
[107] K. Y. Lim, K. J. Yoon, and B. C. Kim, "Highly absorbable lyocell fiber spun from celluloses/hydrolyzed starch-g-PAN solution in NMMO monohydrate," European Polymer Journal 39 (2003), 2115-2120.
[108] S. J. Kadolph and A. L. Langford, Textiles, 9th edition, Pearson Education Inc New Jersey, USA, 2002.
[109] J. C. Cook, Hand Book of Textile Fibre, Nerrow publishing, Watford ,UK, 1964.
[110] W. Klein, Man-mad Fiber and their Processing, The Textile Institute, UK, 1994.
[111] C. A. Lawrence, Advance in Yarn Spinning Technology, Woodhead Publishing Limited, UK, 2010.
[112] P. Lord, Hand Book of Yarn Production: Technology Science and Economics The Textile Institute & CRC & WP England, 2003.
[113] F. Fourne, Synthetic Fibers: Machines and Equipment, Manufacture, Properties, ed, Hanser Publishers, Munich, 1999.
[114] P. Walsh, The Yarn Book, How to understand, design and use yarn, A&C Black Publishers, London, 2006.
[115] S. B. Warner, Fibre Science, Prentice-Hall, Inc, New Jersey, 1995.

[116] Textile ,Fiber and Film Industry Technical conference IEEE 1994 Annual-H2 Paper, USA, 1994.
[117] H. F. Giles, J. R. Wagner, and E. M. Mount, Extrusion: the Definition Processing Guide and Hand Book, William Andrew Inc, Norwich, 2005.
[118] V. Capasso, Mathematical modelling for polymer processing, Springer-Verlag Berlin Heidelberg, New York, 2003.
[119] J. v. Meerveld, M. Hütter, and G. W. M. Petersb, "Continuum model for the simulation of fiber spinning, with quiescent and flow-induced crystallization " Journal of Non-Newtonian Fluid Mechanics, 150:2-3 (2008), 177-195.
[120] B. Tandler, G. Schmack, R. Vogel, D. Blechschmidt, and R. Linder, "Melt Processing of a New Biodegradable Synthetic Polymer in High-Speed Spinning and Underpressure Spunbonding Process," Journal of Polymers and the Environmenta, 9:4 (2001), 149-156.
[121] T. Matsuo, "Speciality Technologies of Fibres and Textiles in Japan," Textile Magazine, 41:4 (2004), 16-19.
[122] R. S. Blackburn, Biodegradable and Sustainable Fibres, Woodhead Publishing, Cambridge, UK, 2005.
[123] G. Tanguchi, Introduction to Quality Engineering, Asian productivity organization, Tokyo, 1986
[124] W. P. Gardiner and G. Gettinby, Experimental Design Techniques in Statistical Practice, A practical Software-Based Approach, Horwood Publishing Limited, Chichester, England, 1998.
[125] J. G. Vlachogiannis and R. K. Roy, "Robust PID controllers by taguchi method " The TOM magazine, 17:5 (2005), 456-466.
[126] K. B. Clark and S. C. Wheelwright, The product development challenge: competing through speed, quality, and creativity, A Harvard business review book, Boston, 1995.
[127] R. H. Lochner and J. E. Mater, Design for Quality, Chapman and Hall, London 1990.
[128] R. Yang, R. R. Mather, and A. F. Fotheringham, "The influence of fiber processing parameters on the structural properties of as-spun polypropylene fibers: A factorial design approach," Journal of Applied Polymer Science, 93:2 (2004), 568-576.
[129] J. C. Moreland, J. L. Sharp, and P. J. Brown, "Lab-Scale Fiber Spinning Experimental Design Cost Comparison," Journal of Engineered Fibers and Fabrics, 5:1 (2010), 39-49.
[130] A. Ziabicki, L. Jarecki, and A. Wasiak, "Dynamic modelling of melt spinning," Computational and Theoretical Polymer Science, 8:1-2 (1998), 143-157.
[131] H. H. George, "Model of steady-state melt spinning at intermediate take-up speeds," Polymer Engineering & Science, 22:5 (1982), 292-299.
[132] S. S. N. Perera, "Viscoelastic Effect in the Non-Isothermal Melt Spinning Processes," Applied Mathematical Sciences, 3:4 (2009), 177 - 186.
[133] R. Yang, R. R. Mather, and A. F. Fotheringham, "Processing, structure, and mechanical properties of as-spun polypropylene filaments—A systematic approach using factorial design and statistical analysis," Journal of Applied Polymer Science, 96:1 (2005), 144-154.
[134] A. Ziabicki, L. Jarecki, and A. Wasiak, "Dynamic modelling of melt spinning," Computational and Theoretical Polymer Science, 8:1/2 (1998), 143-157.
[135] G. X. Wang and E. F. Matthys, "Modelling of rapid solidification by meltspinning: effect of heat transfer in the cooling substrate," Materials Science and Engineering: A, 136 (1991), 85-97.
[136] C. Zhanga, C. Wanga, H. Wanga, and Y. Zhangb, "Multifilament Model of PET Melt Spinning and Prediction of As-spun Fiber's Quality," Journal of Macromolecular Science, Part B: Physics, 46:4 (2007), 193-806.
[137] T. Kotze, Two Dimensional Modelling of PET Melt Spinning: The effects of heat transfer limitations on the quality of PET yarn produced during melt spinning, LAP LAMBERT Academic Publishing, 2010.
[138] N. F. Li, C. W. Yi, and C. S. Wang, "Simulation of Multifilament Superfine Denier Polyester Melt Spinning," Advanced Materials Research, 332:334 (2011), 250-255.
[139] L. Jarecki and Z. Lewandowski, "Mathematical Modelling of the Pneumatic Melt Spinning of Isotactic Polypropylene. Part III. Computations of the Process Dynamics," FIBRES & TEXTILES in Eastern Europe, 17:1 (2009), 75-80.
[140] M. L. Ottone and J. A. Deiber, "Modelling the melt spinning of polyethylene terephthalate " Journal of elastomers and plastics, 32:2 (2000), 119-139.

[141] K. Ravikumar and Y. A. Son, "Process analysis and optimization for the ionic interactions of quaternary ammonium salts with nylon 66 fibers using statistical experimental design," Dyes and Pigments, 75:1 (2007), 199-206.
[142] J. S.-J. Chen and A. A. Tseng, "Modelling and optimization of nozzle design in planar flow melt spinning," manufacturing science and engineering –ASME 1999, 10 (1999), 79-86.
[143] W. He, S. Zhang, and X. Wang, "Mechanical Behavior of Irregular Fibers, Part I: Modeling the Tensile Behavior of Linear Elastic Fibers," Textile Research Journal, 71:6 (2001), 556-560.
[144] A. K. Doufasa, A. J. McHugha, and C. Millerb, "Simulation of melt spinning including flow-induced crystallization: Part I. Model development and predictions," Journal of Non-Newtonian Fluid Mechanics, 92:1 (2000), 27-66.
[145] X. Chen, Modelling and predicting textile behaviour, Woodhead Publishing Ltd, UK, 2010.
[146] S. C. R. Santos and R. A. R. Boaventura, "Adsorption modelling of textile dyes by sepiolite," Applied Clay Science, 42:1-2 (2008), 137-145.
[147] D. Bingol, N. Tekin, and M. Alkan, "Brilliant Yellow dye adsorption onto sepiolite using a full factorial design," Applied Clay Science, 50:3 (2010), 315-321.
[148] T. O. Hanci, I. A. Alaton, and G. Basar, "Multivariate analysis of anionic, cationic and nonionic textile surfactant degradation with the H 2 O 2 /UV-C process by using the capabilities of response surface methodology," Journal of Hazardous Materials, 185,:1 (2011), 193-203.
[149] A. B. Engin, Ö. Özdemir, M. Turan, and A. Z. Turan, "Color removal from textile dyebath effluents in a zeolite fixed bed reactor: Determination of optimum process conditions using Taguchi method," Journal of Hazardous Materials, 159:2-3 (2008), 348-353.
[150] I. Krucinska, "The influence of technological parameters on the filtration efficiency of electret needled non-woven fabrics," Article Journal of Electrostatics, 56:2 (2002), 143-153.
[151] J. P. Chen, K. H. Ho, Y. P. Chiang, and K. W. Wu, "Fabrication of electrospun poly(methyl methacrylate) nanofibrous membranes by statistical approach for application in enzyme immobilization " Journal of Membrane Science, 340:1-2 (2009), 9-15.
[152] A. W. Kaimouz, R. H. Wardman, and R. M. Christie, "Ink-jet printing process for lyocell and cotton fibres. Part 2: The relationship of colour strength and dye fixation to ink penetration," Coloration Technology, 126:6 (2010), 342-347.
[153] E. G. Fisher, extrusion of plastics, The Plastics and Rubber Institute, London, 1976.
[154] C. Rawendaal, Polymer extrusion, HANSER, Munich, 2001.
[155] S. Bruin, D. J. V. Zuilichem, and W. Stolp, "A reveiew of Fundamental and Engineering Aspect of Extrusion of Biopolymers in A single screw Extruder," Journal of Food Process Engineering 2:1 (1978), 1-37.
[156] M. Thuwall, A. Boldizar, and M. Rgdahl, "Extrusion Processing of High Amylose Potato Starch Materials," Carbohydrate Polymers, 65 (2006), 441-446
[157] M. Johnson, N. Tucker, S. Barnes, and K. Kirwan, "Improvement of the Impact performance of a starch Based Biopolymer via the Incorporation of Miscanthus Giganteus Fibres " Industrial Crops and Products, 22 (2005), 175-186.
[158] Y. Li and X.-Q. Dai, Biomechanical engineering of textiles and clothing, Woodhead Publishing Limited, Cambridge, England, 2006.
[159] A. Ziabicki, Fundamental of Fibre Formation, John Wiley &Sons, London, 1976.
[160] A. C. T. Aarts, Analysis of the flow instabilities in the extrusion of polymeric melts, PhD Thesis, Eindhoven University of Technology, Eindhoven,The Netherlands, 1997.
[161] C. Andreoli and F. Freti, Man-made fibres ACIMIT, Italy 2004.
[162] G. M. Ganjyal and M. A. Hanna, "Effect of Extruder Die Nozzle Dimensions on Expansion and Micrographic Characterization during Extrusion of Acetylated Starch " Starch 56:3-4 (2004), 108 -117.
[163] A. V. Shenoy and D. R. Saini, "melt flow index:more than just a quality control parameter:Part 1," advance in polymer technology 6: 1 (1997), 1-50.
[164] B. S. Gupta, Friction in Textile materials, Woodhead Publishing, Cambridge, 2008.
[165] J. W. S. Hearle, L. Hollick, and D. K. Wilson, Yarn texturing technology, Woodhead publishing ltd, Uk 2001.

[166] C.-C. H. a. T.-T. Tang, "Parameter optimization in melt spinning by neural networks and genetic algorithms," The International Journal of Advanced Manufacturing Technology, 27:11-12 (2006), 1113-1118.
[167] L. Hes and P. Ursiny, Yarn Texturizing Technology, EEC Comett program & Eurotex Portugal, 1994
[168] H. Brody, Synthetic fibre materials, Longman group UK limited London, 1994.
[169] E. Cranston, J. Kawada, S. Raymond, F. G. Morin, and R. H. Marchessault, "Cocrystallization Model for Synthetic Biodegradable Poly(butylene adipate-co-butylene terephthalate)," Biomacromolecules, 4 (2003), 995-999.
[170] J. W. S. Hearle and L. W. C. Miles, The Setting of Fibres and Fabrics, Marrow Publishing Co Ltd, England, 1971.
[171] J. A. Brydson, Flow Properties of Polymer Melts 2ed., George Godwin Limited, London, 1981.
[172] B. P. Saville, Physical Testing of Textiles, Woodhead Publishing Ltd, England, 1999.
[173] B. C. Goswami, J. G. Martindale, and F. C. Scardino, Textile Yarns: Technology, structure and application, John Wiley & sons, Inc, USA, 1977.
[174] C. A. Lawrence, Fundamentals of spun yarn technology, CRC Press, New York, 2003.
[175] User's manual, ThermaCAM Research Profesional Edition. Version 2.7, FLIR Systems AB, Sweden, 2003.
[176] Operator's Manual, ThermaCAM SC3000, FLIR Systems AB, Sweden, 1999.
[177] C. Miller, "Effect of filament drawdown on aerodynamic drag and heat transfer in fiber spinning," AIChE Journal, 50:5 (2004), 898-905.
[178] Z. Zhang, "Application of experimental design in new product development," The TQM Magazine, 10:6 (1998), 432 - 437.
[179] D. C. Montgomery, Design and Analysis of Experiments, 7th ed, John Wiley & Sons, New York, 2009.
[180] J. D. Maste, "A methodological comparison of three strategies for quality improvement," nternational journal of quality and reliability management 21:2 (2004), 198-213.
[181] M. R. Ellekjaer and S. Bisgaard, "The use of experimental design in the development of new products," International journal of quality science, 3 3 (1998), 254 - 274.
[182] D. C. Montgomery, Design and Analysis of Experiment, 4th ed., John Wiley and Sons, New York, 1997.
[183] M. S. Phadke, Quality Engineering Using Robust Design, Prentice Hall, Englewood Cliffs, New Jersey, 1989.
[184] Y. E. El-Mogahzy, Engineering textiles: integrating the design and manufacture of textile products, Woodhead Publishing Limited, England, 2009.
[185] J. Antony, D. Perry, C. Wang, and M. Kumar, "An application of taguchi method of experimental design for new product design and development process," Assembly automation 26:1 (2006), 18 - 24.
[186] J. N. Cawse, Experimental Design for Combinatorial and High Throughput Materials Development, John Wiley and Sons, Inc, USA, 2003.
[187] STATGRAPHICS, "STATGRAPHICS Plus Version 5.1," USA (2001).
[188] MINITAB, "Minitab 15.1.0.0," USA (2006).
[189] H. R. Lindman, Analysis of Variance in Experimental Design Springer – Verlag New York, USA, 1992.
[190] "Product user manual, 5 series advanced melt flow systems," Ray-Ran Test Equipment Ltd ,UK (1998).
[191] D. Walton and P. Lorimer, Polymers, Oxford University Press, New York, United States, 2000.
[192] C. D. Han, Rheology in polymer processing, Academic Press New York, 1976.
[193] ANTEC, "ANTEC 1999 Conference Processing," Processing, 1 (1999), 1242-1243.
[194] W. Michaeli, Extrusion Dies for Plastics and Rubber: Design and Engineering, Hanser, Munich, 1990.
[195] M. H. R. Ghoreishy, M. Razavi-Nouri, and G. Naderi, "Finite element analysis of flow of thermoplastic elastomer melt through axisymmetric die with slip boundary condition," Plastics, rubber and composites, 29:5 (2000), 224-228.
[196] I. M. Campbell, Intruduction to Synthetic Polymers, Oxford University Press Inc, United States, 1994.

[197] P. Xing, L. Dong, Y. An, Z. Feng, M. Avella, and E. Martuscelli, "Miscibility and Crystallization of Poly(-hydroxybutyrate) and Poly(p-vinylphenol) Blends," Macromolecules, 30 (1997), 2726 - 2733.
[198] M. H. R. Ghoreishy, M. Razavi-Nouri, and G. Naderi, "Finite element analysis of a thermoplastic elastomer melt flow in the metering region of a single screw extruder," Computational Materials Science, 34 (2005), 389-396.
[199] Z. K. Walczak, Formation of Synthetic Fibres, Gordon and Breach, New York, 1977.
[200] R. H. Gong and R. M. Wreight, Fancy yarns Wood head publishing ltd, England 2002.
[201] H. Hermans, Contribution to the Physics of Cellulose Fibres, Elsevier, Amsterdam, 1946.
[202] M. Pluta, "On the accuracy of microinterferometric measurements of optical-path differences by means of the half-shade method," J. Microscopy, 93:2 (1971), 83-100.
[203] T. Z. N. Sokkar, H. M. El-Dessouky, M. A. Shams-Eldin, and M. A. El-Morsy, "An automatic Fringe Analysis of Two-beam Interference Patterns for Measurement the Refractive Index and Birefringence Profiles of Fibers," Optics & Laser in Engineering, 45:3 (2007), 431.
[204] S. C. Simmens, "Birefringence Determination in Objects of Irregular Cross-sectional Shape and Constant Weight per Unit Length," Nature, 181 (1958), 1260-1261
[205] M. Pluta, Advanced Light Microscopy: Measuring Techniques Vol. 3, PWN-Polish Scientific Publishers, Warsaw, Poland, 1993.
[206] R. Meredith and J. W. S. Hearle, Physical methods of investigating textiles, Textile book publishers, Inc, New York, 1959.
[207] A. Guinier, X-ray diffraction: in crystals, imperfect crystals, and amorphous bodies, Dover Publications, New York, 1994.
[208] R. L. Snyder, J. Fiala, and H. J. Bunge, Defect and Microstructure Analysis by Diffraction, Diffraction-line broadening analysis of strain fields, Oxford University Press, Oxford, 1999.
[209] A. L. Patterson, "The Scherrer Formula for X-Ray Particle Size Determination," The American Physical Society, 56 (1939), 978-982.
[210] B. Fultz and J. M. Howe, Transmission Electron Microscopy and Diffractometry of Materials, Springer, Germany 2007.
[211] W. A. Kalender, Computed Tomography: Fundamentals, System Technology, Image Quality, Applications, Erlangen: Publicis Corporate Publishing, 2005.
[212] H. A. Barnes, J. F. Hutton, and K. Walters, An Introduction to Rheology, Elsevier Science Publisher, The Netherlands, 1989.
[213] S. J. Kadolph and A. L. Langford, Textiles Pearson Education Inc, USA, 2002.
[214] R. S. Lenk, Polymer Rheology, Applied science publishers LTD England, 1978.
[215] C.-Y. Ko, M. Chen, C.-L. Wang, H.-C. Wang, R.-Y. Chen, and I.-M. Tseng, "Poly(trimethylene terephthalate) copolyester containing ethylene glycol moieties. Part 1: Crystallization kinetics and melting behavior," Polymer, 48 (2007), 2415-2424.
[216] T. P. Ryan, Modern engineering statistics, Wiley-Interscience, New Jersey, USA, 2007.
[217] T. Götz, H. Rave, D. Reinel-Bitzer, K. Steiner, and H. Tiemeier, "Simulation of the fiber spinning process," Berichte des Fraunhofer ITWM, 26 (2001), 1-12.
[218] B. Younes and A. Fotheringham, "Factorial Optimisation of the Effects of Extrusion Temperature Profile and Polymer Grade on As-spun Aliphatic-Aromatic Co-Polyester Fibres III. Mechanical Properties," The Journal of the Textile Institute, 103:2 (February 2012), 139-153.
[219] T. Kijchavengkul, R. Auras, M. Rubino, M. Ngouajio, and R. T. Fernandez, "Assessment of aliphatic-aromatic copolyester biodegradable mulch films. Part II: Laboratory simulated conditions " Chemosphere, 71 (2008), 1607-1616.
[220] J. D. Ullman, Principles of database systems, Second Edition, Computer Science Press, Maryland, 1982.
[221] J. v. Meerveld, M. Hutter, and G. W. M. Peters, "Continuum model for the simulation of fiber spinning, with quiescent and flow-induced crystallization," J. Non-Newtonian Fluid Mech, 150 (2008), 177-195.
[222] G. Eder, H. Janeschitz-Kriegl, and S. Liedauer, "Crystallization processes in quiescent and moving polymer melts under heat transfer conditions," Proggress in polymer science, 15:4 (1990), 626-714.

[223] M. J. Stevens, Extruder Principles and Operation, Elsevier Applied Science Publishers LTD, England, UK, 1986.
[224] Z. K. Walczak, Processes of fiber formation, Elsevier Science Ltd, UK, 2002.
[225] H. M. El-Dessouky, A. A. Hamza, A. E. Belal, T. Z. N. Sokkar, and K. M. Yassien, "nterferometric Studies for the Annealing Effects on the Necking Deformation along Polypropylene Fibers," Journal of Engineered Fibers and Fabrics, 2:2 (2007), 1-16.
[226] C. H. Park, E. Y. Hong, and Y. K. Kang, "Effects of spinning speed and heat treatment on the mechanical properties and biodegradability of poly(lactic acid) fibers," Journal of Applied Polymer Science, 103:5 (2007), 3099-3104.
[227] S. Sardag, M. Kanık, and Ö. Özdemir, "The Effect of Vacuum Steaming Processes on Physical and Dyeability Properties of Polyamide 6 Yarns," Textile Research Journal, 80:15 (2010), 1531-15393.
[228] B. Younes and A. Fotheringham, "Statistical modelling of the thermal properties of extruded biodegradable fibres, poster presentation," The 5th International Speciality High Performance Polymer Fibres Conference, Polymer Fibres 2008, Weston Conference Centre, University of Manchester, UK (9-11 July, 2008).